New Experimental Capabilities and Loading Protocols for Seismic Qualification and Fragility Assessment of Nonstructural Systems

by

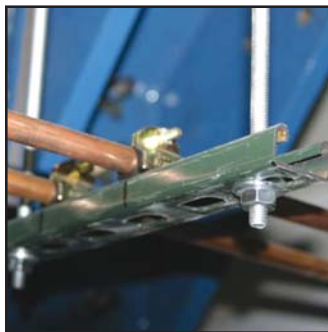## Rodrigo Retamales, Gilberto Mosqueda, Andre Filiatrault and Andrei Reinhorn

NOTICE

New Experimental Capabilities and Loading Protocols for Seismic Qualification and Fragility Assessment of Nonstructural Systems

by

Rodrigo Retamales,[1] Gilberto Mosqueda,[2] Andre Filiatrault[3] and Andrei Reinhorn[3]

1 Post-Doctoral Research Associate, Department of Civil, Structural and Environmental Engineering, University at Buffalo, State University of New York
2 Assistant Professor, Department of Civil, Structural and Environmental Engineering, University at Buffalo, State University of New York
3 Professor, Department of Civil, Structural and Environmental Engineering, University at Buffalo, State University of New York

NTIS DISCLAIMER

Preface

The Multidisciplinary Center for Earthquake Engineering Research (MCEER) is a national center of excellence in advanced technology applications that is dedicated to the reduction of earthquake losses nationwide. Headquartered at the University at Buffalo, State University of New York, the Center was originally established by the National Science Foundation in 1986, as the National Center for Earthquake Engineering Research (NCEER).

Comprising a consortium of researchers from numerous disciplines and institutions throughout the United States, the Center's mission is to reduce earthquake losses through research and the application of advanced technologies that improve engineering, pre-earthquake planning and post-earthquake recovery strategies. Toward this end, the Center coordinates a nationwide program of multidisciplinary team research, education and outreach activities.

MCEER's research is conducted under the sponsorship of two major federal agencies: the National Science Foundation (NSF) and the Federal Highway Administration (FHWA), and the State of New York. Significant support is derived from the Federal Emergency Management Agency (FEMA), other state governments, academic institutions, foreign governments and private industry.

MCEER's NSF-sponsored research objectives are twofold: to increase resilience by developing seismic evaluation and rehabilitation strategies for the post-disaster facilities and systems (hospitals, electrical and water lifelines, and bridges and highways) that society expects to be operational following an earthquake; and to further enhance resilience by developing improved emergency management capabilities to ensure an effective response and recovery following the earthquake (see the figure below).
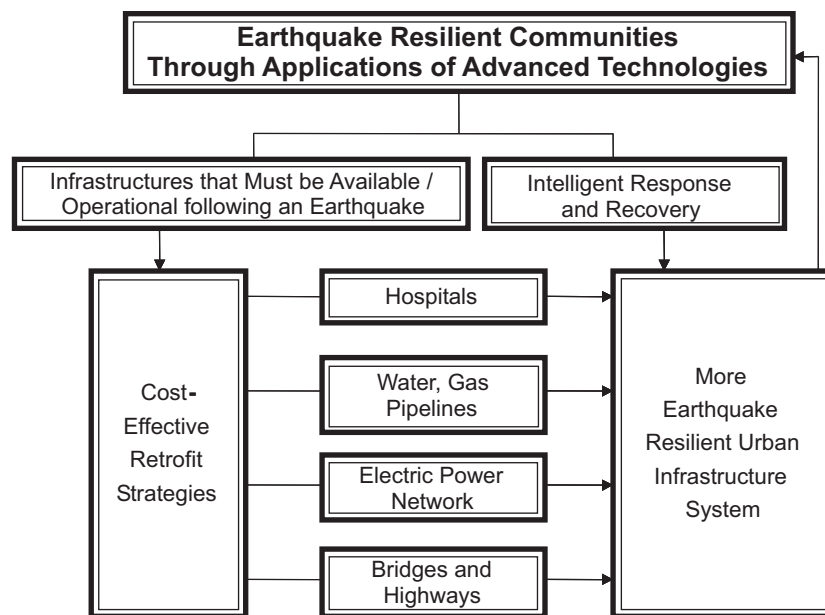
A cross-program activity focuses on the establishment of an effective experimental and analytical network to facilitate the exchange of information between researchers located in various institutions across the country. These are complemented by, and integrated with, other MCEER activities in education, outreach, technology transfer, and industry partnerships.

This report describes the new experimental testing capabilities provided by the University at Buffalo Nonstructural Component Simulator (UB-NCS). The UB-NCS is composed of a two-level testing frame that can subject full-scale nonstructural components and systems to 3g acceleration, 100 in/s (250 m/s) velocity and ±40 in (±1 m) displacement amplitudes. New experimental capabilities are provided for more realistic seismic qualification and seismic fragility assessment of nonstructural systems subjected to both full-scale accelerations and/or interstory drifts demands expected within multistory buildings. An innovative set of testing protocols utilizing the UB-NCS capabilities is proposed for qualification testing and fragility assessment. The proposed protocols complement, and in some cases extend, the capabilities of current protocols such as AC156 and FEMA 461. In particular, new capabilities are provided for testing nonstructural systems that may be displacement and/or acceleration sensitive by simultaneously applying interstory drifts and absolute floor accelerations. The testing capabilities of the UB-NCS are demonstrated through a series of experiments assessing the seismic performance of a full-scale composite hospital emergency room containing typical nonstructural components such as architectural finishes, piping systems and life support medical equipment. In these tests, the seismic performance of individual nonstructural components and medical equipment were evaluated as well as the dynamic interactions between them. The input motions for these tests included the proposed loading protocol and simulated building floor motions.

ABSTRACT

The seismic vulnerability of nonstructural components and equipment with their expensive recovery and/or replacement costs has been demonstrated during past earthquakes. However, there is relatively little research in this field and the data collected from past earthquakes or experimental studies are not sufficient to completely characterize the seismic behavior of nonstructural components and develop effective mitigation measures. In order to better understand the seismic behavior of nonstructural components, the University at Buffalo Nonstructural Component Simulator (UB-NCS) was commissioned to subject nonstructural components to realistic full-scale floor motions. The UB-NCS is composed of a two-level testing frame that can subject nonstructural systems to 3g acceleration, 100 in/s velocity and ± 40 in displacement amplitudes. New experimental capabilities are provided for more realistic seismic qualification and seismic fragility assessment of nonstructural systems subjected to both accelerations and/or interstory drifts demands expected within multi-story buildings.

An innovative set of testing protocols utilizing the UB-NCS capabilities is developed and proposed for qualification testing and fragility assessment. The proposed protocols complement, and in some cases extend, the capabilities of current protocols such as AC156 seismic qualification protocol and the fragility testing methodologies proposed in FEMA 461. In particular, new capabilities are provided for testing nonstructural systems with multiple attachment points that may be displacement and/or acceleration sensitive by simultaneously applying interstory drifts and absolute floor accelerations. The testing capabilities of the UB-NCS and the fidelity to reproduce full-scale seismic floor motions and protocol motions were evaluated through an extensive series of tests. An off-line compensation procedure was developed in order to achieve satisfactory performance.

The unique testing capabilities of the UB-NCS are demonstrated through a series of experiments assessing the seismic performance of a full-scale composite hospital emergency room containing typical nonstructural components such as architectural finishes, piping systems and life support medical equipment. In these tests, the seismic performance of individual nonstructural components and medical equipment was evaluated as well as the dynamic interactions and interdependencies between them. In particular, the seismic behavior of displacement sensitive partition walls and acceleration sensitive wall mounted patient monitors were examined in detail. The input motions for these tests included the proposed loading protocol and simulated building floor motions.

ACKNOWLEDGMENTS

TABLE OF CONTENTS

TABLE OF CONTENTS (CONTINUED)

LIST OF FIGURES

LIST OF FIGURES (CONTINUED)

LIST OF FIGURES (CONTINUED)

LIST OF FIGURES (CONTINUED)

LIST OF FIGURES (CONTINUED)

LIST OF FIGURES (CONTINUED)

LIST OF FIGURES (CONTINUED)

LIST OF FIGURES (CONTINUED)

LIST OF FIGURES (CONTINUED)

LIST OF FIGURES (CONTINUED)

LIST OF FIGURES (CONTINUED)

LIST OF TABLES

LIST OF TABLES (CONTINUED)

SECTION 1

INTRODUCTION

Natural disasters such as the Northridge earthquake (1994), the Kobe earthquake (1995), and more recently, the Hawaii earthquake (2006), have devastated the world for centuries, affecting both engineered and non-engineered infrastructures. In the light of those disasters, many are the cases of partial or global collapse of major and minor structural systems, and many more are the cases involving loss of functionality of critical facilities and essential lifelines; losses which have proved to be as significant as collapse itself. Loss of functionality were mostly caused by severe structural damage and/or the failure of nonstructural components like mechanical equipment, loss of elevators services, damage of water supply systems, and collapse of fixed and movable equipment (McGavin and Patrucco, 1994).

Significant advances have been made in recent years that have provided a better understanding of the seismic behavior of construction materials and structural systems. This has been achieved mainly through improved experimental facilities allowing for the seismic simulation of both scaled and full-scale models and the development of efficient computational tools. Additionally, improved means of communication and electronic documentation have made the transfer of professional experiences and post-disaster field observations more easy and efficient. Certainly, an acceptable level of knowledge has been achieved in the understanding of the structural behavior, which has been partially reflected in current design codes and standard practices.

Nowadays, with the development of performance-based earthquake engineering, achieving a specific building performance objective requires harmonization of performance levels between structural and nonstructural components. Even if the structural components of a building achieve a continuous or immediate occupancy performance level after a seismic event, failure of architectural, mechanical, or electrical components can lower the performance level of the entire building system. This reduction in performance caused by the vulnerability of nonstructural components was recently observed in several buildings during the 2001 Nisqually earthquake in the Seattle-Tacoma area (Filiatrault *et al.*, 2001). Moreover, nonstructural damage has limited the functionality of critical facilities, such as hospitals, as demonstrated by the 1994 Northridge earthquake (McGavin and Patrucco, 1994), the 2001 El Salvador earthquake (Boroschek and Retamales, 2001), and the 2006 Hawaii earthquake (Chock *et al.*, 2006).

According to Taghavi and Miranda (Taghavi and Miranda, 2003), the contents and nonstructural components in office, hotel and hospital buildings compose about 82%, 87% and 92% of the total monetary investment in a building, respectively. Clearly, the investment in nonstructural components and

building contents is far greater than that of structural components and framing. Therefore, it is not surprising that in many past earthquakes, losses from damage to nonstructural building components exceeded losses from structural damage. Furthermore, the failure of nonstructural building components can become a safety hazard or hamper the safe movement of occupants evacuating or rescue workers entering buildings (Villaverde, 2004).

In comparison to structural components and systems, there is relatively limited information on the seismic performance of nonstructural components. Basic research work in this area has been sparse, and the available codes and guidelines (BSSC, 2003a; CSA, 2002; FEMA, 1994; FEMA, 2000a; FEMA, 2000b; FEMA, 2004) are usually, for the most parts, based on past experiences, engineering judgment and intuition, rather than on objective experimental and analytical results. Often, design engineers are forced to start almost from square one after each earthquake event: observe what went wrong and try to prevent repetitions. This is a consequence of the empirical nature of current seismic regulations and guidelines for nonstructural components.

In order to thoroughly assess the seismic performance of full-scale nonstructural components under realistic full-scale seismic floor motions, the Structural Engineering and Earthquake Simulation Laboratory (SEESL) at the University at Buffalo (UB) has commissioned under the National Science Foundation's George E. Brown Junior Network for Earthquake Engineering Simulation (NEES) program a dedicated Nonstructural Component Simulator (UB-NCS). The UB-NCS is a modular and versatile two-level controllable platform for experimental performance evaluation of both displacement and acceleration sensitive nonstructural components, equipment and building contents. The two levels of the UB-NCS can simulate the motions of two consecutive stories in a building, subjecting its contents to full-scale absolute accelerations, velocities and drifts without the need to apply high-pass filters to accommodate the modest stroke capabilities of most existing shake tables in the US.

The input motions for the UB-NCS can be obtained from recorded floor motions of buildings during past earthquakes or the simulated numerical response of a building to a given earthquake record. In order to more broadly assess the seismic performance of nonstructural components, independent of building or earthquake record, a general testing protocol is proposed, capable of simultaneously subjecting test specimens to expected absolute floor accelerations and interstory drifts. The new testing capabilities provide for more realistic simulation and performance assessment of nonstructural components. More importantly, such tests can capture the interaction between various interdependent nonstructural systems that may be present in a building.

The innovative testing capabilities provided by the UB-NCS are demonstrated through a series of experiments evaluating the seismic performance of a full-scale hospital emergency room with various types of nonstructural components and equipment. The emergency room specimen contained architectural finishes (partition walls and suspended ceilings), distributed piping (medical gas and fire suppression), and medical equipment (free standing infusion pumps on poles and wall mounted patient monitors, among others). The model room was subjected to the proposed loading protocol and simulated full-scale building floor motions. These tests allowed for the first time, in a laboratory environment, the close observation of the seismic performance of nonstructural systems in hospitals and the interactions between the various components. By conducting more realistic tests such as these, the UB-NCS is expected to contribute to a better understanding of the seismic behavior of nonstructural components, systems, and equipment that will lead to improved mitigation measures and ultimately reduced losses in future earthquakes.

1.1 Objectives and scope of this report

The objectives of the research described in this report are to develop a methodology and the experimental capabilities for evaluating the seismic behavior of nonstructural systems under realistic demands. To this end, the main contributions of this research include: i) the development of an innovative testing facility specially designed for subjecting nonstructural systems to full-scale floor motions that simultaneously apply story drifts, and absolute floor accelerations and velocities expected at the upper levels of multistory buildings during strong seismic shaking; ii) the development of a methodology for the estimation of the hazard consistent seismic demands expected within multistory buildings and applying these demands through a series of testing protocols suitable for seismic qualification and fragility assessment of nonstructural systems; and iii) the experimental seismic performance evaluation of a full-scale hospital emergency room subjected to full-scale floor motions that captures, for the first time in a laboratory environment, the dynamic interactions between architectural, mechanical and medical equipment and other hospital emergency room contents. These objectives were achieved through the following tasks:

1. Review current code procedures for seismic design of nonstructural components and equipment and identify their limitations.

2. Review experimental testing protocols currently used for seismic qualification and seismic fragility evaluation of nonstructural components and equipment and identify their limitations.

3. Describe the conceptual design criteria and the new testing capabilities provided by the University at Buffalo Nonstructural Component Simulator (UB-NCS).

4. Identify the actual capabilities and limitations of the UB-NCS facility to impose desired full-scale floor motions on full-scale nonstructural component specimens.

5. Propose dynamic and quasi-static testing protocols for experimental seismic qualification and seismic fragility assessment of distributed displacement and/or acceleration sensitive nonstructural components, systems and equipment, taking full advantage of the UB-NCS testing capabilities, and imposing simultaneously absolute floor accelerations and interstory drifts expected within multistory buildings.

6. Experimentally assess the seismic performance of a full-scale emergency room, constructed following standard hospital construction techniques, and fitted with medical equipment critical for patient life support interacting with typical architectural hospital contents.

7. Experimentally assess the efficiency and suitability of the proposed testing protocol to impose, in a controlled way, seismic damage levels compatible with the damage experienced and/or expected during real earthquake events.

In the development of the research plan, the scope of work was limited as follows:

1. Only horizontal components of excitations have been considered in the analysis of seismic demands acting on nonstructural components and equipment, and in the development of the testing protocol. Vertical seismic demands are explicitly not assessed in this research.

2. The UB-NCS performance verification was completed considering only the uni-axial testing configuration. The bi-axial and tri-axial testing configurations will be the subject of future research.

3. The estimation of seismic demands within buildings was performed using a building model with constant stiffness along the height. This assumption may underestimate the interstory drifts demands expected at the uppermost building levels. Furthermore, for estimating the seismic demands, the dynamic interaction between the primary structural system and the nonstructural components is neglected, and therefore, the proposed testing protocol is more suitable for testing light nonstructural components, systems and equipment.

1.2 Organization of this report

The contents of this report are distributed in seven sections (including this one) and one appendix.

Section 2 summarizes the evolutionary process followed by design code provisions from the mid 1990's to the present. A detailed description of the basis and supporting studies for the current seismic design regulations, a summary of the testing protocols currently used for fragility analysis and seismic qualification of nonstructural components and equipment, and a review of the limitations that have been identified in code provisions are presented. Furthermore, a detailed summary of the time and frequency domain analysis tools developed in the past 30 years for the estimation of seismic demands and seismic analysis of nonstructural components and equipment is presented. Methods for exact and approximate solution such as perturbation techniques, modal synthesis and mode acceleration approaches are described. The main assumptions, principles, advantages and drawbacks of each approach are also discussed. Finally, a review of the state-of-the-art of the experimental and analytical studies performed after the year 2000 regarding the seismic performance assessment of nonstructural components and equipment is presented. This review mainly dwells on those experimental studies that could be further investigated by using the capabilities of the UB-NCS.

Section 3 presents a detailed description of the new University at Buffalo Nonstructural Component Simulator (UB-NCS). The criteria considered for the design of the testing frame and the high performance dynamic actuators are discussed. The new testing capabilities provided by the UB-NCS are also presented in this section. Moreover, the results obtained from a series of tests carried out to verify the fidelity and performance capabilities of the UB-NCS are presented. The measured platform motions are compared to the desired floor motions for various signals, including simulated building floor motions, harmonic excitations, and testing protocol histories. A methodology for off-line command input signal compensation is also proposed to improve the fidelity of the UB-NCS. The performance of the UB-NCS with an actual payload consisting of two full-scale C-shaped steel studded gypsum partition walls are described and the behavior of the walls is also analyzed.

Section 4 presents the details of the dynamic and quasi-static testing protocols proposed for experimental seismic qualification and fragility analysis of distributed acceleration and/or displacement sensitive nonstructural components, systems and equipment. A description of the generic building model and the random vibration theory used to estimate the peak seismic demands on nonstructural components located within multistory buildings are presented. Finally, the derivation of the closed-form testing protocol equations, their calibration to impose earthquake compatible damage levels, and several examples of protocol floor motion histories are presented.

Section 5 presents a description of an extensive test series performed on a full-scale mock emergency room (ER). A detailed description of the ER construction process, and the nonstructural components and medical equipment considered in the specimen is presented.

Section 6 presents the analysis of the data obtained during the test series described in Section 5. In this Section, the results of the UB-NCS performance analysis, the observed specimen damage progression, and the fragility analysis of selected acceleration and displacement sensitive nonstructural components and equipment are examined.

Finally, Section 7 presents a summary and conclusions of this research and recommendations for future research. Appendix A of this report presents the details of the geometry of the UB-NCS testing frame.

SECTION 2

LITERATURE REVIEW ON THE SEISMIC BEHAVIOR OF NONSTRUCTURAL COMPONENTS

This section provides a summary of recent research related to nonstructural components through four main subsections. The historical revision of code provisions is included to contrast the level of knowledge about the seismic performance of nonstructural components and the design philosophy considered in the current regulation.

The first subsection of this section presents a description of the evolution of the code provisions used for the seismic design of nonstructural components, from the mid 1990's to the present. The second subsection presents a description of the current methods used for experimental seismic qualification and fragility analysis of nonstructural components. The third subsection describes several analytical tools developed in the last 30 years for estimating the seismic demands acting on nonstructural components and equipment located within multistory buildings. Finally, the fourth subsection summarizes the experimental research on seismic performance of nonstructural components performed in the last eight years (2000-2008).

2.1   Code provisions for seismic design

This subsection presents a summary of the evolution of the code provisions used for seismic design of nonstructural components and equipment from 1994 to the present. The rational, supporting studies and main criticisms to the code provisions are also described and discussed.

2.1.1   Uniform Building Code UBC 1994

The UBC 1994 provisions (ICBO, 1994) for seismic design of structural and nonstructural components were derived from the Structural Engineers Association of California's Blue Book and were based on working-stress design principles. The provisions for nonstructural components were primarily concerned with the design of their attachments to the primary structure, providing minimal standards to safeguard property and public welfare. Post earthquake functionality was indirectly considered through the use of an importance factor in the calculation of the design forces. The UBC 1994 does not require consideration of displacements imposed by the structure in the design of nonstructural components (Drake and Bachman, 1996). The design force F_p for the nonstructural component is calculated as:

$$F_p = ZI_p C_a W_p \qquad (2.1)$$

where Z is the seismic coefficient (function of seismic zone and soil profile type); I_p is the importance factor; C_a is a factor which depends on the flexibility, energy absorption capability and location of the nonstructural component in the building; and W_p is the weight of the component.

2.1.2 NEHRP 1994/ASCE 7-95 provisions

The NEHRP 1994 provisions (BSSC, 1994) were developed by the Building Seismic Safety Council (BSSC) for the Federal Emergency Management Agency (FEMA) and were adopted by the 1995 edition of ASCE-7 (ASCE, 1995). The nonstructural design force requirements are similar to the UBC 1994, but are based on strength design principles. The main difference of this provision resides in that the displacements imposed by the structure on the nonstructural components were explicitly considered.

2.1.2.1 Design forces

In NEHRP 1994, the following equations were proposed for the calculation of design seismic forces:

$$0.5 C_a I_p W_p \leq F_p = \frac{a_p A_p I_p W_p}{R_p} \leq 4.0 C_a I_p W_p \tag{2.2}$$

$$A_p = C_a + \left(A_r - C_a \right)\left(\frac{x}{h} \right) \tag{2.3}$$

$$A_r = 2.0 A_s \leq 4.0 C_a \tag{2.4}$$

where F_p is the seismic design force applied at the center of gravity of the nonstructural component; C_a is the effective peak acceleration seismic coefficient at grade; I_p is the component importance factor, which takes values 1.0 or 1.5; W_p is the component operating weight; a_p is the component amplification factor, which varies from 1.0 to 2.5; A_p is the component acceleration coefficient at attachment point; R_p is the component-response modification factor, which ranges between 1.5 and 6.0; A_r is the component acceleration coefficient at structure roof level; h is the roof elevation; and A_s is the structure response acceleration coefficient, given by:

$$A_s = \frac{1.2 C_v}{T^{2/3}} \leq 2.5 C_a \tag{2.5}$$

where C_v is the peak-velocity related seismic coefficient and T is the effective fundamental period of the primary structure. Example values for a_p, I_p and R_p coefficients are shown in Table 2.1. The seismic design force F_p is to be applied in all directions in combination with dead and operation loads. Conservatively, or in absence of data related to the dynamic properties of the supporting structure, a value $F_p = 4.0 C_a I_p W_p$ can be considered in all design cases. This equation provides adequate design forces for light nonstructural components, but is overly conservative for heavy secondary systems, and therefore, the use of the central

expression shown in equation (2.2) is most suitable in those cases. The design criteria considered in the formulation of the code equations includes: the component weight and mass distribution, the location of the building, the seismic response of the primary structure, the location of the component into the building, the safety level required for the nonstructural system, the importance of the component, and the ductility and energy absorption capability of the component and its anchorages.

Table 2.1. Typical values for a_p, I_p and R_p parameters. After (Drake and Bachman, 1996)

Component	a_p	I_p	R_p
Exit-corridor partitions	1.0	1.5	3.0
Exterior-wall panels	1.0	1.0	3.0
Parapets and chimneys	2.5	1.0	1.5
Suspended lay-in tile ceilings	1.0	1.0	1.5
Mechanical equipment	1.0	1.0	3.0
Piping systems-hazardous contents	2.5	1.5	4.0
Storage tanks on legs (in buildings)	2.5	1.0	2.0
Emergency-power electrical equipment	1.0	1.5	3.0

In equation (2.2), the a_p term accounts for the dynamic amplification of the nonstructural system response due to eventual tuning to the supporting structure and to the ground motion itself. Values for a_p factors are recommended in NEHRP provisions based on the anticipated rigid or flexible behavior of the nonstructural system. Considering that realistic amplification factors are in general not available, the NEHRP provisions propose two values for the component amplification factor: $a_p = 1.0$ (no dynamic amplification is expected) for nonstructural systems with natural periods $T_p < 0.06$ s and $a_p = 2.5$ (dynamic amplification is probable) for nonstructural systems with periods $T_p > 0.06$ s. Details of the study supporting those amplification factor values can be found in Soong and Grigoriu (Soong and Grigoriu, 1993b).

The component acceleration coefficient A_p accounts for the amplification of the acceleration at the ground level along the height of the primary structure.

The seismic coefficient at grade C_a included in this code provision represents the expected peak ground acceleration associated to a local seismic hazard at the site of the building with a 10% probability of exceedance in 50 years. It is the same parameter used in the design of the primary system. The structure-response acceleration coefficient A_s is also the same used for designing the primary system, except that the response modification factor R is not considered. According to references (Drake and Bachman, 1996) and (Bachman and Drake, 1994), the R factor is set equal to 1 because the design of the building may be controlled by other loads or drift requirements, and because there is evidence supporting the insignificant reduction of floor accelerations resulting from yielding of the primary system.

The component acceleration coefficient at roof-level A_r corresponds to the maximum acceleration expected at the roof level of the structure. Consistent with recorded data, the value considered in the provisions corresponds to twice the structural response acceleration, equation (2.4). Moreover, data recorded during strong ground motions show significant increase in the floor acceleration at the uppermost levels of buildings, which can equal four times the acceleration at the grade level. This fact is considered in the right side of equation (2.4) and shown in Figure 2.1. Based on the same recorded data, a trapezoidal distribution of accelerations along the building height was defined in the code, varying from C_a to A_r.
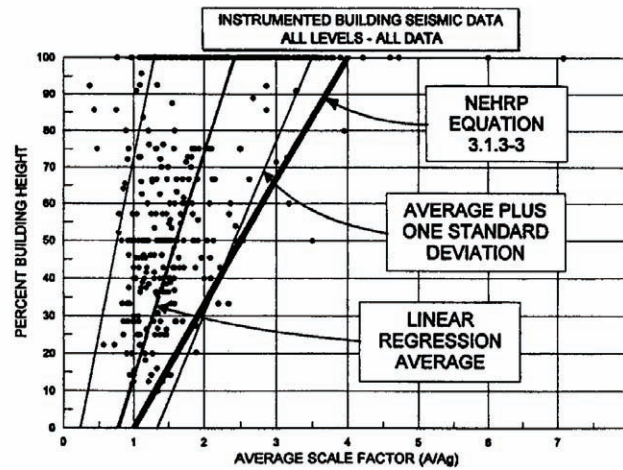
Figure 2.1. Comparison of NEHRP design accelerations and recorded data. Figure taken from Drake and Gillengerten (Drake and Gillengerten, 1994)

Figure 2.1 summarizes the ratios between peak floor and peak grade accelerations along the normalized elevation of the structures for more than 400 recorded data sets obtained from 150 instrumented buildings located in the California region. Sixteen California earthquake events, from the 1971 San Fernando earthquake to the 1994 Northridge earthquake, are included in Figure 2.1 (Drake and Gillengerten, 1994). From the data set, a total of 23 structures that experienced significant ground motions during the 1984 Morgan Hill, 1989 Loma Prieta, and 1992 Landers earthquakes were selected for the development of the code provisions. From these 95 records, 28 were included in the analysis. The selection of records was based on several criteria, including structural type, intensity of ground motion, and observed structural amplification. The peak ground accelerations (PGA) considered in the analysis ranged between 0.03g and 0.39g. The maximum PGA value was recorded in a 4-story building located in Watsonville, struck by the 1984 Morgan Hill earthquake. The peak floor acceleration, 1.24g, was recorded in the same building. The epicentral distance of the records in the database ranged from 18 to 170 km. It is also noted in the study performed by Drake and Gillengerten (Drake and Gillengerten, 1994) that most of the buildings considered in the analysis "exhibited essentially elastic global behavior, although some local inelastic

behavior certainly occurred". In the analysis, all data (A_p's) were normalized with respect to the ground acceleration (A_g's). The amplification ratios, A_p/A_g, were assigned to the nearest quarter building height level. Figure 2.2 shows the recorded data ranges and averages.
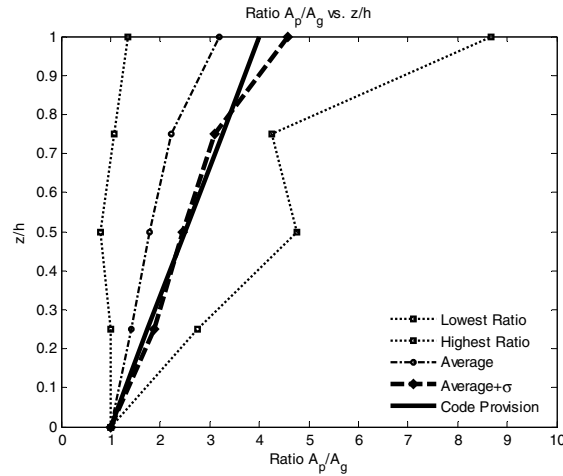
Figure 2.2. Comparison of statistical analysis of recorded data and code provision (After Drake and Gillengerten)

In Figure 2.2 it can be seen that the average values plus one standard deviation fall near the middle point of each range considered. It can also be seen that the code design force given by equation (2.3) follows this trend. It should be noted that the higher amplification factors are associated with the lowest ground shaking intensities. For higher shaking intensities, an increase in the structural damping and limited inelastic behavior are expected to result in lower amplification factors (Drake and Gillengerten, 1994).

The component importance factor I_p accounts for the importance, functionality requirements, difficulty and/or cost of replacement, and potential of component damage. It is intrinsically assumed that a higher design force level implies a higher performance of the nonstructural system. The component response modification factor R_p considers the energy absorption capacity, the overstrength, and the deformability of the nonstructural system and its attachments. The values given in the code were estimated using expert judgment and the following criteria:

Table 2.2. Criteria for selection of R_p factors (After Drake and Gillengerten)

Characteristic of the component	R_p
Brittle or buckling failure mode expected	1.5
Minimal level of energy absorption capability	3.0
Ductile materials and detailing	4.5
Highly ductile materials and detailing	6.0

11

2.1.2.2 Design displacements

The NEHRP 1994 provisions incorporated relative displacement requirements for the design of nonstructural systems. According to these provisions, nonstructural systems should be capable of accommodating the relative displacements D_p imposed at its attachment points (x-th and y-th levels) by the primary system. These displacements are calculated as:

- For connection points at the same building:

$$D_p = min \begin{cases} \delta_{xA} - \delta_{yA} \\ (X - Y)\dfrac{\Delta_{aA}}{h_{sx}} \end{cases} \tag{2.6}$$

- For connection points at different buildings:

$$D_p = min \begin{cases} |\delta_{xA}| + |\delta_{yB}| \\ X\dfrac{\Delta_{aA}}{h_{sx}} + Y\dfrac{\Delta_{aB}}{h_{sx}} \end{cases} \tag{2.7}$$

where δ_{xA} and δ_{yA} are the deflections at the x-th and y-th levels of building A obtained from elastic analysis ($R_{Structure}=1$) multiplied by the C_d factor also defined in the NEHRP provisions; X and Y are the height of the attachment points measured in relation to the grade level; Δ_{aA} is the allowable story drift for building A; and h_{sx} is the interstory height. The other variables are analogously defined. Equations (2.6) and (2.7) allow for estimating the design relative displacement based on information obtained from structural analysis of the building or from the code limits for interstory drifts.

2.1.3 Uniform Building Code UBC 1997

The UBC 1997 provisions (ICBO, 1997) evolved from the NEHRP 1994 design seismic force provisions. The design forces F_p were obtained from:

$$0.7C_a I_p W_p \le F_p = \frac{a_p C_p I_p}{R_p}\left(1 + 3\frac{h_x}{h_r}\right)W_p \le 4.0C_a I_p W_p \tag{2.8}$$

where h_x is the average height of the nonstructural component above the grade level; and h_r is the height of the roof over the grade level. The other parameters have been defined in the previous subsection and take values as seen in the 1994 NEHRP provisions.

The main changes in the design seismic forces included in this standard, in relation to the 1994 NEHRP provisions, were in the minimum design force and in the distribution of accelerations along the height of

the building. The minimum design force was increased from $0.5C_aI_pW_p$ to $0.7C_aI_pW_p$, while the nonstructural component acceleration coefficient A_p was changed by a simpler factor $C_a\left(1+3\dfrac{h_x}{h_r}\right)$.

2.1.4 NEHRP 1997/IBC 2000/ASCE-7 98 provisions

After the decisions in 1994 of the three model code agencies: the International Conference of Building Officials (ICBO), the Building Officials and Code Administrators International (BOCA), and the Southern Building Code Congress International (SBCCI), to form the International Code Council (ICC) and to replace the former design codes, the reference standard for the new International Building Code (IBC) became the ASCE-7 standard (ASCE, 2005), edited by the American Society of Civil Engineers. There was agreement upon that the NEHRP provisions would be used to define the guidelines for the code developed by the ASCE-7 Seismic Task Committee. Therefore, after 1994, the seismic provisions presented in NEHRP 1997, IBC 2000 and ASCE7-98 coincide (Bonneville and Bachman, 2002).

The design provisions in the codes evolved from the 1994 NEHRP provisions. The main contributor for the new provisions was the Building Seismic Safety Council (BSSC). According to the codes, the design forces are calculated as:

$$0.3S_{DS}I_pW_p \le F_p = \frac{0.4a_pS_{DS}}{R_p/I_p}\left(1+2\frac{x}{h}\right)W_p \le 1.6S_{DS}I_pW_p \qquad (2.9)$$

where the new parameters introduced were: $0.4S_{DS}$, a parameter that replaces the C_a parameter in NEHRP 1994, and which corresponds to the mapped design spectral response acceleration at short periods; x, which correspond to the average height over the grade of the nonstructural component; and h, which correspond to the average height over the grade of the roof level. The R_p factors were slightly modified in comparison to the values included in the previous version of the code so that $F_{p_{NEHRP1994}} \approx F_{p_{NEHRP1997}}$ (Bachman and Drake, 1998). In this version of the code, the R_p factor, as defined in subsection 2.1.2, takes values that vary from 1 to 5. The relation which involves the A_p term, equation (2.3), was simplified and replaced by a factor $\left(1+2\frac{x}{h}\right)$. The adjustment of this factor came from the examination of additional building motion records associated to strong motions with peak ground accelerations greater than 0.1g (BSSC, 1997). According to this distribution, the floor accelerations within the building vary linearly from $0.4S_{DS}$ at grade to $1.2S_{DS}$ at the roof level. Additionally, the dependence of the input acceleration with the fundamental period of the primary system, considered in NEHRP 1994 through the structure-response

13

acceleration coefficient A_s, was removed, according to observations of records obtained for buildings with long natural periods (BSSC, 1997).

The most significant difference between NEHRP 1997 and its previous versions reside in the definition of ground motion intensity. In the NEHRP 1997 provisions, the spectral design values are obtained from the maps developed by the BSSC based on the 1996 USGS mapping project (Bonneville and Bachman, 2002) instead of the UBC zonification maps (ICBO, 1994). Those maps, which provide a more current and accurate representation of the local seismic hazard, present Maximum Considered Earthquake (MCE) spectral response accelerations which after scaling by a 2/3 factor are used for seismic design.

The upper and lower bounds of the seismic design force F_p are intended to assure a minimum design force, consistent with the values formerly used by practitioners, and considered in the previous versions of the provisions. No recommendations are given for the vertical component of the seismic design force.

The provisions for designing displacement sensitive nonstructural components attached at multiple building levels are the same as those included in NEHRP 1994, described by equations (2.6) and (2.7) in subsection 2.1.2.2.

2.1.5   NEHRP 2000 provisions

The equations for the estimation of the design seismic force appearing in this version of the provision (BSSC, 2000) are the same as those presented in NEHRP 1997. However, the following alternative method is proposed to be used in lieu of equation (2.9):

$$F_p = \frac{a_i a_p W_p}{R_p / I_p} A_x \tag{2.10}$$

wherein a_i is the acceleration at the i-th level of the structure obtained from modal analysis considering $R_{Structure}=1$; and A_x is the torsional amplification factor calculated as:

$$A_x = \left(\frac{\delta_{Max}}{1.2 \delta_{Avg}} \right)^2 \tag{2.11}$$

where δ_{Max} is the maximum displacement at the x-th level and δ_{Avg} is the average of the displacements at the extreme points at the x-th level of the structure. The lower and upper limits for F_p are the same shown in equation (2.9).

Another important modification seen in this version of the provisions is the increase in conservatism. Accordingly, several component response modification factors R_p were changed.

2.1.6   NEHRP 2003 provisions

The NEHRP 2003 provisions (BSSC, 2003a) have minor changes compared to the NEHRP 2000 edition. One of the important modifications is related to the possibility of reduction in the seismic design force F_p estimated by using either equations (2.9) or (2.10). A reduction of F_p by the ratio T_{flx}/T_p is possible when T_p, the period of the nonstructural component or equipment, is greater than

$$T_{flx} = \left(1 + 0.25 \frac{z}{h} \right) \frac{S_{D1}}{S_{DS}} \qquad (2.12)$$

where S_{D1} is the mapped design spectral response acceleration at one second period. Additionally, a vertical component for the seismic design force F_{p_v} is explicitly specified in the NEHRP 2003 provisions:

$$F_{p_v} = \pm 0.2 S_{DS} I_p W_p \qquad (2.13)$$

No changes are introduced in the requirements for design seismic displacements in equations (2.6) and (2.7), which nonstructural systems should be able to accommodate.

2.1.7   Comments on the code requirements for design of nonstructural components

Several past studies have evaluated the design procedures included in current and recent design codes, and some deficiencies have been identified. FEMA 357 (FEMA, 2000b), for example, identifies general problems which can directly or indirectly affect the seismic design procedures for nonstructural components. These deficiencies are summarized as follows:

- Ground motion pulses are not explicitly considered in current provisions, except for the use of higher spectral acceleration values in regions of active faults. This problem, which is also a concern for designing the primary structural system, can result in the underestimation of the drift demands for designing displacement-sensitive nonstructural systems.

- The effects of the nonstructural systems on the structural system response are not considered. The FEMA document recognizes that there is no guidance in the provisions on how to consider interactions between the two systems. As consequence of this, a cascade design approach is considered.

- Finally, it is recognized that the triangular inverted variation of design accelerations is not fully supported by recorded data or by results of dynamic analyses.

Soong and Grigoriu (Soong and Grigoriu, 1993b), among other researchers, recognized that design codes should prescribe simple and practical formulas to be used by field professionals in design applications. Nevertheless, it was also recognized by Soong et al. that code provisions of the early 1990's did not reflect the level of understanding of the seismic behavior of nonstructural components acquired through experimental and analytical studies. Such a statement can still be considered valid today. For example, numerous studies (Chaudhuri and Hutchinson, 2005; Chong and Soong, 2000; Hutchinson and Chaudhuri, 2006; Lopez Garcia and Soong, 2003; Makris and Konstantinidis, 2003; Makris and Roussos, 1998; Zhang and Makris, 2001) have been performed to identify the conditions triggering the sliding and/or rocking responses of freestanding equipment; however, no clear specifications or guidelines are provided in current codes to prevent or mitigate this type of seismic vulnerability.

Soong and Grigoriu (Soong and Grigoriu, 1993b) also recognize that component amplification factors and response modification factors are mainly based in expert judgment and therefore they are subjectively assigned. The independence of the seismic design forces on the dynamic properties and nonlinear behavior of the primary system is also identified as a deficiency. Current codes do not make a distinction between the inertial forces generated in flexible and stiff buildings, as done when designing the primary resisting system, assuming in both cases nonstructural design forces with the same magnitude. Furthermore, it is noted that the structural period affects the distribution of floor accelerations along the height of the building structure[1] and that period tuning can substantially increase the dynamic response of the nonstructural system. This resonant amplification is partially considered in the dynamic amplification factor. The effect of yielding of the primary system is also not accounted for. While yielding in the primary system can be considered a limiting state case, it is not generally allowed for nonstructural systems because of functionality issues. It is not clear what structural behavior controls the seismic response of nonstructural systems. For example, for a low or moderate mean return period earthquake the ground input energy will be small, but the structure will respond linearly amplifying the input energy transferred to the nonstructural system. On the other hand, for an earthquake providing comparatively larger input energy, the structure will dissipate part of the input energy during its inelastic excursions, reducing the input energy transferred to the nonstructural system.

In order to assess those shortcomings, an equipment amplification factor a_e depending on the nonstructural to primary system period ratio T_e/T_s, and a response modification factor R_s to account for

---

[1] Unfortunately, no guidelines are given to evaluate the variation of acceleration along the height of the building as function of the structural period.

yielding of the primary system (which multiplies the equipment response modification factor) are proposed by Soong and Grigoriu (Soong and Grigoriu, 1993b):

$$
a_c = \begin{cases}
1.0 & \dfrac{T_c}{T_s} \leq 0.5 \wedge \dfrac{T_c}{T_s} \geq 2.0 \\[2ex]
2.5 & 0.7 \leq \dfrac{T_c}{T_s} \leq 1.4 \\[2ex]
-2.75 + 7.5\dfrac{T_c}{T_s} & 0.5 < \dfrac{T_c}{T_s} < 0.7 \\[2ex]
6 - 2.5\dfrac{T_c}{T_s} & 1.4 < \dfrac{T_c}{T_s} < 2.0
\end{cases}
\tag{2.14}
$$

$$
R_s = 1 + \frac{R-1}{7}
\tag{2.15}
$$

where R is the response modification factor for structural design. The amplification factor a_c has been incorporated, in a simplified way, in the design codes for quite some time (see subsection 2.1.2.1). The response modification factor R_s has not been considered due to the reasons described in subsection 2.1.2.1.

2.2   Methods for experimental seismic qualification and fragility analysis

This subsection presents a summary of the testing protocols currently used for the experimental assessment of seismic performance and seismic qualification of building systems and nonstructural components and equipment. A general review of the experimental testing protocols developed for quasi-static cyclic testing of structural components and systems can be found in (Filiatrault *et al.*, 2008).

2.2.1   The ATC-24 testing protocol (1992)

The ATC-24 (Krawinkler, 1992) testing protocol was developed to be used for the seismic performance evaluation of steel structures components under cyclic loads. The loading history recommended by ATC-24 consists of cycles with increasing amplitudes. The amplitude of the protocol cycles is based on a yield deformation δ_y determined using, preferably, a preliminary monotonic test. Details for estimating of the yield displacement δ_y are presented in (Krawinkler, 1992). The loading sequence shown in Figure 2.3 was derived from the analysis of the seismic responses of a set of nonlinear SDOF systems subjected to a set of 15 western United States ground motions (Hadidi-Tamjed, 1987). The number and amplitude of cycles observed in time history analysis were extracted using the "Rainflow" counting algorithm (ASTM, 1997). The recommended number of cycles and peak deformations are given by the following sequence:

- At least 3 cycles with peak deformation amplitude less than δ_y should be imposed.

- At least 3 cycles with peak deformation amplitude equal to δ_y should be imposed.

- At least 3 cycles with peak deformation amplitude equal to $2\delta_y$ should be imposed.

- At least 2 cycles with peak deformation amplitude equal to $3\delta_y$ should be imposed.

- At least 2 cycles with peak deformation amplitude equal to $4\delta_y$ should be imposed.

The loading pattern described above should be continued until severe specimen strength deterioration is evident.
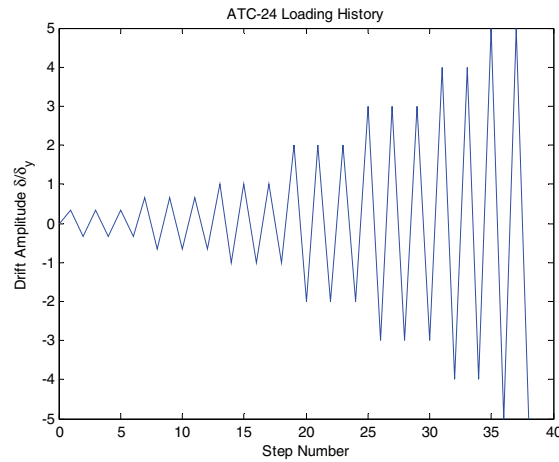
Figure 2.3. ATC-24 loading protocol

2.2.2 The CUREE/Caltech testing protocol (2000)

Krawinkler et al. (Krawinkler *et al.*, 2000) proposed recommendations for performing quasi-static and shake table tests on components of wooden houses for the CUREE/Caltech Woodframe project. The proposed loading histories allow for the assessment of component performance at various performance levels and several failure modes, as well as the development of analytical models. The loading histories are based on results obtained from nonlinear dynamic analyses of representative hysteretic wooden systems subjected to ordinary and near-fault ground motions. Cumulative damage concepts were considered to convert the time history responses into representative displacement and force controlled loading histories. Various testing protocols were proposed, which included: quasi-static deformation controlled (for ordinary and near-fault conditions), quasi-static force controlled and dynamic shake table protocols. The CUREE/Caltech testing protocols were specifically conceived for testing low-rise wood house components, and therefore, it would be necessary to extend its formulation to make it applicable for testing nonstructural components found in more general seismic resistant systems.

2.2.2.1 Deformation controlled quasi-static testing protocol

This protocol is applicable to components whose seismic response is controlled by a deformation parameter such as displacement, rotation and/or shear distortion. It is recognized that the performance of components under cyclic loads is highly dependent on the load history because of cumulative damage considerations. For that reason, the loading history patterns with the capabilities to reproduce the evolution of damage and replicate the global seismic response behavior have been studied extensively (Krawinkler *et al.*, 2000). In order to cover, in a conservative manner, the expected response of structural systems, 84th percentile values (mean values plus one standard deviation for normal distribution) have been considered in the protocols described in this subsection. It is also recognized that the cumulative damage effect has a more significant impact on lower performance levels and, therefore, short return period records are considered preceding the performance evaluation record.

2.2.2.1.1 Basic loading history for ordinary ground motions

This protocol is derived from the statistical analysis of the seismic response of a set of nonlinear systems subjected to a series of ordinary ground motions calibrated to seismic hazards (SH) with a probability of exceedance (PE) of 10% in 50 years. The loading history is composed of three components: initiation cycles, primary cycles and trailing cycles. The initiation cycles are considered to account for small amplitude seismic events and for instrument calibration and initial checks. The primary cycles correspond to cycles larger than all the preceding ones and, the following smaller cycles are called trailing cycles. The amplitude of the trailing cycles is 75% of the preceding primary cycle. The following sequence defines the loading history in terms of Δ, the reference maximum deformation prescribed in the acceptance criteria or a preliminary estimate of the maximum deformation capacity of the component:

- Six initiation cycles with amplitude $0.05\,\Delta$.
- A primary cycle with amplitude $0.075\,\Delta$ followed by six trailing cycles.
- A primary cycle with amplitude $0.1\,\Delta$ followed by six trailing cycles.
- A primary cycle with amplitude $0.2\,\Delta$ followed by three trailing cycles.
- A primary cycle with amplitude $0.3\,\Delta$ followed by three trailing cycles.
- A primary cycle with amplitude $0.4\,\Delta$ followed by two trailing cycles.
- A primary cycle with amplitude $0.7\,\Delta$ followed by two trailing cycles.
- A primary cycle with amplitude $1.0\,\Delta$ followed by two trailing cycles.
- A primary cycle with an increase in amplitude equal to $0.5\,\Delta$ followed by two trailing cycles. The process is continued until the maximum load applied to the component decreases to a small fraction of the maximum load.

In the sequence above, Δ does not correspond necessarily to an acceptable performance level. Krawinkler et al. recommend considering $\Delta = \gamma \Delta_m$, where Δ_m is the displacement at which the applied load drops to 80% of the maximum applied load and γ is a factor which accounts for the difference in the maximum deformation obtained from monotonic and cyclic tests (Figure 2.4). A factor $\gamma = 0.6$ is suggested (Krawinkler *et al.*, 2000). Figure 2.5 shows the proposed protocol for $\Delta = \gamma \Delta_m$.
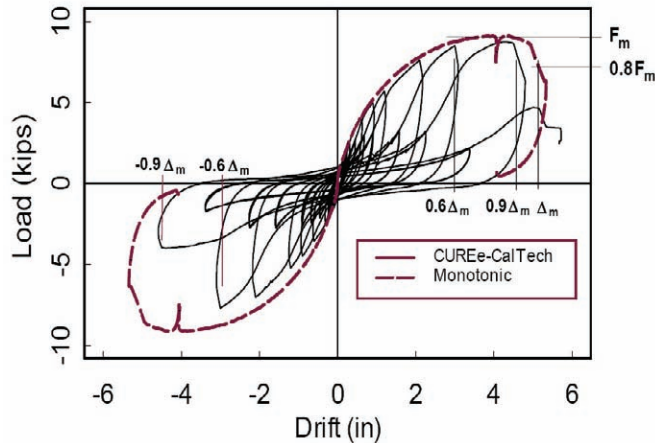
Figure 2.4. Example application of basic loading history. Figure taken from Krawinkler et al. (Krawinkler *et al.*, 2000)

2.2.2.1.2 Abbreviated basic loading history for ordinary ground motions

A simplified version of the basic loading history protocol, which considers a reduced number of cycles, was also proposed:

- Four initiation cycles with amplitude 0.05Δ.
- A primary cycle with amplitude 0.075Δ followed by four trailing cycles.
- A primary cycle with amplitude 0.1Δ followed by four trailing cycles.
- A primary cycle with amplitude 0.2Δ followed by two trailing cycles.
- A primary cycle with amplitude 0.3Δ followed by two trailing cycles.

The process is continued as in the basic loading history. It is expected that the reduction in the number of trailing cycles does not affect the component performance. Figure 2.6 shows the proposed protocol for $\Delta = \gamma \Delta_m$.

2.2.2.1.3 Simplified basic loading history for ordinary ground motions

In this protocol, the amplitude of the trailing cycles is the same of the preceding primary cycle. There is no 25% reduction as in the basic loading history. Figure 2.7 shows the proposed protocol for $\Delta = \gamma \Delta_m$.
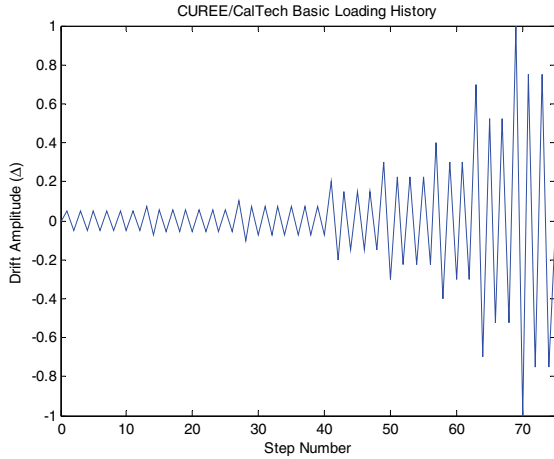
Figure 2.5. Basic loading history protocol (After Krawinkler et al.)
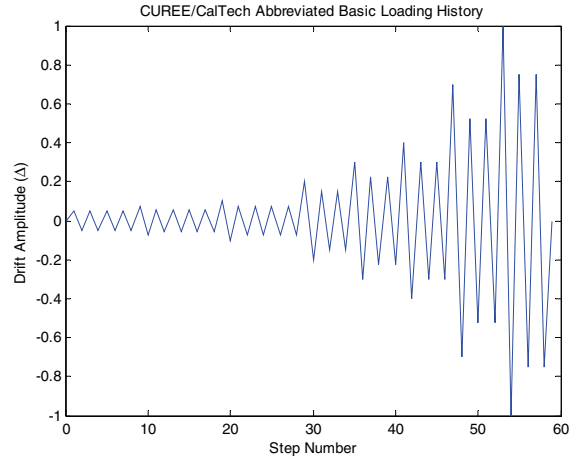
Figure 2.6. Abbreviated basic loading history protocol (After Krawinkler et al.)

2.2.2.1.4 Loading history for near-fault ground motions

The ground motion records considered in the development of this protocol correspond to a seismic hazard (SH) with a probability of exceedance (PE) of 2% in 50 years. The loading history is defined by variations of deformation amplitudes, using a similar deformation parameter Δ_n as in the basic loading history. However, the maximum deformation expected under pulse excitations is close to the value estimated using monotonic loads, and therefore $\Delta_n = \Delta_m$, as shown in Figure 2.8.
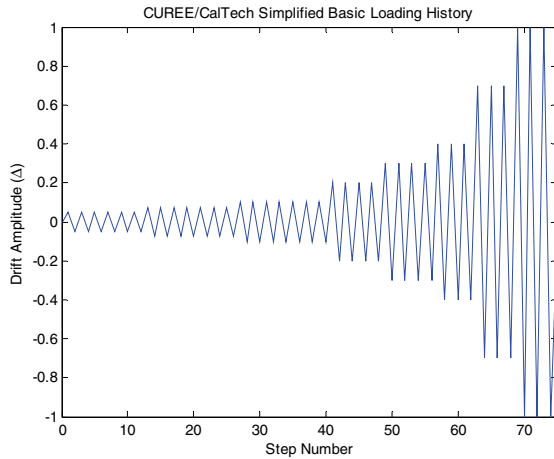
Figure 2.7. Simplified basic loading history protocol (After Krawinkler et al.)
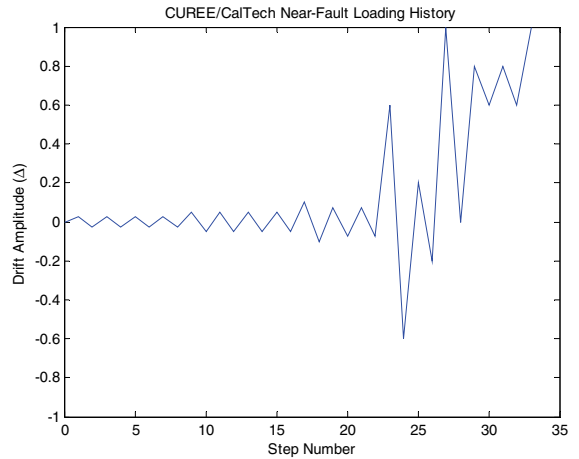
Figure 2.8. Loading history protocol for near-fault ground motions (After Krawinkler et al.)

The sequence followed for the testing protocol is:

- Four cycles with amplitude $0.025\,\Delta_n$.

- Four cycles with amplitude $0.05\,\Delta_n$.

- A primary cycle with amplitude $0.1\,\Delta_n$ followed by two trailing cycles with amplitude $0.075\,\Delta_n$.

- A primary cycle with amplitude $0.6\,\Delta_n$ followed by one trailing cycles with amplitude $0.2\,\Delta_n$.

- A primary positive excursion to $1.0\,\Delta_n$.

- A reversal to zero deformation.

- A positive excursion to $0.8\,\Delta_n$.

- Two cycles with amplitude $0.1\,\Delta_n$ and mean deformation $0.7\,\Delta_n$.

- One positive excursion to the maximum sustainable deformation of the specimen.

2.2.2.2 Loading history for force controlled components

Force controlled testing is recommended only for cases in which a suitable deformation parameter has not been found, which, in general, corresponds to components with brittle failure modes. The objective of this protocol is to estimate the real capacity of components. As in the displacement protocol, the proposed loading history is expected to simulate the real evolution of the damage expected during earthquakes. Given that cumulative damage effects are more significant under ordinary ground motions, only ordinary records calibrated to a SH with a PE of 10% in 50 years have been considered in this protocol. The protocol history is defined in the following way:

- Five cycles with amplitude $0.5\,Q_o$.

- Five cycles with amplitude $0.7\,Q_o$.

- A primary cycle with amplitude $0.8\,Q_o$ followed by two trailing cycles with amplitude $0.6\,Q_o$.

- A primary cycle with amplitude $0.9\,Q_o$ followed by two trailing cycles with amplitude $0.675\,Q_o$.

- A primary cycle with amplitude $0.9\,Q_o$ followed by two trailing cycles with amplitude $0.675\,Q_o$.

- A primary cycle with amplitude $1.0\,Q_o$ followed by two trailing cycles with amplitude $0.75\,Q_o$.

- A primary cycle with amplitude $1.0\,Q_o$ followed by two trailing cycles with amplitude $0.75\,Q_o$.

Additional steps consider increases in amplitude of the primary cycles of $0.1\,Q_o$, followed by two trailing cycles with amplitudes of 0.75 times the amplitude of the previous primary cycle. The process is followed until the component is not able to sustain additional load. The force Q_o is the force expected in the component under the maximum considered earthquake. This force should be estimated before the test by performing monotonic tests on a similar specimen.

2.2.2.3 Protocol for shake table testing

2.2.2.3.1 General description

The CUREE/Caltech protocol defines the criteria for selecting the ground motion histories required for performance assessment of wooden houses. In order to account for cumulative damage effects, it is recommended to perform test series considering ground motions with different return periods. This is recommended because it is not difficult to find structures affected by ground motions with probabilities of exceedance of 10% in 50 years and 2% in 50 years during their lifetimes. If necessary, repairing of the components should be executed during the test series in order to replicate the component conditions at the moment at which the 2%/50yr earthquake strikes.

2.2.2.3.2 Time histories for return periods of 475 years and smaller

In this case, a scaled ordinary record following the shape of the NEHRP ground response spectrum for soil type D, in the period range of interest, should be considered. If possible, three or two components of the record should be considered. Otherwise, the strongest component should be considered.

2.2.2.4 Time histories for long return periods

For long return periods it is recommended to consider near-fault records. If possible, three or two components of the record should be considered. Otherwise, the fault-normal component should be considered. The record used for testing should not be scaled.

2.2.3 ICC-ES AC156 2007 Specification

In January 2007, the Evaluation Service of the International Code Council (ICC-ES) released the latest version of AC156 "Acceptance criteria for seismic qualification by shake-table testing of nonstructural components and systems" (ICC-ES, 2007). This document is currently one of the basic references for seismic qualification of nonstructural components, systems and equipment; and for verification of compliance with section 1621 of IBC 2006 (ICC, 2006). The code specification is applicable to experimental verification of nonstructural components and systems with fundamental frequencies greater than 1.4 Hz.

The information required by the specification to define the testing histories and the compliance criteria include: the equipment attachment elevation with respect to grade, z; the average building roof elevation, h; the spectral response acceleration at short period, S_{DS}; the equipment importance factor, I_p; a description of the functional requirements of the equipment; and a description of mounting conditions, subassemblies, mass distribution, possible equipment variations, and installation instructions.

The preliminary part of the protocol considers a pre-test inspection and verification of functional compliance. Following this, the resonant frequency in each principal direction is searched for by using a single-axis sine loading, sweeping frequencies from 1.3 to 33.3 Hz.

The Required Response Spectrum (RRS) is derived from the IBC2006 formula for total design seismic horizontal force F_p given in equation (2.9). The spectrum for the vertical component is considered equal to 2/3 of the horizontal ground spectrum. The spectra are defined by the parameters A_{FLX} and A_{RIG}, defined in equations (2.16) and (2.17), and shown in Figure 2.9.

In the derivation of the RRS, the ratio R_p/I_p, which is a reduction factor to account for inelastic behavior of the component that is dependent on the energy absorption capacity of the equipment's force-resisting system, is set equal to 1, indicative of unreduced response. This is done because during the experimental testing the equipment will exhibit its intrinsic nonlinear behavior. The importance factor I_p does not increase the shaking intensity but it does affect functionality requirements after the test. The component amplification factor a_p is, by definition, set equal to 1 for rigid components (fundamental frequency greater than 16.7 Hz), and equal to 2.5 for flexible components (fundamental frequency less than 16.7 Hz).
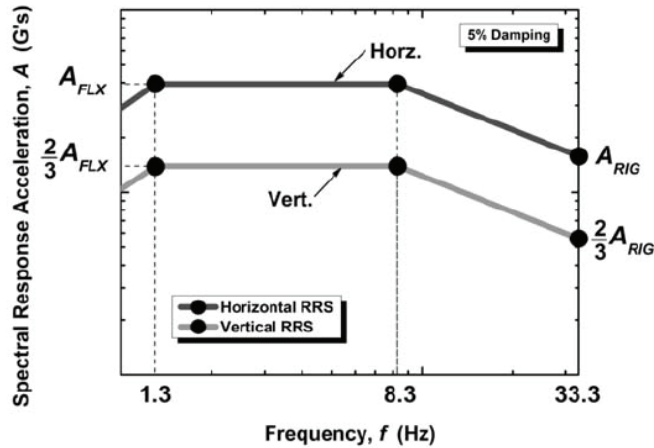
Figure 2.9. Required response spectrum RRS. Figure taken from ICC-ES (ICC, 2006).

$$A_{FLX} = S_{DS}\left(1 + 2\frac{\tilde{z}}{b}\right) \leq 1.6 S_{DS} \tag{2.16}$$

$$A_{RIG} = 0.4 S_{DS}\left(1 + 2\frac{\tilde{z}}{b}\right) \tag{2.17}$$

For vertical RRS, $\tilde{z}$ may be taken equal to 0. Alternatively, the horizontal RRS can be constructed from the information obtained during the structural analysis of the building, equation (2.10), and therefore:

$$A_{FLX} = 2.5 A_x a_i \tag{2.18}$$

24

$$A_{RIG} = A_x a_i \tag{2.19}$$

where A_x is the torsional amplification factor and a_i is the acceleration at the i-th level obtained from the dynamic analysis.

Realizations of non-stationary broadband random excitations having a frequency content ranging between 1.3 and 33.3 Hz matching the required response spectra RRS should be generated. The total duration of the shake table motion should be 30 seconds. The non-stationary character of the input motion is given by a build-hold-decay envelope of 5, 20 and 5 seconds of duration, respectively. The minimum duration of the strong motion should be 20 seconds. Longer strong motion durations are accepted.

2.2.4   The FEMA 461 testing protocols

2.2.4.1 General description

The FEMA 461 document (FEMA, 2006), developed through the collaboration of the three earthquake research centers (Mid-America Earthquake Center, Multidisciplinary Center for Earthquake Engineering Research and Pacific Earthquake Engineering Research Center) defines two testing protocols for experimental seismic fragility assessment of architectural, mechanical and electrical nonstructural components. The report provides, separately, a protocol for quasi-static cyclic testing of displacement-sensitive nonstructural components, and a shake table testing protocol for acceleration-sensitive nonstructural components. The procedures proposed in FEMA 461 are intended to allow for the determination of the median loading conditions at which different damage levels are achieved, and therefore, it is not an attempt to define an equipment qualification level. However, for a given type of nonstructural component, and after developing the fragility curve associated to a given damage state, it is possible to pick the loading level related to a relatively low probability of failure as the loading level for which the component is qualified (FEMA, 2005).

2.2.4.2   The FEMA 461 quasi-static testing protocol

The quasi-static testing protocol should be used for experimental fragility evaluation of displacement sensitive nonstructural components whose behavior is not governed by their dynamic response. This racking testing protocol consists of a set of low rate cyclic displacements or forces which follow a predefined pattern. This protocol can also be used for the characterization of the force-displacement constitutive relationships. This latest process is called testing for modeling because it allows for estimating mechanical properties (strength, stiffness, etc.) and low-cycle fatigue properties.

2.2.4.2.1 Displacement controlled test

The loading history consists of cycles of step-wise increasing displacement amplitudes which allows for the quantification of one or more damage states. Two cycles at each amplitude are performed, as shown in Figure 2.10. Four parameters define this loading history:

- Smallest target deformation Δ_o: Corresponds to the minimum deformation amplitude of the testing protocol. It should be less than the minimum displacement capable of inducing the first damage state. A minimum interstory drift of 0.0015 is recommended.

- Maximum target deformation Δ_m: Corresponds to the deformation level at which the largest damage state is achieved. It should be estimated before the test. A maximum interstory drift of 0.03, in absence or more detailed specimen capacity information, is recommended.

- Number of steps in the loading history n. It should be equal to or greater than 10.

- Amplitude of cycles a_i. The amplitude of the first and last cycle should be $a_1 = \Delta_o$ and $a_n = \Delta_m$, respectively. However, if the final damage state is not observed at the end of the loading history, the loading process should be extended by using additional increments of $0.3\Delta_m$. Nevertheless, the code recommends continuing with the loading protocol even if the last damage state is achieved.

The amplitude a_{i+1} of the displacement history at the $i+1$-th step is given by:

$$\frac{a_{i+1}}{a_n} = 1.4 \frac{a_i}{a_n} \tag{2.20}$$

Figure 2.10 shows the displacement loading history for the case Δ_o=0.0015, Δ_m=0.03, and n=10. If bi-directional testing is required to evaluate the component performance, the elliptical pattern shown in Figure 2.11 should be followed.

In this testing protocol it is essential that interstory drift be the engineering demand parameter (EDP) controlling the component behavior and triggering the different damage states. An adequate step-wise loading history has to be considered in order to sweep all possible damage states, avoiding the activation of more than one damage state at the same time.

The proposed loading protocol history given by equation (2.20) was obtained from statistical analysis of seismic response data of inelastic SDOF and MDOF systems as well as engineering judgment. The protocol is intended to be representative of cumulative damage effects and independent of ground motion

and type of nonstructural component. No near-fault ground motions were considered in its development, as was the case for the CUREE wood loading protocol project (Krawinkler *et al.*, 2000). It is assumed and demonstrated that near-fault motions can generate larger displacement demands in fewer cycles, and therefore, they do not control the number and the sequence of amplitudes in the loading history.
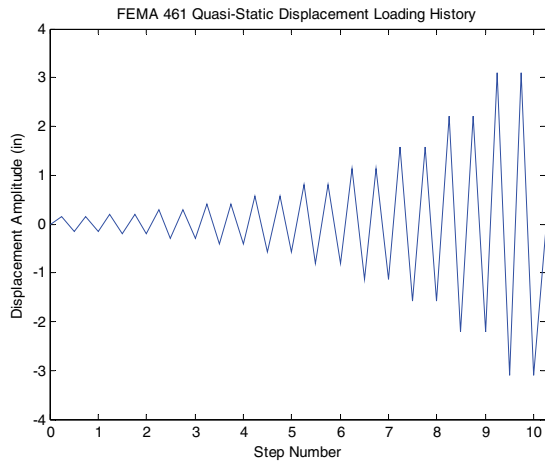
Figure 2.10. Displacement history for Δ_o=0.0015, Δ_m=0.03, and n=10
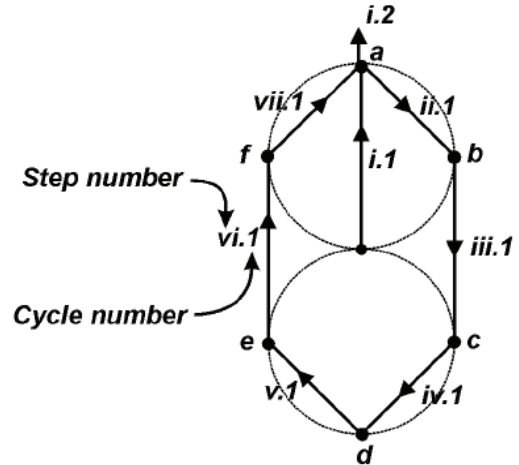
Figure 2.11. Displacement orbit for bidirectional loading test (Figure taken from FEMA 461)

2.2.4.2.2 Force controlled test

Force controlled testing should be performed if forces controls the seismic performance of the component, or if there is no a clear deformation pattern to consider in the damage progression. Given that force demands are highly dependent on the characteristics of each type of component and its boundary conditions, no general protocols are proposed, but some guidelines for its determination are stated in FEMA 461. If the force-deformation relationship for the force-sensitive component is known (from analysis or monotonic test), a cyclic force loading history can be derived by considering the forces associated to the displacements, which follow the series defined by equation (2.20) and shown in Figure 2.12.

(a)

(b)
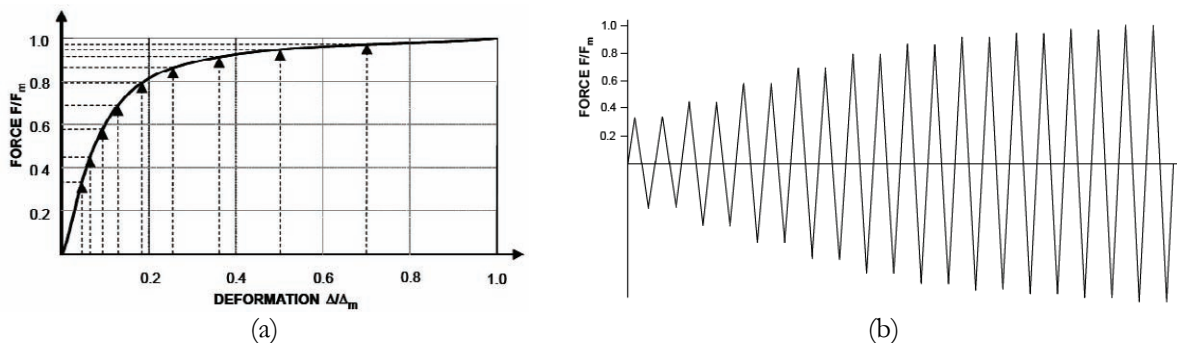
Figure 2.12. Example of force history protocol derived from force-displacement relations: (a) Force-displacement relation; and (b) Force history protocol (Figure taken from FEMA 461)

27

2.2.4.3 The FEMA 461 shake table testing protocol

The shake table testing protocol should be used for fragility evaluation of nonstructural components whose behavior is sensitive to the dynamic motion of a single level in a building structure (FEMA, 2005). Components sensitive to the motion of multiple supports are explicitly not included in the current version of FEMA 461 protocol. The testing procedure is based on the work done in 1997 by Wilcoski et al. at the Construction Engineering Research Laboratory (Wilcoski *et al.*, 1997). The first objective of the shake table testing protocol is to evaluate the seismic response and performance of nonstructural components under simulated floor motions at increasing intensities. A second objective is to characterize the functional performance levels and the damage states of the component to quantify its seismic fragility.

In this protocol, the parameter used to characterize the intensity of the input motion is the peak spectral acceleration. At least three shaking intensities should be used during testing. The intensities for performance evaluation should be selected in order to induce damage states associated to economic losses and downtime. Similarly, in failure tests, the intensity of shaking should be large enough to induce damage states associated to life safety. The increase in intensity level should be constant; with a minimum step size equal to 25% of the previous step.

The performance evaluation and failure tests should be executed using triaxial tests, with motions applied in the principal directions of the specimen. Biaxial tests are possible if the vertical response of the component is negligible, the vertical vibration period is 10 times the horizontal vibration period, or the vertical vibration period falls outside the frequency range of the input motion.

The shake table motions consist of 60 seconds long narrow-band random sweep acceleration records scaled to produce motions which have a relatively smooth response spectra (FEMA, 2005). The band width is one third octave and the center frequency of the records sweeps from 32 Hz down to 0.5 Hz at a rate of 6 octaves[2] per minute. A sweep from high to low frequencies is used to first excite higher vibration modes that have associated failure modes at smaller amplitudes compared to low frequency failure modes. Figure 2.13a and b show examples of acceleration histories recommended for performance evaluation and the corresponding acceleration response spectra, respectively.

The response spectrum for the vertical component history record is approximately 80% of the response spectra of the horizontal component. Visual or monitoring procedures should be considered to identify damage states. The testing time instant at which a given damage state is achieved should be recorded in

---

[2] One octave is defined as the interval between two frequencies that have a frequency ratio of two.

order to identify the center frequency that caused the damage state. The amplitude of motion which caused the damage state is obtained from the Test Response Spectrum (TRS), calculated from the shake table motion up to 10 seconds prior to the observation of the damage state. The peak TRS amplitude is the amplitude causing the damage state. The record responsible for the damage state should be notch-filtered considering the frequency and time at which the damage state was observed, in order to remove the frequencies that have already generated a given damage state. Repeating the test without notch-filtering may amplify the previous damage state. However, once a frequency is removed from the input motion, it will have a negligible effect on higher damage levels, which can be a problem if the higher damage levels are triggered by the removed frequencies but at different amplitudes. Therefore, the use of notch filtering should be assessed for each experimental case. The rules for designing the filter that should be considered are detailed in FEMA 461 (FEMA, 2005).
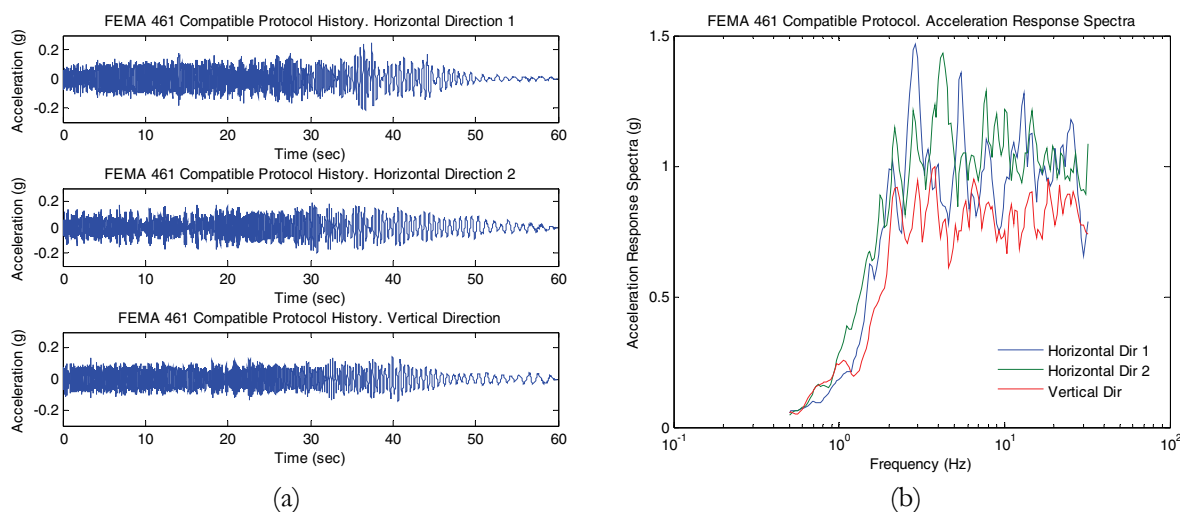
Figure 2.13. FEMA 461 compatible: (a) Shake table acceleration histories; and (b) Acceleration response spectra

2.3   Analytical methods for seismic demands estimation

The seismic response analysis of nonstructural systems constitutes one of the most challenging areas of research in earthquake engineering. In general, the seismic analysis of nonstructural components and equipment is more complex and sophisticated than the seismic analysis of primary systems, largely due to the additional variables that need to be considered. The infinite variety of nonstructural components and equipment configurations makes it difficult to establish general and practical rules for making their seismic design a simple process. Numerous studies have aimed at the estimation of seismic demands on nonstructural components. This subsection presents a summary of the most robust tools available in the literature directed at these estimations. As demonstrated in this subsection, the level of knowledge on the

seismic performance of nonstructural components is not properly reflected in the design code provisions presented in subsection 2.1. The original notation used by the authors is preserved for clarity.

2.3.1   Methods for estimating seismic acceleration demands

2.3.1.1 Exact seismic demands on SDOF nonstructural systems

This subsection presents a summary of the exact solution to the dynamic problem of a combined primary-secondary nonstructural system subjected to a ground motion, as presented by Gupta (Gupta, 1997). The equation of motion for an n-DOF linear classically damped primary system having a nonstructural system attached at its d-th DOF, which can be considered as a linear SDOF system, is given by:

$$M\ddot{x}(t) + C\dot{x}(t) + Kx(t) = -Mr\ddot{u}_g(t) \tag{2.21}$$

where $x(t)$ is the relative displacement vector; $r = \begin{bmatrix} r_p & r_s \end{bmatrix}^T$ is the influence vector; $\ddot{u}_g(t)$ is the time history acceleration record; and M, C and K represent the mass, damping and stiffness matrices of the combined system, given by:

$$M = \begin{bmatrix} M_p & 0_{n \times 1} \\ 0_{1 \times n} & M_s \end{bmatrix}$$

$$C = \begin{bmatrix} C_p & 0_{n \times 1} \\ 0_{1 \times n} & 0 \end{bmatrix} + C_c \tag{2.22}$$

$$K = \begin{bmatrix} K_p & 0_{n \times 1} \\ 0_{1 \times n} & K_s \end{bmatrix} + K_c$$

where M_p, C_p and K_p are the mass, damping and stiffness matrices of the primary system; M_s is the mass of the nonstructural (or "secondary") system; C_c is a damping matrix where the only non-zero elements are $C_{c_{dxd}} = C_{c_{(n+1)x(n+1)}} = -C_{c_{(n+1)xd}} = -C_{c_{dx(n+1)}} = C_s$; $C_s = 2\xi_s \omega_s M_s$ is the damping of the nonstructural system; ξ_s and $\omega_s = \sqrt{K_s / M_s}$ denote the damping ratio and natural frequency of the nonstructural system; K_c is a stiffness matrix where the only non-zero elements are $K_{c_{dxd}} = K_{c_{(n+1)x(n+1)}} = -K_{c_{(n+1)xd}} = -K_{c_{dx(n+1)}} = K_s$; where K_s is the stiffness of the nonstructural SDOF system. Introducing the transformation:

$$x(t) = \Phi_{ps} u(t) \tag{2.23}$$

where $\boldsymbol{\Phi}_{ps} = \begin{bmatrix} \boldsymbol{\Phi}_p & 0 \\ 0 & \phi_s \end{bmatrix}$; $\boldsymbol{\Phi}_p$ denotes the real-valued normalized modal matrix of the primary system only,

normalized in such a way that $\boldsymbol{\Phi}_{ps}^T M \boldsymbol{\Phi}_{ps} = I_{(n+1)\times(n+1)}$, and $\phi_s = 1/\sqrt{M_s}$ is the modal element of the

nonstructural system only. Introducing (2.23) into (2.21):

$$m\ddot{u}(t) + c\dot{u}(t) + ku(t) = -\gamma\ddot{u}_g(t) \tag{2.24}$$

where $m = \boldsymbol{\Phi}_{ps}^T M \boldsymbol{\Phi}_{ps} = I_{(n+1)\times(n+1)}$, $c = \boldsymbol{\Phi}_{ps}^T C \boldsymbol{\Phi}_{ps}$, $k = \boldsymbol{\Phi}_{ps}^T K \boldsymbol{\Phi}_{ps}$, and $\gamma = \boldsymbol{\Phi}_{ps}^T Mr = \begin{bmatrix} \boldsymbol{\Phi}_p^T M_p r_p \\ \phi_s M_s r_s \end{bmatrix}$. To apply

the state space approach, equation (2.24) should be rewritten as:

$$A \begin{bmatrix} \ddot{u}(t) \\ \dot{u}(t) \end{bmatrix} + B \begin{bmatrix} \dot{u}(t) \\ u(t) \end{bmatrix} = -Q\ddot{u}_g(t) \tag{2.25}$$

where $A = \begin{bmatrix} 0_{(n+1)\times(n+1)} & m \\ m & c \end{bmatrix}$, $B = \begin{bmatrix} -m & 0_{(n+1)\times(n+1)} \\ 0_{(n+1)\times(n+1)} & k \end{bmatrix}$, and $Q = \begin{bmatrix} 0_{(n+1)\times1} \\ \gamma \end{bmatrix}$. Assuming solutions of the

form $\begin{bmatrix} \dot{u}(t) \\ u(t) \end{bmatrix} = U_m e^{\mu t}$, substituting into equation (2.25), and considering free vibrations, the following

eigenproblem is obtained:

$$BU_m = -\mu AU_m \tag{2.26}$$

The *2n+2* eigenvalues μ^j *(j=1…2n+2)* are obtained by solving the characteristic equation:

$$|\mu A + B| = 0 \tag{2.27}$$

Since the eigenvectors form a basis for the *2n+2*-dimensional vector space, it is possible to write:

$$\begin{bmatrix} \dot{u}(t) \\ u(t) \end{bmatrix} = \begin{bmatrix} U_m^1, U_m^2, ..., U_m^{2n+2} \end{bmatrix} = \tilde{U}_m z(t) \tag{2.28}$$

where $z(t)$ is the *2n+2* vector of complex-valued principal coordinates and $\tilde{U}_m$ is the complex-valued

modal matrix. Substituting (2.28) into (2.24) and premultiplying by $\tilde{U}_m^T$:

$$\tilde{U}_m^T A \tilde{U}_m \dot{z}(t) + \tilde{U}_m^T B \tilde{U}_m z(t) = -\tilde{U}_m^T Q \ddot{u}_g(t) \tag{2.29}$$

Defining $\tilde{A} = \tilde{U}_m^T A \tilde{U}_m$, $\tilde{B} = \tilde{U}_m^T B \tilde{U}_m$ and $\tilde{Q} = \tilde{U}_m^T Q$, then:

$$\tilde{A}\dot{\underline{z}}(t) + \tilde{B}\underline{z}(t) = -\tilde{Q}\ddot{u}_g(t) \tag{2.30}$$

or

$$\dot{z}^j(t) + \mu^j z^j(t) = -f^j \ddot{u}_g(t) \qquad j=1\ldots2n+2 \tag{2.31}$$

where

$$f^j = \frac{\left[Re(\tilde{A})_{j,j} Re(\tilde{Q})_{j,j} + Im(\tilde{A})_{j,j} Im(\tilde{Q})_{j,j}\right] + i\left[Re(\tilde{A})_{j,j} Im(\tilde{Q})_{j,j} - Im(\tilde{A})_{j,j} Re(\tilde{Q})_{j,j}\right]}{\left[Re(\tilde{A})_{j,j}\right]^2 + \left[Im(\tilde{A})_{j,j}\right]^2} \tag{2.32}$$

The transfer functions $H^j(\omega)$ that relate the j-th principal coordinate $z^j(t)$ to the ground displacement $u_g(t)$ is:

$$H^j(\omega) = -\frac{f^j \omega^2}{\mu^j + i\omega} \qquad j=1\ldots2n+2 \tag{2.33}$$

Now, the transfer function $\aleph^s(\omega)$ for the s-th component of the $u(t)$ vector can be obtained as:

$$\aleph^s(\omega) = -\omega^2 \sum_{j=1}^{2n+2} \frac{U^j_{m_{s+n+1}} f^j (\mu^{*j} + i\omega)}{\tilde{\omega}_j^2 - \omega^2 - 2i\tilde{\xi}_j \tilde{\omega}_j \omega} \qquad s=1\ldots n+1 \tag{2.34}$$

where $\mu^{*j} = -\tilde{\xi}_j \tilde{\omega}_j - i\tilde{\omega}_j \sqrt{1 - \tilde{\xi}_j^2}$ denotes the complex conjugated of the j-th eigenvalue μ^j; $\tilde{\xi}_j$ and $\tilde{\omega}_j$ denote the damping ratio and natural frequency of the j-th vibration mode of the combined system. Finally, the transfer function relating the absolute acceleration of the nonstructural system to the ground acceleration is:

$$\aleph_{a_T}(\omega) = r_s + \phi_s \aleph^{n+1}(\omega) \tag{2.35}$$

The formulation presented above provides an exact solution to the dynamic problem that considers the interaction between primary and secondary (nonstructural) systems. It is limited to nonstructural components and equipment which can be modeled as linear SDOF systems.

2.3.1.2 Floor Response Spectra (FRS)

A widely used practical approach for designing primary structural systems is based on the use of the design response spectra defined in seismic design codes, such as IBC2006 (ICC, 2003) and FEMA450 (BSSC, 2003a). Design spectra are essentially smoothed plots of the statistical peak responses of single

degree of freedom systems excited by a collection of ground motions representative of the seismic hazard at the building site. In a similar fashion, the simplest way to represent the expected demands on nonstructural systems placed within multistory buildings is the Floor Response Spectra (FRS). This concept, originally proposed by Biggs and Roesset (Biggs and Roesset, 1970) in the early 1970's, had its former uses in the design of nonstructural systems for nuclear installations (Lin and Minai, 1987). The approach proposed by Biggs and Roesset consisted of a procedure for estimating the floor response spectra directly from the ground response spectrum without additional time history analyses. In this method, deterministic principles were considered to estimate the amplification of motion as it passes though the primary structure to the nonstructural system. To build upon this deficiency, Singh (Singh, 1976) developed a direct method to generate the floor response spectra accounting for principles of random vibration techniques to characterize the stochastic nature of the input ground motion. Singh's model considered an elastic shear type multistory level classically damped building. According to Singh's procedure, preserving the notation used in the original paper and omitting convoluted derivations, the FRS is obtained as the variance of the absolute acceleration $\ddot{y}_a$:

$$\sigma_{\ddot{y}_a}^2 = C \int_{-\infty}^{\infty} \Phi_u(\omega) \left(4\beta_o^2 \omega_o^2 \omega^2 + \omega_o^4 \right) \left| H_o(\omega) \right|^2 d\omega \qquad (2.36)$$

wherein $\left| H_o(\omega) \right| = 1 \Big/ \sqrt{\left(\omega_o^2 - \omega^2 \right)^2 + 4\beta_o^2 \omega_o^2 \omega^2}$ is the frequency response function of the nonstructural system; ω_o is its natural vibration frequency; and C is a factor to account for the ratio between the expected maximum absolute acceleration and its Root Mean Square (RMS). The author recommends using a factor of $C=3$ as adopted in 1972 by the American National Standards Institute. $\Phi_u(\omega)$ is the one-side Power Spectral Density Function (PSDF) of the stationary floor acceleration response at the u-th level, which is calculated from the dynamic properties of the primary structure, and that according to Singh, it is given by:

$$\Phi_u(\omega) = \sum_{j=1}^{N} \sum_{k=1}^{N} \gamma_j \gamma_k \psi_j(u) \psi_k(u) \left[\omega_j^2 \omega_k^2 + 4\beta_j \beta_k \omega_j \omega_k + 2i\omega \omega_j \omega_k \left(\omega_k \beta_j - \omega_j \beta_k \right) \right] H_j(\omega) H_k^*(\omega) \Phi_g(\omega) \quad (2.37)$$

where N is the number of significant modes considered in the analysis and γ_j, $\psi_j(u)$, β_j, ω_j are the modal participation factor, modal amplitude at u-th story level, the damping ratio and the vibration frequency of the j-th vibration mode of the primary structure, respectively. Furthermore, $H_j(\omega) = 1 \Big/ \left(\omega_j^2 - \omega^2 + 2i\beta_j \omega \omega_j \right)$, where i is the imaginary unit and $*$ denotes the complex conjugate function. $\Phi_g(\omega)$ is the PSDF of the input ground motion. Arguing that power spectral density functions associated to design ground motions are generally unknown and that most design codes specify ground

response spectra, Singh extended his previous method and proposed a procedure to obtain floor acceleration response spectra directly from the ground response spectrum. Nevertheless, several methods are available for the estimation of response spectra compatible PSDF (Singh, 1976). The functional form of the FRS is:

$$
R_u^2(\omega_o) = \begin{cases} \displaystyle\sum_{j=1}^{N} \gamma_j^2 \psi_j^2(u) \Big[\big(A_j + B_j \big) R^2(\omega_o) + \big(C_j + D_j \big) R^2(\omega_j) \Big] + \\[2ex] \displaystyle 2\sum_{j=1}^{N} \sum_{k=j+1}^{N} \gamma_j \gamma_k \psi_j(u) \Big[\big(A_{jk}' + B_{jk}' \big) R^2(\omega_o) + \big(C_{jk}' + D_{jk}' \big) R^2(\omega_j) + \big(E_{jk}' + F_{jk}' \big) R^2(\omega_k) \Big] \end{cases} \tag{2.38}
$$

in which $R_u(\omega_o)$ is the floor response spectrum value at the oscillator frequency ω_o for the u-th level; $R(\omega_o)$ and $R(\omega_j)$ are the code prescribed ground response spectrum at the oscillator and the j-th structural vibration frequencies, respectively; A_j, B_j, C_j, D_j are amplification factors for j-th mode defined in Singh (Singh, 1976); and A_{jk}', B_{jk}', C_{jk}', D_{jk}', E_{jk}', F_{jk}' are amplification factors for j-th and k-th modes, also defined in Singh (Singh, 1976). Both methods remove the problems associated to the non-uniqueness of the results obtained, for example, when spectrum consistent time histories are considered.

In the previous approaches, characterized by their relative simplicity, primary and nonstructural systems are decoupled and individually analyzed. The dynamic properties and the floor responses of the primary structure are estimated neglecting interaction with the nonstructural system. In this approach, the response at the attachment level is considered as the input motion for the estimation of the response of the nonstructural system. This sequence of analysis is also known in the literature as the "cascade" approach because of the transmission path considered. The main shortcoming of the previously presented method resides in that it neglects the interaction between primary and nonstructural systems. This can induce errors greater than 100% in the estimation of seismic demands on nonstructural systems and equipment with large masses and vibration frequencies tuned to the natural frequencies of the primary system (Chen and Soong, 1989). Additionally, the method neglects the effects of non-classical damping and does not yield adequate demands for designing nonstructural systems with multiple attachment points. The possible inelastic behavior of the primary system is not considered either. Several works have been performed in order to assess the aforementioned limitations. The main characteristics of those works are succinctly described in the remainder of this subsection.

The previous approach can not be used directly for the analysis of nonstructural systems with multiple attachment points because, in its original formulation, it does not take into account the cross correlations between the displacements at distinct attachment points. It is important to mention at this point that

current design codes do not consider this situation either. To incorporate this effect, it is necessary to define the cross floor response spectra and the auto floor response spectra. The cross response spectra has two components: the coincidence $R_C(\omega)$ and quadrature spectra $R_Q(\omega)$, which are defined in terms of the real, $\Phi_R(\omega)$, and imaginary, $\Phi_I(\omega)$, parts of the cross spectral density function of two support points (Burdisso and Singh, 1987a; Burdisso and Singh, 1987b; Singh and Burdisso, 1987):

$$R_C^2(\omega_j) = F_1^2 \int_{-\infty}^{\infty} \Phi_R(\omega) |H_j(\omega)|^2 \, d\omega \qquad (2.39)$$

$$R_Q^2(\omega_j) = F_2^2 \int_{-\infty}^{\infty} \Phi_I(\omega) |H_j(\omega)|^2 \, d\omega \qquad (2.40)$$

where F_1 and F_2 are the corresponding peak response factors. Methods to obtain these spectra, directly from the ground response spectra rather than the cross spectral density function are presented in (Burdisso and Singh, 1987a; Burdisso and Singh, 1987b; Singh and Burdisso, 1987). If the interaction between primary and secondary systems may be neglected, as in the case of light equipment, the auto and cross spectra can be directly obtained from the analysis of the primary system.

Methods for spectral peak widening, to account for uncertainties and variations of the structural and ground motion parameters, are extensively described in (Chen and Soong, 1989). For cases of nonstructural systems attached to more than one level, an upper-bound envelope of the individual floor spectra is generally considered.

2.3.1.3 Methods based on perturbation techniques

The interaction between primary and secondary systems can, in principle, be studied through a model of the combined system. However, that approach may result in a system with an excessive number of degrees of freedom which can be difficult or infeasible to analyze. The problem becomes even more difficult and time consuming if different configurations or locations for the secondary system are considered in the evaluation. In 1978, Kelly and Sackman (Sackman and Kelly, 1979) proposed a practical analytical method that allows for including in the analysis the dynamic interaction between primary and secondary systems. In this method, first order perturbation analysis (Bush, 1992; Holmes, 1995) is used to obtain the dynamic properties of the coupled system[3]. The first order perturbation method is valid for the analysis of light

---

[3] Perturbation analysis is a mathematical method used to find approximate solutions to problems difficult to solve analytically, by starting from the exact known solution of a related problem. The analysis can be applied if the problem can be formulated by adding a small term to the mathematical formulation of the problem with a known solution. The solution to the problem is expressed in terms of power series functions of the small term that quantifies the deviation from the solution of the solvable problem.

nonstructural systems. As proposed by Kelly and Sackman, and after the calculation of the eigenproperties of the combined system, a deterministic analysis may be performed to obtain the maximum oscillator modal responses by using ground response spectrum compatible acceleration histories. The modal responses are combined by using an adequate modal combination rule, typically the square root of the sum of the square values rule (SRSS), to obtain the oscillator response. A similar approach was developed by Gupta (Gupta and Jing-Wen, 1986a; Gupta and Jing-Wen, 1986b) and Suarez and Singh (Singh and Suarez, 1986; Suarez and Singh, 1987) to evaluate the eigenproperties of the coupled system by considering second order matrix perturbation techniques (Stewart, 1990). Using this approach, the eigenvalue problem of the combined system can be written as (Lin and Minai, 1987):

$$\left[A_o + \varepsilon A_1 + \varepsilon^2 A_2 \right] \tilde{\psi}_j = p_j \left[B_o + \varepsilon B_1 + \varepsilon^2 B_2 \right] \tilde{\psi}_j \tag{2.41}$$

where ε is the perturbation parameter; A_o and B_o are $O(\varepsilon^0)$ matrices associated to the unperturbed system eigenproblem, defined in terms of the matrices of the decoupled systems; A_1 and B_1 are $O(\varepsilon)$ symmetric non-positive definite matrices; and A_2 and B_2 are $O(\varepsilon^2)$ symmetric non-positive definite matrices. The dimension of all these matrices is $2Nx2N$, where N is the total number of degrees of freedom of the combined system. Also, p_j and $\tilde{\psi}_j$ are the eigenvalues and eigenvectors of the combined system, respectively. For this eigenproblem, the second order eigenvalue is expressed as:

$$p_j = p_{oj} + p_{1j} + p_{2j} \tag{2.42}$$

where p_{oj} is the eigenvalue associated to the unperturbed problem and the first (p_{1j}) and second (p_{2j}) order correction terms are given by:

$$p_{1j} = \tilde{\psi}_{oj}^T \left[A_1 - p_{oj} B_1 \right] \tilde{\psi}_{oj} \tag{2.43}$$

$$p_{2j} = \sum_{\substack{k=1 \\ k \neq j}}^{2N} \frac{p_{1j}^2}{\left(p_{0j} - p_{ok} \right)} + \tilde{\psi}_{oj}^T \left[A_2 - p_{oj} B_2 - p_{1j} B_1 \right] \tilde{\psi}_{oj} \tag{2.44}$$

Similar expressions are developed for the perturbed eigenvectors (Lin and Minai, 1987). However, for heavy nonstructural systems this method does not give accurate results. In such cases, the use of the modal synthesis method is required. In that approach, the modal characteristics of the combined system are calculated synthesizing the dynamic properties of primary and secondary systems. The method allows for finding efficiently and accurately the exact dynamic properties of coupled systems. The floor response spectra can be directly used in designing multiply supported nonstructural system. Uncertainties in structural parameters can be also included in the analysis. The design demands are finally obtained using an adequate modal combination rule.

A method to find a more accurate solution to the eigenproblem of coupled systems was performed in 1987 by Singh and Suarez (Singh and Suarez, 1988). Using such approach, dynamic properties of the combined system can be obtained for classically and unclassically damped primary structures.

2.3.1.4 Mode-acceleration approach for multiply-supported MDOF nonstructural systems

The problem with multiply supported MDOF nonstructural systems is typically assessed following an approach originally proposed by Clough and Penzien (Clough and Penzien, 1993). In that approach, the total response of the nonstructural system is divided into its dynamic and pseudo static parts. Following this concept, Chandra et al. (Chandra *et al.*, 2002) improved the mode-acceleration approach developed by Gupta (Gupta, 1997) for estimating the seismic response of linear, classically-damped, multiply-supported MDOF nonstructural systems, where the primary system is a linear classically-damped multistory building. Floor response transfer functions are formulated in terms of the dynamic properties of a chosen number of fixed-base vibration modes of the primary and nonstructural subsystems. The solved equation of motion accounts for the existing coupling of primary and secondary systems and is valid for both light and heavy nonstructural systems. For a base acceleration $\ddot{z}(t)$, the equation of motion of the combined system is:

$$M\ddot{X}(t) + C\dot{X}(t) + KX(t) = -MR\ddot{z}(t) + f(t) \tag{2.45}$$

where M, C and K are the mass, damping, and stiffness matrices (*nxn*) of the primary system, respectively; $X(t)$ is a vector containing the relative displacements of the primary system with respect to ground; n is the total number of degrees of freedom of the primary system; R is the influence vector (*nx1*); and $f(t)$ is a vector (*nx1*) with the interaction forces between the primary and secondary systems, where the k-th element is given by $\vartheta_k(t) = C_k\dot{u}(t) + K_k u(t)$ with *k=1…a*; where a is the number of attachment points; and $K_1…K_a$ and $C_1…C_a$ are the stiffness and damping constants of the devices connecting the primary and secondary systems. The interaction forces are $\vartheta_k(t) = 0$ for *k=a+1…n*. The $u(t)$ vector (*Nx1*) denotes the displacements of the secondary system, where N is the number of DOF of the secondary system. The first a terms in the $u(t)$ vector are measured relative to the displacements of the primary structure while the remaining are measured relative to the ground. Using the modal expansion $X(t) = \phi\,q(t)$, where ϕ is the real-valued modal matrix of the fixed-base primary system and $q(t)$ is the vector with modal responses, equation (2.45) can be rewritten as:

$$\ddot{q}_r(t) + 2\zeta_r\omega_r\dot{q}_r(t) + \omega_r^2 q_r(t) = -\alpha_r\ddot{z}(t) + \sum_{k=1}^{a}\phi_k^{(r)}\vartheta_k(t) \qquad r=1…n \tag{2.46}$$

37

where $\phi_k^{(r)}$ is the k-th element of the r-th mode shape of the primary system; $\alpha_r = \phi^{(r)T} MR$ is the r-th modal participation factor; ω_r and ζ_r are the natural frequency and damping ratio in the r-th mode. After some algebra, the equation above can be rewritten as:

$$q_r(t) = \frac{1}{\omega_r^2}\left[-\alpha_r \ddot{z}(t) + \sum_{k=1}^{a} \phi_k^{(r)} \vartheta_k(t) - \ddot{q}_r(t) - 2\zeta_r \omega_r \dot{q}_r(t) \right] \qquad r=1\ldots n \tag{2.47}$$

$$X_p(t) = \sum_{r=1}^{n} \frac{\phi_p^{(r)}}{\omega_r^2}\left[-\alpha_r \ddot{z}(t) + \sum_{k=1}^{a} \phi_k^{(r)} \vartheta_k(t) \right] - \sum_{r=1}^{n} \frac{\phi_p^{(r)}}{\omega_r^2}\left[\ddot{q}_r(t) + 2\zeta_r \omega_r \dot{q}_r(t) \right] \qquad p=1\ldots n \tag{2.48}$$

The first sum in this equation represents the pseudo-static part $X_{ps}(t)$ of $X_p(t)$, which can be also obtained from equation (2.46) by dropping the relative velocity and acceleration terms:

$$X_{ps}(t) = -\left[\sum_{i=1}^{n} F_{pi} M_i R_i \right] \ddot{z}(t) + \sum_{k=1}^{a} F_{pk} \vartheta_k(t) \tag{2.49}$$

where M_i is the i-th diagonal term in the M matrix; R_i the i-th term in the R vector; F_{pi} is the (p,i)-th term in the flexibility matrix of the primary system ($F = K^{-1}$). Substituting equation (2.49) into equation (2.48) and considering the first $\hat{n} < n$ modes, the displacement response of the p-th DOF is:

$$X_p(t) = -\left[\sum_{i=1}^{n} F_{pi} M_i R_i \right] \ddot{z}(t) + \sum_{k=1}^{a} F_{pk} \vartheta_k(t) - \sum_{r=1}^{\hat{n}} \frac{\phi_p^{(r)}}{\omega_r^2}\left[\ddot{q}_r(t) + 2\zeta_r \omega_r \dot{q}_r(t) \right] \qquad p=1\ldots n \tag{2.50}$$

which, expressed in frequency domain, is:

$$X_p(\omega) = -\left[\sum_{i=1}^{n} F_{pi} M_i R_i \right] \ddot{z}(\omega) + \sum_{k=1}^{a} F_{pk} \vartheta_k(\omega) - \sum_{r=1}^{\hat{n}} \frac{\phi_p^{(r)}}{\omega_r^2}\left[\omega^2 - 2i\zeta_r \omega \omega_r \right] q_r(\omega) \qquad p=1\ldots n \tag{2.51}$$

where

$$q_r(\omega) = H_r(\omega)\left(-\alpha_r \ddot{z}(\omega) + \sum_{k=1}^{a} \phi_k^{(r)} \vartheta_k(\omega) \right) \qquad r=1\ldots n \tag{2.52}$$

and

$$H_r(\omega) = \frac{1}{\omega_r^2 - \omega^2 + 2i\zeta_r \omega_r \omega} \qquad r=1\ldots n \tag{2.53}$$

Therefore, equation (2.51) becomes:

$$X_p(\omega) = -B_p(\omega) \ddot{z}(\omega) + \sum_{k=1}^{a} (i\omega C_k + K_k) D_{pk}(\omega) u_k(\omega) \tag{2.54}$$

where

$$B_p(\omega) = \sum_{i=1}^{n} F_{pi} M_i R_i + \sum_{r=1}^{\hat{n}} \frac{\phi_p^{(r)}}{\omega_r^2} \left[\omega^2 - 2i\zeta_r\omega\omega_r \right] \alpha_r H_r(\omega) \tag{2.55}$$

$$D_{pk}(\omega) = F_{pk} + \sum_{r=1}^{\hat{n}} \frac{\phi_p^{(r)}}{\omega_r^2} \left[\omega^2 - 2i\zeta_r\omega\omega_r \right] \phi_k^{(r)} H_r(\omega) \tag{2.56}$$

$B_p(\omega)$ represents the transfer function of the displacement response for the p-th DOF if the interaction between primary and secondary systems is neglected. $D_{pk}(\omega)$ represents the transfer function for displacement at the p-th DOF for a force applied along the k-th primary system DOF when both seismic excitation and secondary system are absent.

Now, to complete the solution, the motion of the nonstructural system should be found. The equation of motion of the secondary system is:

$$m\ddot{u}(t) + c\dot{u}(t) + ku(t) = F(t) \tag{2.57}$$

where m, c and k represent the mass, damping and stiffness matrices (NxN) of the secondary system; $F(t)$ is the vector containing the secondary system support excitations:

$$F(t) = -\tilde{m}\ddot{\tilde{X}}(t) - \tilde{c}\dot{\tilde{X}}(t) - \tilde{k}\tilde{X}(t) - mr\ddot{z}(t) \tag{2.58}$$

where $\tilde{m}$, $\tilde{c}$ and $\tilde{k}$ are the mass, damping and stiffness matrices (Nxa). The (i,j)-th element of $\tilde{m}$ is equal to the (i,j)-th element of m; $\tilde{c}$ and $\tilde{k}$ are obtained by considering the first a columns of the c and k matrices, respectively, ignoring the contributions of the stiffness and damping of the attachment devices; $\ddot{\tilde{X}}(t)$, $\dot{\tilde{X}}(t)$ and $\tilde{X}(t)$ are sub-vectors of $\ddot{X}(t)$, $\dot{X}(t)$ and $X(t)$, which consider only the first a elements; and r is the influence vector (Chandra *et al.*, 2002). Using normal coordinates defined as $u(t) = \psi\eta(t)$, equation (2.57) can be rewritten in modal coordinates as:

$$\ddot{\eta}_l(t) + 2\xi_l\Omega_l\dot{\eta}(t) + \Omega_l^2\eta_l(t) = \sum_{i=1}^{N} \psi_i^{(l)} F_i(t) \quad l=1\ldots N \tag{2.59}$$

where Ω_l and ξ_l denote the l-th natural frequency and damping ratio of the secondary system; $\psi_i^{(l)}$ denotes the i-th element of the l-th secondary system modal shape. Therefore, the response at the p-th DOF of the secondary system is:

$$u_p(t) = \sum_{l=1}^{N}\sum_{i=1}^{N} \frac{\psi_p^{(l)}\psi_i^{(l)}}{\Omega_l^2} F_i(t) - \sum_{l=1}^{N} \frac{\psi_p^{(l)}}{\Omega_l^2} \left(\ddot{\eta}_l(t) + 2\xi_l\Omega_l\dot{\eta}(t) \right) \quad p=1\ldots N \tag{2.60}$$

where, again, the first term represents the pseudo-static part u_{ps} of the displacement u_p. Alternatively, u_{ps} can be written as:

$$u_{ps}(t) = \sum_{i=1}^{N} f_{pi} F_i(t) \tag{2.61}$$

where f_{pi} is the (p,i)-th term in the flexibility matrix, $f = k^{-1}$, of the secondary system. Substituting this, considering the first $\hat{N} < N$ terms in the second term, and converting into the frequency domain:

$$u_p(\omega) = \sum_{i=1}^{N} f_{pi} F_i(\omega) + \sum_{l=1}^{\hat{N}} \frac{\psi_p^{(l)}}{\Omega_l^2} \left(\omega^2 - 2i\xi_l \Omega_l \omega\right) \eta_l(\omega) \quad p=1...N \tag{2.62}$$

where $\eta_l(\omega)$ is the Fourier transform of $\eta_l(t)$, and therefore:

$$\eta_l(\omega) = h_l(\omega) \sum_{i=1}^{N} \psi_i^{(l)} F_i(\omega) \tag{2.63}$$

where

$$h_l(\omega) = \frac{1}{\Omega_l^2 - \omega^2 + 2i\xi_l \Omega_l \omega} \tag{2.64}$$

$h_l(\omega)$ is the transfer function relating the l-th modal displacement in the secondary system to the input excitation at its attachments. In frequency domain, the support excitation force can be written as:

$$F_i(\omega) = -m_i r_i \ddot{z}(\omega) + \sum_{j=1}^{a} X_j(\omega) A_{ij}(\omega) \quad i=1...N \tag{2.65}$$

where

$$A_{ij}(\omega) = \omega^2 \tilde{m}_{ij} - i\omega \tilde{x}_{ij} - \tilde{k}_{ij} \tag{2.66}$$

Substituting expressions for $\eta_l(\omega)$ and $F_i(\omega)$ in equation (2.62):

$$u_p(\omega) = \sum_{i=1}^{N} \left[-m_i r_i \ddot{z}(\omega) + \sum_{j=1}^{a} A_{ij}(\omega) X_j(\omega) \right] E_{pi}(\omega) \quad p=1...N \tag{2.67}$$

where

$$E_{pi}(\omega) = \sum_{l=1}^{\hat{N}} \frac{\psi_p^{(l)} \psi_i^{(l)}}{\Omega_l^2} \left(\omega^2 - 2i\xi_l \Omega_l \omega\right) h_l(\omega) + f_{pi} \tag{2.68}$$

40

Finally, a system of equations is obtained in terms of the Fourier spectral amplitude of the primary structure displacements ($p=1…N$):

$$X_p(\omega) - \sum_{j=1}^{a}\left[\sum_{k=1}^{a}D_{pk}(\omega)(i\omega C_k + K_k)\left\{\sum_{i=1}^{N}A_{ij}(\omega)E_{ki}(\omega)\right\}\right]X_j(\omega) = -\left[B_p + \sum_{i=1}^{N}m_i r_i\left\{\sum_{k=1}^{a}(i\omega C_k + K_k)D_{pk}(\omega)E_{ki}(\omega)\right\}\right]\ddot{\chi}(\omega) \quad (2.69)$$

Or in terms of displacements of the secondary system:

$$u_p(\omega) - \sum_{k=1}^{a}\left[\sum_{i=1}^{N}E_{pi}(\omega)(i\omega C_k + K_k)\left\{\sum_{j=1}^{N}A_{ij}(\omega)D_{jk}(\omega)\right\}\right]u_k(\omega) = -\left[\sum_{i=1}^{N}\left(m_i r_i + \sum_{j=1}^{N}A_{ij}(\omega)B_j(\omega)\right)E_{pi}(\omega)\right]\ddot{\chi}(\omega) \quad (2.70)$$

In 2003, Chaudhuri and Gupta (Chaudhuri and Gupta, 2003) extended this theory to include soil-structure interaction in the formulation. In this extension, the base flexibility is considered as a complex-valued impedance function, and the effects of kinematic interaction are assumed to be negligible. To further simplify calculations, only secondary systems which can be modeled as SDOF were considered. Alternatively, Asfura and Kiureghian (Asfura and Der Kiureghian, 1986) developed an analysis approach in which the separation of the response into its dynamic and pseudo-static components is not required.

2.3.1.5 Methods using continuous beam systems

The methods using continuous beam models are attractive because of their relative simplicity and usefulness in developing parametric analyses. This subsection presents the most interesting models of this type found in literature.

2.3.1.5.1 Model by Lavelle et al.

In 1988 Lavelle et al. (Lavelle *et al.*, 1988) proposed a simple exact method to calculate the dynamic response of a combined primary-secondary system. The primary system considered consists of a viscously damped uniform cantilever beam, while the secondary system was modeled as a damped SDOF oscillator attached at some point along the height of the beam (primary system), as shown in Figure 2.14. Both systems were considered to behave linearly. The continuous beam model shown in Figure 2.14 was proposed and studied in the early 1960's by Coull and Choudhury (Coull and Choudhury, 1967a; Coull and Choudhury, 1967b), Heidebrecht and Stafford-Smith (Heidebrecht and Stafford-Smith, 1973), and Stafford-Smith and Coull (Stafford-Smith and Coull, 1991).

The governing equation of motion for the cantilever beam shown in Figure 2.14 is:

$$\rho\ddot{y}(x,t) + C_b\dot{y}(x,t) + EIy^{iv}(x,t) = F(t)\delta(x-h) - \rho\ddot{y}_g(t) \quad (2.71)$$

where ρ is the mass per unit beam length; C_b is the damping per unit beam length and $\delta(x-h)$ denotes the Dirac function; EI is the equivalent rigidity of the flexural beam; and $F(t)$ is the force at the

41

interface between the primary and secondary systems. The equation of motion for the oscillator is given by:

$$M\ddot{z}(t)+C\dot{z}(t)+Kz(t)=C\dot{y}(h,t)+Ky(h,t)-M\ddot{y}_g(t) \tag{2.72}$$

where M, C and K are the mass, damping and stiffness of the secondary system, respectively. The interaction force $F(t)$ is given by:

$$F(t)=C\left[\dot{z}(t)-\dot{y}(h,t)\right]+K\left[z(t)-y(h,t)\right] \tag{2.73}$$
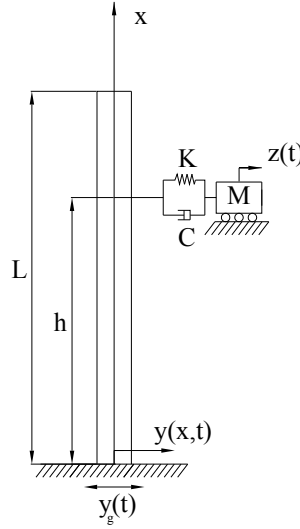
Figure 2.14. Lavelle's continuous beam model

To calculate the modal properties, the damping existing in the system is neglected, and free vibrations are considered. Therefore:

$$\rho\ddot{y}(x,t)+EIy^{iv}(x,t)=K\left[z(t)-y(h,t)\right]\delta(x-h) \tag{2.74}$$

Assuming $y(x,t)=q(t)\psi(x)$, $z(t)=Aq(t)\psi(h)$, and substituting into equation (2.74):

$$\ddot{q}(t)\psi(x)+\frac{EI}{\rho}q(t)\psi^{iv}(x)=\frac{K}{\rho}(A-1)q(t)\psi(h)\delta(x-h) \tag{2.75}$$

from where

$$\frac{\ddot{q}(t)}{q(t)}=\frac{K}{\rho}(A-1)\frac{\psi(h)}{\psi(x)}\delta(x-h)-\frac{EI}{\rho}\frac{\psi^{iv}(x)}{\psi(x)}=-\omega^2 \tag{2.76}$$

42

and therefore $\ddot{q}(t) + \omega^2 q(t) = 0$. After solving to get $A = \dfrac{K}{K - M\omega^2}$, the following equation in terms of $\psi(x)$ is found:

$$\psi^{iv}(x) - \alpha^4 \psi(x) = f(x) \tag{2.77}$$

where $\alpha^4 = \dfrac{\rho\omega^2}{EI}$ and $f(x) = \dfrac{KM\omega^2}{EI}\psi(b)\delta(x - b)$. Equation (2.77) is associated to a Green's function $g(\alpha, L, x, \xi)$, satisfying the same boundary conditions as $\psi(x)$, and also satisfying (Melnikov, 1995; Roach, 1982; Stakgold, 1998):

$$g^{iv}(\alpha, L, x, \xi) - \alpha^4 g(\alpha, L, x, \xi) = \delta(x - \xi) \tag{2.78}$$

which can be solved by using the causal fundamental solution method (Melnikov, 1995). The relation between $\psi(x)$ and $g(\alpha, L, x, \xi)$ is given by (Nicholson and Bergman, 1986):

$$\psi(x) = \int_0^L g(\alpha, L, x, \xi) f(\xi) d\xi \tag{2.79}$$

Substituting for $f(\xi)$ and considering the properties of the Dirac function:

$$\psi(x) = \dfrac{KM\omega^2}{EI}\psi(b) g(\alpha, L, x, b) \tag{2.80}$$

The vibration frequencies of the combined system are obtained after substituting (2.80) into (2.77) and solving for α from the characteristic equation:

$$\left[1 - \dfrac{KM}{\rho}\alpha^4 g(\alpha, L, b, b) \right]\psi(b) = 0 \tag{2.81}$$

Finally, the response of the secondary system $z(t)$ can be obtained from:

$$z(t) = \sum_{n=1}^{\infty} \dfrac{K}{K - M\omega_n^2} q_n(t) \tag{2.82}$$

where the modal shapes have been normalized in such a way that $\psi_n(b) = 1$. The temporal part of the solution is obtained by using the state space approach, after substituting (2.82) into (2.72) and considering a suitable number of modes. It is important to note that a parametric analysis performed using this method should consider six parameters: oscillator to beam mass ratio, natural frequencies and damping of

the oscillator and continuous beam, and location of the oscillator along the height of the building. One limitation is that the method is only applicable to linear structures.

2.3.1.5.2 Model by Miranda et al.

A similar and simpler method to estimate floor acceleration demands in multistory buildings has been used by Miranda and Taghavi (Miranda and Taghavi, 2005), which is based in a building model previously studied by Coull and Choudhury (Coull and Choudhury, 1967a; Coull and Choudhury, 1967b), Heidebrecht and Stafford-Smith (Heidebrecht and Stafford-Smith, 1973), and Stafford-Smith and Coull (Stafford-Smith and Coull, 1991). This method, which is an extension of the approach presented in (Miranda, 1999; Miranda and Reyes, 2002), considers a linear multistory building modeled as a combination of continuous shear and flexure beams with variable stiffness, as shown in Figure 2.15.
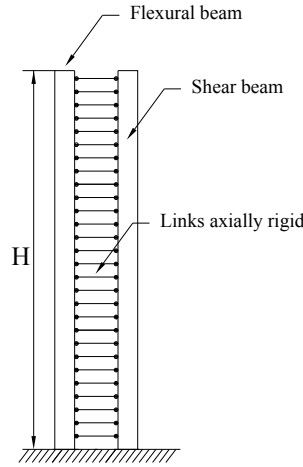
Figure 2.15. Simplified model of multistory building. After Miranda (Miranda, 1999)

The acceleration along the height, x, of the building is calculated according to:

$$\ddot{u}_T\left(x,t\right) \cong \ddot{u}_g\left(t\right) + \sum_{i=1}^{m}\Gamma_i\phi_i\left(x\right)\ddot{D}_i\left(t\right)$$

(2.83)

where the i-th modal participation factor Γ_i is:

$$\Gamma_i = \int_0^1\phi_i\left(x\right)dx \Big/ \int_0^1\phi_i^2\left(x\right)dx$$

(2.84)

and $D_i\left(t\right)$, the i-th modal response, is obtained by solving:

$$\ddot{D}_i\left(t\right) + 2\xi_i\omega_i\dot{D}_i\left(t\right) + \omega_i^2 D_i\left(t\right) = -\ddot{u}_g\left(t\right)$$

(2.85)

where ξ_i is the damping ratio of the i-th vibration mode. Note that in equation (2.83) only the first m vibration modes are included. The modal shapes for the uniform stiffness case $\phi_i''(x)$ are calculated as:

$$\phi_i''(x) = \frac{\sin(\gamma_i x) - \gamma_i\left(\alpha_0^2 + \gamma_i^2\right)^{-\frac{1}{2}} \sinh\left(x\sqrt{\alpha_0^2 + \gamma_i^2}\right) + \eta_i\left[\cosh\left(x\sqrt{\alpha_0^2 + \gamma_i^2}\right) - \cos(\gamma_i x)\right]}{\sin(\gamma_i) - \gamma_i\left(\alpha_0^2 + \gamma_i^2\right)^{-\frac{1}{2}} \sinh\left(\sqrt{\alpha_0^2 + \gamma_i^2}\right) + \eta_i\left[\cosh\left(\sqrt{\alpha_0^2 + \gamma_i^2}\right) - \cos(\gamma_i)\right]} \quad (2.86)$$

where

$$\eta_i = \frac{\gamma_i^2 \sin(\gamma_i) + \gamma_i\sqrt{\alpha_0^2 + \gamma_i^2}\, \sinh\left(\sqrt{\alpha_0^2 + \gamma_i^2}\right)}{\gamma_i^2 \cos(\gamma_i) + \left(\alpha_0^2 + \gamma_i^2\right)\cosh\left(\sqrt{\alpha_0^2 + \gamma_i^2}\right)} \quad (2.87)$$

The γ_i parameters are obtained by solving:

$$2 + \left[2 + \frac{\alpha_0^4}{\gamma_i^2\left(\gamma_i^2 + \alpha_0^2\right)}\right]\cos(\gamma_i)\cosh\left(\sqrt{\gamma_i^2 + \alpha_0^2}\right) + \left[\frac{\alpha_0^4}{\gamma_i\left(\gamma_i^2 + \alpha_0^2\right)}\right]\sin(\gamma_i)\sinh\left(\sqrt{\gamma_i^2 + \alpha_0^2}\right) = 0 \quad (2.88)$$

where $\alpha_0 = H\left(\dfrac{GA_o}{EI_o}\right)^{\frac{1}{2}}$ is a non-dimensional parameter controlling the participation of shear and flexure deformations in the total response of the system; GA_o and EI_o denote the shear and flexural rigidities at the base of the structure, respectively; and H is the total height of the building. Finally, vibration frequencies are obtained from:

$$\omega_i^2 = \frac{EI_o}{\rho H^4}\gamma_i^2\left(\gamma_i^2 + \alpha_0^2\right) \quad (2.89)$$

where ρ is the mass per unit length of the system. In order to account for the stiffness variation along the height of the building, the following modifications to the modal properties are proposed:

$$\phi_i^{nu}(x) = \phi_i''(x) + \left\{(-1)^i\, i^{1.3}\, \sin\left[(i-0.1)\pi x\right]\sqrt{\sin(\pi x)}\right\}\left[\sin\left(\frac{\pi\alpha_0}{60}\right) + 0.4\right]\left(\frac{1-\delta}{9}\right) \quad (2.90)$$

$$\Gamma_i^{nu} = \Gamma_i''\left[1 - \frac{(1-\delta)^{1.2}}{k}\left(\alpha_0^2 - 50\alpha_0 - 200\right)\right] \quad (2.91)$$

$$\left(\frac{T_i}{T_1}\right)_{nu} = \left(\frac{T_i}{T_1}\right)_u\left[1 - \frac{(1-\delta)^{1.2}}{9000}\left(\alpha_0^2 - 50\alpha_0 - 800\right)\right] \quad (2.92)$$

where $\phi_i^{nu}(x)$ and $\phi_i^{u}(x)$ are the i-th modal shape for the systems with non-uniform and uniform stiffness, respectively; and δ is the ratio of the lateral stiffness at the top to the lateral stiffness at the base of the system. Equation (2.91) can be used as an alternative to equation (2.84), wherein $k=8000$, 2000 and 1700 for $i=1$, 2 and 3, respectively.

The advantage of this method is the simplicity of the concepts involved, serving as a fast and efficient tool for preliminary estimation of expected demands. Only four parameters are required in such a parametric analysis: T, ξ, α_0 and δ. Note that for the case of constant stiffness, the response depends only on the three first parameters. According to the analysis shown in (Miranda and Taghavi, 2005) and (Taghavi and Miranda, 2005) the use of only the three first modes ($m=3$) leads to good estimations of acceleration demands. The major limitations of the method are its dependence on specific ground motions and its application to buildings exhibiting linear or almost linear responses. Moreover, this model neglects the dynamic interaction between primary and secondary systems.

2.3.2 Simplified procedures for estimation of seismic acceleration demands

2.3.2.1 Method proposed by Rodriguez et al. (2001)

Rodriguez et al. (Rodriguez *et al.*, 2002) proposed a method to estimate the design accelerations along the height of regular multi-story buildings. The proposed method, called "First mode reduced method", is based on a modal superposition approach modified to account for the inelastic response of the primary system. In this method, the floor acceleration A_n^q at the uppermost level of the building and for the q-th vibration mode is given by:

$$A_n^q = \Gamma_q \phi_n^q \frac{S_a(T_q, \zeta_q)}{R_q} \tag{2.93}$$

where Γ_q is the participation factor for the q-th mode; ϕ_n^q is the amplitude of the q-th mode at level n; $S_a(T_q, \zeta_q)$ is the spectral acceleration; T_q and ζ_q are the period and damping ratio of the q-th mode, respectively; and R_q is a reduction factor to account for the effect of ductility on the primary system. The modal accelerations are calculated using SRSS criteria:

$$A_n = \sqrt{\sum_{q=1}^{r}\left[\Gamma_q \phi_n^q \frac{S_a(T_q, \zeta_q)}{R_q}\right]^2} \tag{2.94}$$

According to numerical simulations, only the first mode is typically affected by ductility demands (Rodriguez *et al.*, 2002), and therefore $R_2 = R_3 = \ldots = R_r = 1$. Thus, equation (2.94) becomes:

$$A_n = \sqrt{\left[\Gamma_1 \phi_n^1 \frac{S_a\left(T_q, \zeta_q\right)}{R_1}\right]^2 + \sum_{q=2}^{r}\left[\Gamma_q \phi_n^q S_a\left(T_q, \zeta_q\right)\right]^2} \tag{2.95}$$

where $R_1 = O_{Me}/O_{Mo}$; and OM_e and OM_o are the overturning moments observed during linear and nonlinear analysis, respectively. To obtain the floor acceleration at the other floors of the building, the following interpolation function is proposed:

$$A_i = \Omega_i A_o \tag{2.96}$$

where A_o is the design peak ground acceleration; and Ω_i is the floor acceleration magnification factor given by:

$$\Omega_i = \begin{cases} 5\dfrac{h_i}{h_n}\left(\dfrac{A_n}{A_o} - 1\right) + 1 & 0 \leq \dfrac{h_i}{h_n} \leq 0.2 \\ \dfrac{A_n}{A_o} & 0.2 < \dfrac{h_i}{h_n} \leq 1 \end{cases} \tag{2.97}$$

where h_i is the height above grade of the *i*-th floor level and h_n is the height above grade of the uppermost building level. Finally, to simplify the design process, a factor $R_1 = \mu/2$ or $R_1 = 1$, whichever is greater, is recommended to be used, where μ is the ductility factor considered in design.

2.3.2.2 Method proposed by Villaverde (2006)

Villaverde (Villaverde, 2006) proposed a simple approximate method to examine the seismic force demands on non-linear light MDOF-secondary systems attached to one or two levels in multi-story nonlinear buildings. In this method, which is essentially a simplification of the method presented in (Villaverde, 1997a), the conventional ground response spectrum technique is used to evaluate the design forces on the secondary system. Dynamic properties (vibration frequencies, modal shapes and damping ratios) of primary and secondary systems are attained independently. Among the simplifications considered in the method are: i) it is assumed that the response of the system is governed by the response of the fundamental vibration mode of the two subsystems; ii) fundamental periods of primary and secondary systems are tuned; iii) the fundamental mode shape of the primary system varies linearly along the height of the building, with zero amplitude at grade and a maximum modal amplitude at the top level; iv) the fundamental mode shape of the secondary system varies linearly along the height of the secondary system, with zero modal amplitude at support points and a maximum modal amplitude at the point where

the maximum deformation is measured when the secondary system is loaded laterally by its own weight; v) the generalized masses in the fundamental modes of both subsystems are equal to their respective total masses; vi) damping ratios are 5% and 0% for primary and secondary systems, respectively; vii) the duration of the strong part of the ground motion is 25 sec; viii) non-linear behavior of primary and secondary systems are independent; and ix) the strength reduction factors for SDOF systems are still valid for MDOF systems with uniform properties vibrating mainly at their first mode. The simplified equations of the method are as follows:

$$F_{p_j} = \frac{w_{p_j} l_j}{\sum_{j=1}^{n} w_{p_j} l_j} V_p \tag{2.98}$$

$$V_p = \frac{C_p}{RR_p} S_a w_p \tag{2.99}$$

$$C_p = \frac{1}{\sqrt{\frac{2w_p}{W} + \frac{(1+0.5T)^2 - 1}{200\Phi_o^2}}} \leq \frac{\sqrt{200\Phi_o}}{1+0.5T} \tag{2.100}$$

$$\Phi_o = \frac{W h_{av}}{\sum_{i=1}^{N} W_i h_i} \tag{2.101}$$

where F_{p_j} denotes the force acting on the j-th mass of the secondary system; w_{p_j} is the weight of the j-th mass of the secondary system; l_j is the distance between the attachment point and the j-th mass of the secondary system; n is the number of lumped masses in the secondary system; S_a is the spectral acceleration amplitude at the fundamental period of the primary system; R and R_p are the strength reduction factors for the primary and secondary systems calculated for the target ductility demands; W and w_p denote the total weight of the primary and secondary systems, respectively; T is the fundamental period of the primary and secondary systems; W_i and h_i are the weight and elevation above the ground of the i-th building level; N is the number of floor levels in the primary system; and h_{av} is the average elevation above the ground of the secondary component. See (Villaverde, 2006) for further details.

2.3.3   Procedures for estimation of drift demands

2.3.3.1 Drift spectrum

A method to estimate interstory drift demands due to ground motion was proposed in 1997 by Iwan (Iwan, 1997). The method, called drift spectrum, is based on a linear system model. Like the typical acceleration response spectrum, the drift spectrum provides a simple indication of the overall drift demand due to earthquake ground motions. The structural system considered in the development of this

model is the continuous shear beam shown in Figure 2.16 rather than the typical SDOF model. This model is considered to adequately capture the effect of the wave propagation response within the building during the strong motion.
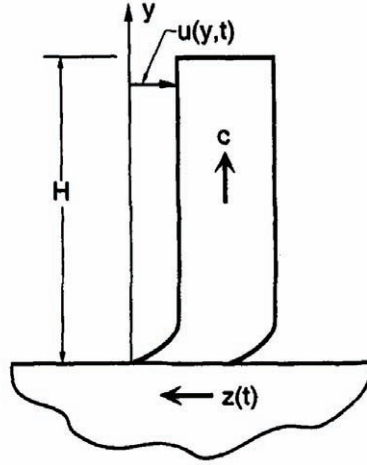
Figure 2.16. Continuous shear beam model. Figure taken from Iwan (Iwan, 1997)

Assuming that the period of the building shown in Figure 2.16 is T, the horizontal displacement along the height of the beam, relative to its base, is given by:

$$u(y,t) = e^{-\alpha t}\phi(y \pm ct)$$

(2.102)

where $\alpha = 2\pi\zeta/T$ is a constant parameter related to the time decaying amplitude of oscillations; ζ is the damping ratio associated to the first vibration mode of the beam; $\phi(y \pm ct)$ denotes the wave traveling upward or downward along the beam; and $c = 4H/T$ is the wave speed. Considering an arbitrary point located at a height $h = \beta H$, where β is a dimensionless height variable $(0 \leq \beta \leq 1)$, and the velocity time history of the ground, $v(t) = \dfrac{dz(t)}{dt}$, the shear-strain at a dimensionless height β is given by:

$$\frac{\partial u}{\partial y}(h,t) = \frac{1}{c}\left\{ \begin{aligned} & e^{-\frac{\pi\beta\zeta}{2}}\left[v\left(t - \frac{\beta T}{4}\right) + \frac{2\pi\zeta}{T} z\left(t - \frac{\beta T}{4}\right)\right] + \\ & \sum_{n=1}^{N \leq \frac{2t}{T} - \frac{\beta}{2}} (-1)^n\, e^{-\left(n\pi + \frac{\beta}{2}\right)\zeta}\left[v\left(t - \frac{nT}{2} - \frac{\beta T}{4}\right) + \frac{2\pi\zeta}{T} z\left(t - \frac{nT}{2} - \frac{\beta T}{4}\right)\right] + \\ & \sum_{n=1}^{N \leq \frac{2t}{T} + \frac{\beta}{2}} (-1)^n\, e^{-\left(n\pi + \frac{\beta}{2}\right)\zeta}\left[v\left(t - \frac{nT}{2} + \frac{\beta T}{4}\right) + \frac{2\pi\zeta}{T} z\left(t - \frac{nT}{2} - \frac{\beta T}{4}\right)\right] \end{aligned} \right\}$$

(2.103)

49

Equation (2.103) considers the superposition of the contributions from all waves traveling upward and downward at height h and time t. The interstory drift demand spectrum, $D(T,\zeta)$, is estimated from the shear strains, and it is defined as:

$$D(T,\zeta) = \max_t \left| \frac{\partial u}{\partial y}(y,t) \right| \tag{2.104}$$

Considering that in many cases the maximum interstory drifts are observed at the base of the buildings ($\beta = 0$), the $D(T,\zeta)$ spectrum can be simplified as (Iwan, 1997):

$$D(T,\zeta) = \max_t \frac{T}{4H} \left| v(t) + \frac{2\pi\zeta}{T} z(t) + 2 \sum_{n=1}^{N \le \frac{2t}{T}} (-1)^n e^{-n\pi\zeta} \left[v\left(t - \frac{nT}{2}\right) + \frac{2\pi\zeta}{T} z\left(t - \frac{nT}{2}\right) \right] \right| \tag{2.105}$$

It is interesting to note that for the calculation of the previous spectrum, only a summation of the ground velocity and displacement time histories is required, and therefore, is much easier to compute than the response spectra (Iwan, 1997). However, ground acceleration time history records should be carefully processed. Some guidelines for that can be found in Boore (Boore, 2001; Boore, 2003b; Boore, 2005), and Boore and Bommer (Boore and Bommer, 2005).

According to Iwan (Iwan, 1997), equation (2.105) can be further simplified considering that the maximum drifts are expected at times when ground velocity $v(t)$ is maximum. At those times, $z(t) \approx 0$ or small, and therefore:

$$D(T,\zeta) \approx \max_t \frac{T}{4H} \left| v(t) + 2 \sum_{n=1}^{N \le \frac{2t}{T}} (-1)^n e^{-n\pi\zeta} v\left(t - \frac{nT}{2}\right) \right| \tag{2.106}$$

If the ground motion can additionally be modeled as an isolated displacement pulse consisting of a positive velocity pulse followed at a time T_p by an identical negative velocity pulse of the same magnitude ($|v_{max}| = |v_{min}|$), with total pulse duration $2T_p$, and such that $t_{min} = t_{max} + T_p$, the maximum interstory drift will occur at a structural period T_p, and it will be given by:

$$D(T_p,\zeta) \approx \frac{T_p}{4H} \left(1 + 2e^{-\pi\zeta}\right) v_{max} \tag{2.107}$$

For an undamped system $\zeta = 0$, and therefore:

50

$$D\left(T_p, \zeta = 0\right) \approx \frac{3T_p}{4H} v_{max}$$

(2.108)

2.3.3.2 Other approximate methods for drift estimations

Another simple method to estimate approximate maximum interstory drift ratios has been proposed by Miranda (Miranda, 1999). In his approach, Miranda considered a model of a limiting case of a multistory building, given by an undamped continuum beam consisting of a combination of flexural and shear cantilever beams, as shown in Figure 2.15. In this method, the solution to the following equation of motion of the combined system is found:

$$\frac{d^4u}{dz^4} - \frac{\alpha^2}{H^2}\frac{d^2u}{dz^2} = \frac{w(z)}{EI}$$

(2.109)

where $\alpha = \sqrt{\dfrac{GAH^2}{EI}}$ is a dimensionless parameter indicating the relative degree of deformability due to shear and flexure. A value of $\alpha = 0$ represents a pure flexural beam model, while a value of $\alpha = \infty$ corresponds to a pure shear beam model. An intermediate value of α represents a typical multistory building deforming in shear and flexure. $w(z)$ represents a generalized equivalent lateral seismic force, given by:

$$w(z) = w_{max}\frac{1 - e^{-\frac{az}{H}}}{1 - e^{-a}}$$

(2.110)

where w_{max} is the intensity of the force at the top of the building and a is a dimensionless parameter that controls the shape of the loading function. Values of $a = 0$ and $a = \infty$ correspond to triangular and uniform load distributions, respectively. A value of $a = 2.13$ approximately represents a parabolic lateral load distribution. The solution to equation (2.109) for the lateral load shown in equation (2.110) is given in (Miranda, 1999):

$$u(z) = \frac{w_{max}H^4}{EI\left(1 - e^{-a}\right)}\left[C_1 \sinh\left(\alpha\frac{z}{H}\right) + C_2 \cosh\left(\alpha\frac{z}{H}\right) + C_3 e^{-\frac{az}{H}} + C_4\left(\frac{z}{H}\right)^2 + C_5\frac{z}{H} + C_6\right]$$

(2.111)

where the constants C_1-C_6 are given by:

$$C_1 = \frac{\alpha^2 e^{-a} - a^2 e^{-a} - a^3 + a\alpha^2 - \alpha^2}{a\alpha^3 \left(a^2 - \alpha^2\right)}$$

$$C_2 = \frac{a^2 e^{-a} - \alpha^2 e^{-a} + a^3 + a\alpha^2 - \alpha^2}{a\alpha^3 \left(a^2 - \alpha^2\right)} \frac{\sinh \alpha}{\cosh \alpha} + \frac{\alpha^2 e^{-a} + a^2 - \alpha^2}{\alpha^4 \left(a^2 - \alpha^2\right)} \frac{1}{\cosh \alpha}$$

$$C_3 = -\frac{1}{a^2 \left(a^2 - \alpha^2\right)}$$

$$C_4 = -\frac{1}{2\alpha^2}$$ (2.112)

$$C_5 = \frac{a^2 e^{-a} - \alpha^2 e^{-a} + a^3 - a\alpha^2}{a\alpha^2 \left(a^2 - \alpha^2\right)}$$

$$C_6 = \frac{\alpha^2 e^{-a} - a^2 e^{-a} - a^3 + a\alpha^2 - \alpha^2}{a\alpha^3 \left(a^2 - \alpha^2\right)} \frac{\sinh \alpha}{\cosh \alpha} + \frac{1}{a^2 \left(a^2 - \alpha^2\right)} - \frac{\alpha^2 e^{-a} + a^2 - \alpha^2}{\alpha^4 \left(a^2 - \alpha^2\right)} \frac{1}{\cosh \alpha}$$

The maximum interstory drift ratio IDR_{max} is defined as:

$$IDR_{max} = max \left| \frac{du(z)}{dz} \right|$$ (2.113)

The height at which the maximum *IDR* occurs is computed from:

$$\frac{d^2 u\left(z/H\right)}{dz^2} = C_1 \alpha^2 \sinh \alpha \frac{z}{H} + C_2 \alpha^2 \cosh \alpha \frac{z}{H} + C_3 a^2 e^{-a\frac{z}{H}} + 2C_4 = 0$$ (2.114)

Equations (2.113) and (2.114) are used to compute the maximum interstory drift ratio demand in the elastic model. An empirical approximated method is also proposed in (Miranda, 1999) to estimate the maximum inelastic drift ratio:

$$IDR_{max_{Inelastic}} = \beta \, max \left| \frac{du(z)}{dz} \right|$$ (2.115)

where

$$\beta = 1 + \frac{\mu}{30} + \frac{N}{200}$$ (2.116)

where μ is the maximum story displacement ductility ratio and N is the number of stories. An extension of this approach was developed by Miranda and Reyes (Miranda and Reyes, 2002) to include a more realistic case of buildings with nonuniform distribution of stiffness.

2.3.4 Other studies related to estimation of seismic demands on nonstructural components

2.3.4.1 Study by Medina et al.

Medina et al. (Medina *et al.*, 2006) performed an analytical study, based on the cascade approach, for the estimation of seismic demands on secondary systems mounted on nonlinear multi-story buildings. Medina's models consider one-bay two-dimensional multistory buildings with the number of levels ranging from 3 to 18 with fundamental vibration periods in the range 0.3-1.8 seconds. The building nonlinearities are considered through the use of demand reduction factors varied between 1 and 8. The secondary systems considered in this analysis correspond to light acceleration-sensitive components which can be represented by elastic SDOF systems. The damping of the secondary system is assumed in the range 0.01% and 5%. Forty ordinary ground motions scaled to the IBC2003 (ICC, 2003) seismic hazard for the California coastal region were considered in the analysis. Further details can be found in (Medina *et al.*, 2006).

In this study, Medina el al. show the direct dependence of the acceleration demands (S_{aC}) on secondary systems on its location along the building and the modal periods, total height, stiffness distribution, and strength of the primary system, in addition to the internal damping and vibration period of the secondary system. The two main deficiencies of the procedure established in the code are assessed: the dependence of seismic demands on both the strength (degree of inelastic behavior) and the dynamic properties (fundamental vibration period) of the supporting structure. It was shown that the code provision used at the time of their study[4] (IBC2003) do not always provide adequate estimations of the seismic demands, especially for secondary systems with vibration periods tuned to one of the natural periods of the primary system. The analysis concludes that as a consequence of the inelastic behavior of the primary system, a significant reduction in the maximum acceleration demands is produced. This situation is not considered in the current design codes. Finally, a modification factor $R_{acc}=S_{aC(elastic)}/S_{aC(inelastic)}$ to be applied on the component amplification factor a_p (Medina *et al.*, 2006) in order to take into account the effects of the inelastic behavior of the primary system is defined. Unfortunately, no closed formulas are given. Only global trends are discussed.

2.3.4.2 Study by Sewell et al.

One of the most relevant and systematic studies on the variables influencing the floor response spectrum FRS used in seismic design of nonstructural components was performed by Sewell et al. (Sewell *et al.*, 1986). In that report, the Floor Response Spectrum Ratio FRSR, defined as the ratio between the FRS's

---

[4] Even if the Study by Medina et al. was performed based on IBC2003, this comment is still valid for current IBC2006 edition.

obtained for the nonlinear multistory system and that obtained for the linear multistory system, is thoroughly studied. It was demonstrated that the FRSR obtained considering both linear and nonlinear SDOF systems may be inaccurate and unconservative at frequencies higher than the natural frequency of the primary system. The level of inaccuracy depends on both the structural configuration and the frequency content of the ground excitation. For broad-band excitations the FRSR estimated using MDOF systems may take values ranging between 2 and 3, while the FSRS estimated using a SDOF model always take values close to 0.7. In the analysis, it was numerically demonstrated that after the inelastic excursions of the primary system, higher vibration modes become relatively more important in the floor acceleration response of nonlinear building than in linear buildings. It is also demonstrated that pinched hysteretic models do not lead to significantly different results when compared to simple bilinear hysteretic models.

Other parameters also investigated in this study were: numerical integration procedure (Newmark, Wilson's Theta, Houbolt and Central Difference methods), hysteretic behavior (bilinear, smooth bilinear, shear wall and smooth shear wall models, pinching and smoothing effects), the structural and equipment damping ratio levels, the location of the secondary system within the building, the number of DOF of the primary system, the location of the nonlinearity and strength distribution along the building, and the characteristics of the input ground motion (input energy and record length). Finally, it is shown that equipment response can be predicted, for a limited structural nonlinearity, from the ground response spectrum.

2.4   Recent studies on seismic performance of nonstructural components and equipment

This subsection presents a brief overview of the recent research on the seismic performance of nonstructural components and equipment. A gracious and succinct description of the experimental research done in this field before 1997 can be found in Villaverde (Villaverde, 1997b). Moreover, the statement of the current objectives and an overview of the nonstructural components research performed at the three U.S. earthquake research centers can be found in Whittaker and Soong (Whittaker and Soong, 2001).

This subsection summarizes those experimental and analytical studies which could be further investigated using the anticipated capabilities of the new University at Buffalo Nonstructural Component Simulator (UB-NCS) presented in Section 3. For that reason, some recent studies on nonstructural components and equipment as for example the assessment of the seismic performance of porcelain transformer bushings (Filiatrault and Matt, 2005; Gilani *et al.*, 2001; Whittaker *et al.*, 2004) are explicitly not included in this subsection. Given the particular typology of those components and/or their location at grade level, they may require testing machinery specifically designed for them or the use of conventional shake tables.

2.4.1   Analytical studies

2.4.1.1   Study by Filiatrault et al. (2004)

Filiatrault et al. (Filiatrault *et al.*, 2004b) developed a methodology that can be used for generating a database of horizontal floor accelerations matching the seismic demands compatible with the Uniform Seismic Hazard (USH) at a given site. The database is recommended for use in shake table testing of critical nonstructural components and equipment mainly sensitive to horizontal accelerations.

2.4.1.2   Study by Hutchinson and Chaudhuri (2006)

Hutchinson and Chaudhuri (Hutchinson and Chaudhuri, 2006) performed an analytical study aimed to find approximate fragility curves for various unattached equipment and building contents. The study focuses in the analysis of rigid scientific equipment, usually placed on top of ceramic laboratory benches. Approximate equations are proposed to estimate fragility curve parameters for bench-mounted sliding-dominated equipment within multistory reinforced concrete and steel framed buildings, for a range of surface's frictional coefficients. The fragility parameter equations are generalized to include the primary building period among their variables. It is demonstrated that the fragility parameters do not depend on the ground motion when realizations match a target response spectrum. The proposed equations can be used to find the possible equipment locations within multistory buildings and estimating possible laboratory economical losses.

2.4.1.3   Study by Overend et al. (2007)

Overend et al. (Overend *et al.*, 2007) performed an analytical study aimed to develop a general crack growing model based in statistical failure theory and linear elastic fracture mechanics. The proposed model allows for determining tensile strength of glass under static perpendicular loads. The capacity of proposed model to predict failure modes is compared to other traditional design methods. Fragility curves to predict glass failure are proposed.

2.4.2   Experimental studies

2.4.2.1   Study by Chong and Soong (2000)

Chong and Soong (Chong and Soong, 2000) conducted an experimental and analytical study aimed at assessing the seismic vulnerability and mitigation measures for unrestrained equipment. The study focused on the sliding response of freestanding rigid equipment under two directional earthquake shaking. A parametric analysis was performed to establish stability bounds for pure sliding response. Fragility curves were developed for several relative displacement thresholds. The study concluded that the values of

friction coefficients and the inclusion of vertical ground motion component play a critical role in the sliding response of freestanding bodies. Finally, experimental and analytical results were compared in order to validate the proposed model and to propose modeling recommendations.

2.4.2.2   Study by Kesti (2000)

Kesti (Kesti, 2000) studied numerically and experimentally the local and distortional buckling behavior of flange and web-stiffened and web-perforated compression members. It was observed that the use of perforations reduces the distortional buckling strength of the section. The objective of Kesti's research was to develop a design method for estimating the compression capacity of perforated steel studs. The influence of the gypsum sheathing on the buckling strength was also taken into account.

2.4.2.3   Study by McMullin and Merrick (2002)

McMullin and Merrick (McMullin and Merrick, 2002) performed a set of seventeen experimental tests for determining the cost-damage relationship of residential gypsum wallboard partition walls. The specimens considered in the tests were 8 ft. high and 16 ft. in length, double sided with ½ in. gypsum wallboard. Among the variables considered for the wall configurations were fastener types and spacing, loading protocol, boundary conditions, opening and fenestration features, and repairing methods. During tests it was observed that maximum loads were sustained at 1 to 1.5% drifts. The two dominant failure modes observed were the loosening of the wallboard from the framing systems due to the pulling of fasteners, and the racking movement of individual panels. Depending on the wall configuration, strength degradation was found to be severe or gradual. It was also observed that monotonic testing protocols predict, with acceptable agreement, the cyclic force-deformation relationships. Damage levels were found to be related to rigidity and strength of boundary elements. Cost-damage relationships are directly related to the number of workers required. Low damage levels can require a single multi-skilled worker, while higher damage levels can involve more complex repairing teams. Total specimen losses were observed at drifts close to 2%.

The results obtained by McMullin and Merrick were used by Kanvinde and Deierlein (Kanvinde and Deierlein, 2006) to generate analytical models to determine the lateral shear strength and initial elastic stiffness of wood-framed gypsum wall panels. These parameters were incorporated into a multi-linear curve which describes the monotonic shear-deformation relationship for gypsum partition walls. The proposed model could be extended to metal studded gypsum partition walls.

2.4.2.4 Study by Bersofsky (2004)

Bersofsky (Bersofsky, 2004) investigated experimentally the seismic fragility of 16 ft long by 8 ft tall light-gage metal-studded gypsum partition walls. In plane shear testing was performed on sixteen wall specimens constructed following current standard practices, including taping, mudding and painting. Return walls 8 ft tall and 4 ft long were attached perpendicular to the direction of testing, at both ends of each wall. The CUREE testing protocol was considered. Parametric fragility models were performed considering several damage measures including gypsum cracking and stud buckling. Three damage states were identified: DS_1) minor damage that can be fixed with tape, mud and paint; DS_2) sections of gypsum need to be cut out and replaced; and DS_3) walls damaged beyond repair. It was observed that DS_1 was triggered at drifts in the range between 0.05 and 0.5%. DS_2 was not observed in all test performed because the gypsum panels got detached from the steel stud frame. DS_3 was observed at drift ratios in the range 1.5 to 3%.

2.4.2.5 Study by Filiatrault et al. (2004b)

Filiatrault et al. (Filiatrault *et al.*, 2004a) conducted a series of shake table tests to evaluate the seismic performance of a combined system composed of a bookcase and a cantilever partition wall system. The seismic response of the combined system is mainly controlled by floor accelerations rather than story drifts. One bookcase fully loaded with books and two different partition wall systems were tested. Seismic hazard consistent floor motions, calculated using the methodology developed by Filiatrault et al. (Filiatrault *et al.*, 2004b), were considered. It was observed that pounding between unanchored bookcases and partition walls is beneficial for the seismic response of the bookcase. The seismic response of the bookcase improves drastically when restraining systems are correctly installed. Fragility curves for overturning of tall bookcases were derived.

2.4.2.6 Study by Goodwin et al. (2004)

Goodwin et al. (Goodwin *et al.*, 2004) investigated the seismic behavior of piping systems typically used in hospital facilities. The objectives of this research were to evaluate the capacity, weak points and failure modes of piping systems. The testing specimen, as recommended by OSHPD, was built after an existing system at UC Davis Medical Center. One hundred feet of 3 and 4 in. diameter ASTM A53 steel pipes and several water heaters and valves were considered in the system. In their research, they performed a series of shake table tests to identify the capacities of cable-braced and unbraced systems. The AC156 protocol was considered for testing. The main findings of this research were that bracings systems limit displacement demands, but the acceleration amplifications are similar in both cases. No significant damage

to the piping systems was found during high intensity motions. Two of eleven braces, two vertical rod hangers, and a flanged connection in the unbraced system failed for the highest input motion level.

2.4.2.7   Study by Badillo-Almaraz et al. (2005)

Badillo-Almaraz et al. (Badillo-Almaraz *et al.*, 2007; Badillo-Almaraz *et al.*, 2000) conducted a series of shake table experiments to evaluate the seismic performance of a set of full-scale suspended ceiling systems. Several system configurations were tested and fragility curves generated. Among the variables considered in the tests were the size and weight of tiles, the use of retainer clips, the use of compression struts, and the physical condition of the grid components.

2.4.2.8   Study by Chaudhuri and Hutchinson (2005)

Chaudhuri and Hutchinson (Chaudhuri and Hutchinson, 2006) performed an experimental and analytical study on the seismic fragility of storage glassware typically found in hospitals and laboratories. Biaxial shake table tests were performed to assess the seismic response of various glassware types. Realistic supporting surfaces were considered during testing (Chaudhuri and Hutchinson, 2005). The effect of both amount and density of the liquid contained in the glassware was assessed. Simulations were performed considering a set of ground motions and two steel buildings. This series of experiments and simulations demonstrates that the seismic response of glassware is mainly dominated by sliding rather than rocking. Nevertheless, significant rotation about the vertical axis was observed. It was concluded that the seismic fragility is dominated by the building flexibility properties.

2.4.2.9   Study by Konstantinidis and Makris (2005)

Konstantinidis and Makris (Konstantinidis and Makris, 2006) conducted a comprehensive analytical and experimental study to assess the seismic response of actual freestanding and restrained laboratory equipment. One incubator and two refrigerators were tested. Freestanding and chained configurations were evaluated using unidirectional shake table motions. The chains were used to prevent equipment from both excessive displacements and rocking. Quasi-static pull tests were performed in order to characterize the mechanical properties of a typical contact surface found in laboratories. The results were used to perform analytical simulations for high intensity ground motions impossible to replicate by using the currently available shake tables. The study demonstrates that using the friction coefficients obtained experimentally in the analytical simulations does not adequately reproduces the response observed during shake table tests. Finally, it was observed that the peak equipment accelerations of the restrained equipment were significantly larger than those observed in the freestanding equipment. Therefore, restraining highly acceleration sensitive laboratory equipment may increase its risk of damage.

2.4.2.10 Study by Lang and Restrepo (2005)

Lang and Restrepo (Lang and Restrepo, 2006) conducted experiments to investigate the seismic fragility of gypsum metal stud partition walls. Two identical full scale specimens were constructed following the current methods and techniques used by practitioners, intending to replicate a typical space found in office, hotel and laboratory buildings. Several damage states were defined and evaluated. The racking protocol defined in ATC-58 (FEMA, 2005) was considered for testing the specimens[5]. The objectives of this research included the assessments of the influence of various wall configurations and boundary conditions in the system performance; and the development of a parametric fragility model relating engineering demand parameters, such as interstory drifts, to damage intensity measures as repairing costs, downtimes, etc. During the test series it was found that the damage progression was highly dependent on the loading protocol considered, and more specifically, on the number of pre-peak loading cycles. After the peak loading, the observed damage was similar using both protocols. The main damage observed were fatigue, pullout and shear of track fasteners. Once the track slip occurred, the damage in partitions walls did not evolve.

2.4.2.11 Study by Nastase et al. (2005)

Nastase et al. (Nastase *et al.*, 2006) performed an experimental evaluation of the dynamic response of nonstructural systems during full-scale building vibration tests. A vacant 4-story building, which resulted highly damaged during the Northridge earthquake, was tested simulating low intensity floor motions and sinusoidal transient motions. The motion was generated using linear and eccentric mass shakers placed at the roof level of the building. The study was focused in the assessment of the vibration response of an actual laboratory space in which nonstructural components, and their respective mounting systems, were considered. Bench-shelf systems composed of cabinets with ceramic countertops and shelves, all attached to a flexible Unistrut steel grid (connected to the upper and bottom floors), were constructed at the fourth level of the building. The force transmission path through floor, counters, shelves and the equipment was studied. Image-based monitoring systems were used to track the dynamic response of the equipment and contents (Hutchinson *et al.*, 2005). In the experiments it was observed that the magnitude of the dynamic amplification measured in bench-shelf systems was significantly affected by its spatial location in plan due to large torsional effects.

---

[5] One of the specimens was tested using the racking protocol appearing in the third draft of ATC-58, and the other one, was tested using the racking protocol defined in a previous draft of ATC-58, where the loading history is calculated as $\frac{a_{i+1}}{a_n} = \left(1.24\frac{a_i}{a_n}\right)^{1.04}$.

2.4.2.12 Study by Lee et al. (2006)

Lee et al. (Lee *et al.*, 2007) studied the seismic performance of four full-scale light-gage steel studded gypsum partition walls constructed following standard Japanese building practice. The specimens were tested considering quasi-static and dynamic cyclic loading protocols. The quasi-static cyclic protocol imposed two cycles per testing amplitude. The dynamic testing protocol consisted in a sinusoidal signal with a constant frequency of 1 second, imposing the same sequence of cycles and drift ratios as the quasi-static testing protocol. Effects of a door opening and intersecting walls were considered in assessing the partition walls performance. It was observed that the damage was concentrated in the walls perimeters and that the dynamic protocol did not amplified the damage observed during the quasi-static protocol. The total loss of the specimens was observed for drift ratios of 2%.

2.4.2.13 Study by Memari et al. (2006)

Memari et al. (Memari *et al.*, 2006) performed a series of full-scale dynamic racking tests to evaluate the seismic vulnerability of architectural glass panel curtain walls. A vulnerability mitigation measure consisting of the modification of corner geometry and edge finishing of conventional glazing curtain walls was proposed. The suggested solution consisted of rounding the glass corners to minimize protrusions and edge roughness. This experiment demonstrates that glass edge and corner finishing have a primary influence on the glass cracking and fallout of curtain walls.

2.4.2.14 Study by Weggel et al. (2007)

Weggel et al. (Weggel *et al.*, 2007) studied the serviceability of an economical, nearly conventional, glass curtain wall system that provides a low level of blast resistance. A conventional mullion system with laminated glass panels was experimentally subjected to static and transient dynamic service loads. A finite element model was developed and calibrated to match the experimental observations. Earthquake loads were not considered in the experimental study of this nearly conventional curtain wall system.

2.4.2.15 Study by Dinehart et al. (2008)

Dinehart et al. (Dinehart *et al.*, 2008) studied an alternative to the conventional screwed sheathing connections used in wood-framed gypsum partition walls. A viscoelastic polymer was introduced between the sheathing and the stud frame. Tests on sheathing connections and shear walls were performed using the CUREE quasi-static testing protocol. It was observed that the viscoelastic connection increases the dissipation of energy and the wall stiffness at large drift levels. The viscoelastic connection improved the wall performance while resisting damage when the specimen was subjected to large drifts ($\approx 3\%$). The viscoelastic connection exhibited less degradation in comparison to the conventional screwed connection.

The experimental study was complemented with the development of a finite element model (Blasetti *et al.*, 2008) used to predict the performance of viscoelastic shear walls, and to optimize the thickness and location of the viscoelastic connections within the walls. It was finally concluded that further research examining the performance of this viscoelastic system throughout dynamic tests is necessary.

2.4.2.16   Study by Fathali and Filiatrault (2008)

Fathali and Filiatrault (Fathali and Filiatrault, 2008) performed an experimental study aimed at evaluating the seismic performance of Isolation/Restraint (I/R) systems for light mechanical equipment. Shake table tests were conducted on an air-handling unit mounted on I/R and rigid systems. It was observed that reducing the displacement of the equipment through using I/R systems amplifies the peak equipment accelerations. Furthermore, it was observed that reducing the gap size improves the seismic performance of the I/R system. Increasing the thickness of the rubber snubbers reduces the forces in the I/R system, but can increase accelerations and displacements in the equipment. It was finally concluded that higher amplification of accelerations are expected for light and flexible equipment than for rugged and heavy equipment.

SECTION 3

DEVELOPMENT OF THE UNIVERSITY AT BUFFALO NONSTRUCTURAL COMPONENT SIMULATOR

The seismic vulnerability of nonstructural components and equipment with their expensive recovery and/or replacement costs has been demonstrated during past earthquakes. The limited data collected during past events are not sufficient to completely characterize the seismic behavior of nonstructural components and develop effective mitigation measures. Moreover, given the complexity of various typologies of nonstructural components subjected to seismic excitations, systematic experimental testing is necessary for a better understanding of their seismic behavior.

Until recently, testing facilities did not have the capability to subject nonstructural components, systems and equipment to both full-scale absolute floor accelerations and story deformations experienced at upper levels of multistory buildings. These motions are typically more demanding compared to those recorded at the ground level, for which earthquake simulators are typically designed. Even for ground shaking, the limited stroke of earthquake simulators typically requires the filtering of low-frequency accelerations that may influence the response of some types of nonstructural components and systems. To address these limitations, the University at Buffalo has commissioned a dedicated Nonstructural Component Simulator (UB-NCS) composed of a two-level testing frame capable of simultaneously subjecting both displacement and acceleration sensitive nonstructural components, systems and equipment to realistic full-scale floor motions expected within multistory buildings.

This section presents a detailed description of the criteria considered for the design of the UB-NCS testing frame and its high performance dynamic actuators. The new testing capabilities provided by the UB-NCS are also detailed. The results obtained from a series of tests carried out to verify the fidelity and performance capabilities of the UB-NCS are presented. A methodology for off-line command input signal compensation is also proposed to improve the fidelity of the UB-NCS in replicating targeted platform motions. The results and observations of a first test performed on two full-scale C-shaped steel studded gypsum partition walls are described.

3.1 UB-NCS design considerations

The main requirements for performing realistic seismic tests of nonstructural components is the ability of the servo-hydraulic equipment to reproduce the absolute floor motions at various levels of a building excited by earthquake motions. In order to assess these equipment requirements, floor motions recorded

in four instrumented buildings during major earthquakes in California were considered (Shakal *et al.*, 1995). One of these buildings was shaken by the 1989 Loma Prieta earthquake, while the other three were shaken by the 1994 Northridge earthquake. Table 3.1 summarizes the peak responses measured and estimated at the roof level of these instrumented buildings. Additionally, the simulation of full-scale near-fault ground motions such as those listed in Table 3.2 also require similar dynamic characteristics compared to building absolute floor motions.

Table 3.1. Peak seismic responses at roof level of four instrumented buildings

Building	Building Description and Location	Measured Peak Roof Accel. (g)	Estimated Fundam. Period T (s)	Estimated Peak Roof Velocity (in/sec)	Estimated Peak Roof Disp. (in)
Pacific Park Plaza	30-story concrete shear wall and moment resisting frame; Emeryville, CA.	0.37 Loma Prieta	2.69	61.0	26.4
Olive View Medical Center	6-story concrete moment resisting frames and steel plate shear walls; Sylmar, CA.	1.50 Northridge	0.33	30.3	1.57
7-story R/C building	Moment resisting frames in perimeter and flat plates and columns in the interior; Van Nuys, CA.	0.58 Northridge	1.98	70.5	22.4
13-story R/C building	Non-ductile moment resisting concrete frames with concrete shear walls in basements; Sherman Oaks, CA	0.45 Northridge	3.00	82.7	39.4

Table 3.2. Peak motion values for 10 historic near-fault ground motion records

Seismic Event	Recording Station	Peak Ground Horizontal Acceleration (g)	Peak Ground Horizontal Velocity (in/sec)	Peak Ground Horizontal Displacement (in)
1994 Northridge	Rinaldi	0.84	64.2	12.2
	Newhall	0.62	47.6	13.4
	Sylmar Converter	0.83	40.2	16.5
	Sylmar Olive View	0.84	46.5	12.2
1995 Kobe	KJMA	0.82	37.8	9.84
	Takatori	0.61	66.9	17.7
1983 Morgan Hill	Coyote LD	1.30	28.0	5.51
1978 Tabas	Tabas	0.85	46.9	35.4
1979 Imperial Valley	El Centro Diff. Array #5	0.52	33.5	25.6
1992 Landers	Lucern Valley	0.79	31.9	24.0

From Table 3.1 and Table 3.2, the envelope responses of the building roof for the four instrumented buildings and the near-fault ground motions are a peak acceleration of 1.5g, a peak velocity of 82.7 in/s, and a peak-to-peak stroke of 78.8 in. To meet these peak demand parameters, the UB-NCS testing frame is activated by four identical high performance dynamic actuators capable of subjecting nonstructural

components and equipment up to 3g horizontal accelerations, 100 in/s velocities and ±40 in displacements for specimens with reactive weights up to 6 kips per level. These dynamic capabilities exceed the peak ground and building response values given in Table 3.1 and Table 3.2, allowing the UB-NCS to reproduce full-scale building floor motions and near-fault ground motions. Each actuator has a load capacity of 22 kips, and is driven by a 950 liters/min servo-valve. Details of the high-performance dynamic actuators are summarized in Table 3.3.

Table 3.3. Actuators properties

Actuator Model	:	MTS ASSY 247.22S
Load capacity (each)	:	22 kips
Stroke		80 in (total)
Minimum static	:	140.3 in
Minimum dynamic	:	141.6 in
Mid-stroke	:	180.9 in
Maximum dynamic	:	220.3 in
Maximum static	:	223.6 in
Servo-valve type	:	256.25 (250 GPM)
Servo controller	:	MTS FlexTest

As illustrated in Figure 3.1, the UB-NCS was designed to accommodate the construction of distributed full-scale nonstructural components, systems and equipment, typically found at the upper levels of multistory buildings, and to subject the specimens to recorded or simulated absolute floor accelerations and interstory drifts.
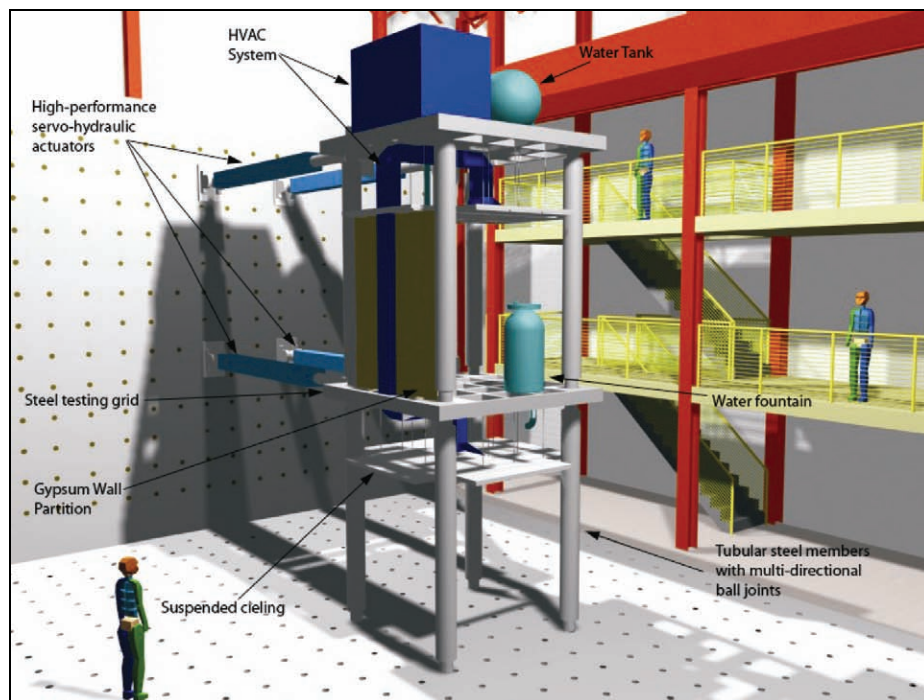
Figure 3.1. Illustration of the UB-NCS

3.2 UB-NCS description

The UB-NCS has a story height of 12 ft in the first level and 14 ft in the second level to accommodate full-scale testing specimens. The platforms at each level are 12.5x12.5 ft with beams typically constructed from HSS8x6x1/2" hollow tube sections. The platform is a 2x2 ft grid with tie-down holes spaced at 1 ft. Additionally, four centrally located cruciform shapes are removable to provide four 3.5x3.5 ft square openings, which can accommodate pass through, tall, or wide, equipment (e.g. heating, ventilating and air conditioning ducts) that may span more than one level. The columns are made of HSS8x8x1/2" and are connected to the platforms by three-dimensional swivels to allow for the unrestrained motion of the testing frame. Figure 3.2 shows a schematic of the elevation and plan view of the testing frame. Figure 3.3 shows photos of the actual frame. Table 3.4 summarizes the dimensions and properties of the UB-NCS.

More detailed construction drawings for the UB-NCS are provided in Appendix A. The set of drawings includes the details of the geometry of the testing frame and the ancillary parking frame system used for restraining the frame in its centered position once the actuators have been shut down.
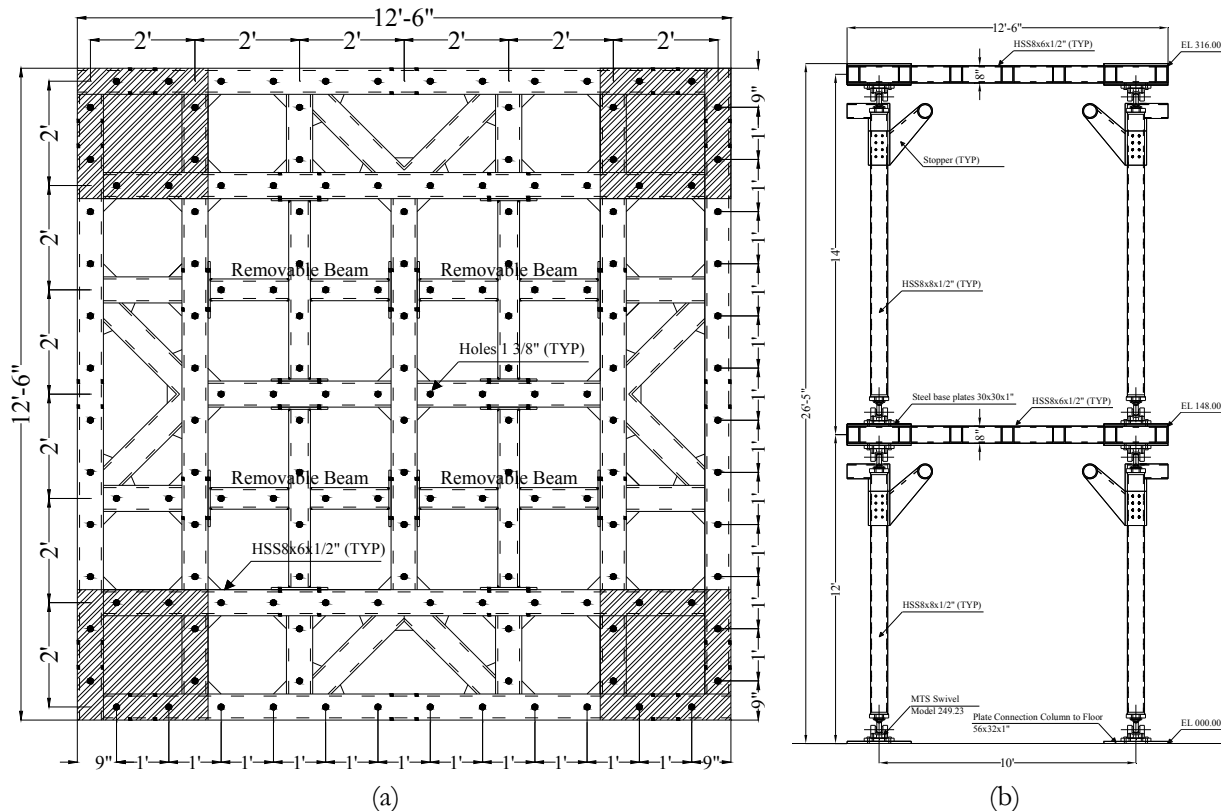
Figure 3.2. Geometry of the UB-NCS: (a) Plan view and (b) Elevation

Table 3.4. Dimensions and properties of the UB-NCS

Platform size	:	12.5x12.5 ft
Opening size	:	3.5x3.5 ft (each)
Number of stories	:	2
Story height 1st level	:	12 ft
Story height 2nd level	:	14 ft
Maximum specimen weight	:	6 kips/level
Degrees of freedom	:	2 horizontal (per floor) + 1 vertical
Frequency of operation	:	0.2-5.0 Hz
Peak displacement	:	± 40 in
Peak velocity	:	100 in/s
Peak acceleration	:	Up to 3g

(a)   (b)

Figure 3.3. Photographs of the UB-NCS: (a) Front view; and (b) Isometric view

3.3   New testing capabilities

The UB-NCS provides the unique capability to replicate, under controlled laboratory conditions, the effects of strong seismic shaking on nonstructural components, systems and equipment located at various floor levels within buildings. This new testing capability constitutes a primary step towards better understanding the progression of damage in nonstructural components and their dependence on various earthquake intensity measures. The knowledge of the seismic performance of several typologies of nonstructural components will allow designers to apply, with reduced uncertainty, performance-based design tools for achieving performance objectives such as building functionality, monetary investment, and/or occupants' life protection, as targeted by stakeholders and investors. The generated fragility data

will also be useful in quantifying and predicting economical loses due to earthquakes and providing the critical data required to support decisions concerning the use of response modification strategies for seismic protection of primary and secondary systems (Miranda, 2006). Moreover, the new testing capabilities will allow for more realistic seismic qualification procedures as required by current codes such as ASCE 7 (ASCE, 2005) and IBC 2006 (ICC, 2006).

The UB-NCS testing facility allows for testing nonstructural components sensitive to interstory drifts, velocities and/or accelerations imposed by the motion of two adjacent floors in multistory buildings during seismic events. Figure 3.4 shows a schematic of the platform motions inputted to the UB-NCS actuators, obtained from the simulated response of a multistory building. Similarly, the platform motions can be obtained from the building floor motions recorded during strong earthquake events. In order to more broadly assess the seismic performance of distributed nonstructural components, systems and equipment, independent of building or ground motion, the testing protocols described in Section 4 have been developed.
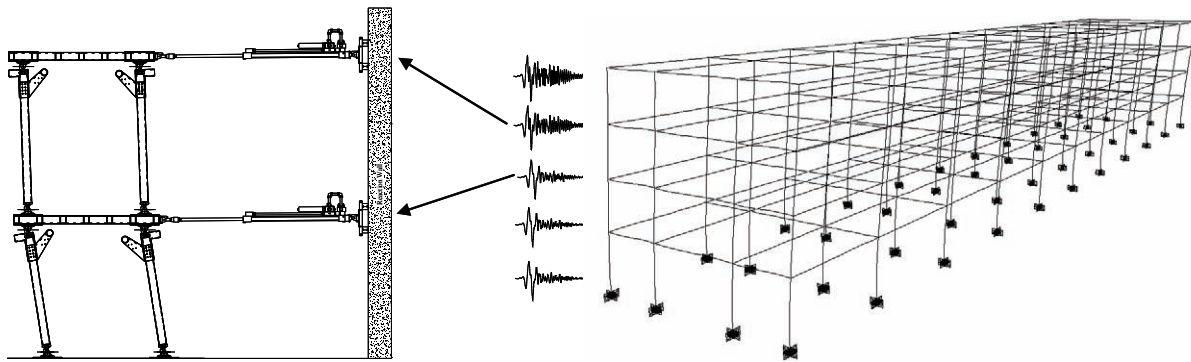
Figure 3.4. Schematic of input motions for UB-NCS platforms

Building contents of several configurations and typologies including partition walls, cladding curtain walls, distributed duct, piping and electrical systems, HVAC systems, suspended ceilings and ceiling mounted equipment can be tested, as illustrated in Figure 3.1. The UB-NCS also allows for testing both anchored and self standing equipment positioned on any of the two platforms and attached to one or both of the platform levels. For example, distributed piping or HVAC systems typically attached at multiple building levels can be spanned between the two UB-NCS platforms to impose simultaneously seismic demands at their upper and bottom attachment points. Recently, a water piping system has been tested considering bottom attachments on conventional shake tables and upper attachments at ancillary reaction frames (Goodwin *et al.*, 2004). This configuration applies accelerations at the bottom supports and drifts on the specimen, but does not impose inertial forces at the upper supports. The modular configuration of the UB-NCS addresses this shortcoming. Further, each platform can also be used as a conventional

earthquake simulator with the capability to reproduce full scale near-fault ground motions, including large displacement/velocity pulses.

The UB-NCS can be extended for biaxial horizontal testing. This configuration will require at least two additional high performance actuators for controlling the three in-plane degrees of freedom at each platform level. Vertical accelerations up to 1.15g can also be included in an experiment by mounting the testing frame on top of one of the two existing 23x23 ft six-degree-of-freedom SEESL earthquake simulators, as shown in Figure 3.5.
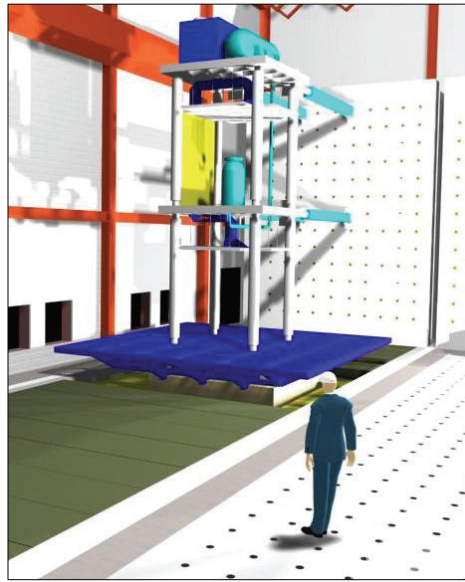
Figure 3.5. UB-NCS mounted on top of SEESL earthquake simulator for vertical acceleration input

The UB-NCS facility can be integrated into the framework for the Real-Time Dynamic Hybrid Testing (RTDHT) developed at UB to investigate the seismic interactions between primary and secondary systems (Reinhorn *et al.*, 2004). The RTDHT is a testing method combining the use of earthquake simulators, dynamic actuators, and computational models for simulating the seismic response of large structures. The prototype structure is divided into one or more physical substructures and one or more computational substructures with the interface boundary forces and displacements imposed by actuators. This new experimental method, capturing the interaction between structural and nonstructural building components, is realized by using the UB-NCS facility in combination with recently developed testing techniques.

3.4   UB-NCS performance verification

The dynamic properties, testing capabilities and actual limitations of the UB-NCS equipment have been experimentally verified through extensive testing using random, harmonic and simulated building floor

motions. This subsection focuses on the capability and fidelity of the UB-NCS to reproduce seismic floor motions and on the actuator control and compensation procedures necessary to adequately replicate these motions.

3.4.1 Dynamic performance of bare actuators

The dynamic performance of the bare actuators was assessed through a series of harmonic excitation tests. Figure 3.6 shows a comparison between nominal and actual capabilities of the high performance actuators. It is observed that the actual capacity of the high performance dynamic actuators is slightly larger than their nominal capacity, in the whole range of frequencies considered in the verification.
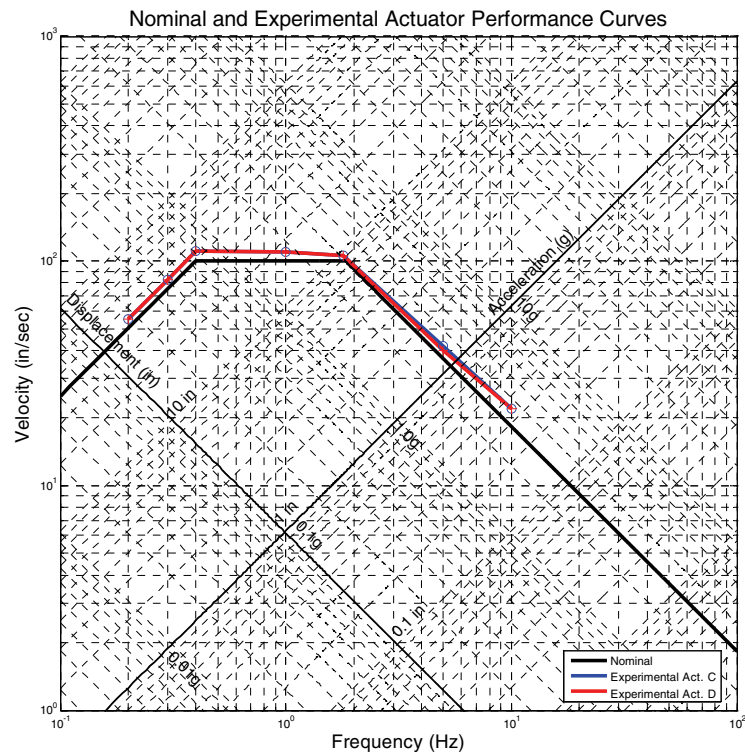
Figure 3.6. Comparison of nominal and measured actuator capacities for harmonic input

3.4.2 Operation frequency limits of UB-NCS

The UB-NCS operation frequency limits were estimated by performing a tests series that included white noise excitations, and vertical and horizontal hammer impacts on the actuators (attached to the testing frame) and on the platform. Table 3.5 shows the natural vibration frequencies identified experimentally.

In Table 3.5 it is observed that the frequency controlling the resonant response of the actuators-platform system is the horizontal bow-string actuator frequency. This frequency and the oil-column frequency are much lower than the frequencies observed in the actuators typically used for experimental earthquake

engineering because of the mechanical and geometrical properties of the long-stroke high-performance actuators required for replicating full-scale building floor motions and near-fault ground motion records. The differences between horizontal and vertical bow-string actuator vibration frequencies are caused by the counterweight system used to compensate the dead weight of the actuators.

Table 3.5. Results experimental tests

Dynamic property	Test			
	Impact on Actuator C	Impact on Actuator D	Impact on Frame	White noise
Vertical bow-string frequency	9.2 Hz	8.7 Hz	-	8.7-9.1 Hz
Horizontal bow-string frequency	6.6 Hz	6.6 Hz	-	-
Oil-column frequency	-	-	12.3-13.6 Hz	-
Frame transverse direction frequency	-	-	38.9-39.3 Hz	-
Platform dish mode frequency	-	-	19.1-20.0 Hz	-

3.4.3 Off-line input command signal compensation process

The input motions for the UB-NCS need to be preconditioned to stay within the operation limits of the equipment and to improve its performance. The floor motions used for developing the necessary command signal compensation procedures were obtained from the simulated response of an existing medical facility located in the San Fernando Valley, in Southern California. This 4-story moment resisting steel framed building model with non-uniform distribution of mass and stiffness has been extensively studied by MCEER (formerly Multidisciplinary Center for Earthquake Engineering Research) investigators (Yuan and Whittaker, 2002). The floor motions were obtained from nonlinear seismic analysis of the building excited by synthetic ground motions corresponding to a seismic hazard with a probability of exceedance of 5% in 50 years (Wanitkorkul and Filiatrault, 2005). The absolute displacement response histories calculated for the 3rd and 4th levels of the building (Figure 3.7) were applied to the bottom and top levels of the UB-NCS, respectively.

The mechanical and geometric properties of the UB-NCS actuators pose several control challenges. These actuators have displacement strokes that are longer and force capacities that are smaller compared to those typically used in structural testing. The geometric configuration of the actuators, as shown in subsection 3.4.2, results in bow-string and oil-column vibration frequencies of approximately 8 and 13 Hz (Table 3.5), respectively, when attached to the testing frame. For this reason, the operating frequency range of the UB-NCS is limited between 0.2-5.0 Hz. Thus, the first step in generating a command signal for the UB-NCS consists of pre-filtering the floor motions to remove all high frequency contents using a Butterworth low-pass filter of order n=50 and cutting frequency f_{cut}=5 Hz. An additional notch filter with central frequency 8 Hz and bandwidth 6.5 Hz is used in the servo-valve control loop to filter the actual electrical signal

provided to the actuators. Both filters are necessary to avoid exciting the system resonant frequencies during testing, while still capturing the first few dominant modes of vibration contributing to the simulated building response. In the discussion that follows, the filtered signal is termed desired floor motion and its associated acceleration response spectrum is named Desired Response Spectrum (DRS).

(a)   (b)
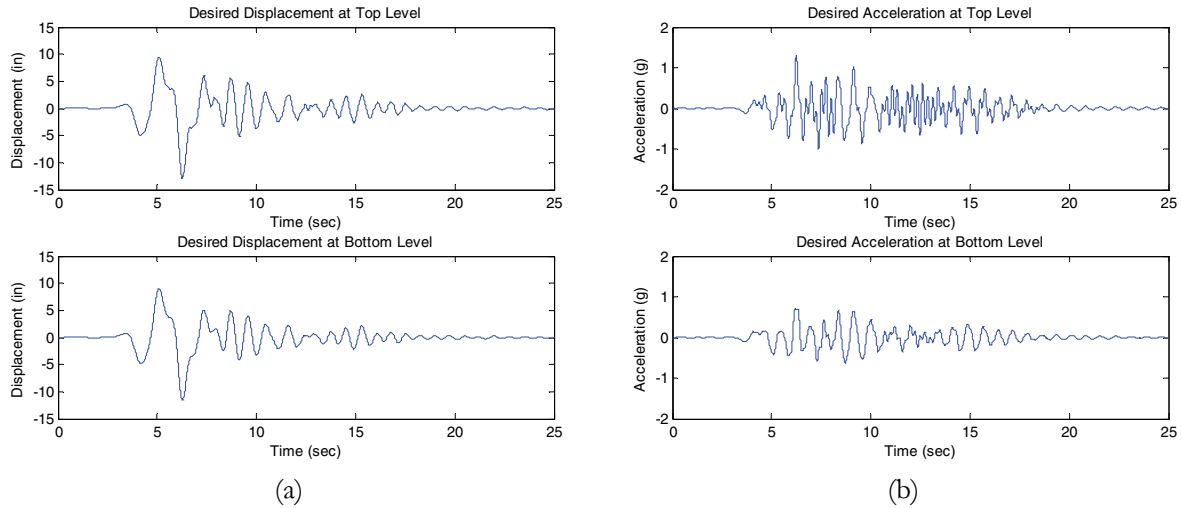
Figure 3.7. Desired floor motions used for evaluation of UB-NCS: (a) displacements and (b) accelerations

The fidelity of the UB-NCS in replicating the desired floor motions depends mainly on adequate tuning of the actuator controllers, training of the real-time Adaptive Inverse Control (AIC) compensator (MTS, 2005), and correct preparation of the input command signal. Tuning of closed loop controllers and AIC compensator is performed before each test series by driving the actuator valves and running the system with a band limited white noise with frequency content in the range of 0.1 to 6 Hz, slightly exceeding the target frequency range of the UB-NCS. The signal Root Mean Square (RMS) amplitude is manually increased from 0.05 to 0.3 inches, with spectral amplitude decreasing with the square of frequency. The tuning process first considers the two actuators located at a same level of the testing frame to minimize differential motions or twist at each level. Then, all four actuators are tuned simultaneously to minimize errors in interstory drifts.

Despite initial efforts to filter control signals and finely tune the actuator controller, the UB-NCS did not completely reproduce the desired floor motions, as shown in Figure 3.8. Figure 3.8a compares the desired and observed bottom level floor motions, indicating a 7.8% overshoots at peak displacements. Figure 3.8b shows that the Observed Response Spectrum (ORS), calculated using the recorded floor accelerations, exceeds the DRS by more than 50% for all frequencies greater than 1.5 Hz. To address these discrepancies, an iterative process was developed to precondition the open loop command signal for better correlation with the Desired Response Spectrum (DRS). A flow chart of the iterative compensation procedure for the command signal, including pre-filtering tasks, is shown in Figure 3.9 and described next.
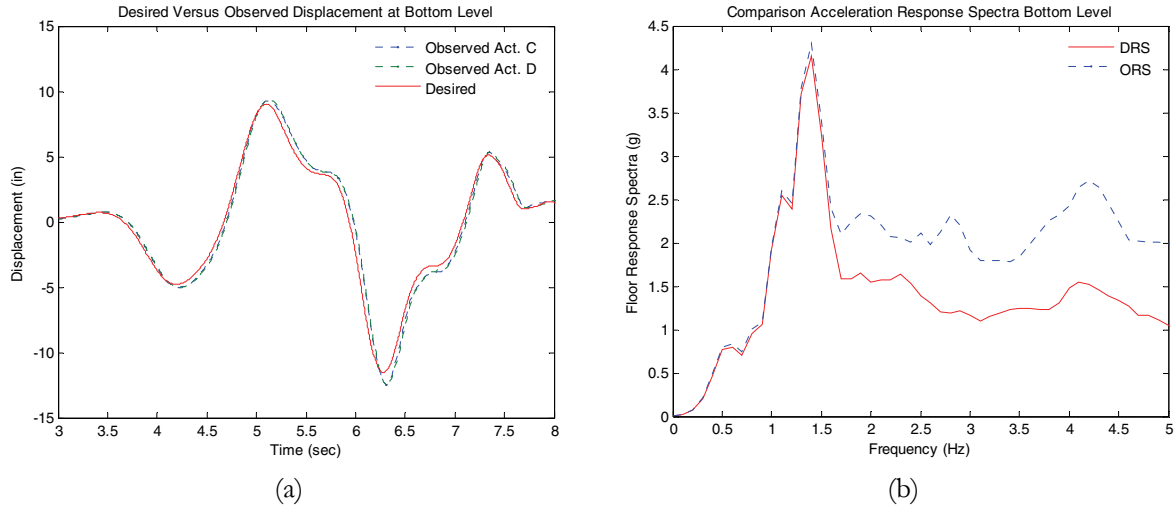
Figure 3.8. Comparison of desired and observed response for simulated floor motions without compensation: (a) displacements at bottom UB-NCS level and (b) desired and observed FRS

In the first off-line iteration of the compensation process for the open loop command signal, the desired floor motion is directly used as command input for running the bare frame. The platform accelerations measured during the test are used to calculate the Observed Response Spectrum (ORS). If the ORS overestimates the DRS by less than 10-20% in the whole range of the UB-NCS operation frequencies (0.2-5 Hz), the command signal is considered acceptable for final specimen testing (Harris, 2001). Otherwise, the command signal is compensated through an iterative process until the aforementioned condition is achieved. In order to prepare the command signal for the next iteration, the Inverse Transfer Function (ITF) between the current command signal and the observed floor motion is calculated. This ITF is used to filter, in the frequency domain, the Fourier spectral amplitudes of the current command signal. Fourier phases are not modified in this process. The resulting compensated command signal in the time domain is considered in the next iteration. This iterative process is followed until convergence is achieved between the DRS and the ORS. Finally, the compensated command signal used in the last iteration is used for final specimen testing.

As shown in Figure 3.8b, the ORS obtained after using the desired floor motions directly as command input overestimates the DRS by more than 50% for all frequencies greater than 1.5 Hz and consequently, a second iteration was necessary. Figure 3.10a shows the ITF between the command and observed displacements used to filter the current command signal FFT for the next iteration. Figure 3.10b shows that the FFT's for the current and compensated command signals are slightly modified. The final results after signal compensation are shown in Figure 3.11. The displacement overshoot in Figure 3.11a is reduced to less than 0.6% of the desired floor motion. The ORS in Figure 3.11b overestimates the DRS by less that 20% for most frequencies except in the range 2.7 to 3.1 Hz, where the amplitude is 45% greater. The command signal at this stage appears acceptable for final specimen testing, though another

73

iteration could be applied if desired. An identical process was simultaneously applied to compensate the UB-NCS top level command signal.
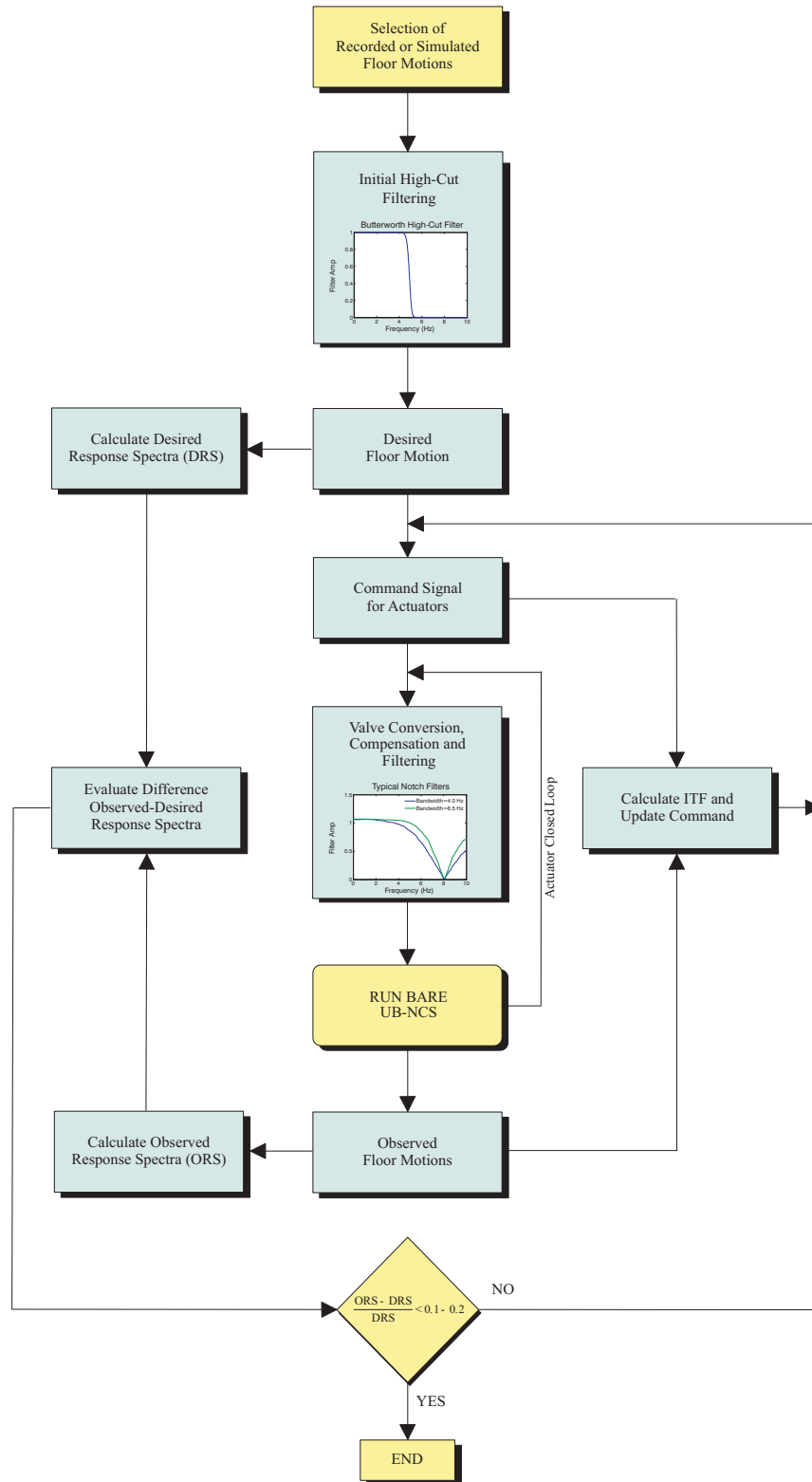
Figure 3.9. Flow chart for off-line iterative process for command signal compensation
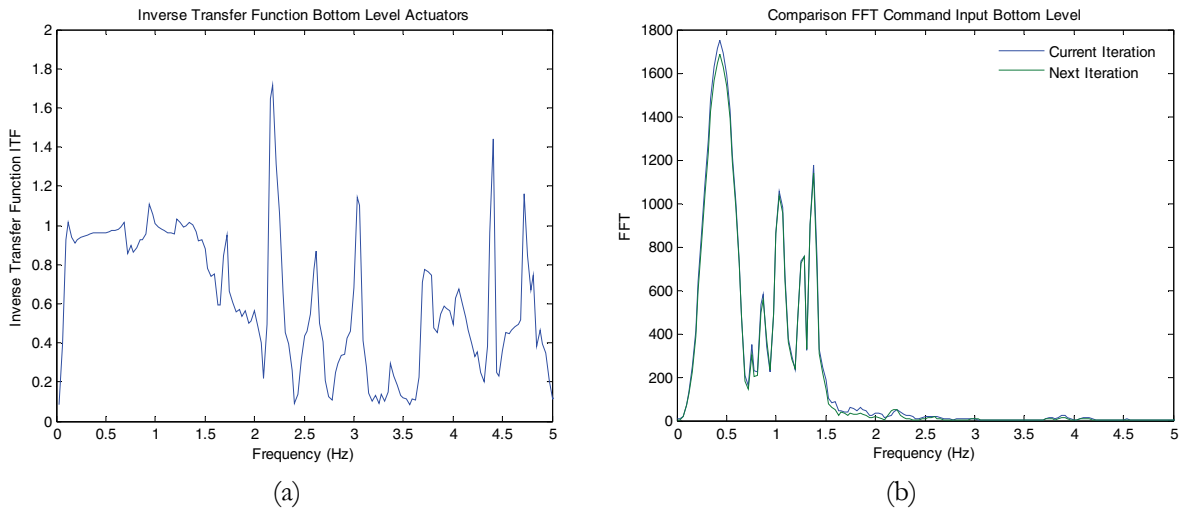
Figure 3.10. Results of first iteration for off-line command signal compensation: (a) inverse transfer function for bottom level actuators; and (b) comparison of FFT for current and compensated command signals
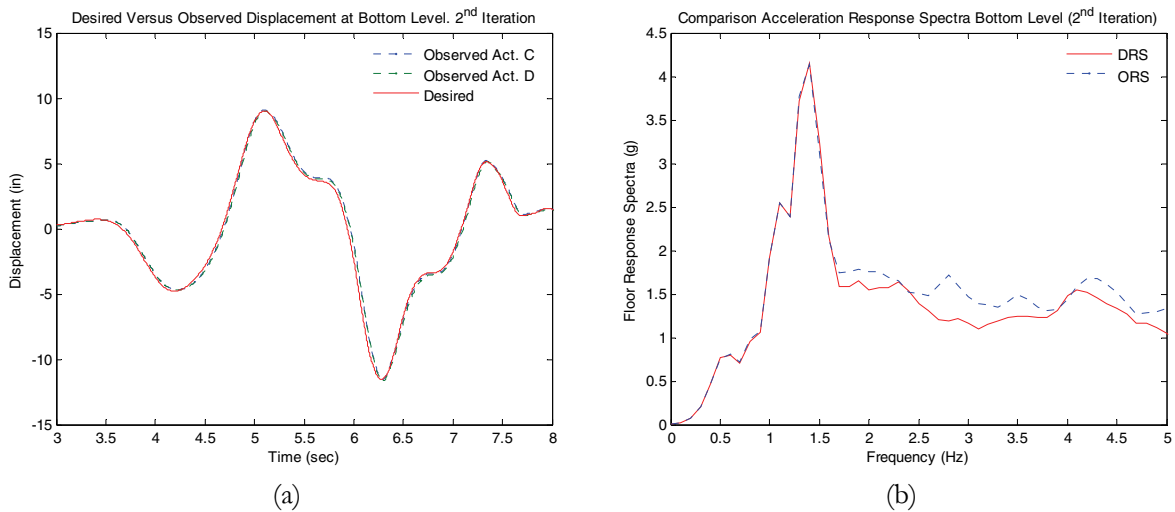
Figure 3.11. Comparison of desired and observed response for simulated floor motions after applying off-line compensation: (a) displacements at bottom level of UB-NCS and (b) desired and observed floor response spectra

3.4.4   Performance evaluation of UB-NCS with payload

The capabilities of the UB-NCS with an actual payload were verified by testing the full-scale steel studded gypsum partition wall specimen shown in Figure 3.12 and detailed in Figure 3.13. The specimen consisted of two identical C-shaped partition walls constructed following standard hospital construction techniques. The walls were constructed between concrete slabs attached to the UB-NCS, as shown in Figure 3.12, to replicate realistic building boundary conditions. The partitions are approximately 10.5 ft in length and 13 ft in height. The steel studs are model SSMA 362S125-43 (18 gauge in thickness) with a typical spacing of 16

inches o.c. and the tracks are model SSMA 362T125-43 (18 gauge in thickness). The tracks were connected to the platform slabs using standard power driven 1½" fasteners, spaced at 12 inches. Gypsum wallboard panels with a thickness of 5/8" were screwed to the studs and finished with corner beads, taping, mud and white paint.

Figure 3.12. Partition walls tested on the UB-NCS with approximate dimensions
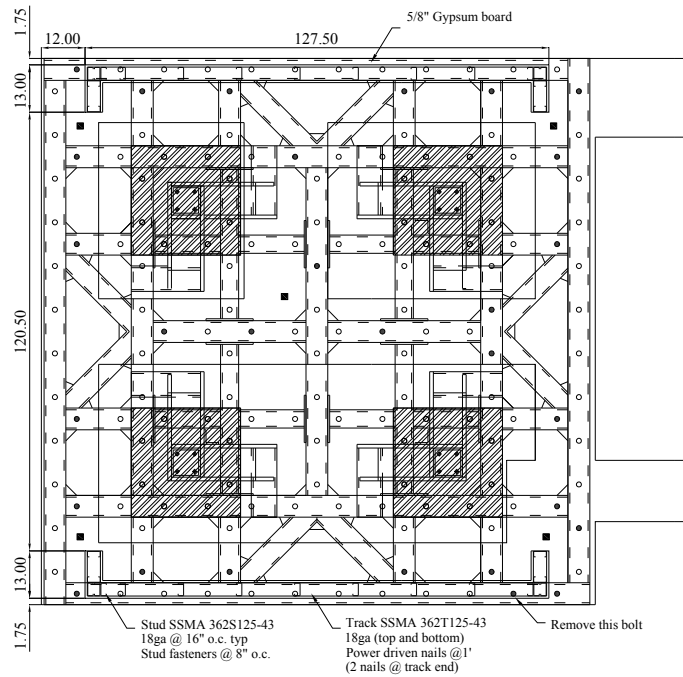
Figure 3.13. Plan layout of partition walls tested using the UB-NCS

A simplified version of the seismic qualification testing protocol presented in Section 4 was considered to assess the seismic performance of the gypsum wall specimen. The testing protocol imposes mean peak seismic demands compatible with a United States Geological Survey (USGS) ground response spectrum associated to a uniform seismic hazard with a probability of exceedance of 10% in 50 years for the city of Northridge, California.

The imposed demands correspond to the mean 84th percentile (mean values plus one standard deviation for normal distribution) demands expected on nonstructural components located within buildings with fundamental periods in the range 0.1 to 5 seconds, and several types of lateral seismic resistant systems (deformation patterns going from pure shear to pure bending). Moreover, the drifts and absolute accelerations imposed by the protocol correspond to the seismic demands expected at a normalized building height $h/H=0.3$, where H denotes the total height of a generic building. This normalized building height corresponds to the building model height that yields the peak mean 84th percentile interstory drifts to be imposed on the predominantly displacement sensitive specimen. Details regarding the estimation of seismic demands distribution within multistory buildings are presented in Section 4.

The closed-form equation for the bottom UB-NCS level displacement protocol (in inches) is given by:

$$x_{Bottom}(t) = 1.95 \, f(t)^{-1.35} \cos\left(\varphi(t)\right) w(t) \tag{3.1}$$

where

$$f(t) = f_{max}\left(\frac{f_{min}^*}{f_{max}}\right)^{\left|\frac{|t-t_d|}{t_d}-1\right|} \tag{3.2}$$

$$t_d = \frac{1}{S_r}\log_2\frac{f_{max}}{f_{min}^*} \tag{3.3}$$

$$f_{min}^* = \frac{S_r \ln 2}{2}\left(\frac{1}{2} - \left\lfloor\frac{4f_{max} - 4f_{min} + 1}{S_r \ln 4}\right\rfloor\right) + f_{max} \tag{3.4}$$

$$\varphi(t) = 2\pi\int_0^t f(\tau)\,d\tau \tag{3.5}$$

and

$$w(t) = \begin{cases} \frac{1}{2}\left[1 - \cos\left(\frac{\pi t}{t_w}\right)\right] & 0 \le t \le t_w \\ 1 & t_w < t < 2t_d - t_w \\ \frac{1}{2}\left[1 - \cos\left(\frac{\pi}{t_w}(t - 2t_d + 2t_w)\right)\right] & 2t_d - t_w \le t \le 2t_d \end{cases} \tag{3.6}$$

$f(t)$, t_d, f_{min}^*, and $\varphi(t)$ in equations (3.2) through (3.5) denote the instantaneous testing frequency, the time instant at which the effective minimum testing frequency is reached, the effective minimum testing frequency, and the instantaneous testing phase, respectively. $w(t)$ in equation (4.105) is a windowing function used to smooth the ramp-up and ramp-down portions of the testing protocol. The other parameters considered for this simplified testing protocol were f_{max} =5 Hz and f_{min} =0.2 Hz, which correspond to the operating limits of the UB-NCS and the frequency content of the responses expected in multistory buildings. A constant frequency sweep rate S_r =12 octaves/min, and a ramp duration t_w=1.5 seconds were used. The resulting protocol shown in Figure 3.14 transitions from high to low frequencies, and then sweeps back to high frequencies. The final high frequency sweep is intended to capture the behavior of components that might be damaged initially by drifts and become sensitive to accelerations (e.g., partition walls acting as a cantilever after failure of top slab connection). Further details on the seismic demand analysis performed to obtain and calibrate the proposed testing protocol are presented in Section 4.

The closed-form equation for the interstory drift (Δ) protocol (in inches) is calculated as:

$$\Delta(t) = \delta\, h_{NCS}\, e^{-\left(\frac{t-t_d}{\sigma}\right)^2} \cos\left(\varphi(t)\right) w(t) \tag{3.7}$$

where $\delta = 1.09\%$ is the maximum interstory drift ratio imposed during testing, h_{NCS} denotes the free interstory height of the testing equipment, and $\sigma = 7.5$ seconds is a factor used to control the number of large and small cycles imposed by the interstory drift protocol.

The protocol displacement history for the top UB-NCS level $\left(x_{Top}\right)$ is calculated as:

$$x_{Top}\left(t, \frac{h}{H}\right) = x_{Bottom}\left(t, \frac{h}{H}\right) + \Delta\left(t, \frac{h}{H}\right) \tag{3.8}$$

Figure 3.14 shows the UB-NCS platform displacements and interstory drift protocol histories used in this test series. For fragility assessment purposes, the protocol was applied on the test specimen using scaling factors of 25, 50, 100, 150 and 200%.

(a)   (b)
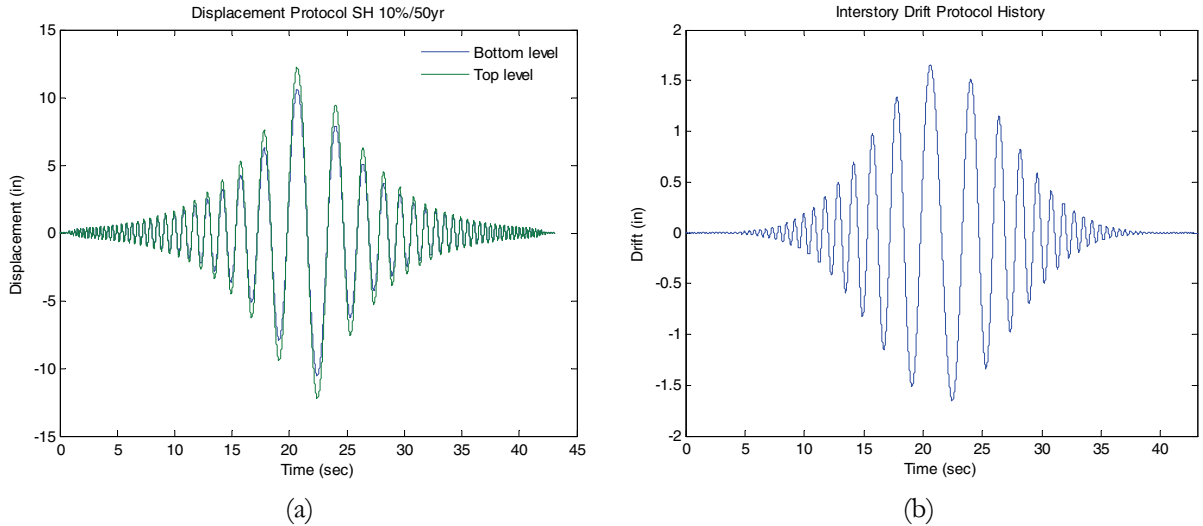
Figure 3.14. Testing Protocol: (a) Floor displacements; and (b) Interstory drift

The input motions for these tests were preconditioned at 100% protocol amplitude with the bare platform, as described in subsection 3.4.3. During the partition wall test series, undershoots in the actuators displacements were observed for frequencies larger than 1 Hz. The error between desired (DRS) and observed (ORS) floor response spectra were on the order of 75%, as observed in Figure 3.15. As a result, it is recommended to perform the actuator tuning process and the off-line input command signal compensation with a similar payload or at small amplitude after the construction of the testing specimen.

78

The full-scale partition wall test series provided valuable information for fragility assessment of the seismic behavior of gypsum partition walls. Table 3.6 summarizes the damage sequence observed in the specimen, while Figure 3.16 shows the ensemble of hysteresis loops measured during the test series. In generating Figure 3.16, the forces in both partition walls are considered to be equal. From Figure 3.16, the maximum force of 9.1 kips in each partition wall is observed at an interstory drift ratio of 0.81%. Strength degradation and pinching response of the partition walls are caused by the cyclic crushing of the gypsum wallboard around the screws connecting the panels to the steel frame. Crushing of the gypsum panels was also observed along the edges of the wall and in between panels. Inspections during demolition of the specimen revealed that the steel-stud frame and connections of the upper and lower track to the concrete slabs were intact, with damage limited mainly to the gypsum panels. Figure 3.17 presents a set of photos showing the damage progression observed in the partition walls.

Table 3.6. Damage evolution in gypsum partition walls

Drift (%)		Damage observed
0.47	:	Raised surface and small cracks around screws at bottom and top of walls. Vertical cracks at top and bottom ends of corner beads.
0.52	:	Initial pop-out of screws at bottom and top of wall. Cracks along tape at sheetrock panel joints. Vertical cracks at top and bottom ends of corner beads propagated. Incipient crushing of wall corners.
1.10	:	Widespread pop-out of screws at center of sheetrock panels. Cracks along most tape at sheetrock panel joints. Permanent gaps (~1/16-1/8") between sheetrock panels. Increased crushing of wall corners.
1.64	:	Widespread pop-out of screws in the whole wall. Edges of sheetrock panels crushed. Smaller sheetrock panels become loose. Permanent gaps (~1/8-1/4) between sheetrock panels. Increased crushing of wall corners.
2.21	:	Screws in all edges of all panels are disconnected. Edges of sheetrock panels continue crushing. Smaller sheetrock panels totally loose. Permanent gaps (~1/4-1/2") in most joints between sheetrock panels.
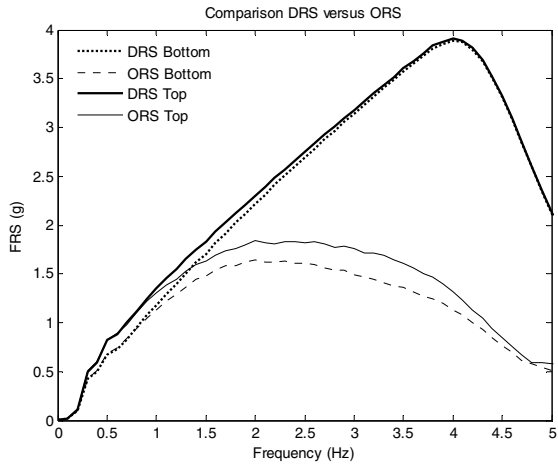
Figure 3.15. Comparison desired (DRS) and observed (ORS) floor response spectra for testing protocol scaled to 100%
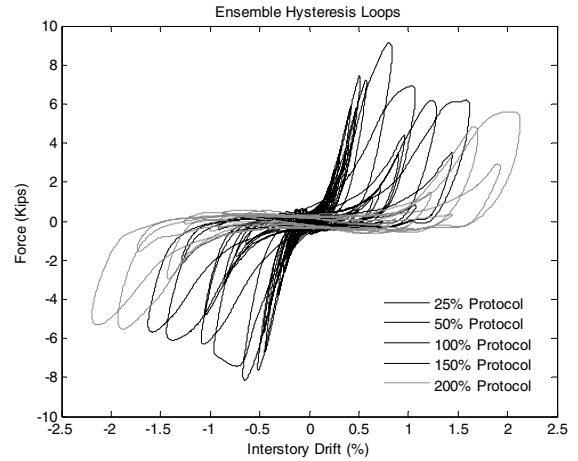
Figure 3.16. Ensemble of measured hysteresis loops of gypsum partition walls using testing protocol in Figure 3.14 at various amplitudes

(a) Screw rising observed at a 0.47% drift ratio

(b) Screw rising observed at a 0.47% drift ratio
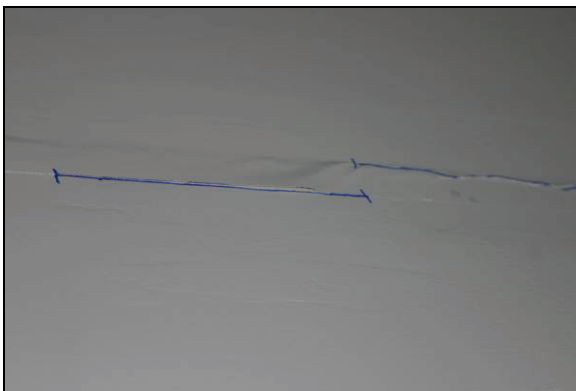
(c) Crack along tape observed at a 0.52% drift ratio
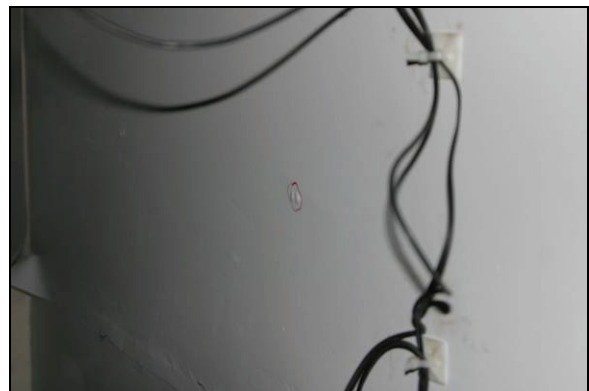
(d) Screw rising observed at a 0.52% drift ratio

Figure 3.17. Photos of damage observed in steel studded gypsum partition walls
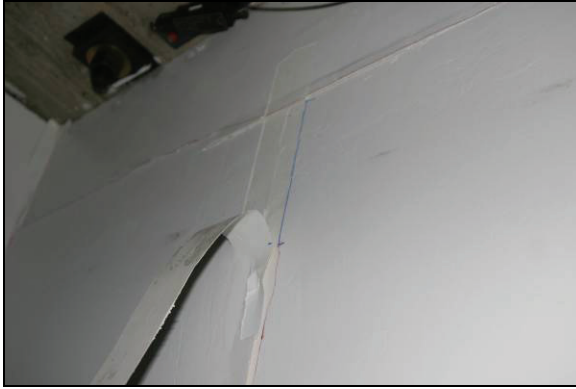
(e) Permanent gaps t~1/16-1/8" between sheetrock panels observed at a 1.10% drift ratio

(f) Permanent gaps t~1/16-1/8" between sheetrock panels observed at a 1.10% drift ratio
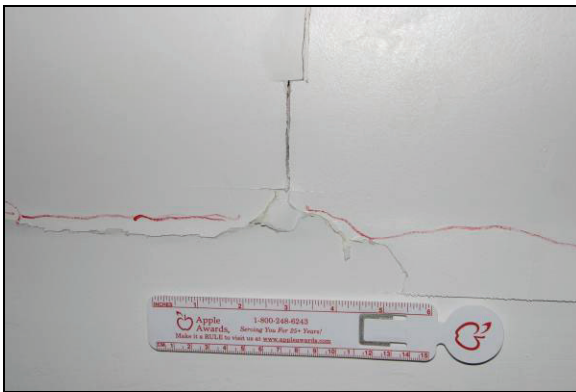
(g) Permanent gaps t~1/8-1/4" between sheetrock panels observed at a 1.64% drift ratio
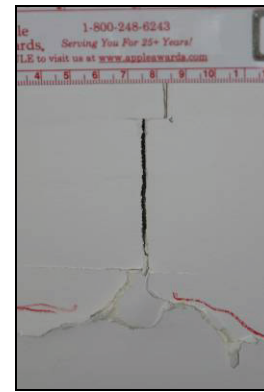
(h) Permanent gaps t~1/8-1/4" between sheetrock panels observed at a 1.64% drift ratio

(i) Permanent gaps t~1/4-1/2" between sheetrock panels observed at a 2.21% drift ratio

(j) Permanent gaps t~1/4-1/2" between sheetrock panels observed at a 2.21% drift ratio

Figure 3.17. Photos of damage observed in steel studded gypsum partition walls (Cont'd)

3.5   Summary

This section presented a description of the new UB-NCS and its testing capabilities. The capability of the testing facility to reproduce desired floor motions has been demonstrated. An off-line iterative process for

input command signal compensation was proposed to match desired floor response spectra in the operational range of the UB-NCS. Finally, the ability of the UB-NCS for evaluating the seismic performance of full-scale testing specimens was demonstrated. Based on the performance of the UB-NCS it was recommended to apply the actuators tuning and the input command signal compensation procedures with an actual payload or at small amplitudes after the construction of the specimen.

Next section will present a testing protocol for seismic qualification and fragility assessment of nonstructural components that imposes simultaneously the seismic hazard consistent absolute floor accelerations and story drifts expected at the upper levels of multistory buildings.

SECTION 4

DEVELOPMENT OF TESTING PROTOCOLS FOR DISTRIBUTED NONSTRUCTURAL COMPONENTS, SYSTEMS AND EQUIPMENT

Recent building design codes and standards, such as IBC 2006 (ICC, 2006) and ASCE 7-05 (ASCE, 2005), now require seismic qualification of mechanical and electrical equipment and its mounting systems in important buildings to ensure they remain functional during and after a seismic event. This requirement has practical consequences on manufacturers and providers of standardized nonstructural components since their products will need to be seismically qualified to a specified level of shaking. Equipment qualification can be accomplished through experimental methods such as shake table testing, analytical methods, or experience data. However, little guidance is provided on actual qualification procedures.

Moreover, with the development of performance-based earthquake engineering, harmonization of performance levels between structural and nonstructural components becomes vital. Even if the structural components of a building achieve a continuous or immediate occupancy performance level after a seismic event, failure of architectural, mechanical, or electrical components can lower the performance level of the entire building system. As consequence, experimental fragility analysis becomes necessary to harmonize the seismic performance of the primary system and building contents.

For experimental seismic qualification and fragility analysis of nonstructural components and equipment, shake table testing protocols have been proposed by AC156 (ICC-ES, 2007), FEMA 461 (FEMA, 2006), and IEEE 693 (IEEE, 2006), and are now being used for this purpose (Badillo-Almaraz *et al.*, 2007; Badillo-Almaraz *et al.*, 2000; Filiatrault and Matt, 2005; Restrepo and Lang, 2005). These protocols have been mainly calibrated to match floor response spectra of linear Single Degree of Freedom (SDOF) systems, considering the limited displacement capabilities of conventional shaking tables. Moreover, these shake table protocols are mainly intended for testing acceleration-sensitive nonstructural components, such as suspended ceiling systems and mechanical equipment, anchored to a single building level. A racking protocol for seismic performance assessment of displacement or drift sensitive components, such as partition walls, is also proposed in FEMA 461.

Nonstructural systems typically found in office, hotel and hospital buildings may be composed of components that individually may be either acceleration or displacement sensitive, but when combined with other systems may become sensitive to both accelerations and interstory drifts. In hospitals, for example, acceleration sensitive patient monitors are typically attached to displacement sensitive partition walls. The seismic performance of individual distributed nonstructural components and the assessment of

interactions between components can be evaluated through a testing protocol taking full advantage of the UB-NCS capabilities.

This section presents a general dynamic testing protocol that can be configured for experimental seismic qualification or experimental seismic fragility evaluation of distributed nonstructural components, systems and equipment. The protocols can be applied dynamically or quasi-statically. The proposed protocol histories are obtained following a seismic demand analysis performed considering a continuous beam model and principles of random vibration theory. The resulting protocol histories impose the mean seismic demands expected within multistory buildings, independent of specific building or ground motion characteristics. Details of the seismic hazard characterization, the random vibration theory concepts, and the building model used for the development of the testing protocol are presented in this section.

4.1   Theoretical background for UB-NCS testing protocol

In order to develop a testing protocol for nonstructural components, the seismic demands are first examined through a generic building model. The seismic excitation input to the building model is characterized through the Uniform Seismic Hazard (USH), a site specific ground response spectrum defined by the United States Geological Survey (USGS). The USGS-USH, which accounts for the Probabilistic Local Seismic Hazard (PLSH), considers the ensemble of all possible earthquake scenarios (characterized by their corresponding earthquake moment magnitude M_w and source-to-site R distance) that can affect the site. A second alternative for characterizing the seismic input for the building model is obtained from the Deterministic Local Seismic Hazard (DLSH), characterized by the site earthquake modal event, the earthquake scenario with the highest probability of occurrence. Under this alternative, pairs M_w-R characterizing the modal event are used as input for the Specific Barrier Model (Halldorsson and Papageorgiou, 2005; Papageorgiou and Aki, 1983b; Papageorgiou and Aki, 1983a; Papageorgiou and Aki, 1984) in estimating the power spectrum input to the generic building model.

In the development that follows, the first alternative will be considered for generating a seismic hazard compatible building model input. However, it is stated that the second alternative can be considered in developing a more general testing protocol accounting for near fault earthquake effects, which is not within the scope of this research.

4.1.1   Principles of stochastic processes

This subsection presents the principles of random vibration theory used to estimate the seismic demands to be imposed by the UB-NCS testing protocol.

4.1.1.1 Statistics of extreme values in random processes

The procedure summarized in this subsection was developed in the 1950's by Cartwright and Longuet-Higgins (Cartwright and Longuet-Higgins, 1956) for studying the statistics of the heights of the maxima in ocean tides. The procedure has been extensively used in engineering applications and here it will be used to estimate the maximum seismic demands expected on nonstructural components.

The first step in the estimation of the peak maxima value for a random process $y(t)$ consists in the estimation of the probability density function for maxima. For this purpose, three random variables $\xi_1 = y$, $\xi_2 = \dfrac{dy}{dt}$ and $\xi_3 = \dfrac{d^2 y}{dt^2}$ are defined. The joint probability density function for ξ_1, ξ_2 and ξ_3, $p(\xi_1, \xi_2, \xi_3)$, can be written in its normal form as (Clough and Penzien, 1993):

$$p(\xi_1, \xi_2, \xi_3) = p(\xi) = \frac{1}{(2\pi)^{3/2}|\mu|^{1/2}} e^{-\frac{1}{2}[\xi - \bar{\xi}]^T \mu^{-1}[\xi - \bar{\xi}]} \tag{4.1}$$

where $\xi = [\xi_1, \xi_2, \xi_3]$, $\bar{\xi} = [\bar{\xi}_1, \bar{\xi}_2, \bar{\xi}_3] = 0$ is the zero mean value vector, and μ is the covariance matrix, whose $\mu_{j,k}$ term is defined by:

$$\mu_{j,k} = E\{\xi_j \xi_k\} \tag{4.2}$$

Defining the n-th moment m_n about the origin of the power spectral density function $S_Y(\omega)$ of the stochastic process $y(t)$ as:

$$m_n = \int_{-\infty}^{\infty} \omega^n S_Y(\omega) d\omega \tag{4.3}$$

The value of m_0 calculated using equation (4.3) corresponds to the square of the root mean square amplitude (Y_{RMS}) of the process $y(t)$. It can be shown that the covariance matrix is given by:

$$\mu = \begin{bmatrix} m_0 & 0 & -m_2 \\ 0 & m_2 & 0 \\ -m_2 & 0 & m_4 \end{bmatrix} \tag{4.4}$$

Substituting (4.4) into equation (4.1):

$$p(\xi_1,\xi_2,\xi_3) = \frac{1}{(2\pi)^{3/2}\left[m_2\left(m_0 m_4 - m_2^2\right)\right]^{1/2}} e^{-\frac{1}{2}\left(\frac{\xi_2^2}{m_2} + \frac{m_4\xi_1^2 + 2m_2\xi_1\xi_3 + m_0\xi_3^2}{m_0 m_4 - m_2^2}\right)}$$ (4.5)

In order to have a positive or negative local maximum in the range $(y, y+dy)$ in the time interval $(t, t+dt)$, the first time derivative of $y(t)$ should be positive (converging to 0) and the second derivative should be negative, both satisfying:

$$0 < \frac{dy}{dt} < \left|\frac{d^2 y}{dt^2}\right| dt$$ (4.6)

which expressed in terms of the new variables is:

$$0 < \xi_2 < |\xi_3| dt$$ (4.7)

Therefore, the probability of finding one maxima lying in the range $(y, y+dy)$ in the time interval $(t, t+dt)$ is given by (Cartwright and Longuet-Higgins, 1956):

$$F(\xi_1) d\xi_1 dt = \left[\int_{-\infty}^{0} p(\xi_1, 0, \xi_3)|\xi_3| d\xi_3\right] d\xi_1 dt$$ (4.8)

where $F(\xi_1)$ is the probability density of finding one maxima lying in the range $(y, y+dy)$ in the time interval $(t, t+dt)$. It follows that the mean frequency of maxima N_1 is given by:

$$N_1 = \int_{-\infty}^{\infty}\int_{-\infty}^{0} p(\xi_1, 0, \xi_3)|\xi_3| d\xi_3 d\xi_1 = \frac{1}{2\pi}\sqrt{\frac{m_4}{m_2}}$$ (4.9)

and therefore, the total number of maxima N in a random process is calculated through:

$$N = N_1 T_d = \frac{T_d}{2\pi}\sqrt{\frac{m_4}{m_2}}$$ (4.10)

where T_d is the total duration of the stochastic process. For the case of earthquake events, T_d is given by:

$$T_d = T_{SR} + 0.05R$$ (4.11)

where R (in km) corresponds to the source-to-site distance; and T_{SR} is the duration of the source rupture process, calculated in terms of the seismic moment M_0 and the global stress drop $\Delta\sigma_G$ during the faulting process using:

$$T_{SR} = \frac{\pi}{2} \left(\frac{7}{16} \frac{M_o}{\Delta\sigma_G} \right)^{1/3}$$

(4.12)

M_o in equation (4.12) is related to the earthquake magnitude M_w, the most common seismological measure of earthquake size, through:

$$M_o = 10^{\frac{3}{2}(M_w + 10.7)}$$

(4.13)

The second term in equation (4.11), proposed by Herrmann (Herrmann, 1985) and also adopted by Boore (Boore, 2003a) and Halldorsson and Papageorgiou (Halldorsson, 2004; Halldorsson and Papageorgiou, 2005), accounts for path-dependent ground motion duration. The pair M_W-R considered in this study corresponds to the modal event (Kramer, 1996) controlling the deterministic local seismic hazard.

Expressing the maxima of the stochastic process in the non-dimensional form $\eta = \xi_1 / \sqrt{m_0} = \xi_1 / Y_{RMS}$ and using (4.5) to solve for the integral in equation (4.8), the probability density function for maxima $p(\eta)$ is obtained as the ratio $F(\xi_1)/N_1$, and it is given by:

$$p(\eta) = \frac{1}{\sqrt{2\pi}} \left[\varepsilon e^{-\frac{\eta^2}{2\varepsilon^2}} + \sqrt{1-\varepsilon^2}\, \eta e^{-\frac{\eta^2}{2}} \int_{-\infty}^{\eta\sqrt{1-\varepsilon^2}/\varepsilon} e^{-x^2/2} dx \right]$$

(4.14)

where

$$\varepsilon^2 = \frac{m_0 m_4 - m_2^2}{m_0 m_4}$$

(4.15)

It can be shown that ε in equation (4.15) takes values in the range $0 < \varepsilon < 1$. The probability of η exceeding a given value $\bar{\eta}$ can be calculated using:

$$q(\bar{\eta}) = \int_{\bar{\eta}}^{\infty} p(\eta) d\eta$$

(4.16)

Substituting (4.14) into (4.16) and integrating, we obtain:

$$q(\eta) = \frac{1}{\sqrt{2\pi}} \left[\int_{\eta/\varepsilon}^{\infty} e^{-x^2/2} dx + \sqrt{1-\varepsilon^2}\, e^{-\eta^2/2} \int_{-\infty}^{\eta\sqrt{1-\varepsilon^2}/\varepsilon} e^{-x^2/2} dx \right]$$

(4.17)

where the dummy variable $\bar{\eta}$ has been replaced by η to simplify the notation. Now, we can calculate the mean peak maxima $\bar{\eta}_{max}$. In order to do so, the probability density function of a random process consisting in that N randomly selected maxima are not larger than a given value η_{max}, is calculated as:

$$p\left(\eta_{max}\right) = \frac{d}{d\eta_{max}}\left[1 - q\left(\eta_{max}\right)\right]^{N} \tag{4.18}$$

The expression shown in equation (4.18) corresponds to the probability density function for the peak maximum of the stochastic process. Now, the mean peak maxima $\bar{\eta}_{max}$ can be calculated as the expectation of the function in equation (4.18):

$$\bar{\eta}_{max}\left(N\right) = \int_{-\infty}^{\infty} \eta \frac{d}{d\eta}\left[1 - q\left(\eta\right)\right]^{N} d\eta \tag{4.19}$$

where, again, the dummy integral variable η_{max} was changed onto η for simplicity. In the case of narrow band processes, as the case of ground motion excitations, the variable ε tends to 0. Introducing $\varepsilon = 0$ in equation (4.17), we obtain a conservative approximation for $q\left(\eta\right)$:

$$\lim_{\varepsilon \to 0} q\left(\eta\right) = \begin{cases} 1 & \eta < 0 \\ e^{-\eta^2/2} & \eta \geq 0 \end{cases} \tag{4.20}$$

Onto substitution of equation (4.20) into equation (4.19) we finally find that:

$$\bar{\eta}_{max}\left(N\right) = \int_{0}^{\infty} N\eta^2 e^{-\eta^2/2}\left[1 - e^{-\eta^2/2}\right]^{N-1} d\eta \tag{4.21}$$

A plot of $\bar{\eta}_{max}\left(N\right)$ in equation (4.21) is shown in Figure 4.1. A simplified procedure for finding an approximate for $\bar{\eta}_{max}\left(N\right)$ for the case $\varepsilon = 0$ was also proposed by Cartwright and Longuet-Higgins (Cartwright and Longuet-Higgins, 1956). They proposed the so called asymptotic approximation:

$$\bar{\eta}_{max}^{appr}\left(N\right) = \sqrt{2ln\left(N\right)} + \frac{\gamma}{\sqrt{2ln\left(N\right)}} \tag{4.22}$$

where γ is the Euler-Mascheroni constant, calculated as $\gamma = -\int_{0}^{\infty} e^{-x} ln\, x dx \approx 0.5772$ (Abramowitz and Stegun, 1972). Equation (4.22) is also plotted in Figure 4.1 for comparison.
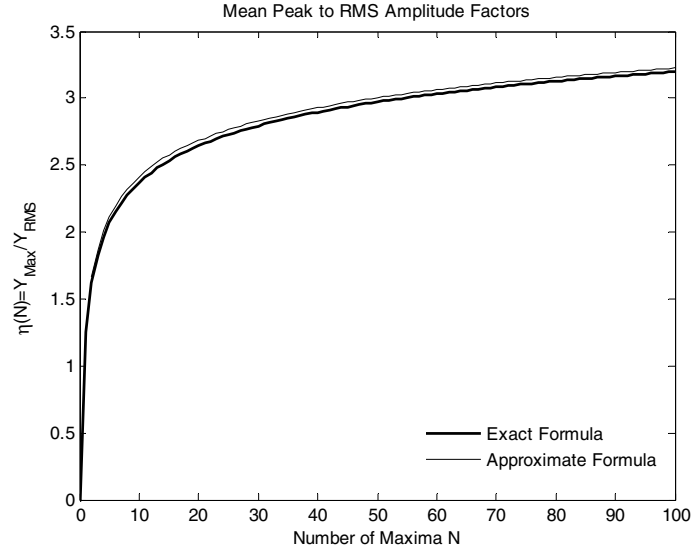
Figure 4.1. Mean peak maxima to root mean square ratio

Finally, it is recalled that the maximum expected amplitude Y_{Max} of the random process $y(t)$ is obtained from the power spectral density moments as:

$$Y_{Max} = \bar{\eta}_{max}(N) Y_{RMS} \tag{4.23}$$

where $\bar{\eta}_{max}(N)$ can be calculated using either equation (4.21) or equation (4.22), N is computed using equation (4.10) and Y_{RMS} is computed using equation (4.3) for $n=0$.

4.1.1.2 Generation of ground response spectrum consistent power spectral density functions

This subsection presents a procedure, combining the method proposed by Gupta and Trifunac (Gupta and Trifunac, 1998) for generating ground response spectrum compatible power spectral density functions and the theory of maxima presented in subsection 4.1.1.1, for generating USGS-USH ground response spectrum consistent power spectral density functions. First, the power spectral density function $S_{\ddot{u}^T}(\omega, \omega_o, \zeta_o)$ for the absolute acceleration response of a SDOF oscillator with natural frequency ω_o and damping ratio ζ_o excited by a ground acceleration stochastic process with power spectral density function $S_{\ddot{u}_g}(\omega, \zeta_o)$ given by (Singh, 1976):

$$S_{\ddot{u}^T}(\omega, \omega_o, \zeta_o) = S_{\ddot{u}_g}(\omega, \zeta_o)\left[4\zeta_o^2\omega_o^2\omega^2 + \omega_o^4\right]\left|H_o(\omega)\right|^2 \tag{4.24}$$

where

89

$$H_o(\omega) = \left(\omega_o^2 - \omega^2 + 2i\zeta_o\omega_o\omega\right)^{-1} \tag{4.25}$$

where $i = \sqrt{-1}$ denotes the imaginary unit. The term $H_o(\omega)$ in equations (4.24) and (4.25) is the frequency response function for the SDOF. Considering that the function $\left|H_o(\omega)\right|^2$ exhibits a single and marked peak at $\omega = \omega_o$, Gupta and Trifunac (Gupta and Trifunac, 1998) proposed to simplify equation (4.24) by considering a constant value obtained from evaluating $\left|H_o(\omega)\right|^2$ at $\omega = \omega_o$ in a range of frequencies with bandwidth $B_w = \pi\zeta_o\omega_o$ centered at ω_o. The bandwidth B_w is selected in such a way that the area under $\left|H_o(\omega)\right|^2$ and the approximate function are the same (Elishakoff, 1983), i.e.:

$$B_w = \frac{\displaystyle\int_0^\infty \left|H_o(\omega)\right|^2}{\left|H_o(\omega_o)\right|^2} = \frac{\dfrac{\pi}{4\zeta_o\omega_o^3}}{\dfrac{1}{4\zeta_o^2\omega_o^4}} = \pi\zeta_o\omega_o \tag{4.26}$$

Moreover, Gupta and Trifunac proposed to replace the term $S_{\ddot{u}_g}(\omega,\zeta_o)$ in equation (4.24) by its value at $\omega = \omega_o$. By introducing those approximations into equation (4.24), the following simplified formula for the absolute acceleration response power spectral density function is obtained:

$$S_{\ddot{u}^T}(\omega,\omega_o,\zeta_o) = S_{\ddot{u}_g}(\omega,\zeta_o)\left[\frac{\omega^2}{\omega_o^2} + \frac{1}{4\zeta_o^2}\right] \tag{4.27}$$

Using equation (4.3), the root mean square amplitude for the absolute acceleration response for a SDOF oscillator with frequency ω_o and damping ratio ζ_o can be calculated as:

$$\ddot{u}_{RMS}^T(\omega_o,\zeta_o) = \sqrt{\int_{-\infty}^\infty S_{\ddot{u}^T}(\omega,\omega_o,\zeta_o)\,d\omega} = \sqrt{2S_{\ddot{u}_g}(\omega,\zeta_o)\int_{\omega_o-\frac{\pi\zeta_o\omega_o}{2}}^{\omega_o+\frac{\pi\zeta_o\omega_o}{2}}\left(\frac{\omega^2}{\omega_o^2} + \frac{1}{4\zeta_o^2}\right)d\omega} \tag{4.28}$$

Calculating the integral at the right side of equation (4.28) we have:

$$\ddot{u}_{RMS}^T(\omega_o,\zeta_o) = \sqrt{\frac{\pi\omega_o S_{\ddot{u}_g}(\omega_o,\zeta_o)}{6\zeta_o}\left(12\zeta_o^2 + \pi^2\zeta_o^4 + 3\right)} \tag{4.29}$$

Now, the expected maximum absolute acceleration response for the SDOF oscillator $\ddot{u}_{Max}^{T}(\omega_o, \zeta_o)$, which corresponds, by definition, to the acceleration response spectrum at a frequency ω_o, $S_a(\omega_o, \zeta_o)$, can be estimated using equation (4.23) and then:

$$S_a(\omega_o, \zeta_o) = \ddot{u}_{Max}^{T}(\omega_o, \zeta_o) = \bar{\eta}_{max}(N)\ddot{u}_{RMS}^{T}(\omega_o, \zeta_o) \tag{4.30}$$

By introducing also the approximation $N \approx \dfrac{T_d \omega_o}{\pi}$ into equation (4.22) and replacing into equation (4.30):

$$S_a(\omega_o, \zeta_o) = \left(\sqrt{2\ln\left(\frac{T_d \omega_o}{\pi}\right)} + \frac{\gamma}{\sqrt{2\ln\left(\frac{T_d \omega_o}{\pi}\right)}} \right) \sqrt{\frac{\pi \omega_o S_{\ddot{u}_g}(\omega_o, \zeta_o)}{6\zeta_o}\left(12\zeta_o^2 + \pi^2 \zeta_o^4 + 3\right)} \tag{4.31}$$

Finally, after simplifying the notation for clarity, the ground acceleration response spectra compatible power spectral density function is obtained as:

$$S_{\ddot{u}_g}(\omega, \zeta) = \frac{6\zeta S_a(\omega, \zeta)^2}{\pi\omega\left(12\zeta^2 + \pi^2\zeta^4 + 3\right)}\left(\sqrt{2\ln\left(\frac{T_d \omega}{\pi}\right)} + \frac{\gamma}{\sqrt{2\ln\left(\frac{T_d \omega}{\pi}\right)}} \right)^{-2} \tag{4.32}$$

where T_d is, for simplicity, the estimated duration of the random earthquake process, equation (4.11), although, for the sake of exactness, it should correspond to the SDOF response process duration. Equation (4.32) can also be expressed in terms of the SDOF natural period instead of natural frequency as commonly used in engineering applications.

Information presented until this point is sufficient to generate ground acceleration realizations $\ddot{u}_g(t)$ using, for example, the procedure presented by Soong and Grigoriu (Soong and Grigoriu, 1993a):

$$\ddot{u}_g(t) = \sum_{k=1}^{m} \sqrt{S_{\ddot{u}_g}(\omega_k, \zeta)\Delta\omega}\left[V_k \cos(\omega_k t) + W_k \sin(\omega_k t)\right] \tag{4.33}$$

where V_k and W_k are independent realizations of Gaussian processes with zero mean and unit standard deviation; m is the number of non-overlapping intervals of width $\Delta\omega$ considered in discretizing the power spectrum $S_{\ddot{u}_g}(\omega, \zeta)$; and ω_k is the central frequency of the kth interval.

4.1.2 Structural model for parametric seismic demand analysis

4.1.2.1 Model description

The building model considered for the seismic demands analysis consists of a continuous elastic cantilever beam combining a flexural beam (Bernoulli's beam) and a shear beam, both connected throughout an infinite number of axially rigid links distributed along the height of the model, as illustrated in Figure 4.2. In this continuous model, shear and flexural beams undergo the same deformations, allowing for modeling of generic buildings whose seismic resistant systems are composed of a combination of shear walls and moment resisting frames. This model, proposed and studied in the early 1960's by Coull and Choudhury (Coull and Choudhury, 1967a; Coull and Choudhury, 1967b), Heidebrecht and Stafford-Smith (Heidebrecht and Stafford-Smith, 1973), and Stafford-Smith and Coull (Stafford-Smith and Coull, 1991), has been extensively studied by other researchers (Akkar *et al.*, 2005; Chopra and Chintanapakdee, 2001; Iwan, 1997; Kim and Collins, 2002; Kim *et al.*, 2006; Lavelle *et al.*, 1988; Miranda, 1999; Miranda and Akkar, 2006; Miranda and Reyes, 2002; Miranda and Taghavi, 2005; Nicholson and Bergman, 1986; Reinoso and Miranda, 2005; Taghavi and Miranda, 2005; Taghavi and Miranda, 2006; Wang *et al.*, 1992), and recently has shown promising results in simulating the seismic responses observed in multistory buildings during real ground motions (Reinoso and Miranda, 2005; Taghavi and Miranda, 2006).
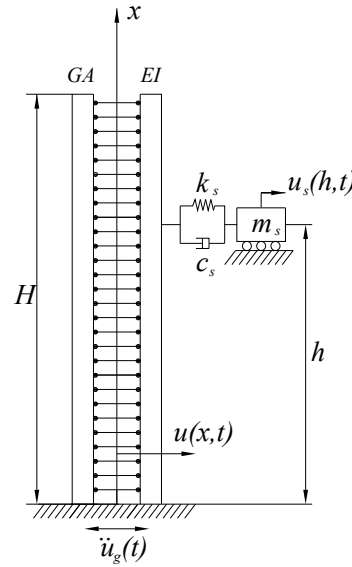
Figure 4.2. Continuous flexural-shear beam model

The differential equation of motion governing the undamped dynamic response of the system is:

$$m(x)\frac{\partial^2 u(x,t)}{\partial t^2} + EI(x)\frac{\partial^4 u(x,t)}{\partial x^4} - GA(x)\frac{\partial^2 u(x,t)}{\partial x^2} = -m(x)\frac{\partial^2 u_g(t)}{\partial t^2} \tag{4.34}$$

where $m(x)$, $I(x)$ and $A(x)$ are the mass per unit length, and sectional inertia and area along the height of the beam; and E and G are the Young and shear modulus of the material, respectively. In order to simplify the following discussion, properties and materials will be considered uniform along the beam, and therefore $m(x) = \bar{m}$, $I(x) = I$ and $A(x) = A$. Introducing these simplifications into equation (4.34) yields:

$$\bar{m}\frac{\partial^2 u(x,t)}{\partial t^2} + EI\frac{\partial^4 u(x,t)}{\partial x^4} - GA\frac{\partial^2 u(x,t)}{\partial x^2} = -\bar{m}\frac{\partial^2 u_g(t)}{\partial t^2} \tag{4.35}$$

For the case of undamped free vibrations, equation (4.35) can be rewritten as:

$$\frac{\bar{m}}{EI}\frac{\partial^2 u(x,t)}{\partial t^2} + \frac{\partial^4 u(x,t)}{\partial x^4} - \frac{GA}{EI}\frac{\partial^2 u(x,t)}{\partial x^2} = 0 \tag{4.36}$$

By using separation of variables to solve equation (4.36) and considering the change of variables $u(x,t) = \varphi(x)\,y(t)$, equation (4.36) can be rewritten as:

$$\frac{\bar{m}}{EI}\varphi(x)\frac{\partial^2 y(t)}{\partial t^2} + \frac{\partial^4 \varphi(x)}{\partial x^4}y(t) - \alpha^2\frac{\partial^2 \varphi(x)}{\partial x^2}y(t) = 0 \tag{4.37}$$

where $\alpha = \sqrt{GA/EI}$ is a parameter accounting for the relative stiffness of the shear and flexural beams considered in the model. A limiting value $\alpha = 0$ allows for replicating the deformation pattern associated to pure flexural beams; while a value $\alpha = \infty$ represents a pure shear beam, typically used to model structures with beams significantly stiffer than columns (Miranda and Akkar, 2006). By separating variables in equation (4.37) we have:

$$\frac{\ddot{y}(t)}{y(t)} = -\frac{EI}{\bar{m}}\frac{\varphi^{iv}(x)}{\varphi(x)} + \alpha^2\frac{EI}{\bar{m}}\frac{\varphi''(x)}{\varphi(x)} = -\omega^2 \tag{4.38}$$

and then,

$$\ddot{y}(t) + \omega^2 y(t) = 0 \tag{4.39}$$

$$\varphi^{iv}(x) - \alpha^2\varphi''(x) - k^4\varphi(x) = 0 \tag{4.40}$$

where

$$k^4 = \frac{\omega^2\bar{m}}{EI} \tag{4.41}$$

The general solution to equation (4.40) is given by:

$$\varphi(x) = A\cos(\lambda_1 x) + B\sin(\lambda_1 x) + C\cosh(\lambda_2 x) + D\sinh(\lambda_2 x) \tag{4.42}$$

where

$$\lambda_1^2 = \frac{\sqrt{\alpha^4 + 4k^4} - \alpha^2}{2} \tag{4.43}$$

$$\lambda_2^2 = \frac{\sqrt{\alpha^4 + 4k^4} + \alpha^2}{2} \tag{4.44}$$

From equations (4.43) and (4.44):

$$\lambda_2^2 = \lambda_1^2 + \alpha^2 \tag{4.45}$$

The constants A, B, C and D in equation (4.42) are obtained by imposing the boundary conditions for displacements, rotations, bending moments and shear forces at free and clamped ends of the continuous beam model:

$$\varphi(0) = 0 \tag{4.46}$$
$$\varphi'(0) = 0 \tag{4.47}$$
$$\varphi''(H) = 0 \tag{4.48}$$
$$\varphi'''(H) - \alpha^2 \varphi'(H) = 0 \tag{4.49}$$

In equations (4.48) and (4.49) the term H denotes the total height of the cantilever beam. After some algebra, and after introducing the change of variables $\overline{\lambda}_1 = \lambda_1 H$ and $\overline{\lambda}_2 = \lambda_2 H$, the normalized (in terms of total beam height H) n-th modal shape is obtained:

$$\varphi_n(x) = \cos\left(\frac{\overline{\lambda}_{n1}x}{H}\right) - \cosh\left(\frac{\overline{\lambda}_{n2}x}{H}\right) - \frac{\overline{\lambda}_{n1}^2 \cos\left(\overline{\lambda}_{n1}\right) + \overline{\lambda}_{n2}^2 \cosh\left(\overline{\lambda}_{n2}\right)}{\overline{\lambda}_{n1}^2 \sin\left(\overline{\lambda}_{n1}\right) + \overline{\lambda}_{n1}\overline{\lambda}_{n2} \sinh\left(\overline{\lambda}_{n2}\right)}\left[\sin\left(\frac{\overline{\lambda}_{n1}x}{H}\right) - \frac{\overline{\lambda}_{n1}}{\overline{\lambda}_{n2}} \sinh\left(\frac{\overline{\lambda}_{n2}x}{H}\right)\right] \tag{4.50}$$

The $\overline{\lambda}_{n1}$ term shown in equation (4.50) is obtained by solving the following characteristic equation:

$$2 + \left(\frac{2\overline{\lambda}_{n1}^4 + 2\overline{\lambda}_{n1}^2\alpha_o^2 + \alpha_o^4}{\overline{\lambda}_{n1}^4 + \overline{\lambda}_{n1}^2\alpha_o^2}\right)\cosh\left(\sqrt{\overline{\lambda}_{n1}^2 + \alpha_o^2}\right)\cos\left(\overline{\lambda}_{n1}\right) + \frac{\alpha_o^2}{\overline{\lambda}_{n1}\sqrt{\overline{\lambda}_{n1}^2 + \alpha_o^2}}\sinh\left(\sqrt{\overline{\lambda}_{n1}^2 + \alpha_o^2}\right)\sin\left(\overline{\lambda}_{n1}\right) = 0 \tag{4.51}$$

where the variable $\alpha_o = \alpha H$ is a dimensionless parameter which takes values in the range 1.5 to 6 for most of real structures (Miranda and Akkar, 2006). The term $\overline{\lambda}_{n2}$ in equation (4.50) is calculated combining equations (4.45) and (4.51).

By combining equations (4.41) and (4.43) a relation between the fundamental period of the system and higher mode vibration periods can be found as:

$$T_n = T_t \sqrt{\frac{(kH)_t^4}{(kH)_n^4}} \qquad (4.52)$$

where

$$(kH)_n^4 = \bar{\lambda}_{n1}^4 + \bar{\lambda}_{n1}^2 \alpha_o^2 \qquad (4.53)$$

Finally, using modal superposition, the solution to equation (4.36) can be written as:

$$u(x,t) = \sum_{n=1}^{\infty} \gamma_n \varphi_n(x) y_n(t) \approx \sum_{n=1}^{N_m} \gamma_n \varphi_n(x) y_n(t) \qquad (4.54)$$

where N_m is the number of significant modes considered in the analysis and γ_n is the modal participation factor, defined as:

$$\gamma_n = \frac{\int_0^H \varphi_n(x)\,dx}{\int_0^H \left(\varphi_n(x)\right)^2 dx} \qquad (4.55)$$

The n-th modal response $y_n(t)$ can be found by solving the N_m uncoupled damped modal equations of motion:

$$\ddot{y}_n(t) + 2\zeta_n \omega_n \dot{y}_n(t) + \omega_n^2 y_n(t) = -\ddot{u}_g(t) \qquad (4.56)$$

where ζ_n and ω_n are the modal damping and the modal angular vibration frequency, respectively.

4.1.2.2 Estimation of peak absolute accelerations and peak interstory drifts

The following subsections present the methodologies for estimating peak absolute accelerations and peak interstory drifts along height of the building model described in subsection 4.1.2.1 excited by ground motions represented by a ground response spectrum compatible power spectral density function.

4.1.2.2.1 Estimation of peak absolute accelerations

The procedure described in this subsection is an extension of the floor response spectrum (FRS) approach developed by Singh (Singh, 1976) using the structural model described in subsection 4.1.2.1. The objective here is to estimate the mean peak absolute accelerations in the response of a SDOF secondary system attached at any level along the height of the building model. The method described in subsection 4.1.1.1, used here to compute peak absolute acceleration demands, requires knowing the corresponding power

spectral density function. In order to obtain this PSDF, the absolute acceleration $\ddot{u}^T(x,t)$ along the height of the building is first defined as:

$$\ddot{u}^T(x,t) = \frac{\partial^2 u(x,t)}{\partial t^2} + \ddot{u}_g(t) = \sum_{n=1}^{\infty} \gamma_n \varphi_n(x) \ddot{y}_n(t) + \ddot{u}_g(t) \tag{4.57}$$

Equation (4.57) can be simplified by considering a reduced number of significant modes N_m as:

$$\ddot{u}^T(x,t) \approx \sum_{n=1}^{N_m} \gamma_n \varphi_n(x) \ddot{y}_n(t) + \ddot{u}_g(t) \tag{4.58}$$

On the other hand, from equation (4.56):

$$\ddot{y}_n(t) = -\ddot{u}_g(t) - 2\zeta_n \omega_n \dot{y}_n(t) - \omega_n^2 y_n(t) \tag{4.59}$$

Onto substitution of equation (4.59) into equation (4.58):

$$\ddot{u}^T(x,t) \approx -\sum_{n=1}^{N_m} \gamma_n \varphi_n(x) \left[\ddot{u}_g(t) + 2\zeta_n \omega_n \dot{y}_n(t) + \omega_n^2 y_n(t) \right] + \ddot{u}_g(t) \tag{4.60}$$

$$\ddot{u}^T(x,t) \approx \underbrace{\ddot{u}_g(t) \left[1 - \sum_{n=1}^{N_m} \gamma_n \varphi_n(x) \right]}_{f_1(t)} - \underbrace{\sum_{n=1}^{N_m} \gamma_n \varphi_n(x) \left[2\zeta_n \omega_n \dot{y}_n(t) + \omega_n^2 y_n(t) \right]}_{f_2(t)} \tag{4.61}$$

By omitting the dependence on x of the expressions for $\varphi_n(x)$, just to simplify notation, the correlation function for the absolute acceleration process is calculated from:

$$E\left\{ \ddot{u}^T(x,t_1) \ddot{u}^T(x,t_2) \right\} = E\left\{ \left[f_1(t_1) - f_2(t_1) \right] \left[f_1(t_2) - f_2(t_2) \right] \right\} \tag{4.62}$$

$$E\left\{ \ddot{u}^T(x,t_1) \ddot{u}^T(x,t_2) \right\} = E\left\{ f_1(t_1) f_1(t_2) \right\} - E\left\{ f_1(t_1) f_2(t_2) \right\} - E\left\{ f_2(t_1) f_1(t_2) \right\} + E\left\{ f_2(t_1) f_2(t_2) \right\} \tag{4.63}$$

The first term at the right side of equation (4.63) is calculated as:

$$E\left\{ f_1(t_1) f_1(t_2) \right\} = E\left\{ \ddot{u}_g(t_1) \left[1 - \sum_{n=1}^{N_m} \gamma_n \varphi_n \right] \ddot{u}_g(t_2) \left[1 - \sum_{m=1}^{N_m} \gamma_m \varphi_m \right] \right\} \tag{4.64}$$

$$E\left\{ f_1(t_1) f_1(t_2) \right\} = \left[1 - 2\sum_{n=1}^{N_m} \gamma_n \varphi_n + \sum_{n=1}^{N_m} \sum_{m=1}^{N_m} \gamma_n \gamma_m \varphi_n \varphi_m \right] E\left\{ \ddot{u}_g(t_1) \ddot{u}_g(t_2) \right\} \tag{4.65}$$

$$E\left\{ f_1(t_1) f_1(t_2) \right\} = \left[1 - 2\sum_{n=1}^{N_m} \gamma_n \varphi_n + \sum_{n=1}^{N_m} \sum_{m=1}^{N_m} \gamma_n \gamma_m \varphi_n \varphi_m \right] \int_{-\infty}^{\infty} S_{\ddot{u}_g}(\omega) e^{i\omega(t_1 - t_2)} d\omega \tag{4.66}$$

The second term at the right side of equation (4.63) is given by:

$$E\left\{ f_1(t_1) f_2(t_2) \right\} = E\left\{ \ddot{u}_g(t_1) \left[1 - \sum_{n=1}^{N_m} \gamma_n \varphi_n \right] \left[\sum_{m=1}^{N_m} \gamma_m \varphi_m \left[2\zeta_m \omega_m \dot{y}_m(t_2) + \omega_m^2 y_m(t_2) \right] \right] \right\} \tag{4.67}$$

96

$$E\left\{f_1(t_1)f_2(t_2)\right\} = E\left\{\ddot{u}_g(t_1)\sum_{n=1}^{N_m}\gamma_n\varphi_n\left[2\zeta_n\omega_n\dot{y}_n(t_2)+\omega_n^2 y_n(t_2)\right]\right\}+\cdots$$

$$\cdots-E\left\{\ddot{u}_g(t_1)\sum_{n=1}^{N_m}\sum_{m=1}^{N_m}\gamma_n\gamma_m\varphi_n\varphi_m\left[2\zeta_m\omega_m\dot{y}_m(t_2)+\omega_m^2 y_m(t_2)\right]\right\} \tag{4.68}$$

where the first term in $E\left\{f_1(t_1)f_2(t_2)\right\}$, equation (4.68), is given by:

$$E\left\{\ddot{u}_g(t_1)\sum_{n=1}^{N_m}\gamma_n\varphi_n\left[2\zeta_n\omega_n\dot{y}_n(t_2)+\omega_n^2 y_n(t_2)\right]\right\}=\begin{cases}2E\left\{\ddot{u}_g(t_1)\sum_{n=1}^{N_m}\gamma_n\varphi_n\zeta_n\omega_n\dot{y}_n(t_2)\right\}+\cdots\\[2ex]\cdots+E\left\{\ddot{u}_g(t_1)\sum_{n=1}^{N_m}\gamma_n\varphi_n\omega_n^2 y_n(t_2)\right\}\end{cases} \tag{4.69}$$

where

$$2E\left\{\ddot{u}_g(t_1)\sum_{n=1}^{N_m}\gamma_n\varphi_n\zeta_n\omega_n\dot{y}_n(t_2)\right\}=2\sum_{n=1}^{N_m}\gamma_n\varphi_n\zeta_n\omega_n\int_{-\infty}^{\infty}i\omega S_{\ddot{u}_g}(\omega)H_n(\omega)e^{i\omega(t_1-t_2)}d\omega \tag{4.70}$$

and

$$E\left\{\ddot{u}_g(t_1)\sum_{n=1}^{N_m}\gamma_n\varphi_n\omega_n^2 y_n(t_2)\right\}=\sum_{n=1}^{N_m}\gamma_n\varphi_n\omega_n^2\int_{-\infty}^{\infty}S_{\ddot{u}_g}(\omega)H_n(\omega)e^{i\omega(t_1-t_2)}d\omega \tag{4.71}$$

In equations (4.70) and (4.71) the term $H_n(\omega)$ corresponds to the n-th modal complex frequency response function, and is given by:

$$H_n(\omega)=\left(\omega_n^2-\omega^2+2i\zeta_n\omega\omega_n\right)^{-1} \tag{4.72}$$

The second term in $E\left\{f_1(t_1)f_2(t_2)\right\}$, equation (4.68), is given by:

$$E\left\{\ddot{u}_g(t_1)\sum_{n=1}^{N_m}\sum_{m=1}^{N_m}\gamma_n\gamma_m\varphi_n\varphi_m\left[2\zeta_m\omega_m\dot{y}_m(t_2)+\omega_m^2 y_m(t_2)\right]\right\}=2E\left\{\ddot{u}_g(t_1)\sum_{n=1}^{N_m}\sum_{m=1}^{N_m}\gamma_n\gamma_m\varphi_n\varphi_m\zeta_m\omega_m\dot{y}_m(t_2)\right\}+$$

$$\cdots+E\left\{\ddot{u}_g(t_1)\sum_{n=1}^{N_m}\sum_{m=1}^{N_m}\gamma_n\gamma_m\varphi_n\varphi_m\omega_m^2 y_m(t_2)\right\} \tag{4.73}$$

where

$$E\left\{\ddot{u}_g(t_1)\sum_{n=1}^{N_m}\sum_{m=1}^{N_m}\gamma_n\gamma_m\varphi_n\varphi_m\zeta_m\omega_m\dot{y}_m(t_2)\right\}=\sum_{n=1}^{N_m}\sum_{m=1}^{N_m}\gamma_n\gamma_m\varphi_n\varphi_m\zeta_m\omega_m\int_{-\infty}^{\infty}i\omega S_{\ddot{u}_g}(\omega)H_n(\omega)e^{i\omega(t_1-t_2)}d\omega \tag{4.74}$$

and

$$E\left\{\ddot{u}_g(t_1)\sum_{n=1}^{N_m}\sum_{m=1}^{N_m}\gamma_n\gamma_m\varphi_n\varphi_m\omega_m^2 y_m(t_2)\right\}=\sum_{n=1}^{N_m}\sum_{m=1}^{N_m}\gamma_n\gamma_m\varphi_n\varphi_m\omega_m^2\int_{-\infty}^{\infty}S_{\ddot{u}_g}(\omega)H_n(\omega)e^{i\omega(t_1-t_2)}d\omega \tag{4.75}$$

The third term at the right side of equation (4.63) is given by:

$$E\left\{f_2(t_1)f_1(t_2)\right\}=E\left\{f_1(t_1)f_2(t_2)\right\} \tag{4.76}$$

The result shown in equation (4.76) arises directly from the property of symmetry of correlation matrices. The fourth term in equation (4.63) is given by Singh (Singh, 1976):

$$E\left\{f_2(t_1)f_2(t_2)\right\}=\sum_{n=1}^{N_m}\sum_{m=1}^{N_m}\gamma_n\gamma_m\varphi_n\varphi_m\omega_n\omega_m\left[\omega_n\omega_m+4\zeta_n\zeta_m+2i\omega(\omega_m\zeta_n-\omega_n\zeta_m)\right]\int_{-\infty}^{\infty}S_{\ddot{u}_g}(\omega)H_n(\omega)H_m^*(\omega)e^{i\omega(t_1-t_2)}d\omega \tag{4.77}$$

Finally, merging the results in equations (4.66), (4.70), (4.71), (4.74), (4.75) and (4.77), the power spectral density function for the absolute acceleration along the height of the building model is obtained as:

$$S_{\ddot{u}^T}(x,\omega)=\begin{cases}S_{\ddot{u}_g}(\omega)-2S_{\ddot{u}_g}(\omega)\sum_{n=1}^{N_m}\gamma_n\varphi_n(x)\left[1+H_n(\omega)\left(\omega_n^2+2i\zeta_n\omega\omega_n\right)\right]+\cdots\\[2mm] S_{\ddot{u}_g}(\omega)\sum_{n=1}^{N_m}\sum_{m=1}^{N_m}\gamma_n\gamma_m\varphi_n(x)\varphi_m(x)\left[1-2H_n(\omega)\left(\omega_n^2+2i\zeta_n\omega\omega_n\right)\right]+\cdots\\[2mm] \sum_{n=1}^{N_m}\sum_{m=1}^{N_m}\gamma_n\gamma_m\varphi_n(x)\varphi_m(x)\omega_n\omega_m\left[\omega_n\omega_m+4\zeta_n\zeta_m+2i\omega(\omega_m\zeta_n-\omega_n\zeta_m)\right]S_{\ddot{u}_g}(\omega)H_n(\omega)H_m^*(\omega)\end{cases} \tag{4.78}$$

Equation (4.78) corresponds to the PSDF for the absolute accelerations along the height of the building model. The PSDF for the absolute acceleration response of a secondary component modeled as a SDOF system, attached at a single point located at a height h, arbitrary along the height of the building, and that does not interact dynamically with the primary system (cascade approach), is given by (Singh, 1976):

$$S_{\ddot{u}_s^T}(h,\omega,\omega_s)=S_{\ddot{u}^T}(h,\omega)\left(4\zeta_s^2\omega_s^2\omega^2+\omega_s^4\right)H_s(\omega)H_s^*(\omega) \tag{4.79}$$

where ζ_s and ω_s are the damping ratio and the natural angular vibration frequency of the secondary component, respectively, and $H_s(\omega)$ is the frequency response function for the secondary component, given by:

$$H_s(\omega)=\left(\omega_s^2-\omega^2+2i\zeta_s\omega\omega_s\right)^{-1} \tag{4.80}$$

Finally, using the principles described in subsection 4.1.1.1, the mean peak absolute acceleration demands acting on acceleration sensitive components with different dynamic properties and located at different heights along a building can be found.

4.1.2.2.2 Estimation of peak generalized drifts

The theory of generalized drift considered herein is based on the concept originally proposed by Iwan (Iwan, 1997) and recently extended and discussed by Miranda and Akkar (Miranda and Akkar, 2006), Chopra and Chintanapakdee (Chopra and Chintanapakdee, 2001), Akkar et al. (Akkar *et al.*, 2005), Kim and Collins (Kim and Collins, 2002), Kim et al. (Kim *et al.*, 2006), and Nicholson and Bergman (Nicholson and Bergman, 1986), among other researchers. The generalized drift concept provides an estimation of the distortion expected along the height of a building during strong motion. The concept is particularly suitable for building systems modeled as continuum beams. In this research, the original concept has been extended for use with the shear-flexure beam model in combination with the stochastic method for estimating peak distortions along the building height. The generalized drift $\theta(x,t)$ along the height of the beam model is defined as:

$$\theta(x,t) = \frac{\partial u(x,t)}{\partial x} = \sum_{n=1}^{\infty} \gamma_n \frac{d\varphi_n(x)}{dx} y_n(t) \approx \sum_{n=1}^{N_m} \gamma_n \frac{d\varphi_n(x)}{dx} y_n(t) \tag{4.81}$$

In equation (4.81) the term $\dfrac{d\varphi_n(x)}{dx}$ is obtained after derivation of equation (4.50) as:

$$\frac{d\varphi_n(x)}{dx} = \frac{\bar{\lambda}_{n}}{H}\left\{ sin\left(\frac{\bar{\lambda}_{n}x}{H}\right) + \frac{\bar{\lambda}_{n2}}{\bar{\lambda}_{n1}} sinh\left(\frac{\bar{\lambda}_{n2}x}{H}\right) + \frac{cos\left(\bar{\lambda}_{n1}\right) + \frac{\bar{\lambda}_{n2}^2}{\bar{\lambda}_{n1}^2} cosh\left(\bar{\lambda}_{n2}\right)}{sin\left(\bar{\lambda}_{n1}\right) + \frac{\bar{\lambda}_{n2}}{\bar{\lambda}_{n1}} sinh\left(\bar{\lambda}_{n2}\right)} \left[cos\left(\frac{\bar{\lambda}_{n1}x}{H}\right) + cosh\left(\frac{\bar{\lambda}_{n2}x}{H}\right) \right] \right\} \tag{4.82}$$

For estimating the mean peak generalized drift spectrum by using the method described in subsection 4.1.1.1, the power spectral density function for the generalized drifts is required. The PSDF for generalized drifts along the height of the building model are calculated as:

$$E\{\theta(x,t_1)\theta(x,t_2)\} = E\left\{ \sum_{n=1}^{N_m} \gamma_n \frac{d\varphi_n(x)}{dx} y_n(t_1) \sum_{m=1}^{N_m} \gamma_m \frac{d\varphi_m(x)}{dx} y_m(t_2) \right\} \tag{4.83}$$

$$E\{\theta(x,t_1)\theta(x,t_2)\} = E\left\{ \sum_{n=1}^{N_m} \sum_{m=1}^{N_m} \gamma_n \gamma_m \frac{d\varphi_n}{dx}(x) \frac{d\varphi_m}{dx}(x) y_n(t_1) y_m(t_2) \right\} \tag{4.84}$$

$$E\{\theta(x,t_1)\theta(x,t_2)\} = \sum_{n=1}^{N_m} \sum_{m=1}^{N_m} \gamma_n \gamma_m \varphi_n'(x) \varphi_m'(x) \int_{-\infty}^{\infty} S_{\ddot{u}_g}(\omega) H_n(\omega) H_m^*(\omega) e^{i\omega(t_1-t_2)} d\omega \tag{4.85}$$

The PSDF for generalized drift along the height of the building $S_\theta(x,\omega)$ can be obtained from:

$$S_\theta(x,\omega) = S_{\ddot{u}_g}(\omega) \sum_{n=1}^{N_m} \sum_{m=1}^{N_m} \gamma_n \gamma_m \frac{d\varphi_n}{dx}(x) \frac{d\varphi_m}{dx}(x) H_n(\omega) H_m^*(\omega) \tag{4.86}$$

Finally, using the methodology described in subsection 4.1.1.1, the mean peak drift demands acting on displacement sensitive components can be found.

4.2 Estimation of seismic demands on nonstructural components along building height

The continuous beam model presented in subsection 4.1.2 was considered to model a generic multistory building and to describe the seismic loading path traveling from the ground to both acceleration and displacement sensitive nonstructural components. The input ground motion was characterized by a Power Spectral Density Function (PSDF) compatible with the USGS Uniform Seismic Hazard (USH). The USH is considered here to account for the aggregated local seismic hazard and generating a broadband PSDF, consistent with the seismic hazard defined by current code provisions. Considering a modal event, in combination with the Specific Barrier Model (SBM), would be more suitable for estimating a narrow band PSDF, associated to near fault excitations, which are not directly considered in current code provisions.

For the analysis presented here, a USH with a Probability of Exceedance (PE) of 10% in 50 years for the city of Northridge, California, was selected. The input/output relations for the combined primary/secondary system derived in subsection 4.1.2.2 are used to compute the PSDF for the secondary system demands. The principles presented in subsection 4.1.1.1 are used to estimate the mean peak seismic demands expected on nonstructural components.

In the estimation of seismic demands, a Seismic Hazard (SH) with PE of 10% in 50 years is considered representative of broadband ground motion excitations typically observed in fault parallel components of strong ground motion records. This approach is consistent with that used by Krawinkler et al. (Krawinkler *et al.*, 2000).

4.2.1 Characterization of seismic hazard

For the estimation of seismic demands representative of relatively short return periods, a seismic hazard with a probability of exceedance of 10% in 50 years for a rock site (site class B according to ASCE 7-05) in the city of Northridge (longitude 118.518 W, latitude 34.237 N), obtained from the USGS website[6], was considered. This city is chosen as representative of a largely populated high seismicity urban area (Wanitkorkul and Filiatrault, 2005). Other site locations will be considered later to evaluate more general seismic demands. Table 4.1 shows the events with contributions larger than 1% to the disaggregated SH

---

for a PE of 10% in 50 years. Figure 4.3 shows all pairs R-M_w (source to site distance-moment magnitude) contributing to the local SH (with contributions up to 0.05%).

Table 4.1. Disaggregated SH for City of Northridge (Only contributions up to 1%)

Source-to-Site Distance R (km)	Moment Magnitude M_w	Contribution to Local SH (%)
7.6	6.48	13.3
7.9	**6.64**	**51.7**
11.7	6.65	2.06
7.9	6.85	21.0
11.0	6.84	1.45
7.7	7.05	4.48

In Table 4.1 it can be seen that the modal event, the event with the higher contribution to the local SH (Kramer, 1996), is an earthquake with a moment magnitude M_w^* =6.64 occurring at a distance R^* =7.9 km from the selected site. This event is identified to occur along the Santa Susana fault and controls the deterministic local seismic hazard (DLSH). This modal event is used along with equation (4.11) to estimate the duration of the ground motion process.
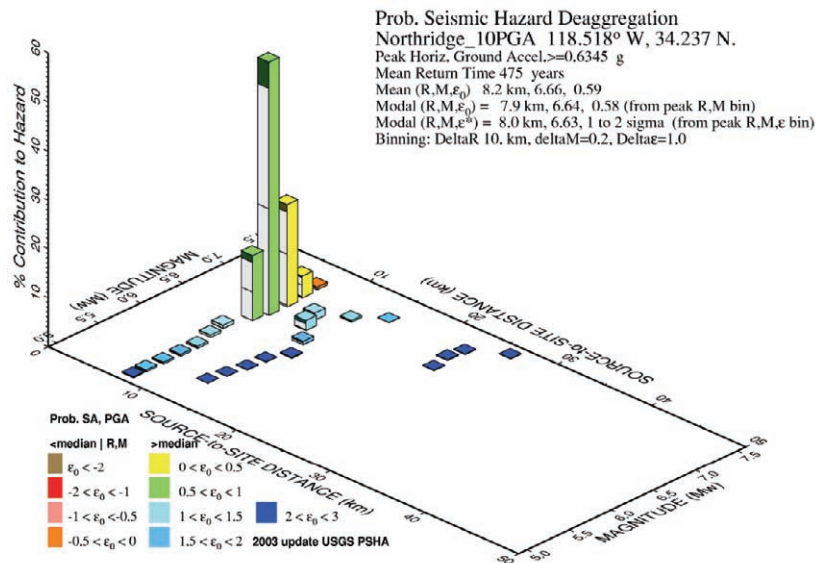
Figure 4.3. Probabilistic seismic hazard with a probability of exceedance of 10%/50yrs for the City of Northridge (From USGS interactive disaggregation website, 2002)

Table 4.2 shows the USGS-USH ground acceleration response spectra coordinates for a SH with a PE of 10% in 50 years. Those values, plotted in Figure 4.4, account for the aggregated probabilistic local seismic hazard (PLSH) in the site under study. In order to apply the random vibration theory presented in subsection 4.1.1, the USH ground acceleration compatible PSDF is required. Before applying equation

(4.32), the USGS-USH ground response spectrum data is interpolated using the following spectral shape function:

$$S_a(T) = \frac{A_o}{1 + \dfrac{T}{0.1T_o + \dfrac{T}{R}}} \frac{1 + 4.5\left(\dfrac{T}{T_o}\right)^p}{1 + \left(\dfrac{T}{T_o}\right)^q} \tag{4.87}$$

where A_o represents the peak ground acceleration (PGA), T_o is the period at peak spectral acceleration (T_o =0.2 seconds in this case), and the parameters R, p and q are estimated using best fit techniques. Table 4.3 summarizes the mean values for the best fit coefficients calculated considering 95% confidence bounds. The interpolated acceleration spectrum best fitting the USGS seismic hazard is also shown in Figure 4.4.

Table 4.2. USGS-UHS spectral acceleration amplitudes for a SH with PE 10%/50yrs

Period T (sec)	Spectral Amplitude (g)
0.0	0.63
0.1	1.22
0.2	1.51
0.3	1.34
0.5	0.96
1.0	0.50
2.0	0.22

Table 4.3. Best fit parameters for USGS-USH ground response acceleration spectrum

Parameter	Best Fit Value
A_o	0.63g
T_o	0.2 sec
R	0.160
p	1.472
q	2.471

Upon calculation of the interpolated (best fit) continuous USGS-USH ground acceleration response spectrum, the procedure described in subsection 4.1.1.2 and given by equation (4.32) is used to estimate the corresponding hazard compatible ground acceleration PSDF. Figure 4.5 shows the PSDF's obtained from the USGS-USH that will be used as input for the upcoming calculations of seismic demands acting on nonstructural components within buildings.

4.2.2 Building model

The continuous flexural-shear building model described in subsection 4.1.2.1 and shown in Figure 4.2 has been considered for estimating the seismic demands expected in acceleration and displacement sensitive nonstructural systems located at different elevations of a generic building. Three values for the parameter α_o controlling the deformation pattern of the building, α_o = 0, 5 and 10, have been selected to perform the seismic demand analysis. Figure 4.6 compares the modal shapes governing the deformation patterns

for the flexural-shear beam (for the case $\alpha_o = 10$), the pure flexural beam ($\alpha_o = 0$), and the pure shear beam ($\alpha_o = \infty$).
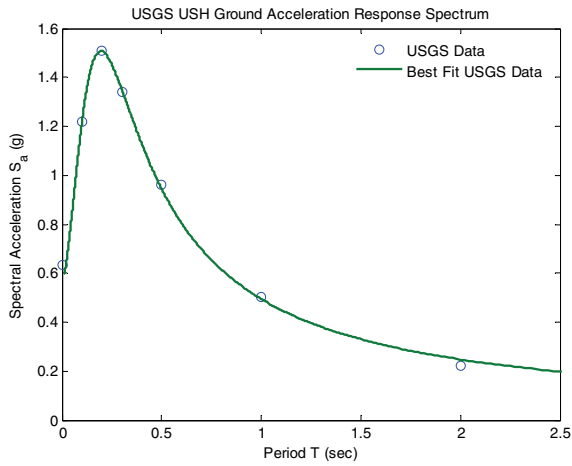
Figure 4.4. USGS USH ground acceleration response spectrum
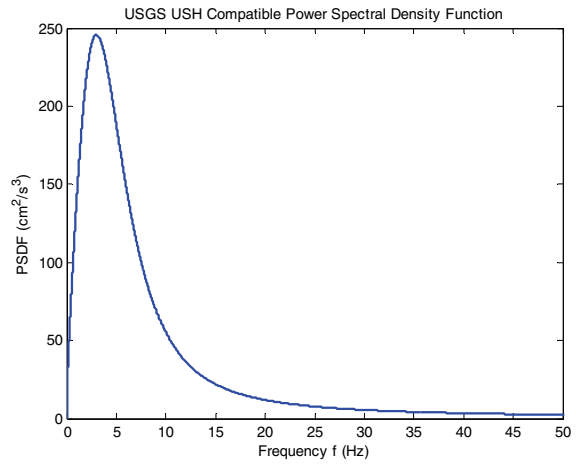
Figure 4.5. USGS USH ground acceleration response spectrum compatible PSDF
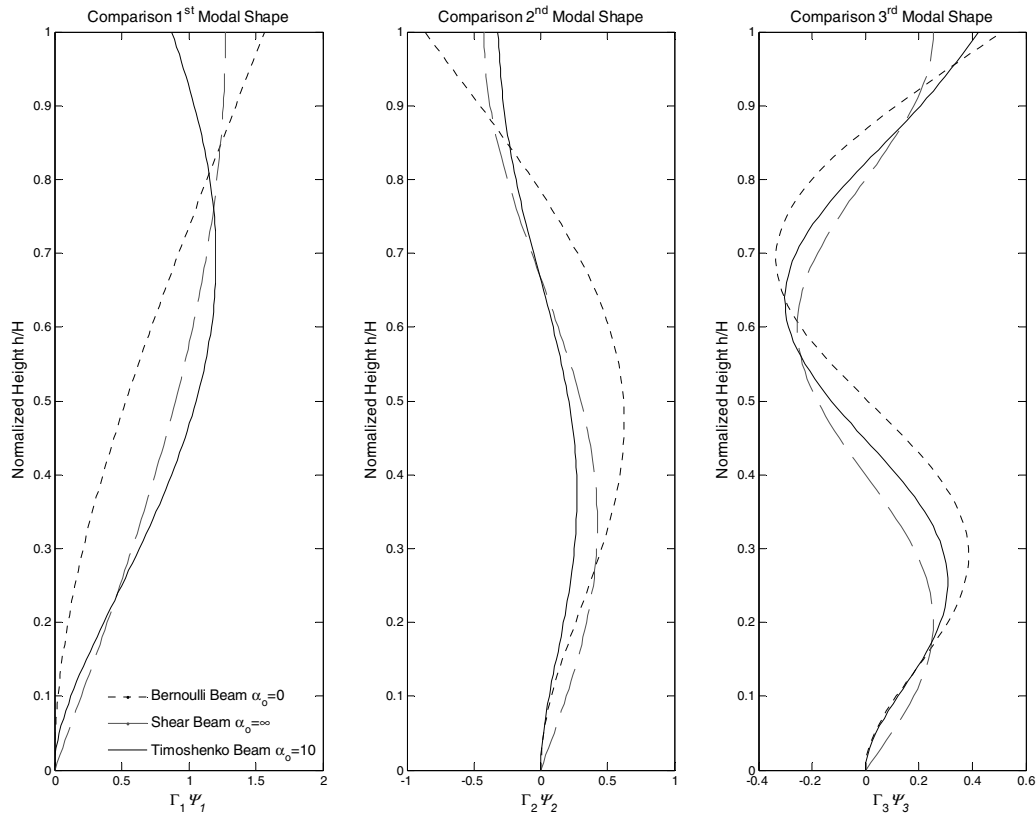
Figure 4.6. Comparison of modal shapes for the flexural-shear beam ($\alpha_o = 10$), the pure flexural (Bernoulli) beam ($\alpha_o = 0$), and the pure shear beam ($\alpha_o = \infty$).

4.2.3   Estimation of absolute acceleration demands

The procedure summarized in subsection 4.1.2.2.1 is used to estimate: i) the PSDF of absolute accelerations along the height of the building model, and ii) the PSDF for absolute acceleration responses of acceleration-sensitive secondary systems attached at a single level (single point) along the height of the building. A "cascade" type approach was intrinsically considered in equations presented in subsection 4.1.2.2.1, neglecting dynamic interactions between primary and secondary systems. That assumption is valid for estimating the seismic demands acting on relatively light nonstructural components and equipment, which is the case of the nonstructural components and systems that can be tested using the UB-NCS. The first ten vibration modes ($N_m = 10$) of the primary system were considered in the computation of the secondary system's mean peak acceleration responses.

Figure 4.7 shows the three dimensional absolute acceleration floor response spectra (3D FRS'), obtained for the case $\alpha_o = 5$, for primary systems with fundamental vibration periods T_p ranging between 0 and 5 seconds and SDOF secondary systems with vibration periods T_s ranging also between 0 and 5 seconds. The 3D FRS' are shown at 10 specific levels along the height of the building. The graph shown in the upper left corner of Figure 4.7 for the ground level corresponds to the three dimensional representation of the interpolated USGS-USH ground response spectra shown in Figure 4.4.

Similar 3D FRS's are obtained for the other α_o's considered in the analysis, as shown in Figure 4.8. In Figure 4.7 and Figure 4.8 it can be seen that the peak response accelerations of secondary components increase from grade to the building roof level. Significant amplification effects are also evident for secondary systems with natural vibration periods coupled either with the natural period of the primary system or the dominant period of the ground motion. Effects of amplification due to coupling with ground period are significant for peak acceleration observed on systems placed at the bottom third of the building. At higher elevations, the maximum acceleration amplifications are observed for secondary systems with periods similar to the primary system. The peak maximum amplitudes are observed for the cases in which both primary and secondary systems have simultaneously natural periods in the range of the dominant ground motion period. In those cases the acceleration in the secondary system can reach a maximum peak value approximately 23 times the peak ground acceleration.
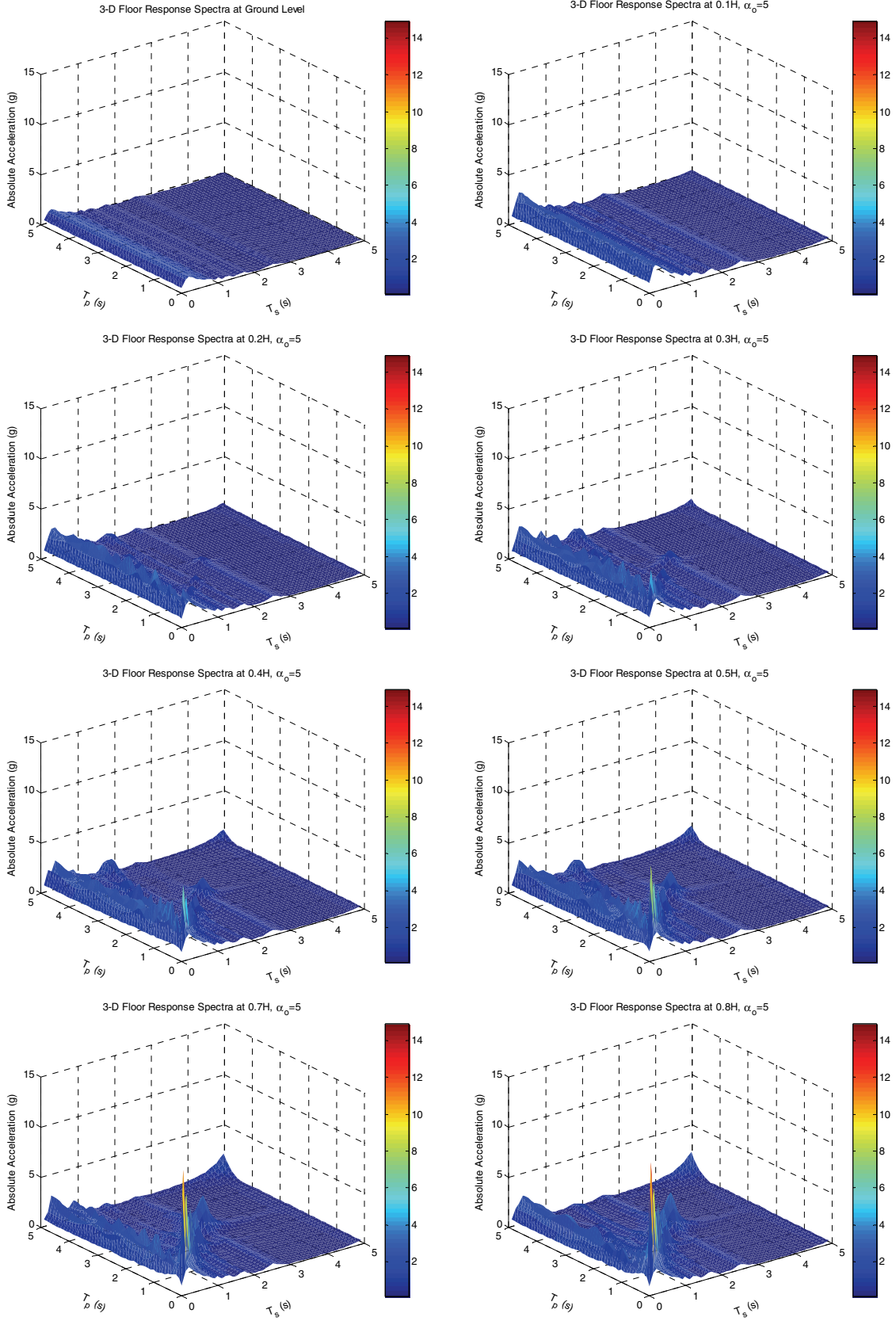
Figure 4.7. Three dimensional absolute acceleration floor responses spectra for α_o=5
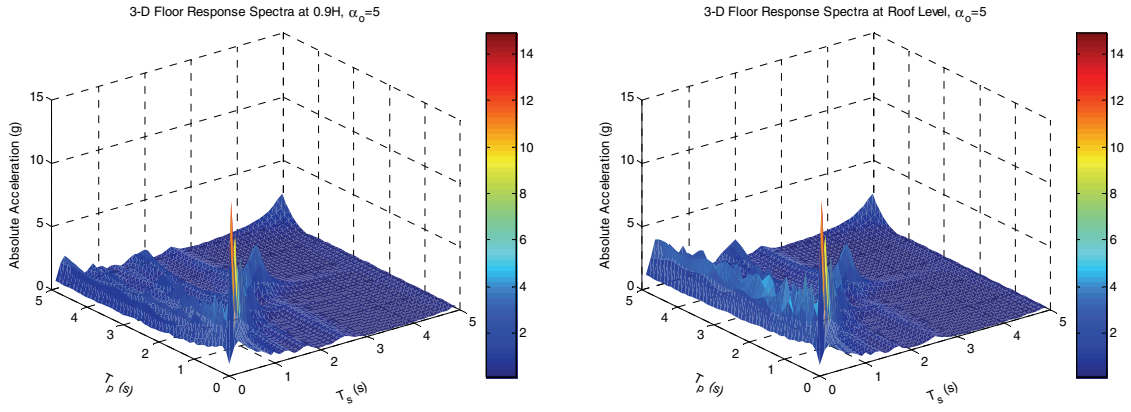
Figure 4.7. Three dimensional absolute acceleration floor responses spectra for α_o=5 (Cont'd)
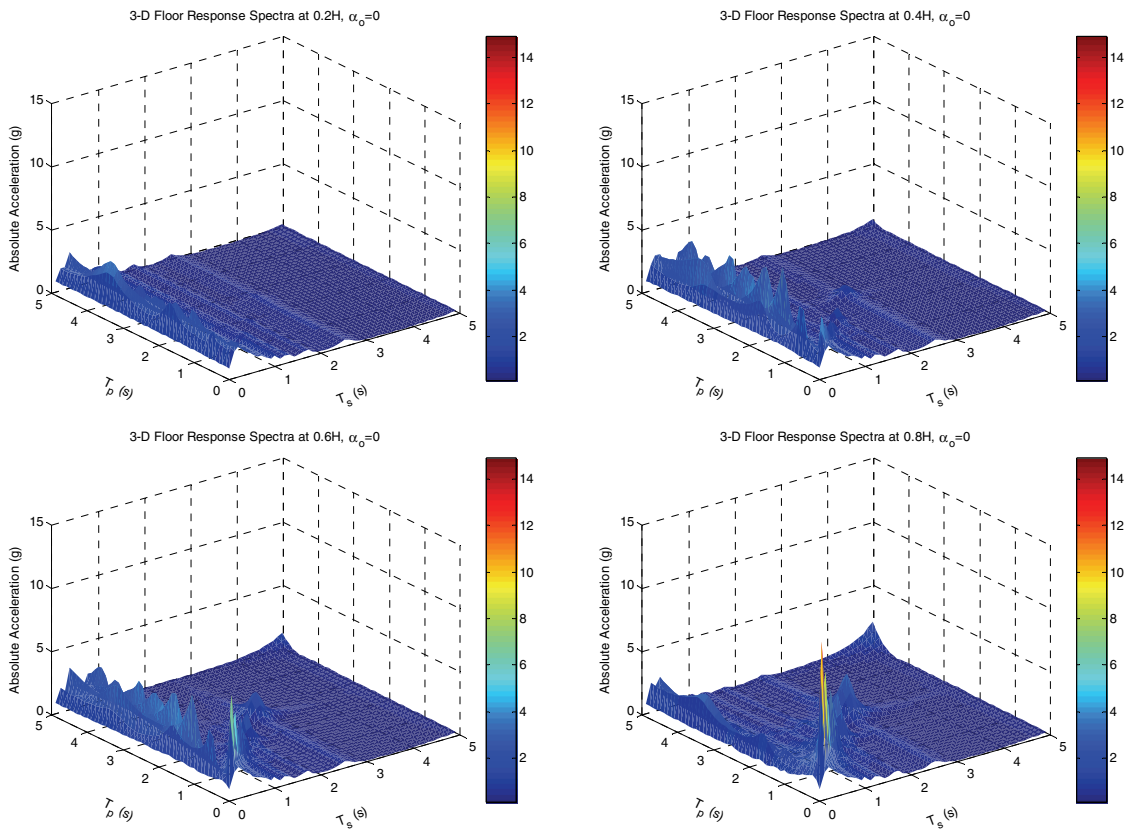
Figure 4.8. Three dimensional absolute acceleration floor response spectra for α_o=0 and α_o=10
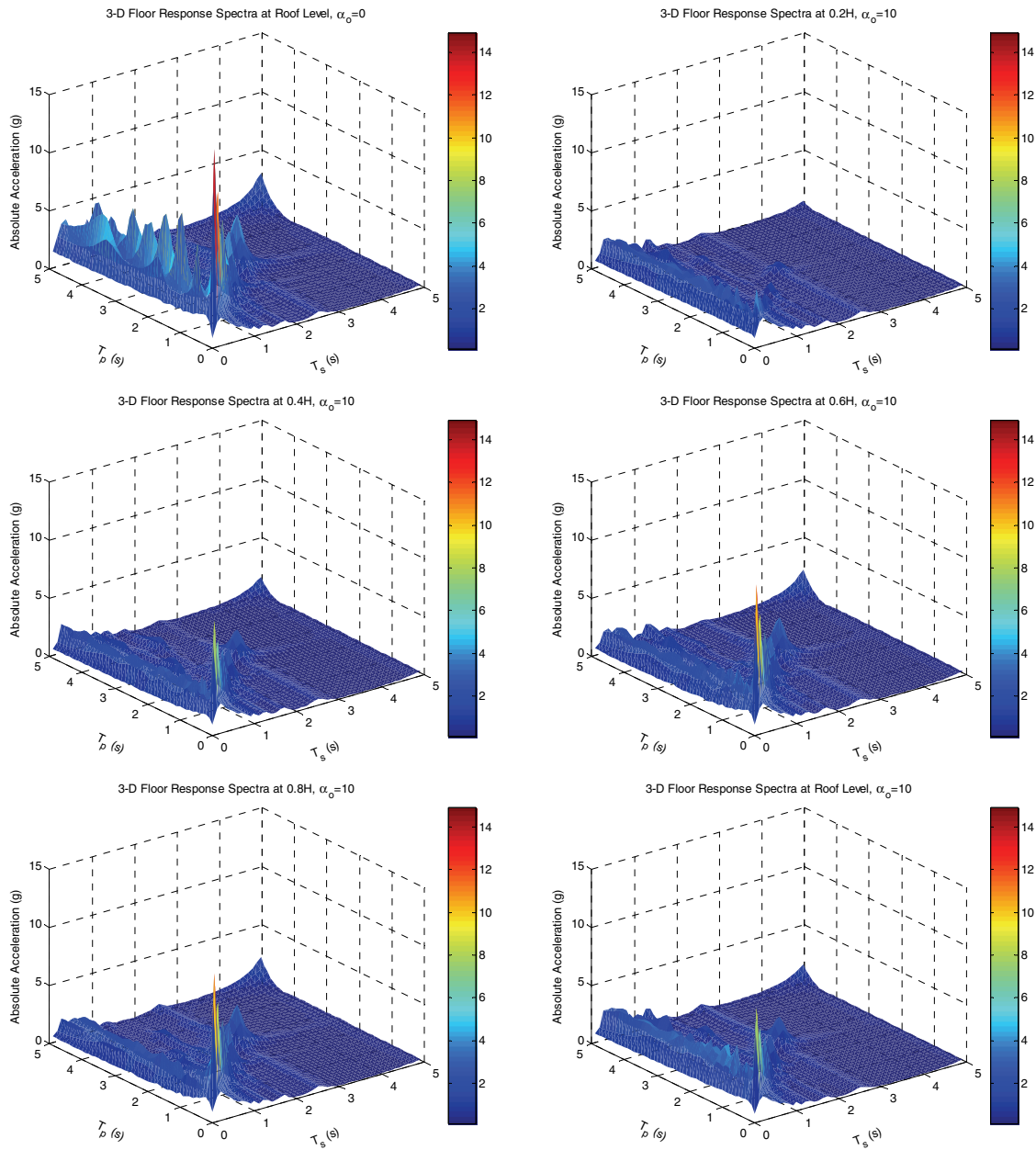
Figure 4.8. Three dimensional absolute acceleration floor response spectra for α_o=0 and α_o=10 (Cont'd)

The data shown in Figure 4.7 and Figure 4.8 have been statistically processed to be used in general testing protocols capable of subjecting nonstructural systems, to conservative but realistic hazard compatible seismic demands. The resulting demands are independent of building deformation patterns, seismic resistant system and primary system fundamental vibration period. The dependency of demands on normalized building height within a multistory building is considered.

The peak absolute accelerations shown in the three dimensional response spectra in Figure 4.7 and Figure 4.8 were further processed to get a single absolute acceleration response spectrum for each building height. In order to do so, the period of the secondary system T_s and its location along the building height h were kept variable and statistic analysis was performed over the entire range of primary system fundamental periods T_p considered in the parametric analysis. Figure 4.9 shows the 84th percentile acceleration response spectra for the secondary system obtained from the statistical analysis of buildings with several deformation patterns (α_o = 0, 5 and 10).
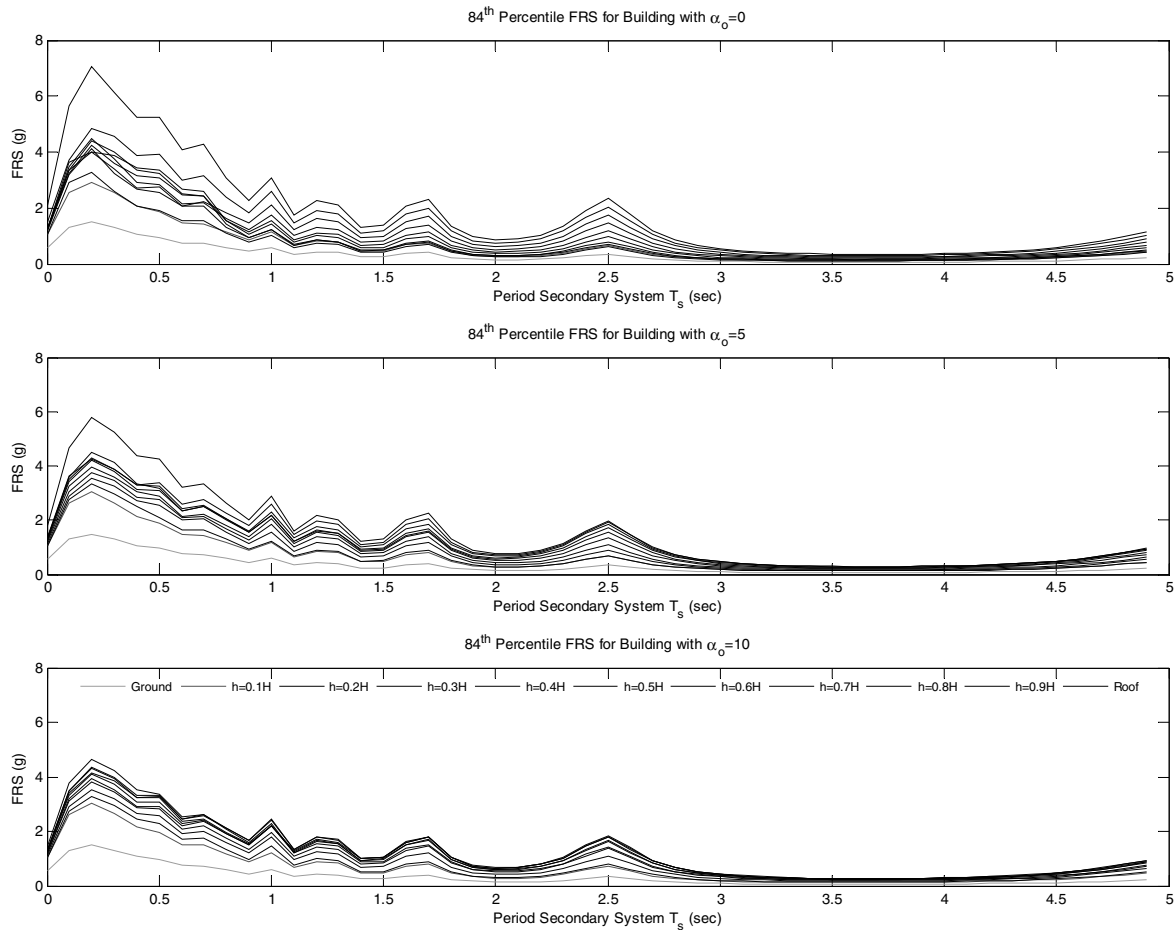
Figure 4.9. 84th Percentile FRS along height of buildings with several deformation patterns

Data presented in Figure 4.9 has been further processed to get the mean, over all α_o values considered in the analysis, 84th percentile spectral acceleration demands, as shown in Figure 4.10. In Figure 4.10, the amplification of spectral acceleration demands along the building height can be observed. Figure 4.11 shows the ratios of the mean 84th % FRS's along the height of the building to the ground response spectrum.
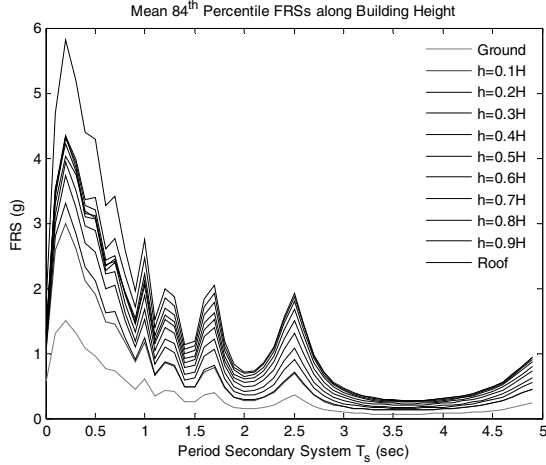
Figure 4.10. Mean 84th percentile FRS along building height
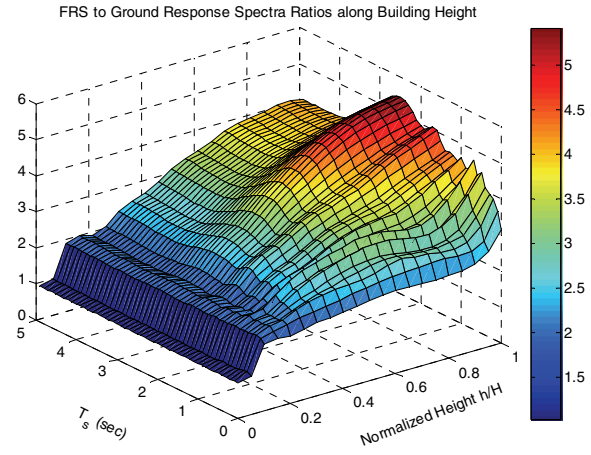
Figure 4.11. FRS to ground response spectrum ratios along building height

Figure 4.12 shows the variation of the ratios of the peak values of the mean 84th % FRS's to the peak value of the ground response spectrum along the building height. Given that the peak spectral responses are, in all cases, observed at a secondary system period $T_s = 0.2$ sec, the data presented in Figure 4.12 is equivalent to a profile of Figure 4.11 at a period $T_s = 0.2$ sec. Using best fit techniques, a function $FRS_{Factor}(h/H)$ interpolating the data presented in Figure 4.12 is used to extrapolate the ground response spectrum, matching the peak values of the mean 84th % FRS's along the height of the building model. The function $FRS_{Factor}(h/H)$ reflects the amplification effects of ground acceleration along the building height. The obtained best fit curve is given by:

$$FRS_{Factor}\left(\frac{h}{H}\right) = 1 + 10\frac{h}{H} - 19.4\left(\frac{h}{H}\right)^2 + 12.4\left(\frac{h}{H}\right)^3 \qquad (4.88)$$

The extrapolated mean 84th percentile floor response spectrum along the building height, shown in Figure 4.13, is calculated using:

$$FRS\left(T_s, \xi, \frac{h}{H}\right) = FRS_{Factor}\left(\frac{h}{H}\right)S_a\left(T_s, \xi\right) \qquad (4.89)$$

where $S_a(T_s, \xi)$ denotes the ground response spectrum calculated, in this case, using equation (4.87).

Figure 4.14 shows a comparison between the mean 84th percentile FRS's estimated using the continuous beam model in combination with principles of RVT, the smoothened (extrapolated) mean 84th percentile FRS's estimated according to equations (4.87), (4.88) and (4.89), the AC156 (ICC-ES, 2007) testing protocol floor response spectra, currently used for seismic qualification of equipment, and the floor

response spectrum recommended in FEMA450 (BSSC, 2003a) for the site under study. Upper and lower limits of AC156 and FEMA450 floor response spectra are not included in the plots.
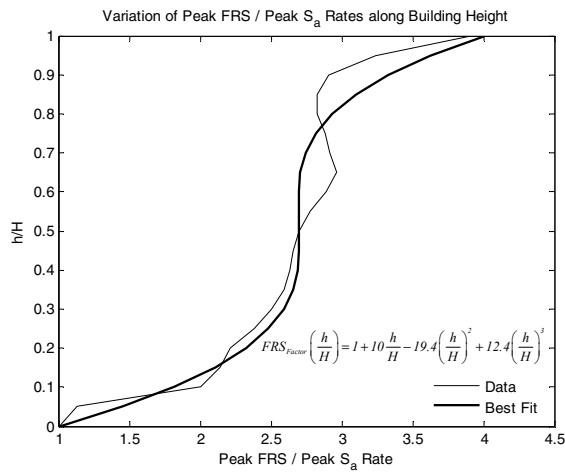
Figure 4.12. Variation of peak FRS's to peak ground response spectrum values along building height
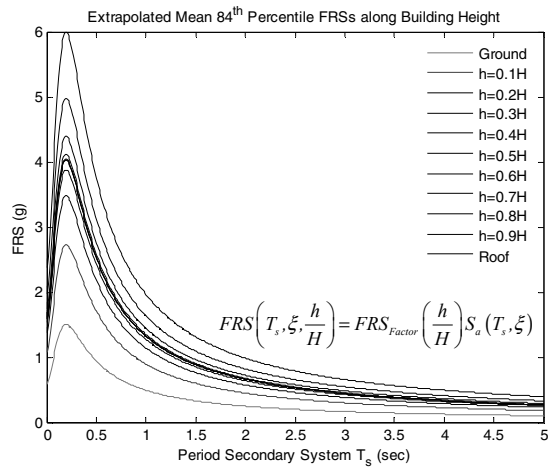
Figure 4.13. Extrapolated (smoothened) mean 84th % FRS along building height
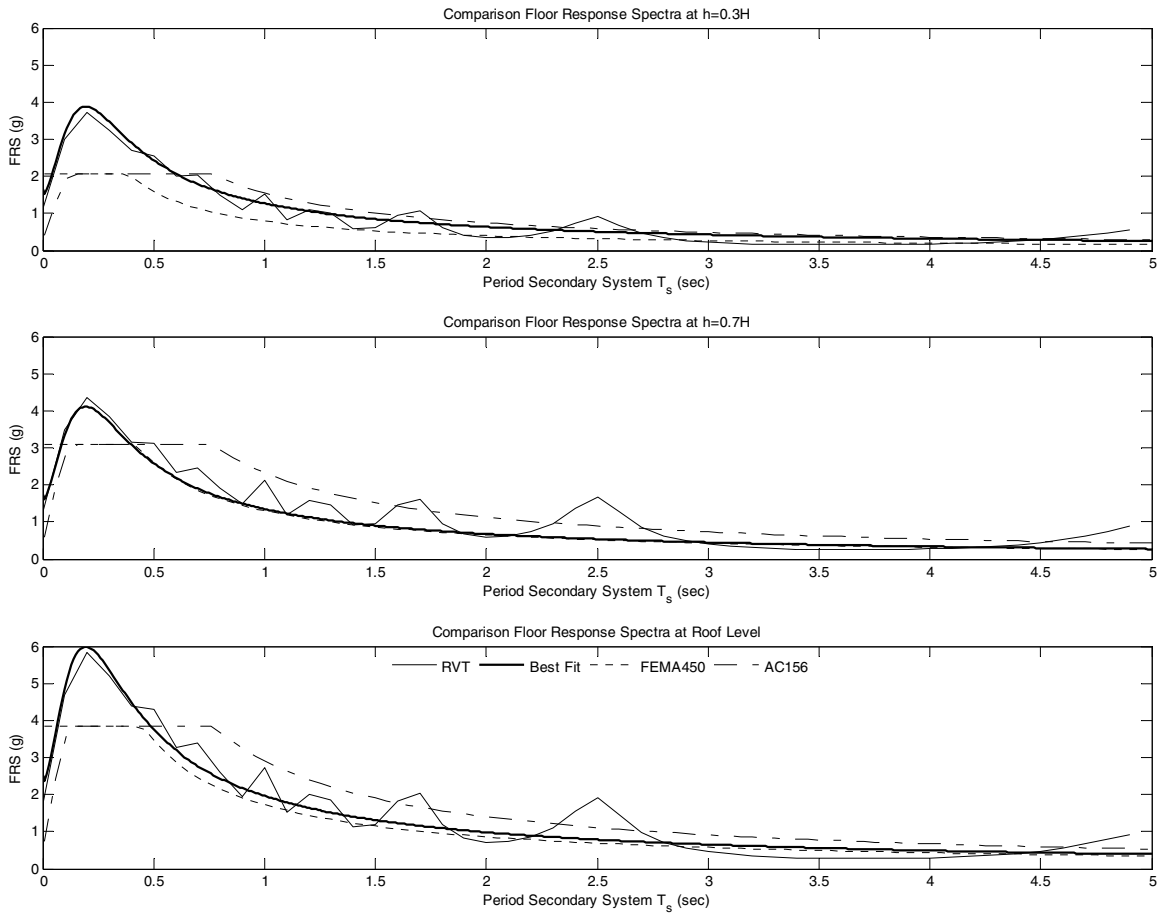
Figure 4.14. Comparison FRS's at several building levels

In Figure 4.14, it can be seen that the extrapolated mean 84th percentile FRS properly smoothes and matches the random vibration theory results. Furthermore, the extrapolated FRS's closely match the FEMA450 spectra at the uppermost building levels, for periods greater than 0.4 sec. For periods smaller than 0.4 sec, the RVT (random vibration theory) and extrapolated spectrum based on equation (4.89) overestimate the AC156 and FEMA450 floor response spectra since the latter two consider inelastic building response. The AC156 floor response spectrum seems to be the most conservative spectrum for periods greater than 0.7 seconds.

4.2.4   Estimation of generalized drift demands

Using the procedure described in subsection 4.1.2.2.2, the PSDF for generalized drifts has been calculated. The first $N_m = 10$ vibration modes of the continuous beam model were considered in those calculations. Buildings with deformation patterns defined by parameters $\alpha_o = 0$, 5 and 10 were considered. Using the procedure described in subsection 4.1.1.1 the peak generalized drifts, or simply the Generalized Drift Spectrum (GDS), were calculated for buildings with fundamental periods T_p ranging between 0 and 5 seconds. In order to apply equation (4.82) it is necessary to find a relation between the total height H of the building and its fundamental vibration period T_p. The T_p-H relation used to calculate the GDS was derived from the following relations proposed by Chopra and Goel (Chopra and Goel, 2000):

$$T_{SMRF} = 0.035H^{0.8}$$ (4.90)

$$T_{CMRF} = 0.018H^{0.9}$$ (4.91)

$$T_{RCSW} = \frac{0.0023}{\sqrt{\overline{A}_e}}H$$ (4.92)

where T_{SMRF}, T_{CMRF} and T_{RCSW} are the fundamental vibration periods of steel moment resisting frames (SMRF), concrete moment resisting frames (CMRF), and reinforced concrete shear wall buildings (RCSW), respectively. H (in ft) is the total height of the building and $\overline{A}_e$, the equivalent shear area, is calculated as a percentage of the building plan area A_B as:

$$\overline{A}_e = \frac{100}{A_B}\sum_{i=1}^{N_w}\left(\frac{H}{H_i}\right)^2\frac{A_i}{1+0.83\left(\frac{H_i}{D_i}\right)^2}$$ (4.93)

where A_i, H_i and D_i are the area, height, and dimension of the ith shear wall, respectively; and N_w is the total number of shear walls. The empirical formulas given by equations (4.90), (4.91) and (4.92) were estimated by Chopra and Goel through best fit regression analysis of the data recorded in 42 SMRF, 27

CMRF and 16 RCSW buildings during strong motions in which the structures responded in the elastic range.

Equations (4.90) through (4.93) are used instead of equations recommended in Section 12.8 of ASCE 7-05 (ASCE, 2005), also derived by Chopra and Goel, because the code equations were intentionally calibrated to underestimate structural periods and conservatively calculate pseudo-spectral accelerations and subsequent design seismic forces. However, these formulae are not conservative for estimating building displacement demands (Chopra and Goel, 2000), and therefore, the mean values obtained in Chopra and Goel's regression are used instead. Assuming that the proportion of instrumented buildings studied by Chopra and Goel is representative of the actual proportion among structural seismic resistant systems, the following approximate relation between H and T_p was used:

$$T_{Approx} = \frac{42T_{SMRF} + 27T_{CMRF} + 16T_{RCSW}}{85} \tag{4.94}$$

The term T_{RCSW} in equation (4.94) has been calculated considering a value $\overline{A}_e = 2.5\%$. Figure 4.15 shows a comparison between the T_p-H relations shown in equations (4.90) to (4.94).
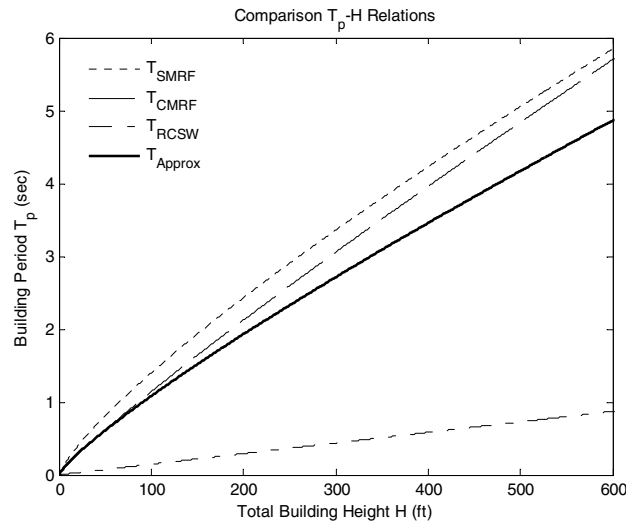
Figure 4.15. Building natural period T_p – Total building height H relations

From the data shown in Figure 4.15, it is seen that the range of periods for the primary system (T_p=0-5 sec) considered for developing the testing protocol is associated with buildings having total heights up to 620 ft, or equivalently, up to 50 story levels. Figure 4.16 shows the generalized drift spectra calculated for buildings with parameters $\alpha_o = 0$, 5 and 10. The GDS' presented in Figure 4.16 were further processed to eliminate the dependence of seismic drift demands on the period of the primary system T_p. Accordingly,

the 84th percentile drift demands were calculated along building height for each deformation pattern α_o, as shown in Figure 4.17.
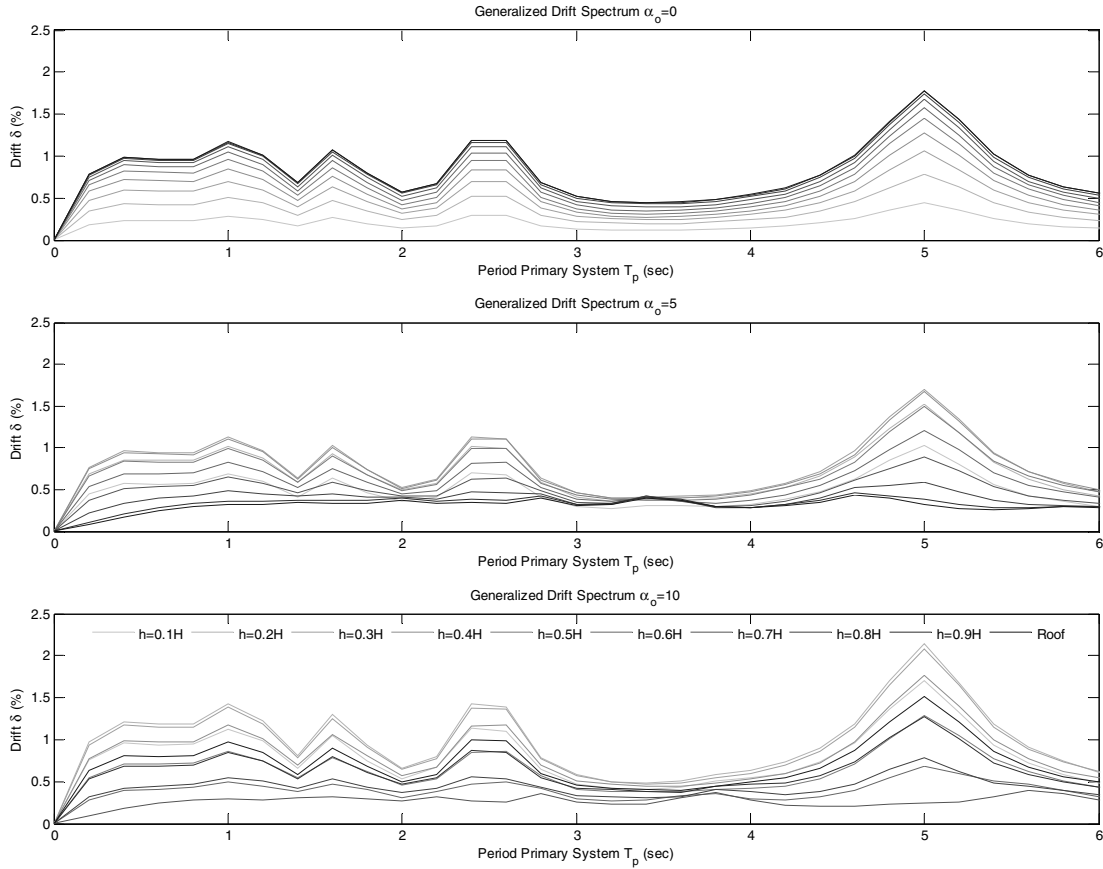
Figure 4.16. Generalized drift spectra at several building heights (α_o = 0, 5 and 10)

The data presented in Figure 4.17 was statistically analyzed to get the mean, over all α_o considered in the analysis, 84th percentile generalized drift demands shown in Figure 4.18. In Figure 4.18 it can be seen that the maximum mean 84th percentile generalized drift reaches 1.09% at a height equal to 0.3 times the total height of the building (h/H=0.3). At the roof level (h/H=1), the mean 84th % generalized drift reaches a value equal to 0.86%. Those values are associated to a seismic hazard with a probability of exceedance of 10% in 50 years. Equation (4.95) shows the best fit interpolation curve for the mean 84th percentile generalized drift along the building height. Equation (4.95) is also plotted in Figure 4.18.

$$\delta\left(\frac{h}{H}\right) = \frac{1}{4}sin\left(7\frac{h}{H}\right) - \frac{6}{5}\left(\frac{h}{H}\right)^2 + 1.9\left(\frac{h}{H}\right)^{0.55} \tag{4.95}$$

Recognizing that the zero mean 84th percentile generalized drift observed in Figure 4.18 at the base of the generic building model $\left(\delta(0)=0\right)$ corresponds to a numerical limitation of the continuous beam model,

the following distribution of generalized drift ratio along building height, in terms of percentage, is proposed:

$$\delta\left(\frac{h}{H}\right)=\begin{cases}1.09 & \frac{h}{H}\leq 0.3 \\ \frac{1}{4}sin\left(7\frac{h}{H}\right)-\frac{6}{5}\left(\frac{h}{H}\right)^2+1.9\left(\frac{h}{H}\right)^{0.55} & \frac{h}{H}>0.3\end{cases} \tag{4.96}$$

The generalized drift distribution described by equation (4.96) is also plotted in Figure 4.18.
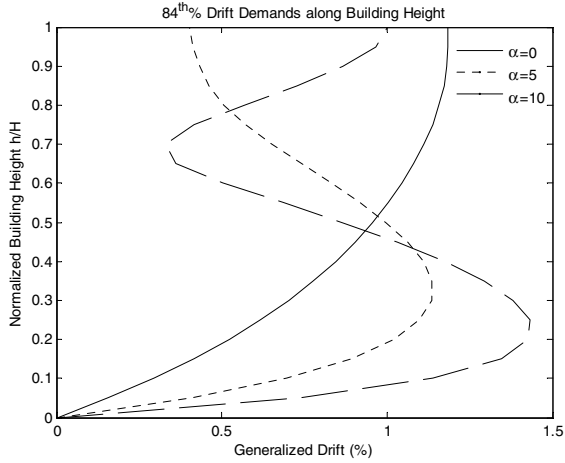
Figure 4.17. 84th % Generalized drifts along building height ($\alpha_0 = 0$, 5 and 10)
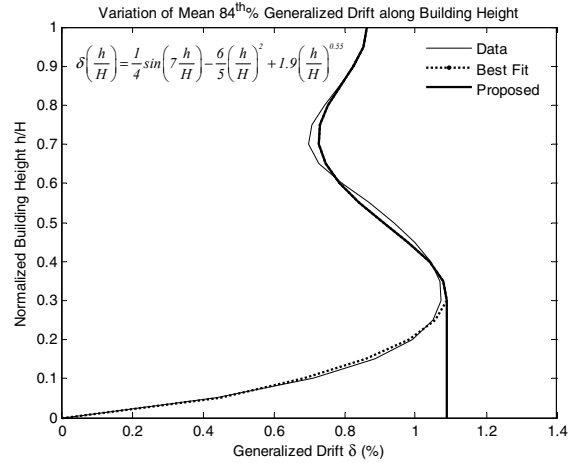
Figure 4.18. Mean 84th % generalized drift along building height

4.3 Testing protocol for seismic qualification

Testing protocols currently used for the seismic qualification of nonstructural components and equipment focus either on displacement or acceleration sensitive components, through racking or shake table protocols. However, some nonstructural systems may be sensitive to both displacement and accelerations. Nonstructural systems typically found in office, hotel and hospital buildings may be composed of components that individually may be either acceleration or displacement sensitive, but when combined with other systems may become sensitive to both accelerations and interstory drifts.

The seismic performance of individual distributed nonstructural components and the interactions between components composing a nonstructural system can be evaluated through a testing protocol that simultaneously imposes the expected drift and acceleration demands. This subsection proposes a general dynamic testing protocol for experimental seismic qualification of acceleration, displacement and acceleration/displacement sensitive nonstructural components, systems and equipment. The testing protocol was mainly developed for use with the Nonstructural Component Simulator developed in the

Structural Engineering and Earthquake Simulation Laboratory (SEESL) at the University at Buffalo (UB-NCS), taking full advantage of its testing capabilities. However, the methodology proposed herein can also be extended and used for experimental seismic qualification of acceleration sensitive nonstructural components and equipment performed using conventional shake tables. Previous research developed by Krawinkler et al. (Krawinkler *et al.*, 2000) and Wilcoski et al. (Wilcoski *et al.*, 1997), among others, constitute the basis for the development of this testing protocol. Similarly, the applicable aspects of current testing protocols such as AC156 (ICC-ES, 2007), IEEE 693 (IEEE, 2006) and FEMA 461 (FEMA, 2006) have been considered. The proposed testing protocol complements the current provisions in AC156 for seismic qualification of distributed displacement and/or displacement sensitive components, systems and equipment. Furthermore, the proposed protocol extends the minimum testing frequency that can be considered in an experiment from 1.3 Hz, as in current AC156 procedure, to 0.2 Hz, approximately, allowing for more realistic testing of nonstructural components and systems sensitive to low frequency actions.

The proposed protocol consists of a pair of displacement histories for the bottom and top levels of the UB-NCS that simultaneously matches: i) a target acceleration response spectrum with peak values mainly dominated by high frequencies, and ii) a generalized interstory drift with peak amplitudes applied at low frequencies. Both the target spectral accelerations and drifts can be specified based on the expected values at a given normalized building height h/H, where h is the height above grade where the nonstructural component is located, and H is the total height of the building. The seismic hazard can be specified using the USGS-USH as in the previous subsection. However, here the protocol motions are developed based on the ASCE 7-05 design ground response spectrum, in order to generate code compliant seismic demands.

The qualification testing protocol is presented as a set of closed-form equations, which considers as variables: (i) the location of the nonstructural component along the height of the building (through the parameter h/H); (ii) the range of frequencies to be assessed during testing ($f_{min} - f_{max}$); and (iii) the ASCE 7-05 mapped design spectral coordinates at 0.2 second period, S_{DS}, and at one second period, S_{D1}. The testing protocol is calibrated to induce and impose on components attached at a single or at two levels of a building (represented by the two UB-NCS platforms) a number of cycles consistent with the number of cycles induced and imposed by the floor motions recorded in real multistory buildings during relatively strong shaking. The considered recorded floor motions were obtained from the California Strong Motion Instrumentation Program (CSMIP) database (Naeim *et al.*, 2005).

4.3.1 Generation of hazard consistent floor displacement histories

The qualification testing protocol histories are generated considering the amplification path of the peak values of the mean 84th % floor acceleration response spectrum along building height, given by equation (4.88); and the profile of mean 84th % generalized interstory drifts given by equation (4.96); both scaled to the seismic hazard level associated with the ASCE 7-05 design spectral coordinates S_{DS} and S_{D1}, to impose realistic and code compliant seismic demands on nonstructural systems. The key parameters for the protocol displacement histories are the normalized location of the component along building height h/H; and the mapped spectral demands S_{DS} and S_{D1}.

4.3.1.1 Frequency content of loading protocol

The frequency content targeted for the seismic qualification testing protocol covers the range of frequencies between $f_{min} = 1/6$ Hz and $f_{max} = 5$ Hz, equivalent to periods ranging between 0.2 and 6 sec, which corresponds to the operating frequency range of the UB-NCS and the expected fundamental periods of typical multistory buildings, including some higher vibration modes. The instantaneous loading frequency $f(t)$ considered in the proposed testing protocol corresponds to an extension of the logarithmic variation proposed by Wilcoski et al. (Wilcoski *et al.*, 1997), given by:

$$f(t) = f_{max} \left(\frac{f_{min}^*}{f_{max}} \right)^{\left| \frac{|t-t_d|}{t_d} - 1 \right|}$$

(4.97)

where

$$f_{min}^* = \frac{S_r \, ln \, 2}{2} \left(\frac{1}{2} - \left\lfloor \frac{4 f_{max} - 4 f_{min} + 1}{S_r \, ln \, 4} \right\rfloor \right) + f_{max}$$

(4.98)

In equations (4.97) and (4.98), f_{max}, f_{min} and $f_{min}^* \approx 0.2$ Hz correspond to the maximum, and minimum target and actual testing frequencies, respectively; and $\lfloor \ \rfloor$ denotes the floor function. The total duration of the testing protocol is $2t_d$, where t_d is the time at which the actual minimum testing frequency f_{min}^* (or peak generalized drift) is reached and is given by:

$$t_d = \frac{1}{S_r} log_2 \frac{f_{max}}{f_{min}^*}$$

(4.99)

where S_r denotes a constant sweep rate calibrated to induce the same number of "Rainflow" cycles (ASTM, 1997) on acceleration sensitive nonstructural components and equipment as would be experienced during real seismic floor motions (Naeim *et al.*, 2005).

Equation (4.97) provides the instantaneous testing frequency transitioning from high to low frequencies, then back to high frequencies. The final high frequency sweep is intended to capture the behavior of components that might be damaged initially by drifts and become sensitive to accelerations (e.g., partition walls acting as a cantilever after failure of top slab connections). Figure 4.19 shows a typical instantaneous testing frequency variation, for the case $f_{min} = 1/6$ Hz, $f_{max} = 5.0$ Hz, and $S_r = 12$ octaves/min.
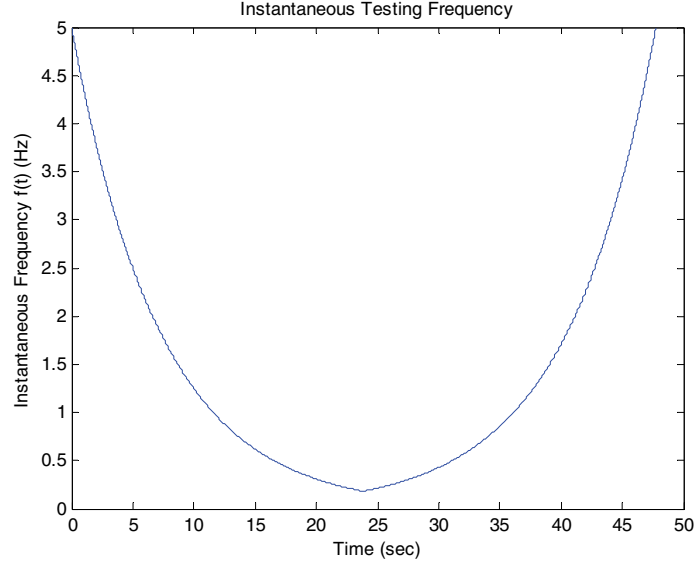
Figure 4.19. Typical instantaneous testing frequency variation

4.3.1.2 Qualification protocol histories

4.3.1.2.1 Displacement history for UB-NCS bottom level

The displacement testing protocol proposed for the UB-NCS bottom level $\left(x_{Bottom}\right)$ closely matches the floor response spectrum specified by FEMA 450 for acceleration sensitive nonstructural components placed at a given normalized building height $h/H > 0$. The testing protocol has also been calibrated to approximate the ASCE 7-05 ground response spectrum, and therefore, it allows for evaluating the seismic performance of nonstructural systems located at the grade level ($h/H = 0$). The closed-form equation for the bottom level qualification testing protocol time history is expressed as:

$$x_{Bottom}\left(t, \frac{h}{H}, S_{DS}, S_{DI}\right) = \alpha\left(t, \frac{h}{H}, S_{DS}, S_{DI}\right) f(t)^{\beta} \cos\left(\varphi(t)\right) w(t) FRS_{Factor}\left(\frac{h}{H}\right) \tag{4.100}$$

In equation (4.100), $f(t)$ is the instantaneous loading frequency given by equation (4.97). The factor $FRS_{Factor}\left(h/H\right)$, equation (4.88), is used to amplify the amplitude of the UB-NCS platform motions in

order to match the ASCE 7-05 ground response spectrum and the FEMA 450 floor response spectrum at a specified normalized height h/H.

The function $\alpha(t, h/H, S_{DS}, S_{D1})$ in equation (4.100) is used to control the shape of the protocol response spectrum, and is given by:

$$\alpha\left(t, \frac{h}{H}, S_{DS}, S_{D1}\right) = \frac{3S_{D1}}{2g} \begin{cases} sin\left(\dfrac{\pi t}{2t_{T_{Flex}}}\right) & 0 \le t < t_{T_{Flex}} \\ 1 & t_{T_{Flex}} \le t \le 2t_d - t_{T_{Flex}} \\ sin\left(\dfrac{\pi}{2t_{T_{Flex}}}\left(t - 2t_d + 2t_{T_{Flex}}\right)\right) & 2t_d - t_{T_{Flex}} < t \le 2t_d \end{cases}$$ (4.101)

where

$$T_{Flex} = \left(1 + 0.25\frac{h}{H}\right)\frac{S_{D1}}{S_{DS}}$$ (4.102)

$$t_{T_{Flex}} = \frac{1}{S_r} log_2\left(f_{max} T_{Flex}\right)$$ (4.103)

The parameter T_{Flex} defined in equation (4.102) corresponds to the corner period of the ground or floor response spectrum, as defined by ASCE 7-05 and FEMA 450, respectively. The larger the ratio S_{D1}/S_{DS}, as typically observed for soft soils, the larger the corner period T_{Flex}. Similarly, it is observed that the higher the location of the nonstructural component or equipment within the building, the larger the corner period. The parameter $t_{T_{Flex}}$ defined in equation (4.103) corresponds to the time at which the instantaneous testing period, the inverse of the instantaneous testing frequency, sweeps the corner period T_{Flex}. The parameter $t_{T_{Flex}}$ controls the period at which the peak spectral response is observed.

The function $\alpha(t, h/H, S_{DS}, S_{D1})$ in equation (4.101) has not a rigorous theoretical foundation, but its effectiveness in modulating the shape of the protocol response spectrum is demonstrated later in subsection 4.3.3 through a series of examples.

The coefficient $\beta = -1.25$ in equation (4.100) is a calibration factor used to minimize the error observed in matching the target (ground or floor) acceleration response spectrum in the long period range ($T > T_{Flex}$). The function $\varphi(t)$ in equation (4.100) is the instantaneous testing phase, given by:

$$\varphi(t) = 2\pi \int_0^t f(\tau)d\tau = \begin{cases} \dfrac{2\pi f_{max}}{S_r \ln 2}\left[1 - \left(\dfrac{f_{min}^*}{f_{max}}\right)^{\frac{t}{t_d}}\right] & 0 \le t \le t_d \\[20pt] \dfrac{2\pi}{S_r \ln 2}f_{max} + \dfrac{2\pi f_{min}^*}{S_r \ln 2}\left[\left(\dfrac{f_{max}}{f_{min}^*}\right)^{\frac{t}{t_d}-1} - 2\right] & t_d < t \le 2t_d \end{cases} \tag{4.104}$$

The function $w(t)$ in equation (4.100) is a sinusoidal windowing function used to smooth the ramp-up and ramp-down portions of the testing protocol, given by:

$$w(t) = \begin{cases} \dfrac{1}{2}\left[1 - \cos\left(\dfrac{\pi t}{t_w}\right)\right] & 0 \le t \le t_w \\[14pt] 1 & t_w < t < 2t_d - t_w \\[14pt] \dfrac{1}{2}\left[1 - \cos\left(\dfrac{\pi}{t_w}(t - 2t_d + 2t_w)\right)\right] & 2t_d - t_w \le t \le 2t_d \end{cases} \tag{4.105}$$

where t_w is the duration of the ramp-up and ramp-down portions of the floor displacement histories, which typically takes values between 0.5 and 2 seconds.

4.3.1.2.2 Interstory drift protocol

The interstory drift protocol is calibrated to impose a controlled number of small and large amplitude cycles. The peak interstory drift reached during testing matches the mean 84th percentile generalized drift expected at a given normalized building height h/H, as calculated in subsection 4.2.4, scaled to the ASCE 7-05 site dependent design seismic hazard level. The closed-form equation for the proposed interstory drift $(\varDelta)$ protocol time history is:

$$\varDelta\left(t, \frac{h}{H}, S_{D1}\right) = h_{NCS}\frac{S_{D1}}{0.5g}e^{-\left(\frac{t-t_d}{\sigma}\right)^2}\delta\left(\frac{h}{H}\right)\cos(\varphi(t))w(t) \tag{4.106}$$

where $\delta(h/H)$ is the mean 84th percentile generalized drift at a given normalized height h/H, equation (4.96), and h_{NCS} denotes the free interstory height of the testing equipment (approximately 13 ft).

The function $e^{-\left(\frac{t-t_d}{\sigma}\right)^2}$ is a Gaussian-shaped modulating function in which σ is a constant factor calibrated to control the number of total and large (damaging) cycles imposed by the interstory drift protocol. The term $S_{D1}/0.5g$ corresponds to the scaling factor, where $0.5g$ is the USGS-USH spectral coordinate at one

second period for the site considered in the generalized drift demand estimation. $\varphi(t)$ and $w(t)$ were previously defined in equations (4.104) and (4.105), respectively.

4.3.1.2.3 Displacement history for UB-NCS top level

The protocol displacement history for the top UB-NCS level $\left(x_{Top} \right)$ is calculated based on the bottom level and interstory drift protocol histories. The closed-form equation for the top level displacement protocol is:

$$x_{Top}\left(t,\frac{h}{H},S_{DS},S_{DI} \right) = x_{Bottom}\left(t,\frac{h}{H},S_{DS},S_{DI} \right) + \varDelta\left(t,\frac{h}{H},S_{DI} \right) \tag{4.107}$$

Displacements for the top and bottom UB-NCS levels are, in consequence, in phase.

4.3.2 Examples of testing protocol histories

This subsection presents examples of testing protocol displacement histories proposed for the experimental seismic qualification of distributed nonstructural components, systems and equipment. Table 4.4 shows a summary of the three examples considered.

Table 4.4. Summary testing protocol examples

Example	City	Coordinates		Mapped Spectral Demands			Norm.
		Longitude	Latitude	Site class	S_{DS}	S_{DI}	Height h/H
1	Northridge	-118.52	34.237	B	1.283g	0.461g	0.0
2	Northridge	-118.52	34.237	B	1.283g	0.461g	1.0
3	New York	-73.920	40.867	D	0.365g	0.114g	1.0

4.3.2.1 Testing protocol histories for example 1

As a first case, protocol displacement histories are generated for a site characterized by ASCE 7-05 mapped spectral coordinates S_{DS}=1.283g and S_{DI}=0.461g. The parameter h/H is chosen to be equal to 0. At this building level, the imposed generalized drift is maximum and the floor motion histories match the ASCE 7-05 design ground response spectrum. This type of floor motions are recommended for testing nonstructural components and systems predominantly displacement sensitive and/or placed at the grade level. Figure 4.20 shows the proposed floor displacement, velocity and acceleration histories for the bottom and top UB-NCS levels. Five-point numerical differentiation with local cubic polynomial fit is used to compute floor velocity and acceleration histories. Figure 4.21 shows the interstory drift protocol history obtained from equation (4.106). Figure 4.22 shows the response spectra for the UB-NCS bottom

and top level floor motions. In Figure 4.22 it is observed that the mean response spectrum for the bottom and top level platform motions closely matches the ASCE 7-05 ground response spectrum in the range of periods of engineering interest and within the operating range of the UB-NCS (0.2-5.0 sec). Table 4.5 summarizes the peak motion values for this testing protocol.
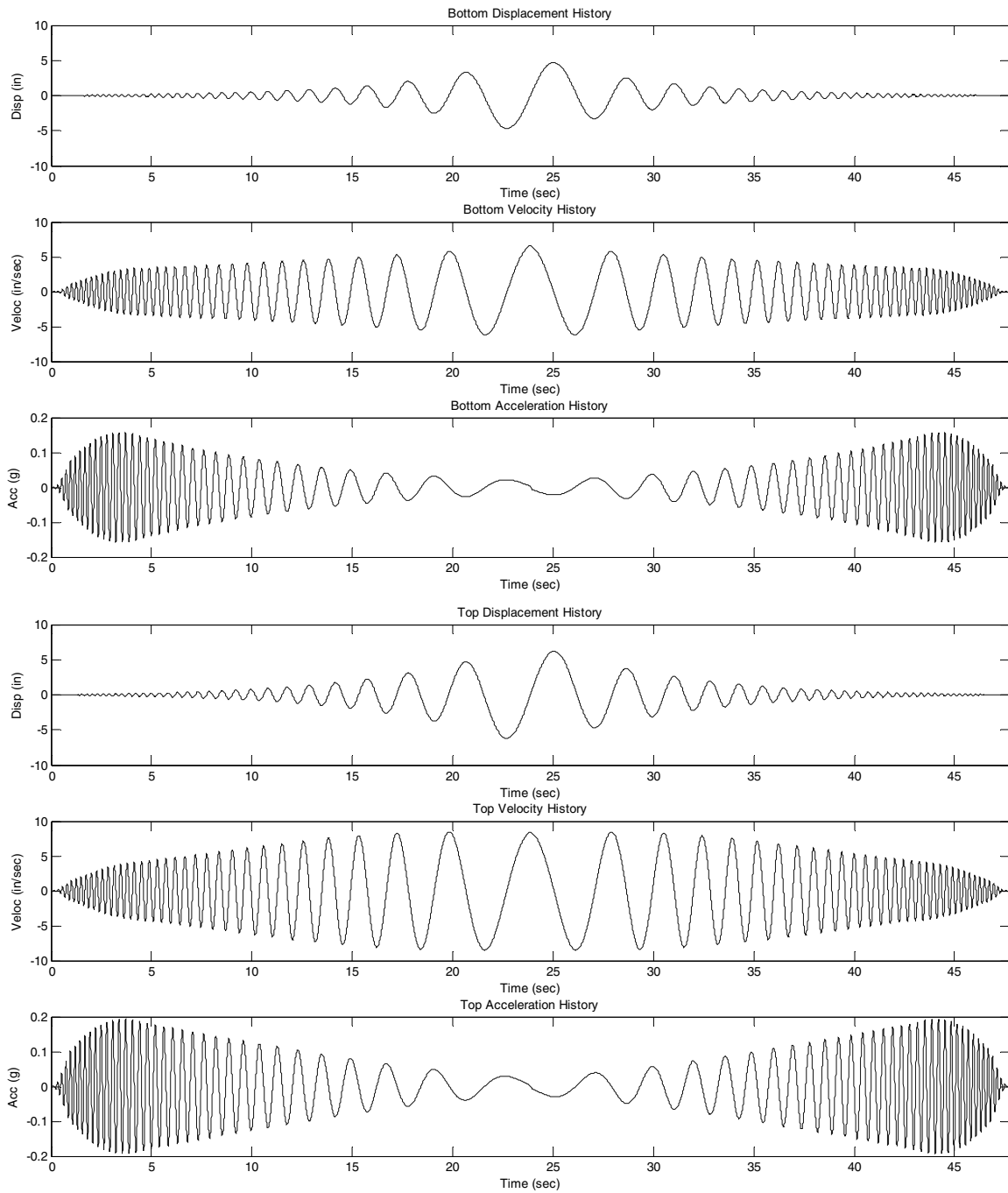
Figure 4.20. Proposed protocol floor motions for S_{DS}=1.283g, S_{D1}=0.461g, and h/H =0
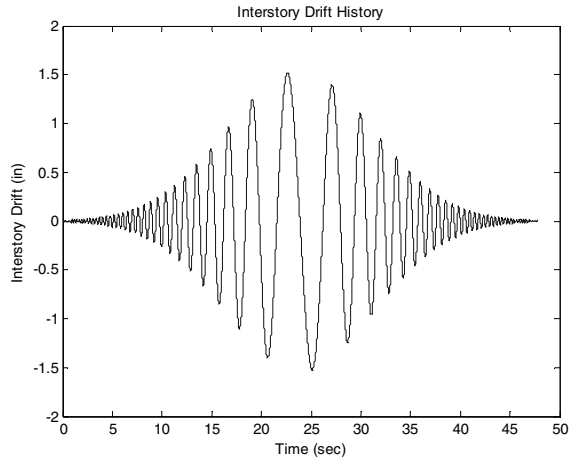
Figure 4.21. Proposed interstory drift testing protocol for S_{DS}=1.283g, S_{D1}=0.461g, and h/H =0
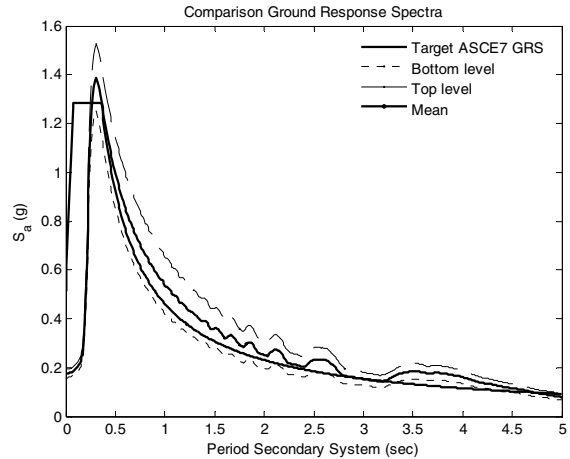
Figure 4.22. Comparison target and protocol FRS for S_{DS}=1.283g, S_{D1}=0.461g, and h/H =0

Table 4.5. Envelope floor motions testing protocol for S_{DS}=1.283g, S_{D1}=0.461g, and h/H =0

Peak Displacements		Peak Interstory Drift		Peak Velocities		Peak Accelerations	
$D_{Max\ Bot}$ (in)	$D_{Max\ Top}$ (in)	Δ_{Max} (in)	δ_{Max} (%)	$V_{Max\ Bot}$ (in/s)	$V_{Max\ Top}$ (in/s)	$A_{Max\ Bot}$ (g)	$A_{Max\ Top}$ (g)
4.70	6.21	1.52	1.00	6.64	8.49	0.16	0.19

4.3.2.2 Testing protocol histories for example 2

In the second example, protocol displacement histories are generated for a site characterized by ASCE 7-05 mapped spectral coordinates S_{DS}=1.283g and S_{D1}=0.461g. The parameter h/H is chosen to be equal to 1 in this case, which corresponds to a building roof level. At this level, the accelerations imposed on specimens are maximum and the protocol floor motions match the FEMA 450 floor response spectrum at the roof level. This protocol history is recommended for testing nonstructural components and systems predominantly sensitive to floor accelerations.

Figure 4.23 shows the proposed floor displacement, velocity and acceleration histories for the bottom and top UB-NCS levels. Figure 4.24 shows the interstory drift protocol history estimated using equation (4.106). Figure 4.25 shows the floor response spectra for the bottom and top UB-NCS level floor motions. In Figure 4.25 it is observed that the mean FRS for the platform motions closely matches the FEMA 450 FRS at roof level in the range of periods of engineering interest (0.2-5.0 sec). Table 4.6 summarizes the peak motion values for this testing protocol.

122

Table 4.6. Envelope floor motions testing protocol for S_{DS}=1.283g, S_{D1}=0.461g, and h/H =1

Peak Displacements		Peak Interstory Drift		Peak Velocities		Peak Accelerations	
$D_{Max\ Bot}$ (in)	$D_{Max\ Top}$ (in)	Δ_{Max} (in)	δ_{Max} (%)	$V_{Max\ Bot}$ (in/s)	$V_{Max\ Top}$ (in/s)	$A_{Max\ Bot}$ (g)	$A_{Max\ Top}$ (g)
18.8	20.0	1.21	0.79	26.6	28.0	0.55	0.58
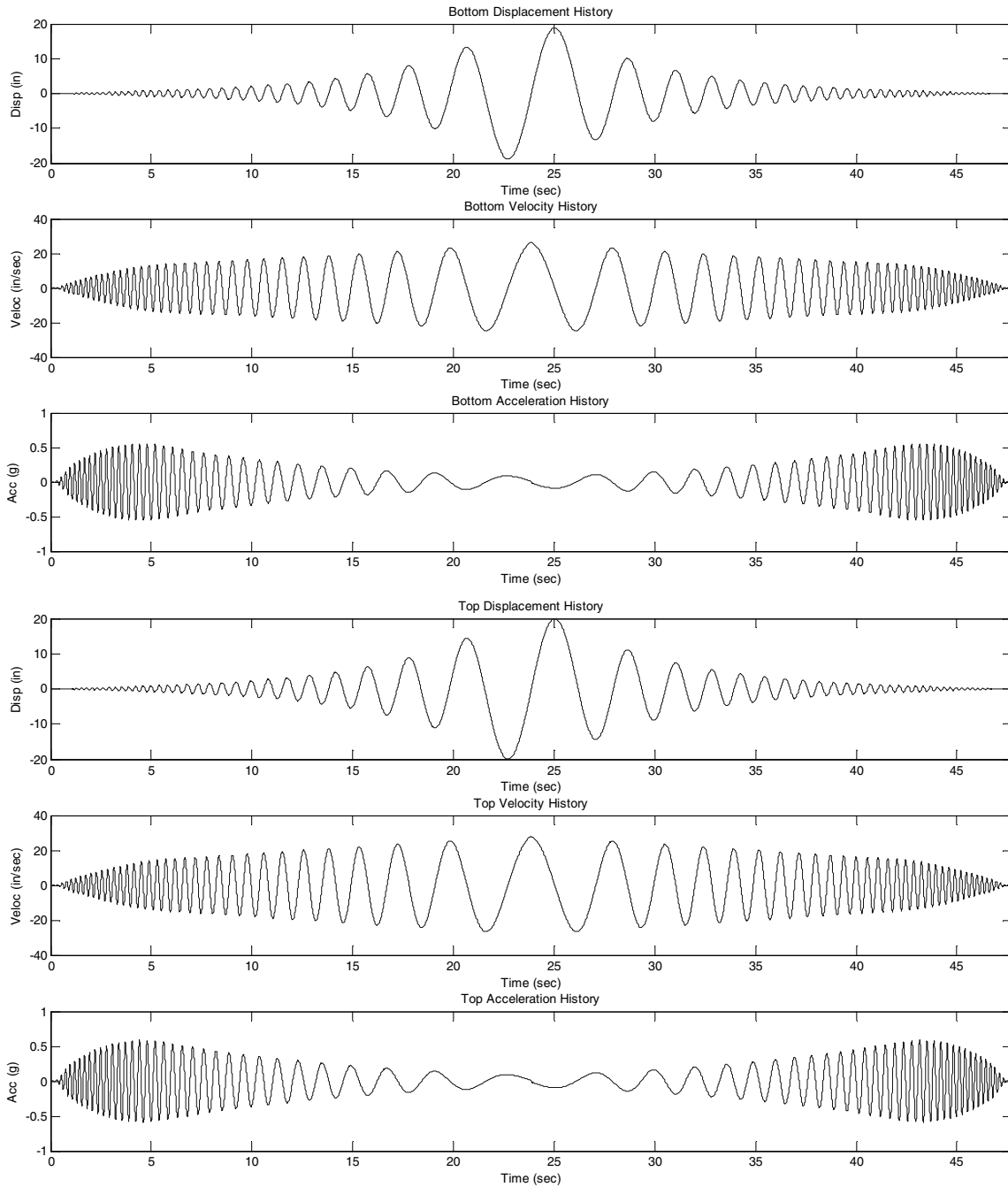
Figure 4.23. Proposed testing protocol floor motions for S_{DS}=1.283g, S_{D1}=0.461g, and h/H =1 (roof level)
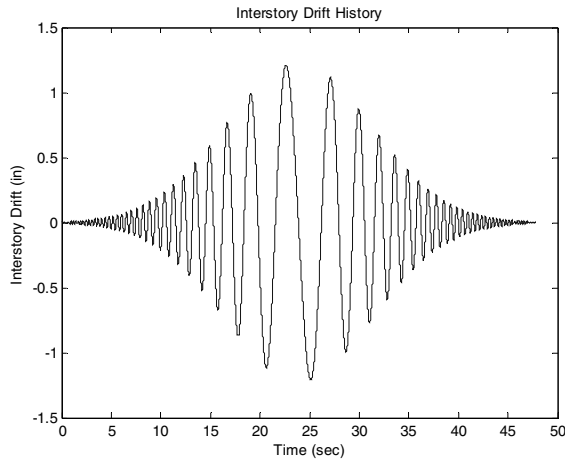
Figure 4.24. Proposed interstory drift testing protocol for S_{DS}=1.283g, S_{D1}=0.461g, and h/H =1
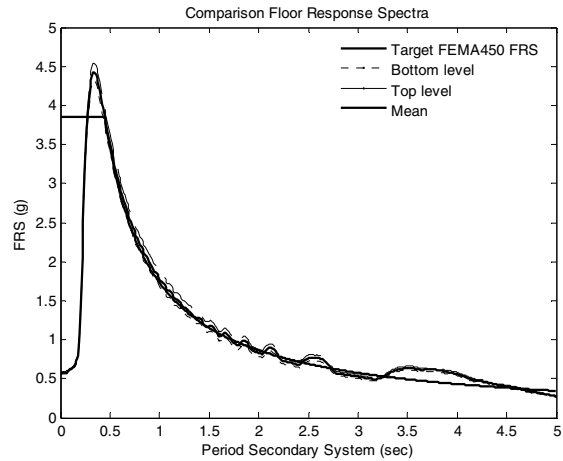
Figure 4.25. Comparison target and protocol FRS for S_{DS}=1.283g, S_{D1}=0.461g, and h/H =1

4.3.2.3   Testing protocol histories for example 3

In this example, protocol displacement histories are generated for a site characterized by ASCE 7-05 mapped spectral coordinates S_{DS}=0.365g and S_{D1}=0.114g. The parameter h/H is chosen to be equal to 1, as in the previous example. This example illustrates typical testing protocol time histories recommended for seismic qualification of nonstructural components, equipment and systems to be used in regions of low seismicity. The resulting floor motions for the bottom and top platform levels and the interstory drift protocol history are shown in Figure 4.26 and Figure 4.27. Figure 4.28 shows the FRS's for the bottom and top UB-NCS level floor motions, and again, it is observed that the mean FRS for the platform motions closely matches the FEMA 450 FRS at roof level. Table 4.7 summarizes the peak motion values for this testing protocol.

Table 4.7. Envelope floor motions testing protocol for S_{DS}=0.365g, S_{D1}=0.114g, and h/H =1

Peak Displacements		Peak Interstory Drift		Peak Velocities		Peak Accelerations	
$D_{Max\ Bot}$ (in)	$D_{Max\ Top}$ (in)	Δ_{Max} (in)	δ_{Max} (%)	$V_{Max\ Bot}$ (in/s)	$V_{Max\ Top}$ (in/s)	$A_{Max\ Bot}$ (g)	$A_{Max\ Top}$ (g)
4.65	4.95	0.30	0.20	6.57	6.92	0.15	0.16
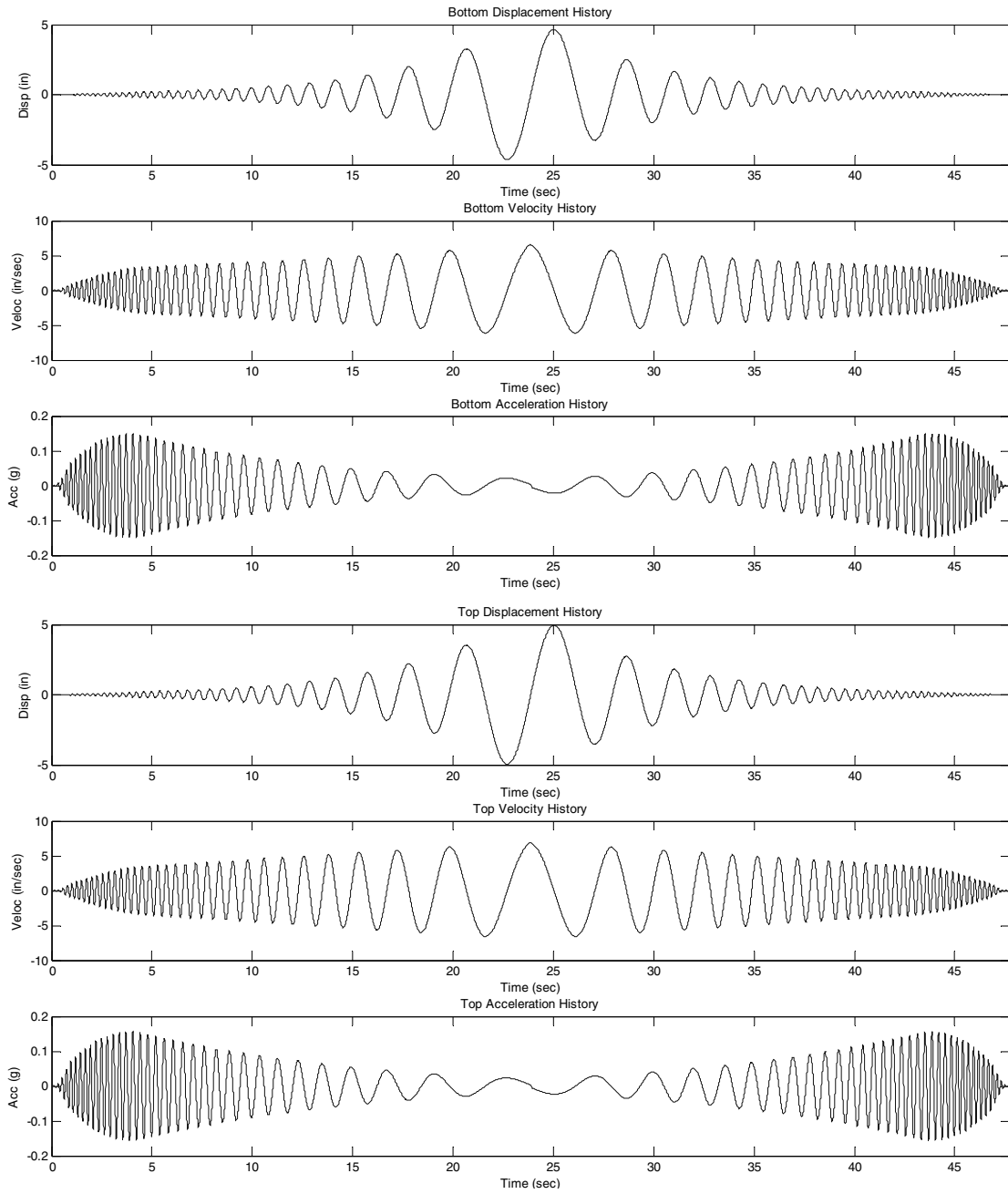
Figure 4.26. Proposed testing protocol floor motions for S_{DS}=0.365g, S_{D1}=0.114g, and h/H =1 (roof level)
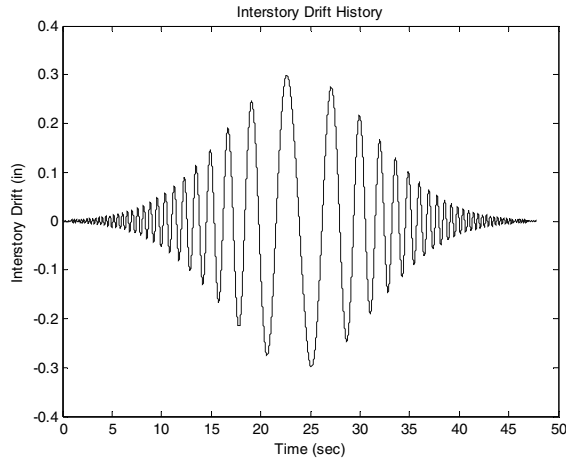
Figure 4.27. Proposed interstory drift testing protocol for S_{DS}=0.365g, S_{D1}=0.114g, and h/H =1
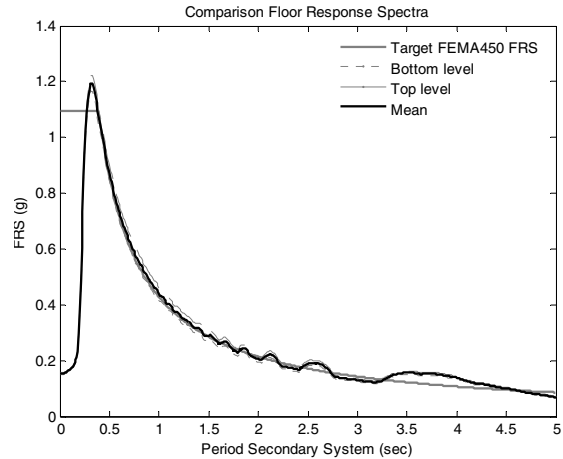
Figure 4.28. Comparison target and protocol FRS for S_{DS}=0.365g, S_{D1}=0.114g, and h/H =1

4.3.3 Calibration of testing protocol for general seismic hazard levels

This subsection describes the ability of the proposed testing protocol to match target ASCE 7-05 ground and FEMA 450 floor response spectra. In particular, the adequacy of the function $\alpha(t,h/H,S_{DS},S_{D1})$ presented in equation (4.101) to control the shape of the protocol response spectra is assessed. The versatility of the $\alpha(t,h/H,S_{DS},S_{D1})$ function is demonstrated in Figure 4.29, which compares the ASCE 7-05 ground response spectrum for soils class B at different sites and the mean (for both platform motions) protocol response spectra.
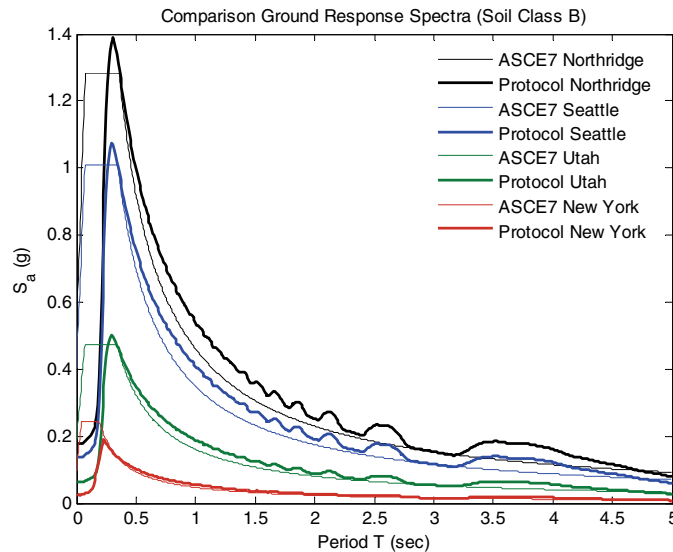
Figure 4.29. Testing protocol imposing ground response spectral demands

126

Figure 4.30 and Figure 4.31 demonstrate the ability of the testing protocol to impose spectral accelerations associated with several soil conditions. A comparison of target ASCE 7-05 ground response spectra and mean protocol response spectra for a city with high seismicity such as Northridge (Latitude 34.237, Longitude -118.518) is shown in Figure 4.30. The same comparison is shown in Figure 4.31 for a city with low seismicity such as New York City (Latitude 40.867, Longitude -73.920).
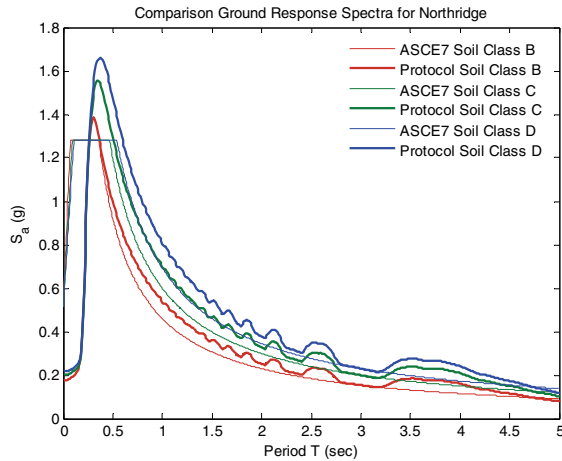
Figure 4.30. Testing protocol to imposing ground response spectral demands for several soil conditions (Northridge)
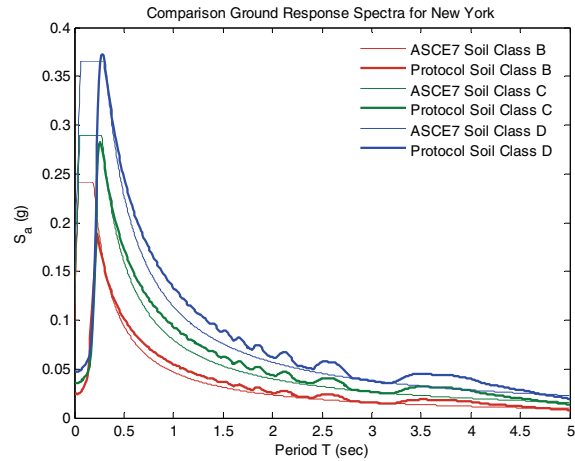
Figure 4.31. Testing protocol to imposing ground response spectral demands for several soil conditions (New York City)

Finally, Figure 4.32 and Figure 4.33 show comparisons of FEMA 450 floor response spectra (for soil class C) and mean (for both platform levels) testing protocol response spectra for normalized building heights h/H=0.25, 0.50, 0.75 and 1.0.
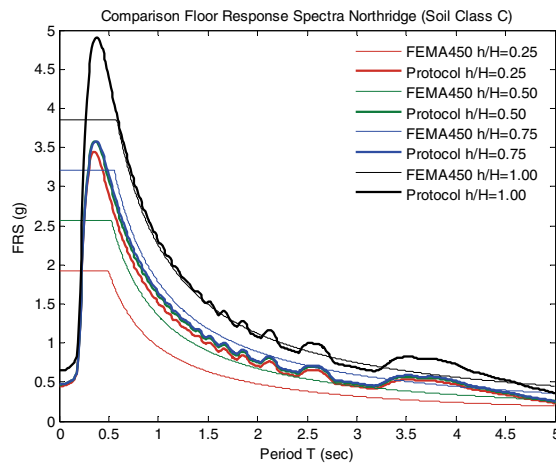
Figure 4.32. Testing protocol imposing floor response spectral demands for several building heights (Northridge)
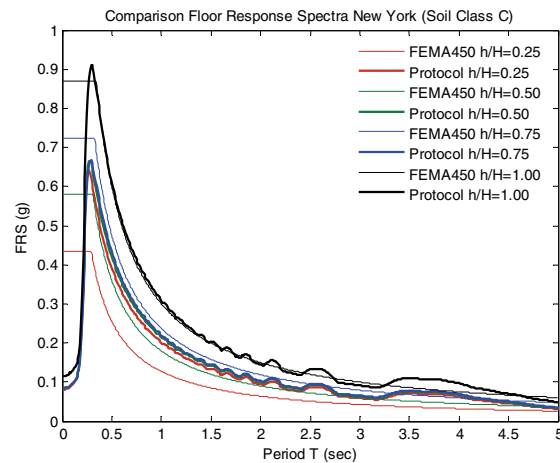
Figure 4.33. Testing protocol imposing floor response spectral demands for several building heights (New York City)

In Figure 4.32 and Figure 4.33 it is observed that the testing protocol closely matches the FEMA 450 FRS for normalized building heights h/H greater than 0.5. At lower levels, the differences observed in floor response spectra are caused by the disagreement between the triangular inverted distribution of accelerations considered by current code provisions and the distribution considered by the proposed testing protocol (see equation (4.88)) obtained using principles of random vibration theory. In Figure 4.29 through Figure 4.33, the upper and lower limits for ASCE 7-05 ground and FEMA 450 floor response spectra were not included.

4.3.4 Calibration of induced/imposed vibration cycles

Cumulative damage effects of nonstructural components subjected to earthquake loading are dependent on the number and amplitude of vibration cycles induced (on acceleration sensitive components) and imposed (on displacement sensitive components) during the seismic action. For this reason, it is important to examine and compare the number of cycles induced and imposed by the loading protocol and recorded building floor motions. The number of cycles induced and imposed by the testing protocol depends on the instantaneous frequency variation function $f(t)$, the constant sweep rate S_r, and the parameter σ controlling the interstory drift qualification protocol's shape.

Floor motion histories recorded during historical earthquakes at the upper levels of 6 instrumented buildings selected from the California Strong Motion Instrumentation Program (CSMIP) database have been considered.

In the building selection, buildings with several number of floor levels, with different seismic resistant systems and natural vibration periods, designed and built between 1960's and 1990's, affected by a variety of historical strong ground motions, and with distance to earthquake sources less than 15 km, were considered. Buildings located in sites with different geological conditions, with the highest recorded ground and floor accelerations, and with several uses, were also selected for the calibration process.

Table 4.8 lists the characteristics of the set of buildings considered in the cycle counting analysis. Photos of the instrumented buildings considered in the cycle counting analysis are shown in Figure 4.34. More detailed schematics of the floor plans and details of the instrumentation schemes are provided in Figure 4.35.

Table 4.8. CSMIP Instrumented buildings selected for cycle counting analysis

CSMIP Station ID	City	Building Structural System	Number of Stories	Building Period (s)	Type	Design Date	Site Geology	Recorded Earthquakes in Station	Min. Distance to Source (km)	Max. PGA (g)	Max. PFA (g)
24464	North Hollywood	Reinforced concrete columns and beams	20	2.56	Hotel	1967	Sandstone, shale	Whittier Northridge	15	0.30	0.65
24514	Sylmar	Concrete slab, metal deck, steel frames	6	0.40	Hospital	1976	Alluvium	Whittier Northridge	13	0.80	1.50
24629	Los Angeles	Concrete slabs, steel frames and deck	54	6.20	Office	1988	Alluvium over sedimentary rock	Northridge	32	0.13	0.18
47459	Watsonville	Concrete slabs and shear walls	4	0.37	Commercial	-	Fill over alluvium	Loma Prieta	17	0.58	1.20
24322	Sherman Oaks	Concrete slabs, beams, and columns	13	0.84	Commercial	1964	Alluvium	Whittier Landers Northridge	13	0.75	0.42
24386	Van Nuys	Concrete slabs, columns, spandrel beams	7	1.58	Hotel	1965	Alluvium	Landers Big Bear Northridge	7	0.45	0.58

Building 24464

Building 24514

Building 24629

Building 47459

Figure 4.34. Pictures of buildings considered for cycle counting analysis (Taken from CSMIP database)

Building 24322   Building 24386

Figure 4.34. Pictures of buildings considered for cycle counting analysis (Taken from CSMIP database) (Cont'd)

Figure 4.35. Detail instrumentation of buildings considered for cycle counting analysis (Taken from CSMIP database)

Figure 4.35. Detail instrumentation of buildings considered for cycle counting analysis (Taken from CSMIP database) (Cont'd)

131

Figure 4.35. Detail instrumentation of buildings considered for cycle counting analysis (Taken from CSMIP database) (Cont'd)

4.3.4.1 Number of cycles induced on acceleration sensitive nonstructural components

In order to compute the number of cycles induced on acceleration sensitive nonstructural components during earthquakes, linear elastic analyses of SDOF systems have been performed considering the bin of recorded building floor accelerations and the proposed testing protocol. A damping ratio equal to 5% has been considered for the SDOF oscillator. The "Rainflow" counting algorithm (ASTM, 1997) was used to simplify the SDOF's response excursion amplitudes. This counting method has been extensively used in the past for estimating the number and amplitude of cycles imposed by the ATC-24 and CUREE/Caltech testing protocols proposed by Krawinkler (Krawinkler, 1992) and Krawinkler et al. (Krawinkler *et al.*, 2000), respectively. In order to induce and impose a controlled number of cycles using the testing protocol, a parameter N_λ, defined as:

$$N_\lambda = N_{Cycles} \mid A_{Cycle} \geq \lambda A_{Max} \tag{4.108}$$

is considered to calibrate the testing protocol sweeping rate. N_λ corresponds to the number of rainflow cycles N_{Cycles} with amplitude A_{Cycle} larger than $\lambda\%$ times the maximum rainflow amplitude A_{Max} observed in response of the SDOF oscillator. In particular, two statistical parameters are calculated, N_{10} (number of excursions with rainflow amplitude greater than 10% the largest rainflow excursion amplitude) and N_{50} (number of excursions with rainflow amplitude greater than 50% the largest rainflow excursion amplitude), representative of the total number of damaging excursions and the number of large excursions observed in the SDOF's response, respectively.

Figure 4.36 through Figure 4.39 show comparisons between the number of rainflow cycles induced by the testing protocol (for a constant sweeping rate S_r =12 octaves/minute) and the mean and 84th percentile number of rainflow cycles induced by the set of recorded building floor accelerations on SDOF with frequencies in the UB-NCS operating range (0.2-5 Hz).
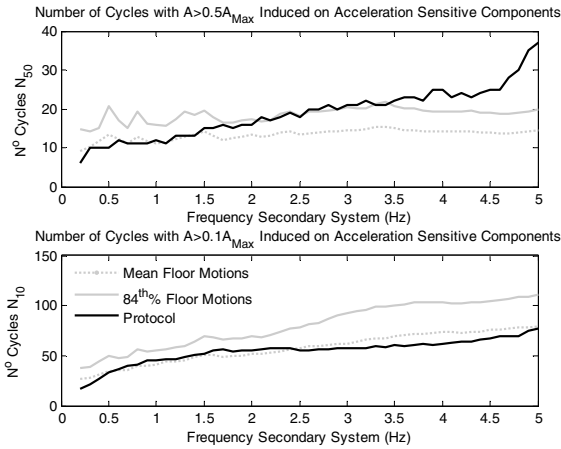
Figure 4.36. N_{10} and N_{50} number of rainflow cycles induced by recorded building floor motions and testing protocol for Northridge S_{DS}=1.283g, S_{D1}=0.461g, and h/H =0
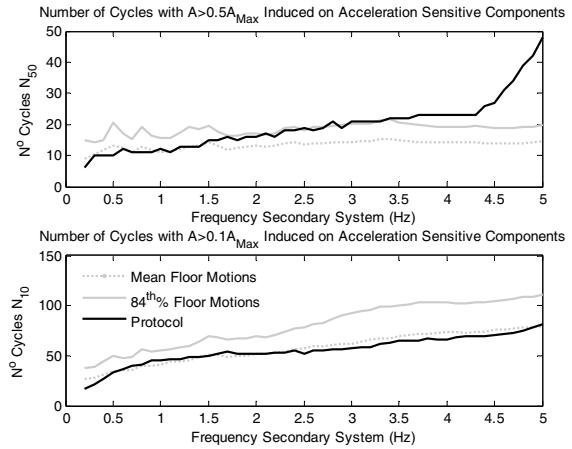
Figure 4.37. N_{10} and N_{50} number of rainflow cycles induced by recorded building floor motions and testing protocol for Northridge S_{DS}=1.283g, S_{D1}=0.461g, and h/H =1
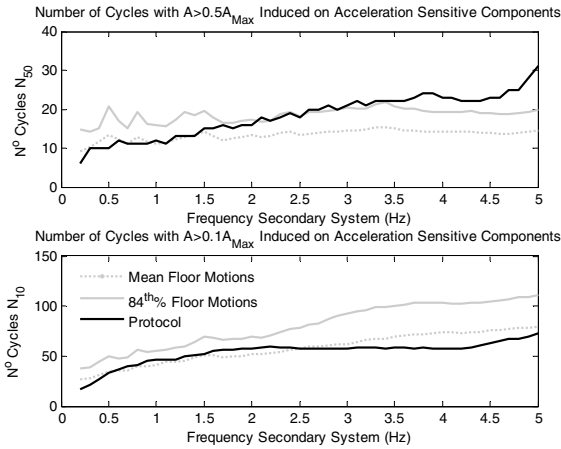
Figure 4.38. N_{10} and N_{50} number of rainflow cycles induced by recorded building floor motions and testing protocol for New York S_{DS}=0.365g, S_{D1}=0.114g, and h/H =0
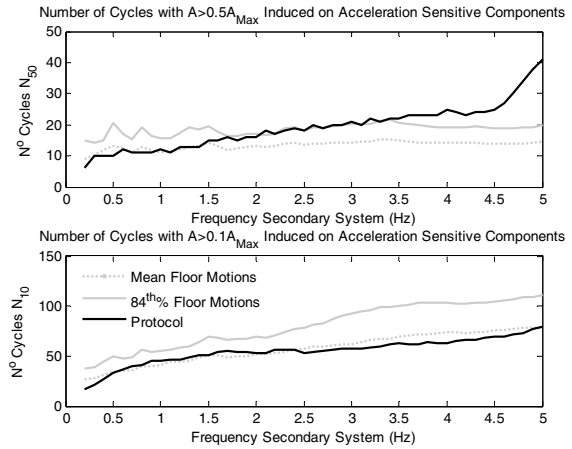
Figure 4.39. N_{10} and N_{50} number of rainflow cycles induced by recorded building floor motions and testing protocol for New York S_{DS}=0.365g, S_{D1}=0.114g, and h/H =1

Figure 4.36 through Figure 4.39 show comparisons of the effectiveness of the calibrated protocol for sites with several seismic hazard levels. It can be seen that for systems with frequencies lower than 1.5 Hz, the proposed testing protocol closely matches the mean number of large cycles (N_{50}) induced by the recorded floor motions. For SDOF systems with frequencies larger that 1.5 Hz, the testing protocol closely matches the 84th percentile number of large cycles induced by real floor motions. The testing protocol

overestimates the 84th percentile number of large cycles induced by real floor motions for oscillators with natural frequencies larger than 4.5 Hz. Similarly, it is observed that the testing protocol closely matches the mean total number of damaging excursions (N_{10}) for oscillators with natural frequencies in the range of interest (0.2-5 Hz).

4.3.4.2 Number of cycles induced on displacement sensitive nonstructural components

This subsection describes the procedure used to calibrate the factor σ controlling the shape of the Gaussian function used to envelope the interstory drift qualification protocol history presented in equation (4.106) and shown in Figure 4.21, Figure 4.24 and Figure 4.27.

The rainflow counting algorithm was used to compute the number of cycles N_λ, as defined in equation (4.108), observed in the interstory drift histories. The interstory drift histories were calculated from the displacement histories obtained after integration and baseline correction of the floor acceleration histories recorded (CSMIP database) at the upper levels of the selected buildings (Naeim *et al.*, 2005). The "Rainflow" counting algorithm was also applied to the proposed interstory drift protocol, iteratively, considering several values for the parameter σ until achieving convergence with the recorded data. Figure 4.40 shows the results of the calibration process for the proposed testing protocol. Dots in Figure 4.40 denote individually processed data. The optimal value found for the parameter σ is 10.5 seconds.
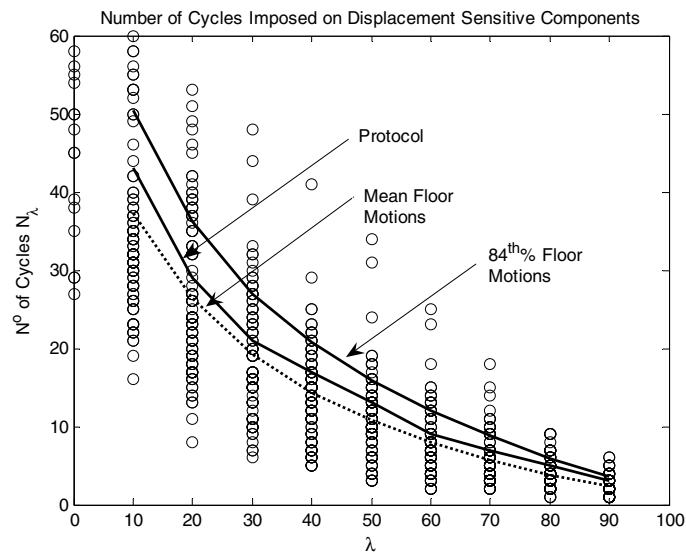
Figure 4.40. Comparison of number of rainflow cycles imposed by recorded building interstory drifts and testing protocol

In Figure 4.40 it is seen that the number of rainflow cycles imposed by the interstory drift protocol closely matches the mean number of rainflow cycles imposed by real building interstory drift histories. It is seen that the combined use of the calibrated Gaussian window and the proposed instantaneous frequency

function allows for closely matching the mean number of cycles in the whole profile of cycle amplitudes, for which λ varies between 10 and 90. The profile of cycle amplitudes shown in Figure 4.40 only depends on the parameter σ, and therefore, it is independent of the seismic hazard level associated to the protocol history, or peak drift ratio reached during testing.

4.4   Testing protocols for fragility assessment

Testing protocols currently used for experimental fragility assessment of nonstructural components and equipment are mainly based on the recommendations of the FEMA 461 document (FEMA, 2006). FEMA 461 proposes two separate testing protocols for fragility assessment of acceleration and displacement sensitive nonstructural components. The protocol for acceleration sensitive nonstructural components consists of a shake table protocol, suitable for testing building contents and self-supported equipment with attachments at a single building level. The seismic fragility is assessed by applying the testing protocol consecutively at increasing amplitudes, which can induce undesired low cycle fatigue damage on the tested specimens. The protocol recommended for testing displacement sensitive nonstructural components consists of a quasi-static racking protocol suitable for testing components attached at more than one level, but whose seismic performance is independent on the dynamic actions. This subsection proposes two general testing protocols, based on the FEMA 461 protocols, suitable for testing nonstructural components, systems and equipment that may be sensitive to both floor accelerations and interstory drifts.

 The first fragility testing protocol, consisting of a pair of dynamic floor motions for the UB-NCS platforms, is recommended for fragility analysis of nonstructural components and systems that may be simultaneously sensitive to the interstory drifts, and absolute velocities and accelerations imposed by the dynamic action of two adjacent levels in a multistory building. The proposed protocol allows for assessing the seismic performance of individual nonstructural components and equipment, and the dynamic interactions between components of a nonstructural system or equipment. This protocol attempts to find the seismic demands triggering all potential specimen damage states by performing a single test, reducing the risk of inducing low cycle fatigue damage on the tested component.

The second testing protocol proposed for fragility assessment consists of a quasi-static interstory drift testing history that is recommended for fragility assessment of nonstructural components, systems and equipment not sensitive to the loading rate. The proposed quasi-static protocol is consistent with the proposed dynamic fragility testing protocol and is presented here as an alternative to the FEMA 461 quasi-static testing protocol. The main reason for proposing the alternative quasi-static testing protocol is to have a baseline for comparing quasi-static and dynamic test results.

4.4.1 Dynamic fragility testing protocol

The fundamental objective of the dynamic fragility testing protocol is to find the median seismic demands (interstory drifts, absolute velocities or absolute accelerations) triggering the different damage states of displacement and/or acceleration sensitive nonstructural components, systems and equipment. In order to find a relation between the demand parameters, the maximum seismic demands expected within a set of buildings with fundamental periods ranging between 0.1 and 5 seconds, representatives of several seismic resistant structural systems, are examined. The general testing protocol is developed for a generic site characterized by seismic design spectral coordinates $S_{DS}=1g$ and $S_{D1}=0.6g$. The challenge is to develop a single protocol that will trigger all potential damage states without having to repeat the load history at increased amplitude.

4.4.1.1 Frequency content of testing protocol

The instantaneous frequency for the dynamic fragility testing protocol is given by equation (4.97). The target frequency limits for the protocol are set equal to $f_{min}=1/6$ Hz and $f_{max}=5.5$ Hz, and therefore, the effective minimum testing frequency calculated according to equation (4.98) is $f_{min}^{*}=0.20$ Hz. The maximum testing frequency f_{max} is set slightly higher than 5 Hz in order to better control the number of large vibration cycles induced on acceleration sensitive nonstructural components with natural vibration frequencies in the range between 4.5 and 5 Hz.

4.4.1.2 Estimation of protocol target peak demands

This subsection presents the process for estimating the maximum peak accelerations and the maximum peak generalized drift to be imposed by the protocol histories.

4.4.1.2.1 Maximum peak spectral acceleration amplification along building height

The maximum peak spectral acceleration amplification along building height, $FRS_{Factor_{Max}}$, calculated from the factor $FRS_{Factor}(h/H)$ given in equation (4.88) and shown in Figure 4.12, is given by:

$$FRS_{Factor_{Max}} = max\left\{FRS_{Factor}\left(\frac{h}{H}\right)\right\} = FRS_{Factor}(1) = 4 \qquad (4.109)$$

4.4.1.2.2 Mean spectral acceleration shape

In order to define a conservative but rational testing protocol history, a target spectral shape, controlled by the function $\alpha(t, h/H, S_{DS}, S_{D1})$ presented in equation (4.101), should be specified. An enveloping

spectral acceleration shape is estimated assuming a factor $h/H = 1$, corresponding to a building roof level. Substituting this value into equation (4.102), a corner period $T_{Flex} = 0.75$ seconds is obtained. Accordingly, using equation (4.103), a factor $t_{T_{Flex}} = 10.2$ seconds is calculated. Finally, merging all these results into equation (4.101) a function $\alpha_F(t)$ is obtained:

$$\alpha_F(t) = 0.9 \begin{cases} sin(0.154t) & 0 \leq t < 10.2 \\ 1 & 10.2 \leq t \leq 2t_d - 10.2 \\ sin(\pi + 0.154(t - 2t_d)) & 2t_d - 10.2 < t \leq 2t_d \end{cases} \tag{4.110}$$

where $t_d = 24$ seconds is calculated using equation (4.99); and a constant sweep rate $S_r = 12$ octaves/min has been considered.

4.4.1.2.3 Maximum peak generalized drift along building height

In analogy with the calculations presented in subsection 4.4.1.2.1, the maximum peak generalized drift along building height is computed from equation (4.96):

$$\delta_{Max}^* = max\left\{\delta\left(\frac{h}{H}\right)\right\} = \delta(0) = 1.09 \% \tag{4.111}$$

4.4.1.2.4 Testing protocol modification factor

The dynamic testing protocol proposed for seismic fragility assessment incorporates a ductility modification factor, R_μ, to account for potential nonlinearities in the seismic response of the primary system. The R_μ factor allows for controlling the relation between the peak accelerations and the peak interstory drift imposed on the specimen. Subsection 4.4.1.6 describes the alternatives for applying this testing protocol for assessing the seismic fragility of distributed nonstructural components. The ductility modification factor is defined as:

$$R_\mu = \frac{R}{\Omega_o} \tag{4.112}$$

where R and Ω_o denote the response modification coefficient and the system overstrength factor, respectively. The R factor is commonly used in engineering practice to design structures under reduced elastic force levels. The R factor typically takes values between 1 and 8 (ASCE, 2005), depending on the type and characteristics of the primary structural system. Figure 4.41 shows a typical force-displacement relation used in structural design. F_E in Figure 4.41 denotes a design force level required for the structure

to remain essentially elastic, associated with a deformation level δ_E. $F_S = F_E/R$ denotes a typical reduced force level for which a structure is normally designed, with corresponding deformation level $\delta_S = \delta_E/R$.

The system overstrength factor Ω_o accounts for the expected variations of the strength of the materials used in construction, the safety factors used in structural design and the intrinsic structural system overstrength, among other factors. Typical values for the overstrength factor are in the range between 1.25 and 3. In consequence, typical values for the R_μ factor are in the range between 1 and 4. A detailed description of the parameters R and Ω_o is presented in the commentary of FEMA 450 (BSSC, 2003b).

As shown in Figure 4.41, the expected maximum force in the nonlinear system, $F_Y = \Omega_o F_S = F_E/R_\mu$, is associated with the elastic displacement $\delta_Y = \Omega_o \delta_S = \delta_E/R_\mu$. The actual maximum displacement experienced by the nonlinear system is then $\delta_{max} = \mu\delta_Y$, where μ denotes the structural ductility factor. A relation between R_μ and μ was proposed by Newmark and Hall (Newmark and Hall, 1982):

$$\mu = \begin{cases} \dfrac{R_\mu^2 + 1}{2} & \textit{In the velocity and displacement spectral regions} \\ R_\mu & \textit{In the acceleration spectral region} \end{cases} \tag{4.113}$$

The relation between R_μ and μ can be used to estimate the maximum system force and displacement:

$$F_Y = F_x\left(R_\mu\right)F_E \tag{4.114}$$

where

$$F_x\left(R_\mu\right) = \frac{1}{R_\mu} \tag{4.115}$$

and

$$\delta_{max} = \mu\delta_Y = \frac{\mu}{R_\mu}\delta_E = \begin{cases} \dfrac{R_\mu^2 + 1}{2R_\mu}\delta_E & \textit{In the velocity and displacement spectral regions} \\ \delta_E & \textit{In the acceleration spectral region} \end{cases} \tag{4.116}$$

A conservative estimate for displacement is then:

$$\delta_{max} = \frac{R_\mu^2 + 1}{2R_\mu}\delta_E \tag{4.117}$$

The $F_x(R_\mu)$ factor will be considered later to modify the platform displacement histories (and in consequence platform absolute accelerations), while a factor:

$$F_\Delta(R_\mu) = \frac{R_\mu^2 + 1}{2R_\mu}$$

(4.118)

will be used to modify the interstory drift ratios computed for the linear elastic continuous beam model studied in subsection 4.1.2. Figure 4.42 shows a plot of the $F_\Delta(R_\mu)$ factor. Finally, the R_μ factor can be selected to control the relation between the maximum absolute acceleration and interstory drift imposed by the dynamic fragility testing protocol. A more thorough discussion about the R_μ and μ parameters can be found in Uang (Uang, 1991).

4.4.1.3 Dynamic fragility protocol histories

The equations presented in subsection 4.3.1 for the qualification protocol are modified here to be used for general dynamic fragility assessment. The modifications adjust the peak interstory drifts and accelerations imposed by the protocol. However the same shape of the loading history is maintained since the number of induced and imposed cycles have been carefully calibrated.
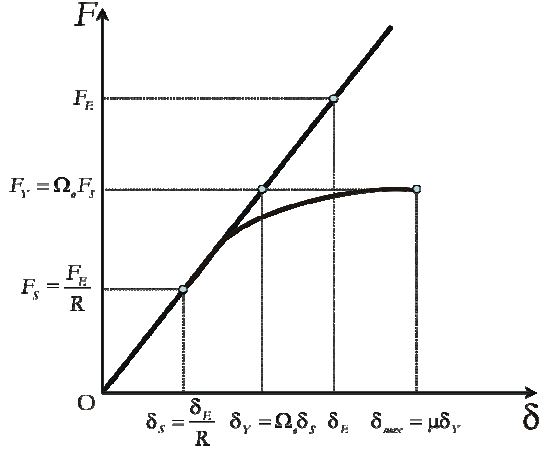
Figure 4.41. Typical force-displacement relation
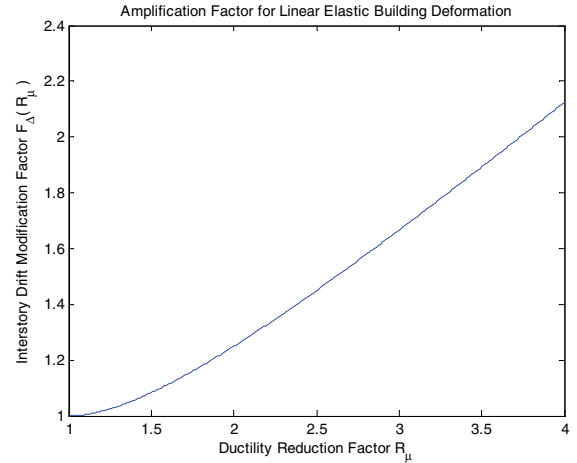
Figure 4.42. Interstory drift modification factor

4.4.1.3.1 Displacement history for UB-NCS bottom level

The closed-form equation for the displacement protocol history proposed for the UB-NCS bottom level $\left(x_{Bottom}^{Fragility}\right)$ is expressed as:

$$x_{Bottom}^{Fragility}(t) = F_x(R_\mu) FRS_{Factor_{Max}} \alpha_F(t) f(t)^\beta \cos(\varphi(t)) w(t)$$

(4.119)

where $FRS_{Factor_{Max}}$ =4 as calculated in subsection 4.4.1.2.1; $F_x(R_\mu)$ is the acceleration modification factor defined in equation (4.115); R_μ is the ductility reduction factor typically ranging between 1 and 4, corresponding to structural ductility factors μ between 1 and 8; $\alpha_F(t)$ is the spectral shape modulating function given in equation (4.110); $f(t)$ is given in equation (4.97); β = -1.25 is a constant parameter controlling the spectral shape at long periods; and $\varphi(t)$ and $w(t)$ are given in equations (4.104) and (4.105), respectively.

Conservatively, it is recommended to consider a value R_μ =1 for calculating the $F_x(R_\mu)$ factor used for generating the bottom level platform displacement history, and therefore, equation (4.119) becomes:

$$x_{Bottom}^{Fragility}(t) = FRS_{Factor_{Max}} \, \alpha_F(t) f(t)^\beta \cos(\varphi(t)) w(t) \tag{4.120}$$

Subsection 4.4.1.4 presents examples of dynamic fragility protocol histories.

4.4.1.3.2 Interstory drift protocol history

The closed-form equation for the interstory drift fragility protocol history $(\varDelta^{Fragility})$ is given by:

$$\varDelta^{Fragility}(t) = \varDelta_{Max} e^{-\left(\frac{t-t_d}{\sigma_F}\right)^2} \cos(\varphi(t)) w(t) \tag{4.121}$$

where $\varphi(t)$ and $w(t)$ are given in equations (4.104) and (4.105), respectively; and σ_F =9.8 seconds is a constant factor calibrated to impose the same mean number of total and damaging cycles imposed by the floor motions recorded in instrumented multistory buildings during strong shaking (see subsection 4.3.4). One alternative to compute maximum interstory drift to be imposed during testing, $\varDelta_{Max}$, is:

$$\varDelta_{Max} = h_{NCS} F_\varDelta(R_\mu) \frac{S_{DI}}{0.5\,g} \delta_{Max}^* \tag{4.122}$$

where h_{NCS} is the free interstory height of the UB-NCS testing facility; and $F_\varDelta(R_\mu)$ is given in equation (4.118). After substitution of S_{DI}=0.6g and δ_{Max}^* =1.09 % (maximum generalized drift ratio as calculated in subsection 4.4.1.2.3), equation (4.122) becomes:

$$\varDelta_{Max} = 1.3 h_{NCS} F_\varDelta(R_\mu) \tag{4.123}$$

where the $F_\varDelta(R_\mu)$ factor is given in equation (4.118). The ductility reduction factor R_μ takes values in the range 1 to 4, for structural ductilities in the range 1 to 8.

Conservatively, a ductility reduction factor $R_\mu = 4$, associated to a structural ductility $\mu = 8$, is recommended to be considered for generating the interstory drift protocol history. However, it is important to consider the maximum possible drift so that all possible damage states are triggered.

A second alternative for estimating the peak interstory drift Δ_{Max} to be imposed by the fragility protocol is provided in (Krawinkler *et al.*, 2000). The method, originally proposed for estimating the maximum deformation to be imposed on wood-frame components during cyclic tests, consists in performing a preliminary monotonic test to obtain the specimen deformation capacity, Δ_{Max}. This Δ_{Max} is defined as the deformation at which the load in the component drops for the first time below 80% of the maximum load sustained by the component. This approach for estimating Δ_{Max} is preferred to ensure that sufficient interstory drift is applied on the specimen to trigger all potential damage states.

The interstory drift protocol defined by equation (4.121) is symmetric about a time instant t_d, and therefore, one half of the cycles imposed by the protocol corresponds to primary cycles, while the other half, applied after reaching the target peak drift, corresponds to trailing cycles. Nevertheless the total number of rainflow cycles imposed by the protocol closely matches the median total number of rainflow cycles imposed by recorded building floor motions, as discussed in subsection 4.4.1.5. Subsection 4.4.1.4 presents examples of dynamic interstory drift fragility protocol histories.

4.4.1.3.3 Displacement history for UB-NCS top level

The fragility displacement history for the top UB-NCS level $\left(x_{Top}^{Fragility} \right)$ is calculated based on the bottom level and interstory drift fragility protocol histories. The closed-form equation for the top level protocol is:

$$x_{Top}^{Fragility}\left(t\right) = x_{Bottom}^{Fragility}\left(t\right) + \Delta^{Fragility}\left(t\right) \tag{4.124}$$

Displacements for the top and bottom UB-NCS levels are, in consequence, in phase. Subsection 4.4.1.4 presents examples of dynamic fragility protocol histories.

4.4.1.4 Example histories for dynamic fragility testing protocol

This subsection presents a series of examples of dynamic fragility testing histories. The first three cases studied consider ductility reduction factors $R_\mu = 1$, 2.5 and 4, associated to structural ductilities $\mu = 1$, 3.6 and 8.5, to modify both platform displacement and interstory drift protocol histories. A fourth case study considers a ductility reduction factor $R_\mu = 1$ for computing the bottom platform displacement history, equation (4.120); and a targeted maximum interstory drift ratio $\Delta_{Max} = 3\%$ directly substituted into equation

(4.121) for computing the interstory drift protocol history. Figure 4.43 through Figure 4.46 illustrate several key characteristics of the proposed fragility protocol for all cases studied. Table 4.9 summarizes the peak motion values for the dynamic fragility testing protocols shown in Figure 4.43 through Figure 4.46. As observed in Table 4.9 and in Figure 4.43 through Figure 4.45, the peak platform accelerations drop drastically as the R_μ factor is increased, while the imposed peak drift slowly increases. Consequently, for nonstructural systems whose seismic performance is simultaneously controlled by both accelerations and interstory drifts, it may be convenient to consider, conservatively, a ductility factor $R_\mu = 1$ (associated to an unreduced acceleration level) for calculating the bottom platform displacement history given in equation (4.119); and a value $R_\mu \geq 4$ in equation (4.123), for computing the interstory drift protocol history. This scenario is assessed in the fourth case study, whose protocol histories are shown in Figure 4.46.

Table 4.9. Envelope floor motions dynamic fragility testing protocol

Ductility Red. Factor R_μ	Peak Displacements		Peak Interstory Drift		Peak Velocities		Peak Accelerations	
	$D_{Max\ Bot}$ (in)	$D_{Max\ Top}$ (in)	Δ_{Max} (in)	δ_{Max} (%)	$V_{Max\ Bot}$ (in/s)	$V_{Max\ Top}$ (in/s)	$A_{Max\ Bot}$ (g)	$A_{Max\ Top}$ (g)
1	22.5	24.3	1.79	1.30	33.9	36.1	0.57	0.60
2.5	9.00	11.6	2.60	1.89	13.6	16.9	0.23	0.28
4	5.63	9.43	3.80	2.76	8.48	14.5	0.14	0.23
1*	22.5	26.6	4.14	3.00	33.9	39.1	0.57	0.65

* This case considers a factor R_μ=1 only for computing bottom level displacement history.

4.4.1.5 Calibration of cycles imposed/induced on specimens

This subsection assesses the number of cycles imposed and induced by the displacement and interstory drift protocols, respectively. Figure 4.47 shows comparisons between the number of rainflow cycles induced by the fragility testing protocol (for a constant sweeping rate $S_r = 12$ oct/minute) and the mean and 84th% number of rainflow cycles induced by the set of recorded building floor accelerations (described in Subsection 4.3.4) on SDOF with frequencies in the UB-NCS operating range (0.2-5 Hz). In Figure 4.47, it can be seen that for systems with frequencies lower than 1.5 Hz, the proposed testing protocol closely matches the mean number of large cycles (N_{50}) induced by the recorded floor motions. For SDOF systems with frequencies in the range 1.5 to 3.5 Hz, the testing protocol closely matches the 84th percentile number of large cycles induced by real building floor motions. For oscillators with natural frequencies larger than 3.5 Hz, the testing protocol overestimates the 84th percentile number of large cycles induced by real floor motions. More importantly, it is observed that the testing protocol closely matches the mean total number of damaging excursions (N_{10}) for oscillators with natural frequencies in the range of interest (0.2-5 Hz).
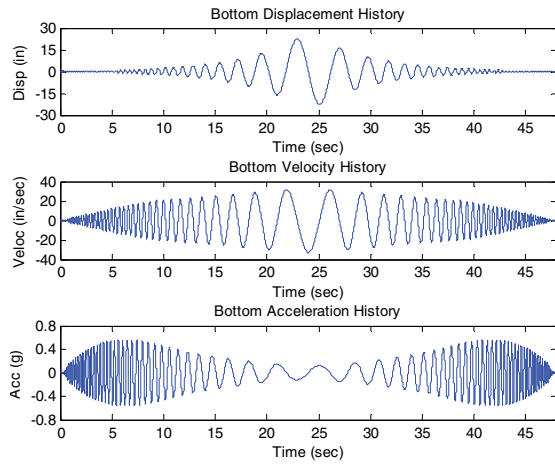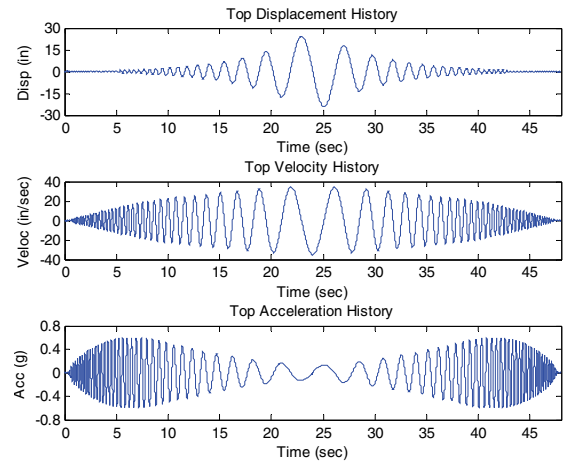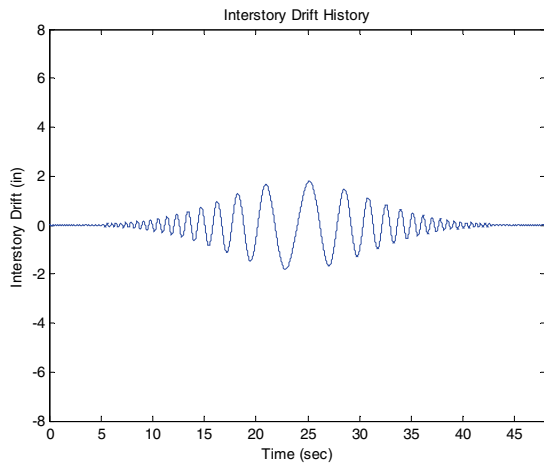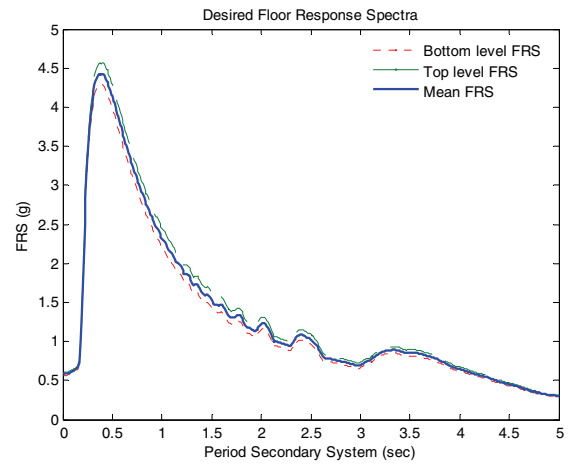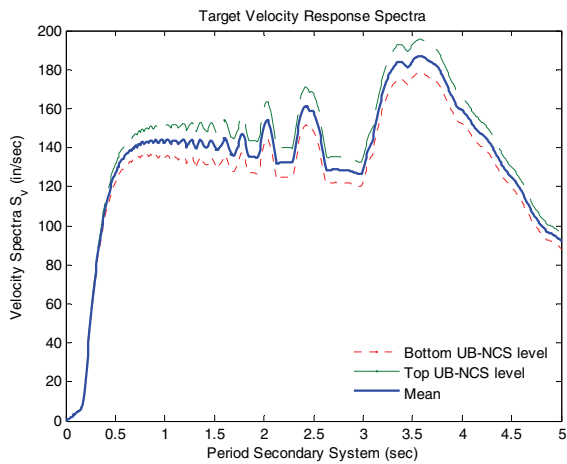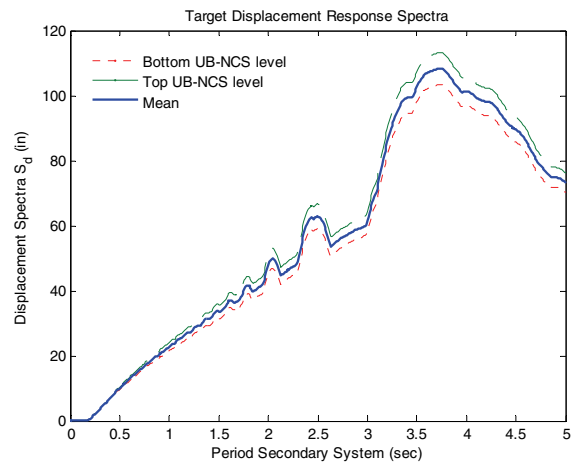
Figure 4.43. Proposed dynamic fragility protocol, R_μ=1: (a) Bottom platform motions; (b) Top platform motions; (c) Interstory drift history; (d) Acceleration response spectrum; (e) Velocity response spectrum; and (f) Displacement response spectrum
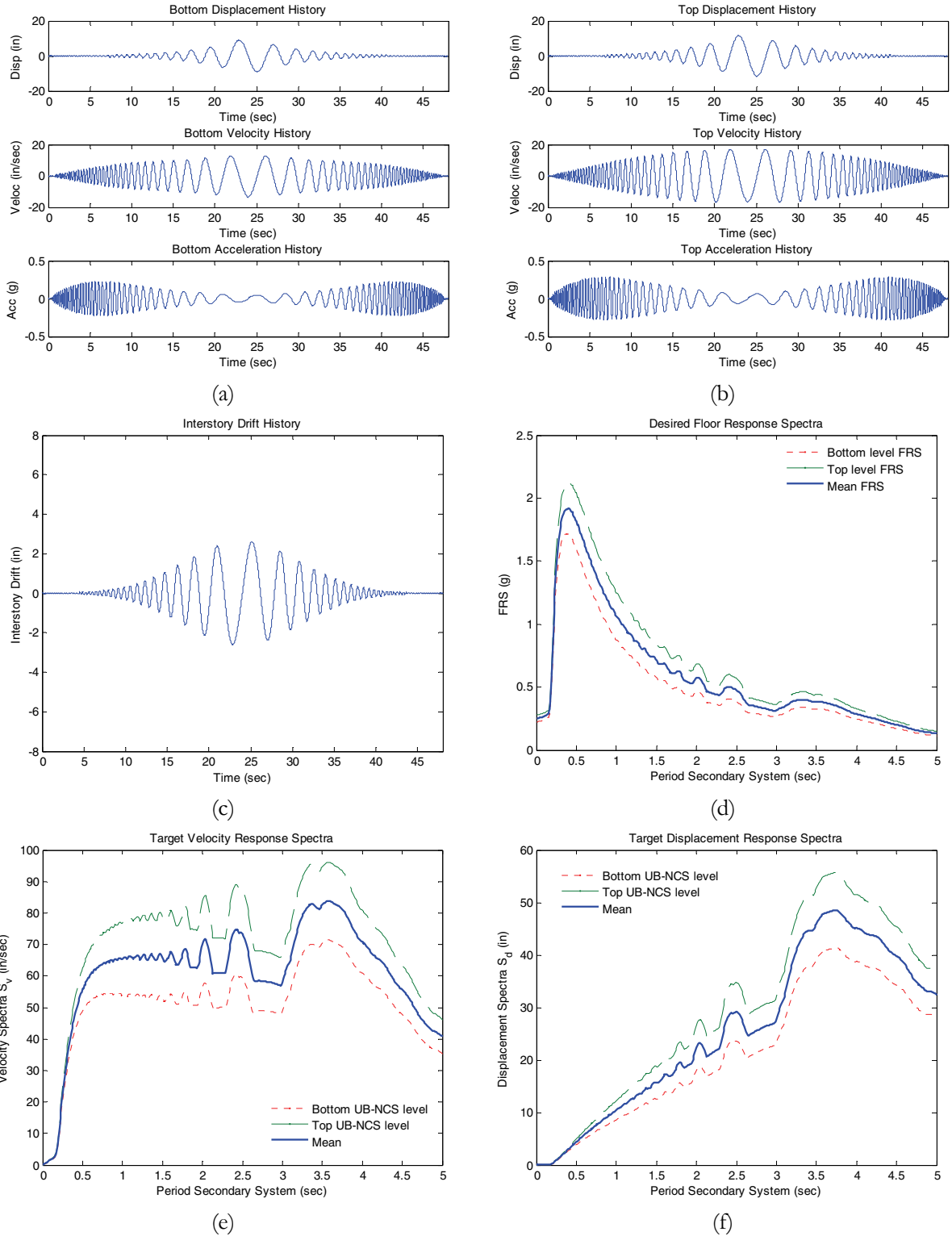
Figure 4.44. Proposed dynamic fragility protocol, R_μ=2.5: (a) Bottom platform motions; (b) Top platform motions; (c) Interstory drift history; (d) Acceleration response spectrum; (e) Velocity response spectrum; and (f) Displacement response spectrum
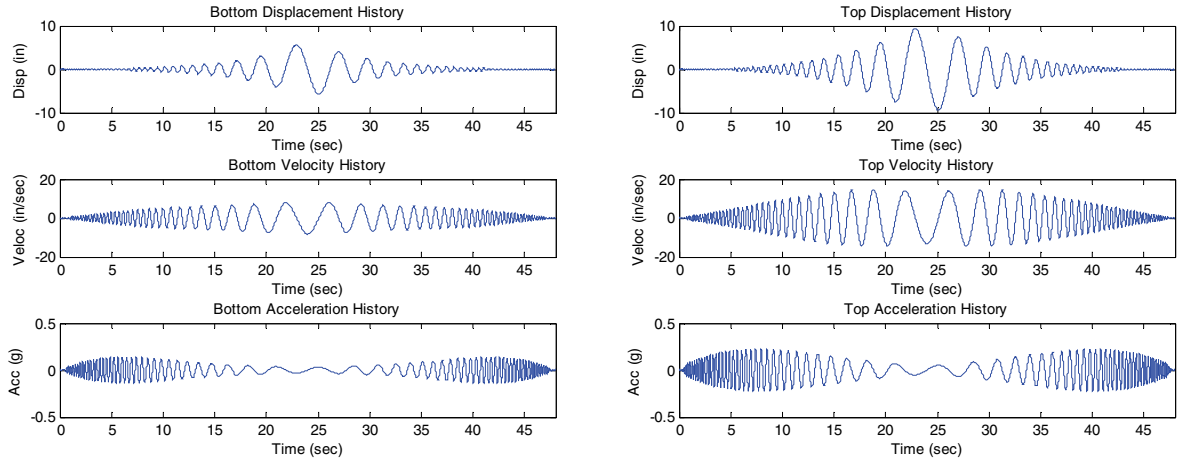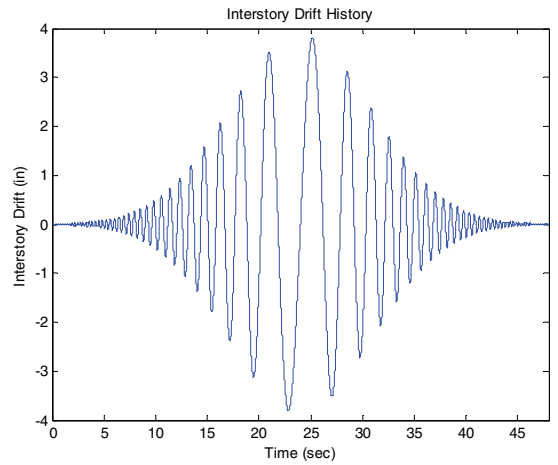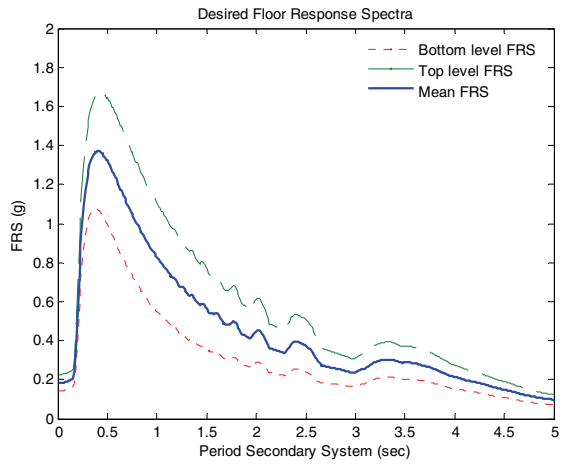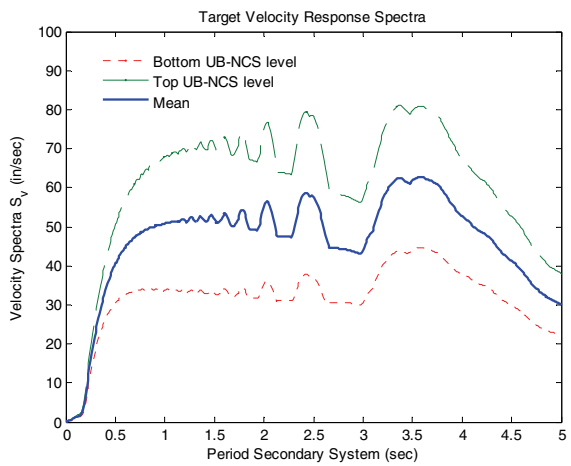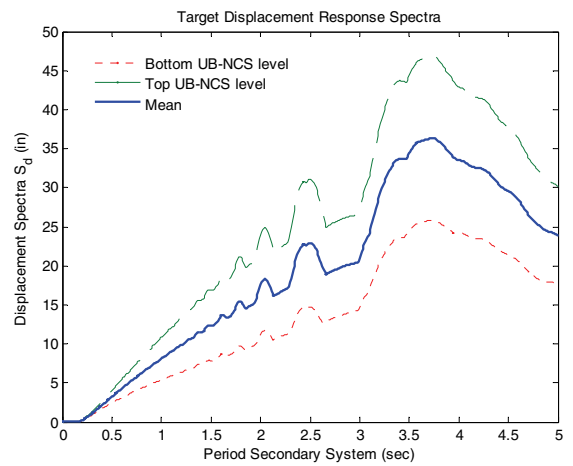
Figure 4.45. Proposed dynamic fragility protocol, R_μ=4: (a) Bottom platform motions; (b) Top platform motions; (c) Interstory drift history; (d) Acceleration response spectrum; (e) Velocity response spectrum; and (f) Displacement response spectrum
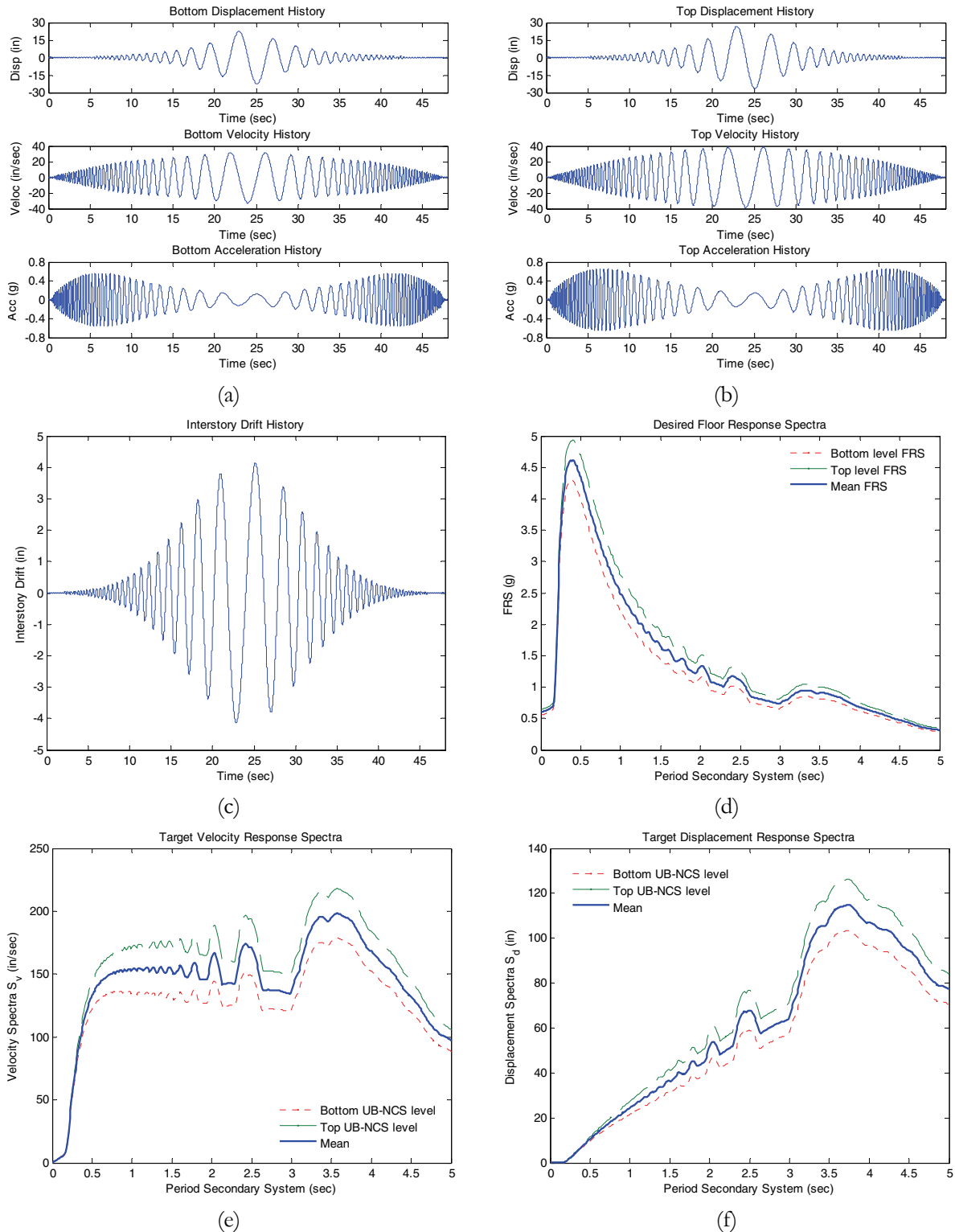
Figure 4.46. Proposed dynamic fragility protocol, $R_\mu=1$ and $\Delta_{Max}=3\%$: (a) Bottom platform motions; (b) Top platform motions; (c) Interstory drift history; (d) Acceleration response spectrum; (e) Velocity response spectrum; and (f) Displacement response spectrum

The "Rainflow" counting algorithm was also applied to the proposed interstory drift dynamic fragility protocol to verify the adequacy of the parameter $\sigma_F = 9.8$ seconds, controlling the shape of the Gaussian enveloping function, considered in equation (4.123). Figure 4.48 compares the number of rainflow cycles imposed by the proposed testing protocol and by recorded building floor motions. The adequacy of the value considered for the parameter σ_F is demonstrated in Figure 4.48. In Figure 4.48 it is seen that the number of rainflow cycles imposed by the interstory drift protocol closely matches the mean number of rainflow cycles imposed by real building interstory drift histories. It is seen that the combined use of the calibrated Gaussian window and the proposed instantaneous frequency function allows for closely matching the mean number of cycles in the whole profile of cycle amplitudes, for which λ varies between 10 and 90.
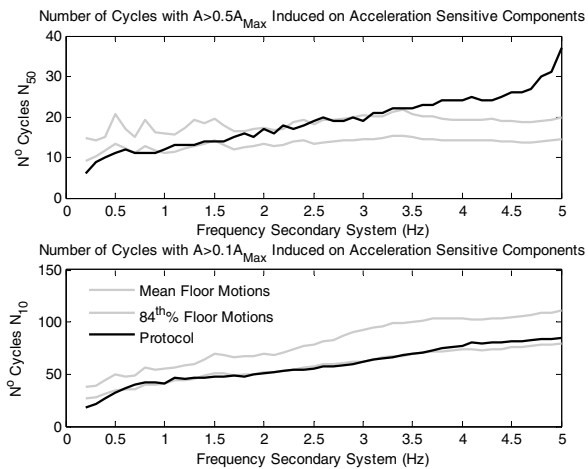
Figure 4.47. N_{10} and N_{50} number of rainflow cycles induced by dynamic fragility platform protocol motions
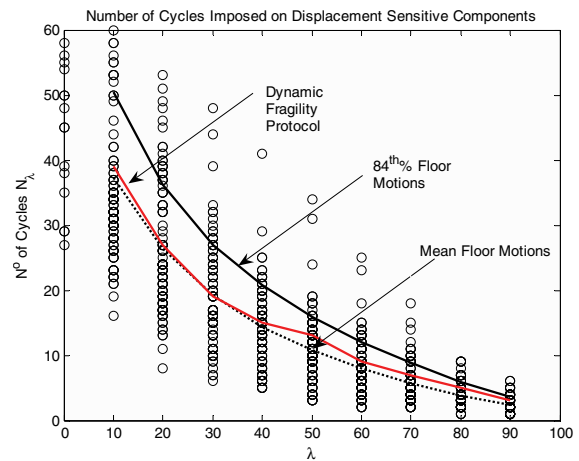
Figure 4.48. Number of rainflow cycles imposed by recorded building interstory drifts and dynamic fragility drift protocol

The number of rainflow cycles shown in both Figure 4.47 and Figure 4.48 are valid for the proposed fragility protocol, independent of the R_μ factor considered for generating the floor and interstory drift histories.

4.4.1.6 Recommendations for using dynamic fragility testing protocol

Two options are described in this subsection for using the proposed dynamic fragility testing protocol for assessing the seismic performance of distributed nonstructural components, systems and equipment sensitive to both absolute floor accelerations and interstory drifts. The options depend on the damage characteristics of the specimens and their sensitivity to low amplitude cycles.

4.4.1.6.1 Equipment sensitive to low cycle fatigue damage

For nonstructural components, systems and equipment susceptible of exhibiting low cycle fatigue damage, the experimental seismic fragility should be evaluated through a single test. In order to capture the instant at which each damage state is triggered, time-stamped high definition videos should be used to correlate with the applied accelerations, velocities and interstory drifts. Extensive instrumentation is required all along the specimen's components for characterizing the seismic demand path traveling from the platforms to the specimen's components.

Nevertheless, a low intensity test will be required for compensating the input command signal to be used in the single final test and for checking the functionality of the data acquisition system.

4.4.1.6.2 Equipment not sensitive to low cycle fatigue damage

In the case that the nonstructural component, system or equipment is not sensitive to low cycle fatigue damage, a procedure similar to the one described in FEMA 461 can be used. The protocol can be applied at several increasing levels of shaking in order to populate the fragility data curves for all damage states anticipated for the specimen. The minimum testing amplitude, generally performed for checking the functionality of the data acquisition system, should be large enough to allow for an appropriate compensation of the equipment's command input signal; while the maximum testing amplitude should be within the operational limits of the equipment. Moreover, the number of tests to be carried out during the experimental fragility test series should be carefully selected. Section 5 presents a detailed example of the application of the proposed methodology for assessing experimentally the seismic performance of displacement and acceleration sensitive components included in a full scale composite hospital emergency room.

4.4.2 Quasi-static fragility testing protocol

The main objective of the quasi-static fragility testing protocol is to assess the median seismic demands triggering the different damage states of distributed nonstructural components, systems and equipment which are not loading rate dependent. The proposed protocol is intended to be consistent with the protocol included in the current version of FEMA 461 (FEMA, 2006) and the testing procedures previously presented in this section. The basic difference resides in that this alternative testing protocol has been calibrated to impose a number of cycles matching observations of recorded building floor motions. The philosophy and methodology for applying the proposed quasi-static testing protocol are identical to the ones described in FEMA 461.

The interstory drift protocol history presented in this subsection consists of a simple but general loading pattern that can be applied by using any displacement-controlled testing equipment. In particular, the protocol can be imposed on full-scale specimens by using the UB-NCS testing facility, inputting the protocol history at the top platform and keeping the bottom platform at rest.

All cycles imposed by the quasi-static fragility protocol are primary cycles. No trailing cycles are considered in the proposed history. Furthermore, and in order to use the same principles described along this section, all parameters controlling the shape of the testing protocol have been recalibrated.

4.4.2.1 Quasi-static fragility testing protocol histories

The closed form equation for the quasi-static fragility testing protocol is given by:

$$\Delta_{QS}(t) = \Delta_{Max} e^{-\left(\frac{t-t_{QS}^*}{\sigma_{QS}}\right)^2} cos\left(\varphi_{QS}(t)\right) \qquad t_{min}^{QS} \leq t \leq t_d^{QS} \tag{4.125}$$

where Δ_{Max} is the maximum interstory drift ratio imposed by the testing protocol, typically set equal to 3 or 4%, or according to the methods described in subsection 4.4.1.2.3. The parameter $\sigma_{QS} = 258.9$ seconds controls the shape of the testing protocol envelope. The parameter t_{QS}^* corresponds to the time at which the peak drift is reached, calculated as:

$$t_{QS}^* = -\frac{1}{S_r^{QS} ln2} ln\left(1 - \left\lfloor 2\frac{f_{max}^{QS} - f_{min}^{QS}}{S_r^{QS} ln2} + \frac{1}{2}\right\rfloor \frac{S_r^{QS} ln2}{2 f_{max}^{QS}}\right) \tag{4.126}$$

where the parameters $S_r^{QS} = 0.467$ octaves/min, $f_{max}^{QS} = 0.167$ Hz, and $f_{min}^{QS} = 0.011$ Hz have been calibrated to impose a controlled number of cycles on displacement sensitive nonstructural components. Although it is recognized that the low frequencies considered in equation (4.126) do not have any effect on the specimen performance, their relation, in conjunction with the value of the sweep rate S_r^{QS}, controls the number of large and small cycles imposed by the protocol. The operator $\lfloor \ \rfloor$ in equation (4.126) denotes the floor function. The function $\varphi_{QS}(t)$ in equation (4.125), derived from equation (4.104), is the instant testing phase, given by:

$$\varphi_{QS}(t) = \frac{2\pi f_{max}^{QS}}{S_r^{QS}}\left[1 - \left(\frac{f_{min}^{*QS}}{f_{max}^{QS}}\right)^{\frac{t}{t_d^{QS}}}\right] \qquad t_{min}^{QS} \leq t \leq t_d^{QS} \tag{4.127}$$

where f_{min}^{*QS} denotes the effective minimum testing frequency, and which in analogy with the dynamic case, is calculated using:

$$f_{min}^{*\,QS} = \frac{S_r^{QS}\,ln\,2}{2}\left(\frac{1}{2} - \left\lfloor \frac{4\,f_{max}^{QS} - 4\,f_{min}^{QS} + 1}{S_r^{QS}\,ln\,4} \right\rfloor\right) + f_{max}^{QS} \tag{4.128}$$

The limits of equation (4.125) and (4.127) are given by:

$$t_d^{QS} = \frac{1}{S_r^{QS}}\,log_2\,\frac{f_{max}^{QS}}{f_{min}^{*\,QS}} \tag{4.129}$$

$$t_{min}^{QS} = -\frac{1}{S_r^{QS}\,ln\,2}\,ln\left\{1 - \frac{S_r^{QS}\,ln\,2}{4\,f_{max}^{QS}}\left(\left\lfloor\frac{2\,f_{max}^{QS}}{S_r^{QS}\,ln\,2}\left[1 - \left(\frac{f_{min}^{*\,QS}}{f_{max}^{QS}}\right)^{\frac{t_{QS}^* - \sigma_{QS}\sqrt{ln\frac{1}{\chi}}}{t_d^{QS}}}\right] + \frac{1}{2}\right\rfloor - 1\right)\right\} \tag{4.130}$$

The parameter t_d^{QS} defined in equation (4.129) denotes the total duration of the quasi-static protocol. The parameter χ in equation (4.130), accounts for the minimum drift amplitude considered in the test history, expressed as a fraction of the maximum drift Δ_{max}. A value $\chi = \Delta_{min}/\Delta_{max} = 0.05$ is recommended here, as in FEMA 461. The parameter t_{min}^{QS} defined in equation (4.130) corresponds to the time at which the protocol defined in equation (4.125) crosses the horizontal axis (zero interstory drift ratio) before reaching for first time the minimum interstory drift ratio considered in testing. All the aforementioned calculations can be performed using standard mathematical worksheets. Figure 4.49 shows examples of interstory drift histories for a target interstory drift ratio $\Delta_{Max} = 3\%$, and for parameters $\chi = 0.05$ and 0.10.
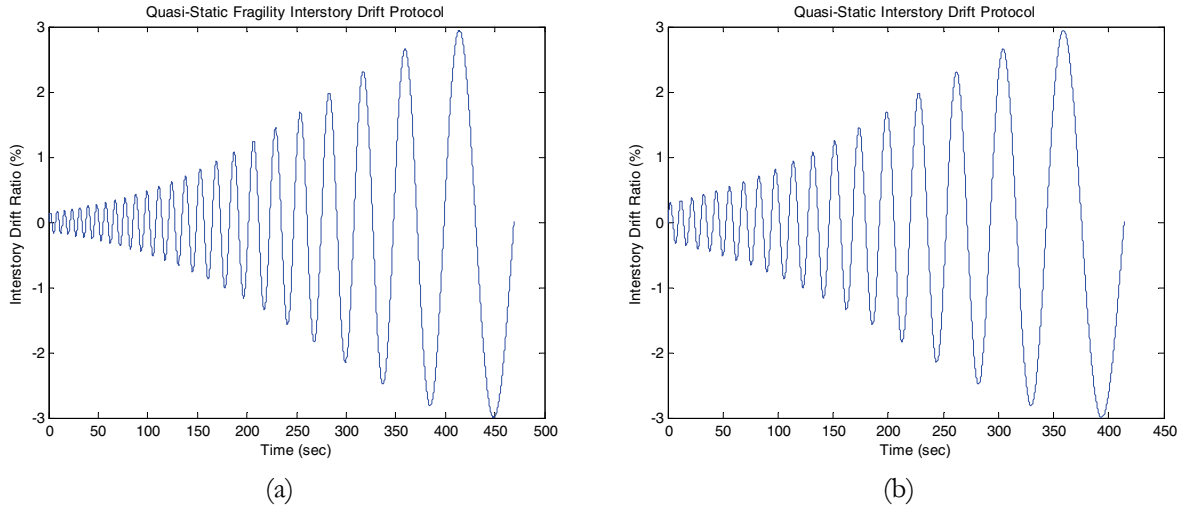
Figure 4.49. Quasi-static fragility interstory drift history for: (a) $\chi = 0.05$ and (b) $\chi = 0.10$

The time scale shown in Figure 4.49 is only illustrative of the total duration of the test. The time variable has been included in equations (4.125) through (4.130) for consistency with the equations presented in

preceding subsections and for protocol calibration purposes. In Figure 4.49, it is observed that all cycles imposed by the quasi-static fragility protocol are primary cycles.

4.4.2.2 Additional comments on the proposed quasi-static fragility testing protocol

The testing protocol presented in the previous subsection is recommended for use following the same methodology detailed in FEMA 461 and therefore, further details are not presented here.

The parameters controlling the shape of the quasi-static fragility protocol were calibrated to impose a controlled number of "rainflow" cycles on displacement sensitive components, systems and equipment. Figure 4.50 compares the number of rainflow cycles imposed by the proposed testing protocol and by recorded building floor motions. The number of cycles with $N_\lambda \geq 10$ imposed by the protocol histories generated for $\chi = 0.05$ and 0.10 are the same, and therefore, only one curve is shown. In Figure 4.50, it is observed that the number of rainflow cycles imposed by the interstory drift protocol matches the mean number of rainflow cycles imposed by real building interstory drift histories, in the whole profile of cycle amplitudes. It is also observed that the FEMA 461 protocol imposes a reduced number of cycles with amplitude smaller than 50% of the maximum drift (lower number of small cycles). Figure 4.51 shows a comparison of the normalized (with respect to the first and last cycle amplitudes) cycle amplitude increase for the quasi-static protocol for the cases $\chi = 0.05$ and 0.10 and for the FEMA 461 protocol.
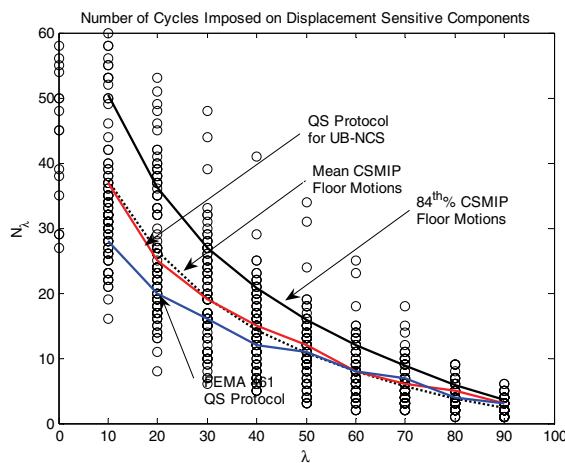
Figure 4.50. Number of rainflow cycles imposed by recorded building interstory drifts and quasi-static fragility drift protocol
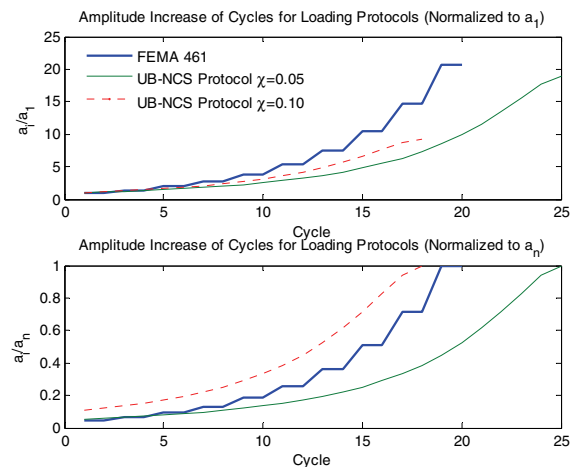
Figure 4.51. Comparison of cycle amplitude increase for UB-NCS quasi-static fragility protocol and FEMA461 quasi-static testing protocol

In Figure 4.51 it is observed that the cycle amplitude, normalized with respect to the amplitude of the first cycle, increases faster in the FEMA 461 testing protocol than in the UB-NCS testing protocol. This is a consequence of the lower number of small cycles imposed by the FEMA protocol. In the case in which the cycle amplitude is normalized with respect to the maximum imposed interstory drift, the protocol for

$\chi = 0.10$ exhibits a similar rate of increase as the FEMA 461 quasi-static protocol. It is also observed that by increasing the value of χ, the total number of cycles imposed by the UB-NCS quasi-static fragility protocol is reduced from $n=25$ to $n=18$. However, the ratio a_n/a_1 becomes significantly different.

4.5   Summary

A detailed methodology for estimating the hazard consistent seismic demands expected along the height of linear elastic multistory buildings has been presented. The seismic demands were derived by applying the theory of random vibration processes to continuous building models. The estimated absolute accelerations and story drift demands were incorporated into a set of testing protocols equations specially calibrated to impose simultaneously those seismic demands for the seismic qualification and fragility assessment of nonstructural components, systems and equipment located within multistory buildings. The testing methodology proposed here will be used in section 5 for evaluating the seismic performance of a typical hospital emergency room and assessing the dynamic interactions between its architectural components and medical equipment.

SECTION 5

SEISMIC PERFORMANCE ASSESSMENT OF A FULL-SCALE HOSPITAL EMERGENCY ROOM

This section describes the first large-scale experimental tests performed using the University at Buffalo Nonstructural Component Simulator (UB-NCS). A model hospital emergency room was constructed and subjected to two types of excitations: (i) the proposed qualification protocol (see subsection 4.3) that applies seismic demands consistent with building floor motions, and (ii) simulated floor motions obtained from a four story building model excited by hazard consistent ground motion realizations. The emergency room specimen included architectural finishes, distributed piping systems for medical gas and fire extinguishing systems, and content such as life support medical equipment. These experiments also serve to demonstrate the actual testing capabilities of the UB-NCS, subjecting various nonstructural systems to realistic floor motion demands.

The main objectives and scopes of the experimental program are described in Subsection 5.1. Subsection 5.2 presents a description of the test specimen, including construction details, and Subsection 5.3 summarizes the tests program and the instrumentation used to monitor the response of the specimen. Subsection 5.4 presents the results and observations from the experiments.

The analysis and discussion of the results and experimental observations described in this Section are presented in Section 6.

5.1   Objectives and scope of experiment

The main objectives of the full-scale hospital test series were: (i) to valuate the actual capabilities and limitations of the UB-NCS in subjecting full-scale nonstructural components and systems to full-scale floor motions; (ii) to evaluate the seismic performance of a full-scale hospital emergency room and assess the seismic behavior of individual components as well as the seismic interactions among the various nonstructural components and medical equipment typically found in an emergency room setting; and (iii) to evaluate the feasibility and efficiency of the novel testing protocol described in Section 4 specifically developed to assess the seismic performance of nonstructural components, systems and contents sensitive to accelerations and/or displacements.

The seismic performance of the test specimen was assessed considering floor motions obtained from a suitable testing protocol, as described in Subsection 5.3.1, and the simulated seismic response of a four story medical facility. Recorded building floor motions are not directly used in the test series but their

properties (frequency content, number of cycles induced and imposed, etc.) are implicit in the properties of the testing protocol considered.

5.2   Description of Emergency Room (ER) test specimen

A full-scale Emergency Room (ER) mock up was constructed for seismic testing under full-scale floor motions. Only the nonstructural components, content and equipment were included in the experiment. The room was enclosed by steel studded gypsum partition walls with a layout similar to a specimen previously tested by Restrepo and Lang (Lang, 2007; Lang and Restrepo, 2006; Restrepo and Lang, 2005) using the FEMA 461 pseudo-static loading protocol. The reason for constructing a similar specimen was to compare the behavior of partitions walls when subjected to a dynamic loading protocol. Minor modifications were made to the original design in order to fit the specimen within the UB-NCS (Keller and Mosqueda, 2005). The walls were constructed between concrete slabs attached to the UB-NCS as shown in Figure 5.1. The room was approximately 4.4 m (14'-6") in length, 3.2 m (10'-7") in width, and 3.85 m (12'-6") in height, as shown in Figure 5.2.

Figure 5.1. Photograph of UB-NCS with concrete slabs
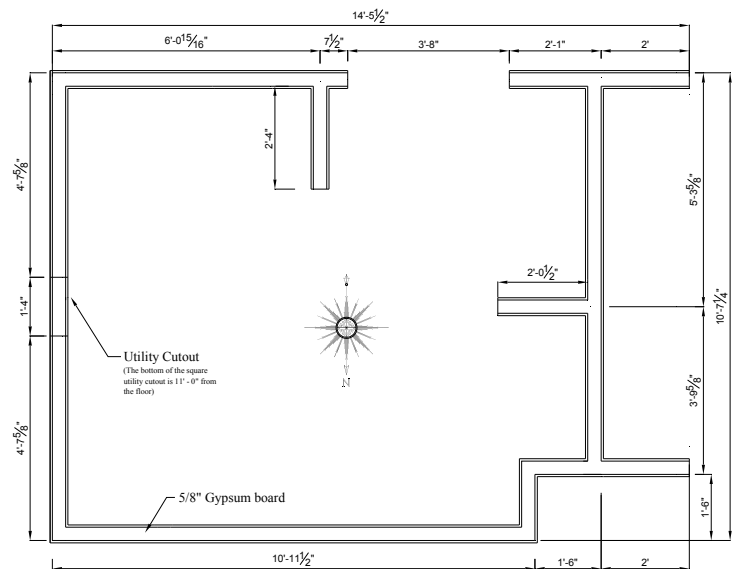
Figure 5.2. Geometry of specimen for the UB-NCS demonstration project

The simulated emergency room was furnished with medical equipment critical for inpatients' life support following a seismic event (Myrtle *et al.*, 2005). Medical equipment found in other hospital critical services was also considered for demonstration purposes. The nonstructural components and systems, along with the medical equipment included in these experiments, are listed in Table 5.1.

Table 5.1. Nonstructural components and medical equipment included in specimen

	Nonstructural components and equipment
1	Steel stud framed gypsum partition walls
2	Suspended ceiling and suspended light
3	Flooring
4	Sprinkler system
5	Medical gas pipes with in-wall outlets
6	Wall mounted patient monitors
7	Freestanding poles with IV infusion pumps
8	Ceiling mounted surgical light
9	Operating room video equipment rack
10	Gurney
11	Medical cart on casters
12	180 lb crash dummy

Detailed descriptions of the key items listed in Table 5.1 are presented in the following subsections. Figure 5.3 shows a general layout of the medical equipment included in the experiment and Figure 5.4 shows several photographs of the interior of the emergency room.
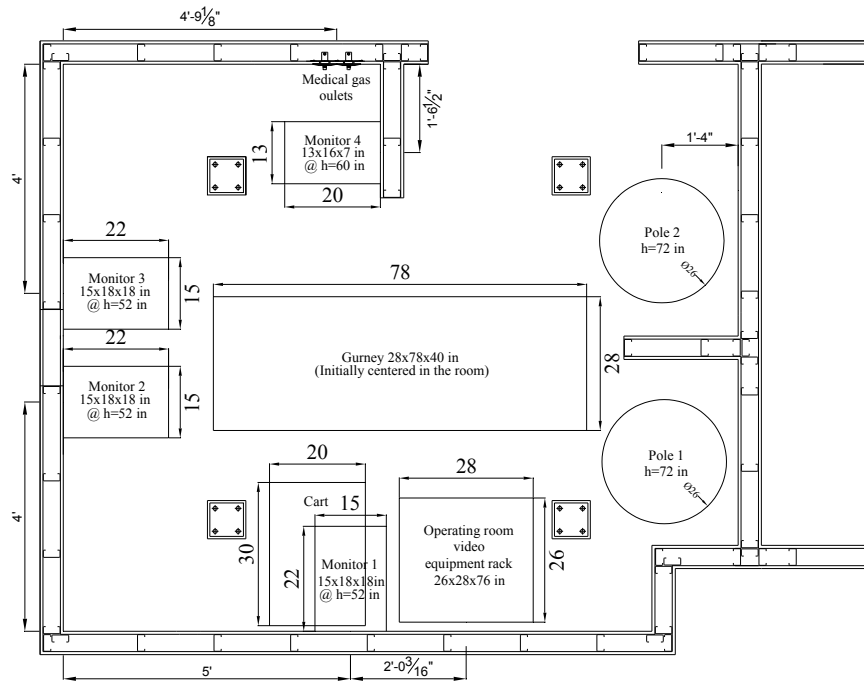
Figure 5.3. Plan layout for equipment in emergency room tests

155
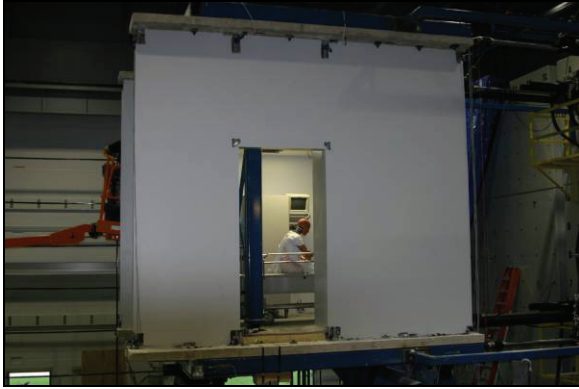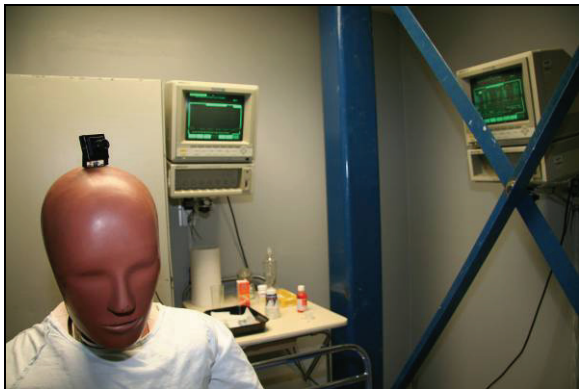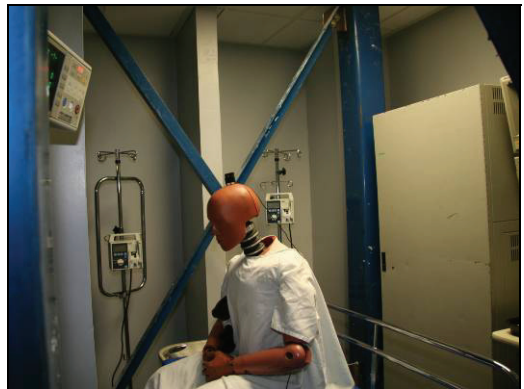
Figure 5.4. Photographs of interior of emergency room: (a) view through door opening; (b) dummy sitting on gurney, video rack, and monitor 1; (c) monitors 1 and 2, and medical cart; and (d) dummy, poles 1 and 2, and video rack

For fragility assessment purposes, the hospital emergency room was subjected to increasing levels of shaking including design and maximum considered earthquake level motions, as detailed in Subsection 5.3. The floor displacement histories considered for these tests were obtained from the simulated response of an existing medical facility located in the San Fernando Valley, in Southern California, and from a simplified version of the qualification testing protocol described in Subsection 4.3.

5.2.1   Partition walls

Figure 5.5 shows the elevations and dimensions of the gypsum partition walls enclosing the emergency room. Figure 5.6 and Figure 5.7 show isometric views of the steel stud framing system and the finished specimen, respectively.
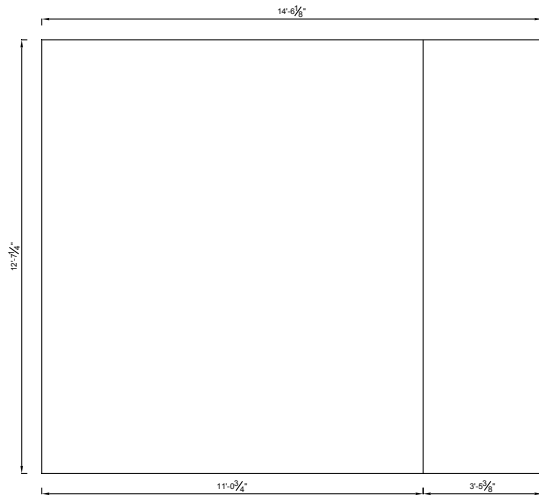
Exterior View North Wall
Scale: -
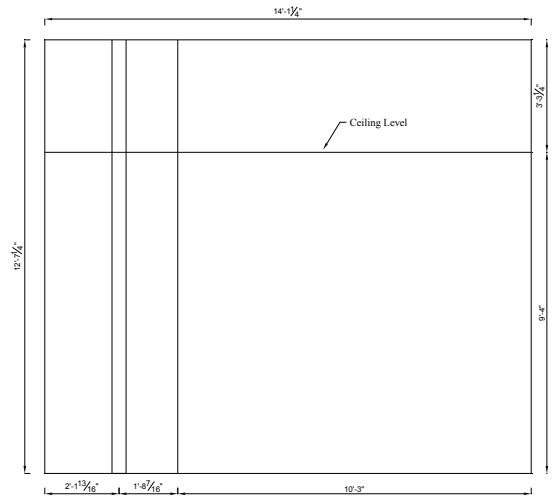
Interior View North Wall
Scale: -
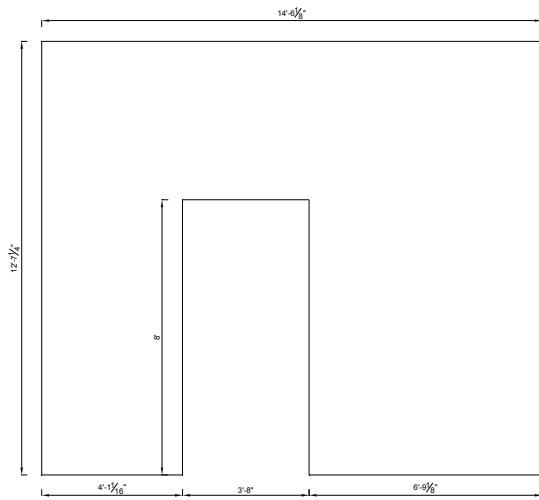
Exterior View South Wall
Scale: -
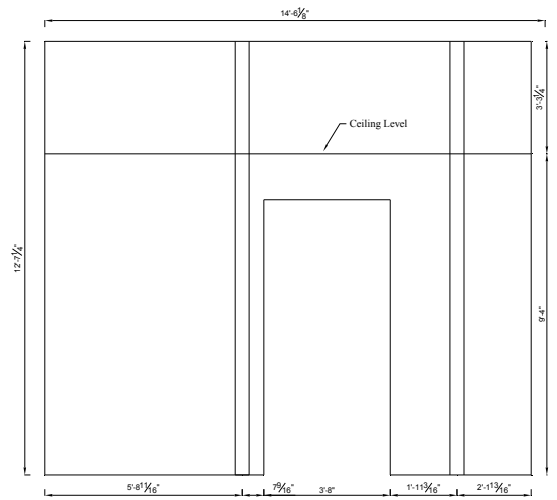
Interior View South Wall
Scale: -
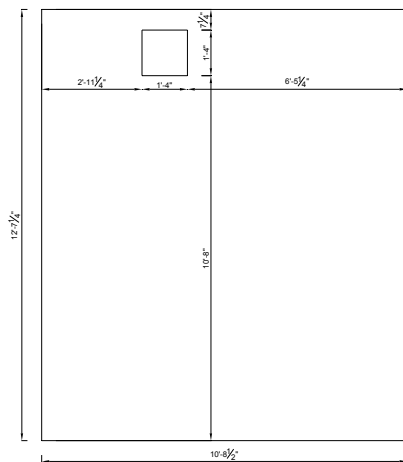
Exterior View East Wall
Scale: -
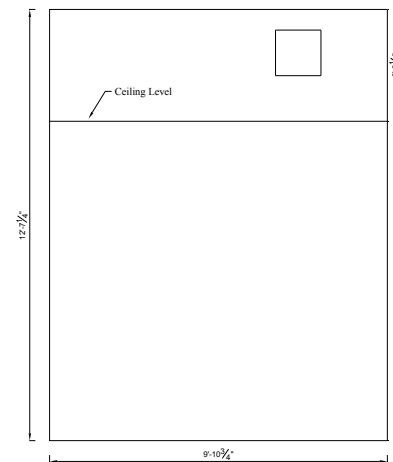
Interior View East Wall
Scale: -

Figure 5.5. Elevations partition walls

157

Exterior View West Wall
Scale: -

Interior View West Wall
Scale: -
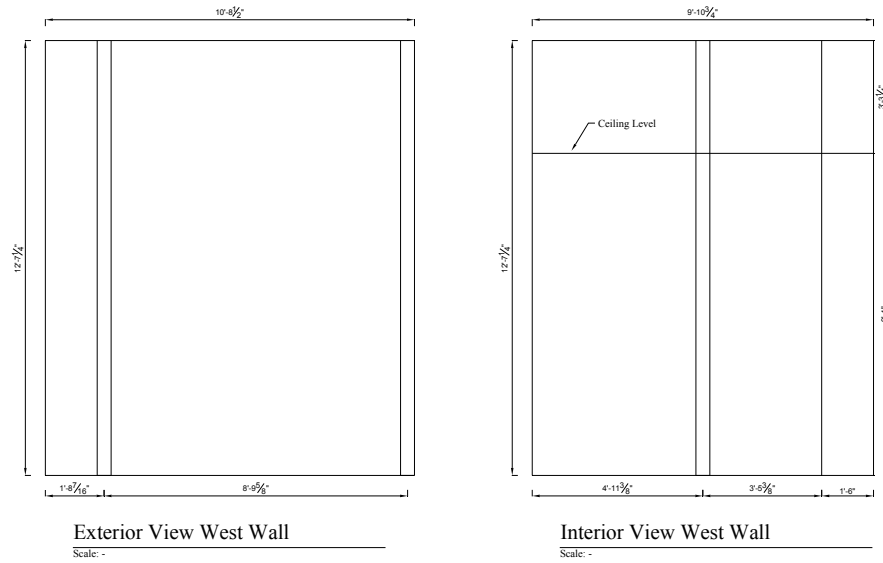
Figure 5.5. Elevations partition walls (Cont'd)

Figure 5.6. Isometric view of steel stud framing

Figure 5.7. Isometric view of finished specimen

The partition wall frame was constructed using steel studs model SSMA 362S125-43 (18 gauges in thickness) with a typical spacing of 40 cm (16") and slotted tracks model SSMA 362T125-43 (18 gauges in thickness). The tracks were connected to the 4" in thickness concrete platform slabs (cylindrical strength $f'_c \approx$ 3.3-4.0 ksi) detailed in Figure 5.8 and Figure 5.9 using standard power driven 25 mm (1")

fasteners, spaced at 30 cm (1') using a Ramset gun model SA-270 and Ramset .27 caliber shots. Two fasteners were used at the track ends and wall intersections. Studs were screwed to bottom and top tracks and to adjacent studs at wall intersections (with a spacing of 18" o.c.) using standard Phillips self-drilling #8 screws, as shown in Figure 5.10. A gap of approximately 1/8" was left in the connection between the top ends of studs and top tracks. The construction of the steel stud framing followed specifications contained in the Steel Stud Manufacturers Association manual (SSMA, 2001).

Figure 5.8. Detail geometry of concrete slab

Figure 5.9. Detail reinforcement of concrete slab

Figure 5.10 shows typical stud arrangements at wall intersections. Figure 5.11 shows the detail of the bottom and top stud to track and gypsum to stud and track connections. Figure 5.12 shows a photograph of the typical connections of studs to tracks and studs to studs at wall intersections. Figure 5.13 shows the details of the door frame around the opening, including the connections to the main steel stud frame. Figure 5.14 shows the detail of the connection of the top track to the concrete slab, including the typical distribution of fasteners. A general view of the completed steel stud framing system is provided in Figure 5.15.

Figure 5.10. Stud arrangement at wall intersections

Figure 5.11. Stud to track and gypsum to stud and track connections details

Gypsum wallboard panels (4'x8') with a thickness of 15 mm (5/8") were screwed to the studs using standard Phillips self-drilling #6 screws. Typical spacing for screws was 12 and 8 inches for field and perimeter screws, respectively. Drywall panel joints were offset on opposite faces of partition walls. Gypsum wallboards were screwed to the top and bottom tracks. The partition walls were finished with metal corner beads (1-1/4"), drywall paper joint tape (2-1/16" in width), mud and water-based semi-gloss paint. Figure 5.16 and Figure 5.17 show general views of the installed gypsum drywall panels on the south, and east and north walls, respectively.
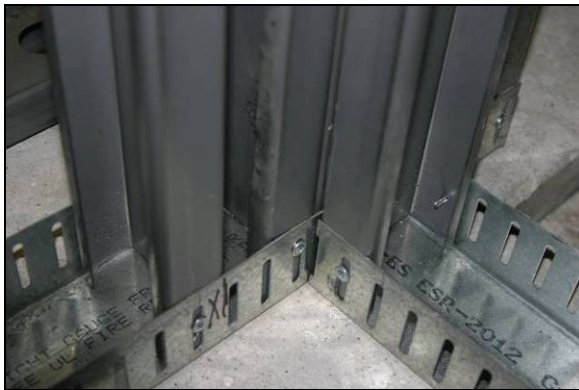
Figure 5.12. Wall intersection detail

Figure 5.13. General view of door opening frame

Figure 5.14. Top track connection detail

Figure 5.15. General view of steel stud framing

160

Figure 5.16. General view of gypsum wallboards panels in south wall
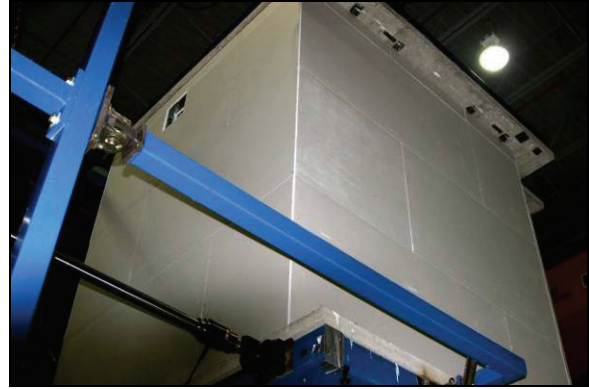
Figure 5.17. General view of gypsum wallboard panels in east and north walls

5.2.2 Suspended ceiling

A suspended ceiling system was installed for finishing the interior of the emergency room. The ceiling was placed at a height of 9' above the finished floor level. The main beams and cross tees were Armstrong model Prelude XL 15/16" Fire Resistant, exposed tee. The wall moldings used were 2"x2" angle sections. The main runners were installed in the east-west direction at spacing of 4' on center. Four ft. cross runners were installed in the north-south direction at spacing of 2' on center, whereas 2' cross runners were installed in the east-west direction at spacing of 2' on center. The tiles used were 24"x24" Fine Fissured with Angled Tegular edge profile. Figure 5.18 shows the layout of the ceiling grid.
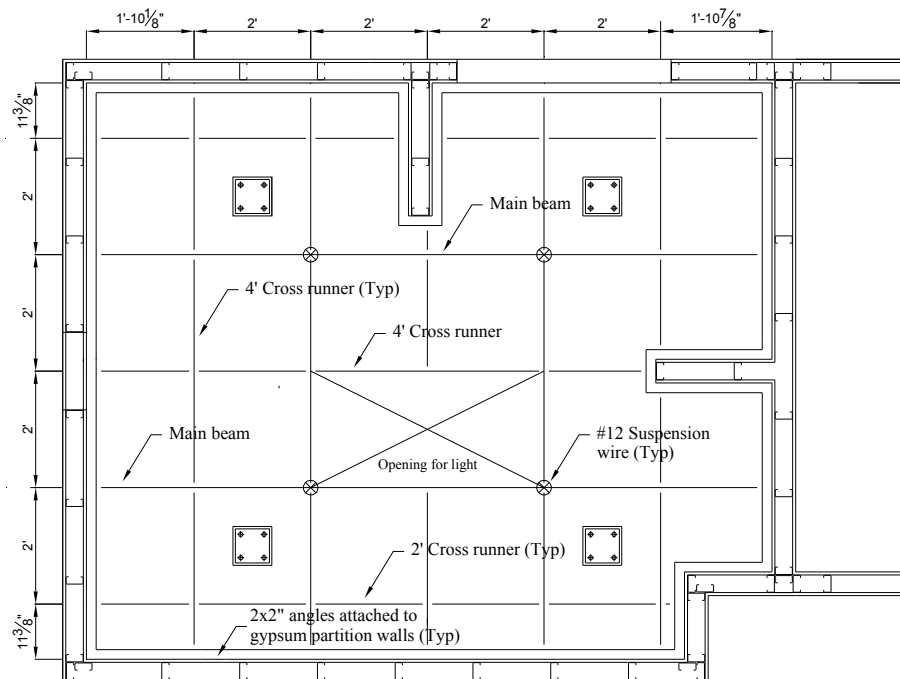
Figure 5.18. Layout of suspended ceiling grid

Standard steel hanger wires #12 in gage were used to support the main beams at the points indicated in Figure 5.18. The spacing between wire hangers was 4' in both directions. A 24x48" light was installed in the opening shown in Figure 5.18, with its weight supported by the ceiling grid.

Figure 5.19 shows a detail of the connection between the main beams and the 4' in length cross tees. The connection detail of the wire used to suspend the ceiling grid and the light attached to the grid is also shown. The wall molding angle supporting the perimeter of the ceiling can be seen in Figure 5.20. Figure 5.21 shows a general view of the installed ceiling while Figure 5.22 shows the detail of the ceiling around one of the UB-NCS columns.
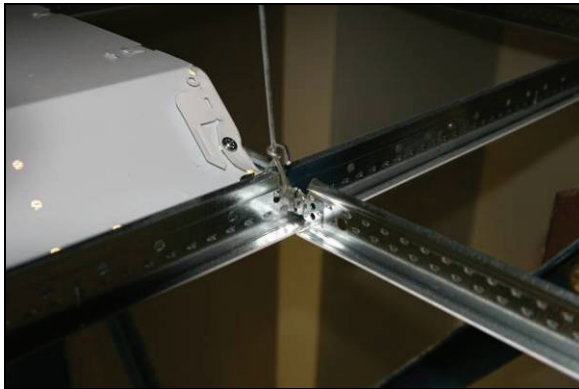
Figure 5.19. Main runner and grid hanger detail

Figure 5.20. Ceiling grid and wall molding detail
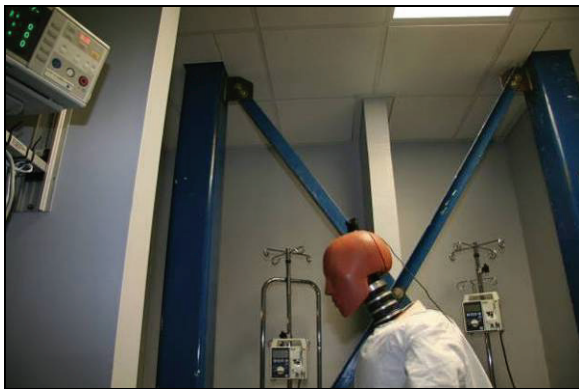
Figure 5.21. General view of suspended ceiling
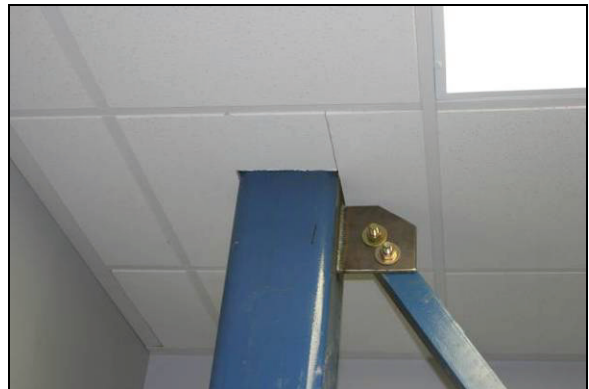
Figure 5.22. Detail of ceiling around UB-NCS column

5.2.3 Fire extinguishing system

A fire extinguishing system, composed of vertical and horizontal schedule 40 pipe runs, ½" in diameter, was considered for the test specimen. Figure 5.24 and Figure 5.23 present elevation and plan views of the pipe runs. The rising portion of the pipe run was attached to the UB-NCS concrete slabs using a combination of flanges and pipe clamps as shown in Figure 5.25. The horizontal sprinkler pipe run was attached to the partition walls using a combination of flanges and pipe clamps as shown in Figure 5.26,

and to the top UB-NCS concrete slab using 3/8" all threaded rod hangers 7" in length, as shown in Figure 5.27. Figure 5.28 shows a general view of the fire suppression pipe runs. A Standard Spray Pendant sprinkler head model Rasco F1 with glass bulb type LPC-VdS (rated for response at 155°F) was considered to interact with the suspended ceiling system (Figure 5.29). During testing, the fire extinguishing system was connected to a hydrant providing typical working pressure.
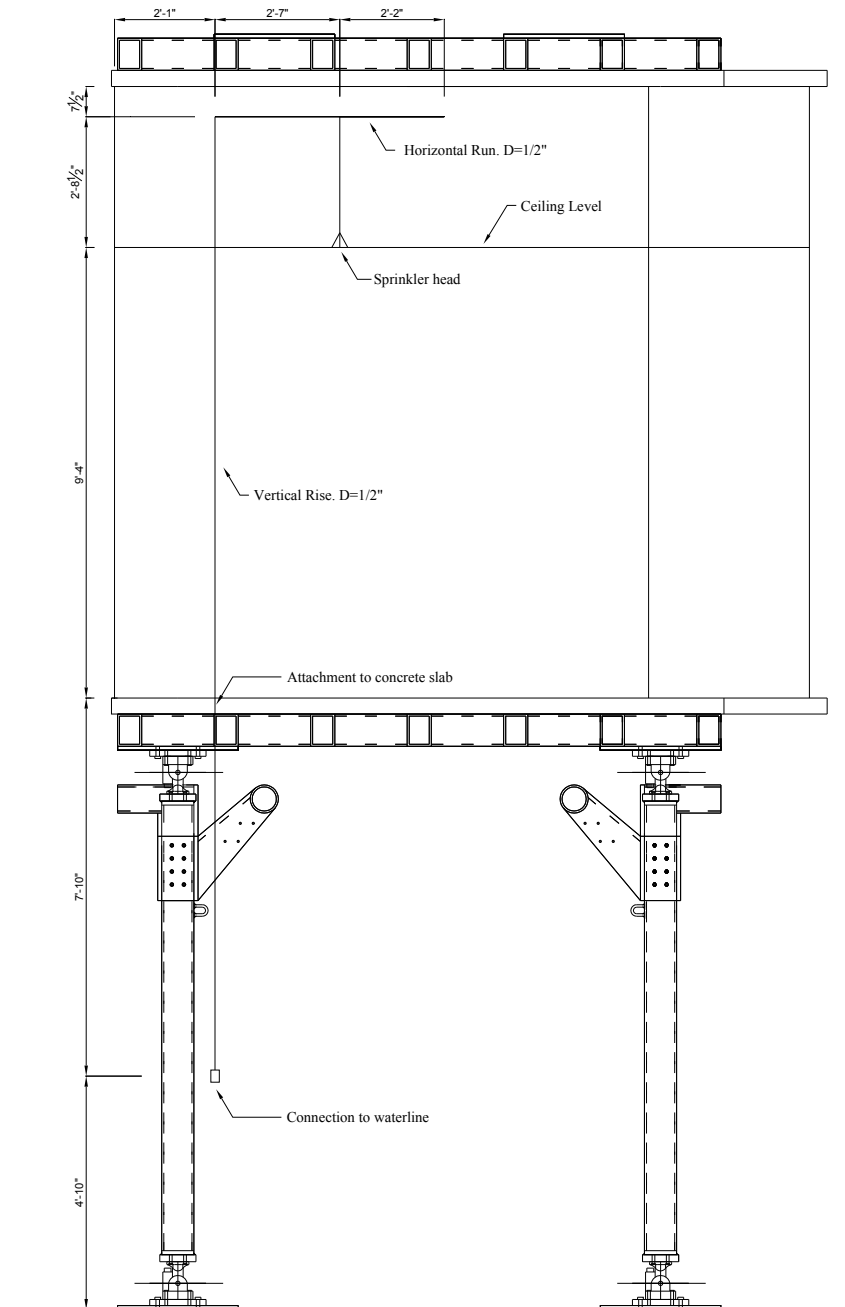
Figure 5.23. Elevation of sprinkler pipe runs
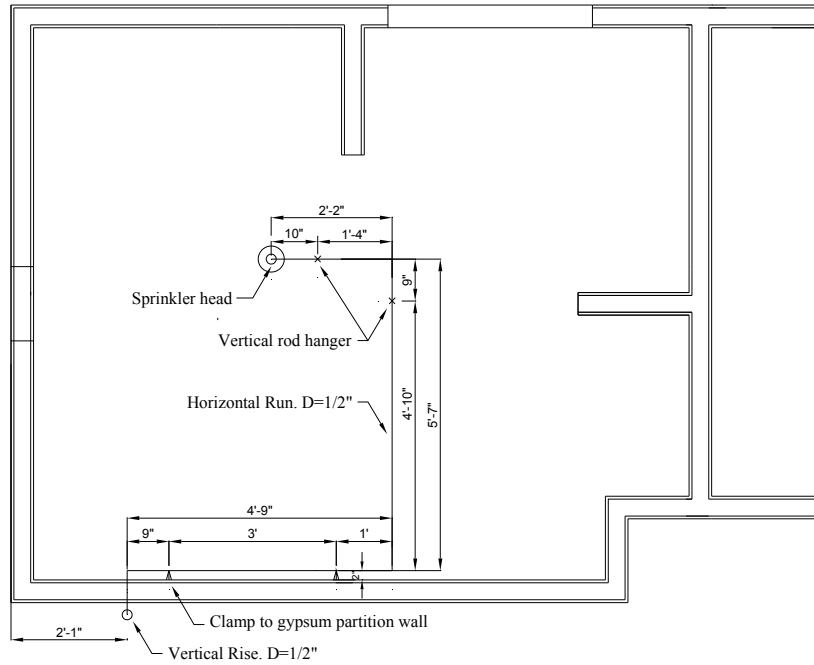
Figure 5.24. Plan view of sprinkler pipe runs

Figure 5.25. Attachment detail of vertical pipe run to UB-NCS concrete slab

Figure 5.26. Detail of sprinkler run crossing partition wall

Figure 5.27. Vertical rod hanger detail
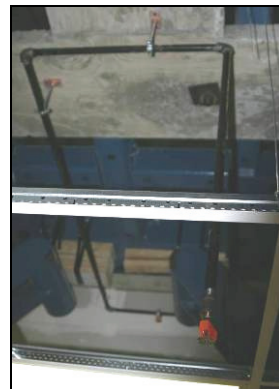
Figure 5.28. General view of sprinkler pipe runs

Figure 5.29. Sprinkler head

5.2.4   Medical gas piping

A medical gas distribution system was also installed within the emergency room test specimen. The piping layout is shown in Figure 5.30.
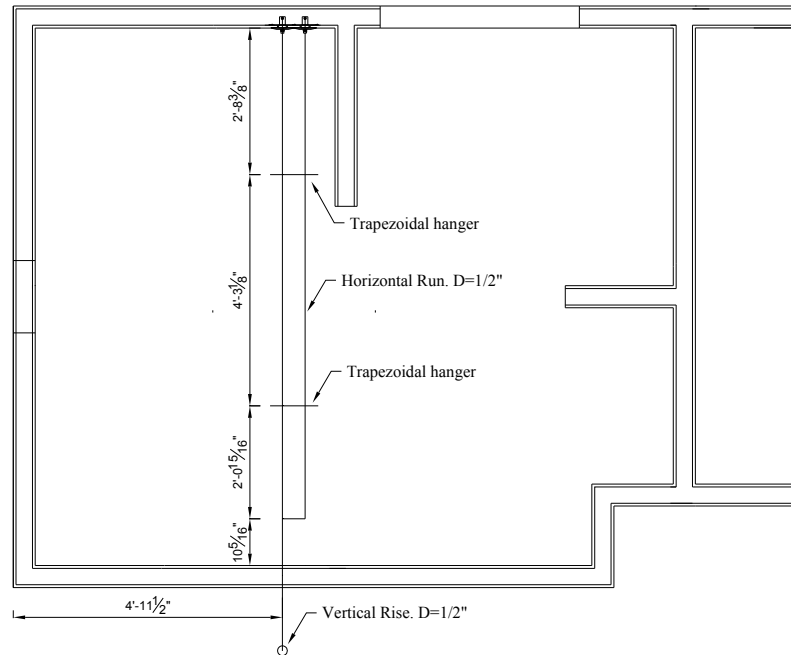
Figure 5.30. Plan view of medical gas pipes

The copper pipes used were ½" in diameter. The vertical pipe run was attached to the UB-NCS concrete slab, similar to the sprinkler horizontal run, as shown in Figure 5.25. The horizontal runs were hanged from the top slab using trapezoidal hangers with 3/8" in diameter all-thread rods (35" in length) inserted into the top concrete slab using standard drop-in devices. Bracing systems were deliberately not considered for the trapezoidal hanger.

Figure 5.31 and Figure 5.32 show details of the hanging system including the clamp used to connect the medical pipe to the trapeze and the drop-in device used to attach the threaded rod to the concrete slab. Figure 5.33 shows a general view of the medical pipes within the partition walls and the in-wall mounted outlets, installed using standard hospital construction techniques. Details of the in-wall mounted outlets geometry are shown in Figure 5.34. In order to reproduce normal ER operation conditions, the medical pipes were pressurized through an air line during testing. The free space between the horizontal medical gas run and the sprinkler vertical run was approximately 5".
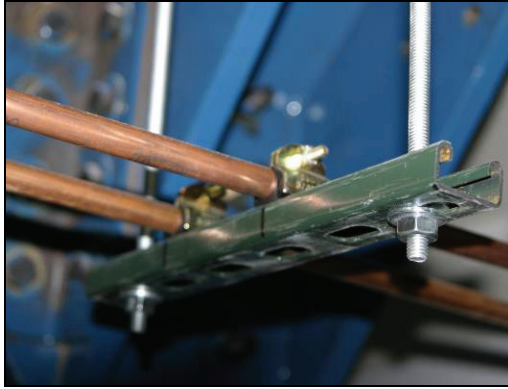
Figure 5.31. Detail of clamp connecting pipe to hanger

Figure 5.32. Connection hanger to top concrete slab

Figure 5.33. In-wall outlets mounting detail
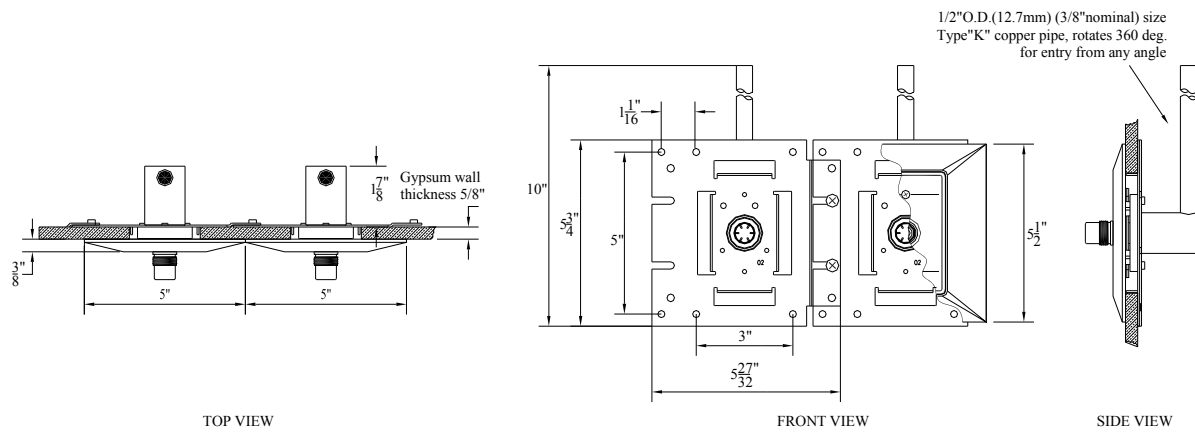
Figure 5.34. Geometric details of in-wall mounted medical gas outlets

5.2.5 Wall mounted patient monitors

Four wall mounted patient monitors were installed in the emergency room as indicated in Figure 5.3. Monitors 1, 2 and 3, were multi-parameter electrocardiogram monitors (ECG) Hewlett Packard model HP M1176A; and Monitor 4, was a multi-parameter vital signal monitor Hewlett Packard model HP 78352C. Table 5.2 summarizes the geometric properties and the weights of these monitors and photographs are provided in Figure 5.35.

Table 5.2. Geometric properties and weights of wall mounted patient monitors

Monitor	Model	Dimensions (in)			Weight (lbf)
		Height	Width	Depth	
1, 2 and 3	HP M1176A	19.7	14.6	17.8	57.2
4	HP 78352C	7.0	13.0	16.0	19.0

The monitors were installed using GCX PolyMount instrument mounting systems. The wall channels for Monitors 1, 2 and 4 were installed following the OSHPD pre-approved seismic anchorage (OPA-0079) detailed in Figure 5.36 and shown in the photographs in Figure 5.38. The wall channel for Monitor 3 was intentionally installed using the deficient anchorage shown in Figure 5.37. The detail shown in Figure 5.37 does not consider an effective anchorage of 6 of the 7 #10x2.0" oval head sheet metal screws installed at both sides of the wall channel. Figure 5.38 also shows the differences between the mounting plates for large/heavy monitors (Monitors 1, 2 and 3) and for small/light monitors (Monitor 4). The wall channels were installed at wall heights indicated by the manufacturer. Accordingly, the base for the wall channels were installed at 52 and 60" above the emergency room floor, for the large and the small monitors, respectively.

(a) Monitors 1, 2 and 3   (b) Monitor 4
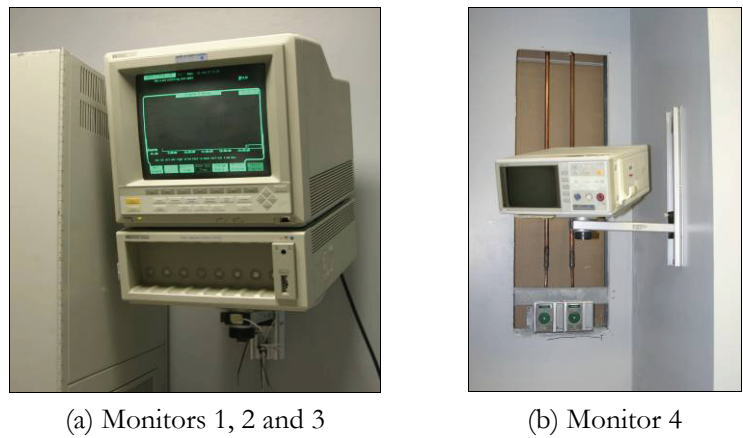
Figure 5.35. Wall-mounted patient monitors
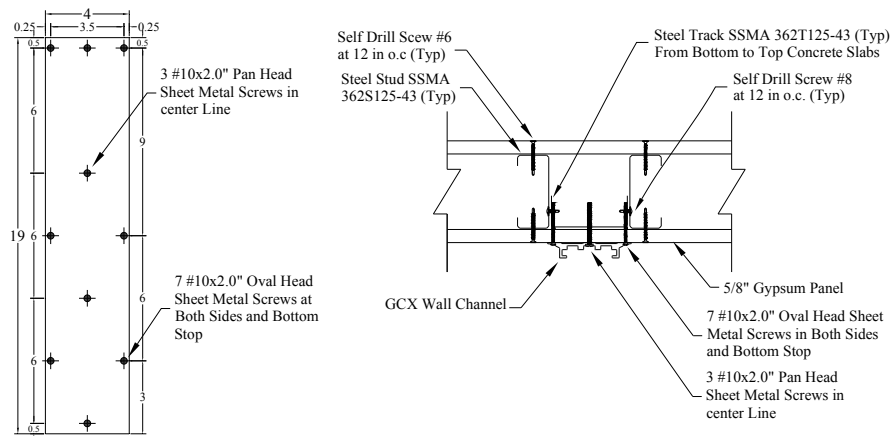
Figure 5.36. Details installation GCX wall channels for Monitors 1, 2 and 4
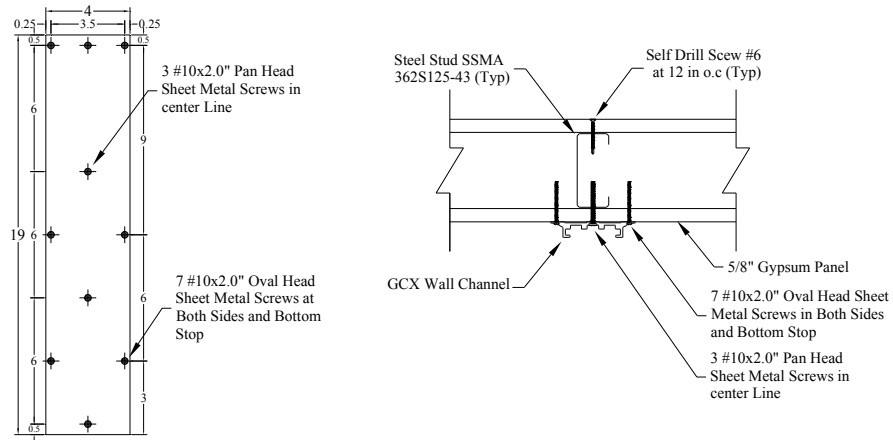
Figure 5.37. Details installation GCX wall channels for Monitor 3

| (a) | (b) | (c) |
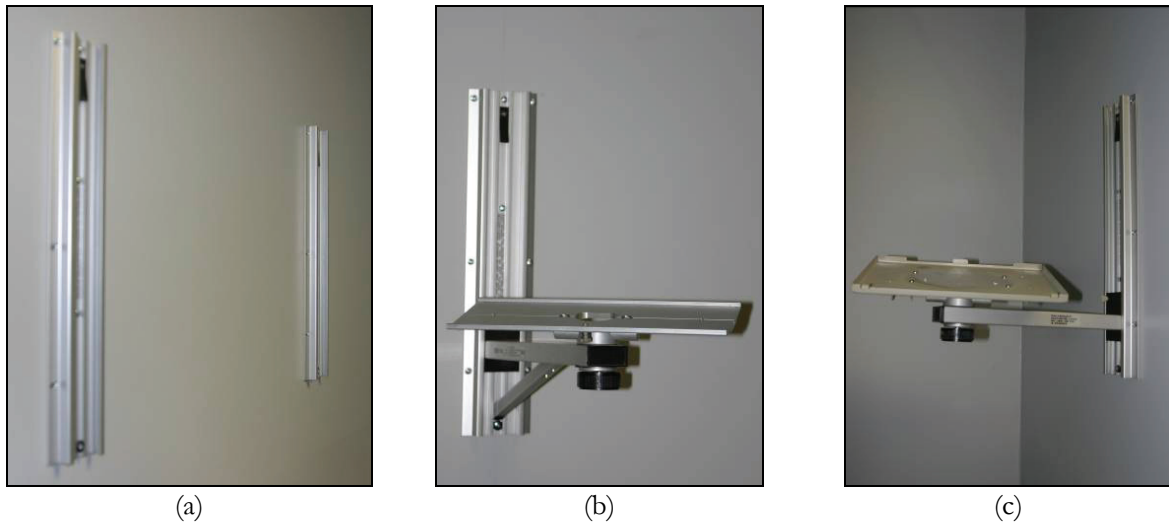
Figure 5.38. Detail of mounting systems: (a) Wall channels for Monitors 2 and 3; (b) Mounting systems for Monitors 1, 2 and 3; and (c) Mounting system for Monitor 4

5.2.6   Freestanding poles with IV infusion pumps

Two movable freestanding poles with IV infusion pumps were included in the test series. The poles, shown in Figure 5.39, were positioned in the emergency room as indicated in Figure 5.3. Both IV infusion pumps were Abbott model Plum XL. Table 5.3 summarizes the geometric properties and the weights of these infusion pumps. Both IV infusion pump stands have a total adjusted height of 72" (operating position), and a 26" diameter base, which incorporates five 3" in diameter casters. The bases of the poles weight approximately 20 lbf each. The IV infusion pumps where located at a height of approximately 45" above the floor. It should be noted that the infusion pumps had limited clearance to move freely during the test.

(a) IV infusion pump pole 1 (in the background)   (b) IV infusion pump pole 2

Figure 5.39. Freestanding poles with IV infusion pumps

Table 5.3. Geometric properties and weight of IV infusion pumps

Model	Dimensions (in)			Weight (lbf)
	Height	Width	Depth	
Abbott Plum XL	8.25	7.5	8.75	7.75

5.2.7   Ceiling mounted surgical light

The surgical light shown in Figure 5.40 installed at the Niagara Falls Memorial Medical Center was mounted hanging from the bottom UB-NCS platform, as shown in Figure 5.41.
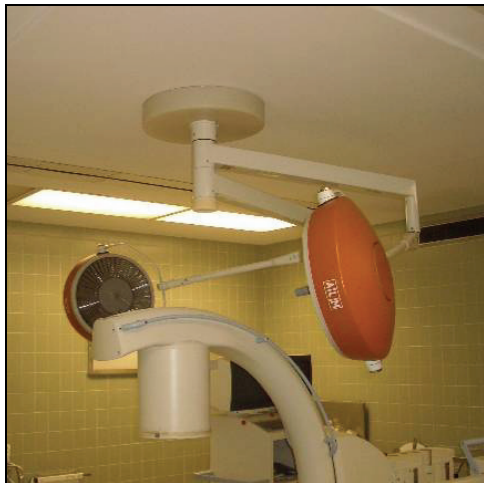
Figure 5.40. Surgical light in operating theater at Niagara Falls Memorial Medical Center

Figure 5.41. Surgical light hanging from bottom UB-NCS platform

The surgical light shown is model ALM 751, with capacity for rotating 360 degrees. The light heads were connected to the arms using standard 3/16" in diameter socket cap screws.

5.2.8   Operating room video equipment rack

The operating room video equipment rack on casters shown in Figure 5.42 and Figure 5.43 was included in the tests. The metal video rack is 76" in height, 28" in width and 26" in depth. A detail showing the dimensions of the rack is shown in Figure 5.44. The rack was filled with the operating theater equipment shown in Figure 5.42, including, from top to bottom: a TV monitor, a surgical CO_2 insufflator, a color video printer, and a digital signal processing system. All equipment has rubber bearings at its base with no additional attachments. The position of the video rack inside the emergency room, shown in Figure 5.3, was intentionally selected to evaluate the seismic interaction with Monitor 1. The rack is mounted on top of swivel casters whose break devices were activated prior to testing. The rack door was also locked shut during testing. The geometric properties of the equipment inside the video rack are listed in Table 5.4.

Figure 5.42. General view of interior of video equipment rack

Figure 5.43. General view of exterior of video equipment rack

Table 5.4. Geometric properties and weights equipment on video rack

Item	Dimensions (in)		
	Height	Width	Depth
TV monitor	17	18	19
CO_2 insufflator	6	14.5	9.5
Video printer	5	17	16
Digital signal processing	3	12	12

5.2.9 Medical gurney and dummy

A 180-pound crash dummy sitting on a medical gurney was included in the test series, as shown in Figure 5.45. The gross dimensions and location of the gurney inside the emergency room are shown in Figure 5.3. The gurney's breaking system was activated before and after each test to simulate typical gurney operating conditions.
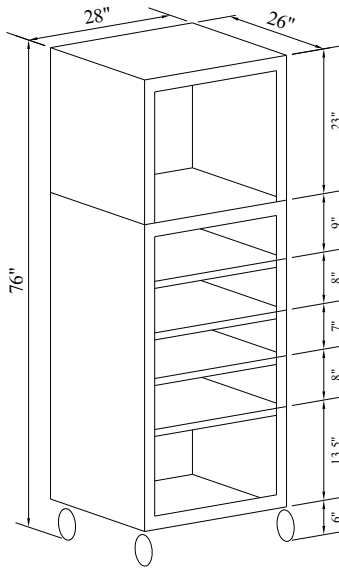
Figure 5.44. Detail geometry operating theater video rack

Figure 5.45. Crash dummy sitting on medical gurney

5.2.10 Medical cart

A medical cart on casters was placed in the room with various items on the top shelf to demonstrate the response of free-standing content. The medical cart is shown in Figure 5.43. Among the medical accessories put on top of the cart are a bottle of water, a glass, paper towel, pills, medicine bottles, and a recipient with medical supplies.

5.3   Testing program

The emergency room test specimen was subjected to increasing levels of a simplified version of the qualification testing protocol presented in Section 4. For comparison purposes the specimen was also subjected to the floor motions obtained from the simulated seismic response of a four story steel framed medical facility. Finally, the specimen was loaded with a simplified version of the qualification interstory drift protocol described in Section 4, applied quasi-statically, and considering scaling factors to reach a target peak interstory drift ratio of 3%.

5.3.1   Seismic qualification protocol

The simplified version of the closed-form equation for the bottom UB-NCS level displacement history considered in this test series is given by:

$$x_{Bottom}\left(t, \frac{h}{H}\right) = \bar{\alpha} f(t)^{\beta} \cos\left(\varphi(t)\right) w(t) FRS_{Factor}\left(\frac{h}{H}\right) \tag{5.1}$$

where $\bar{\alpha}$=0.75 and β=-1.35 are constant calibration parameters controlling the shape of the target response spectrum. A normalized building height h/H=1, corresponding to the roof building level, was substituted into equation (5.1). At this normalized building height the absolute acceleration imposed by the testing protocol is the greatest. The functions $f(t)$, $\varphi(t)$, $w(t)$ and $FRS_{Factor}(h/H)$ were given in equations (4.97), (4.104), (4.105) and (4.88), respectively. The minimum and maximum frequencies included in the test series were f_{min}=0.2 Hz and f_{max}=5 Hz, respectively. The constant sweep rate considered was S_r=12 octaves/min.

The simplified version of the closed-form equation for the qualification interstory drift protocol history is given by:

$$\Delta\left(t, \frac{h}{H}\right) = h_{NCS} e^{-\left(\frac{t-t_d}{\sigma}\right)^2} \delta\left(\frac{h}{H}\right) \cos\left(\varphi(t)\right) w(t) \tag{5.2}$$

where σ=9.8 seconds is a constant parameter calibrated to impose a controlled number of large and total cycles on displacement sensitive nonstructural components and systems; t_d is calculated using equation (4.99); and $\delta(h/H)$ was given in equation (4.96).

The dynamic loading protocol used in the test series is shown in Figure 5.46. The figure shows the instantaneous loading frequency and the motion histories for the top and bottom levels of the UB-NCS. This dynamic testing protocol was applied at various amplitude scales including 10, 25, 50, 100 and 150%.

Figure 5.47a shows a comparison between bottom and top platform displacement histories while Figure 5.47b shows the dynamic interstory drift protocol history. Table 5.5 lists the tests series performed and the corresponding expected peak platform motion values. In Table 5.5, the 100% scaled protocol histories, also shown in Figure 5.46 and Figure 5.47, are inherently associated to a seismic hazard (SH) with a probability of exceedance (PE) of 10% in 50 years, which corresponds to as design earthquake level; while the 150% scaled protocol histories impose demands expected with an earthquake having a PE of 2% in 50 years, commonly referred to as maximum considered earthquake (BSSC, 2003a).
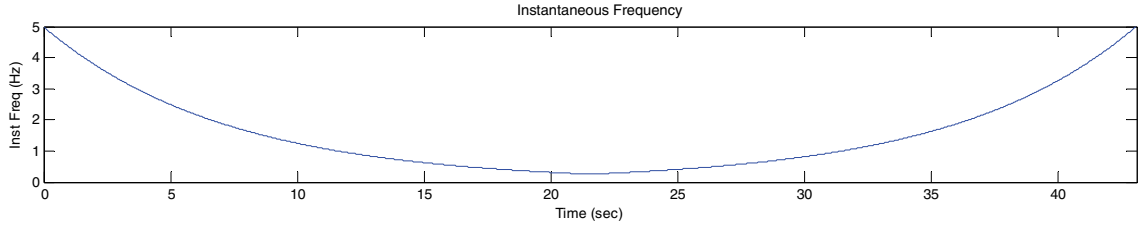
(a) Instantaneous testing frequency
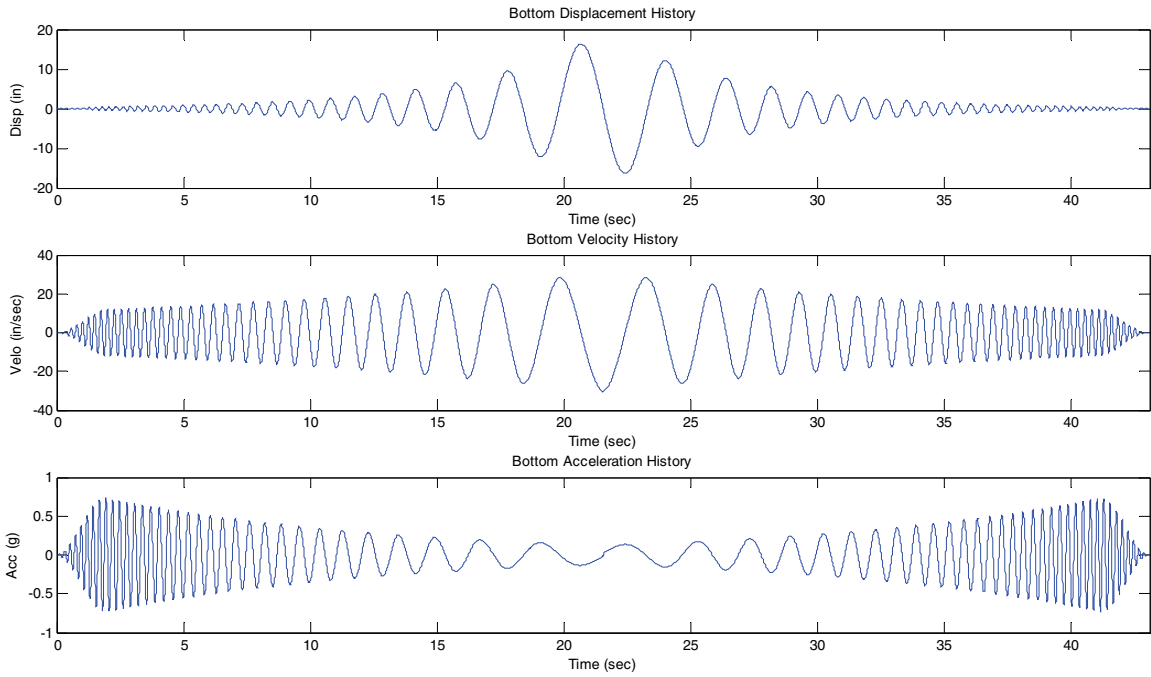
(b) Bottom UB-NCS level floor motions
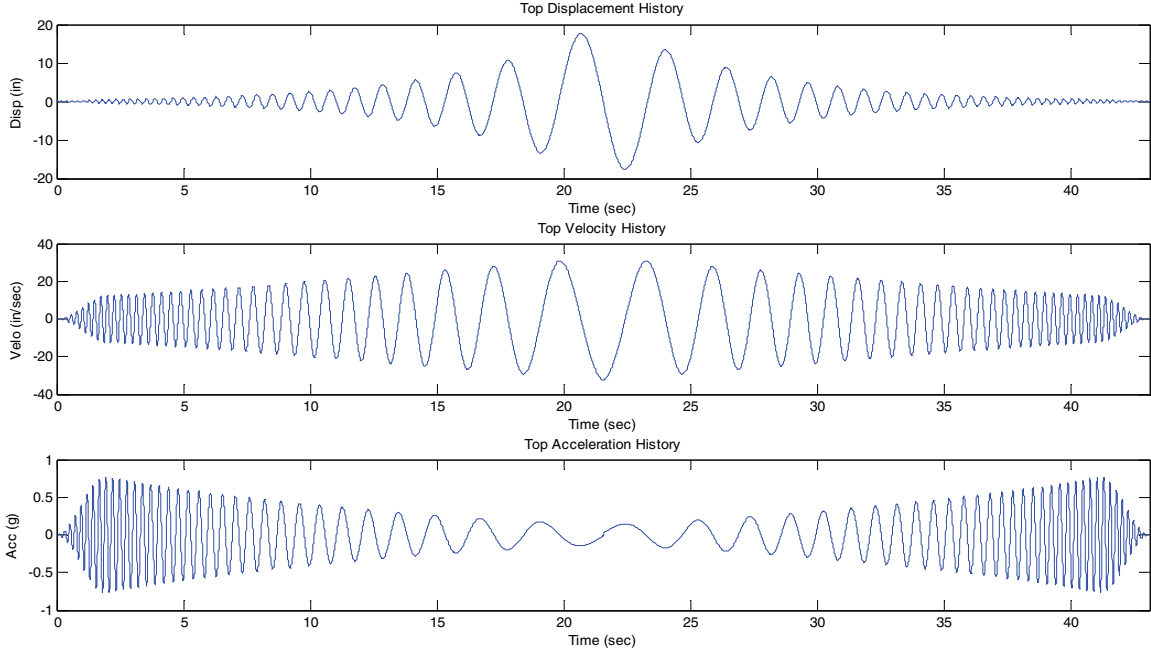
(c) Top UB-NCS level floor motions

Figure 5.46. Testing protocol floor motions for nonstructural systems located at roof level (h/H=1)
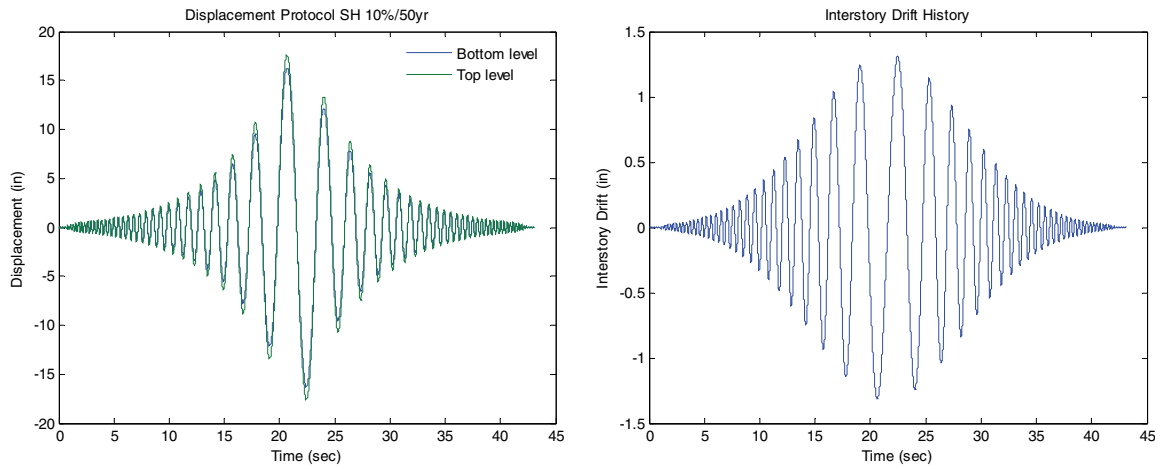
(a) Comparison of floor displacements histories   (b) Interstory drift protocol history

Figure 5.47. Testing protocol at 100% scale for nonstructural systems located at roof level (*h/H*=1)

Table 5.5. List of tests performed and envelope of peak floor motion for dynamic protocol

Test	Scaling Factor	Peak Displacements		Peak Interstory Drift		Peak Velocities		Peak Accelerations	
		$D_{Max\ Bot}$ (in)	$D_{Max\ Top}$ (in)	d_{Max} (in)	δ_{Max} (%)	$V_{Max\ Bot}$ (in/s)	$V_{Max\ Top}$ (in/s)	$A_{Max\ Bot}$ (g)	$A_{Max\ Top}$ (g)
1	10%	1.63	1.76	0.13	0.09%	3.1	3.3	0.07	0.08
2	25%	4.08	4.4	0.33	0.22%	7.6	8.2	0.18	0.19
3	50%	8.15	8.80	0.66	0.43%	15.3	16.3	0.37	0.39
4	**100%**	**16.3**	**17.6**	**1.31**	**0.87%**	**30.5**	**32.6**	**0.73**	**0.77**
5	150%	24.5	26.4	1.97	1.30%	45.8	48.9	1.10	1.16

5.3.2   Simulated building floor motions

In order to validate the suitability of the testing protocol to impose earthquake compatible damage levels, the specimen was also subjected to the floor motions obtained from the simulated response of an existing four story steel framed medical facility located in the San Fernando Valley in California (Wanitkorkul and Filiatrault, 2005). This four story steel framed building model with non-uniform distribution of mass and stiffness, shown in Figure 5.48, has been extensively studied by MCEER investigators (Yuan and Whittaker, 2002).

The floor motions were obtained from nonlinear seismic analysis of the building excited by synthetic ground motions corresponding to seismic hazards with probabilities of exceedance of 10% in 50 years and 2% in 50 years. The absolute displacement response histories calculated for the 4th and roof levels of the building, shown in Figure 5.49 and Figure 5.50, were applied to the bottom and top levels of the UB-NCS, respectively. Figure 5.49 shows the response histories along with other relevant properties computed for the simulated building response associated to a SH with a PE of 10% in 50 years. Figure 5.49a illustrates the floor displacement histories observed at the 4th and roof building levels, while Figure

5.49b shows the interstory drift history for the uppermost building level. Figure 5.49c and Figure 5.49d show the floor velocity and acceleration histories, respectively. Figure 5.49e presents a comparison between the Fast Fourier Transforms (FFT's) computed for the simulated building floor motions and the testing protocol (scaled to 100%). In Figure 5.49e, the dominant period of $T \approx 0.8$ seconds for the four story building can be identified. Figure 5.49f shows a comparison between the floor response spectra (FRS's) computed for the simulated building floor motions and the testing protocol (scaled to 100%). Figure 5.49g and Figure 5.49h show comparisons of the number of "Rainflow" cycles induced and imposed by the simulated floor motions and the testing protocol (scaled to 100%) on acceleration and displacement sensitive nonstructural components, respectively.
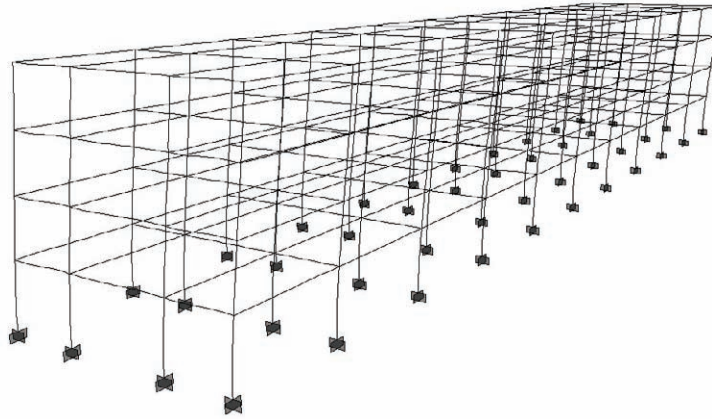
Figure 5.48. Four story building model used to simulate building floor motions.
After Yuan and Whittaker (Yuan and Whittaker, 2002)

In Figure 5.49f it can be observed that the spectral demands imposed by the simulated building floor motions exceed the spectral demands imposed by the testing protocol for frequencies close to the dominant building frequency. This is expected since the protocol averages the response of buildings with different periods. In Figure 5.49g it can be observed that the number of cycles induced by the simulated building floor motions exceed the number of large cycles (N_{50}) induced by the testing protocol on acceleration sensitive nonstructural components with natural frequencies tuned with the natural frequency of the building. The parameters λ and N_λ plotted in Figure 5.49h were previously defined in Subsection 4.3.4. In Figure 5.49h it can be observed that the number of cycles imposed by the simulated building floor motions on displacement sensitive nonstructural systems is only slightly lower than the number of cycles imposed by the testing protocol.
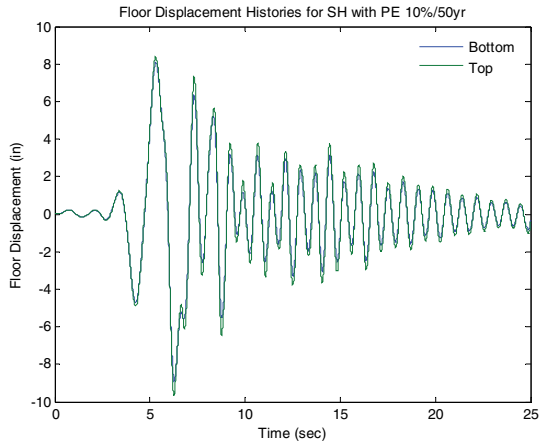
(a) Floor displacements histories
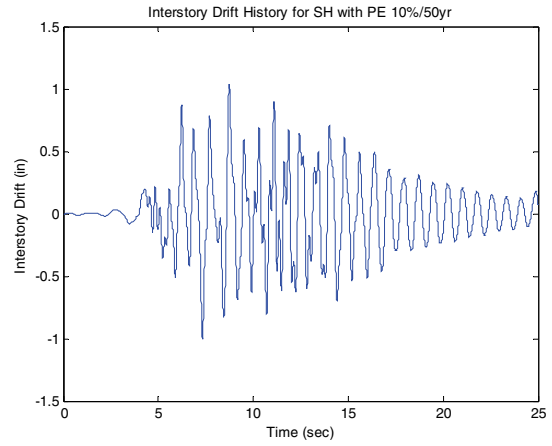
(b) Interstory drift history
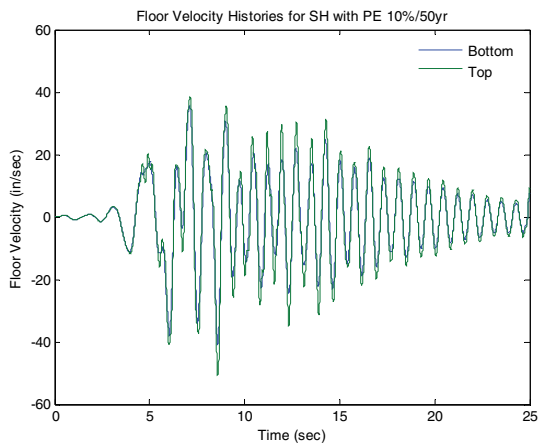
(c) Floor velocity histories
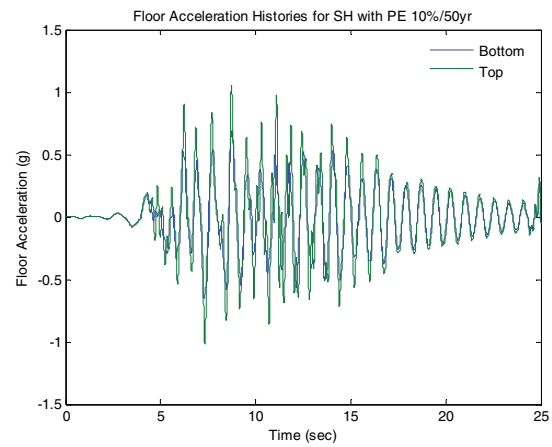
(d) Floor acceleration histories
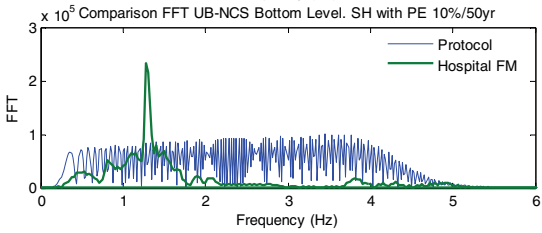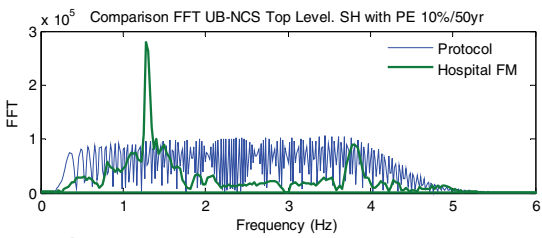
(e) Comparison of FFT's
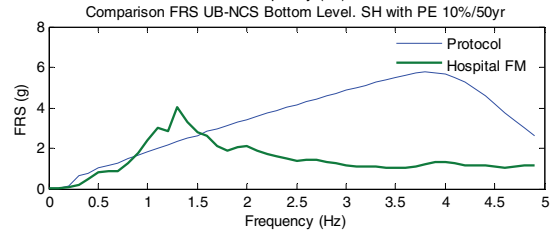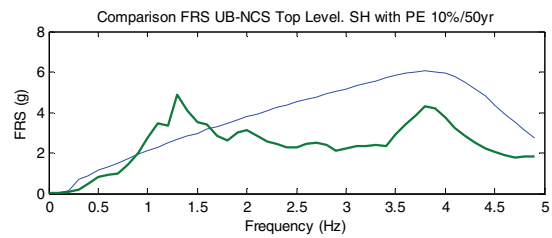
(f) Comparison of FRS's

Figure 5.49. Simulated building floor motions (FM) for earthquake event with PE of 10% in 50 yrs
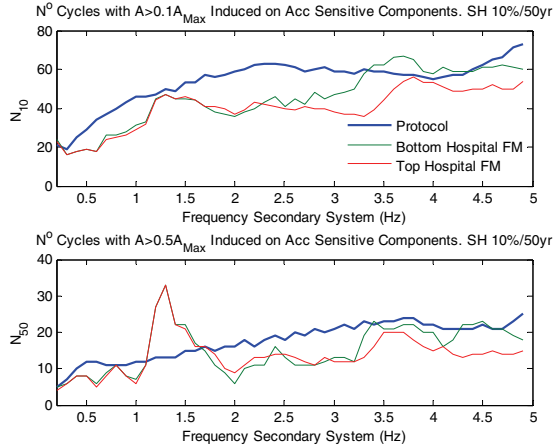
(g) Comparison of number of cycles induced on acceleration sensitive NSC's
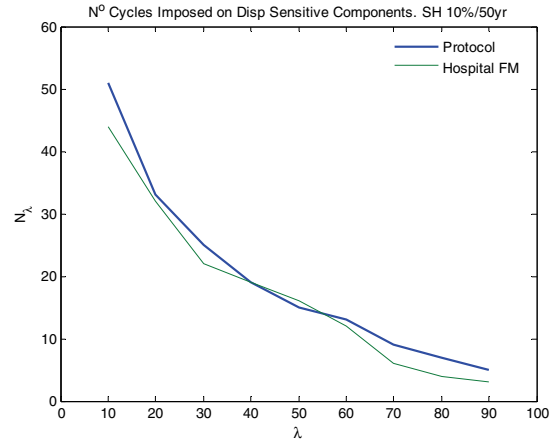
(h) Comparison of number of cycles imposed on displacement sensitive NSC's

Figure 5.49. Simulated building floor motions (FM) for earthquake event with PE of 10% in 50 yr (Cont'd)

Similar plots are shown in Figure 5.50 for the simulated building floor motions corresponding to a PE of 2% in 50 years. In Figure 5.50, the protocol FFT's and FRS's have been amplified by a factor 1.5 to account for a compatible seismic hazard level. Figure 5.50e, f, g, and h exhibit the same trends observed in Figure 5.49e, f, g, and h, respectively.

Table 5.6 summarizes the tests series performed considering the simulated building floor motions and the expected peak platform motion values.
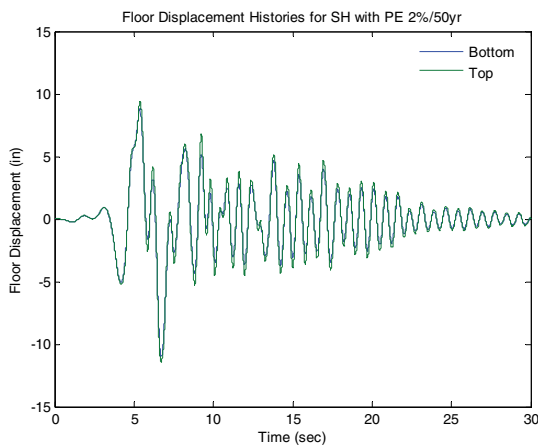
(a) Floor displacement histories
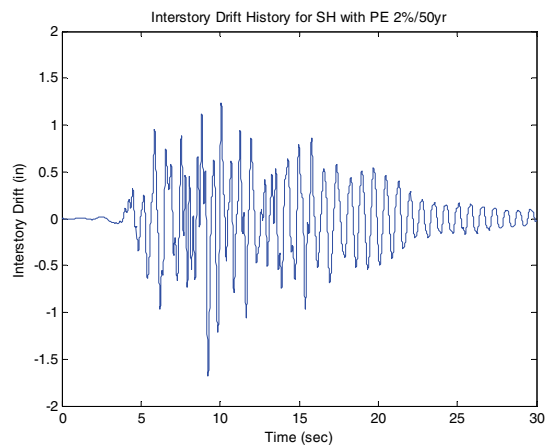
(b) Interstory drift history

Figure 5.50. Simulated building floor motions (FM) for earthquake event with PE of 2% in 50 yr
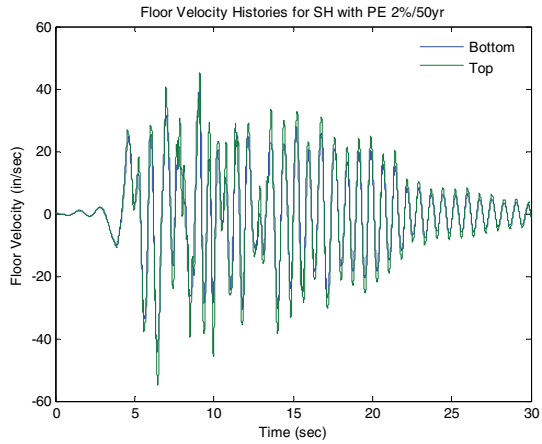
(c) Floor velocity histories
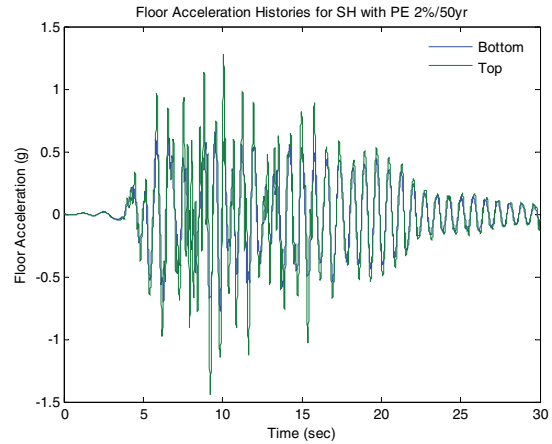
(d) Floor acceleration histories
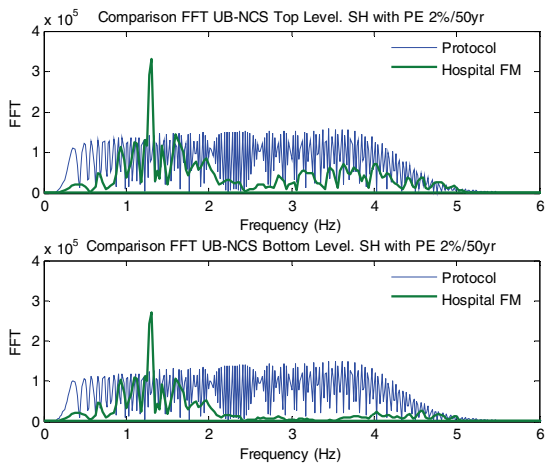
(e) Comparison FFT's
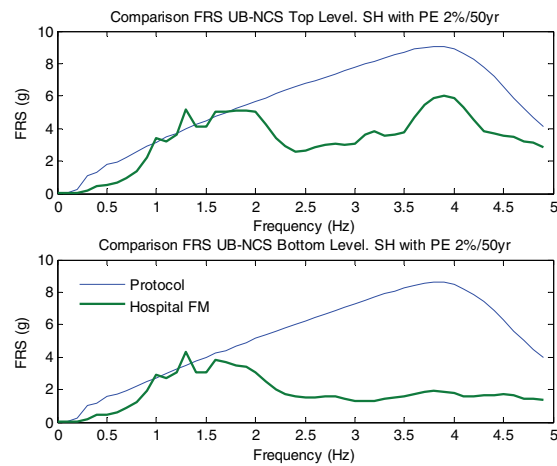
(f) Comparison FRS's
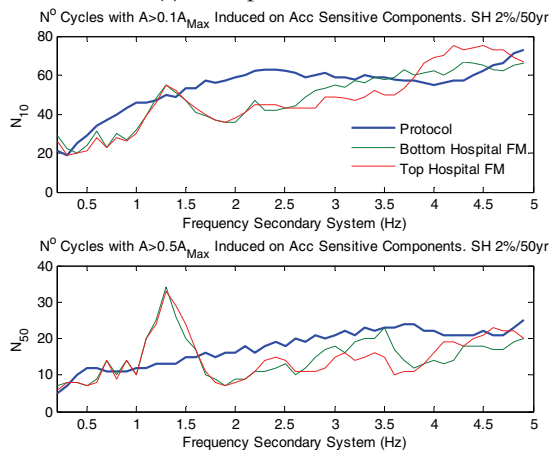
(g) Comparison of number of cycles induced on acceleration sensitive NSC's
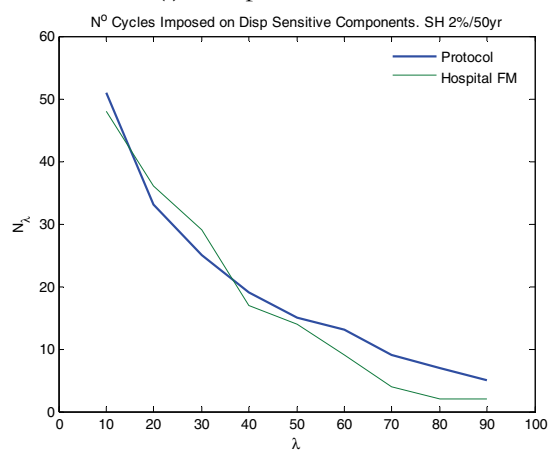
(h) Comparison of number of cycles imposed on displacement sensitive NSC's

Figure 5.50. Simulated building floor motions (FM) for earthquake event with PE of 2% in 50 yr (Cont'd)

178

Table 5.6. List of tests and envelope of peak floor motions for simulated building floor motions

Test	Test Description	Scaling Factor	Peak Displacements		Peak Interstory Drift		Peak Velocities		Peak Accelerations	
			$D_{Max\ Bot}$ (in)	$D_{Max\ Top}$ (in)	d_{Max} (in)	δ_{Max} (%)	$V_{Max\ Bot}$ (in/s)	$V_{Max\ Top}$ (in/s)	$A_{Max\ Bot}$ (g)	$A_{Max\ Top}$ (g)
6	Floor Motion PE 10%/50yr	25%	2.23	2.42	0.26	0.17%	10.3	12.7	0.17	0.27
7	Floor Motion PE 10%/50yr	50%	4.45	4.83	0.53	0.35%	20.5	25.5	0.35	0.53
8	Floor Motion PE 10%/50yr	100%	8.90	9.66	1.05	0.70%	41.0	50.9	0.69	1.06
9	Floor Motion PE 2%/50yr	25%	2.78	2.85	0.42	0.28%	11.1	13.7	0.19	0.36
10	Floor Motion PE 2%/50yr	50%	5.55	5.70	0.84	0.55%	22.2	27.4	0.39	0.72
11	Floor Motion PE 2%/50yr	100%	11.1	11.4	1.67	1.11%	44.4	54.8	0.77	1.44

5.3.3   Quasi-static tests

In order to assess the seismic performance of displacement sensitive components and damage states at interstory drift levels larger than those imposed by dynamic testing as listed in Table 5.5 and

Table 5.6, larger drifts were applied quasi-statically. The loading history is similar to the interstory drift applied in the dynamic protocol shown in Figure 5.47b, but with the time scale extended by a factor of 10. Figure 5.51 shows the resulting full-scale drift protocol for quasi-static testing. The drift was applied by maintaining the bottom level actuators under constant zero displacement and imposing the protocol as a displacement command to the top level UB-NCS actuators. Table 5.7 summarizes the test series with scaling factors and peak demands applied during each test.
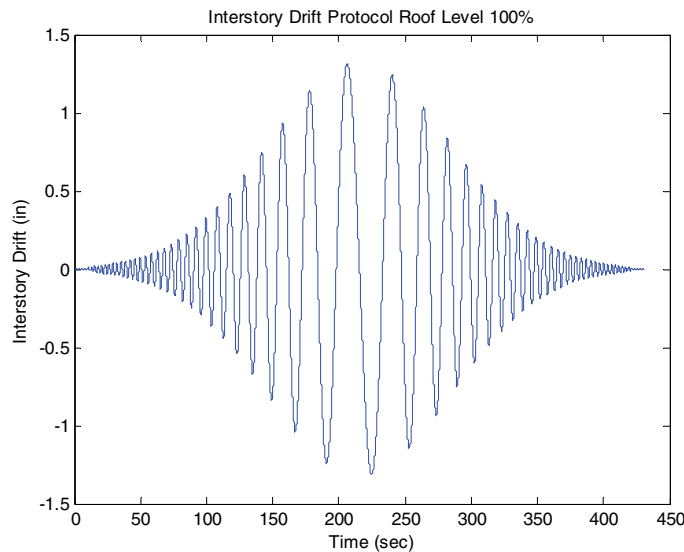
Figure 5.51. Quasi-static interstory drift protocol (scaled to 100%)

Table 5.7. List of tests performed and envelope of peak floor motions for quasi-static protocol

Test	Test Description	Scaling Factor	Peak Displacements		Peak Interstory Drift		Peak Velocities		Peak Accelerations	
			$D_{Max\ Bot}$ (in)	$D_{Max\ Top}$ (in)	d_{Max} (in)	δ_{Max} (%)	$V_{Max\ Bot}$ (in/s)	$V_{Max\ Top}$ (in/s)	$A_{Max\ Bot}$ (g)	$A_{Max\ Top}$ (g)
12	Drift Protocol (Quasi-static)	200%	-	2.62	2.62	1.73%	-	-	-	-
13	Drift Protocol (Quasi-static)	250%	-	3.28	3.28	2.17%	-	-	-	-
14	Drift Protocol (Quasi-static)	300%	-	3.93	3.93	2.60%	-	-	-	-
15	Drift Protocol (Quasi-static)	350%	-	4.59	4.59	3.03%	-	-	-	-

179

5.3.4   Instrumentation setup

The instrumentation scheme focused on measuring the responses of the UB-NCS platforms, wall mounted vital sign patient monitors and gypsum partition walls. Table 5.8 lists the instruments used in these tests and Figure 5.52 through Figure 5.60 illustrate the location of the instruments within the test specimen. More specifically, the instrumentation included: load cells on the actuators to record the forces imposed on the UB-NCS; accelerometers to record the longitudinal, transverse and vertical accelerations of both UB-NCS platforms (Figure 5.52), tri-axial accelerometers at the base of the wall-mounted patient monitors (Figure 5.53); and string potentiometers to measure wall deformations in the direction of loading (East-West direction). Additional potentiometers were installed to closely monitor the behavior of the partition walls including relative slip between bottom and top steel tracks and concrete slabs, and to capture wall rocking effects. The rocking effects were evaluated by using potentiometers to measure relative displacements between the studs located at the wall boundaries and tracks and concrete slabs, as shown in Figure 5.54. Figure 5.54 also summarizes the notation for the instrumentation listed in Table 5.8.

The photographs in Figure 5.55 through Figure 5.60 show details of the instrumentation installation. The three accelerometers installed at the base of Monitor 1 (M1AVb, M1ANSb and M1AEWb) were used to measure the dynamic amplifications of the platform motions due to the partition wall system flexibility. Figure 5.56 shows a detail of the string potentiometer installed to measure the diagonal deformations of the central portion of the south wall (SCWD2), and the hook end of the potentiometer used to record diagonal deformations of the eastern portion of the south wall (SEWD1). Furthermore, Figure 5.56 shows the potentiometer used to record the relative slip of the south wall top track (SCWLT). Figure 5.57 shows a detail of the instrumentation of the partition walls around the bottom right corner of the doorway. In Figure 5.57, the string potentiometer used to measure the diagonal deformations of the eastern portion of the south wall (SEWD2), and the potentiometers used to measure the relative motion between the corner stud and track (SEWVBWi) and the corner stud and the concrete slab (SEWVBW), are shown. Figure 5.58 shows a detail of the instrumentation of the partition walls around the bottom left corner of the door. Figure 5.58 shows the string pot used to measure the diagonal deformations of the western portion of the south wall (SWWD1), and the potentiometer used to measure the relative motion between the corner stud and the concrete slab (SWWVBE). Figure 5.59 and Figure 5.60 show details of the potentiometers installed to measure the relative slip of the bottom (NEWLB) and top (NEWLT) tracks of the eastern portion of the north wall, respectively. The sampling rate for the dynamic and quasi-static test series listed in Table 5.5, Table 5.6 and Table 5.7 were 256, 256 and 32 Hz, respectively.
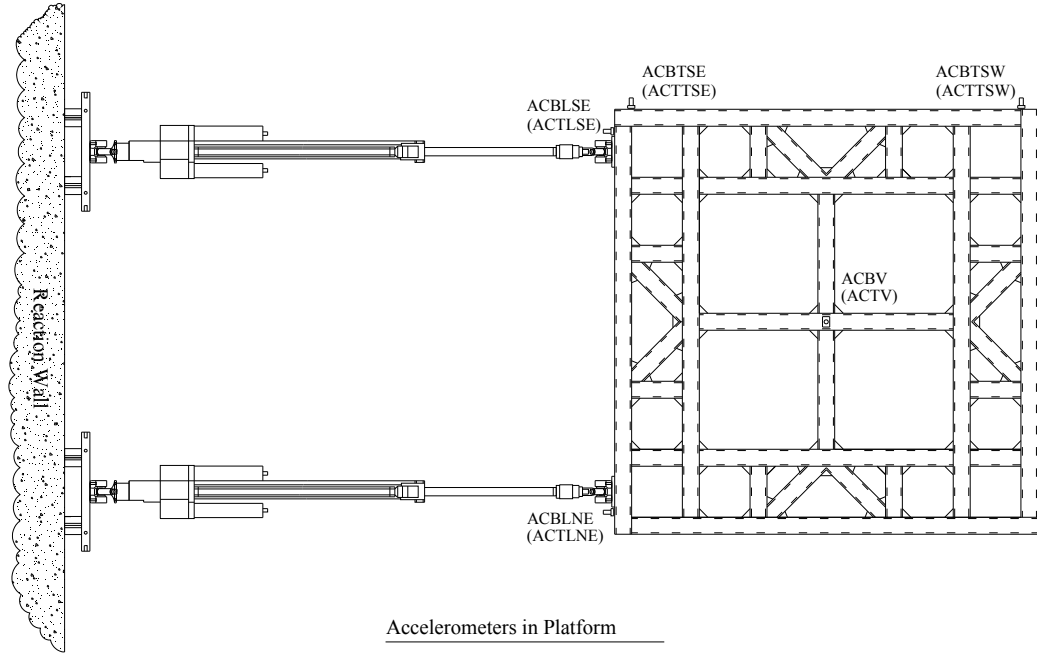
Figure 5.52. Instrumentation of UB-NCS platforms
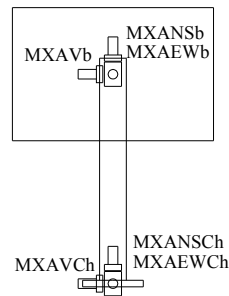
Figure 5.53. Instrumentation of wall-mounted patient monitors
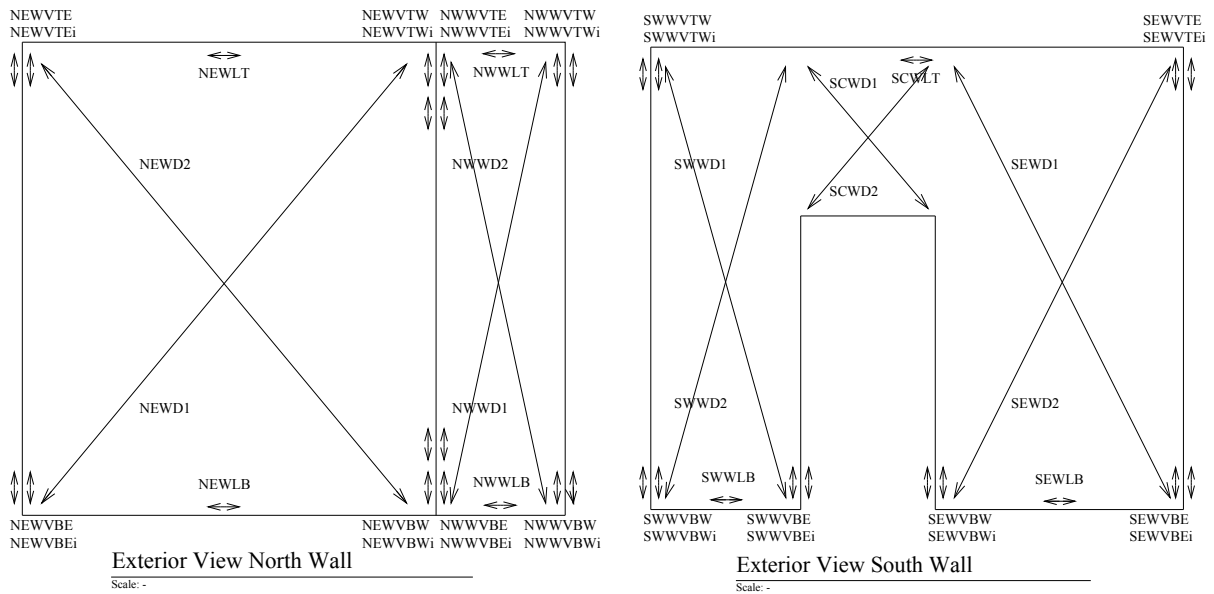
Figure 5.54. Instrumentation of gypsum partition walls

Table 5.8. Instrumentation list

Channel	ID	Instrument	Response quantity	Min Operation Limits	Orientation	Location and comment
Data acquired from Actuators
1	Time		Time			
2	ComActA		Actuator Disp	±40in		Actuator A command
3	ComActB		Actuator Disp	±40in		Actuator B command
4	ComActC		Actuator Disp	±40in		Actuator C command
5	ComActD		Actuator Disp	±40in		Actuator D command
6	DispActA		Actuator Disp	±40in		Actuator A displacement
7	DispActB		Actuator Disp	±40in		Actuator B displacement
8	DispActC		Actuator Disp	±40in		Actuator C displacement
9	DispActD		Actuator Disp	±40in		Actuator D displacement
10	ForceA		Actuator Force	±50kip		Actuator A
11	ForceB		Actuator Force	±50kip		Actuator B
12	ForceC		Actuator Force	±50kip		Actuator C
13	ForceD		Actuator Force	±50kip		Actuator D
Accelerometers in Platforms
14	ACBLNE	Accelerometer	Acceleration	±10g	EW	Bottom Platform
15	ACBLSE	Accelerometer	Acceleration	±10g	EW	Bottom Platform
16	ACBTSW	Accelerometer	Acceleration	±10g	NS	Bottom Platform
17	ACBTSE	Accelerometer	Acceleration	±10g	NS	Bottom Platform
18	ACBV	Accelerometer	Acceleration	±10g	V	Bottom Platform
19	ACTLNE	Accelerometer	Acceleration	±10g	EW	Top Platform
20	ACTLSE	Accelerometer	Acceleration	±10g	EW	Top Platform
21	ACTTSW	Accelerometer	Acceleration	±10g	NS	Top Platform
22	ACTTSE	Accelerometer	Acceleration	±10g	NS	Top Platform
23	ACTV	Accelerometer	Acceleration	±10g	V	Top Platform
Instrumentation North East Wall
24	NEWD1	String Pot	Displacement	±6 in	Diagonal	Diagonal north east wall
25	NEWD2	String Pot	Displacement	±6 in	Diagonal	Diagonal north east wall
26	NEWVTE	Potentiometer	Disp uplift	±1 in	V	North east wall top east end (stud to concrete)
27	NEWVTEi	Potentiometer	Disp uplift	±1 in	V	North east wall top east end (stud to track)
28	NEWVTW	Potentiometer	Disp uplift	±1 in	V	North east wall top west end (stud to concrete)
29	NEWVTWi	Potentiometer	Disp uplift	±1 in	V	North east wall top west end (stud to track)
30	NEWVBE	Potentiometer	Disp uplift	±1 in	V	North east wall bottom east end (stud to concrete)
31	NEWVBEi	Potentiometer	Disp uplift	±1 in	V	North east wall bottom east end (stud to track)
32	NEWVBW	Potentiometer	Disp uplift	±1 in	V	North east wall bottom west end (stud to concrete)
33	NEWVBWi	Potentiometer	Disp uplift	±1 in	V	North east wall bottom west end (stud to track)
34	NEWLT	String Pot	Displacement	±6 in	EW	North east wall relative motion top track
35	NEWLB	String Pot	Displacement	±6 in	EW	North east wall relative motion bottom track
Instrumentation North West Wall
36	NWWD1	String Pot	Displacement	±6 in	Diagonal	Diagonal north west wall
37	NWWD2	String Pot	Displacement	±6 in	Diagonal	Diagonal north west wall
38	NWWVTE	Potentiometer	Disp uplift	±1 in	V	North west wall top east end (stud to concrete)
39	NWWVTEi	Potentiometer	Disp uplift	±1 in	V	North west wall top east end (stud to track)
40	NWWVTW	Potentiometer	Disp uplift	±1 in	V	North west wall top west end (stud to concrete)
41	NWWVTWi	Potentiometer	Disp uplift	±1 in	V	North west wall top west end (stud to track)
42	NWWVBE	Potentiometer	Disp uplift	±1 in	V	North west wall bottom east end (stud to concrete)
43	NWWVBEi	Potentiometer	Disp uplift	±1 in	V	North west wall bottom east end (stud to track)
44	NWWVBW	Potentiometer	Disp uplift	±1 in	V	North west wall bottom west end (stud to concrete)
45	NWWVBWi	Potentiometer	Disp uplift	±1 in	V	North west wall bottom west end (stud to track)
46	NWWLT	String Pot	Displacement	±6 in	EW	North west wall relative motion top track
47	NWWLB	String Pot	Displacement	±6 in	EW	North west wall relative motion bottom track
Instrumentation South West Wall
48	SWWD1	String Pot	Displacement	±6 in	Diagonal	Diagonal south west wall
49	SWWD2	String Pot	Displacement	±6 in	Diagonal	Diagonal south west wall
50	SWWVTW	Potentiometer	Disp uplift	±1 in	V	South west wall top west end (stud to concrete)
51	SWWVTWi	Potentiometer	Disp uplift	±1 in	V	South west wall top west end (stud to track)
52	SWWVBW	Potentiometer	Disp uplift	±1 in	V	South west wall bottom west end (stud to concrete)
53	SWWVBWi	Potentiometer	Disp uplift	±1 in	V	South west wall bottom west end (stud to track)
54	SWWVBE	Potentiometer	Disp uplift	±1 in	V	South west wall bottom east end (stud to concrete)
55	SWWVBEi	Potentiometer	Disp uplift	±1 in	V	South west wall bottom east end (stud to track)
56	SWWLB	String Pot	Displacement	±6 in	EW	South west wall relative motion bottom track
Instrumentation South East Wall
57	SEWD1	String Pot	Displacement	±6 in	Diagonal	Diagonal south east wall
58	SEWD2	String Pot	Displacement	±6 in	Diagonal	Diagonal south east wall
59	SEWVTE	Potentiometer	Disp uplift	±1 in	V	South east wall top east end (stud to concrete)
60	SEWVTEi	Potentiometer	Disp uplift	±1 in	V	South east wall top east end (stud to track)
61	SEWVBW	Potentiometer	Disp uplift	±1 in	V	South east wall bottom west end (stud to concrete)
62	SEWVBWi	Potentiometer	Disp uplift	±1 in	V	South east wall bottom west end (stud to track)
63	SEWVBE	Potentiometer	Disp uplift	±1 in	V	South east wall bottom east end (stud to concrete)
64	SEWVBEi	Potentiometer	Disp uplift	±1 in	V	South east wall bottom east end (stud to track)
65	SEWLB	String Pot	Displacement	±6 in	EW	South east wall relative motion bottom track
Instrumentation South Central Wall
66	SCWD1	String Pot	Displacement	±6 in	Diagonal	Diagonal south central wall
67	SCWD2	String Pot	Displacement	±6 in	Diagonal	Diagonal south central wall
68	SCWLT	String Pot	Displacement	±6 in	EW	Sputh central wall relative motion top track
Instrumentation Monitor X
69	MXAVCh	Accelerometer	Acceleration	±10g	V	Chanel instrumentation
70	MXANSCh	Accelerometer	Acceleration	±10g	NS	Chanel instrumentation
71	MXAEWCh	Accelerometer	Acceleration	±10g	EW	Chanel instrumentation
72	MXAVb	Accelerometer	Acceleration	±10g	V	Bottom equipment instrumentation
73	MXANSb	Accelerometer	Acceleration	±10g	NS	Bottom equipment instrumentation
74	MXAEWb	Accelerometer	Acceleration	±10g	EW	Bottom equipment instrumentation

Figure 5.55. Detail of instrumentation at the base of wall mounted vital sign monitors. In the photo: accelerometers M1AVb, M1ANSb and M1AEWb
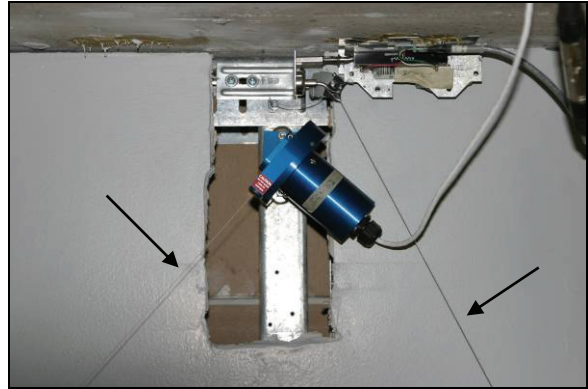
Figure 5.56. Detail of instrumentation of wall diagonal and track slip. In the photo: string pot SCWD2 and potentiometer SCWLT. Hook for string pot SEWD1 is also shown

Figure 5.57. Detail of instrumentation at wall boundary. In the photo: string pot SEWD2, and potentiometers SEWVBW and SEWVBWi
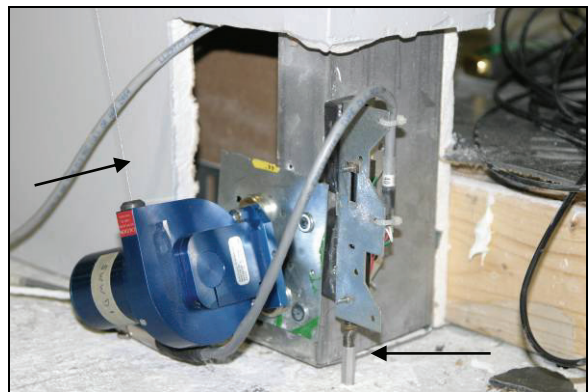
Figure 5.58. Detail of instrumentation at wall boundary. In the photo: string pot SWWD1, and potentiometers SWWVBE and SWWVBEi
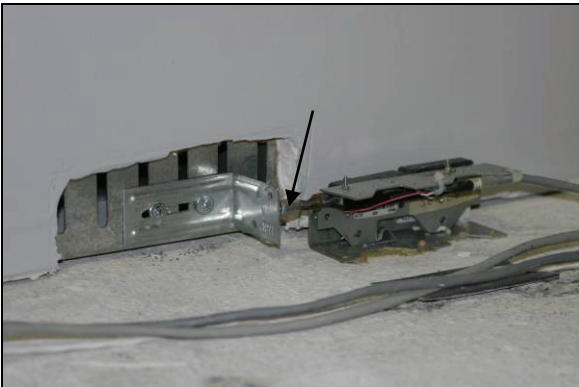
Figure 5.59. Detail of instrumentation for bottom track slip. In the photo: potentiometer NEWLB
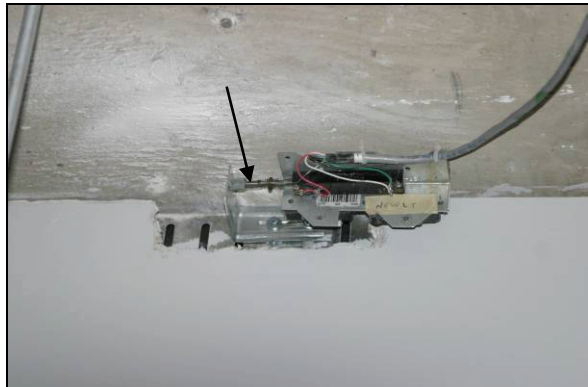
Figure 5.60. Detail of instrumentation for top track slip. In the photo: potentiometer NEWLT

5.3.5　Damage observations

Detailed damage investigations were conducted after most tests in order to identify the progression of damage, the different damage states, and the level of excitation at which the damage states occurred. Measured data and video were collected during each test. After some of the tests, a detailed damage assessment was conducted, consisting of visual observations and high resolution photographs. Table 5.9 summarizes the damage assessment method used following each of the tests performed in this research.

Table 5.9. Damage assessment method

Test type	Test description	Measured Data	Damage assessment		
			Video	Photo	Detailed inspection
Dynamic testing protocol	Scaled to 10%	✓			
	Scaled to 25%	✓	✓	✓	✓
	Scaled to 50%	✓	✓	✓	✓
	Scaled to 100% (Design earthquake level)	✓	✓	✓	
	Scaled to 150% (MCE level)	✓	✓	✓	✓
Simulated building floor motions	Design earthquake level scaled to 25%	✓	✓		
	Design earthquake level scaled to 50%	✓	✓		
	Design earthquake level scaled to 100%	✓	✓	✓	✓
	MCE level scaled to 25%	✓	✓		
	MCE level scaled to 50%	✓	✓		
	MCE level scaled to 100%	✓	✓	✓	✓
Quasi-static testing protocol	Scaled to 200%	✓	✓	✓	✓
	Scaled to 250%	✓	✓	✓	✓
	Scaled to 300%	✓	✓	✓	✓
	Scaled to 350%	✓	✓	✓	✓

5.4　Experimental results

This subsection presents the detailed qualitative and quantitative results and observations obtained from the test series performed on the mock emergency room described in Subsection 5.2. The seismic performance of the specimen and the fidelity of the UB-NCS for replicating the desired floor motions are discussed in Section 6. The findings presented here are based on the data collected during the experiments as summarized in Table 5.9. All recorded data channels have been filtered using a low-pass Butterworth filter of order 50 with a cutting frequency of 5 Hz. The observations presented in this subsection are later used in Section 6 to evaluate the overall progression of damage to the various components of the emergency room and perform fragility analysis.

5.4.1　Results and observations for seismic qualification protocol floor histories

This subsection presents the observations and results of the tests performed using the floor motion histories described in Subsection 5.3.1, corresponding to the proposed seismic qualification protocol.

5.4.1.1 Dynamic testing protocol scaled to 10%

This low-level test was performed mainly to verify the operation of the test setup including control and data acquisition systems. A brief inspection of the room was performed following the experiment. No damage was observed in any of the acceleration or displacement sensitive nonstructural components.

5.4.1.2 Dynamic testing protocol scaled to 25%

The purpose of the 25% amplitude scaled testing protocol was mainly to evaluate the fidelity of the UB-NCS in applying the command motions. A compensated input motion to be used as the command signal for the UB-NCS platforms in subsequent tests was generated based on this test. Nevertheless, damage investigations were conducted to identify any noticeable damage experienced at this intensity.

5.4.1.2.1 Command signal compensation

The iterative command signal compensation procedure described in Section 3 was used to prepare the floor motions to be used at larger intensity test levels. Figure 5.61 summarizes the preliminary results of the 25% scaled test performed using the non compensated signals shown in Figure 5.46b and Figure 5.46c. Figure 5.61a shows a comparison between desired and observed platform displacements while Figure 5.61b compares desired and observed interstory drift histories. Although not perceptible in Figure 5.61a, undershoots were observed at low amplitude-high frequency platform motions. Figure 5.61c shows the relative displacements between actuators placed at a same platform level. In Figure 5.61c it is seen that the relative displacements do not exceed 1/8 of an inch, the limiting value observed during the shake-down process. Figure 5.61d shows the forces imposed by each UB-NCS actuator, from where the residual force capacity, available to load the test specimen, can be estimated. Note that the peak actuator force is 22 kip. Figure 5.61e and Figure 5.61f compare the desired (DRS) and observed (ORS) floor response spectra (FRS's) for the bottom and top UB-NCS platform levels, respectively. The ORS underestimated the DRS for both bottom and top UB-NCS platforms by more than 50%. This is believed to be a direct consequence of the displacement undershoots observed for frequencies greater than 1 Hz. Based on the criteria and methodology for command signal compensation described in Section 3, the UB-NCS platform input motions required compensation. Figure 5.61g and Figure 5.61h show the compensated signals with amplified displacement amplitudes at frequencies larger than 1 Hz, for the next (second) iteration. The modified signal amplifies the displacement input at higher frequencies in order to achieve the desired response spectrum.
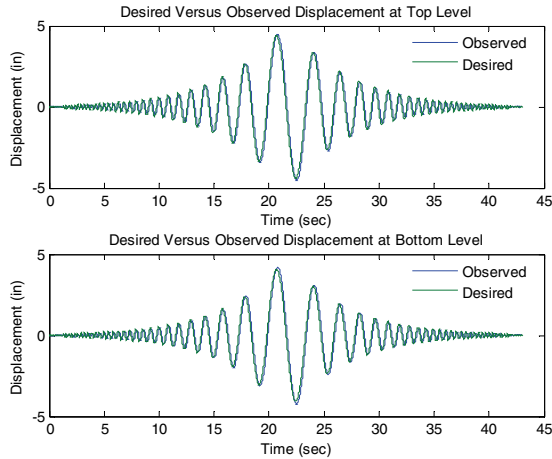
(a) Comparison of desired and observed platform displacements
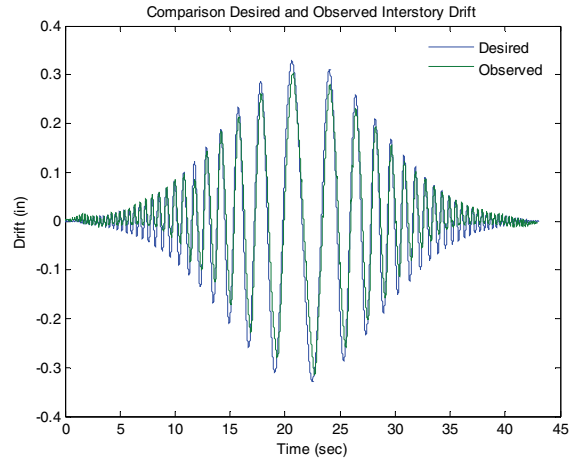
(b) Comparison of desired and observed interstory drift
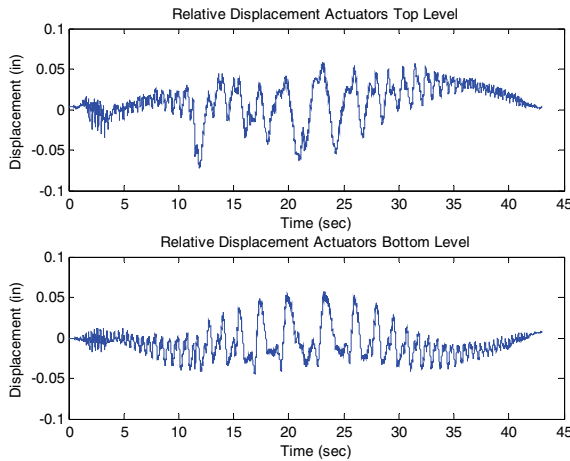
(c) Relative displacement between actuators
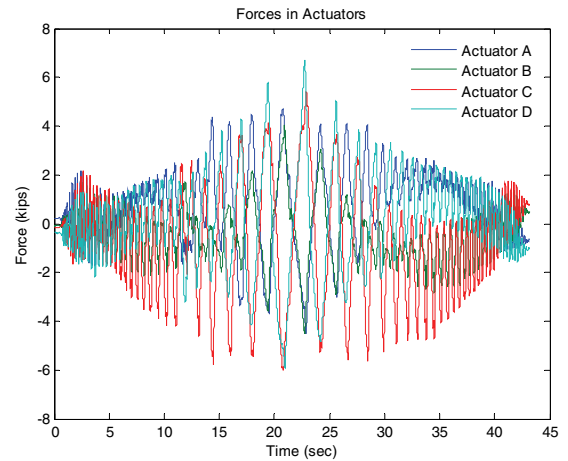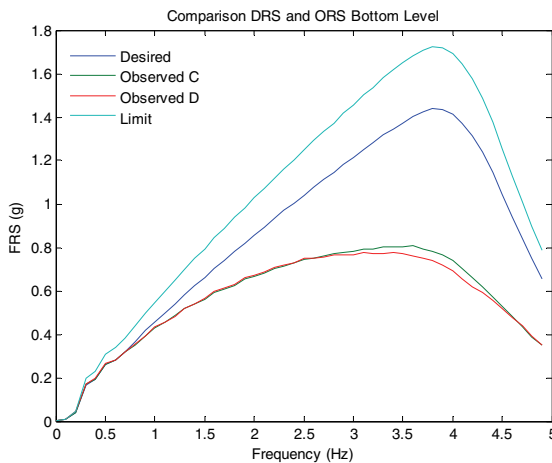
(d) Actuator force histories

(e) Comparison of DRS and ORS bottom level
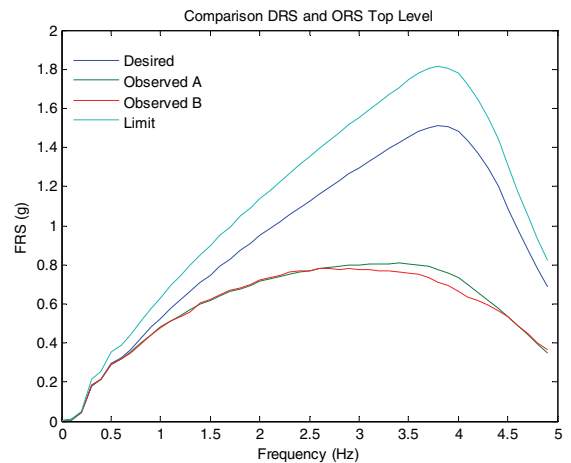
(f) Comparison of DRS and ORS top level

Figure 5.61. Experimental results dynamic testing protocol scaled to 25%, before compensation
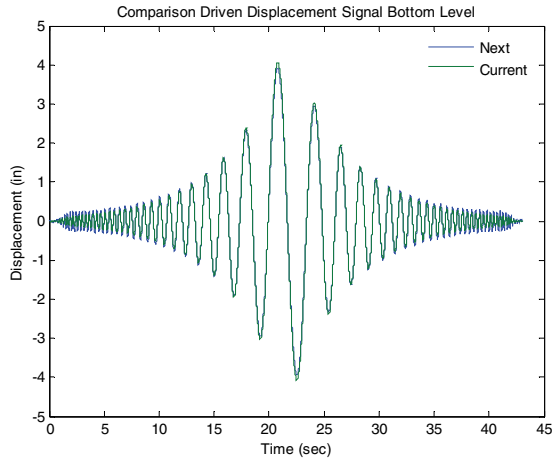
(g) Comparison current and next command signal for bottom level
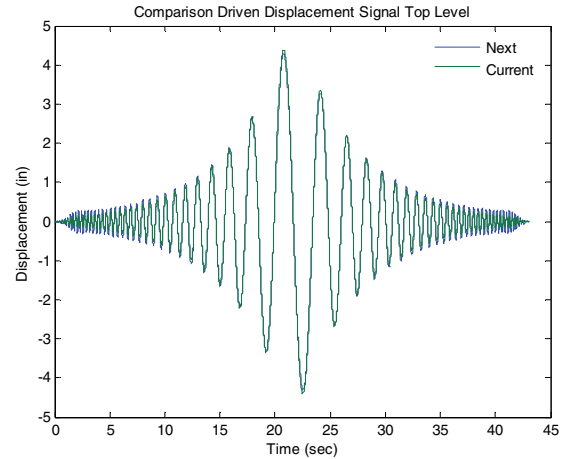
(h) Comparison current and next command signal for top level

Figure 5.61. Experimental results dynamic testing protocol scaled to 25%, before compensation (Cont'd)

Figure 5.62 compares the DRS and ORS after compensating the platform displacement command inputs. After signal compensation, the ORS closely matches the DRS for the whole range of frequencies of interest. The iterative process was stopped at this point and the compensated input motions were used for larger amplitude tests.
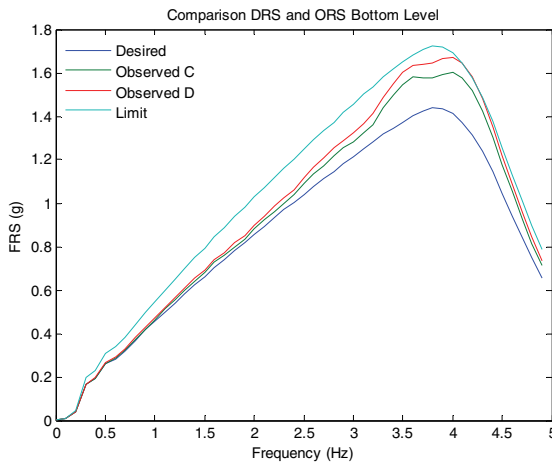
(a)
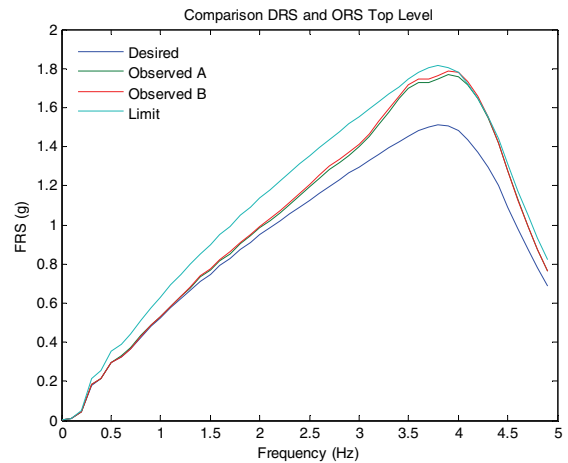
(b)

Figure 5.62. Comparison of DRS and ORS for (a) bottom level platform; and (b) top level platform for dynamic testing protocol scaled to 25% after command input compensation

5.4.1.2.2 Tests results and damage observations

Table 5.10 summarizes the envelope of desired and observed peak floor response parameters recorded during the 25% scaled test carried out using the compensated dynamic testing protocol. From Table 5.10

it can be observed that the errors in replicating floor displacements[7], velocities, and interstory drifts histories are less than 5%. However, errors up to 20% are observed in replicating top platform accelerations. The acceleration overshoots are evident in Figure 5.63, and are likely due to the compensation procedure to match the desired response spectra in Figure 5.62.

Table 5.10. Envelope of peak floor motions for dynamic testing protocol scaled to 25%

Response	Peak Platform Displacement (in)		Peak Interstory Drift δ_{Max}		Peak Platform Velocity (in/sec)		Peak Platform Acceleration (g)	
	$D_{Max\ Bot}$	$D_{Max\ Top}$	(in)	(%)	$V_{Max\ Bot}$	$V_{Max\ Top}$	$A_{Max\ Bot}$	$A_{Max\ Top}$
Desired	4.07	4.40	0.33	0.22	7.63	8.16	0.18	0.19
Observed	4.11	4.43	0.34	0.23	7.60	8.11	0.22	0.24
Error (%)	0.82	0.71	4.02	4.02	0.42	0.62	16.6	20.4

The key results from the 25% scaled dynamic protocol test are shown in Figure 5.63. A comparison between the desired and observed response histories for displacement, drift and acceleration demonstrate that the UB-NCS performed adequately after command signal compensation. Figure 5.63e shows the force history imposed on the partition wall specimen. The force history in the partition walls, $F_p(t)$, shown in Figure 5.63e, is calculated using:

$$F_P(t) = \frac{1}{2}\left(F_{P_T}(t) - F_{P_B}(t)\right) \tag{5.3}$$

where $F_{P_T}(t)$ and $F_{P_B}(t)$ denote the forces in the partition walls computed using the accelerations and forces recorded at top and bottom UB-NCS platform levels. These forces are computed by subtracting the inertial forces generated by the platform mass from the total force applied by the actuators.

$$F_{P_T}(t) = F_T(t) - \left(W_T + \frac{W_S}{2}\right)\frac{a_T(t)}{g} \tag{5.4}$$

$$F_{P_B}(t) = F_B(t) - \left(W_B + \frac{W_S}{2}\right)\frac{a_B(t)}{g} \tag{5.5}$$

The forces $F_T(t)$ and $F_B(t)$ denote the total force applied by the actuators located at top and bottom UB-NCS levels, respectively; W_T = 14.6 kips, W_B = 15.3 kips, and W_S = 4.0 kips denote the reactive weight of the top and bottom UB-NCS platforms (including concrete slabs), and of the test specimen, respectively. $a_T(t)$ and $a_B(t)$ denote the average accelerations recorded at top (channels ACTLSE and

---

[7] Note that the maximum errors in replicating floor displacements are observed at small-high frequency displacements, and not at peak displacements.

ACTLNE) and bottom (channels ACBLSE and ACBLNE) platform levels, respectively, and *g* denotes acceleration due to gravity. Figure 5.63f shows the resulting hysteresis loop based on the estimated forces in the partition walls $F_p(t)$ and the measured drift. Pinching of the hysteresis is evident even at this low interstory drift level.
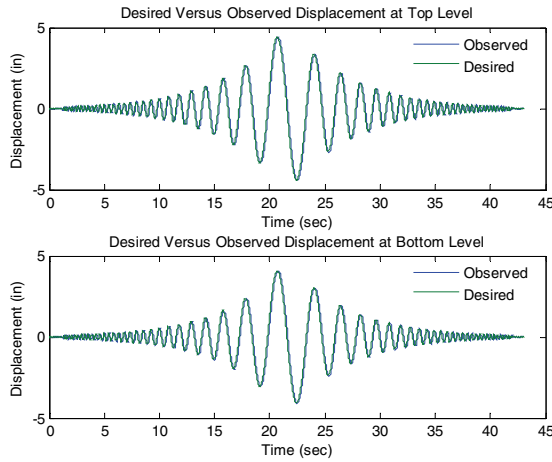
(a) Comparison of desired and observed platform displacements
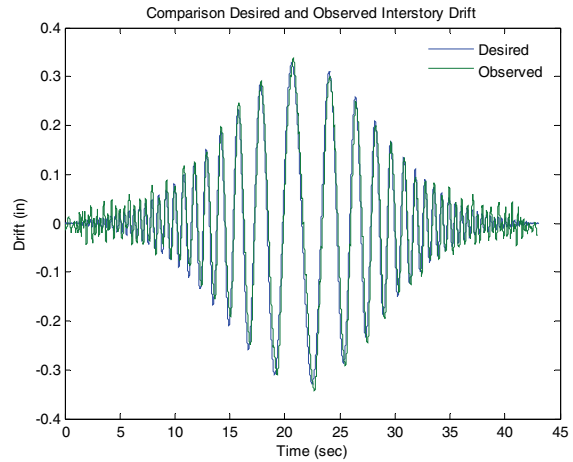
(b) Comparison of desired and observed interstory drifts
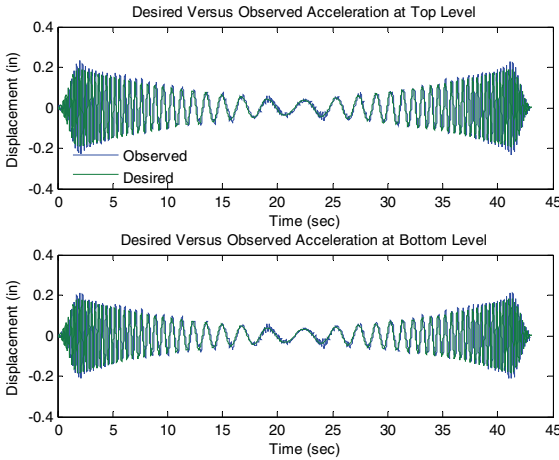
(c) Comparison of desired and observed accelerations
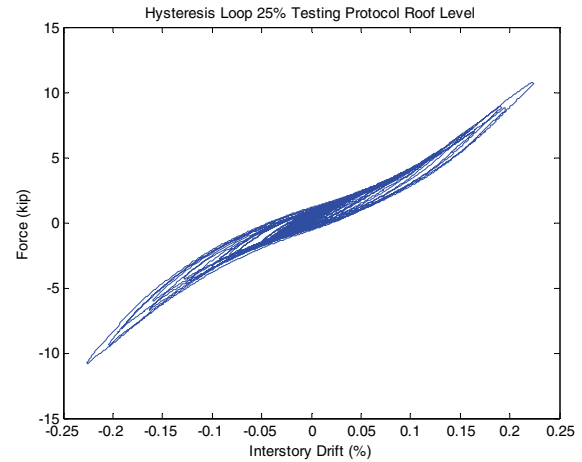
(d) Specimen hysteresis loop

Figure 5.63. Experimental results for dynamic protocol scaled to 25%, after command input compensation

The initial stiffness of the specimen, K_I, can be estimated by using the information presented in Figure 5.63f and:

$$K_I = \frac{\left|F_{\Delta_{Max}^+}\right| + \left|F_{\Delta_{Min}^-}\right|}{\left|\Delta_{Max}^+\right| + \left|\Delta_{Min}^-\right|} \tag{5.6}$$

where, according to Figure 5.63f, $F_{\Delta^+_{Max}}$ = 10.7 kips, $F_{\Delta^-_{Min}}$ = -10.8 kips, Δ^+_{Max} = 0.34 in (0.22 %), and Δ^-_{Min} = -0.34 in (0.23 %). After replacing those values into equation (5.6), an initial stiffness K_I = 31.6 kips/in is obtained. The stiffness is similar to the initial stiffness computed by Lang and Restrepo (Lang, 2007; Lang and Restrepo, 2006): K_I = 25.5 kips/in. The discrepancy in the stiffness values is partially due to the difference in specimen height, which for the case of the UCSD's specimen was 14 ft and for the UB-NCS test series was 12.6 ft.

During this test, some incipient damage was induced in the gypsum partition walls, as summarized in Figure 5.64. On the exterior side of the north wall, some slight screw pop-out was observed at the base of the wall. On the exterior of the south wall, a 4' hairline crack starting at the base of the south east corner of the specimen was observed along the corner bead. A photograph of this damage is shown in Figure 5.65a. A vertical crack was also observed along the joint of the gypsum wallboard over the upper right corner of the door opening, as shown in Figure 5.65b. Furthermore, a 1' in length crack, inclined approximately 30 degrees, was observed at the top left corner of the south wall opening, as shown in Figure 5.65c. Similar minor damage was observed in the interior face of the south wall.
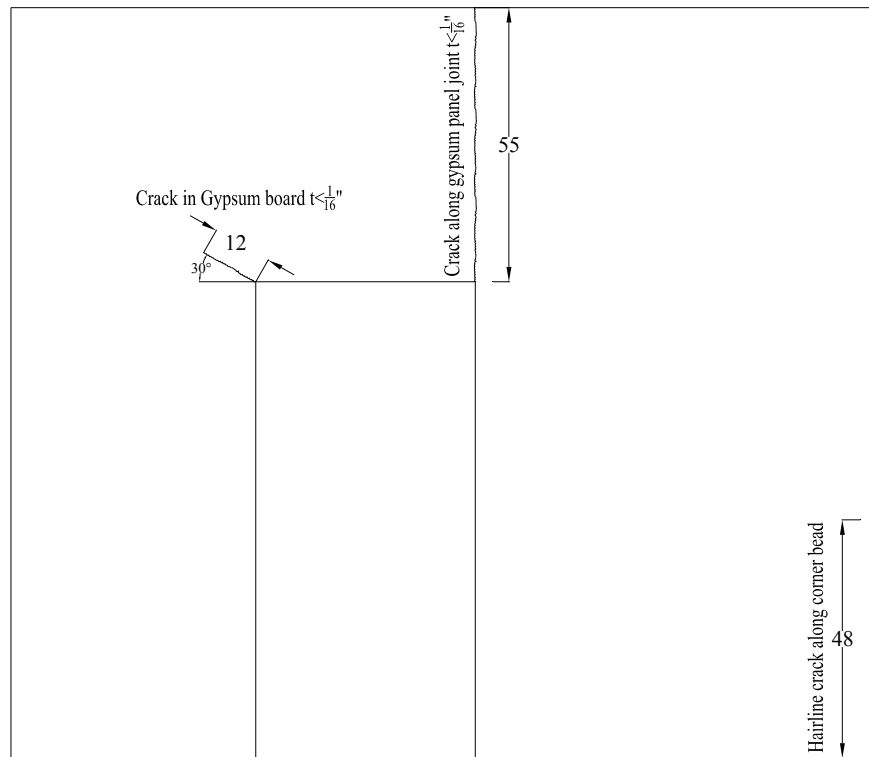
(a) Damage to exterior south wall

Figure 5.64. Damage observed in partition walls during dynamic testing protocol scaled to 25%
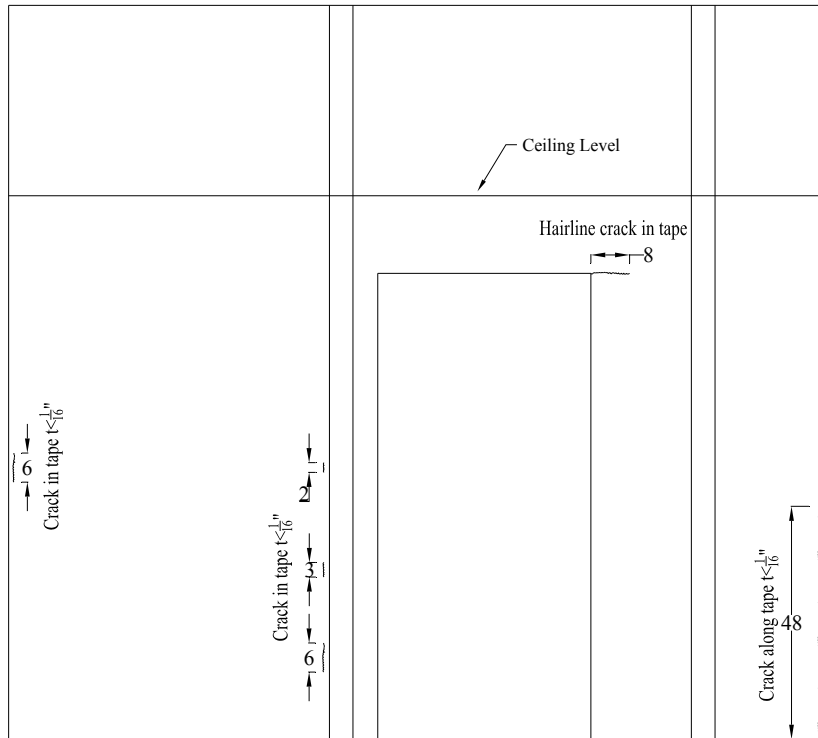
(b) Damage to interior south wall. Note that north wall (not shown) did not exhibited significant damage

Figure 5.64. Damage observed in partition walls during dynamic testing protocol scaled to 25% (Cont'd)
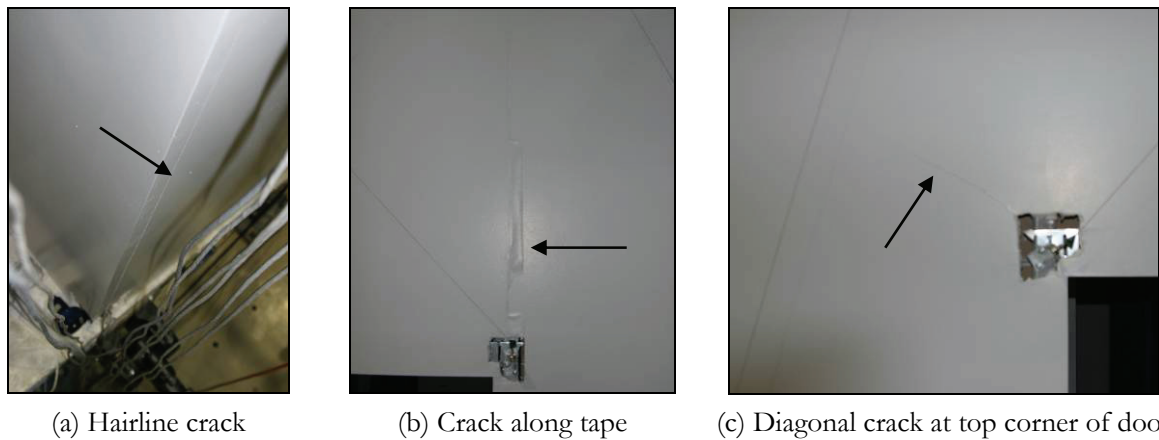
(a) Hairline crack   (b) Crack along tape   (c) Diagonal crack at top corner of door

Figure 5.65. Example of damage observed in gypsum partition walls

Table 5.11 summarizes the damage observations in the exterior face of the partition walls oriented in the direction of loading. The damage observed on the exterior faces of the partition walls is considered in the fragility analysis given that: i) it is representative of the global level of damage of the whole room, and ii) the experimental observations database is more populated for this case.

Table 5.11. Quantification of partition wall damage during dynamic testing protocol scaled to 25%

Damage measure	Quantified damage (Total length)
Hairline cracks	48 in
Cracks $t \leq \frac{1}{16}''$	67 in

The seismic behavior of Monitor 2 (Figure 5.3), one of the two monitors attached to the partition wall perpendicular to the direction of testing, was closely examined for this test. This piece of equipment is examined further because: i) it is a clear example of an acceleration sensitive component interacting dynamically with a displacement sensitive component (partition wall); ii) it demonstrates the unique testing capabilities provided by the UB-NCS; iii) it allows for the validation of the proposed testing protocol; and iv) it failed at the design earthquake level test. Figure 5.66 shows a set of plots summarizing the seismic performance of the monitor. Figure 5.66a shows the longitudinal (EW direction) acceleration histories of the bottom and top platforms and the base of Monitor 2. Little acceleration amplification is observed in Figure 5.66a, demonstrating the high out-of-plane stiffness of the partition wall configuration tested. Figure 5.66b shows the vertical acceleration histories of the bottom platform, the wall channel and the base of the monitor, clearly showing the amplification at the base of the monitor. Figure 5.66c presents the Fast Fourier Transforms (FFT's) for the triaxial response accelerations recorded at the base of Monitor 2 (channels M2AEWB for longitudinal, M2ANSB for transverse, and M2AVB for vertical accelerations, respectively). In Figure 5.66c it can be observed, in both transverse and vertical response FFT's, a dominant frequency at 2.5 Hz. Figure 5.66d shows the transfer functions (TF's) for longitudinal and vertical accelerations at the base of Monitor 2.
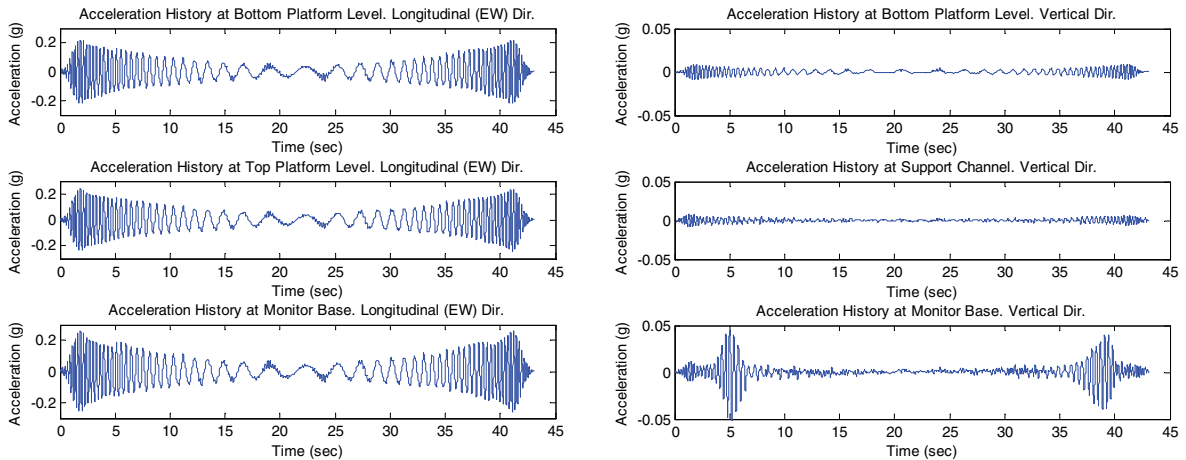
(a) Longitudinal acceleration amplification through partition walls

(b) Vertical acceleration amplification through partition walls and monitor supporting system

Figure 5.66. Experimental results of Monitor 2 for dynamic testing protocol scaled to 25%, after command input compensation
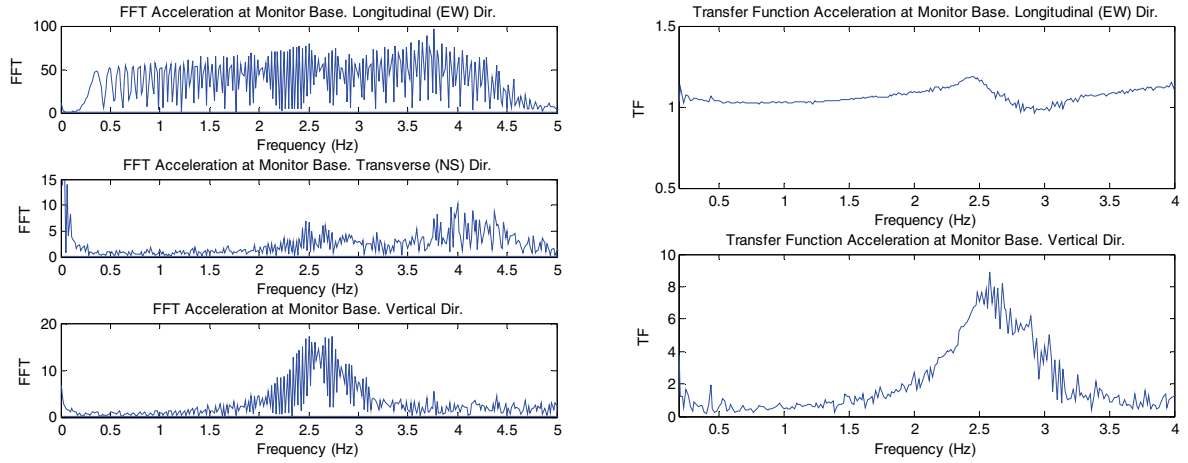
(c) FFT's for responses at the base of monitor

(d) Transfer function for longitudinal and vertical accelerations at the base of monitor

Figure 5.66. Experimental results of Monitor 2 for dynamic testing protocol scaled to 25%, after command input compensation (Cont'd)

The input vertical acceleration considered in the calculation of the vertical TF's corresponds to the acceleration history recorded at the center point of the bottom UB-NCS platform (Channel ACBV in Figure 5.52). In Figure 5.66d, peak amplifications are observed around a frequency of 2.5 Hz.

5.4.1.3 Dynamic testing protocol scaled to 50%

A test using the dynamic protocol scaled to 50% amplitude was performed mainly to populate the damage progression database required for constructing the fragility curves described in Subsection 5.5.

Table 5.12 summarizes the envelope of desired and observed peak floor motions recorded during the 50% scaled test using the dynamic testing protocol. In Table 5.12 it can be observed that the errors in replicating floor displacements, floor velocities, and interstory drifts histories are less than 8%. As in the previous test, errors close to 23% are observed for the platform accelerations.

Table 5.12. Envelope of peak floor motions for dynamic testing protocol scaled to 50%

Response	Peak Platform Displacement (in)		Peak Interstory Drift δ_{Max}		Peak Platform Velocity (in/sec)		Peak Platform Acceleration (g)	
	$D_{Max\,Bot}$	$D_{Max\,Top}$	(in)	(%)	$V_{Max\,Bot}$	$V_{Max\,Top}$	$A_{Max\,Bot}$	$A_{Max\,Top}$
Desired	8.15	8.80	0.66	0.43	15.3	16.3	0.37	0.38
Observed	8.26	8.91	0.71	0.47	15.2	16.2	0.46	0.50
Error (%)	1.32	1.18	7.57	7.57	0.56	0.69	19.7	23.7

Figure 5.67 illustrates the key results obtained from this test. In Figure 5.67e and Figure 5.67f it can be seen that the ORS slightly exceed the DRS limits recommended in Section 3. Incipient pinching is observed in the hysteresis loop shown in Figure 5.67h.
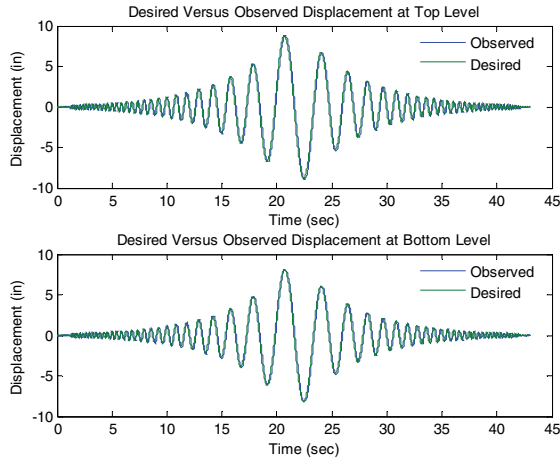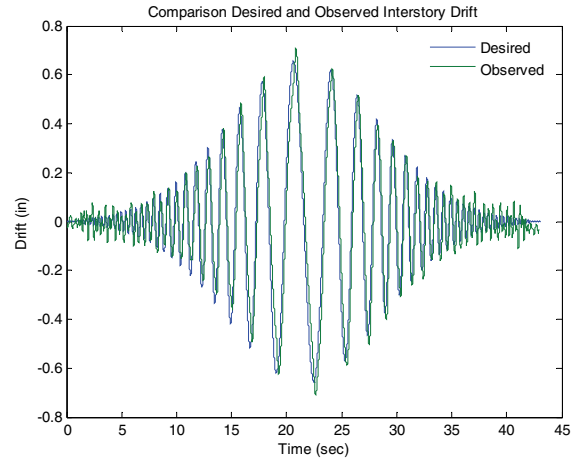
193

(a) Comparison of desired and observed displacements

(b) Comparison of desired and observed interstory drifts
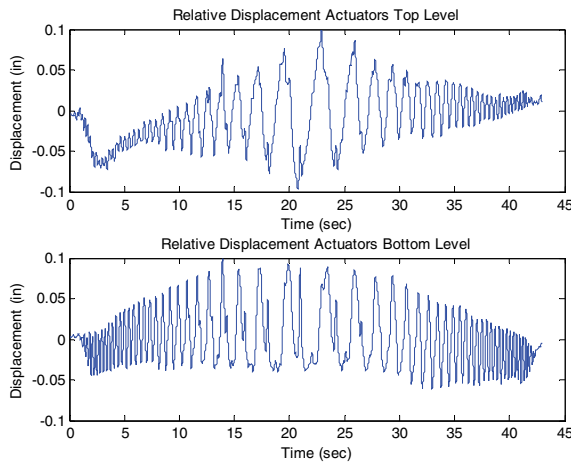
(c) Relative displacements between actuators
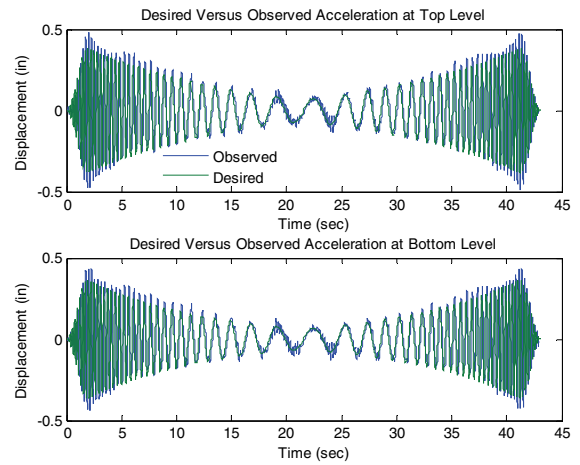
(d) Comp. of desired and observed accelerations
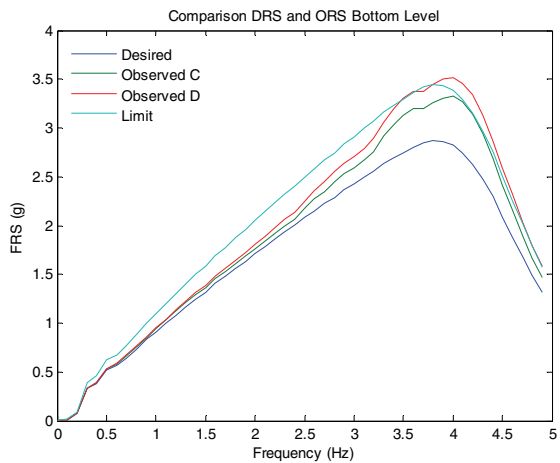
(e) Comparison of DRS and ORS bottom level
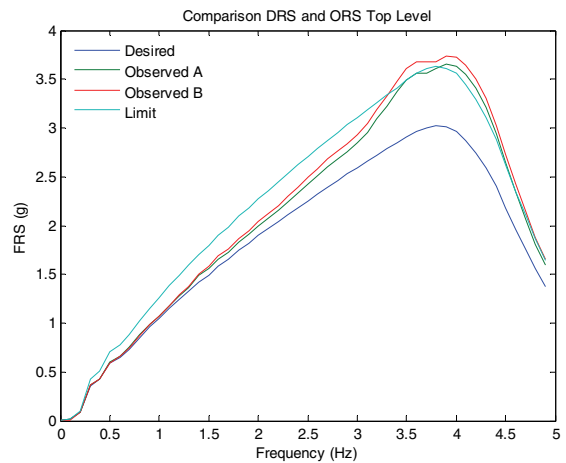
(f) Comparison of DRS and ORS top level

Figure 5.67. Experimental results for dynamic testing protocol scaled to 50%
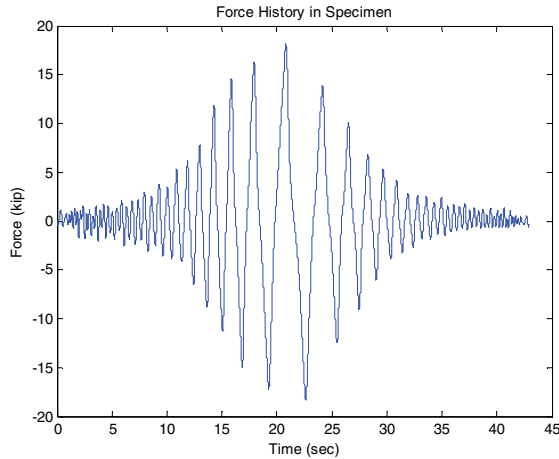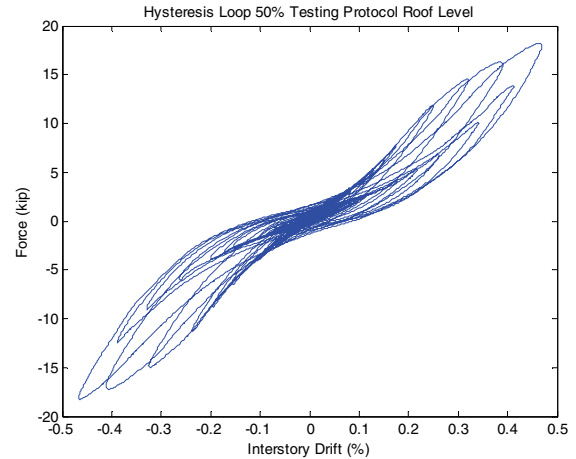
(g) Force history in specimen   (h) Specimen hysteresis loop

Figure 5.67. Experimental results for dynamic testing protocol scaled to 50% (Cont'd)

During this test, damage in both the north and south walls was observed mainly along cornerbeads (exterior walls faces) and paper tape along vertical joints at wall boundaries (interior walls faces), as shown in Figure 5.68. Note that it is probable that the damage observed on the interior surfaces of the walls, as shown in Figure 5.68, has extended beyond the ceiling level. Similar damage was observed in both north and south walls. On the exterior surface of the north wall, some screw pop out was observed at the connection of the gypsum boards to the bottom track. On the exterior surface of the south wall, the 1' in length crack observed at the end of the previous test at the top left corner of the door opening propagated reaching a length of 18 inches (Figure 5.70a). Moreover, the hairline crack shown in Figure 5.70b appeared in the door frame.

Table 5.13 summarizes the quantification of the damage observed on the exterior of the partition walls oriented in the loading direction. In Table 5.13, the damage measure "Screws pop-out area" corresponds to the total gypsum wallboard with raised or popped out surface are that may require repairs.

Table 5.13. Quantification of partition wall damage during dynamic testing protocol scaled to 50%

Damage measure	Quantified damage (Total length or surface)
Hairline cracks	549 in
Cracks t ≤ $\frac{1}{16}$″	73 in
Screws pop-out area	1701 in²
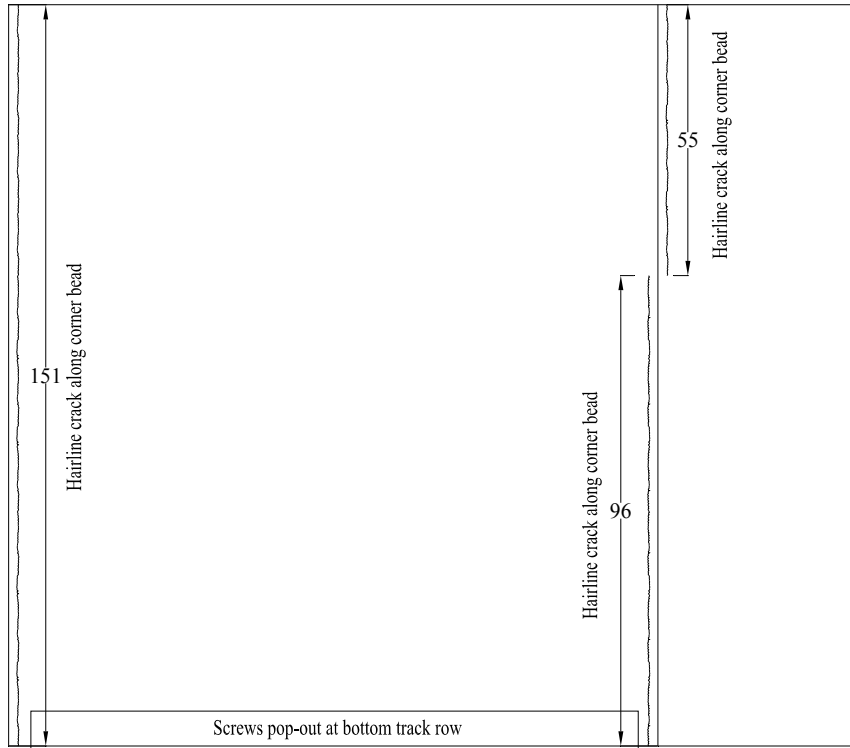
(a) Damage exterior north wall
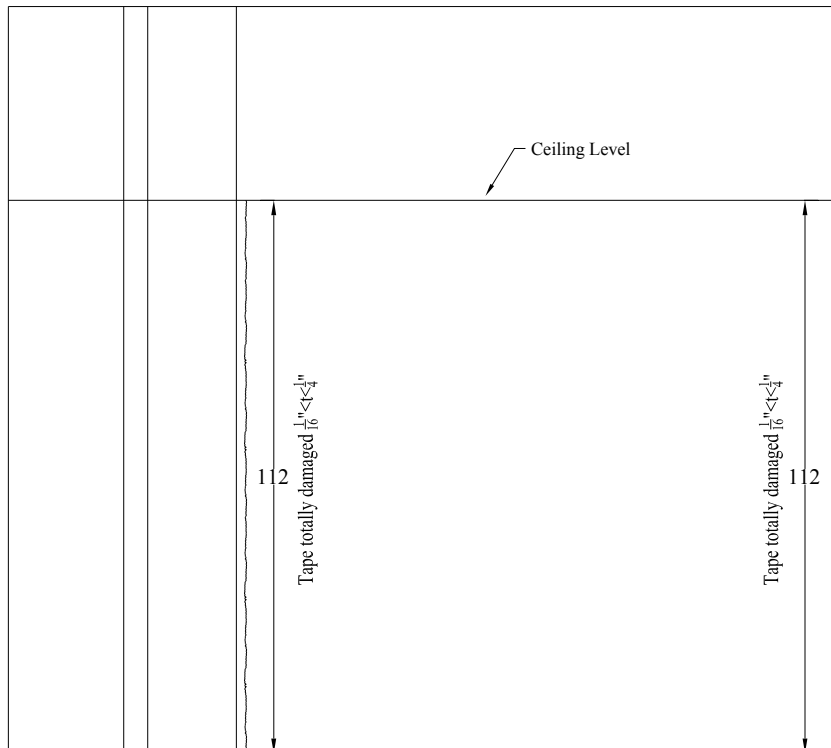
(b) Damage interior north wall

Figure 5.68. Damage observed in partition walls during dynamic testing protocol scaled to 50%

Crack in Gypsum board $t<\frac{1}{16}$"

18

30°

Crack along gypsum panel joint $t<\frac{1}{16}$"

55

Hairline rack along corner bead

96

Hairline rack along corner bead

151

Screws pop-out at bottom track row

(c) Damage exterior south wall

Ceiling Level

Crack in joint $t<\frac{1}{16}$"

5

12

Crack in joint $t<\frac{1}{16}$"

Tape totally damaged $\frac{1}{16}$"$<t<\frac{1}{4}$"

112

Tape totally damaged $\frac{1}{16}$"$<t<\frac{1}{4}$"

112

Crack along tape $t<\frac{1}{16}$"

48
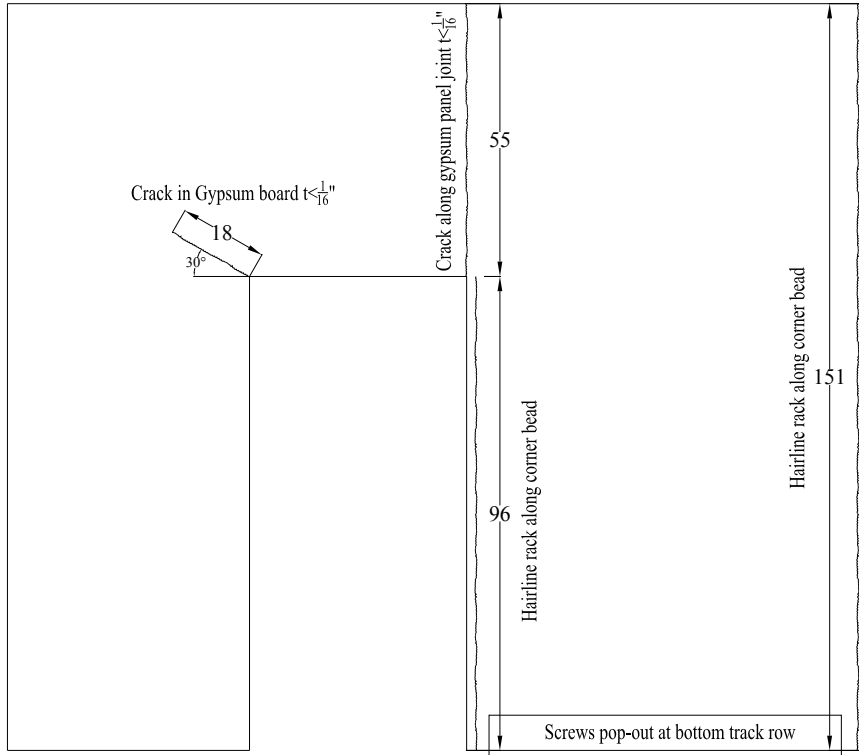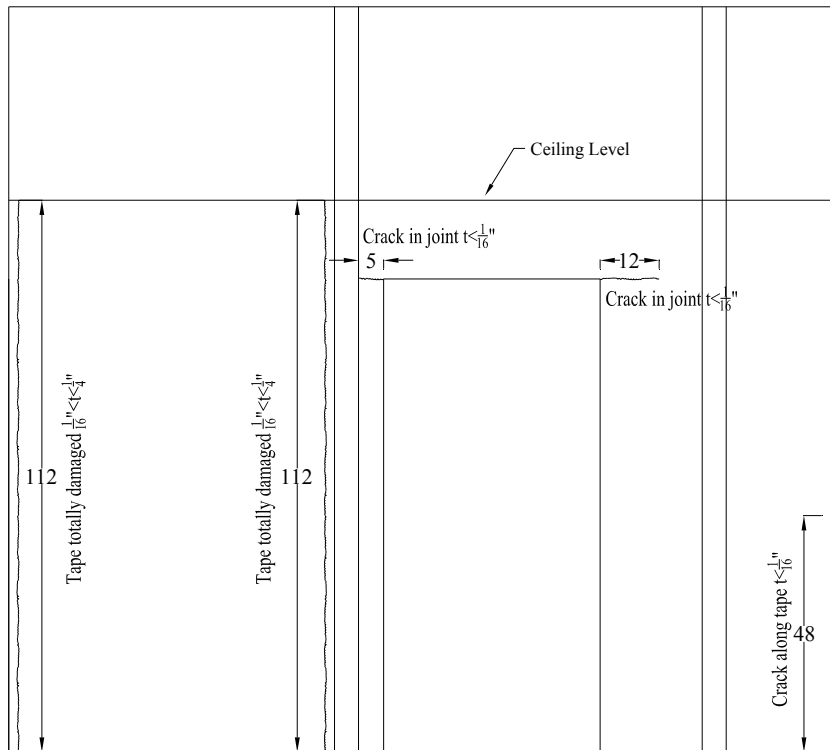
(d) Damage interior south wall

Figure 5.68. Damage observed in partition walls during dynamic testing protocol scaled to 50% (Cont'd)

Figure 5.69 shows a set of plots summarizing the seismic performance of Monitor 2 during the test performed considering the dynamic testing protocol scaled to 50%. Figure 5.69b clearly shows the amplification of vertical accelerations at the base of the monitor. In Figure 5.69c and d, a dominant equipment frequency of 2.4 Hz is identified.
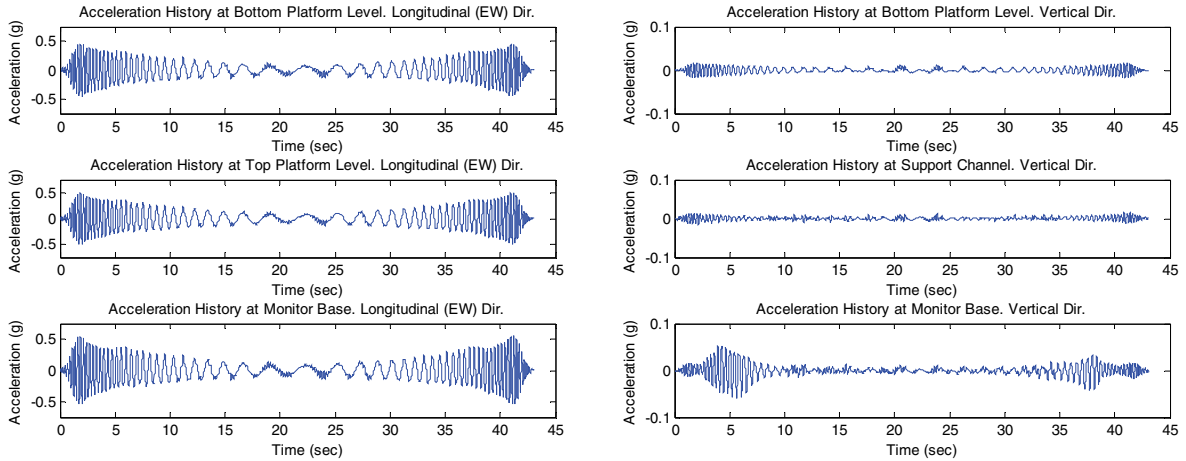
(a) Longitudinal acceleration amplification through partition walls

(b) Vertical acceleration amplification through partition walls and monitor supporting system
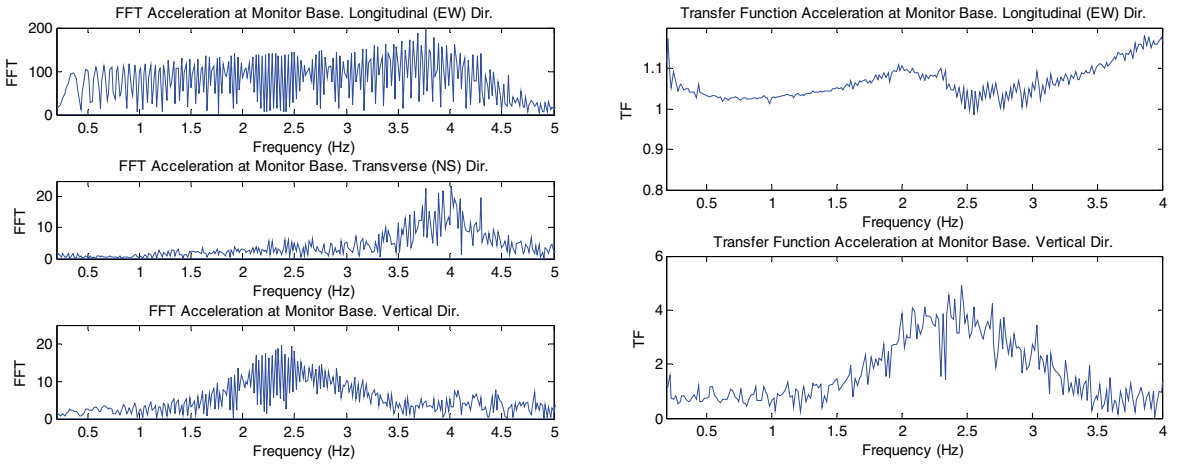
(c) FFT's for responses at the base of monitor

(d) Transfer function for longitudinal and vertical accelerations at the base of monitor

Figure 5.69. Experimental results of Monitor 2 for dynamic testing protocol scaled to 50%

In addition, it was observed that the bulb in the larger light of the surgical lamp burned out after impacting four times with one of the UB-NCS columns. The light bulb was replaced before the next test. Furthermore, Monitor 4 was dismounted from its retention clip device, as shown in Figure 5.70c, but did not fall to the floor. In the videos recorded during the test, excessive rocking of the video equipment rack and up to 4" displacement can be observed.

(a) Crack propagation at top left corner of door opening

(b) Hairline crack along door opening corner bead

(c) Monitor removed from its supporting device
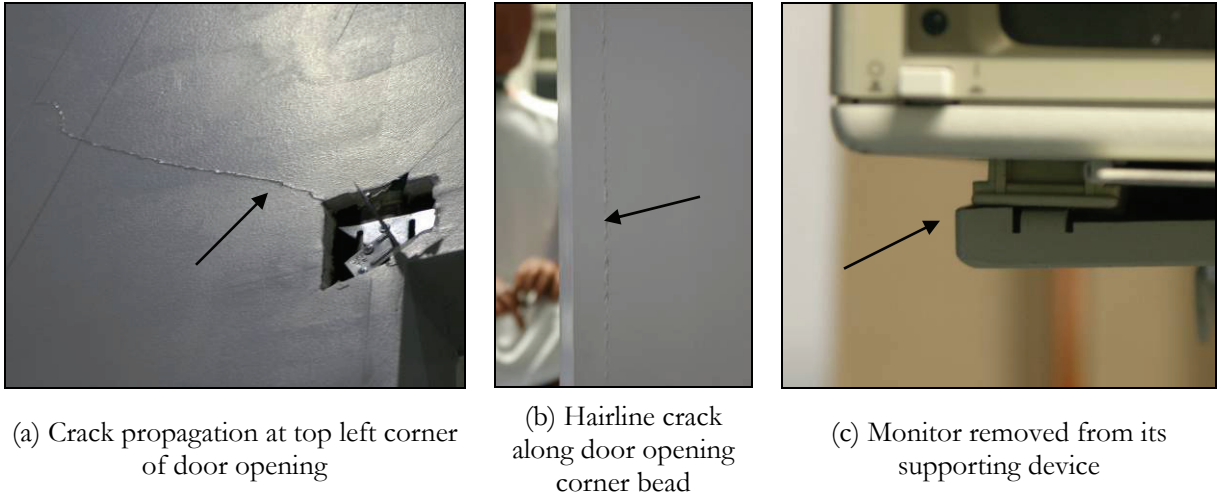
Figure 5.70. Examples of damage observed in specimen during dynamic testing protocol scaled to 50%

By the end of the test, the rack was displaced 3" from its initial position. Moreover, the equipment inside the rack displaced between 1.5 and 2.5". The medical gurney rotated gradually until reaching an angle of approximately 30 degrees. The infusion pumps poles displaced up to 12".

5.4.1.4 Dynamic testing protocol scaled to 100% (design earthquake level)

This test used the seismic qualification testing protocol calibrated to impose, on displacement and acceleration sensitive nonstructural components, the mean 84th percentile seismic demands expected at the roof level of multistory buildings, during a design level earthquake. The design level seismic hazard is associated with earthquake events with PE of 10% in 50 years. Table 5.14 summarizes the envelope of the desired and observed peak floor motions recorded during the test performed considering the dynamic testing protocol scaled to 100%. In Table 5.14 it can be observed that the errors in replicating floor displacements and velocities, and interstory drifts histories are less than 8%. Nevertheless, errors up to 33% are observed in replicating top platform accelerations.

Table 5.14. Envelope of peak floor motions for dynamic testing protocol scaled to 100%

Response	Peak Platform Displacement (in)		Peak Interstory Drift δ_{Max}		Peak Platform Velocity (in/sec)		Peak Platform Acceleration (g)	
	$D_{Max\ Bot}$	$D_{Max\ Top}$	(in)	(%)	$V_{Max\ Bot}$	$V_{Max\ Top}$	$A_{Max\ Bot}$	$A_{Max\ Top}$
Desired	16.3	17.6	1.31	0.87	30.5	32.6	0.73	0.77
Observed	16.6	17.9	1.42	0.94	30.5	32.5	1.09	1.15
Error (%)	1.87	1.53	7.67	7.67	0.22	0.52	32.7	33.1

Figure 5.71 presents the most relevant results obtained from this test. The results observed in Figure 5.71 follow the same trends described for Figure 5.67. One exception is that the errors in matching the DRS increase to about 20%. Thus the overshooting errors appear to increase with increasing amplitude.
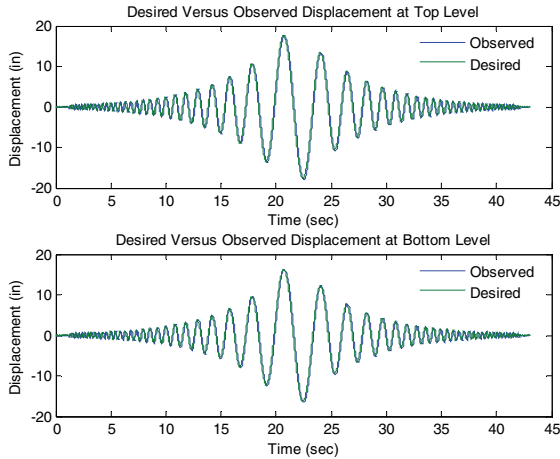
(a) Comparison of desired and observed platform displacements
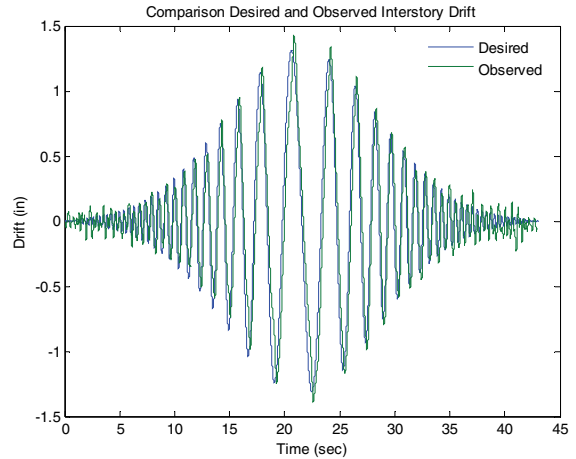
(b) Comparison of desired and observed interstory drifts
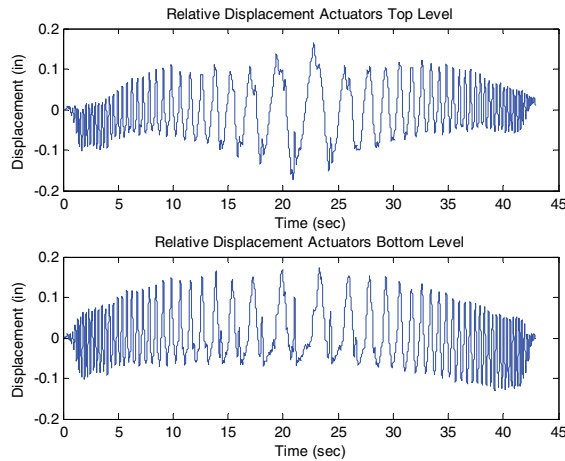
(c) Relative displacements between actuators
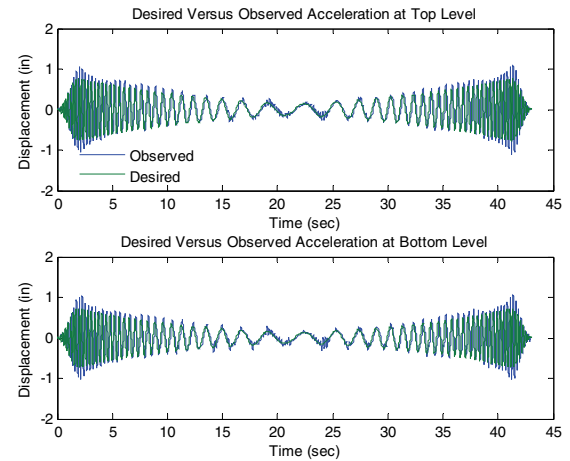
(d) Comp. of desired and observed accelerations
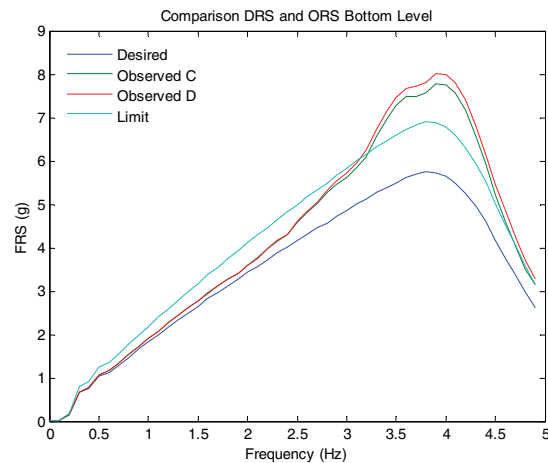
(e) Comparison of DRS and ORS bottom level
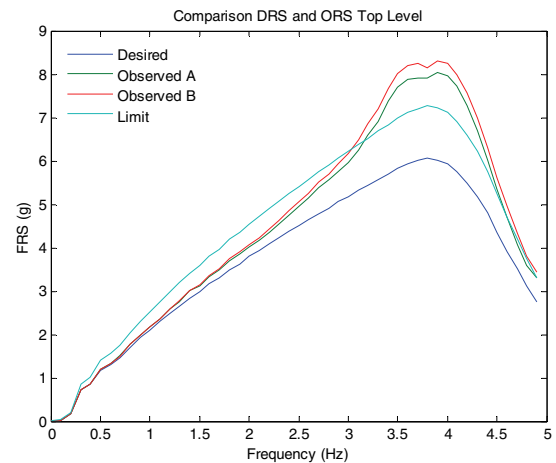
(f) Comparison of DRS and ORS top platform

Figure 5.71. Experimental results for dynamic testing protocol scaled to 100%, design earthquake level
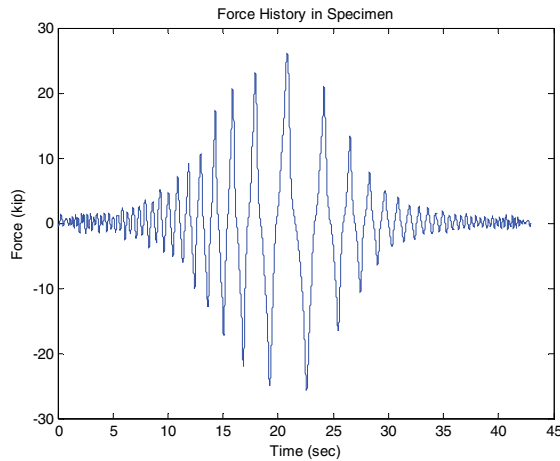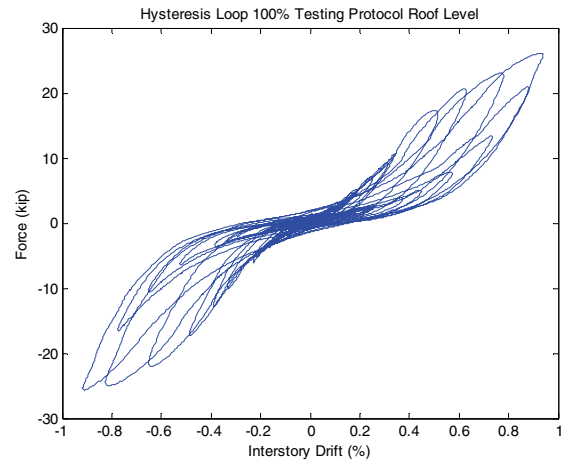
(g) Force history in specimen   (h) Specimen hysteresis loop

Figure 5.71. Experimental results for dynamic testing protocol scaled to 100%, design earthquake level (Cont'd)

During this test, at a time of 35 seconds, Monitor 2 and Monitor 3 (Figure 5.35b) broke off their supporting systems. In both monitors, the failure was observed in the screws connecting the monitor mounting plate to the horizontal pin in the swivel-tilt head. Figure 5.72 shows a set of plots summarizing the seismic performance of Monitor 2. Only the first 21 seconds of the recorded accelerations were considered to develop Figure 5.72c and Figure 5.72d because of the failure of the monitor supporting system.

During this design level test, extensive cracks were observed along corner beads and joints between gypsum wallboards in both the north and south partition walls. Unfortunately, the pre-established testing program did not allow for capturing detailed damage progression. Nevertheless, important information regarding the overall seismic performance of the emergency room was obtained from the videos recorded during the test. The number of popped out screws increased, as shown in Figure 5.73c, which shows this damage at the base of the exterior surface of the north wall. The largest light in the surgical lamp shown in Figure 5.41 broke off its support after exhibiting excessive displacement and hitting the UB-NCS columns several times (Figure 5.73d). Furthermore, one of the drop-in devices attaching the medical gas piping hangers to the top concrete slab (Figure 5.32) pulled out from the concrete slab, as shown in Figure 5.73e. The gurney shown in Figure 5.45 exhibited excessive motion after deactivation of its breaking system due to the strong shaking. The crash test dummy was thrown off the gurney. Severe impact was observed between the video cabinet and the patient monitor shown in Figure 5.43. Most of the medical supplies placed on top of the medical cart also shown in Figure 5.43 fell off the cart, as shown in Figure 5.73f.
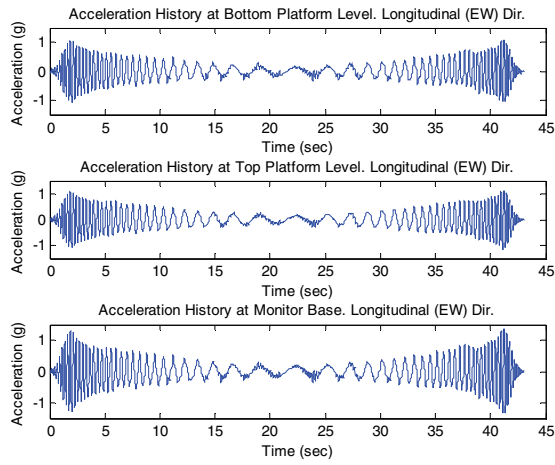
(a) Longitudinal acceleration amplification through partition walls
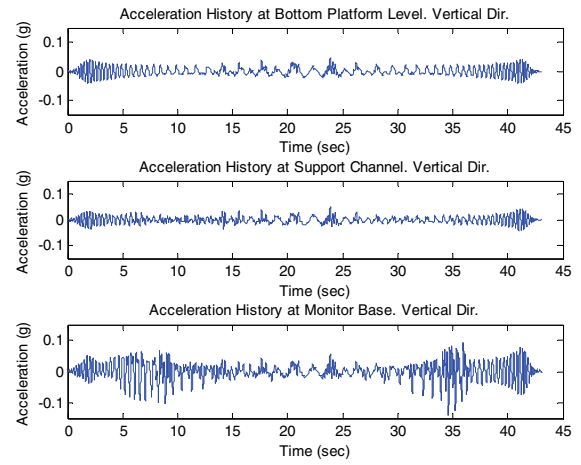
(b) Vertical acceleration amplification through partition walls and monitor supporting system
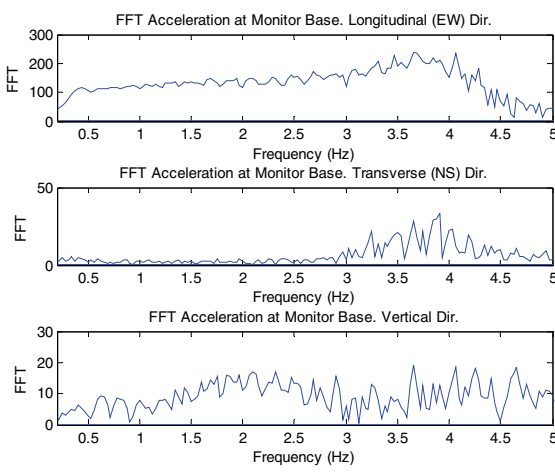
(c) FFT's for responses at the base of monitor
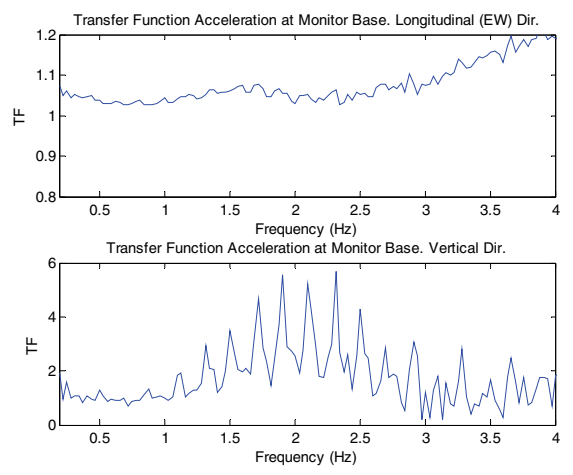
(d) Transfer function for longitudinal and vertical accelerations at the base of monitor

Figure 5.72. Experimental results of Monitor 2 for dynamic testing protocol scaled to 100%, design earthquake level
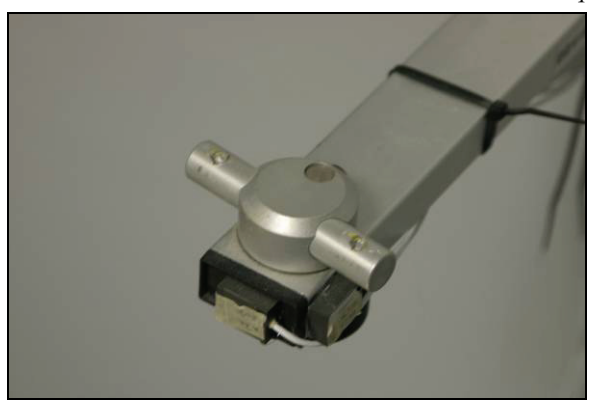
(a) Broken screws at monitor's supporting system

(b) Collapsed monitors

Figure 5.73. Examples of damage observed in specimen components during dynamic testing protocol scaled to 100% (design earthquake level)
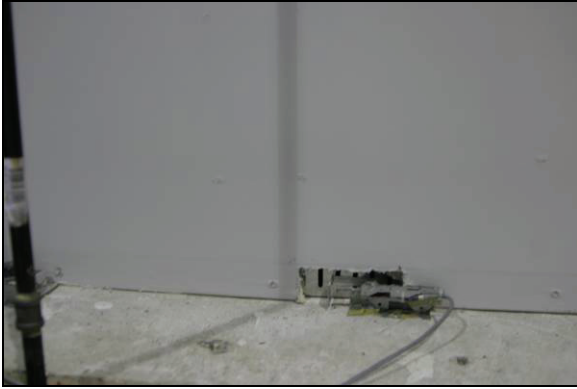
(c) Increased number of popped-out screws at the base of north wall (exterior)
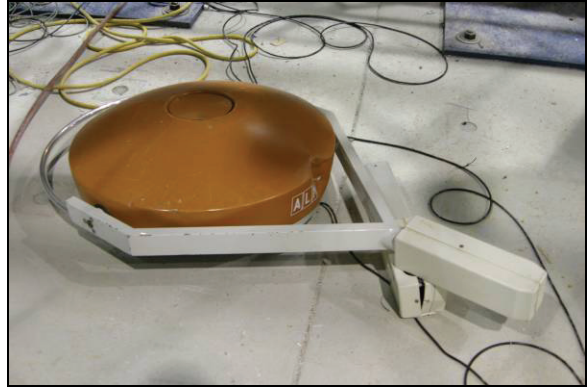
(d) Collapsed light in surgical lamp

(e) Pulled-out of drop-in device

(f) Medical supplies fell down from medical cart

Figure 5.73. Examples of damage observed in specimen components during dynamic testing protocol scaled to 100% (design earthquake level). (Cont'd)

5.4.1.5 Dynamic testing protocol scaled to 150% (maximum considered earthquake level)

This test used the seismic qualification testing protocol calibrated to impose, on displacement and acceleration sensitive nonstructural components, the mean 84th percentile seismic demands expected at the roof level of multistory buildings, during an earthquake event associated to a maximum considered seismic hazard. This seismic hazard level is associated to earthquake events with a probability of exceedance of 2% in 50 years.

Table 5.15 summarizes the envelope of the desired and observed peak floor motions, recorded during the test performed considering the dynamic testing protocol scaled to 150%. In Table 5.15 it can be observed that the errors in replicating floor displacements and velocities, and interstory drifts histories are less than 8.5%. Nevertheless, errors up to 50% are observed in replicating top platform accelerations. Figure 5.74 illustrates the key results obtained from this test. Figure 5.74d shows the overshots in acceleration histories described in Table 5.15. Overshoots of the same magnitude are observed in the ORS for the

bottom and top UB-NCS platforms. Clearly, the input motions overcompensated for the response of the UB-NCS. The hysteresis loop shown Figure 5.74h exhibits severe pinching due mainly to the extensive propagation of cracks along gypsum panel joints described later.

Table 5.15. Envelope of peak floor motions for dynamic testing protocol scaled to 150%

Response	Peak Platform Displacement (in)		Peak Interstory Drift δ_{Max}		Peak Platform Velocity (in/sec)		Peak Platform Acceleration (g)	
	$D_{Max\ Bot}$	$D_{Max\ Top}$	(in)	(%)	$V_{Max\ Bot}$	$V_{Max\ Top}$	$A_{Max\ Bot}$	$A_{Max\ Top}$
Desired	24.5	26.4	1.97	1.30	45.8	48.9	1.10	1.15
Observed	24.9	26.9	2.15	1.42	46.4	49.1	2.13	1.94
Error (%)	1.96	1.92	8.39	8.39	1.30	0.35	48.4	40.7
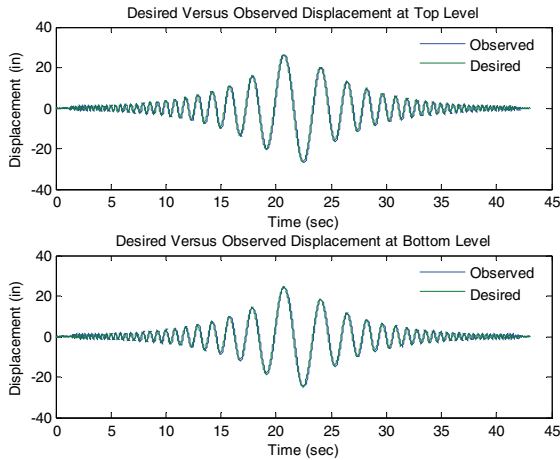
(a) Comparison of desired and observed platform displacements
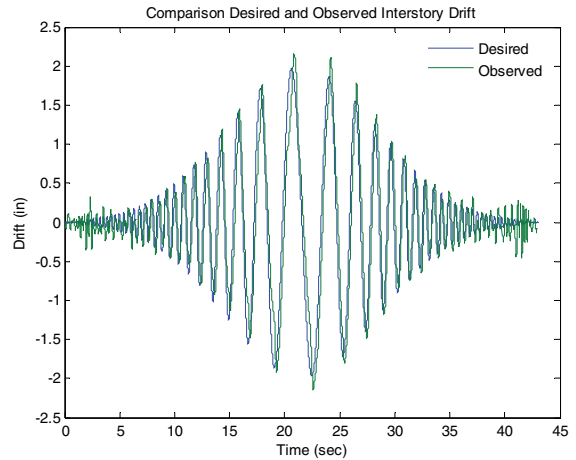
(b) Comparison of desired and observed interstory drifts
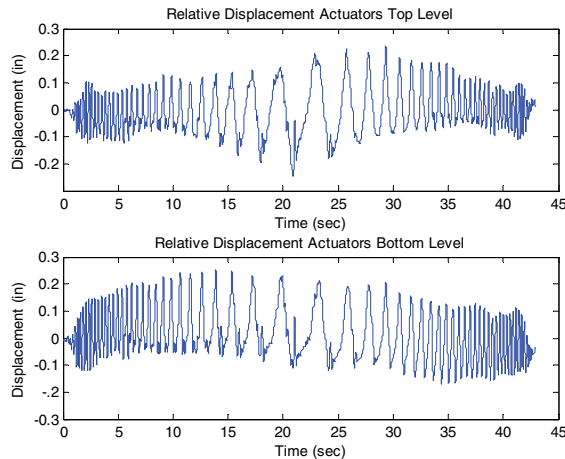
(c) Relative displacements between actuators
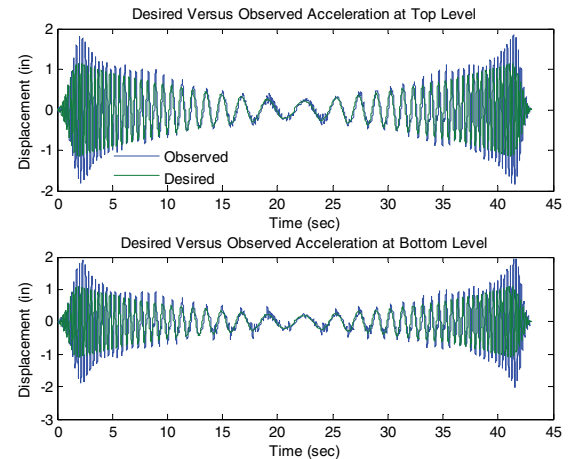
(d) Comparison of desired and observed accel.

Figure 5.74. Experimental results for dynamic testing protocol scaled to 150% (maximum credible earthquake level)

(e) Comparison of DRS and ORS bottom level
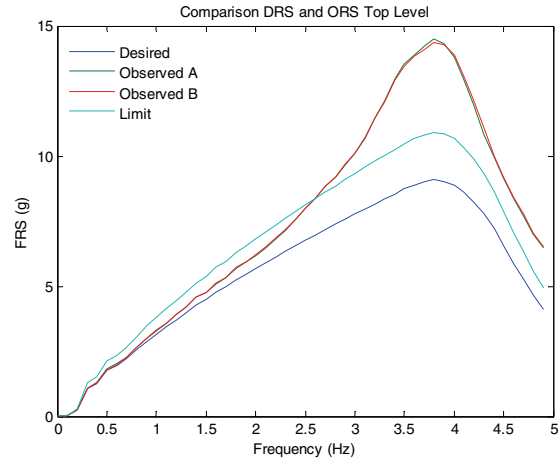
(f) Comparison of DRS and ORS top level
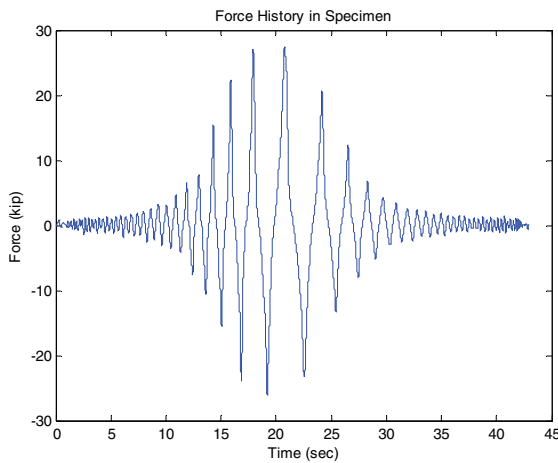
(g) Force history in specimen
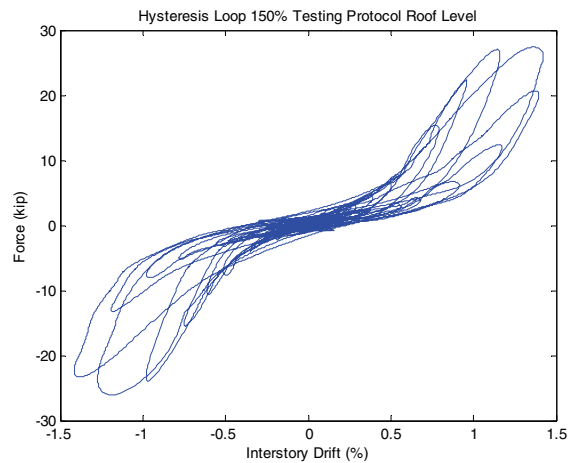
(h) Specimen hysteresis loop

Figure 5.74. Experimental results for dynamic testing protocol scaled to 150% (maximum credible earthquake level) (Cont'd)

During this test, severe damage to both the north and south walls was observed, as detailed in Figure 5.75 and Figure 5.76. It is considered highly probable that the damage observed in the interior of the emergency room was extended beyond the ceiling level. Similar damage was observed on both the north and south walls. Extensive residual crack openings (~1/8-1/4") were observed along all cornerbeads (Figure 5.76a through Figure 5.76d) and severe damage was observed along gypsum panel joints (Figure 5.76e through Figure 5.76i). A significant increase in the number of rocking and popped-out screws was observed, as shown in Figure 5.76a, Figure 5.76d, Figure 5.76j and Figure 5.76k. The cracks observed at the top corners of the door opening continued propagating as shown in Figure 5.76l and Figure 5.76m. Table 5.16 summarizes the quantification of the damage observed in the exterior of the partition walls oriented in the direction of loading.

Screws pop-out at top track row

Crack along corner bead (Residual gap of $\frac{1}{16}$")

55

Crack along corner bead (Residual gap of $\frac{1}{4}$")

151

Crack along corner bead (Residual gap of $\frac{1}{4}$")

96

Screws pop-out around 3 bottom rows

(a) Damage exterior north wall

Ceiling Level

27

Tape totally damaged $\frac{1}{16}$"$<$t$<\frac{1}{4}$"

Tape totally damaged $\frac{1}{16}$"$<$t$<\frac{1}{4}$"

48

112

Permanent gap $\frac{1}{8}$"-$\frac{1}{4}$"

123

112

Permanent gap $\frac{1}{8}$"

48

Tape totally damaged $\frac{1}{16}$"$<$t$<\frac{1}{4}$"
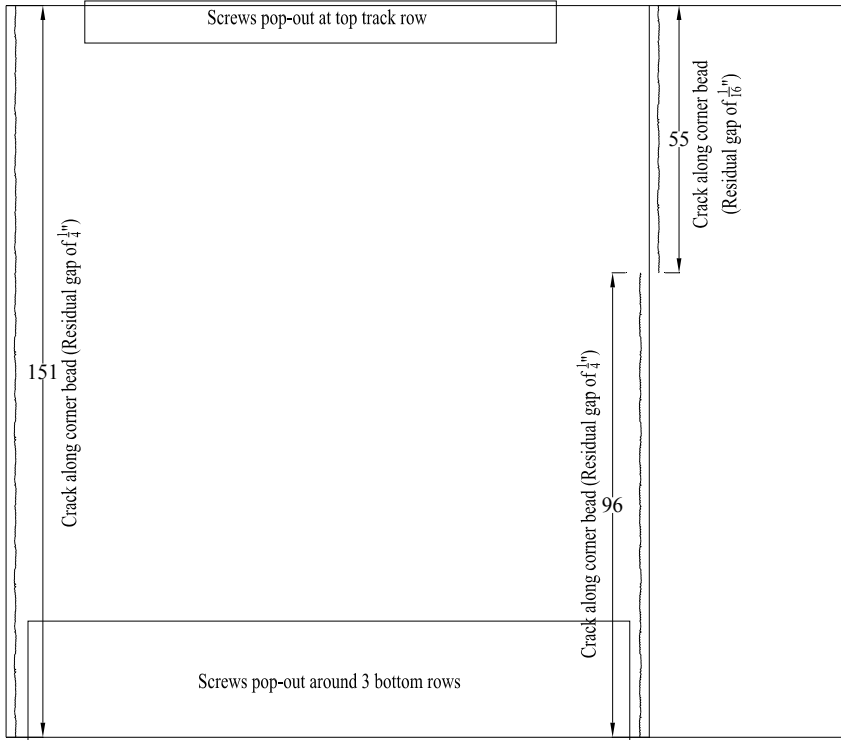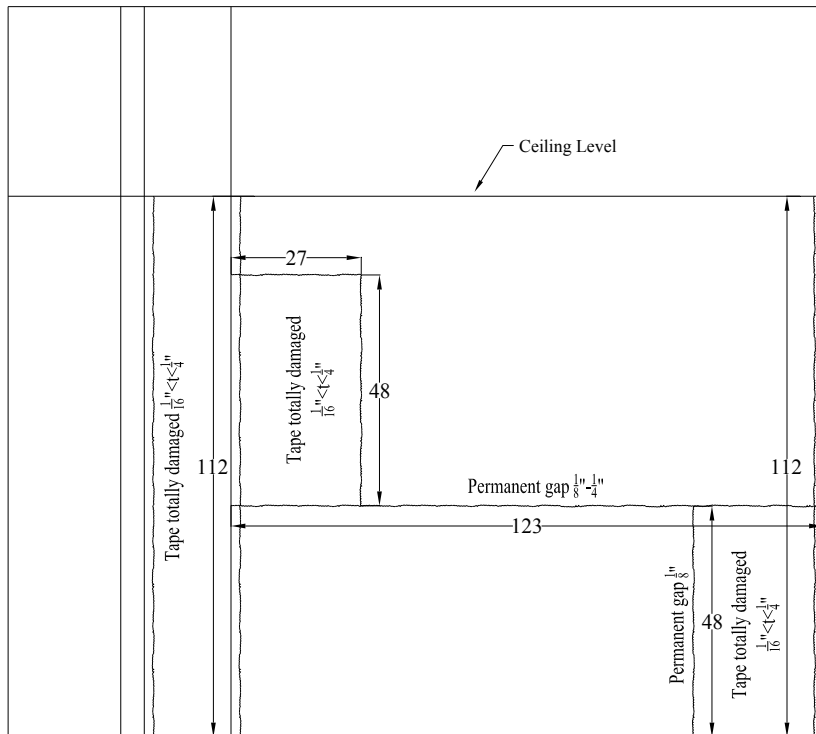
(b) Damage interior north wall

Figure 5.75. Damage observed in partition walls during dynamic testing protocol scaled to 150%, maximum considered earthquake level
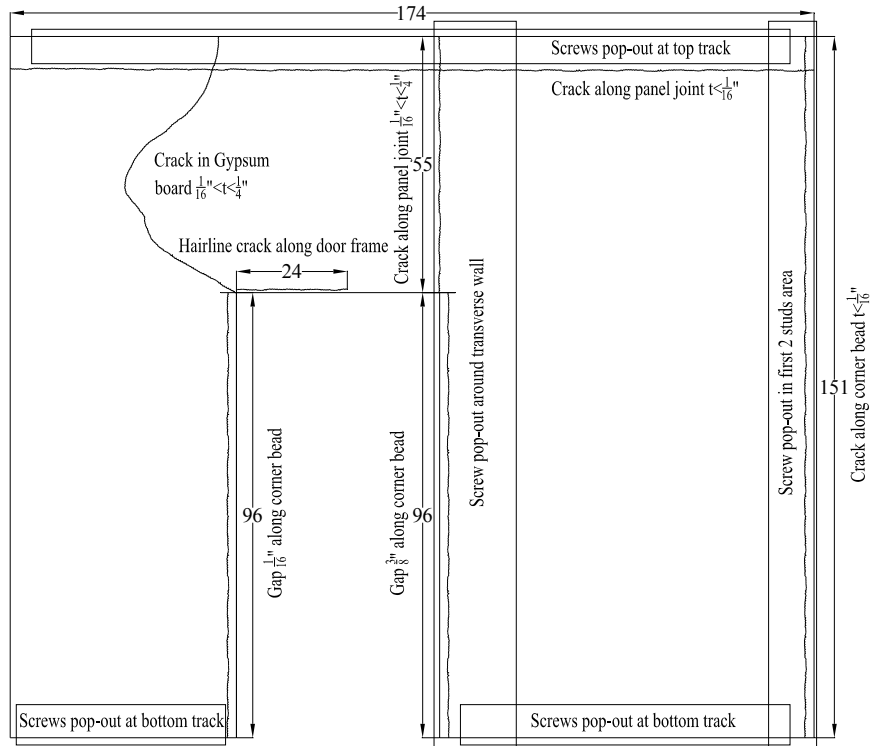
(c) Damage exterior south wall
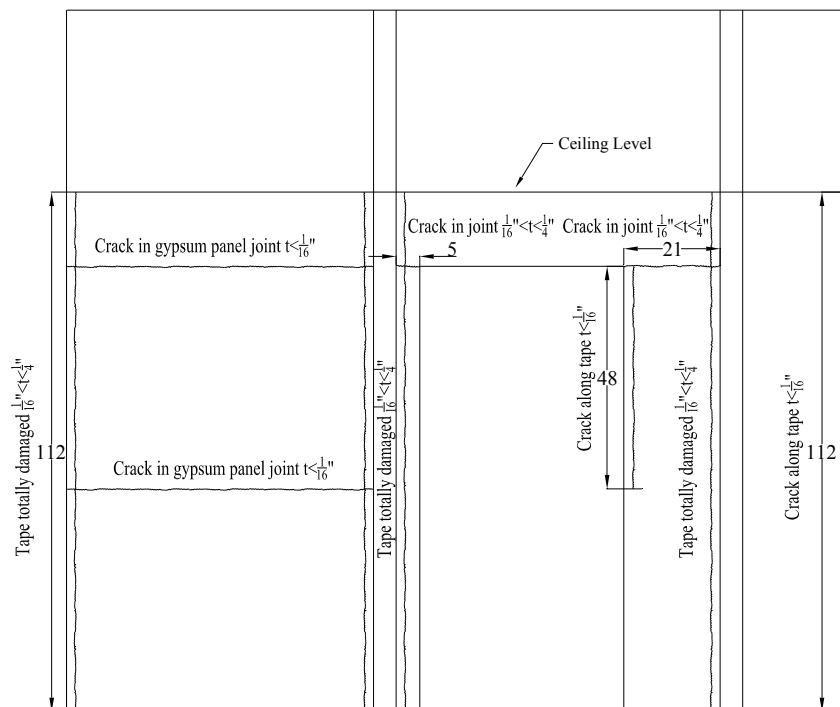
(d) Damage interior south wall

Figure 5.75. Damage observed in partition walls during dynamic testing protocol scaled to 150%, maximum considered earthquake level (Cont'd)
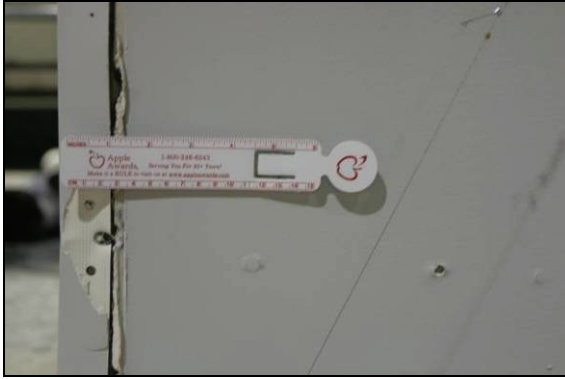
(a) Damage observed along cornerbeads at door frame (right)

(b) Damage observed along cornerbeads at door frame (left)

(c) Damage observed along cornerbeads at northwest corner
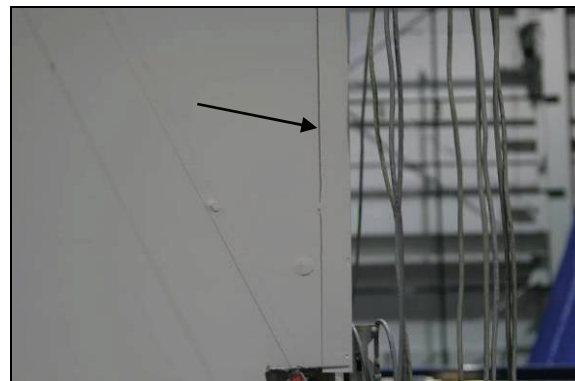
(d) Damage observed along cornerbeads at southeast corner

(e) Damage of gypsum panel joints at interior surface of north wall
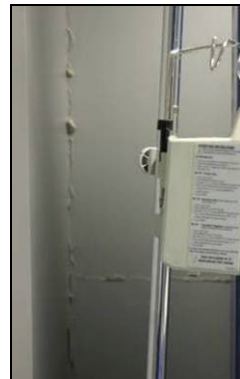
(f) Damage of gypsum panel joints at interior surface of north wall
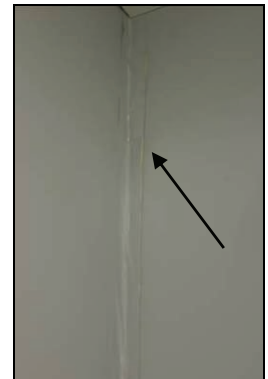
(g) Damage of gypsum panel joints at interior surface of south wall

Figure 5.76. Examples of damage observed on partition walls during dynamic testing protocol scaled to 150%, maximum considered earthquake level
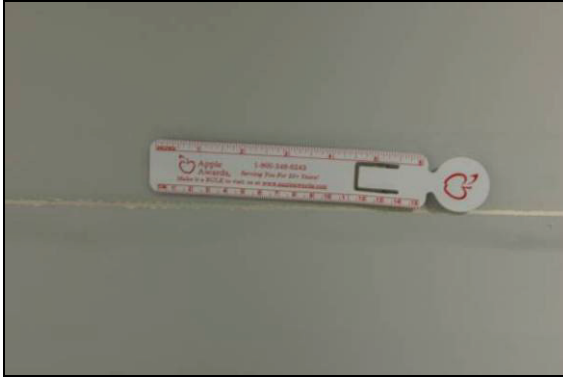
(h) Damage of gypsum panel joints at interior surface of south wall

(i) Damage of gypsum panel joints at interior surface of south wall

(j) Screw pop-out examples
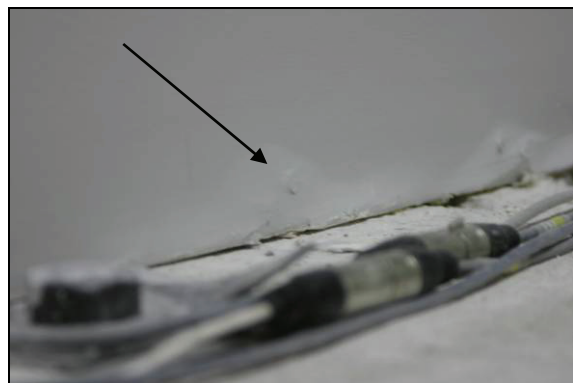
(k) Screw pop-out examples

(l) Diagonal and vertical cracks at top left door opening corners

(m) Diagonal and vertical cracks at top right door opening corners

Figure 5.76. Examples of damage observed on partition walls during dynamic testing protocol scaled to 150%, maximum considered earthquake level (Cont'd)

During the test imposing demands compatible with the maximum considered earthquake, an increased level of damage was observed in other components. Monitor 4 (see Figure 5.35c) fell down from its supporting system (Figure 5.77a). Moreover, at the end of the test, a permanent vertical drop of approximately 0.25 inches respect to the wall channel was measured in the supporting arm (Figure 5.77b).

Noticeable residual deformations were observed in the medical gas pipes, as shown in Figure 5.77c. At this point, it is recalled that the medical gas supporting system failed during the design earthquake level test. As in the previous test, the gurney exhibited excessive motion after deactivation of its breaking system (Figure 5.77d), and the dummy was thrown off the gurney and almost out of the room, as shown in Figure 5.77e. The IV pump pole 2 overturned and fell down over the dummy, as shown in Figure 5.77e. The IV pump pole 1, shown in Figure 5.3 and Figure 5.39a, exhibited excessive displacements (over 10 inches), and impacted and damaged the base of the gypsum panels, as shown in Figure 5.77f. All medical supplies on the medical cart shown in Figure 5.43 fell down during the test (Figure 5.77g). Some minor damage was observed in the suspended ceiling system. Figure 5.77h shows the only tile that fell down during the test. Figure 5.77i and Figure 5.77j show two of the ceiling tiles dislocated from their original installation position. Figure 5.77j also shows the deformation of the ceiling supporting frame. Figure 5.77k shows the minor damage along the edge of several ceiling tiles located in the perimeter of the emergency room. Excessive rotations and displacements up to 7 inches of the equipment inside the surgical video rack were observed, as shown in Figure 5.77l.

Table 5.16. Quantification of specimen's damage during dynamic testing protocol scaled to 150%

Damage measure	Quantified damage (Total length or area)
Hairline cracks	24 in
Cracks t ≤ $\frac{1}{16}''$	466 in
Cracks $\frac{1}{16}'' <$ t $< \frac{1}{4}''$	405 in
Cracks t ≥ $\frac{1}{4}''$	96 in
Screws pop-out area	10666 in^2

(a) Monitor 4 fell down

(b) Permanent vertical displacement of mounting arm of Monitor 4

Figure 5.77. Examples of damage observed in specimen components during dynamic testing protocol scaled to 150% (maximum credible earthquake level)
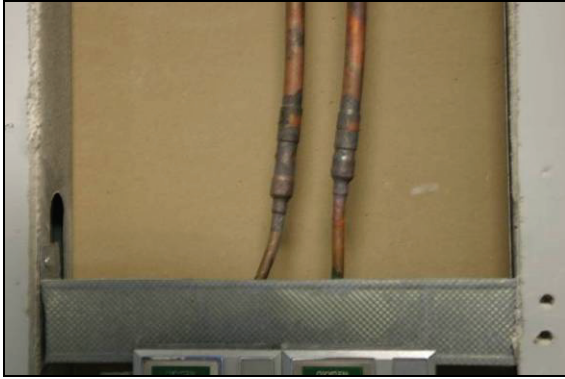
(c) Bending of medical gas pipes

(d) Excessive displacement of medical gurney

(e) Dummy thrown off medical gurney and pole fell down over dummy

(f) Gypsum wallboard damaged by IV pump pole impact
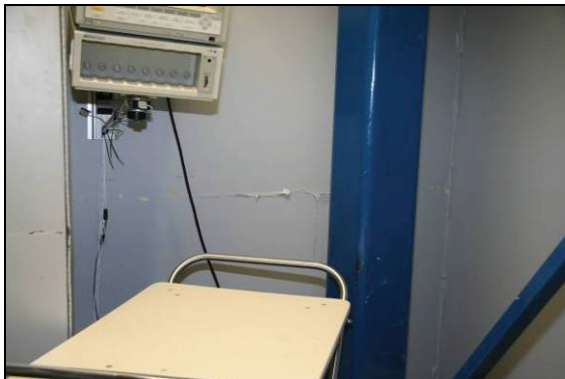
(g) Medical supplies fell down from medical cart

(h) Ceiling tile fell down

Figure 5.77. Examples of damage observed in specimen components during dynamic testing protocol scaled to 150% (maximum credible earthquake level) (Cont'd)
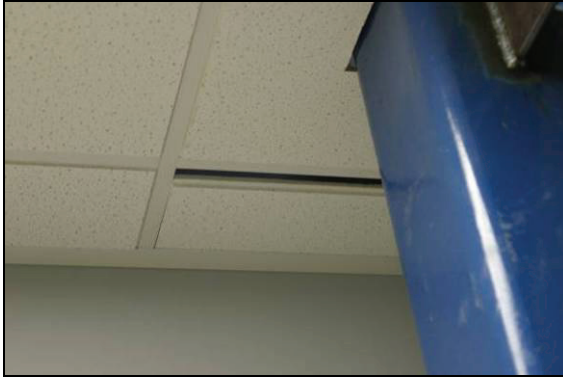
(i) Permanent displacement of ceiling tiles

(j) Deformation of ceiling grid

(k) Damage along ceiling tile edges

(l) Excessive displacement and rotation of surgical video rack contents

Figure 5.77. Examples of damage observed in specimen components during dynamic testing protocol scaled to 150% (maximum credible earthquake level) (Cont'd)

5.4.2   Results and observations for simulated building floor motions

This subsection presents the observations and results of the tests performed considering the floor motion histories described in Subsection 5.3.2, corresponding to the simulated floor response of a four story steel framed medical facility. Before running this test series, new mounting brackets were installed for Monitors 2, 3 and 4, and new (fully functional) monitors were mounted. The medical gurney, the dummy and the infusion pump poles were relocated in their original positions, as indicated in Figure 5.3. All surgical video rack contents were also repositioned to their original location inside the rack. The medical supplies were repositioned on top of the medical cart.

5.4.2.1 Simulated building floor motions for a SH with PE of 10% in 50 years, scaled to 25%

This test was performed mainly to compensate the input command signal for the UB-NCS platforms in subsequent tests. Nevertheless, some observations regarding the testing frame fidelity and seismic performance of the testing specimen are presented.

5.4.2.1.1 Command signal compensation

The iterative command signal compensation procedure described in Section 3 was used to compensate the floor motions to be used in this test series. Figure 5.78 summarizes the main results of the test performed considering the original (before compensation) signals shown in Figure 5.49, scaled to 25%. Figure 5.78e and Figure 5.78f show that the ORS underestimate the DRS for both bottom and top UB-NCS platforms in the whole range of frequencies of interest. A poorer performance is observed in the actuators located at the top platform level. Based on the criteria and methodology for command signal compensation described in Section 3, the UB-NCS platform input motions were compensated. Figure 5.78g and Figure 5.78h show the compensated signals to be used in larger amplitude tests. The effectiveness of using the compensated signal for running larger amplitude tests is demonstrated later.
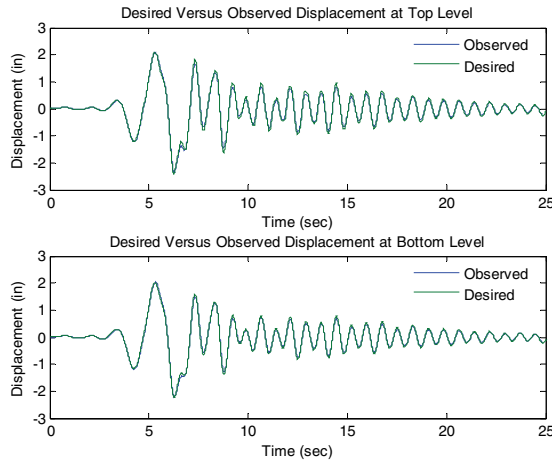
(a) Comparison of desired and observed platform displacements

(b) Comparison of desired and observed interstory drift histories
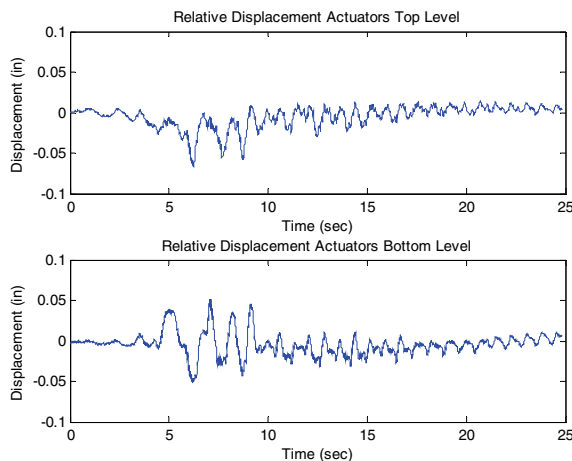
(c) Relative displacements between actuators

(d) Actuator force histories

Figure 5.78. Experimental results for simulated building floor motions for SH with PE 10% in 50 years, scaled to 25%, before command input compensation
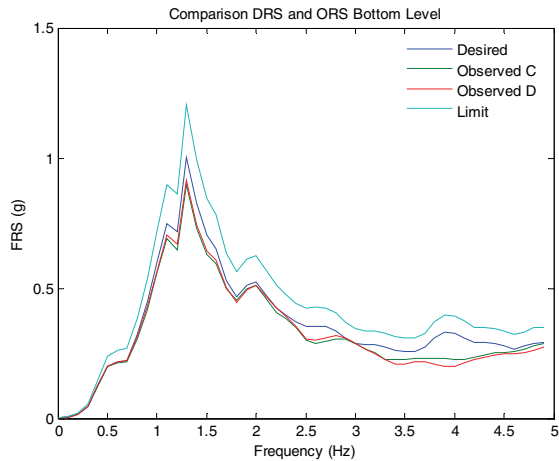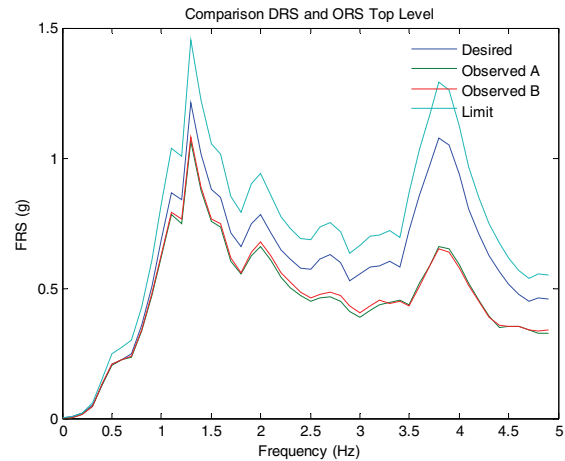
(e) Comparison of DRS and ORS bottom level   (f) Comparison of DRS and ORS top level
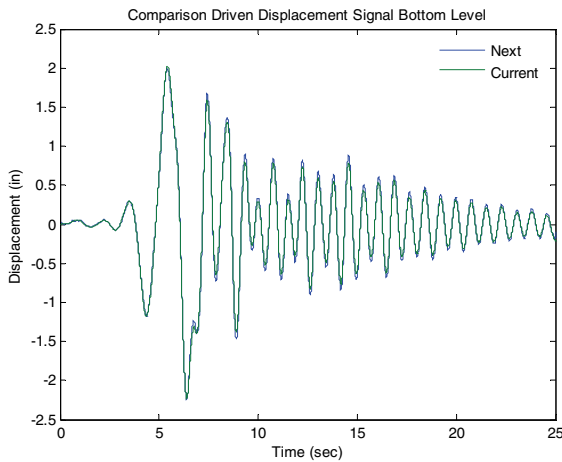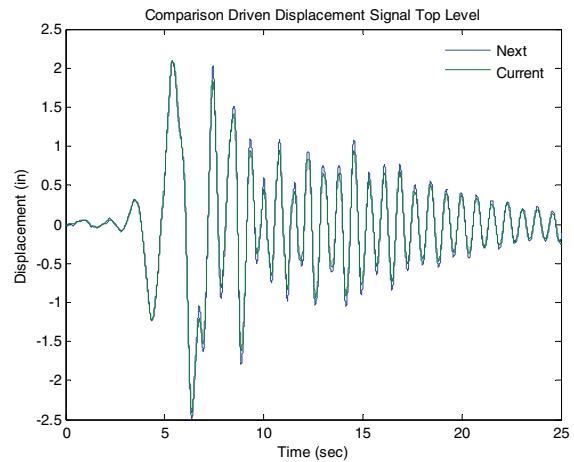
(g) Comparison of current and next command signal for bottom level   (h) Comparison of current and next command signal for top level

Figure 5.78. Experimental results for simulated building floor motions for SH with PE 10% in 50 years, scaled to 25%, before command input compensation (Cont'd)

5.4.2.1.2 Test results and observed damage

Table 5.17 summarizes the envelope of the desired and observed peak floor motions, recorded during this test. In Table 5.17 it can be observed that the errors in replicating floor displacements and velocities are less than 4%. Nevertheless, errors up to 36% and 16% are observed in replicating interstory drifts and platform accelerations, respectively.

5.4.2.2 Simulated building floor motions for a SH with PE of 10% in 50 years, scaled to 50%

This subsection presents the main results and observations obtained during the test performed using the simulated seismic response of the building, for a SH associated with a PE of 10% in 50 years, scaled to 50%.

Table 5.17. Envelope of peak simulated building floor motions for PE 10%/50yr scaled to 25%

Response	Peak Platform Displacement (in)		Peak Interstory Drift δ_{Max}		Peak Platform Velocity (in/sec)		Peak Platform Acceleration (g)	
	$D_{Max\ Bot}$	$D_{Max\ Top}$	(in)	(%)	$V_{Max\ Bot}$	$V_{Max\ Top}$	$A_{Max\ Bot}$	$A_{Max\ Top}$
Desired	2.22	2.41	0.26	0.17	10.3	12.7	0.17	0.27
Observed	2.22	2.34	0.19	0.13	9.54	11.3	0.18	0.23
Error (%)	0.31	3.00	36.0	36.0	7.46	12.6	3.73	16.2

Table 5.18 summarizes the envelope of desired and observed peak floor motions, recorded during this test. In Table 5.18 it can be observed that the errors in replicating floor displacements and velocities, and interstory drifts histories are less than 4%. Errors up to 16% are observed in replicating peak platform accelerations. Figure 5.79 illustrates the key results obtained from this test. In Figure 5.79a, b, d, e and f it is observed that the UB-NCS platform accelerations closely match the desired floor response spectra in the whole range of frequencies of interest. The measured hysteretic response of the partition walls is not as clear as for the loading protocol. This is because the wall was already severely damaged. Also, the cyclic nature of the protocol allows for better extraction of hysteresis from recorded data.

Table 5.18. Envelope of peak simulated building floor motions for PE 10%/50yr, scaled to 50%

| Response	Peak Platform Displacement (in)		Peak Interstory Drift δ_{Max}		Peak Platform Velocity (in/sec)		Peak Platform Acceleration (g)	
	$D_{Max\ Bot}$	$D_{Max\ Top}$	(in)	(%)	$V_{Max\ Bot}$	$V_{Max\ Top}$	$A_{Max\ Bot}$	$A_{Max\ Top}$
Desired	4.45	4.83	0.52	0.34	20.5	25.4	0.34	0.53
Observed	4.47	4.79	0.50	0.33	20.3	25.5	0.41	0.60
Error (%)	0.45	0.85	4.05	4.05	0.85	0.11	16.5	11.7
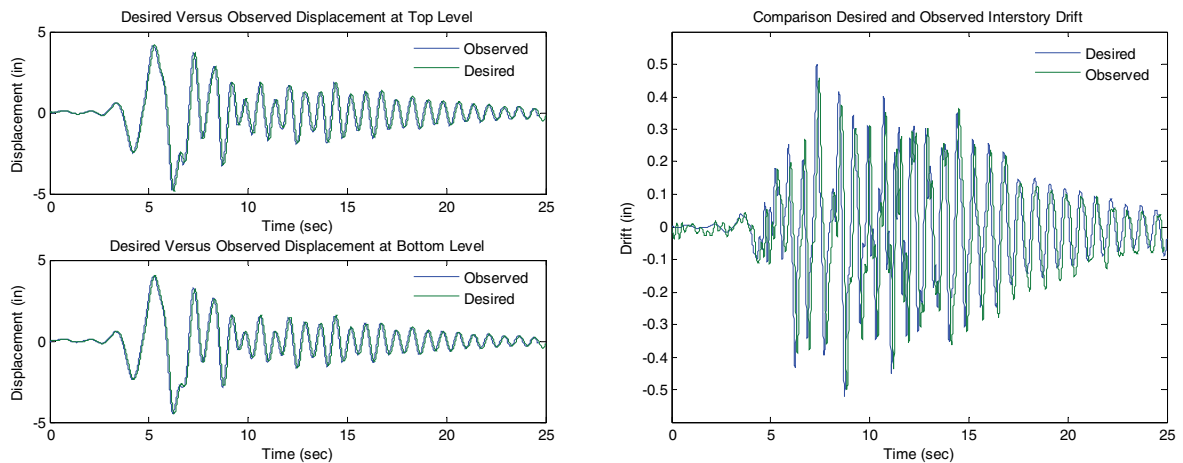
(a) Comparison of desired and observed platform displacements

(b) Comparison of desired and observed interstory drifts

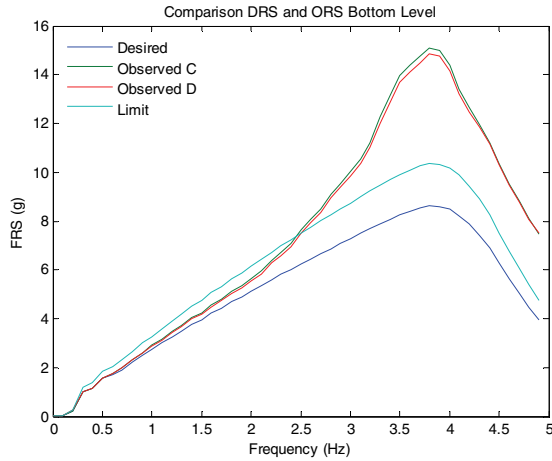Figure 5.79. Experimental results for simulated building floor motions for SH with PE 10% in 50 years, scaled to 50%
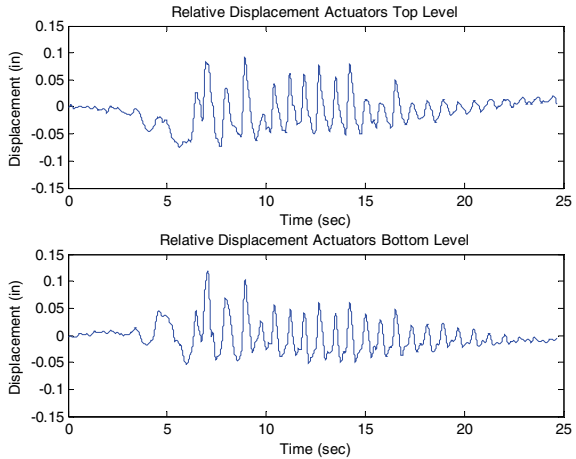
(c) Relative displacements between actuators

(d) Comp. of desired and observed accelerations

(e) Comparison of DRS and ORS bottom level
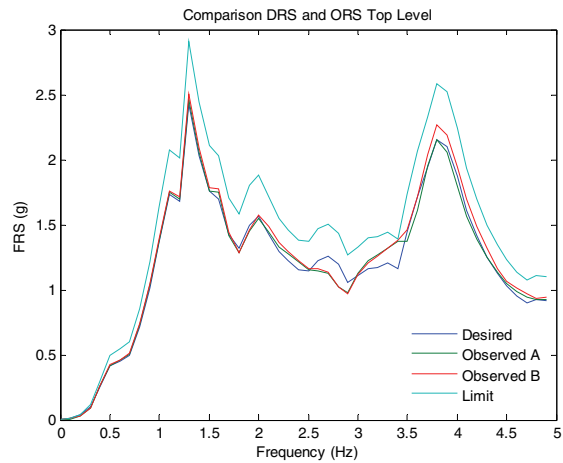
(f) Comparison of DRS and ORS top level
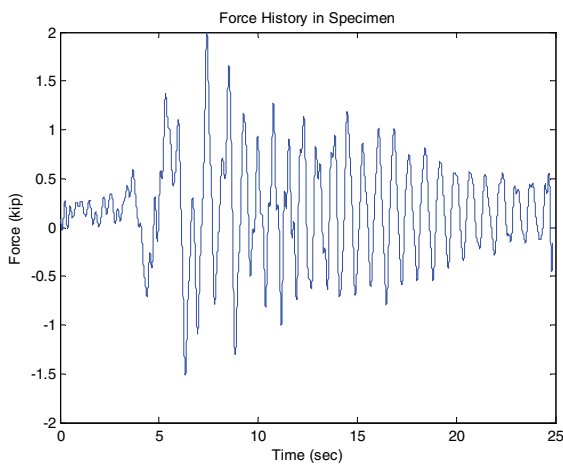
(g) Force history in specimen
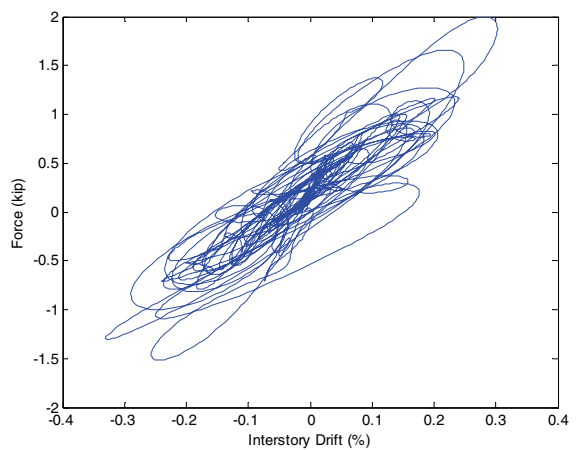
(h) Specimen hysteresis loop

Figure 5.79. Experimental results for simulated building floor motions for SH with PE 10% in 50 years, scaled to 50% (Cont'd)

Figure 5.80 shows a set of plots summarizing the seismic performance of Monitor 2. In Figure 5.80c, dominant frequencies of 1.3, 2.6 and 3.8 Hz are observed. Figure 5.80a shows the amplification of the

vertical accelerations measured at the base of the monitor due to the flexibility of the partition walls and the supporting arm system. Figure 5.80d shows the TF's for longitudinal and vertical accelerations at the base of Monitor 2. It is observed that there is no correlation between the dominant frequencies in Figure 5.80c and Figure 5.80d.
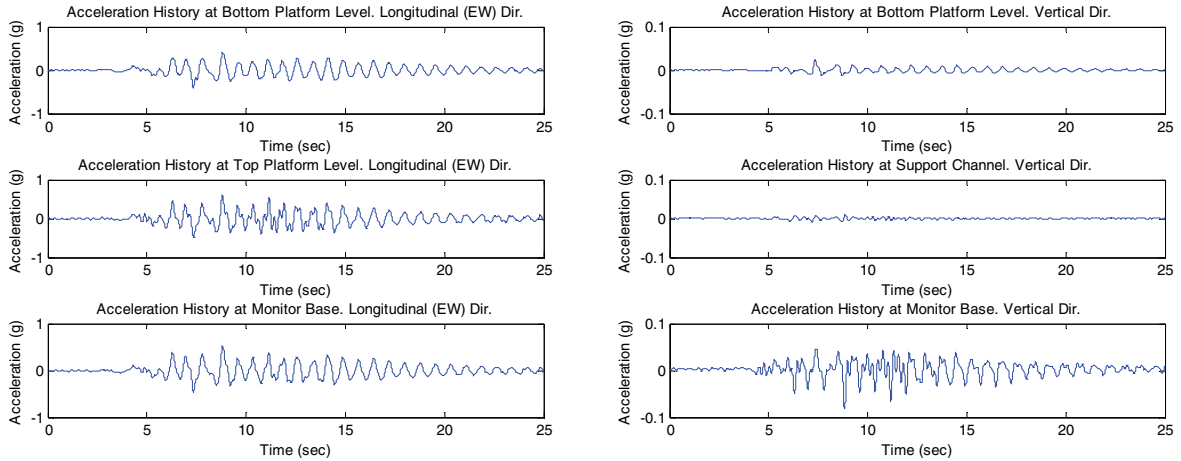
(a) Longitudinal acceleration amplification through partition walls

(b) Vertical acceleration amplification through partition walls and monitor supporting system

(c) FFT's for responses at the base of monitor

(d) Transfer function for longitudinal and vertical accelerations at the base of monitor

Figure 5.80. Experimental results Monitor 2 for simulated building floor motions for SH with PE 10% in 50 years, scaled to 50%

During this test, severe impact between the surgical video rack and Monitor 1 (Figure 5.3 and Figure 5.35a) was observed. Also, the medical gurney displaced substantially but the crash dummy remained on the gurney. One half of the medical supplies settled on top of the medical cart fell down. Up to 10" of displacements were observed in IV pump poles 1 and 2.

5.4.2.3 Simulated building floor motions for a SH with PE of 10% in 50 years, scaled to 100%

This subsection presents the main results and observations obtained during the test performed using the simulated seismic response of the building, for a SH associated with a PE of 10% in 50 years, scaled to 100%. This set of floor motions imposes on the specimen seismic demands associated to a seismic hazard corresponding to a design earthquake level. Table 5.19 summarizes the envelope of desired and observed peak floor motions, recorded during this test. It can be observed that the errors in replicating floor displacements and velocities, and interstory drifts histories are less than 4 and 1%, respectively. Errors up to 36 and 23% are observed in replicating peak bottom and top platform accelerations, respectively. A peak error of 12% is observed in reaching peak interstory drifts.

Table 5.19. Envelope of peak simulated building floor motions for PE 10%/50yr scaled to 100%

Response	Peak Platform Displacement in)		Peak Interstory Drift δ_{Max}		Peak Platform Velocity (in/sec)		Peak Platform Acceleration (g)	
	$D_{Max\ Bot}$	$D_{Max\ Top}$	(in)	(%)	$V_{Max\ Bot}$	$V_{Max\ Top}$	$A_{Max\ Bot}$	$A_{Max\ Top}$
Desired	8.90	9.66	1.04	0.69	41.0	50.7	0.69	1.06
Observed	9.25	9.66	0.92	0.61	40.7	50.6	1.08	1.38
Error (%)	3.77	0.02	12.7	12.7	0.89	0.58	36.4	23.2

Figure 5.81 illustrates the key results obtained from this test. In Figure 5.81e it can be observed that the bottom level actuators do not properly match the desired response spectrum for frequencies larger than 2.5 Hz. Figure 5.81f shows that at the top level, the actuators properly match the desired floor response spectrum in the whole range of frequencies of interest.
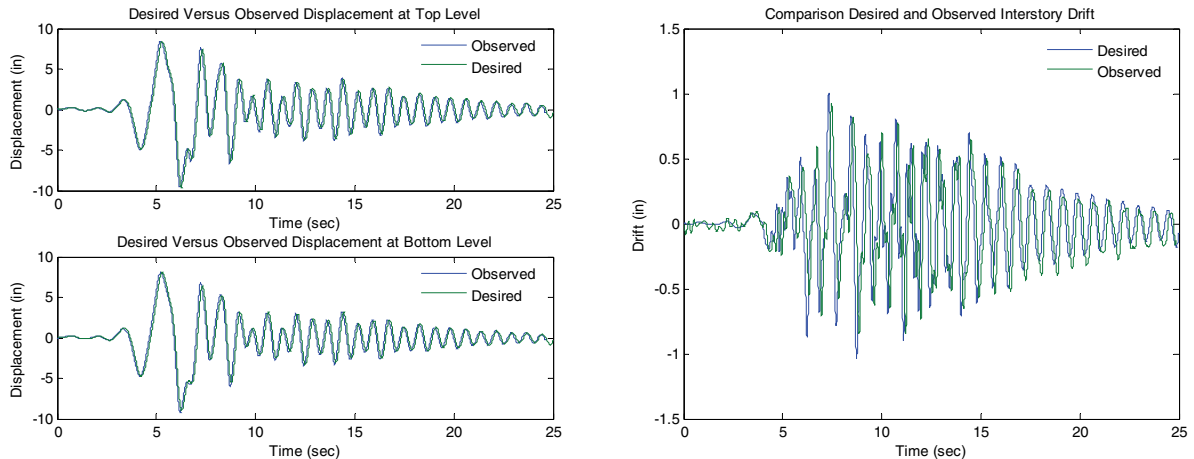
(a) Comparison of desired and observed platform displacements

(b) Comparison of desired and observed interstory drifts

Figure 5.81. Experimental results for simulated building floor motions for SH with PE 10% in 50 years, scaled to 100%
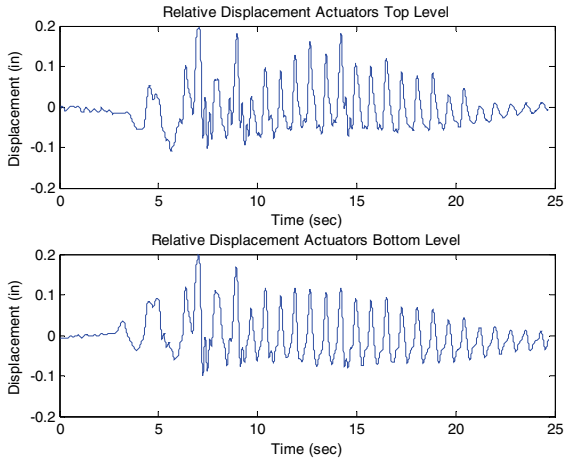
(c) Relative displacements between actuators
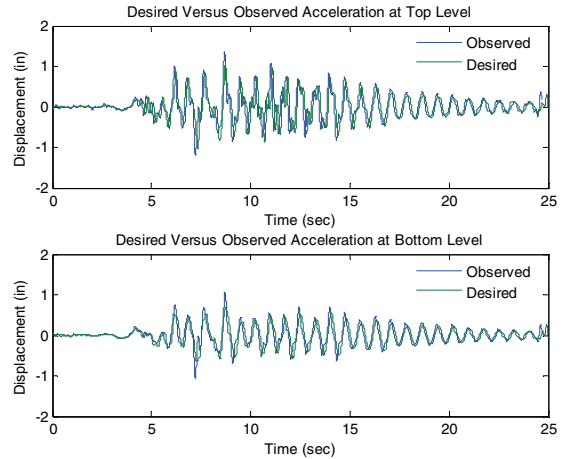
(d) Comp. of desired and observed accelerations
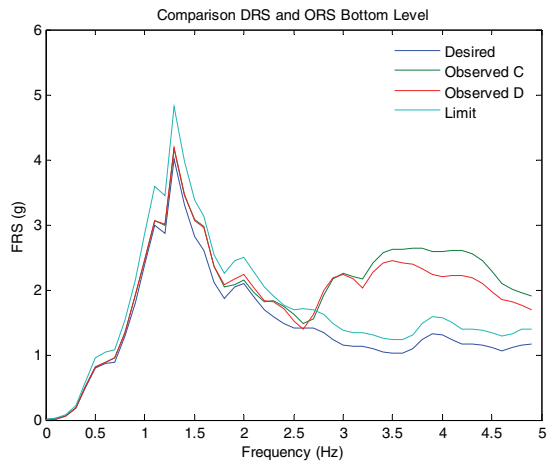
(e) Comparison of DRS and ORS bottom level
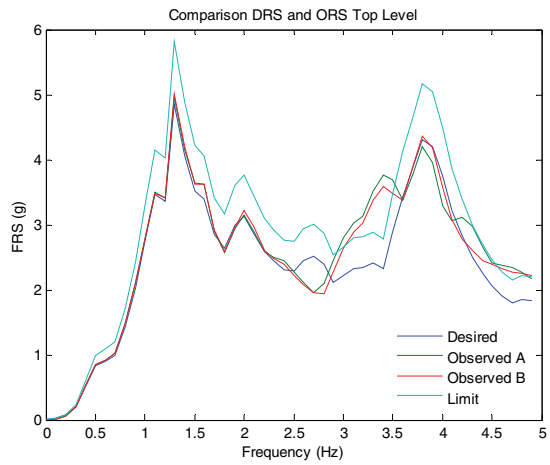
(f) Comparison of DRS and ORS top level
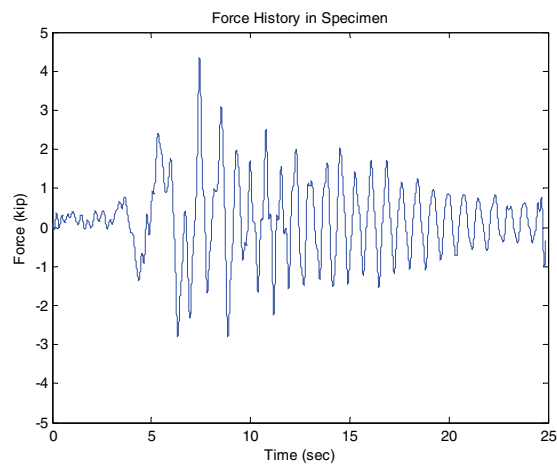
(g) Force history in specimen
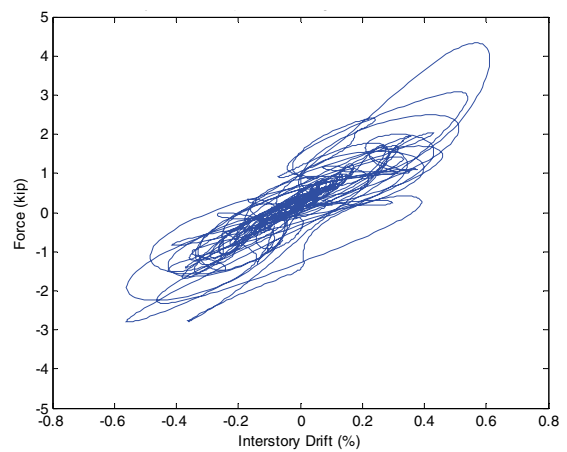
(h) Specimen hysteresis loop

Figure 5.81. Experimental results for simulated building floor motions for SH with PE 10% in 50 years, scaled to 100% (Cont'd)

Figure 5.82 shows a set of plots summarizing the seismic performance of Monitor 2. The trends observed are similar to the observed in Figure 5.80.
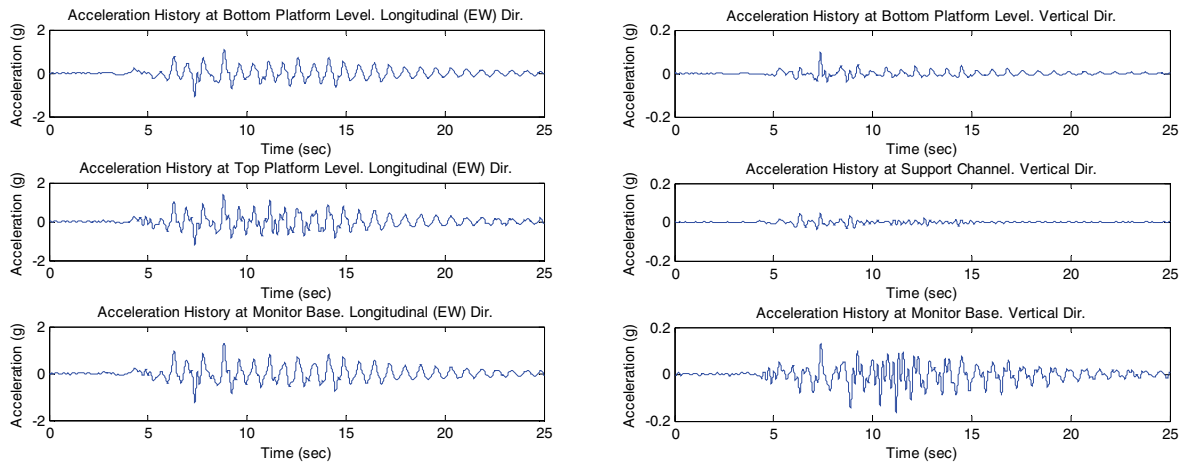
(a) Longitudinal acceleration amplification through partition walls

(b) Vertical acceleration amplification through partition walls and monitor supporting system
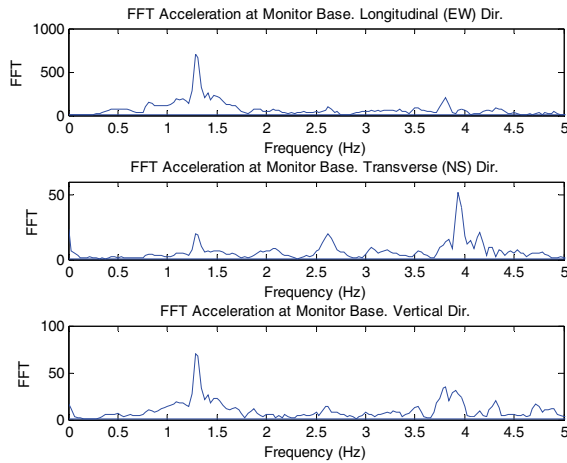
(c) FFT's for responses at the base of monitor
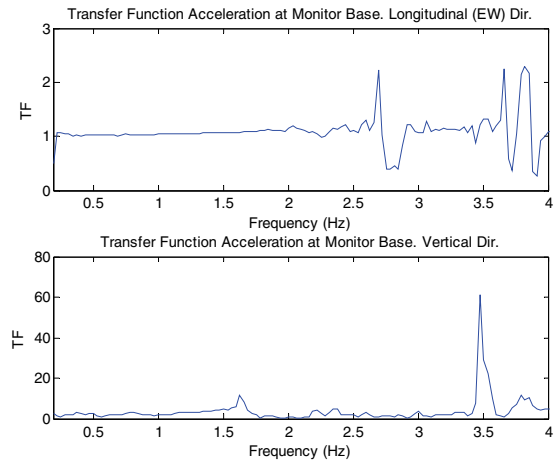
(d) Transfer function for longitudinal and vertical accelerations at the base of monitor

Figure 5.82. Experimental results Monitor 2 for simulated building floor motions for SH with PE 10% in 50 years, scaled to 100%

Several additional observations were found regarding other equipment. Extremely severe impact between the surgical video rack and Monitor 1 (Figure 5.3 and Figure 5.35a) was observed. Excessive displacement of the medical gurney was observed, as shown in Figure 5.83a. All medical supplies settled on top of the medical cart fell down (Figure 5.83a). Up to 10" displacements were observed in IV pump poles 1 and 2 (Figure 5.83b). Furthermore, the IV pump poles impacted and severely damaged the base of the west partition wall.

(a) Excessive displacement of gurney and medical cart

(b) Excessive motion of infusion pump pole

Figure 5.83. Examples of damage observed in specimen components during simulated building floor motions for SH with PE 10% in 50 years, scaled to 100%

5.4.2.4 Simulated building floor motions for a SH with PE of 2% in 50 years, scaled to 25%

This test was performed mainly to compensate the command signal to be inputted to the UB-NCS platforms in subsequent tests. Nevertheless, some observations regarding the testing frame fidelity and seismic performance of the testing specimen are presented.

5.4.2.4.1 Command signal compensation

The iterative command signal compensation process was used to prepare the floor motions to be used in the following tests. Figure 5.84 summarizes the main results of the test performed considering the non compensated signals shown in Figure 5.50, scaled to 25%. Figure 5.84e and Figure 5.84f show that the ORS underestimate the DRS for both bottom and top UB-NCS platforms in the whole range of frequencies of interest, and therefore, the input signals needed to be compensated using the methodology described in Section 3. Figure 5.84g and Figure 5.84h show the compensated signals to be used in larger amplitude tests. The effectiveness of using the compensated signal for running larger amplitude tests is demonstrated in subsection 5.4.2.5.
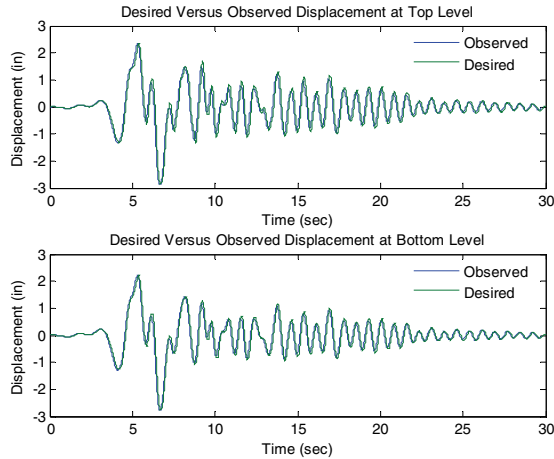
(a) Comparison of desired and observed platform displacements
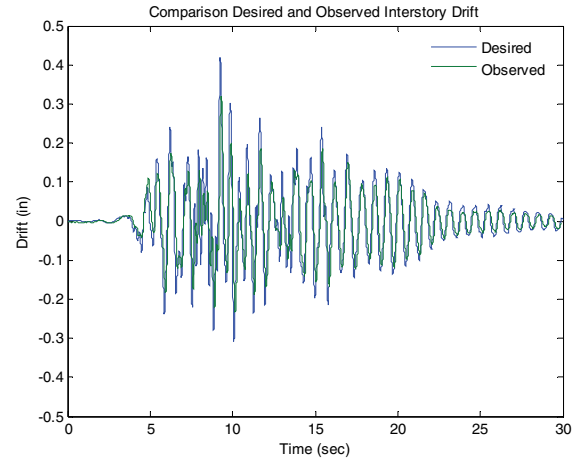
(b) Comparison of desired and observed interstory drift histories
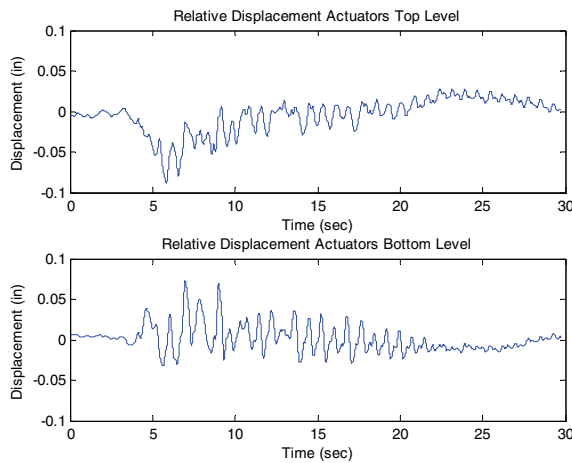
(c) Relative displacements between actuators
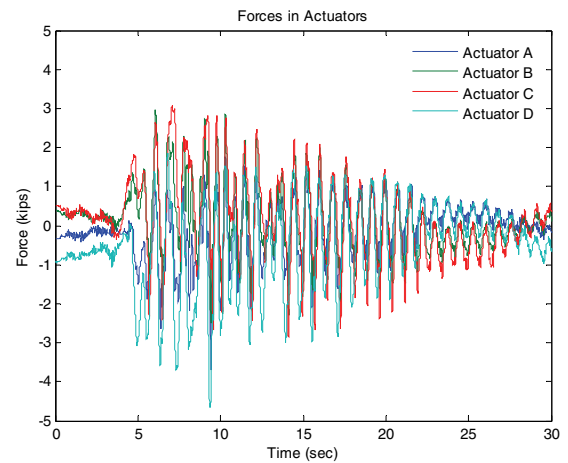
(d) Actuator force histories
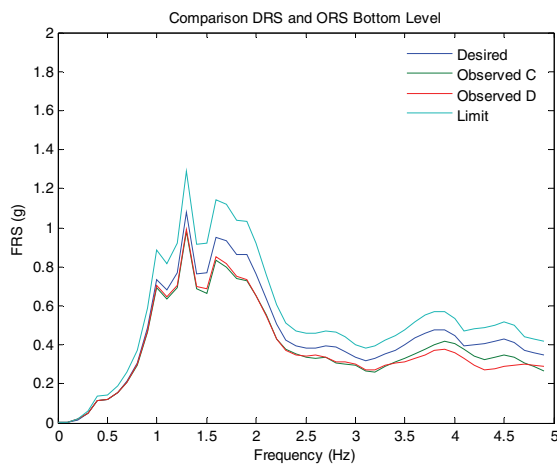
(e) Comparison DRS and ORS bottom level platform
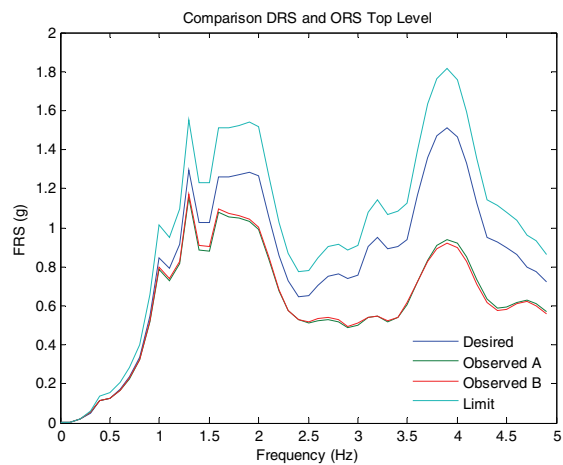
(f) Comparison of DRS and ORS top level platform

Figure 5.84. Experimental results for simulated building floor motions for SH with PE 2% in 50 years, scaled to 25%, before command input compensation
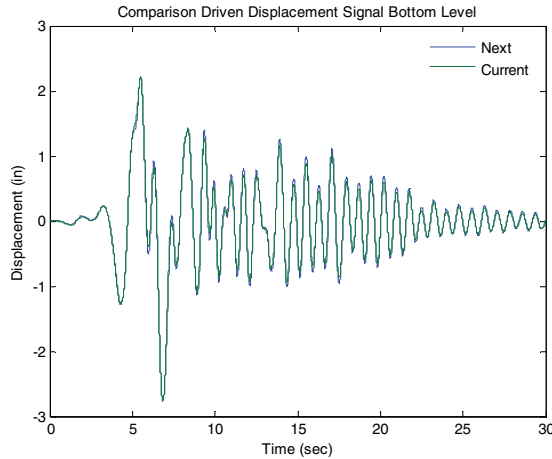
(g) Comparison of current and next command
signal for bottom level
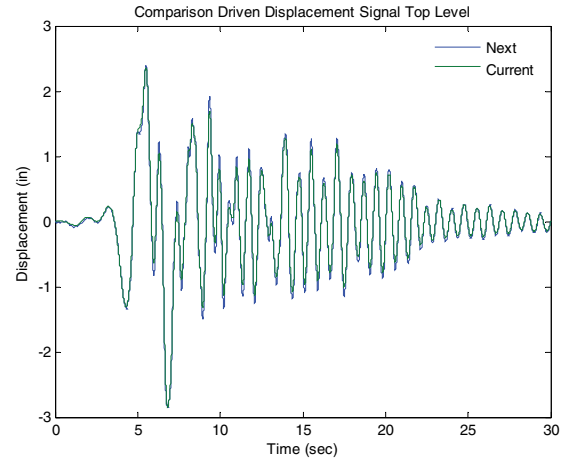
(h) Comparison of current and next command
signal for top level

Figure 5.84. Experimental results for simulated building floor motions for SH with PE 2% in 50 years,
scaled to 25%, before command input compensation (Cont'd)

5.4.2.4.2 Test results and observed damage

Table 5.20 summarizes the envelope of desired and observed peak floor motions, recorded during this
test, before command signal compensation. In Table 5.20 it can be observed that the errors in replicating
floor displacements and velocities are less than 1 and 11%, respectively. Nevertheless, errors up to 30 and
37% are observed in replicating interstory drifts and platform accelerations, respectively.

Table 5.20. Envelope of peak simulated building floor motions for PE 2%/50yr, scaled to 25%

Response	Peak Platform Displacement (in)		Peak Interstory Drift δ_{Max}		Peak Platform Velocity (in/sec)		Peak Platform Acceleration (g)	
	$D_{Max Bot}$	$D_{Max Top}$	(in)	(%)	$V_{Max Bot}$	$V_{Max Top}$	$A_{Max Bot}$	$A_{Max Top}$
Desired	2.76	2.85	0.42	0.28	11.1	13.7	0.19	0.36
Observed	2.79	2.88	0.32	0.21	10.6	12.4	0.17	0.26
Error (%)	1.06	1.02	30.8	30.8	4.40	10.8	16.3	37.3

5.4.2.5 Simulated building floor motions for a SH with PE of 2% in 50 years, scaled to 50%

Table 5.21 summarizes the envelope of desired and observed peak floor motions, recorded during the
test performed using the simulated building seismic response for a SH associated with a PE of 2% in 50
years, scaled to 50%. In Table 5.21 it can be observed that the errors in replicating floor displacements
and velocities, and interstory drifts histories are less than 2, 3 and 12%, respectively. Errors up to 10% are
observed in replicating peak platform accelerations.

Table 5.21. Envelope of peak simulated building floor motions for PE 2%/50yr, scaled to 50%

Response	Peak Platform Displacement (in)		Peak Interstory Drift δ_{Max}		Peak Platform Velocity (in/sec)		Peak Platform Acceleration (g)	
	$D_{Max\ Bot}$	$D_{Max\ Top}$	(in)	(%)	$V_{Max\ Bot}$	$V_{Max\ Top}$	$A_{Max\ Bot}$	$A_{Max\ Top}$
Desired	5.53	5.70	0.84	0.55	22.2	27.4	0.39	0.72
Observed	5.63	5.76	0.75	0.50	22.8	27.3	0.43	0.77
Error (%)	1.90	0.99	11.4	11.4	2.40	0.62	9.48	5.95

Figure 5.85 illustrates the most important results obtained from this test. In Figure 5.85a, b, and d it can be seen that the UB-NCS can adequately reproduce desired floor motions, story drifts and absolute floor accelerations, respectively. In Figure 5.85e and f it is demonstrated that the testing frame can achieve desired floor response spectra after properly compensating command input signals.
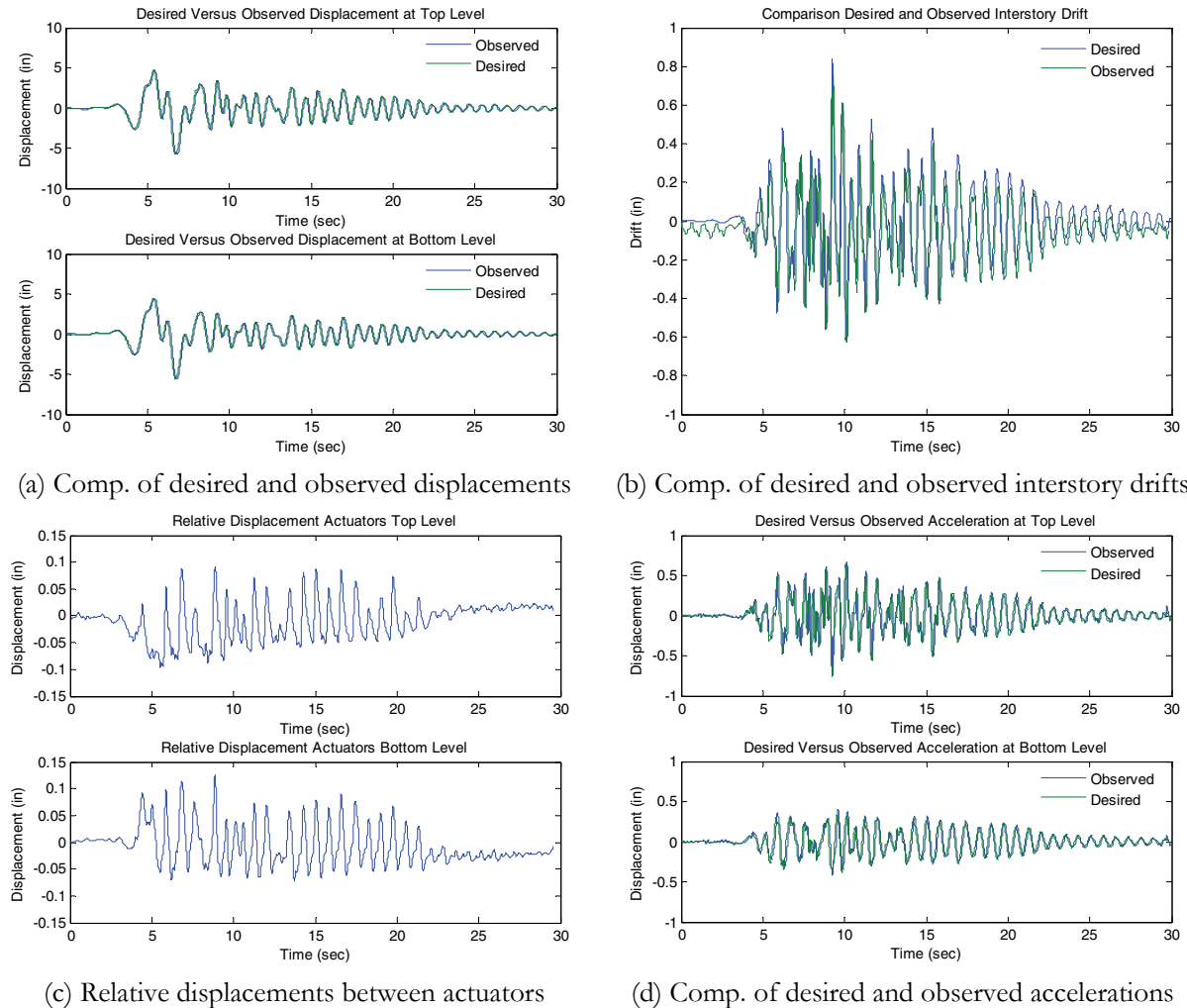
(a) Comp. of desired and observed displacements

(b) Comp. of desired and observed interstory drifts

(c) Relative displacements between actuators

(d) Comp. of desired and observed accelerations

Figure 5.85. Experimental results for simulated building floor motions for SH with PE 2% in 50 years, scaled to 50%
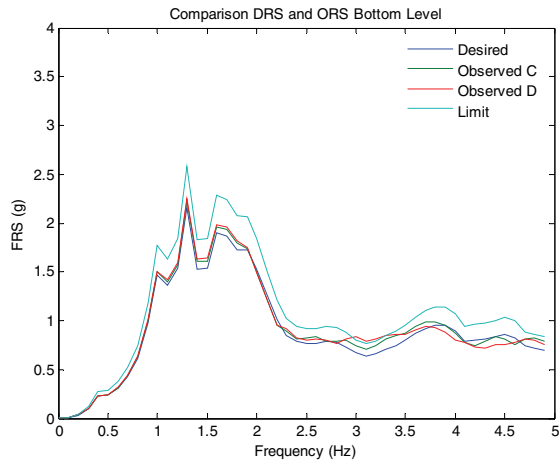
(e) Comparison of DRS and ORS bottom level
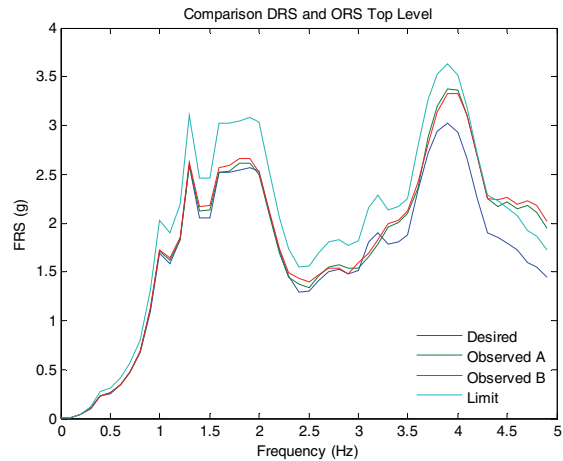
(f) Comparison of DRS and ORS top level
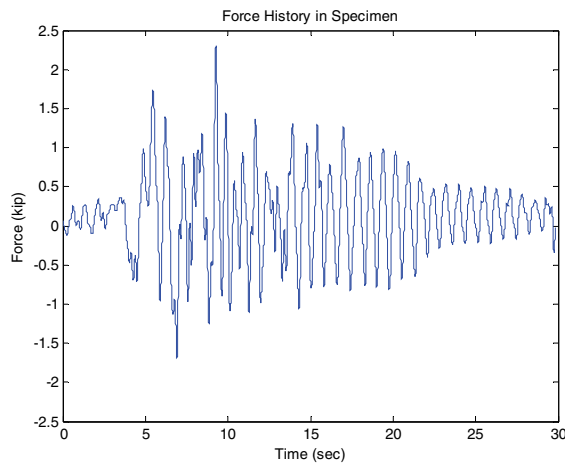
(g) Force history in specimen
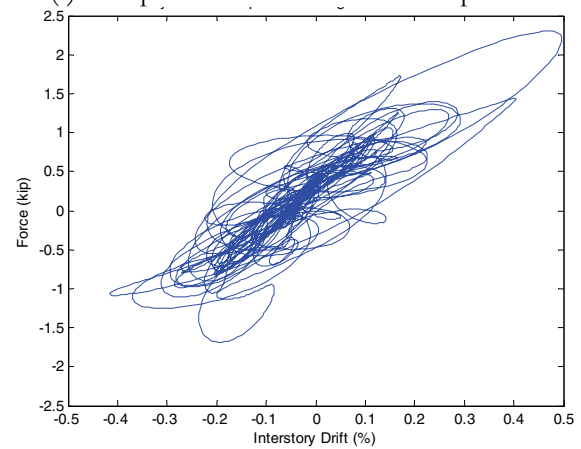
(h) Specimen hysteresis loop

Figure 5.85. Experimental results for simulated building floor motions for SH with PE 2% in 50 years, scaled to 50% (Cont'd)

During this test several additional observations were made. Impact between the surgical video rack and Monitor 1 shown in Figure 5.3 and Figure 5.35a was observed. At the end of the test, the medical video rack was rotated 45 degrees in relation to its original position. Excessive displacement of the medical gurney and the medical cart was observed. Nevertheless the crash dummy did not fall from the gurney. All supplies settled on top of the medical cart were thrown off. Up to 15 inches displacements were observed in both IV pump poles 1 and 2, which impacted the UB-NCS columns and the base of the west gypsum partition wall.

Figure 5.86 shows a set of plots summarizing the seismic performance of Monitor 2. In Figure 5.86 it is clearly observed that the vertical accelerations were amplified at the base of Monitor 2. In Figure 5.86,

dominant frequencies are observed around 1.3, 2.6 and 3.2 Hz. The frequency 1.3 Hz is close to the natural vibration frequency of the studied building.
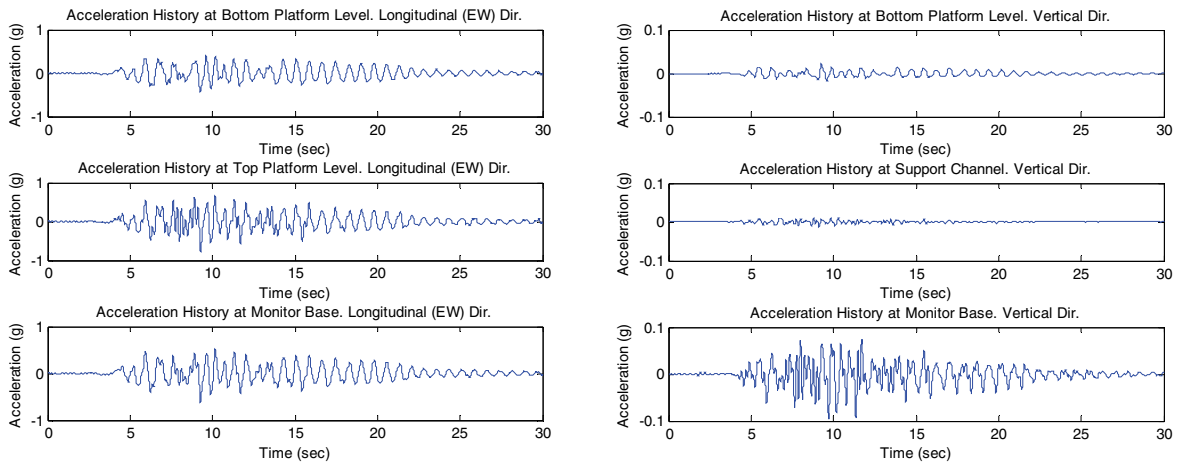
(a) Longitudinal acceleration amplification through partition walls

(b) Vertical acceleration amplification through partition walls and monitor supporting system
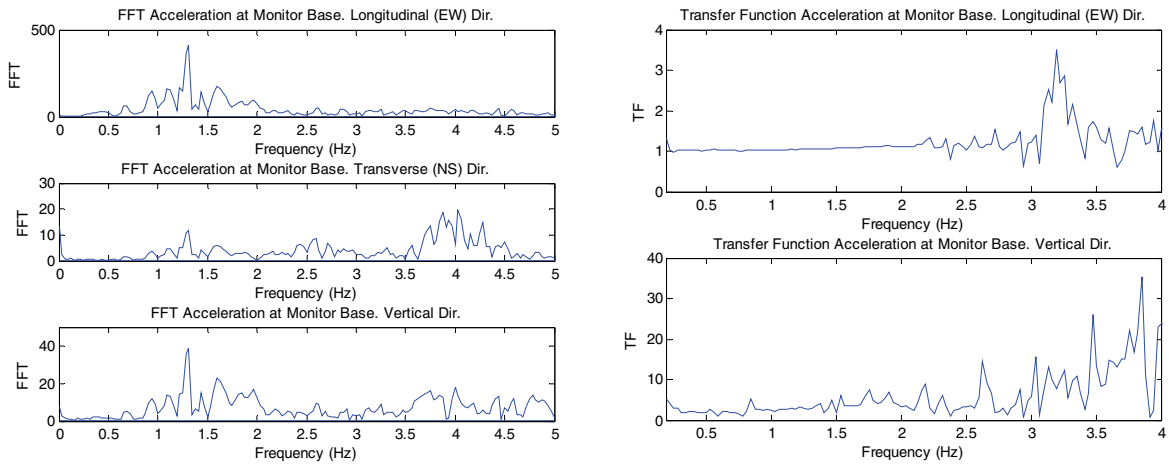
(c) FFT's for responses at the base of monitor

(d) Transfer function for longitudinal and vertical accelerations at the base of monitor

Figure 5.86. Experimental results Monitor 2 for simulated building floor motions for SH with PE 2% in 50 years, scaled to 50%

5.4.2.6 Simulated building floor motions for a SH with PE of 2% in 50 years, scaled to 100%

This subsection presents the main results and observations obtained during the test performed using the simulated building seismic response for a SH associated with a PE of 2% in 50 years, scaled to 100%. This set of floor motions imposes on the testing specimen the seismic demands associated with a maximum considered earthquake level. Table 5.22 summarizes the envelope of desired and observed peak floor motions, recorded during this test. It can be observed that the errors in replicating both floor

displacements and velocities are less than 5 %. Errors up to 17 and 34% are observed in replicating peak interstory drifts and peak platform accelerations, respectively.

Table 5.22. Envelope of peak simulated building floor motions for PE 2%/50yr, scaled to 100%

Response	Peak Platform Displacement (in)		Peak Interstory Drift δ_{Max}		Peak Platform Velocity (in/sec)		Peak Platform Acceleration (g)	
	$D_{Max\ Bot}$	$D_{Max\ Top}$	(in)	(%)	$V_{Max\ Bot}$	$V_{Max\ Top}$	$A_{Max\ Bot}$	$A_{Max\ Top}$
Desired	11.1	11.4	1.67	1.11	44.4	54.8	0.77	1.44
Observed	11.6	11.6	1.43	0.94	46.7	54.7	1.17	1.85
Error (%)	4.80	1.77	17.1	17.1	4.86	0.31	33.9	21.9

Figure 5.87 provides the key results obtained from this test. In Figure 5.87 it is observed that the maximum relative displacement between actuators located at a same platform level are 0.25 and 0.3 inches approximately, for the bottom and top levels, respectively. In Figure 5.87e and f it is observed that at this test amplitude level, the bottom platform actuators impose floor accelerations that overestimate the DRS for frequencies larger than 2.3 Hz and that the top platform actuators impose accelerations that overestimate the DRS for frequencies larger than 3.6 Hz.

During this test, Monitors 2 and 3 broke off their supporting systems, as was the case during the test performed using the dynamic testing protocol scaled to 100%. Figure 5.88 shows a set of plots summarizing the seismic performance of Monitor 2. In Figure 5.88b, the dynamic amplification of the vertical accelerations recorded at the base of the monitor is observed, with a dominant frequency around 1.3 Hz, as indicated in Figure 5.88c.
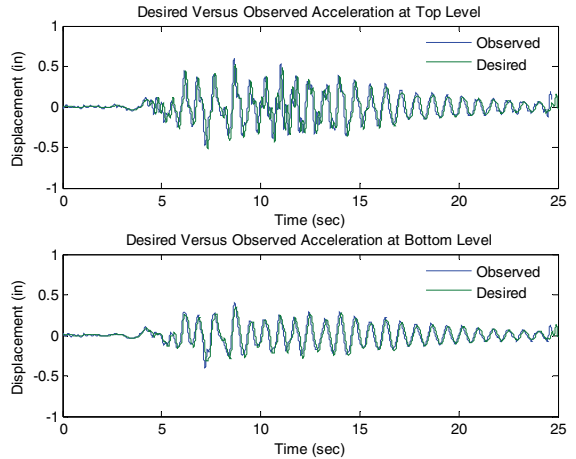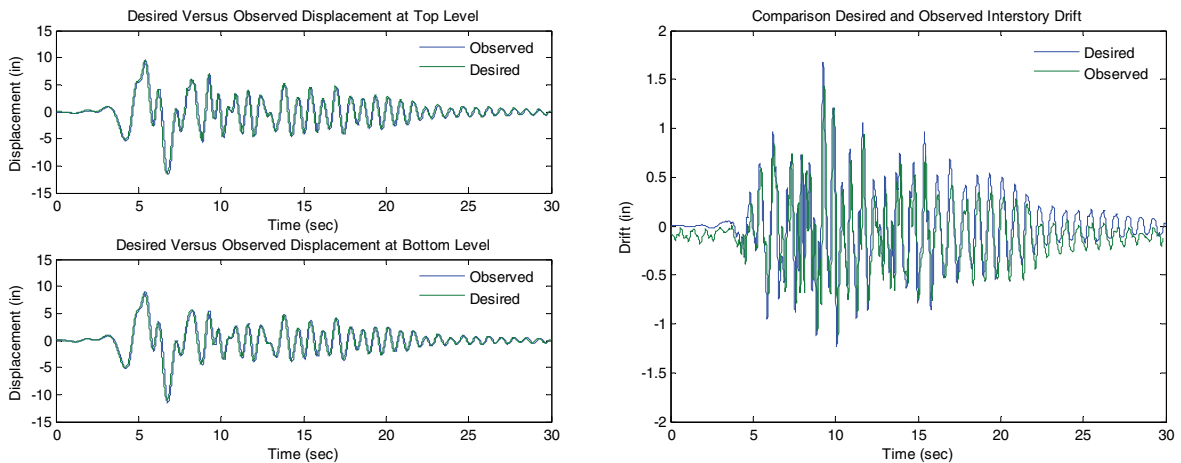

(a) Comp. of desired and observed displacements   (b) Comp. of desired and observed interstory drifts
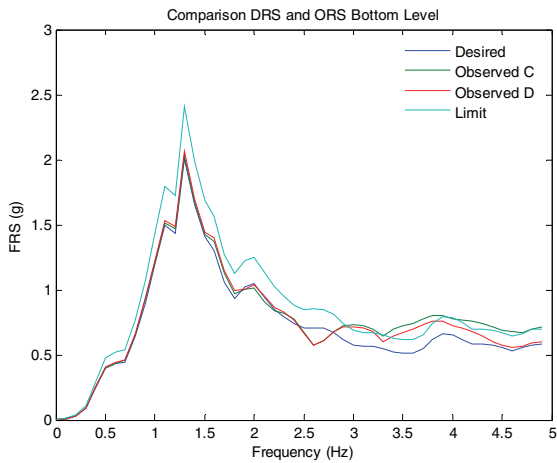
Figure 5.87. Experimental results for simulated building floor motions for SH with PE 10% in 50 years, scaled to 100%
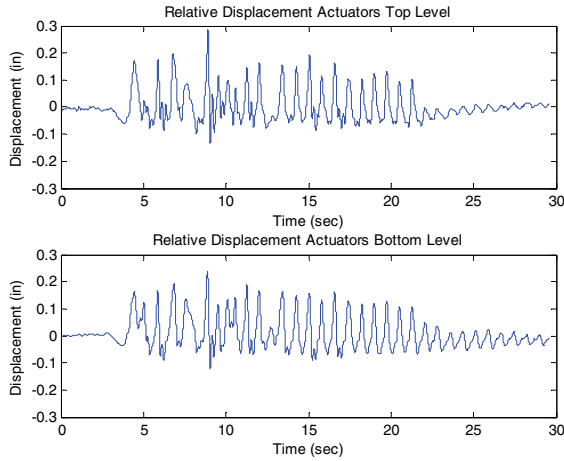
(c) Relative displacements between actuators
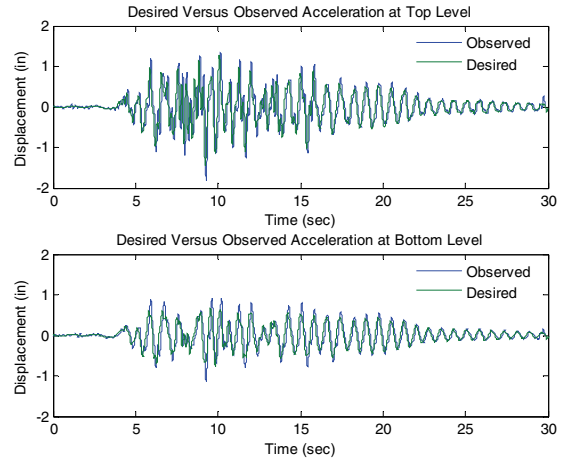
(d) Comp. of desired and observed accelerations
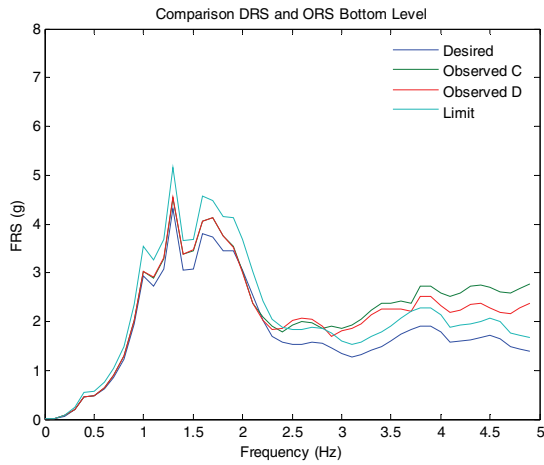
(e) Comparison of DRS and ORS bottom level
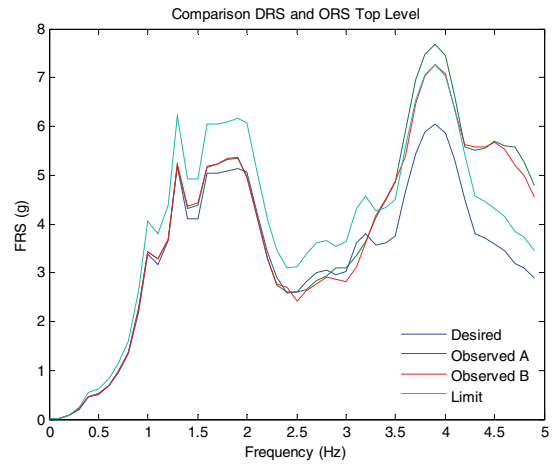
(f) Comparison of DRS and ORS top level
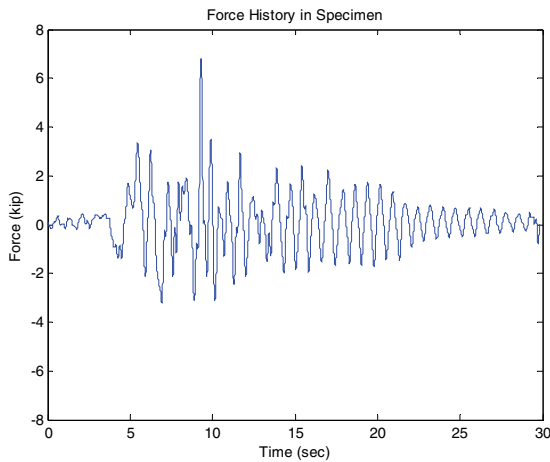
(g) Force history in specimen
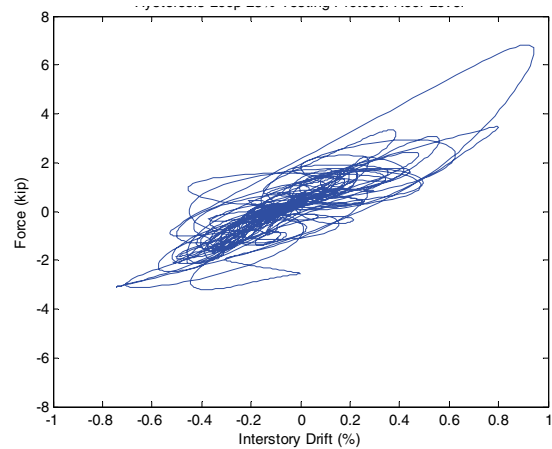
(h) Specimen hysteresis loop

Figure 5.87. Experimental results for simulated building floor motions for SH with PE 10% in 50 years, scaled to 100% (Cont'd)
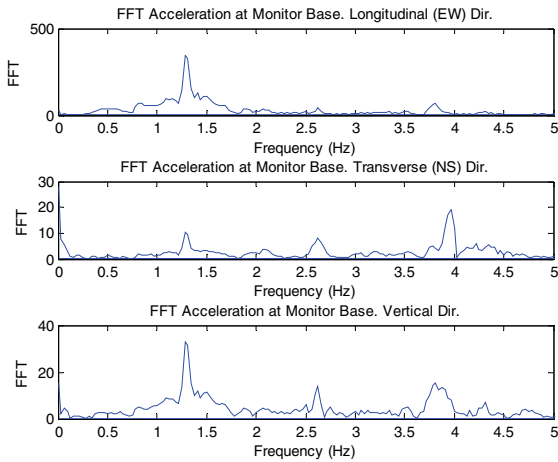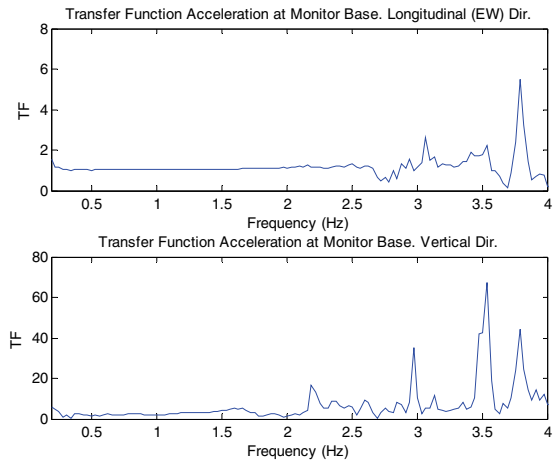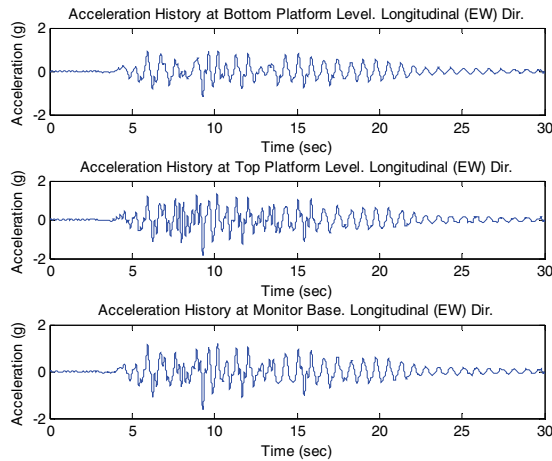
(a) Longitudinal acceleration amplification through partition walls
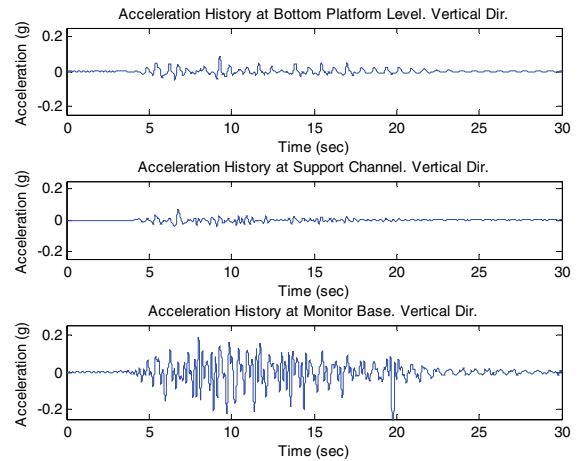
(b) Vertical acceleration amplification through partition walls and monitor supporting system
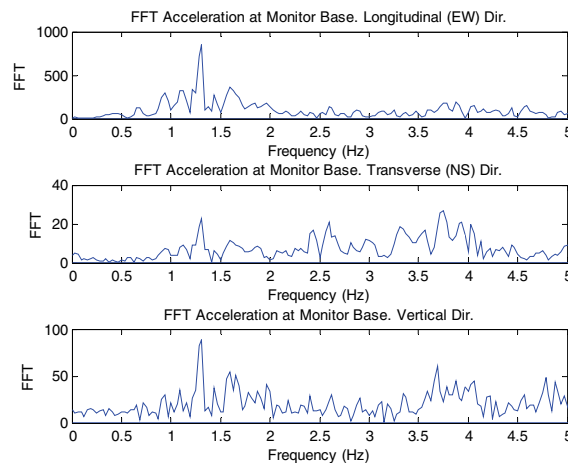
(c) FFT's for responses at the base of monitor
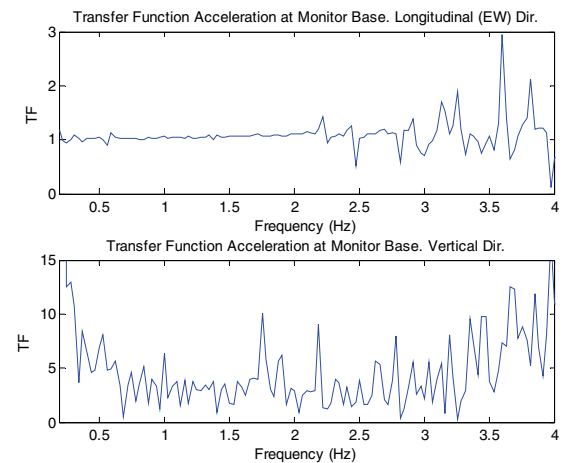
(d) Transfer function for longitudinal and vertical accelerations at the base of monitor

Figure 5.88. Measured response of Monitor 2 for simulated building floor motions for SH with PE 2% in 50 years, scaled to 100

Following this test, a detailed inspection of the test specimen was performed. In addition to the failure of monitor supports, shown in Figure 5.89a, extremely severe impact between the surgical video rack and Monitor 1 (Figure 5.3 and Figure 5.35a) was observed. Figure 5.89b shows the final condition of Monitor 1, which can be compared to its original condition, shown in Figure 5.35a. Excessive displacement of the medical gurney was observed (Figure 5.89a). For this platform motion intensity, the crash dummy was thrown off the gurney, as sown in Figure 5.89c. All medical supplies settled on top of the medical cart fell (Figure 5.89a). Up to 15" displacements were observed in IV pump poles 1 and 2, as shown in Figure 5.89d. Furthermore, the poles impacted and severely damaged the base of the west partition walls, as

shown in Figure 5.89e. Finally, excessive displacement of the surgical video rack contents was observed (Figure 5.89f).

(a) Monitors broke off supporting systems

(b) Final condition of Monitor 1 after impact of surgical video rack

(c) Dummy thrown off gurney

(d) Excessive displacement of infusion pump poles
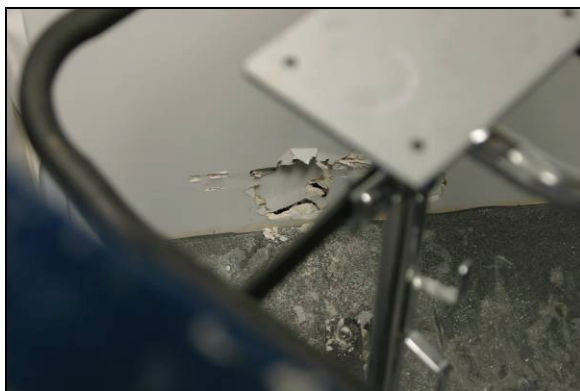
(e) Damage in base of partition walls resulting from poles impact
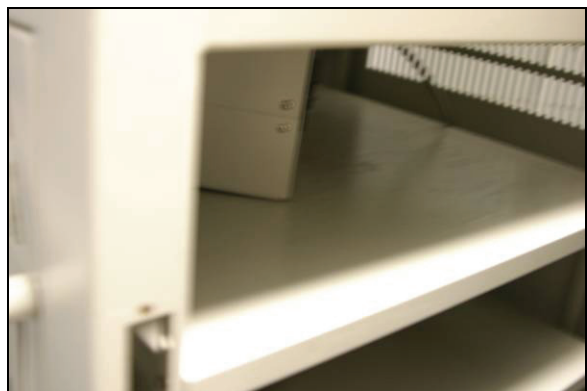
(f) Shifting of video rack contents

Figure 5.89. Examples of damage observed in specimen components during simulated building floor motions for SH with PE 2% in 50 years, scaled to 100%

5.4.3   Results and observations for quasi-static protocol tests

This subsection presents the main observations and results of the tests series performed using the quasi-static testing protocol further described in Subsection 5.3.3. The testing protocol was applied at 200, 250 and 300% amplitude scales. After each quasi-static test, a detailed inspection of the partition walls and the analysis of the progression of damage were carried out.

5.4.3.1   Quasi-static protocol test scaled to 200%

This test used the interstory drift protocol, applied quasi-statically, with a target peak interstory drift of 2.63 inches, equivalent to 1.74% of the free interstory height. Table 5.23 compares the peak desired and observed interstory drifts, recorded during the quasi-static testing protocol scaled to 200%. In Table 5.23 it is observed that even under the quasi-static condition the error between the desired and observed story drifts reached 1.7%. Figure 5.90 presents the key results obtained during this test. Figure 5.90a shows interstory drift and specimen force histories. Figure 5.90b shows the hysteresis loop observed during this test, where an increased level of pinching of the gypsum partition walls is observed. Figure 5.91 summarizes the damage observed in the exterior surface of the walls oriented in the loading direction.

Table 5.23. Envelope of interstory drifts for quasi-static testing protocol, scaled to 200%

Response	Peak Interstory Drift δ_{Max}	
	(in)	(%)
Desired	2.63	1.74
Observed	2.67	1.77
Error (%)	1.70	1.70

(a) Interstory drift and specimen force histories   (b) Specimen hysteresis loop
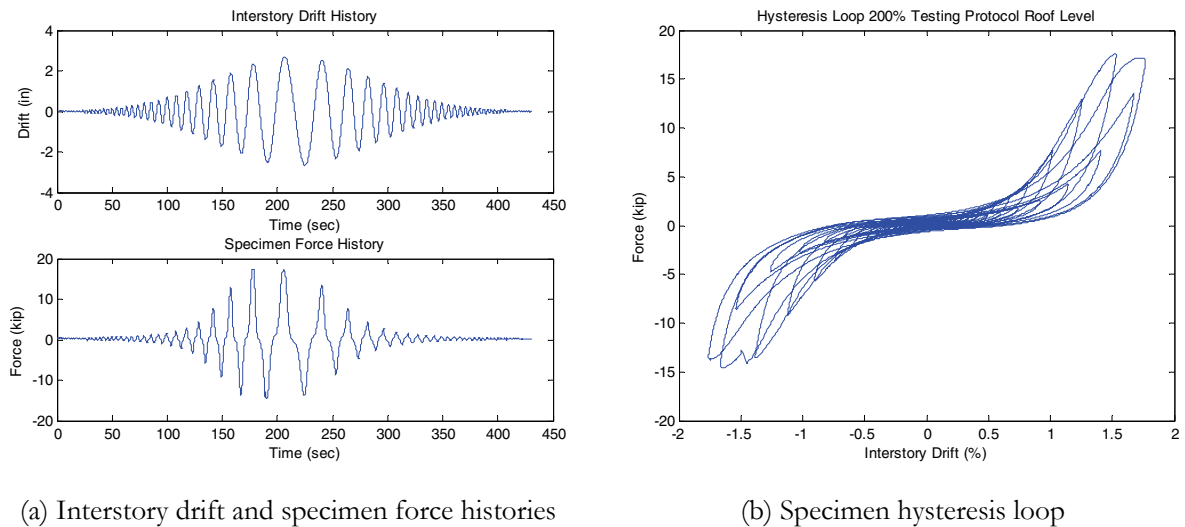
Figure 5.90. Experimental results of quasi-static testing protocol, scaled to 200%

Screws pop-out at top track row

Crack along corner bead (Residual gap of $\frac{1}{4}$")

151

Generalized screw pop-out around wall corner

Crack along corner bead (Residual gap $\frac{1}{16}$"<t<$\frac{1}{4}$")

55

Crack along corner bead (Residual gap of $\frac{1}{2}$")

Crack all along gypsum panel joint t<$\frac{1}{16}$"

96

96

Generalized screws pop-out in first gypsum board panel

(a) Damage in north wall

174

Screws pop-out at top track

Crack in Gypsum board. Panel detached from steel stud frame

Crack along gypsum panel joint t>$\frac{1}{4}$"

Crack along panel joint $\frac{1}{16}$"<t<$\frac{1}{4}$"

55

Crack along door frame t<$\frac{1}{16}$"

24

Screw pop-out around transverse wall

Screw pop-out in first 2 studs area

151

Crack along corner bead $\frac{1}{16}$"<t<$\frac{1}{4}$"

Gap $\frac{1}{16}$"<t<$\frac{1}{4}$" along corner bead

96

Gap t>$\frac{3}{8}$" along corner bead

96

Crack along gypsum panel joint $\frac{1}{16}$"<t<$\frac{1}{4}$"

81

Almost generalized screws pop-out in this panel

Screws pop-out at bottom track

(b) Damage in south wall

Figure 5.91. Damage observed in partition walls during quasi-static testing protocol, scaled to 200%

Table 5.24 summarizes the quantification of the damage observed in the specimen at the drift level of 1.74%, as shown in Figure 5.91.

Table 5.24. Quantification of specimen damage during quasi-static testing protocol, scaled to 200%

Damage measure	Quantified damage (Total length or surface)
Hairline cracks	0 in
Cracks $t \leq \frac{1}{16}''$	24 in
Cracks $\frac{1}{16}'' < t < \frac{1}{4}''$	653 in
Cracks $t \geq \frac{1}{4}''$	398 in
Screws pop-out area	10666 in^2
Detached area	5140 in^2

Figure 5.92 shows some examples of the damage observed, which is mainly characterized by residual gaps along corner beads larger than ½" in thickness, and significant damage along joints between gypsum panels. A more generalized level of screw pop-out was observed in the walls.

(a) Damage in panel joint in south wall
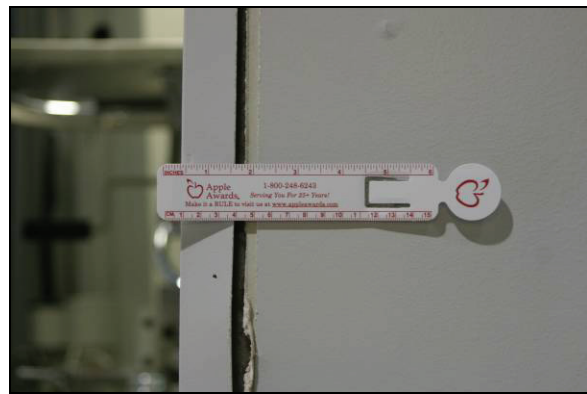
(b) Damage in corner bead in door frame

(c) Damage in panel joint in north wall
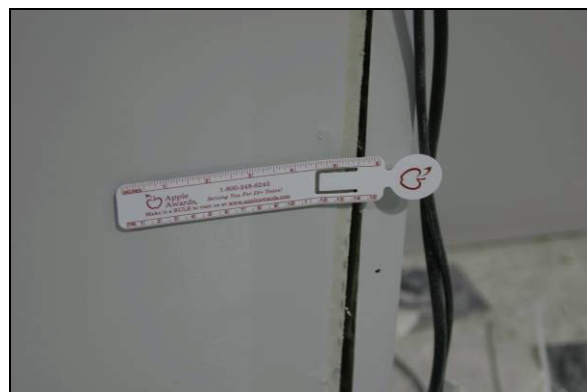
(d) Damage in corner bead in north wall

Figure 5.92. Examples of damage observed in gypsum partition walls during quasi-static testing protocol, scaled to 200%

5.4.3.2 Quasi-static protocol test scaled to 250%

The quasi-static interstory drift protocol applied a peak interstory drift of 3.28 inches, equivalent to 2.17% of the free UB-NCS interstory height. Table 5.25 compares the peak desired and observed interstory drifts, recorded during the quasi-static testing protocol scaled to 250%. In Table 5.25 it is observed that even under the quasi-static condition the error of the actuators reaches 2.3%.

Table 5.25. Envelope of interstory drifts for quasi-static testing protocol, scaled to 250%

Response	Peak Interstory Drift δ_{Max}	
	(in)	(%)
Desired	3.28	2.17
Observed	3.36	2.22
Error (%)	2.28	2.28

Figure 5.93 presents the key results obtained during this test. In Figure 5.93b, an increased level of pinching of the gypsum partition walls is observed.
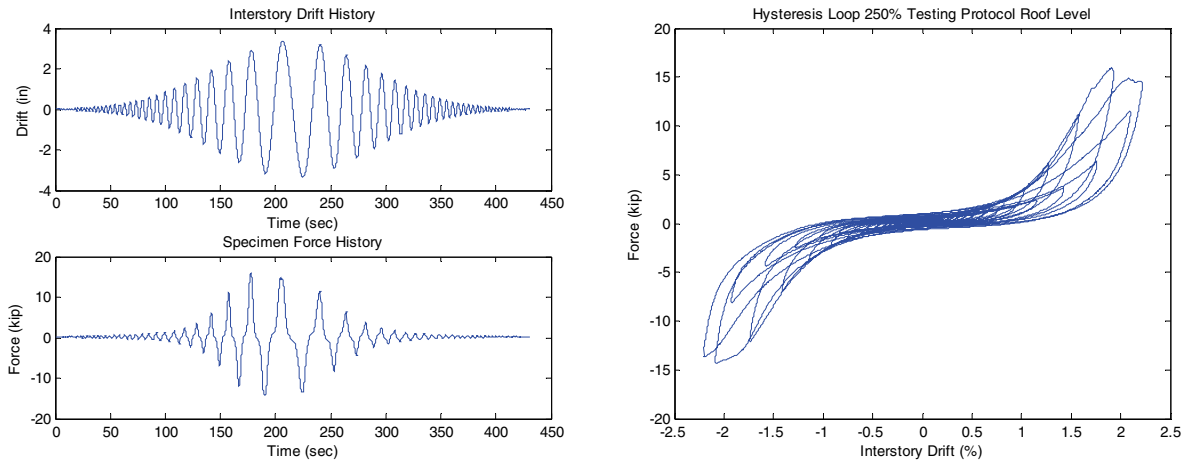
(a) Interstory drift and specimen force histories   (b) Specimen hysteresis loop

Figure 5.93. Experimental results quasi-static testing protocol, scaled to 250%

Figure 5.94 summarizes the damage observed in the exterior surfaces of the walls oriented in the loading direction, while Table 5.26 summarizes the quantification of the damage shown in Figure 5.94.

Figure 5.95 shows some examples of the damage observed during this test, which is mainly characterized by residual gaps along corner beads larger than ½" in thickness, and significant damage, including crushing, along joints between gypsum panels; and diagonal cracks and detachment of several gypsum panels. Most of the surfaces of the walls exhibit pop-out of screws.

Screws pop-out at top track row

Crack along corner bead (Residual gap $t>\frac{1}{4}$")

Crack along corner bead (Residual gap $\frac{1}{16}$"$<t<\frac{1}{4}$")

55

Generalized screw pop-out around wall corner

Portion of gypsum board detached from steel stud frame

Panel joint damaged $t>\frac{1}{4}$"

48

Crack all along gypsum panel joint $t>\frac{1}{4}$"

96

151

Crack along corner bead (Residual gap $t>\frac{1}{2}$")

96

Generalized screws pop-out in first gypsum board panel. Gypsum panels detached from steel stud frame

Permanent gap $t>\frac{1}{4}$"

48

(a) Damage in north wall

174

Screws pop-out at top track

Crack along panel joint $t>\frac{1}{4}$"

Crack in Gypsum board. Panel detached from steel stud frame

Crack along gypsum panel joint $t>\frac{1}{4}$"

55

Crack along door frame $\frac{1}{16}$"$<t<\frac{1}{4}$"

24

Screw pop-out around transverse wall

Screw pop-out in first 2 studs area

Corner bead totally damaged Gap $t>\frac{1}{2}$"

151

Gap $\frac{1}{16}$"$<t<\frac{1}{4}$" along corner bead

96

Gap $t>\frac{3}{8}$" along corner bead

96

Crack along gypsum panel joint $t>\frac{1}{4}$"

81

Gypsum panel detached from steel stud frame

Screws pop-out at bottom track

(b) Damage in south wall

Figure 5.94. Damage observed in partition walls during quasi-static testing protocol, scaled to 250%
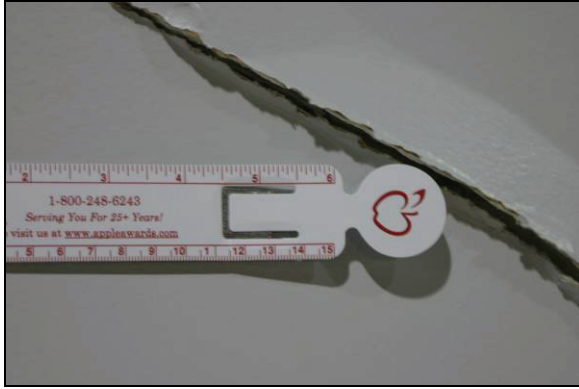
(a) Diagonal crack in exterior south wall

(b) Crushing of gypsum panel along corner bead around door opening

(c) Detached panel and diagonal cracking in north wall

(d) Zoom of detached panel and diagonal cracking in north wall

(e) Horizontal crack along joint of gypsum panels in north wall
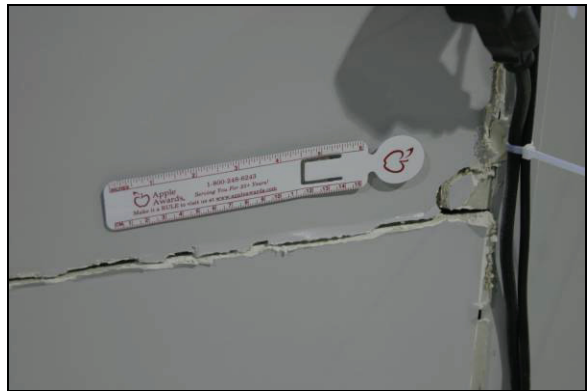
(f) Permanent gap and crushing along horizontal joint and corner bead in north wall

Figure 5.95. Examples of damage observed in gypsum partition walls during quasi-static testing protocol, scaled to 250%

Table 5.26. Quantification of partition wall damage after quasi-static testing protocol, scaled to 250%

Damage measure	Quantified damage (Total length or surface)
Hairline cracks	0 in
Cracks $t \leq \frac{1}{16}''$	0 in
Cracks $\frac{1}{16}'' < t < \frac{1}{4}''$	175 in
Cracks $t \geq \frac{1}{4}''$	1421 in
Screws pop-out area	28459 in²
Detached area	28065 in²

5.4.3.3 Quasi-static protocol test scaled to 300%

This test used the interstory drift protocol, applied quasi-statically, with a target peak interstory drift of 3.94 inches, equivalent to 2.61% of the free interstory height. Table 5.27 compares the peak desired and observed interstory drifts, recorded during the quasi-static testing protocol scaled to 300%. In Table 5.27 it is observed that even under the quasi-static condition the error of the interstory drift imposed by the actuators reaches 2.3%.

Table 5.27. Envelope of interstory drifts for quasi-static testing protocol, scaled to 300%

Response	Peak Interstory Drift δ_{Max}	
	(in)	(%)
Desired	3.94	2.61
Observed	4.03	2.67
Error (%)	2.27	2.27

Figure 5.96 presents the key results obtained during this test. In Figure 5.96 it is observed that the partition walls do not carry loads for drift ratios lower than approximately 1.2% due to pinching effects.
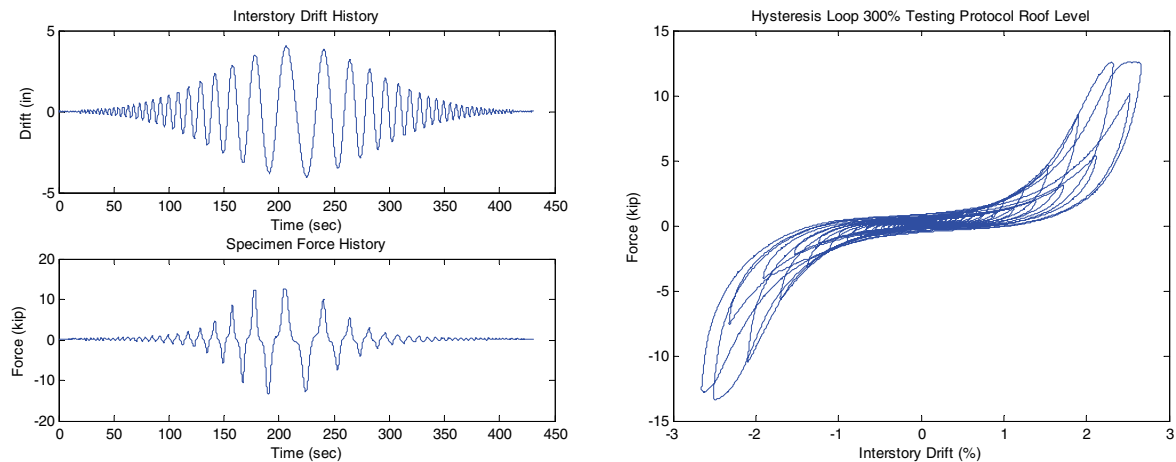
(a) Interstory drift and specimen force histories   (b) Specimen hysteresis loop

Figure 5.96. Experimental results quasi-static testing protocol, scaled to 300%

Figure 5.97 shows some examples of the damage observed during this test. The observed damage can be categorized as total damage or complete loss of the partition walls. The damage generally includes residual gaps along corner beads, crushing along joints between gypsum panels, and diagonal cracks and detachment of most gypsum panels. The gypsum partition walls need to be replaced in order to repair the walls. However, no damage was observed in the steel stud framing.
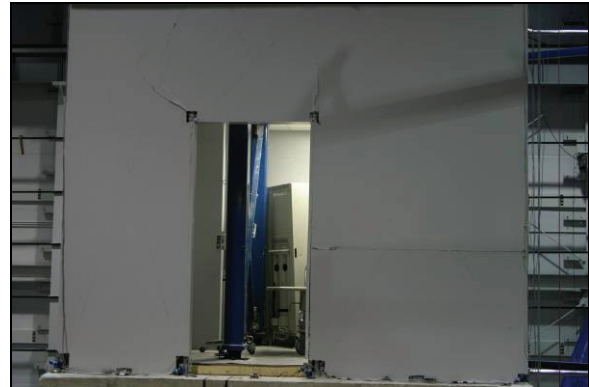
(a) Generalized damage of north wall (b) Generalized damage of south wall

Figure 5.97. Examples of damage observed in gypsum partition walls during quasi-static testing protocol, scaled to 300%

5.4.3.4 Quasi-static protocol test scaled to 350%

This test used the interstory drift protocol, applied quasi-statically, with a target peak interstory drift of 4.60 inches, equivalent to 3.04% of the free interstory height. This test was performed mainly to observe the reserve capacity of the partition walls and any additional damage states in the already badly damaged test specimen. Table 5.28 compares the peak desired and observed interstory drifts, recorded during the quasi-static testing protocol scaled to 350%. In Table 5.28 it is observed that under quasi-static condition the error of the actuators reaches 2.4%.

Table 5.28. Envelope of interstory drifts for quasi-static testing protocol, scaled to 350%

Response	Peak Interstory Drift δ_{Max}	
	(in)	(%)
Desired	4.60	3.04
Observed	4.71	3.11
Error (%)	2.37	2.37

Figure 5.98 presents the key results obtained during this test. In Figure 5.98 it is observed that the partition walls do not carry loads for drift ratios lower than approximately 1.5% due to pinching effects. Figure 5.99 shows some examples of the damage observed during this test. The observed damage can be categorized as general damage, as in the previous test.
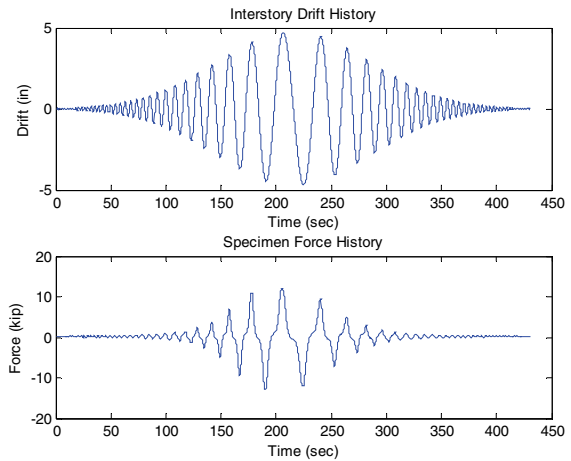
(a) Interstory drift and specimen force histories
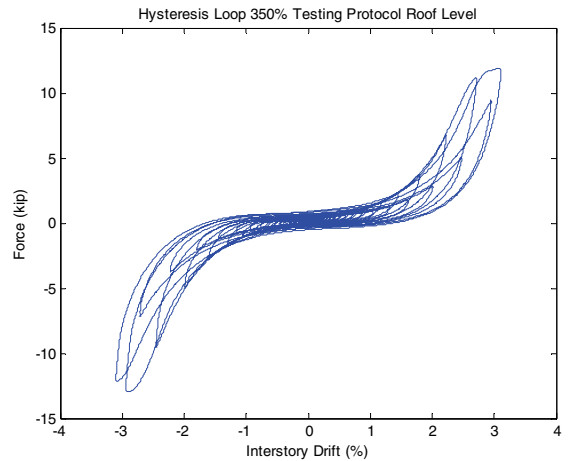
(b) Specimen hysteresis loop

Figure 5.98. Experimental results quasi-static testing protocol, scaled to 350%
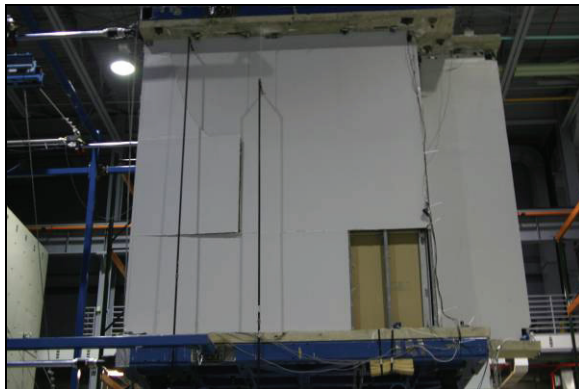
(a) Generalized damage of north wall
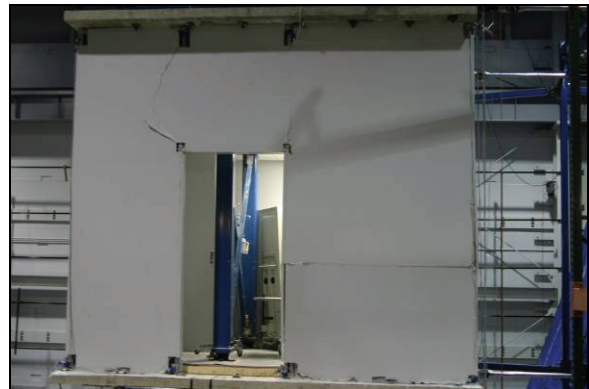
(b) Generalized damage of south wall

(c) Crushing at edge of detached panel in south wall

(d) Damage around interior corner of door opening

Figure 5.99. Examples of damage observed in gypsum partition walls during quasi-static testing protocol, scaled to 350%

(e) Crushing of gypsum board around screw   (f) Crushing of gypsum panel joint

Figure 5.99. Examples of damage observed in gypsum partition walls during quasi-static testing protocol, scaled to 350% (Cont'd)

SECTION 6

ANALYSIS AND DISCUSSION OF EXPERIMENTAL RESULTS

This Section presents the analysis and discussion of the experimental results described in Section 5. Subsection 6.1 presents further analyses of the seismic performance of the hospital emergency room replica, focusing mainly on the damage progression of the gypsum partition walls, and the seismic fragility analysis of wall-mounted inpatient monitors. Subsection 6.2 analyses the fidelity of the UB-NCS in replicating the desired floor motions. Finally, the key conclusions from the test series described in Section 5 are presented in Subsection 6.3.

6.1   Specimen global performance analysis

In order to better understand the progression of damage in the fully equipped emergency room, the results from the series of quasi-static and dynamic tests are combined to identify suitable damage measures for key components and the instance at which these damage states occur. First, the observed damage on all components included in the experiment and the corresponding drifts and accelerations at which the damage occurred are summarized. A comparison is made between the intensity levels at which damage was observed for the testing protocol and the simulated building floor motions. Following the global damage survey, a more detailed analysis is conducted for gypsum partition walls (displacement sensitive component) and wall-mounted patient monitors (acceleration sensitive component) in order to derive experimental fragility curves for their identified damage states.

6.1.1   Global performance of components

As detailed in Subsection 5.4, most of the components in the hospital test specimen exhibited certain degree of damage during the test series. This subsection summarizes the experimental damage observations as a function of the seismic demands imposed on the test specimen. Table 6.1 summarizes the test damage observations. The first two columns of Table 6.1 present the mean peak acceleration recorded at the top and bottom UB-NCS platforms (PFA) and the observed peak interstory drift ratio.

During all tests included in this experimental test series, no damage was observed in the fire suppression system, including the vertical and horizontal pipe runs, and in the sprinkler head. Only one drop in device used to connect one medical gas pipe hanger was pulled out the concrete slab (see subsection 5.4.1.4). At the end of the test series, no damage was observed in the steel studded frame.

Table 6.1. Summary of damage observations in mock emergency room

PFA (g)	Drift Ratio (%)		Observed Damage
0.07	0.09	:	No visible damage in specimen's components.
0.23	0.23	:	Incipient hairline cracks along base of cornerbeads and gypsum panel joints.
0.48	0.47	:	Raised areas and small cracks around screws near bottom and top tracks. Hairline cracks all along of corner beads and door fenestration, and vertical cracks along wall boundary panel joints. One bulb in surgical lamp ran out of service after impacting four times one of the UB-NCS columns. Monitor 4 moved out of its supporting system retention clip, without falling. Significant motion of surgical video rack. Medical gurney rotates 30 degrees from its initial position. Infusion pumps displaced up to 12 inches from its initial position.
1.12	0.94	:	Monitor 2 and Monitor 3 broke off their mounting systems. Extensive cracks along cornerbeads and at joints between gypsum panels. The largest light in the surgical lamp broke off its supporting system after exhibiting excessive displacements and hitting the UB-NCS columns several times. One of the drop-in devices used to attach the medical gas pipes to the top concrete slab was pulled out from the concrete. The gurney exhibited excessive motion after deactivation of its breaking system. The crash dummy was thrown off the gurney. Severe impact was observed between surgical video rack and Monitor 1. Most of medical supplies placed on top of the medical cart fell down the cart.
2.04	1.42	:	Widespread screws pop-out around wall boundaries was observed. The tape covering vertical wall boundaries were completely damaged. Permanent gaps were observed along cornerbeads, some horizontal gypsum panel joints, and door opening. Monitor 4 fell down from its clipped supporting system. Noticeable residual deformations are observed in vertical runs of the medical gas pipes. The gurney exhibited a larger level of displacements after deactivation of its breaking system and the crash dummy was thrown off the gurney and almost out of the room. IV pump Pole 2 overturned and fell down over the crash dummy. IV pump Pole 1 exhibited excessive motion (up to 12 inches) impacting and damaging the base of the gypsum panels. All medical supplies placed on top of the medical cart fell down. Some slight damage was observed in the suspended ceiling system: One ceiling tile fell down, permanent displacements of ceiling tiles, deformations of ceiling grid, and damage along ceiling tile edges. Excessive displacement of the equipment inside the surgical video rack was observed.
-	1.77	:	Widespread pop-out of screws in the whole specimen. The paper tape covering vertical wall boundaries was completely damaged. Permanent gaps were observed along cornerbeads, horizontal gypsum panel joints, and door opening. Initiated gypsum panel detachment from steel studded frame.
-	2.22	:	Generalized screws pop-out in the whole specimen. The tape covering vertical wall boundaries was completely damaged. Large permanent gaps and crushing of joint compound along cornerbeads, horizontal gypsum panel joints, and door fenestration. Gypsum panels detached from steel studded frame.
-	2.67	:	Total damage of partition wall specimen: most of gypsum panels were detached from the steel studded frame, and extensive crushing of gypsum along panel joints and cornerbeads.

6.1.2 Comparison of observed damage for testing protocol and simulated building floor motions

A couple of quantitative and several qualitative observations allow for validating the adequacy of the proposed testing protocol to induce and impose damage on nonstructural components compatible with that induced and imposed by simulated building floor motions. The quantitative aspects include:

- The damage imposed by the proposed testing protocol and by the simulated building floor motions are, in principle, compatible given that they impose/induce similar number of cycles on displacement/acceleration sensitive nonstructural components, as shown and compared in Figure 5.49.

- For the case of protocol floor histories, the collapse of Monitors 2 and 3 was observed for a peak acceleration at the base of the monitor of 1.38g, while for the simulated building floor motions, the collapse was observed for an acceleration equal to 1.62g. The difference in the peak acceleration triggering the damage of the monitor's supporting system is less than 15%.

The qualitative aspects include:

- The amplitudes and characteristics of the displacements observed in the gurney, medical cart and infusion pump poles are comparable for both design and maximum considered earthquake levels, for the testing protocol and simulated floor motions.

- The magnitude of the damage imposed on the base of the gypsum partition walls by the excessive motion and impact of the infusion pump poles is similar for both testing protocol and simulated building floor motions.

- The characteristics of the interaction observed (basically impact) between the surgical video rack and Monitor 1 during the protocol and simulated floor motion excitations are comparable, for both design and maximum considered earthquake levels.

- The characteristics of the excessive displacement of the equipment placed inside the surgical video rack is similar for the maximum considered earthquake, for both protocol and simulated building floor motion histories.

- Similar effects on the medical supplies placed on top of the medical cart were observed for both protocol and simulated building floor motion histories, associated to design and maximum considered earthquake levels.

It is important to highlight that the protocol is intended to be representative of various floor motions and should impose conservative seismic demands.

6.1.3 Seismic performance of gypsum partition walls

This subsection presents the ensemble of hysteresis loops observed during the dynamic and the quasi-static tests performed with the proposed testing protocol. A summary of the progression of damage in the gypsum walls is presented as a function of the imposed interstory drift.

6.1.3.1 Force-displacement response

Figure 6.1 shows the ensemble of partition walls hysteresis loops observed during the dynamic and the quasi-static (QS) tests carried out using the testing protocol proposed in subsections 5.3.1 and 5.3.3, respectively. The peak resisting force of approximately 28 kips is more than double the peak force obtained during the quasi-static tests performed by Lang et al. (Lang, 2007) using a similar specimen (~13 kips). Moreover, the drift ratio value at which the peak force is achieved shifts from the 0.6 % observed by Lang et al. to 1.2 % observed during the dynamic tests using the UB-NCS. Note that at a drift of 0.6 %, the peak force in Figure 6.1 is approximately 20 kips. The large difference in peak resisting force is partially explained by the different failure modes observed in the two tests. While the top track connection failed in the tests by Lang et al., the steel stud frame and tracks remained intact during the UB-NCS tests. The different failure modes were likely caused by the different spacing used for the track fasteners: Lang et al. used a spacing of 24 inches while a 12 inch spacing was used for the UB-NCS tests.

In Figure 6.1, the peak drift imposed by the 150 % dynamic protocol is 1.42 %, the larger cycles shown in the figure correspond purely to QS loading. Coincidently, the transition from dynamic to quasi-static tests coincides with the instant of major damage in the partition wall, indicated by the significant drop in peak resisting force.
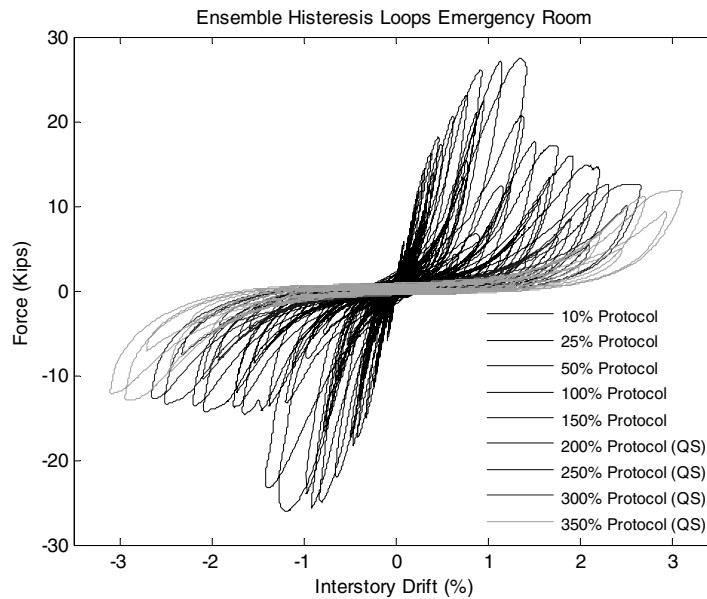
Figure 6.1. Ensemble hysteresis loops for steel studded gypsum partition walls

244

6.1.3.2 Progression of damage

The progression of damage observed in the gypsum partition walls during the dynamic and quasi-static tests performed using the proposed testing protocol is summarized in Table 6.2. The observed damage progression correlates well with observations obtained from previous tests described in Section 3, that were performed using specimens with similar geometry, materials and construction methods.

Table 6.2. Progression of damage in steel studded gypsum partition walls

Drift Ratio (%)		Observed Damage
0.09	:	No visible damage in specimen
0.23	:	Minimum level of damage observed
		Incipient hairline cracks along base of cornerbeads and gypsum panel joints
0.47	:	Raised areas and small cracks around screws near bottom and top tracks
		Hairline cracks along corner beads
		Vertical cracks $t \leq 1/16''$ along wall boundary panel joints
		Small hairline cracks around door fenestration
1.42	:	Widespread pop-out of screws around wall boundaries
		Tape covering vertical wall boundaries completely damaged
		Permanent gaps $1/16'' \leq t \leq 1/4''$ along cornerbeads, some horizontal gypsum panel joints, and door fenestration
1.77	:	Widespread pop-out of screws in the whole specimen
		Tape covering vertical wall boundaries completely damaged
		Permanent gaps $1/16'' \leq t \leq 1/4''$ along cornerbeads, horizontal gypsum panel joints, and door opening
		Some permanent gaps $t \geq 1/4''$ along cornerbeads
		Initiated gypsum panel detachment from steel studded frame
2.22	:	Generalized pop-out of screws in the whole specimen
		Tape covering vertical wall boundaries completely damaged
		Permanent gaps $t \geq 1/4''$ and crushing of joint compound along cornerbeads, horizontal gypsum panel joints, and door fenestration
		Gypsum panel detached from steel studded frame
2.67	:	Total damage of specimen
		Most gypsum panels detached from steel stud frame
		Extensive crushing of gypsum along panel joints and cornerbeads

6.1.3.3 Study of damage states

Damage progression curves were computed for the steel studded gypsum partition walls considered in this research. Fragility analysis could not be directly performed given that only a single specimen was tested, and therefore, the information required for statistically assessing the seismic demands triggering each Damage State (DS) was not available. Nevertheless, a procedure is proposed later in this subsection for estimating, in an approximate way, a statistical parameter that has shown promise in predicting the demand parameters triggering the various DS's identified for the gypsum partition wall systems.

Four DS's were identified based on the information provided in Table 6.2 and are listed in Table 6.3. The type of repair that would be required and the potential effects on functionality of an emergency room

enclosed by partition walls were also considered in selecting the DS. Table 6.3 is similar to the one proposed by Taghavi and Miranda (Taghavi and Miranda, 2003) for drywall wood studded partition walls, with some adjustments to the particular characteristics and observed damage of the tested specimen. The last column in Table 6.3 includes a Damage Measure (DM) for each DS that allows for the quantification or measurement of each damage state based on the specimen damage. The Damage Measures (DM) have been carefully selected based on experimental observations and quantities that could be measured after the experiments, such as crack lengths and widths. Note that two damage measures are considered for damage states DS_3 and DS_4. The most suitable damage descriptor for each damage state is later investigated through statistical analysis of the experimentally collected data.

Table 6.3. Definition of Damage States (DS) for steel studded gypsum partition walls

Damage State (DS)	Description of Damage State	Potential Effects on ER Operations (Boroschek and Retamales, 2004)	Repair Actions	Damage Measure (DM)
DS_1	Hairline cracks along corner beads and paper joint tape.	Service remains fully functional; Interruptions minimal during the repairing process.	One coat of paint to cover hairline cracks (optional).	Cumulative Length of hairline cracks
DS_2	Minor permanent gaps ($t \leq \frac{1}{16}$ ") between gypsum boards and between corner beads and gypsum boards; Raised screws noticeable at gypsum panel edges.	Service remains functional; Critical inpatients may need to be moved to a cleaner room during the repair.	Re-screwing of fasteners (as necessary); One coat of mudding and two coats of paint may be necessary.	Length of minor gaps $t \leq 1/16''$
DS_3	Major permanent gaps ($\frac{1}{16}$ " $\leq t \leq \frac{1}{4}$ ") between gypsum boards and between corner beads and gypsum boards; Crushing along gypsum panel edges; Screws pop out.	Minor interruption of services due to aseptic issues; Service out of function for a couple of days.	Removal of crushed material along gypsum board; Replacement of fasteners, mudding and painting; Replacement of corner beads may be necessary; Gypsum panel joints taping, mudding and painting.	Length of gaps $1/16'' \leq t \leq 1/4''$ or Area of popped out screws
DS_4	Permanent gaps $t \geq 1/4''$; Gypsum panels detached from steel stud frame.	Interruption of normal operation is expected due to safety reasons. Service out of function for a couple of weeks.	Replacement of damaged gypsum panels and corner beads; Gypsum panel joints taping, mudding and painting.	Length of gaps $t \geq 1/4''$ or Area of detached gypsum panels

Table 6.4 summarizes the quantification of damage observed during each test for which the damage was assessed in detail, as specified in Table 5.9 and described in Subsection 5.4. The numbers provided in the table correspond to the total length or area that was observed to be damaged in post test observations. The numbers decrease from preliminary damage states such as 'hairline cracks' because these cracks opened up in subsequent tests and instead were categorized as larger cracks. No new hairline cracks were

observed at larger amplitudes since all new cracks had wide openings at that drift level. The complete failure of the partition walls was observed during the test imposing a drift ratio of 2.67%, and therefore, the damage shown in the last column of Table 6.4, corresponds to the total "damageable" joint lengths or panel surfaces of the specimen.

Table 6.4. Quantification of damage observed during tests

Damage Measure (DM)	Damage Quantification					
	δ_{Max}=0.23 %	δ_{Max}=0.47 %	δ_{Max}=1.42 %	δ_{Max}=1.77 %	δ_{Max}=2.22 %	δ_{Max}=2.67 %
Hairline cracks (in)	48	549	24	-	-	-
Cracks t ≤ $\frac{1}{16}$″ (in)	67	73	466	24	-	-
Cracks $\frac{1}{16}$″ < t < $\frac{1}{4}$″ (in)	-	-	405	653	175	-
Cracks t ≥ $\frac{1}{4}$″ (in)	-	-	96	398	1421	2304
Screws pop-out area (in²)	-	1701	10666	19494	28459	-
Detached area (in²)	-	-	-	5140	28065	48324

As stated in Subsection 5.4, only the damage observed in the exterior walls has been considered in the analysis because: i) for those walls the observed damage database is more populated, and ii) the damage observed is representative of the global specimen damage.

Table 6.5 shows the accumulated damage observed in the specimen. Several considerations are taken into account for populating Table 6.5, which include:

- All observed cracks with width $t \le 1/16$″ are assumed to contribute to the total length of hairlines.

- All observed cracks with width $1/16$″ $\le t \le 1/4$″ are assumed to contribute to the total length of cracks with width $t \le 1/16$″ and hairline cracks.

- All observed cracks with width $t \ge 1/4$″ are assumed to contribute to the total length of cracks with width $1/16$″ $\le t \le 1/4$″, $t \le 1/16$″, and hairlines.

- All panel joints around detached areas of gypsum panels are assumed to contribute to the total length of cracks with width $t \ge 1/4$″, $1/16$″ $\le t \le 1/4$″, $t \le 1/16$″, and hairlines.

- At the ultimate condition (δ_{Max} = 2.67 %), all specimen joints and panel areas are damaged.

Table 6.5. Quantification of cumulated damage observed during tests

Damage Measure	Damage Quantification					
	δ_{Max}=0.23 %	δ_{Max}=0.47 %	δ_{Max}=1.42 %	δ_{Max}=1.77 %	δ_{Max}=2.22 %	δ_{Max}=2.67 %
Hairline cracks (in)	115	622	991	1223	1596	2304
Cracks t ≤ $\frac{1}{16}$″ (in)	67	73	967	1223	1596	2304
Cracks $\frac{1}{16}$″ < t < $\frac{1}{4}$″ (in)	0	0	501	1199	1596	2304
Cracks t ≥ $\frac{1}{4}$″ (in)	0	0	96	546	1421	2304
Screws pop-out area (in²)	0	1701	10666	24634	28459	48324
Detached area (in²)	0	0	0	5140	28065	48324

Figure 6.2 plots the experimental cumulative damage progression data summarized in Table 6.5, expressed as the percentage of the total "damageable" length of crack or wallboard surface shown in the last column of Table 6.5. The best fit standard lognormal cumulative distribution curve, $F_X(x)$, is computed for each damage state (or for each damage measure) using:

$$F_X(x) = \frac{1}{2}\left[1 + erf\left(\frac{ln(x) - \mu}{\sigma\sqrt{2}}\right)\right] \tag{6.1}$$

where $erf(\ )$ denotes error function; x denotes the Engineering Demand Parameter (EDP) controlling the progression of damage, which in this case corresponds to interstory drift ratio; and μ and σ denote the mean and standard deviation of the natural logarithm of the seismic demand for which the 50% of the testing specimen exhibits a specific damage state. In terms of these variables, the median θ and the dispersion β of the seismic demand at which the 50% of the component will reach or exceed a specified damage state are given by (Soong, 1981):

$$\theta = e^{\mu} \tag{6.2}$$

and

$$\beta = \left(e^{\sigma^2} - 1\right)e^{2\mu+\sigma^2} \tag{6.3}$$

The curves in Figure 6.2 presents the percentage of wallboard exhibiting a given damage state. These are not conventional fragility curves that provide the probability of achieving or initiating a given damage state. Instead they describe the distribution (as percentage) of damage through the partition walls. Examining hairline cracks for example, given a drift ratio, these curves provide the expected crack length expressed as a percentage of the total length of joints along the wall that can crack.

Table 6.6 lists the values of the best fit parameters resulting from the estimation process. In Table 6.6, the parameter $EDP_{\gamma=5\%}$ is a reference parameter denoting the seismic demand associated with achieving 5% of a given damage state. This parameter has been shown to correlate well with the seismic demand at which a given damage state is first observed. The parameter $EDP_{\gamma=5\%}$ ($\gamma=0.05$) is calculated using:

$$EDP_{\gamma} = e^{\mu+\sigma\sqrt{2}\,erf^{-1}(2\gamma-1)} \tag{6.4}$$

where $erf^{-1}(\ )$ denotes the inverse error function. From the analysis of the results presented in Table 6.6 it is concluded that the most suitable damage measure indices (associated to the lowest dispersion

values β), for the damage states DS$_3$ and DS$_4$, as defined in Table 6.3, are the length of cracks with widths $\frac{1}{16}'' < t < \frac{1}{4}''$, and the surface of detached gypsum panels, respectively.
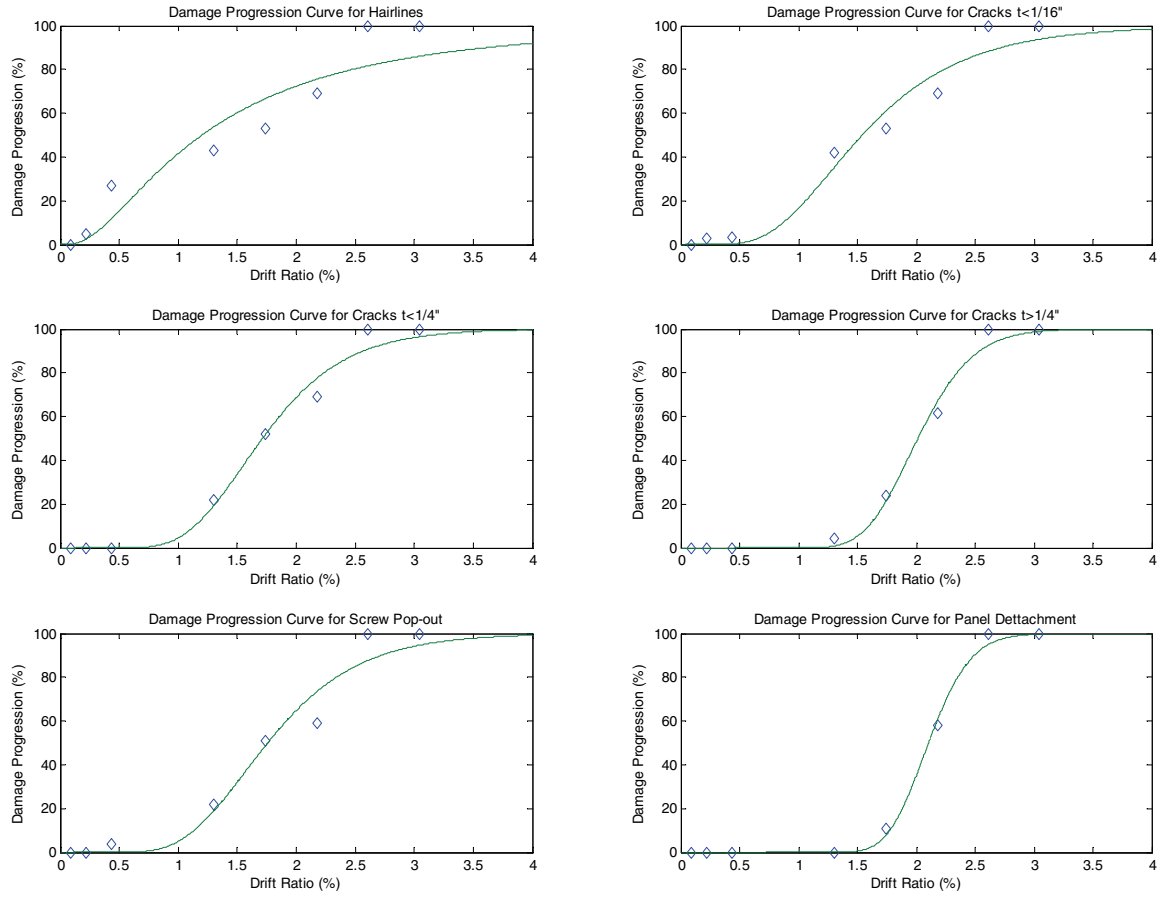
Figure 6.2. Damage progression data and best fit damage progression curves

Table 6.6. Best fit parameter estimation

Damage Measure	Damage State Associated	Best Fit Parameter for Drift Ratio (%)				
		μ	σ	θ	β	$EDP_{\gamma=5\%}$
Hairline cracks	**DS$_1$**	**0.18**	**0.86**	**1.20**	**3.29**	**0.29**
Cracks $t \leq \frac{1}{16}''$	**DS$_2$**	**0.43**	**0.44**	**1.54**	**0.63**	**0.74**
Cracks $\frac{1}{16}'' < t < \frac{1}{4}''$	**DS$_3$**	**0.54**	**0.32**	**1.71**	**0.34**	**1.02**
Cracks $t \geq \frac{1}{4}''$	DS$_4$	0.70	0.18	2.01	0.14	1.49
Screws pop-out area	DS$_3$	0.56	0.34	1.76	0.43	1.00
Detached area	**DS$_4$**	**0.74**	**0.13**	**2.10**	**0.08**	**1.69**

Figure 6.3 shows a comparison of the damage progression curves computed for the different damage states identified in this experimental test series. From the inspection of the results presented in Table 6.6 and plotted in Figure 6.3 it is observed that lower damage levels (DS$_1$ and DS$_2$) have associated larger dispersions of the median seismic demands for which 50% of the specimen (in terms of joint length or

wallboard surface) has reached a given damage state. In the case of hairline cracks for example, the lowest damage level identified in this research, the dispersion β of the median drift ratio for which the specimen would reach the DS_1, with a probability of 50%, is 1.2%. This result is compatible with experimental observations in the sense that, for example, hairline crack propagation does not continue at high interstory drift levels as could be expected, because other higher damage states (such as DS_2 or DS_3) are initiated instead. This result is consistent with previous observations by Lang et al. (Lang, 2007) and Bersofsky (Bersofsky, 2004). On the other hand, the highest damage level considered, consisting in the detachment of gypsum board panels, has a relatively low dispersion due to, mainly, the clear interstory drift amplitude at which the partition wall system is completely destroyed.
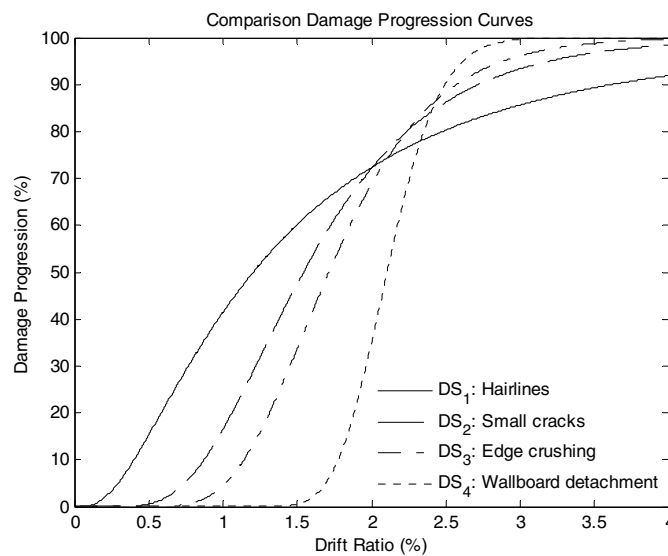
Figure 6.3. Damage progression curves for damage states of gypsum partition walls

The statistical parameter EDP_γ, as defined in equation (6.4), has shown a prominent capability to predict the drift amplitude at which damage states are first observed. For example, according to the last column of Table 6.6, the drift ratio at which the gypsum panel detachment starts (DS_4) is 1.69%, while according to Table 6.2, panel detachment started for a drift ratio in the range 1.42 to 1.77%. Furthermore, and according to Table 6.6, cracks with widths in the range $\frac{1}{16}'' < t < \frac{1}{4}''$, representative of large residual cracks in the gypsum partition walls (Table 6.3), are triggered at a drift ratio of 1.02%, which is consistent with the range provided in Table 6.2. This establishes that large residual cracks started for drift amplitudes in the range 0.47 to 1.42%. Similar analyses can be performed to cross the experimental observations presented in Table 6.2, the damage states defined in Table 6.3, and the prediction values presented in Table 6.6.

In terms of the potential effects of partition walls damage on the emergency room serviceability, according to definitions in Table 6.3, it can be concluded that the normal service functionality will not be interrupted during seismic events imposing drift ratios less than 0.74%. Of course, the ER operations will also be dependent on various other components, however, only the effects of the partition walls are considered here. Interruptions of the ER functionality are expected for drifts ratios in the range 1.02 to 1.76%, drifts for which DS_2 and DS_3 are triggered. Finally, from Table 6.6, it can be concluded that 50% of the partition walls (DS_4), will be completely destroyed at interstory drift ratios larger than 2.1%, although the detaching of panels will be observed at an imposed interstory drift ratio of 1.69%.

6.1.4 Seismic performance of wall-mounted patient monitors

This subsection presents the fragility analysis of the wall-mounted patient monitors. In the experiments, some of the patient monitors fell from their support using both the testing protocol and the simulated building floor motions as input motions. This equipment is examined further because its response is believed to be controlled mainly by acceleration, providing an acceleration sensitive component interacting with the drift sensitive gypsum partition walls.

6.1.4.1 Fragility analysis

Figure 6.4a shows the peak horizontal accelerations recorded at the base of Monitor 2 during dynamic tests. It is recalled herein that the supporting devices for Monitors 2 and 3 failed during the tests performed using: i) the dynamic testing protocol scaled to 100%; and ii) the simulated building floor motions associated to a seismic hazard with a probability of exceedance of 2% in 50 years, scaled to 100%. The best fit fragility curve for the damage state consisting of the failure of the monitor's supporting device, is shown in Figure 6.4a. The fragility curve has been estimated using the methodology proposed by Porter and Bachman (Porter and Bachman, 2006) using only a single damage state. Table 6.7 summarizes the best fit parameters obtained following the optimization process. A constraint value for the dispersion $\beta \geq 0.2$ has been considered in the analysis, as recommended in (Porter and Bachman, 2006). Figure 6.4b complements the fragility curve presented in Figure 6.4a by showing the probability density function for the only damage state assessed in this case. From inspection of Figure 6.4 and Table 6.7, it can be concluded that an acceleration of 1.35g at the base of the equipment has a 50% probability to induce failure of the monitor supporting devices.
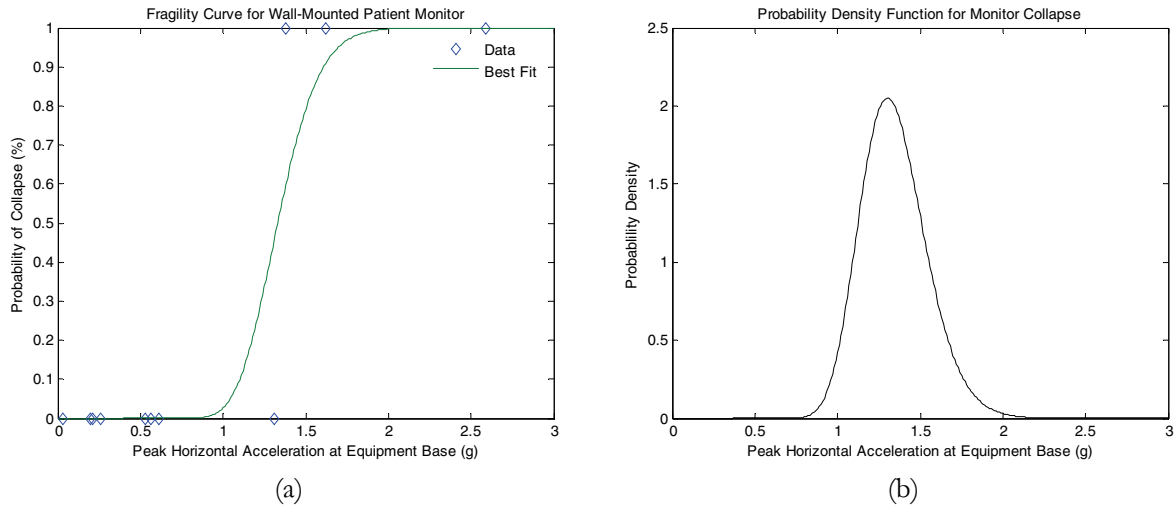
Figure 6.4. (a) Fragility curve for failure of wall-mounted patient monitor; and (b) Probability density functions for failure of wall-mounted patient monitor

Table 6.7. Best fit parameter estimation for wall-mounted patient monitors

Damage Measure	Damage State Associated	Best Fit Parameter for Monitor Base Acceleration (g)			
		μ	σ	θ	β
Peak acceleration at base of monitor	Monitor's supporting device failure	0.29	0.15	1.35	0.20

6.2   UB-NCS performance analysis

This subsection presents a succinct analysis of the performance of the UB-NCS testing facility to impose target floor motions. The level of demands imposed during the test series presented in this report was unique, by far exceeding the demands considered during the equipment shake-down process, and therefore, it provides valuable information for improving the strategy currently used for controlling the testing equipment.

Figure 6.5 shows plots of the peak relative displacement error observed between two actuators placed at a same platform level as a function of the peak velocity imposed by the actuators for all dynamic tests. The motion of the pair of actuators at each level should ideally be synchronized to avoid undesired random twist (yaw) of the testing platform. It is observed that the error varies linearly with the observed peak platform velocity. For platform velocities up to 50 inches/sec, the relative displacement between actuators is approximately ¼ of an inch.
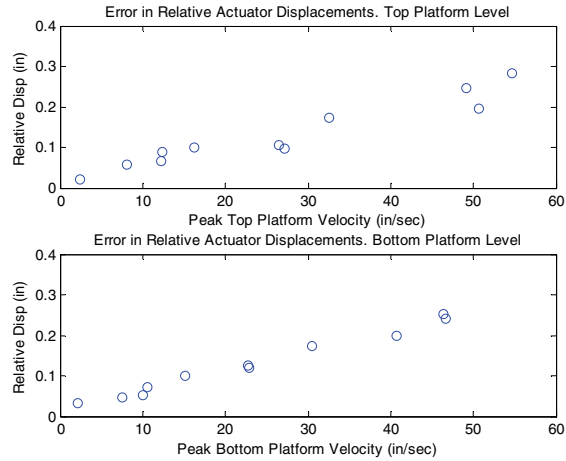
Figure 6.5. Relative displacements between actuators

Figure 6.6 summarizes the errors observed in the peak interstory drifts imposed during the dynamic tests as a function of peak test velocity. The test velocity in this case is computed as the average of observed top and bottom peak platform velocities. Although the dispersion of data around the best fit curve shown in Figure 6.6 is significant, the trend of the collected data can be clearly identified. Moreover, extrapolation of the data shown in Figure 6.6, through its best fit line, to the zero mean platform velocity point, properly yields the observations made during the quasi-static test series, as shown in Table 5.23, Table 5.25, Table 5.27 and Table 5.28.

Finally, Figure 6.7 shows the errors observed in the bottom and top platform accelerations as function of the target peak platform velocity. Only data recorded after command signal compensation was included in Figure 6.7. In Figure 6.7 it is observed than the higher the target platform velocity, the higher the error in the observed platform acceleration. For target velocities close to 50 inches/sec, the error observed in the recorded accelerations, in relation to the target acceleration, is approximately 40%. The errors observed in peak accelerations are proportional and representative of the errors observed in matching desired response spectra.

Based on this analysis, it can be concluded that the errors in the imposed interstory drifts are not significant. For example, an error of 14% in the interstory drift imposed on a specimen subjected to a target interstory drift of 3% during a floor motion characterized by a target peak platform velocity of 50 in/sec, would result in a 3x1.14=3.42% actual imposed drift. Such a difference is expected to have minor influence in the accuracy of the specimen fragility analysis. Further, the actual measured drifts can be considered in the fragility analysis instead of the desired drift.
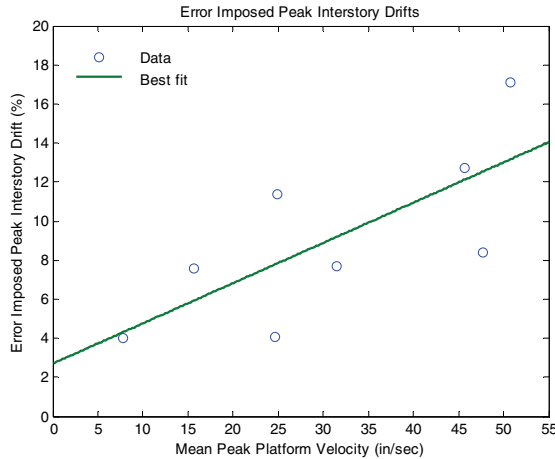
Figure 6.6. Errors observed in imposed peak interstory drifts
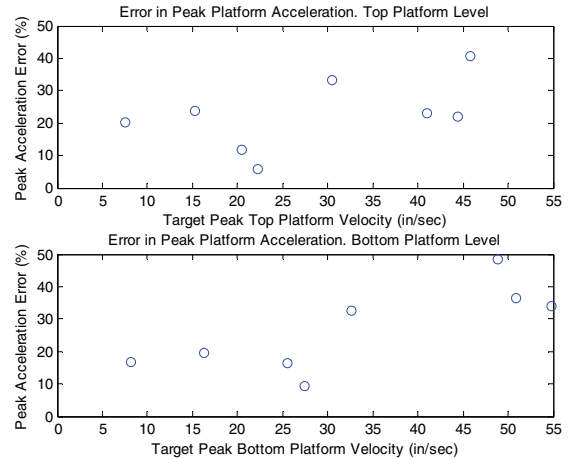
Figure 6.7. Errors observed in imposed platform accelerations

The errors observed in simulating platform acceleration histories are more severe, particularly for qualification type testing. However, the errors in imposed accelerations could be lowered by reducing the tolerance currently considered by the iterative off-line command input compensation process. As observed during this test series, after degradation of the specimen's stiffness, the input command signals seem to be "overcompensated". A second alternative, or an additional measure, might be to perform the compensation process using the 50% design earthquake level floor motions. Alternatively, the UB-NCS can be compensated with dead weight to simulate the specimen pay load as is done for shake table tuning.

6.3   Summary and conclusions of full-scale emergency room test series

Extensive testing has been performed to investigate the seismic performance of a full-scale mock emergency room by using a testing protocol that has been calibrated to impose and induce hazard consistent seismic demands on displacement and/or acceleration sensitive nonstructural components, and the simulated response of a multistory moment resistant steel framed building. Complementary quasi-static tests were carried out to assess the performance of displacement sensitive component undergoing higher interstory drift ratios. The experimental series was also useful to evaluate the fidelity of the UB-NCS equipment to impose target full scale floor motions. The conclusions of this test series are detailed as follows:

1.   The UB-NCS has demonstrated its ability to impose, under controlled laboratory conditions, the full-scale floor motions required to assess the seismic performance of full scale nonstructural components and systems. However, some important facts should be considered in future experiments, and some improvements to the proposed control strategy are suggested:

254

1.1. The errors observed in the imposed interstory drift histories vary linearly in the range 2.5 to 14%, for mean peak platform velocities ranging between 0 and 55 inches/sec. Therefore, for floor motion histories reaching high platform velocities, it may be desired to compensate the target interstory drift history accordingly.

1.2. The maximum relative displacement between actuators located at a same platform level reaches 0.25 inches for peak platform velocities up to 50 inches/sec.

1.3. During the test series it was observed that the higher the target peak platform velocity, the higher the error in the observed peak platform accelerations. The errors in peak platform accelerations reach 50% for peak target platform velocities up to 50 inches/sec, denoting significant overshoots for large amplitude tests. Nevertheless, high platform velocities were reached for the tests at which the specimen stiffness was already degraded, and therefore, two solutions are proposed:

1.3.1. Perform the offline iterative input command compensation process considering, at least, the floor motions corresponding to 50% of the target floor motions. Even if the specimen may be damaged during the command compensation process, more accurate results will be obtained during target and higher amplitude floor motions tests.

1.3.2. The minimum errors observed in replicating target peak platform accelerations, consistent with the errors found in observed response spectra (ORS's), are on the order of 20% approximately. This error could be lowered by reducing the tolerance currently considered by the offline input compensation process.

2. Several degrees of damage were observed in both displacement and acceleration sensitive nonstructural components included within the emergency room.

2.1. The observed damage, for the design and lower earthquake levels, includes:

2.1.1. Partition walls. Extensive cracks along cornerbeads and at joints between gypsum panels. Popped-out screws were observed around top and bottom tracks.

2.1.2. Wall mounted monitors. Monitor 1 was severely impacted by the surgical video rack. Monitors 2 and 3 simultaneously broke off their supporting systems. Monitor 4 moved out of its supporting system's retention clip.

2.1.3.   Surgical lamp. Severe impact was observed between the surgical lamp lights and the UB-NCS columns. As consequence of the impact, one bulb burned out and one of the lamps broke off its supporting system.

2.1.4.   Medical gas. One of the drop-in devices used to attach the hangers for the medical pipes horizontal runs was pulled out from the top concrete slab. Furthermore, excessive horizontal displacement was observed. The gas pipes impacted the sprinkler head several times without causing any damage.

2.1.5.   Medical gurney. The medical gurney exhibited excessive motion after deactivation of its breaking system.

2.1.6.   Crash dummy. The crash dummy was thrown off the medical gurney.

2.1.7.   Medical cart. One half of the medical supplies placed on top of the medical cart fell down from their original position.

2.1.8.   Surgical video rack. Severe impact between the surgical video rack and Monitor 1 was observed. Excessive displacement of the rack was observed.

2.1.9.   Infusion pumps poles. Excessive displacement of poles was observed.

2.2.   The additional damage observed, for the maximum considered earthquake level, includes:

2.2.1.   Partition walls. Permanent gaps were observed along cornerbeads, at horizontal joints between gypsum panels, and around door fenestration. Paper tape covering wall boundaries were completely damaged. Widespread screws pop-out was observed around wall boundaries.

2.2.2.   Wall mounted monitors. Monitor 1 was severely impacted by the surgical video rack and it almost fell down. Monitors 2 and 3, which were repositioned on top of new mounting systems after collapsing during the design earthquake level test (protocol loading), again broke off their supporting systems with the simulated building floor motions. Monitor 4 fell down from its supporting device (protocol loading).

2.2.3.   Medical gas. The medical pipe runs exhibited excessive horizontal displacements, impacting several times the sprinkler head, without inducing any damage. Permanent

deformations were observed in the vertical runs (within the gypsum wall) of the medical gas pipes.

2.2.4. Medical gurney. The medical gurney exhibited a larger level of displacements after deactivation of its breaking system.

2.2.5. Crash dummy. The crash dummy was thrown off the medical gurney and almost out of the emergency room.

2.2.6. Medical cart. All medical supplies placed on top of the medical cart fell down.

2.2.7. Surgical video rack. Severe impact between the surgical video rack and Monitor 1 was observed. Monitor 1 almost fell due to the intensity of the impact. Excessive displacement of the rack was observed. Furthermore, excessive displacement of the equipment inside the rack was observed.

2.2.8. Infusion pumps poles. Excessive displacement of poles was observed. The poles impacted and severely damaged the base of the gypsum partition walls.

2.2.9. Ceiling system. One ceiling tile fell down, permanent displacements of ceiling tiles, deformations of ceiling grid, and damage along ceiling tiles edges were observed.

3. The damage progression of gypsum partition walls, as a function of the interstory drift ratio imposed on the specimen, was examined in detail. The main observations were:

3.1. For a drift ratio of 0.09%, there was no perceptible damage in the specimen.

3.2. For a drift ratio of 0.23%, incipient hairline cracks were observed at the top and bottom ends of cornerbeads.

3.3. For a drift ratio of 0.47%, hairline cracks were observed all along cornerbeads. Small vertical cracks and paper tape damage were observed all along wall boundary panel joints.

3.4. For a drift ratio of 1.42%, widespread screw pop-out was observed around wall boundaries. The paper tape covering the wall boundaries was totally damaged. Permanent gaps were observed along cornerbeads, some horizontal gypsum panel joints, and door fenestration.

3.5. For a drift ratio of 1.77%, widespread screw pop-out was observed in the whole specimen. Some incipient large gaps are observed along cornerbeads. Detachment of gypsum boards from steel studded frame initiated.

3.6. For a drift ratio of 2.22%, large gaps and joint compound material crushing was observed along cornerbeads, gypsum panel joints and door fenestration. Gypsum boards were detached from the steel studded frame.

3.7. For a drift ratio of 2.67%, the damage observed in the partition wall system was total.

4. Damage progression and fragility analysis were performed for one sample of displacement sensitive (steel studded frame gypsum partition walls) and one sample of acceleration sensitive (wall-mounted patient monitors) nonstructural components, respectively.

4.1. For the gypsum partition walls, four damage states (DS), with their corresponding damage measures (DM), were identified.

4.1.1. DS_1, corresponding to the hairline cracks appearing in the wall and its DM was the total length of hairline cracks observed. It can be repaired with paint.

4.1.2. DS_2 corresponding to minor permanent gaps observed between gypsum panels and cornerbeads, and its DM was the total length of cracks with width $t \leq 1/16''$. It must be repaired with mud and paint.

4.1.3. DS_3 consisting of major permanent gaps with crushing of joint panel compound, and its DM was the length of cracks with width $1/16'' \leq t \leq 1/4''$. The crushed material must be removed from panel joints. New mudding, taping and painting are required.

4.1.4. Finally, DS_4 corresponding to detachment of gypsum panels, and its DM was the surface of detached gypsum panels. The gypsum panels should be completely replaced.

4.2. The parameter $EDP_{\gamma=5\%}$ proposed for estimating the seismic demand at which the damage state will be observed for first time has shown prominent capability to predict experimental observations.

4.3. According to the fragility (damage progression) analysis results, the partition wall system will be lost, with a probability of 50%, during a seismic event imposing an interstory drift ratio of 2.1%. Nevertheless, the total loss of the partition walls could be observed for interstory drifts of 1.69%. Moreover, the serviceability of the emergency room can be significantly affected, with a probability of 50%, during seismic events imposing drift ratios of 1.71%. Nevertheless, the service functionality could be affected if drifts ratios as low as 1.02% are observed.

4.4. For the wall-mounted patient monitors, only one damage state, consisting in the failure of the monitor's supporting system, was identified and assessed. The engineering demand parameter considered in this case was the peak acceleration measured at the base of the equipment, which includes dynamic amplifications due to flexibility of the partition walls. From the fragility analysis, it was observed that a peak horizontal acceleration at the base of the monitor of 1.35g would have 50% probability of inducing collapse of the equipment's mounting system.

5. The adequacy and suitability of the proposed testing protocol to impose, under controlled laboratory conditions, the hazard compatible seismic damage expected on displacement and/or acceleration sensitive nonstructural components, systems and equipment has been assessed. Both qualitative and quantitative parameters have been considered.

5.1. The damage imposed by the proposed testing protocol and by the simulated building floor motions is compatible in the sense that they impose/induce a similar number of cycles on displacement/acceleration sensitive nonstructural components. The testing protocol floor motions have been calibrated to impose/induce a number of cycles compatible with the number of cycles imposed/induced by the floor motions recorded at the upper levels of multistory buildings during strong earthquake events.

5.2. During the tests performed using the protocol floor histories, the collapse of Monitors 2 and 3 was observed at a peak acceleration measured at the base of the monitor of 1.38g, while during the tests carried out using the simulated building floor motions, the collapse was observed at a peak acceleration of 1.62g. The difference in the peak acceleration triggering the damage of the monitor's supporting system is less than 15%.

5.3. The amplitudes and characteristics of the displacements observed in the gurney, medical cart and infusion pump poles were comparable for both design and maximum considered earthquake levels, for both testing protocol and simulated building floor motions.

5.4. The magnitude of the damage imposed at the base of the gypsum partition walls by the excessive motion and impact of the infusion pump poles was similar for both protocol and simulated building floor motions.

5.5. The observed interaction between the surgical video rack and Monitor 1, during the protocol and the simulated floor motion excitations, was similar, for both design and maximum considered earthquake levels.

5.6. The characteristics of the motions of the equipment inside the surgical video rack was similar for the maximum considered earthquake, for both testing protocol and simulated building floor motion histories.

5.7. Similar effects on the medical supplies placed on top of the medical cart were observed for both testing protocol and simulated building floor motion histories, associated to design and maximum considered earthquake levels.

SECTION 7

SUMMARY, CONCLUSIONS AND RECOMMENDATIONS

The research presented in this report provides a critical step in a methodology for better understanding the seismic behavior of nonstructural components, systems and equipment through more realistic testing procedures. A short summary of this research and the resulting conclusions of this work are provided here. Recommendations for future research are also presented at the end of this section.

7.1   Summary and conclusions

In order to better understand the seismic behavior of nonstructural components, the University at Buffalo Nonstructural Component Simulator (UB-NCS) has been commissioned to subject nonstructural components to realistic full-scale floor motions. This new equipment provides improved experimental capabilities for more realistic qualification testing and fragility assessment of nonstructural components. Full-scale, anchored or self-supported equipment and building contents, with attachment points at one or two consecutive levels can be tested. Most important, equipment and combined nonstructural systems that may be sensitive to both accelerations and/or interstory drifts can be rigorously evaluated under realistic loading conditions to evaluate interdependencies as well as the interaction with the primary structural system.

An extensive test series was performed to identify the actual capabilities and limitations of the UB-NCS. The fidelity of the testing facility to reproduce, under controlled laboratory conditions, full-scale seismic floor motions expected in multistory buildings, and other random and harmonic motions was demonstrated. In order to achieve a satisfactory performance of the equipment, an off-line compensation procedure was developed and recommended for testing of full-scale nonstructural specimens.

A set of innovative testing protocols taking full advantage of the UB-NCS testing capabilities has been developed and proposed for experimental seismic qualification and fragility assessment of acceleration and/or displacement sensitive nonstructural components, systems and equipment. The proposed testing protocols are characterized by their simplicity, versatility and closed-form equations. The qualification protocol histories have been calibrated to impose, simultaneously, seismic hazard consistent absolute floor accelerations and interstory drifts acting on nonstructural components and contents located within multistory buildings. Moreover, the protocol histories were adjusted to impose and induce the same number of "rainflow" cycles on displacement and acceleration sensitive nonstructural components, respectively, as observed for building floor motions recorded during strong earthquake shaking. It was demonstrated that the seismic qualification testing protocol is capable of imposing seismic demands

compatible with both the ASCE 7-05 ground response spectrum and the FEMA 450 floor response spectrum at a specified normalized building height, for sites with a given seismic hazard level. Furthermore, the proposed protocol imposes peak interstory drifts compatible with the seismic hazard specified in current code provisions.

The proposed fragility testing protocol consists of a simplified version of the seismic qualification protocol. The seismic hazard was chosen consistent with an area of high seismicity in order to impose on the specimens conservative but realistic absolute floor accelerations and interstory drifts. This protocol incorporates response modification factors that amplify story drift demands to account for nonlinear building response. A quasi-static fragility testing protocol, compatible with the dynamic version of the fragility protocol, was also proposed for evaluating the seismic performance of displacement sensitive nonstructural components that are not loading rate dependent.

The proposed qualification protocol extends the current capabilities of the AC156 qualification procedure for testing of distributed nonstructural components with multiple attachment points and sensitive to both absolute floor accelerations and story drifts. Similarly, the proposed fragility testing protocol supplements the current FEMA 461 testing methodologies.

The proposed qualification testing protocol was used to successfully assess the seismic performance of a full-scale composite emergency room. Damage progression curves were generated for displacement sensitive steel studded gypsum partition walls, and seismic fragility analysis was performed for critical acceleration sensitive medical equipment. The observations from these experiments were used to characterize the dynamic interactions between nonstructural components and the medical equipment included in the experiments.

From the observations of damage progression for the gypsum partition walls, four damage states, with their respective damage measures, were identified. The damage states were defined considering the type of repair that would be required and the potential effects on the functionality of the emergency room. Moreover, the damage measures were carefully selected based on experimental observations and quantities that could be measured after the experiments. The effectiveness of a statistical parameter proposed to anticipate the interstory drift ratios triggering each damage state was demonstrated. Severe interruptions of the emergency room functionality, due to damage in the gypsum partition wall system, are expected, with a probability of 50%, at interstory drift ratios of 1.71%. Nevertheless, serviceability interruptions could be expected, with a probability of 5%, for interstory drift ratios as low as 1.02%. Total loss of the gypsum partition wall system, with a probability of 50%, is expected for an interstory drift ratio of 2.10%.

However, total loss of the gypsum partition wall system could be expected, with a probability of 5%, during earthquake events imposing interstory drift ratios as low as 1.69%.

From the experimental observations of the seismic performance of wall-mounted vital sign patient monitors, only one damage state was identified, consisting of the failure of the mounting system. The data recoded during tests was used to generate the fragility curve for the identified damage state. The resulting fragility curves indicate that a horizontal acceleration of 1.35g at the base of the monitor would have 50% probability to induce failure of the monitor's supporting system.

The test series performed with the emergency room provided important information regarding the suitability of the proposed testing protocol to impose and induce, in a controlled way, the hazard compatible seismic damage observed in nonstructural components during tests carried out using simulated building floor motions. Both qualitative and quantitative observations were considered and discussed to validate the adequacy of the damage imposed by the testing protocol. It was observed that both the protocol and simulated building floor motion histories induced failure of the monitor's supporting system at approximately the same peak horizontal accelerations measured at the base of the monitors. Moreover, the characteristics of the motion observed in freestanding equipment and the seismic interactions between nonstructural components and medical equipment were similar.

7.2   Recommendations for future research

A rigorous stochastic analysis was performed in this investigation to estimate the mean 84th percentile peak seismic demands acting on nonstructural components located within multistory buildings. Vertical components of seismic demands were not included in this analysis. Nevertheless, the same principles and methodology described here could be used to estimate the mean 84th percentile peak vertical seismic demands. Moreover, the "rainflow" counting algorithm should be applied to vertical components of recorded building floor motions to calibrate the vertical excitation sweeping rate. Finally, the functional form of the proposed testing protocols could be recalibrated for defining vertical motion histories.

The testing procedures proposed in this research, and in particular the functional closed-form protocol equations, could be adapted and recalibrated for use with conventional shake tables. Freestanding nonstructural systems and/or equipment attached to a single building level that exceed the payload capacity or frequency limits of the UB-NCS may benefit from this approach.

The theory used to develop the qualification protocol presented in this report can be further extended to generate a testing protocol suitable for assessing the effects of near fault ground motions on nonstructural components. The use of a deterministic hazard model was recommended for this approach.

SECTION 8

REFERENCES

Abramowitz, M. and I.A. Stegun (1972). <u>Handbook of Mathematical Functions with Formulas, Graphs, and mathematical Tables, 9th printing</u>. New York, Dover Publications.

Akkar, S., U. Yazgan and P. Gulkan (2005). "Drift Estimates in Frame Buildings Subjected to Near-Fault Ground Motions." <u>Journal of Structural Engineering</u> **131**(7): 1014-1024.

ASCE (1995). <u>ASCE 7-95: Minimum design loads for buildings and other structures</u>. New York, American Society of Civil Engineers.

ASCE (2005). <u>ASCE 7-2005: Minimum design loads for buildings and other structures</u>. New York, American Society of Civil Engineers.

Asfura, A. and A. Der Kiureghian (1986). "Floor response spectrum method for seismic analysis of multiple supported secondary systems." <u>Journal of Earthquake Engineering and Structural Dynamics</u> **14**: 245-265.

ASTM (1997). ASTM E1049-85 (R1997) Standard practices for cycle counting in fatigue analysis, American Society of Testing Materials.

Bachman, R.E. and R.M. Drake (1994). <u>1994 NEHRP provisions for architectural, mechanical and electrical components</u>. Proceedings 5th U.S. National conference on earthquake engineering. Earthquake Engineering Research Institute. July 10-14, Chicago, Ill.

Bachman, R.E. and R.M. Drake (1998). <u>Design force provisions for nonstructural elements and model codes</u>. Proceedings 6th U.S. National conference on earthquake engineering. Earthquake Engineering Research Institute, Seattle.

Badillo-Almaraz, H., A.S. Whittaker and A.M. Reinhorn (2007). "Seismic Fragility of Suspended Ceiling Systems." <u>Earthquake Spectra</u> **23**(1): 21-40.

Badillo-Almaraz, H., A.S. Whittaker, A.M. Reinhorn and G.P. Cimellaro (2000). Report MCEER-2006-0001: Seismic Fragility of Suspended Ceiling Systems. Buffalo, National Center for Earthquake Engineering Research. State University of New York. University at Buffalo.

Bersofsky, A. (2004). Performance Evaluation of Gypsum Wallboard Partitions. <u>Master of Science Thesis, Department of Structural Engineering</u>. San Diego, University of California, San Diego. **Master of Science:** 147.

Biggs, J.M. and J.M. Roesset (1970). <u>Seismic analysis of equipment mounted on a massive structure</u>. Cambridge, Mass.

Blasetti, A.S., R.M. Hoffman and D.W. Dinehart (2008). "Simplified Hysteretic Finite-Element Model for Wood and Viscoelastic Polymer Connections for the Dynamic Analysis of Shear Walls." <u>Journal of Structural Engineering</u> **134**(1): 77-86.

Bonneville, D.R. and R.E. Bachman (2002). <u>The evolving process of US seismic code development</u>. Proceedings 7th U.S. National conference on earthquake engineering. Earthquake Engineering Research Institute, Boston.

Boore, D. (2003a). "Simulation of ground motions using the stochastic method." <u>Pure and Applied Geophysics</u> **160**: 635-676.

Boore, D.M. (2001). "Effect of baseline corrections on displacements and response spectra for several recordings of the 1999 Chi-Chi, Taiwan, Earthquake." <u>Bulletin of the Seismological Society of America</u> **91**(5): 1199-1211.

Boore, D.M. (2003b). "Analog-to-digital conversion as a source of drifts in displacements derived from digital recordings of ground acceleration." <u>Bulletin of the Seismological Society of America</u> **35**(5): 2017-2024.

Boore, D.M. (2005). "On pads and filters: Processing strong-motion data." <u>Bulletin of the Seismological Society of America</u> **95**(2): 745-750.

Boore, D.M. and J.J. Bommer (2005). "Processing of strong-motion accelerograms: needs, options and consequences." <u>Soil Dynamics and Earthquake Engineering</u> **25**(2): 93-115.

Boroschek, R. and R. Retamales (2001). Damage Observed in the El Salvador's Public Hospital System during the January 13, 2001 Earthquake. Santiago, Chile, WHO/PAHO Collaborating Center for Disaster Mitigation in Health Facilities.

Boroschek, R. and R. Retamales (2004). <u>Guidelines for vulnerability reduction in the design of new health facilities</u>. Washington, D.C., PAHO/World Bank.

BSSC (1994). <u>FEMA 222: NEHRP Recommended provisions for seismic regulations for new buildings</u>. Washington, D.C., Building Seismic Safety Council.

BSSC (1997). <u>FEMA 303: NEHRP Recommended provisions for seismic regulations for new buildings and other structures. Part 2: Commentary</u>. Washington, D.C., Building Seismic Safety Council.

BSSC (2000). FEMA 368: NEHRP Recommended provisions for seismic regulations for new buildings and other structures. Washington, D.C., Building Seismic Safety Council. Federal Emergency Management Agency.

BSSC (2003a). FEMA 450-1: NEHRP Recommended provisions for seismic regulations for new buildings and other structures. Part 2: Provisions. Washington, D.C., Building Seismic Safety Council. Federal Emergency Management Agency.

BSSC (2003b). FEMA 450-2: NEHRP Recommended provisions for seismic regulations for new buildings and other structures. Part 2: Commentary. Washington, D.C., Building Seismic Safety Council. Federal Emergency Management Agency.

Burdisso, R.A. and M.P. Singh (1987a). "Multiply supported secondary systems, Part I: response spectrum analysis." <u>Journal of Earthquake Engineering and Structural Dynamics</u> **15**: 55-72.

Burdisso, R.A. and M.P. Singh (1987b). "Seismic analysis of multiply supported secondary systems with dynamic interaction effects." <u>Journal of Earthquake Engineering and Structural Dynamics</u> **15**: 1005-1022.

Bush, A.W. (1992). Perturbation methods for engineers and scientists. Boca Raton, CRC Press.

Cartwright, D.E. and M.S. Longuet-Higgins (1956). "The statistical distribution of the maxima of a random function." Proceedings of the Royal Society of London. Series A, Mathematical and Physical Sciences **237**(1209): 212-232.

Chandra, V., R.S. Chaudury and V. Gupta (2002). "Mode-acceleration approach to seismic response of multiply-supported secondary systems." Earthquake engineering and structural dynamics **31**: 1603-1621.

Chaudhuri, S.R. and V.K. Gupta (2003). "Mode acceleration approach for generation of floor spectra including soil-structure interaction." ISET Journal of earthquake technology **40**(2-4): 99-115.

Chaudhuri, S.R. and T.C. Hutchinson (2005). "Characterizing frictional behavior for use in predicting the seismic response of unattached equipment." Soil Dynamics and Earthquake Engineering **25**(7-10): 591-604.

Chaudhuri, S.R. and T.C. Hutchinson (2006). "Seismic damage assessment of hazardous storage glassware using experimental and numerical simulations." Proceedings 8th US National conference on earthquake engineering. April 18-21, San Francisco, California.

Chen, Y.Q. and T.T. Soong (1989). Seismic behavior and response sensitivity of secondary structural systems. Technical Report NCEER 89-0030, National Center for Earthquake Engineering Research. Buffalo, University at Buffalo. **Technical report NCEER 89-0030**.

Chock, G., I. Robertson, P. Nicholson, H. Brandes, E. Medley, P. Okubo, B. Hirshorn, J. Sumada, T. Kindred, G. Linurna, A. Sarwar, J. Dal Pino and W. Holmes (2006). Compilation of Observations of the October 15, 2006, Kiholo Bay (Mw 6.7) and Mahukona (Mw 6.0) Earthquakes, Hawai'i, Earthquake Engineering Research Institute.

Chong, W.H. and T.T. Soong (2000). Report NCEER-2000-0005: Sliding Fragility of Unrestrained Equipment in Critical Facilities. Buffalo, National Center for Earthquake Engineering Research. State University of New York. University at Buffalo.

Chopra, A.K. and R.K. Goel (2000). "Building Period Formulas for Estimating Seismic Displacements." Earthquake Spectra **16**(2): 533-536.

Chopra, A.K. and C. Chintanapakdee (2001). "Drift Spectrum vs. Modal Analysis of Structural Response to Near-Fault Ground Motions." Earthquake Spectra **17**(2): 221-234.

Clough, R. and J. Penzien (1993). Dynamics of Structures. New York, McGraw-Hill.

Coull, A. and J.R. Choudhury (1967a). "Analysis of Coupled Shear Walls." ACI Journal **Proceeding Vol 64**(N 9): 587-593.

Coull, A. and J.R. Choudhury (1967b). "Stresses and Deflections in Coupled Shear Walls." ACI Journal **Proceeding Vol 64**(N 2): 65-72.

CSA (2002). Guideline for Seismic Risk Reduction of Operational and Functional Components (OFCs) of Buildings. Standard CSA S832-01. Mississagua, Ontario, Canadian Standard Association.

Dinehart, D.W., A.S. Blasetti and H.W. Shenton (2008). "Experimental Cyclic Performance of Viscoelastic Gypsum Connections and Shear Walls." Journal of Structural Engineering **134**(1): 87-95.

Drake, R.M. and J.D. Gillengerten (1994). Examination of CDMG ground motion data in support of the 1994 NEHRP provisions. Proceedings 5th U.S. National conference on earthquake engineering. Earthquake Engineering Research Institute. July 10-14, Chicago, Ill.

Drake, R.M. and R.E. Bachman (1996). "NEHRP provisions for 1994 for nonstructural components." Journal of architectural Engineering **2**(1): 26-31.

Elishakoff, I. (1983). Probabilistic theory of structures. New York, Dover Publications.

Fathali, S. and A. Filiatrault (2008). Experimental Seismic Performance Evaluation of Isolation/Restraint Systems for Mechanical Equipment Part 2: Light Equipment Study. Technical Report MCEER-22-2007. Buffalo, NY, University at Buffalo, State University of New York**:** 174.

FEMA (1994). FEMA 74: Reducing the risk of nonstructural earthquake damage. Washington, D.C., Federal Emergency Management Agency.

FEMA (2000a). FEMA 356: Prestandard and commentary for the seismic rehabilitation of buildings. Washington, D.C., Federal Emergency Management Agency.

FEMA (2000b). FEMA 357: Global topics on the prestandard and commentary for the seismic rehabilitation of buildings, American Society of Civil Engineers. Federal Emergency Management Agency.

FEMA (2004). Installing Seismic Restraints for Electrical Equipment. Report No. FEMA 450. Washington, D.C., Federal Emergency Management Agency.

FEMA (2005). ATC-58: Interim Protocols for Seismic Performance Testing of Architectural, Mechanical and Electrical Components (Third draft), Mid-America Center for Earthquake Engineering Research, Multidisciplinary Center for Earthquake Engineering Research and Pacific Earthquake Engineering Research Center.

FEMA (2006). FEMA461: Interim protocols for determining seismic performance characteristics of structural and nonstructural components through laboratory testing, Applied Technology Council. Federal Emergency Management Agency.

Filiatrault, A. and H. Matt (2005). "Experimental Seismic Response of High-Voltage Transformer-Bushing Systems." Earthquake Spectra **21**(4): 1009-1025.

Filiatrault, A., S. Kuan and R. Tremblay (2004a). "Shake Table Testing of Bookcase-partition Wall Systems." Canadian Journal of Civil Engineering **31**(4): 664-676.

Filiatrault, A., R. Tremblay and S. Kuan (2004b). "Generation of Floor Accelerations for Seismic Testing of Operational and Functional Building Components." Canadian Journal of Civil Engineering **31**(4): 646-663.

Filiatrault, A., A. Wanitkorkul and M. Constantinou (2008). Development and Appraisal of a Numerical Cyclic Loading Protocol for Quantifying Building System Performance. Technical Report MCEER-08-0013. Buffalo, New York., University at Buffalo**:** 91.

Filiatrault, A., C.-M. Uang, B. Folz, C. Christopulos and K. Gatto (2001). Reconnaissance Report of the February 28, 2001 Nisqually (Seattle-Olympia) Earthquake. Structural Systems Research Project Report N SSRP-2000/15, Department of Structural Engineering, University California, San Diego, La Jolla, CA. **22**.

Gilani, A.S., A.S. Whittaker and G.L. Fenves (2001). "Seismic Evaluation and Retrofit of 230-kV Porcelain Transformer Bushings." Earthquake Spectra **17**(4): 597-616.

Goodwin, E., E. Maragakis and A. Itani (2004). Seismic evaluation of hospital piping systems. Proceedings 13th World conference on earthquake engineering., Vancouver, B.C., Canada.

Gupta, A.K. and J. Jing-Wen (1986a). "Coupled response spectrum analysis of secondary systems using uncoupled modal properties." Nuclear engineering and design **92**: 61-68.

Gupta, A.K. and J. Jing-Wen (1986b). "A new instructive response spectrum (IRS) method for multiply connected secondary systems with coupling effects." Nuclear engineering and design **96**: 63-80.

Gupta, I.D. and M.D. Trifunac (1998). "Defining equivalent stationary PSDF to account for nonstationarity of earthquake ground motion." Soil Dynamics and Earthquake Engineering **17**(2): 89-99.

Gupta, V. (1997). "Acceleration transfer function of secondary systems." Journal of engineering mechanics **123**(7): 678-685.

Hadidi-Tamjed, H. (1987). Statistical Response of Inelastic SDOF Systems Subjected to Earthquakes. PhD Dissertation, Department of Civil Engineering Stanford, Stanford University.

Halldorsson, B. (2004). The specific barrier model: Its calibration to earthquakes of different tectonic regions and the synthesis of strong ground motions for earthquake engineering applications. Department of Civil, Structural and Environmental Engineering. Buffalo, State University of New York at Buffalo. **Doctor of Philosophy:** 415.

Halldorsson, B. and A.S. Papageorgiou (2005). "Calibration of the Specific Barrier Model to Earthquakes of Different Tectonic Regions." Bulletin of the Seismological Society of America **95**(4): 1276-1300.

Harris, C., Ed. (2001). Shock and Vibration Handbook. New York, McGraw-Hill Professional.

Heidebrecht, A.C. and B. Stafford-Smith (1973). "Approximate analysis of tall wall-frame structures." ASCE Journal of Structural Engineering **99**(2): 199-221.

Herrmann, R.B. (1985). "An extension of random vibration theory estimates of strong ground motion to large distances." Bulletin of the Seismological Society of America **75**(5): 1447-1453.

Holmes, M. (1995). Introduction to perturbation methods. New York, Springer-Verlag.

Hutchinson, T.C. and S.R. Chaudhuri (2006). "Simplified Expression for Seismic Fragility Estimation of Sliding-Dominated Equipment and Contents." Earthquake Spectra **22**(3): 709-732.

Hutchinson, T.C., S.R. Chaudhuri, F. Kuester and S. Auduong (2005). "Light-Based Motion Tracking of Equipment Subjected to Earthquake Motions." Journal of Computing in Civil Engineering **19**(3): 292-303.

ICBO (1994). <u>Uniform building code</u>. Whittier, CA, International Conference of Building Officials.

ICBO (1997). <u>Uniform building code</u>. Whittier, CA, International Conference of Building Officials.

ICC-ES (2007). AC156: Acceptance criteria for seismic qualification by shake-table testing of nonstructural components and systems, International Code Council Evaluation Service.

ICC (2003). <u>International Building Code</u>. Whittier, CA, International Code Council.

ICC (2006). <u>International Building Code</u>. Whittier, CA, International Code Council.

IEEE (2006). <u>IEEE Recommended Practice for Seismic Design of Substations. IEEE Std 693</u>, Institute of Electrical and Electronic Engineers.

Iwan, W.D. (1997). "Drift spectrum: Measure on demand for earthquake ground motions." <u>Journal of structural engineering</u> **123**(4): 397-404.

Kanvinde, A.M. and G.G. Deierlein (2006). "Analytical Models for the Seismic Performance of Gypsum Drywall Partitions." <u>Earthquake Spectra</u> **22**(2): 391-411.

Keller, D. and G. Mosqueda (2005). <u>Nonstructural Component Simulator: Specimen Design and Preliminary Study of Damage Mechanisms</u>. 2005 Earthquake Engineering Symposium for Young Researchers, Peppermill Hotel - Reno, Nevada.

Kesti, J. (2000). Local and Distortional Buckling of Perforated Steel Wall Studs. <u>Dissertation for the degree of Doctor of Science in Technology, Department of Civil and Environmental Engineering</u>. Helsinki, Helsinki University of Technology**:** 101.

Kim, J. and K.R. Collins (2002). "Closer Look at the Drift Demand Spectrum." <u>Journal of Structural Engineering</u> **128**(7): 942-945.

Kim, J., K.R. Collins and Y.-M. Lim (2006). "Application of Internally Damped Shearbeam Model to Analysis of Buildings under Earthquakes: Robust Procedure for Quick Evaluation of Seismic Performance." <u>Journal of Structural Engineering</u> **132**(7): 1139-1149.

Konstantinidis, D. and N. Makris (2006). "Experimental and analytical studies on the seismic response of freestanding and restrained laboratory equipment." <u>Proceedings 8th US National conference on earthquake engineering. April 18-21, San Francisco, California</u>.

Kramer, S.L. (1996). <u>Geotechnical earthquake engineering</u>, Pearson Education.

Krawinkler, H. (1992). ATC-24: Guidelines for Cyclic Seismic Testing of Components of Steel Structures. Redwood City, Report prepared for the Applied Technology Council.

Krawinkler, H., F. Parisi, L. Ibarra, A. Ayoub and R. Medina (2000). CUREE-Caltech Woodframe Project Publication W-02: Development of a testing protocol for wood frame structures. Palo Alto, California, Consortium of Universities for Research in Earthquake Engineering.

Lang, A.F. (2007). Seismic Performance Evaluation of Gypsum Wallboard Partitions. San Diego, Thesis Master of Science in Structural Engineering. University of California, San Diego. **Master of Science:** 136.

Lang, A.F. and J.I. Restrepo (2006). <u>Seismic performance evaluation of gypsum wallboard partitions</u>. Proceedings 8th US National conference on earthquake engineering, San Francisco, California.

Lavelle, F.M., L.A. Bergman and P.D. Spanos (1988). "Seismic floor response spectra for a combined system by Green's function." <u>National Center for Earthquake Engineering Research</u> **Technical report NCEER 88-0011**.

Lee, T.-H., M. Kato, T. Matsumiya, K. Suita and M. Nakashima (2007). "Seismic performance evaluation of non-structural components: drywall partitions." <u>Earthquake Engineering & Structural Dynamics</u> **36**(3): 367-382.

Lin, Y.K. and R. Minai (1987). <u>Lecture notes in engineering</u>. U.S.-Japan Joint seminar on stochastic approaches in earthquake engineering, Boca Raton, Florida, USA.

Lopez Garcia, D. and T.T. Soong (2003). "Sliding fragility of block-type non-structural components. Part 1: Unrestrained components." <u>Earthquake Engineering & Structural Dynamics</u> **32**(1): 111-129.

Makris, N. and Y. Roussos (1998). PEER Report 1998-05: Rocking response and overturning of equipment under horizontal pulse-type motions. Berkeley, Pacific Earthquake Engineering Research Center. College of Engineering. University of California, Berkeley.

Makris, N. and D. Konstantinidis (2003). "The rocking spectrum and the limitations of practical design methodologies." <u>Earthquake Engineering & Structural Dynamics</u> **32**(2): 265-289.

McGavin, G. and H. Patrucco (1994). Survey of Non Structural Damage to Healthcare Facilities in the January 17, 1994, Northridge Earthquake. Ontario, CA, HMC Group.

McMullin, K.M. and D. Merrick (2002). CUREE-Caltech Woodframe Project Publication W-15: Seismic performance of gypsum walls: experimental test program, Consortium of Universities for Research in Earthquake Engineering.

Medina, R.A., R. Sankaranarayanan and K.M. Kingston (2006). "Floor response spectra for light components mounted on regular moment-resisting frame structures." <u>Engineering Structures</u> **In Press, Corrected Proof**.

Melnikov, Y.A. (1995). <u>Green's functions in applied mechanics</u>. Boston, Computational Mechanics Publications.

Memari, A.M., P.A. Kremer and R.A. Behr (2006). "Architectural Glass Panels with Rounded Corners to Mitigate Earthquake Damage." <u>Earthquake Spectra</u> **22**(1): 129-150.

Miranda, E. (1999). "Approximate seismic lateral deformation demands in multistory buildings." <u>ASCE Journal of structural engineering</u> **125**(4): 417-425.

Miranda, E. (2006). "Use of probability-based measures for automated damage assessment." <u>The Structural Design of Tall and Special Buildings</u> **15**(1): 35-50.

Miranda, E. and C. Reyes (2002). "Approximate lateral drift demands in multistory buildings with nonuniform stiffness." <u>ASCE Journal of structural engineering</u> **128**(7): 840-849.

Miranda, E. and S. Taghavi (2005). "Approximate floor acceleration demands in multistory buildings. I: Formulation." <u>ASCE Journal of structural engineering</u> **131**(2): 203-211.

Miranda, E. and S.D. Akkar (2006). "Generalized Interstory Drift Spectrum." <u>ASCE Journal of Structural Engineering</u> **132**(6): 840-852.

MTS (2005). <u>Model 793.00 System Software. Volume 1. Introduction Station Manager. User Information and Software Reference</u>. Eden Prairie, MN, MTS Systems Corporation.

Myrtle, R.C., S.F. Masri, R.L. Nigbor and J.P. Caffrey (2005). "Classification and Prioritization of Essential Systems in Hospitals under Extreme Events." <u>Earthquake Spectra</u> **21**(3): 779-802.

Naeim, F., H. Lee, H. Bhatia, S. Hagie and K. Skliros (2005). CSMIP-3DV Technical Manual, John A. Marin & Associated, Inc.

Nastase, D., T.C. Hutchinson, F. Kuester and K. Doerr (2006). <u>Response of nonstructural elements and systems during full-scale building vibration tests</u>. Proceedings 8th US National conference on earthquake engineering San Francisco, California.

Newmark, N.M. and W.J. Hall (1982). Earthquake Spectra and Design. El Cerrito, California, Earthquake Engineering Research Institute.

Nicholson, J.W. and L.A. Bergman (1986). "Free vibration of combined dynamical systems." <u>Journal of engineering mechanics</u> **112**(1): 1-14.

Overend, M., G.A.R. Parke and D. Buhagiar (2007). "Predicting Failure in Glass: A General Crack Growth Model." <u>Journal of Structural Engineering</u> **133**(8): 1146-1155.

Papageorgiou, A.S. and K. Aki (1983a). "A specific barrier model for the quantitative description of inhomogeneous faulting and the prediction of strong ground motion. Part II. Applications of the model." <u>Bulletin of the Seismological Society of America</u> **73**(4): 953-978.

Papageorgiou, A.S. and K. Aki (1983b). "A specific barrier model for the quantitative description of inhomogeneous faulting and the prediction of strong ground motion. I. Description of the model." <u>Bulletin of the Seismological Society of America</u> **73**(3): 693-722.

Papageorgiou, A.S. and K. Aki (1984). "Erratum." <u>Bulletin of the Seismological Society of America</u> **74**(2): 794-795.

Porter, K.A., Kennedy, R.P. and R.E. Bachman (2006). Developing Fragility Functions for Building Components. A Report to ATC-58. Redwood City, CA., Applied Technology Council.

Reinhorn, A.M., M.V. Sivaselvan, Z. Liang and X. Shao (2004). <u>Real-Time Dynamic Hybrid Testing of Structural Systems</u>. 13th World Conference in Earthquake Engineering, Vancouver, B.C., Canada.

Reinoso, E. and E. Miranda (2005). "Estimation of floor acceleration demands in high-rise buildings during earthquakes." <u>The Structural Design of Tall and Special Buildings</u> **14**(2): 107-130.

Restrepo, J.I. and A.F. Lang (2005). Interim report to PEER advisory board. Year 7: Performance evaluation of gypsum wallboard partitions. Results of test 1. San Diego, Department of Structural Engineering. University of California, San Diego.

Roach, G.F. (1982). <u>Green's functions</u>. Cambridge, Cambridge University Press.

Rodriguez, M.E., J.I. Restrepo and A.J. Carr (2002). "Earthquake-induced floor horizontal accelerations in buildings." Earthquake engineering and structural dynamics **31**: 693-718.

Sackman, J.L. and J.M. Kelly (1979). "Seismic analysis of internal equipment and component in structures." Engineering Structures **1**(4): 179-190.

Sewell, R.T., C.A. Cornell, G.R. Toro and R.K. McGuire (1986). Report No 82: A study of factors influencing floor response spectra in nonlinear multi-degree-of-freedom structures. Stanford, California, The John A. Blume Earthquake Engineering Center. Department of Civil and Environmental Engineering. Stanford University.

Shakal, A.F., M.J. Huang, M.J. Huang, R.B. Darragh, A.G. Brady, M.D. Trifunac, C.E. Lindvall, D.J. Wald, T.H. Heaton and J.J. Mori (1995). "Recorded ground and structure motions." Earthquake Spectra **11**(S2): 13-96.

Singh, M. (1976). "Generation of seismic floor spectra." Journal of the engineering mechanics division **101**(EM5): 593-607.

Singh, M.P. and L.E. Suarez (1986). "Perturbation analysis of structure-equipment system." Nuclear engineering and design **97**(2): 167-186.

Singh, M.P. and R.A. Burdisso (1987). "Multiply supported secondary systems, Part I: seismic inputs." Journal of Earthquake Engineering and Structural Dynamics **15**: 73-90.

Singh, M.P. and L.E. Suarez (1988). "A method for dynamic coupling with nonclassical damping effect." Journal of Sound and Vibration **22**(1).

Soong, T.T. (1981). Probabilistic Modeling and Analysis in Science and Engineering. New York, John Wiley & Sons.

Soong, T.T. and M. Grigoriu (1993a). Random vibration of mechanical and structural systems. New York, PTR Prentice Hall.

Soong, T.T., Chen, G., Wu, Z., Zhang, R-H. and M. Grigoriu (1993b). Assessment of the 1991 NEHRP provisions for nonstructural components and recommended revisions. Technical Report NCEER 93-00003. Buffalo, National Center for Earthquake Engineering Research, University at Buffalo. **Technical report NCEER 93-0003**.

SSMA (2001). Product Technical Information. ICBO ER-4943P, Steel Stud Manufacturers Association.

Stafford-Smith, B. and A. Coull (1991). Tall building structures: Analysis and design. New York.

Stakgold, I. (1998). Green's functions and boundary value problems, John Wiley & Sons Inc.

Stewart, G.W. (1990). Matrix perturbation theory. Boston, Academic Press.

Suarez, L.E. and M.P. Singh (1987). "Perturbed complex eigenproperties of classically damped primary structure and equipment by a perturbation approach." Journal of Sound and Vibration **116**(2).

Taghavi, S. and E. Miranda (2003). PEER Report 2003/05: Response assessment of nonstructural building elements. Berkeley, Pacific Earthquake Engineering Research Center. College of Engineering. University of California, Berkeley.

Taghavi, S. and E. Miranda (2005). "Approximate floor acceleration demands in multistory buildings. II: Applications." ASCE Journal of structural engineering **131**(2): 212-220.

Taghavi, S. and E. Miranda (2006). "Seismic demand assessment on acceleration-sensitive building nonstructural components." Proceedings 8th US National conference on earthquake engineering. April 18-21, San Francisco, California.

Uang, C.-M. (1991). "Establishing R (or Rw) and Cd Factors for Building Seismic Provisions." Journal of Structural Engineering **117**(1): 19-28.

Villaverde, R. (1997a). "Method to improve seismic provisions for nonstructural components in buildings." Journal of structural engineering **123**(4): 432-439.

Villaverde, R. (1997b). "Seismic design of secondary structures: State of the art." Journal of structural engineering **123**(8): 1011-1019.

Villaverde, R. (2004). Seismic Analysis and Design of Nonstructural Elements. Earthquake Engineering: From Engineering Seismology to Performance Based Engineering. Y. Bozorgnia and V. Bertero. Boca Raton, CRC Press LLC.

Villaverde, R. (2006). "Simple method to estimate the seismic nonlinear response of nonstructural components in buildings." Engineering Structures **28**(8): 1209-1221.

Wang, Y.P., A.M. Reinhorn and T.T. Soong (1992). "Development of Design Spectra for Actively Controlled Wall-Frame Buildings." Journal of Engineering Mechanics **118**(6): 1201-1220.

Wanitkorkul, A. and A. Filiatrault (2005). Report MCEER 05-0005: Simulation of strong ground motions for seismic fragility evaluation of nonstructural components in hospitals, Multidisciplinary Center for Earthquake Engineering Research. State University of New York. University at Buffalo.

Weggel, D.C., B.J. Zapata and M.J. Kiefer (2007). "Properties and Dynamic Behavior of Glass Curtain Walls with Split Screw Spline Mullions." Journal of Structural Engineering **133**(10): 1415-1425.

Whittaker, A.S. and T.T. Soong (2001). An overview of nonstructural components research at three US earthquake engineering research centers. Proceedings of seminar on seismic design, performance and retrofit of nonstructural components in critical facilities, Applied Technology Council.

Whittaker, A.S., G.L. Fenves and A.S.J. Gilani (2004). "Earthquake Performance of Porcelain Transformer Bushings." Earthquake Spectra **20**(1): 205-223.

Wilcoski, J., J.B. Gambill and S.J. Smith (1997). The CERL Equipment fragility and protection procedure (CEFAPP), USACERL Technical report 97/58. Champaign, Illinois, U.S. Army Corps of Engineers.

Yuan, T. and A.S. Whittaker (2002). MCEER demonstration hospitals: Mathematical models and preliminary analysis results. Buffalo, Department of Civil, Structural and Environmental Engineering. University at Buffalo.

Zhang, J. and N. Makris (2001). "Rocking Response of Free-Standing Blocks under Cycloidal Pulses." Journal of Engineering Mechanics **127**(5): 473-483.

APPENDIX A. UB-NCS DRAWINGS

Steel base plates 30x30x1"
in corner bays (top and bottom)

Removable Beam
Removable Beam
Removable Beam
Removable Beam

DET 2 (TYP) DET 1 (TYP)

Holes 1 3/8" (TYP)

HSS8x6x1/2" (TYP)

DET 3 (TYP)

DET 6 (TYP) DET 4 (TYP)

DET 5 (TYP)

24   24   24   24   24   24

6 12 6 6 12 6 6 12 12 12 6 6 12 6 6 12 6
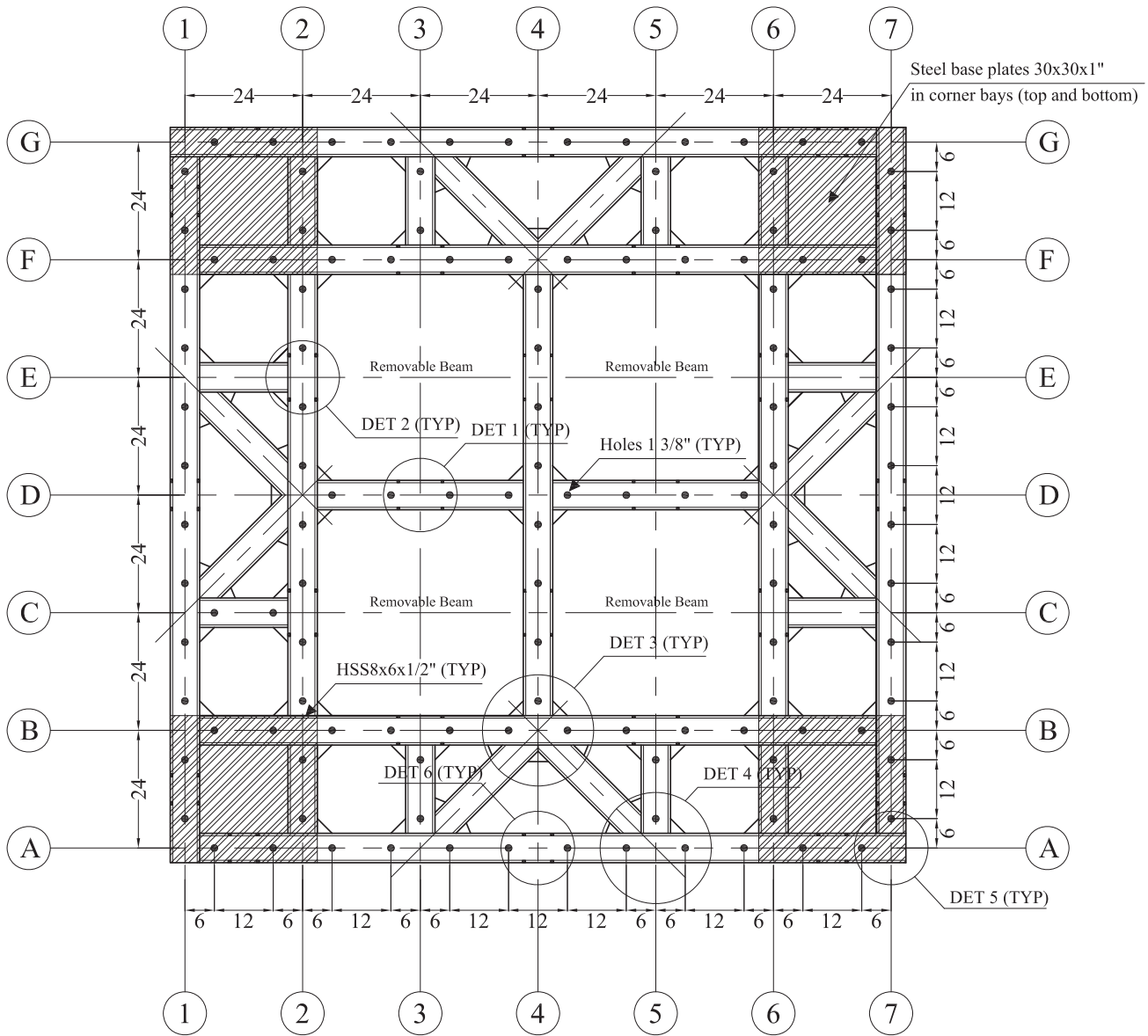
Plan View Platform EL 148.00 & EL 316.00
Scale: 1:30

University at Buffalo		DRAWING N°:
PROJECT: Platform Design	CONTENT: Platform Plan View	1
BY: Rodrigo Retamales	REV: 06/01/2008	DATE: 04/27/2005
		SCALE: Indicated

Figure A.1. Platform plan view

Figure A.2. Elevation frame

Text labels visible in the figure:

12'-6"

HSS8x6x1/2" (TYP)

EL 316.00

8"

Stopper (TYP)

14'

HSS8x8x1/2" (TYP)

26'-5"

Steel base plates 9x9x1 3/4"

Steel plates 14x14x1 1/2"

Steel base plates 30x30x1"

HSS8x6x1/2" (TYP)

EL 148.00

8"

12'

HSS8x8x1/2" (TYP)

MTS Swivel
Model 249.23

Plate Connection Column to Floor
56x32x1"

EL 000.00

10'
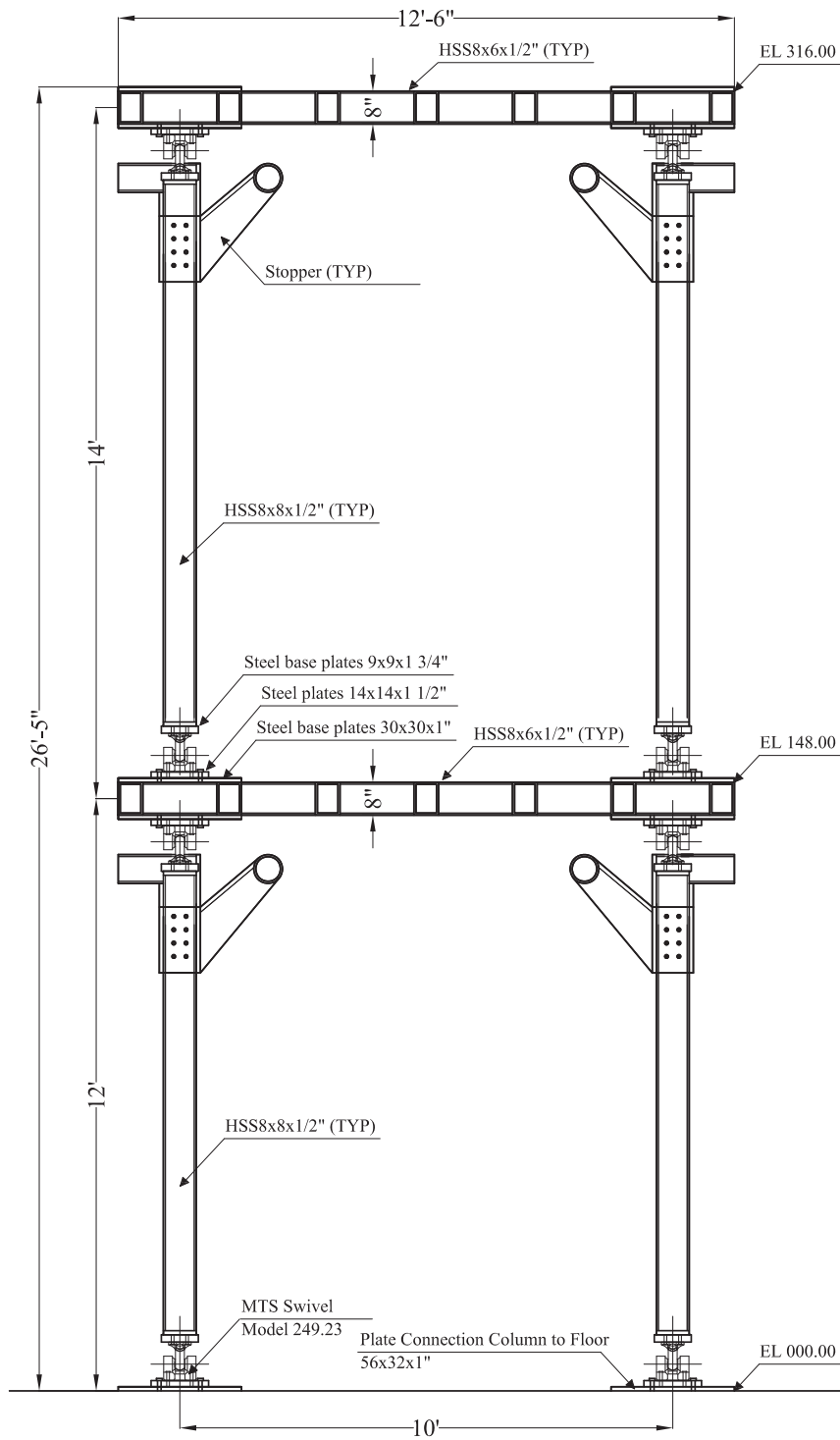
Elevation Frame

Scale: 1:40

Title block:

University at Buffalo

PROJECT: Platform Design

CONTENT: Elevation Frame

BY: Rodrigo Retamales

DATE: 05/23/2005

REV: 06/01/2008

DRAWING Nº: 2

SCALE: Indicated

Detail 1 (TYP)
Scale: 1:10

- 2 Holes for Bolts 5/8"
- (ASTM A325)
- Holes 1 3/8" (TYP)
- 2 Holes for Bolts 5/8"
- (ASTM A325)
- HSS8x6x1/2" (TYP)

Detail 2 (TYP)
Scale: 1:10

- 2 Holes for Bolts 5/8"
- (ASTM A325)
- HSS8x6x1/2" (TYP)
- Holes 1 3/8" (TYP)
- Steel stiffeners 3x3x1" (TYP)

University at Buffalo

PROJECT: Platform Design	CONTENT: Details 1 & 2	DRAWING Nº: 3
BY: Rodrigo Retamales	REV: 06/01/2008	DATE: 04/27/2005	SCALE: Indicated

Figure A.3. Details 1 & 2
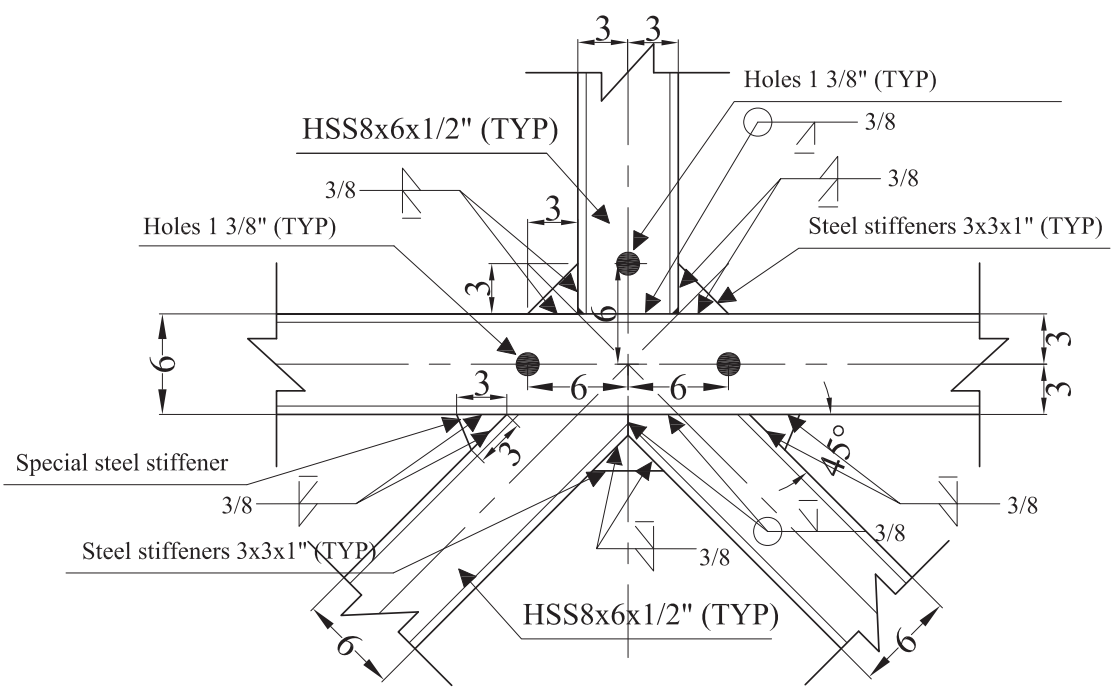
Detail 3 (TYP)
Scale: 1:10
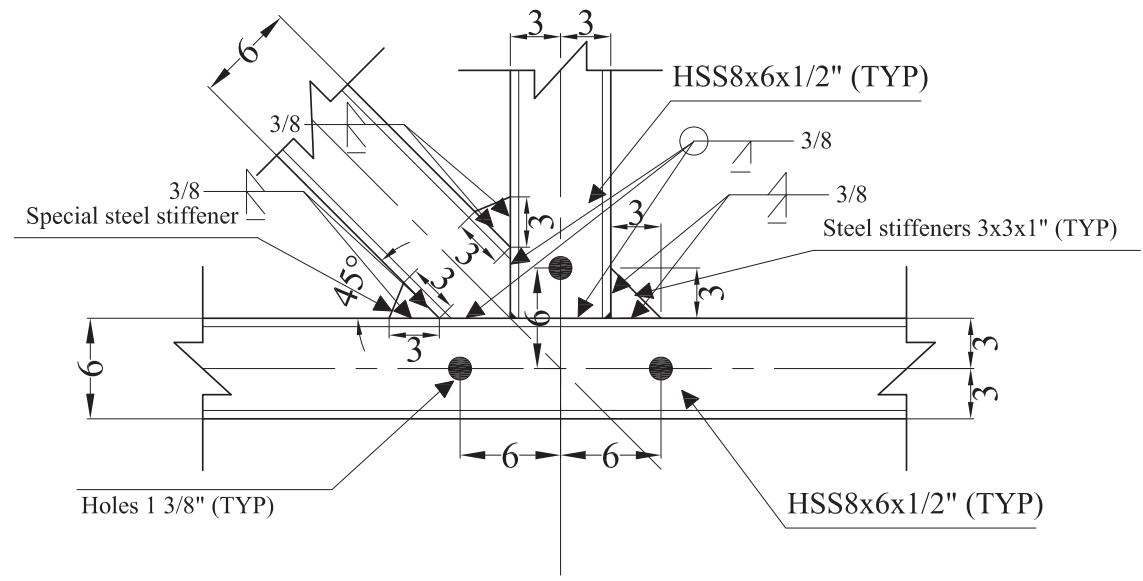
Detail 4 (TYP)
Scale: 1:10

Figure A.4. Details 3 & 4

University at Buffalo

DRAWING N°: 4

SCALE: Indicated

CONTENT: Details 3 & 4

DATE: 04/27/2005

PROJECT: Platform Design

REV: 06/01/2008

BY: Rodrigo Retamales

Figure A.5. Detail 5

The technical drawing contains the following labels and annotations:

- HSS8x6x1/2" (TYP)
- Steel base plates 30x30x1" in all corner bays (top and bottom)
- 4 Holes for Bolts 5/8-11 Grade SAE 8 (According to Swivel Fabricator Specification)
- Holes 1 3/8" (TYP)
- Steel stiffeners 3x3x1" (TYP)

Dimensions: 3, 3, 6, 6, 3.125, 5.750, 3.125, 3/8

Detail 5 (TYP)
Scale: 1:10

Detail 6 (TYP)

Scale: 1:10

HSS8x6x1/2" (TYP)

3/8

Special steel stiffener

Special steel stiffener

Steel stiffeners 3x3x1" (TYP)

HSS8x6x1/2" (TYP)

Holes 1 3/8" (TYP)

4 Holes for Bolts 5/8-11 Grade SAE 8
(According to Swivel Fabricator Specification)

Figure A.6. Detail 6

View A-A
Section HSS8x6x1/2" (TYP)
Scale: 1:8

View B-B
Section HSS8x6x1/2" (TYP)
Scale: 1:8

View C-C
Section HSS8x6x1/2" (TYP)
Scale: 1:8

View D-D
Section HSS8x6x1/2" (TYP)
Scale: 1:8

View E-E
Section HSS8x6x1/2" (TYP)
Scale: 1:8

Holes 1 3/8" (TYP)
Removable walking mesh (t=1")
(in all bays)
Steel stiffeners 3x3x1" (TYP)
Holes for Bolts 5/8"
(ASTM A325)
4 Holes for Bolts 5/8-11 Grade SAE 8
(According to Swivel Fabricator Specification)
Steel base plate 30x30x1"
in all corner bays

University at Buffalo

		DRAWING Nº:
PROJECT:	CONTENT:	7
Platform Design	Detail Views A-A, B-B, C-C, D-D & E-E	
BY:	REV:	DATE:	SCALE:
Rodrigo Retamales	06/01/2008	04/27/2005	Indicated

Figure A.7. Detail views A-A, B-B, C-C, D-D & E-E

282

Removable Beam Section HSS7x5x1/2" (TYP)

Top View Removable Beam (TYP)
Scale: 1:10

View F-F
Scale: 1:8

View G-G
Scale: 1:8

	University at Buffalo	DRAWING Nº:
		8
PROJECT:	CONTENT:	SCALE:
Platform Design	Removable Beam	Indicated
BY:	REV:	DATE:
Rodrigo Retamales	06/01/2008	04/27/2005
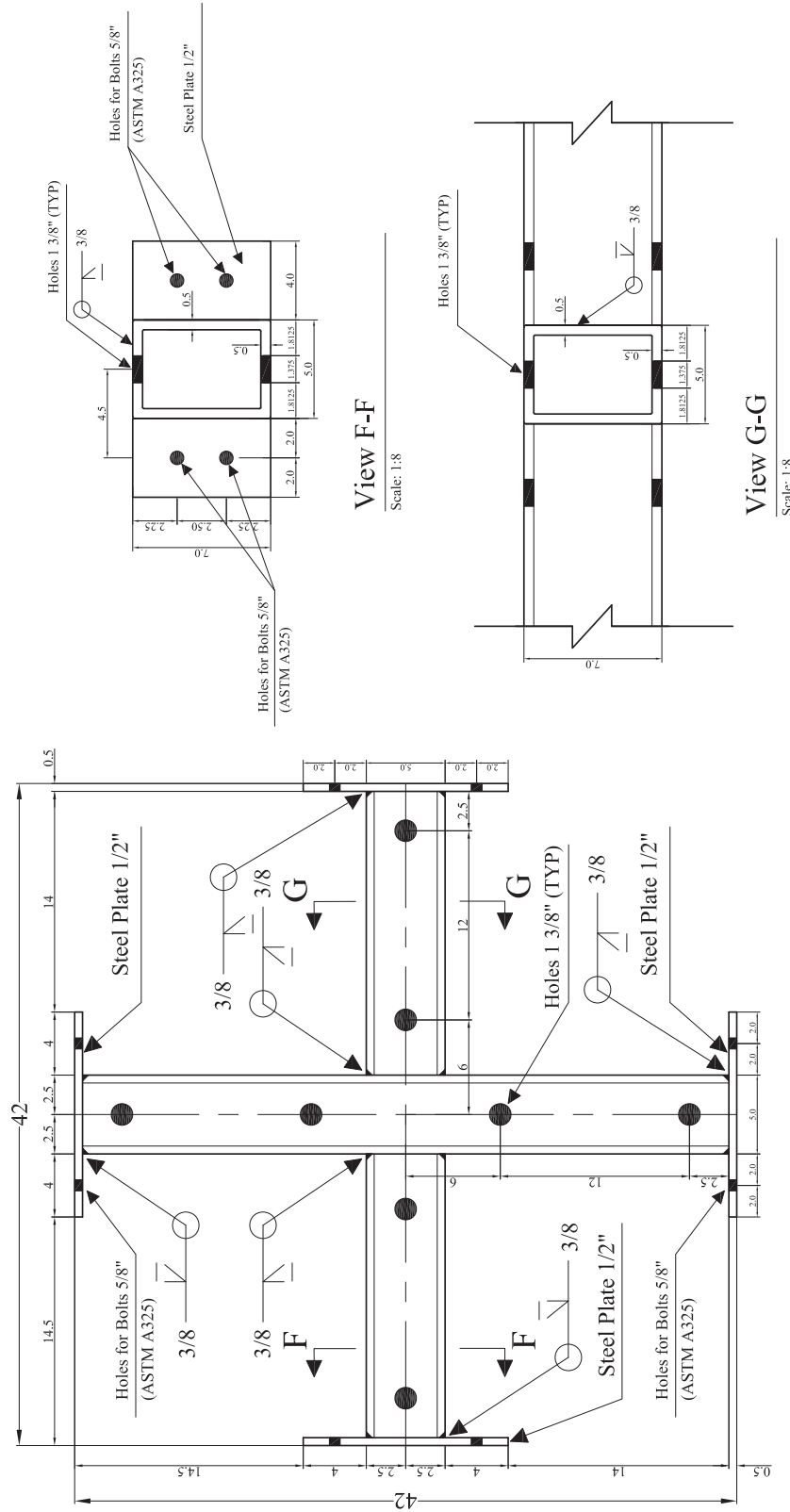
Figure A.8. Removable beam

283

Swivel MTS 249.23
Approximated Geometry (except as indicated)
Scale: 1:8

Swivel to Platform Connection
Scale: 1:10
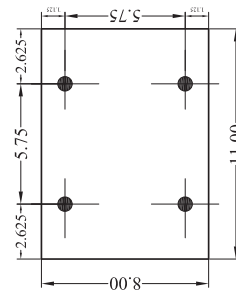
Detail Steel Plate 11x8x1"
For Swivels - Platform connections
Scale: 1:8

4 Holes for Bolts 5/8-11 Grade SAE 8
(According to Swivel Fabricator Specification)

Steel Plate 11x8x1"

Steel Plate 11x8x1"

University at Buffalo

PROJECT: Platform Design

CONTENT: Actuator swivel - Platform Connection

BY: Rodrigo Retamales

REV: 06/01/2008

DATE: 04/27/2005

DRAWING N°: 9

SCALE: Indicated

Figure A.9. Actuator swivel platform connection
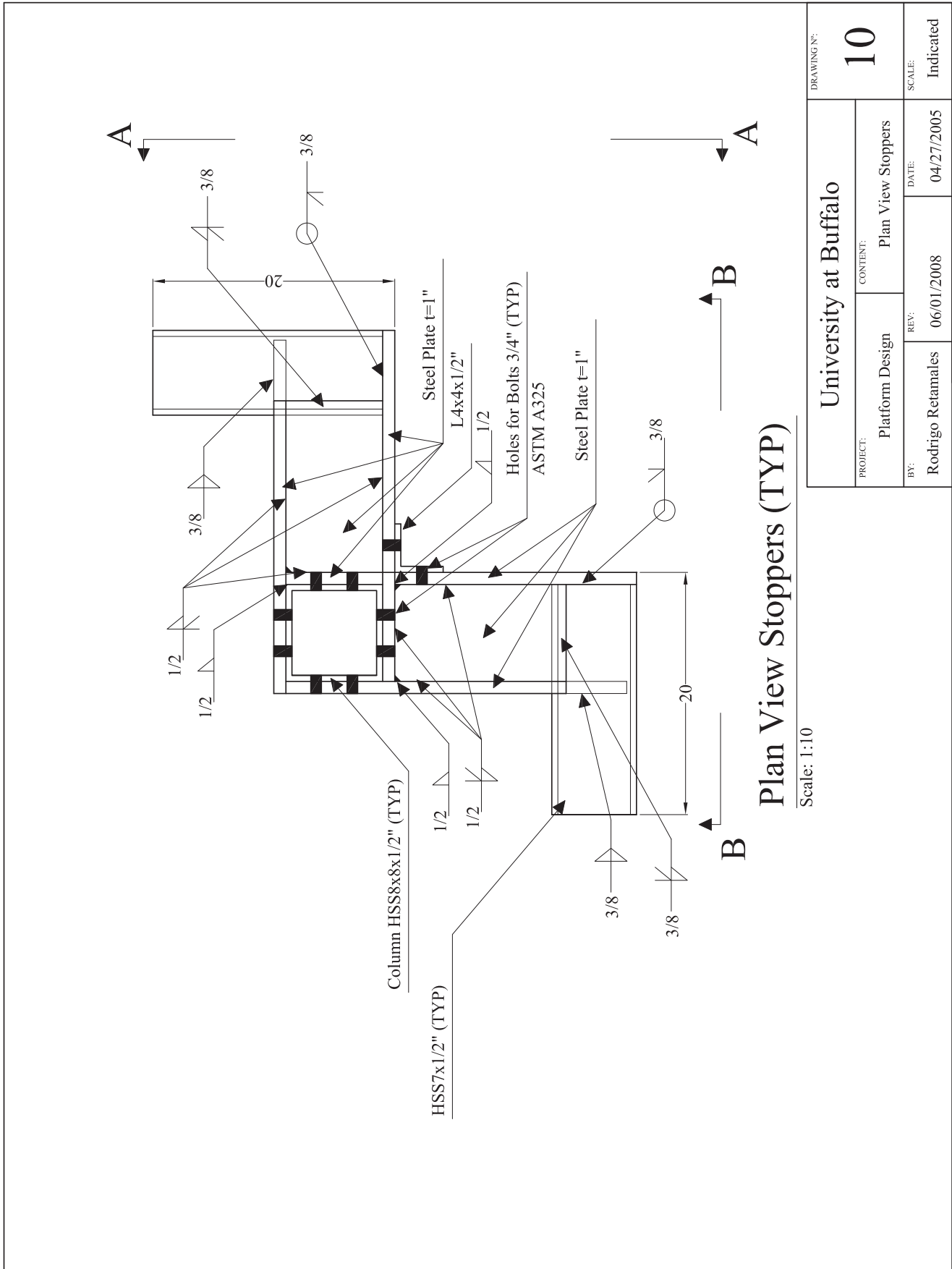
Figure A.10. Plan view stoppers

Labels visible in the figure:

- DRAWING N°: 10
- SCALE: Indicated
- University at Buffalo
- CONTENT: Plan View Stoppers
- PROJECT: Platform Design
- DATE: 04/27/2005
- BY: Rodrigo Retamales
- REV: 06/01/2008
- Plan View Stoppers (TYP)
- Plan View Stoppers
- Scale: 1:10
- Steel Plate t=1"
- L4x4x1/2"
- Holes for Bolts 3/4" (TYP)
- ASTM A325
- Steel Plate t=1"
- Column HSS8x8x1/2" (TYP)
- HSS7x1/2" (TYP)
- 20
- 3/8
- 1/2
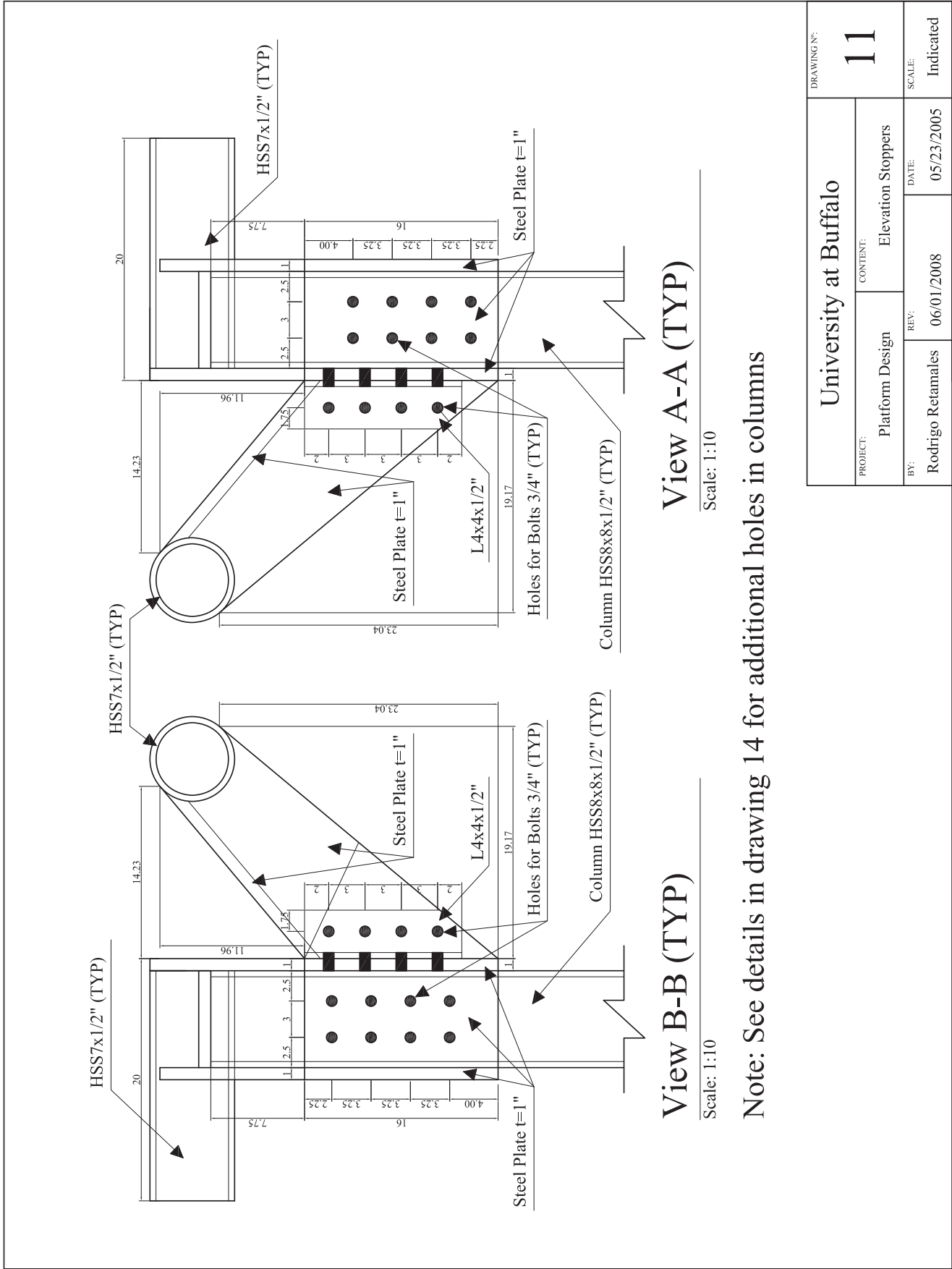
Figure A.11. Elevation stoppers
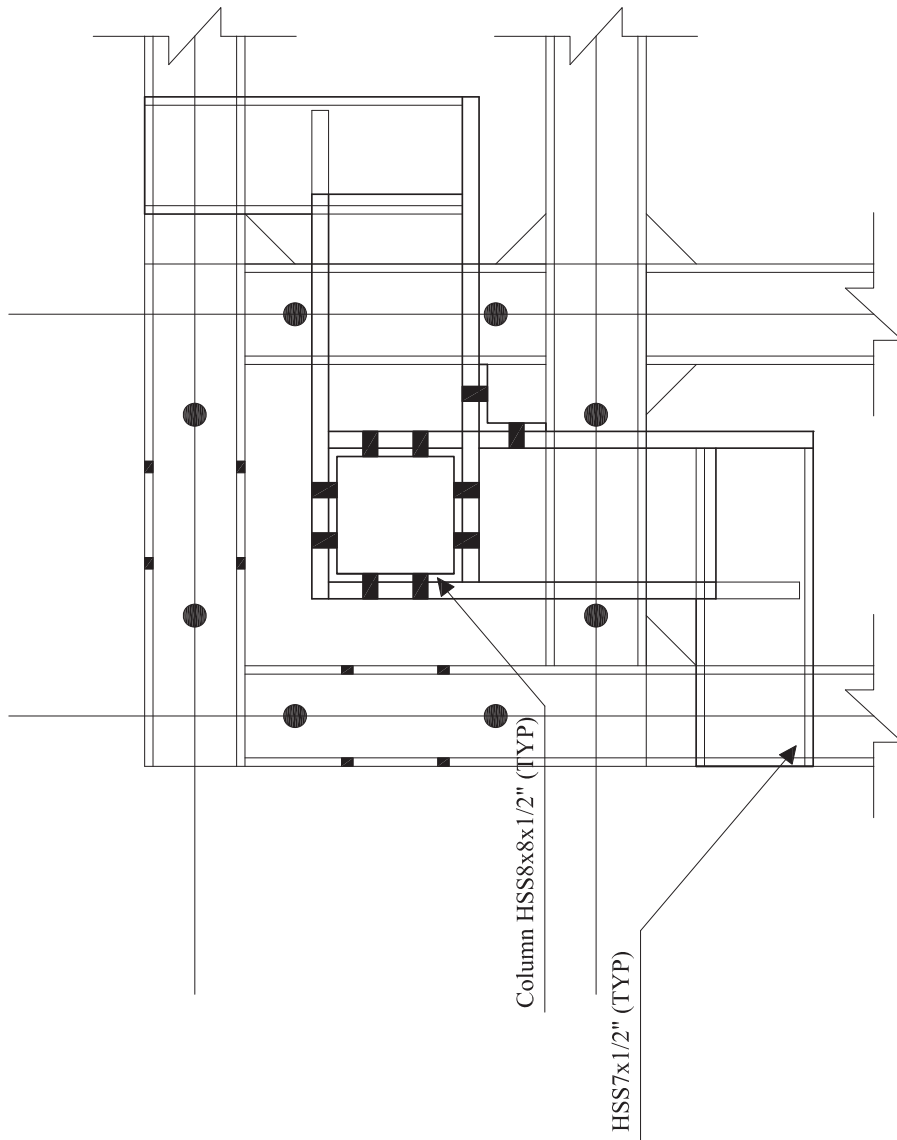
Interaction Stopper-Platform

Scale: 1:10

Column HSS8x8x1/2" (TYP)

HSS7x1/2" (TYP)

University at Buffalo

PROJECT:	CONTENT:		DRAWING N°:
Platform Design	Interaction Stopper-Platform		12
BY:	REV:	DATE:	SCALE:
Rodrigo Retamales	06/01/2008	04/27/2005	Indicated

Figure A.12. Interaction platform-stoppers

Detail Swivel Connection
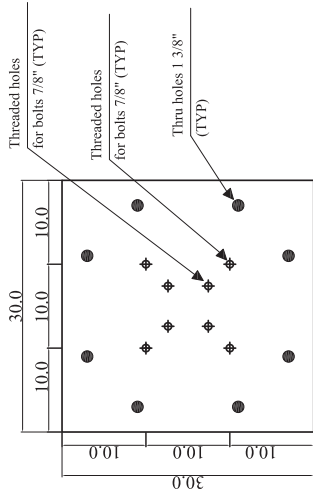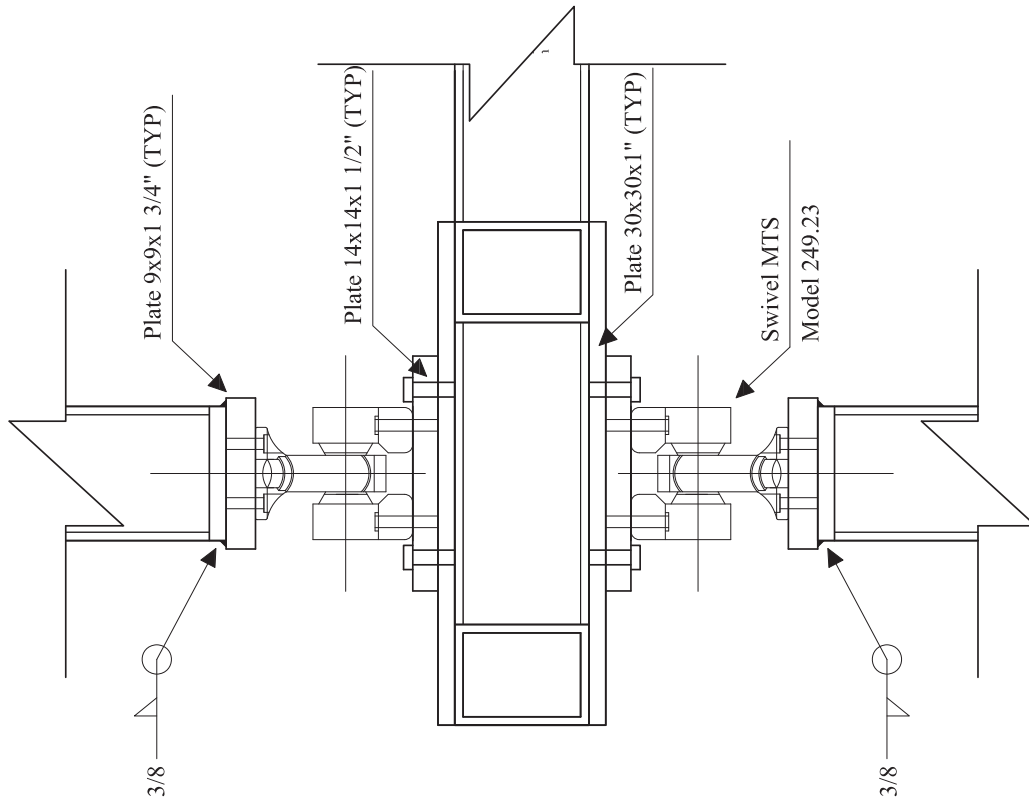
Scale: 1:10

Detail holes in Steel Plates 30x30x1" (TYP)
Scale: 1:20

Threaded holes for bolts 7/8" (TYP)

Threaded holes for bolts 7/8" (TYP)

Thru holes 1 3/8" (TYP)

30.0
10.0 10.0 10.0

30.0
10.0 10.0 10.0

Detail Plate 9x9x1 3/4"
Connection Swivel to columns (TYP) (16 Units)
Scale: 1:20

Threaded holes for Bolts 5/8-11 (TYP)

9.00

2.73 3.54 2.73
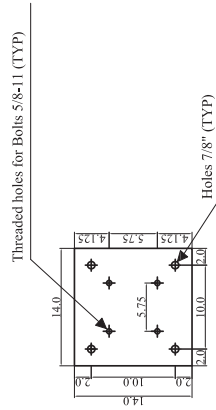
Detail Plate 14x14x1 1/2"
Connection Swivel to base plates (TYP) (16 Units)
Scale: 1:20

Threaded holes for Bolts 5/8-11 (TYP)

Holes 7/8" (TYP)

14.0
2.0 10.0 2.0

14.0
2.0 10.0 2.0

4.125 5.75 4.125

5.75

Plate 9x9x1 3/4" (TYP)

Plate 14x14x1 1/2" (TYP)

Plate 30x30x1" (TYP)

Swivel MTS Model 249.23

3/8

3/8

DRAWING Nº:					13

University at Buffalo			
CONTENT:	Detail Swivel Connection & Connection Plates		
PROJECT:	Platform Design		
BY:	Rodrigo Retamales	REV: 06/01/2008	DATE: 04/27/2005
			SCALE: Indicated

Figure A.13. Detail swivel connection & connection plates

288
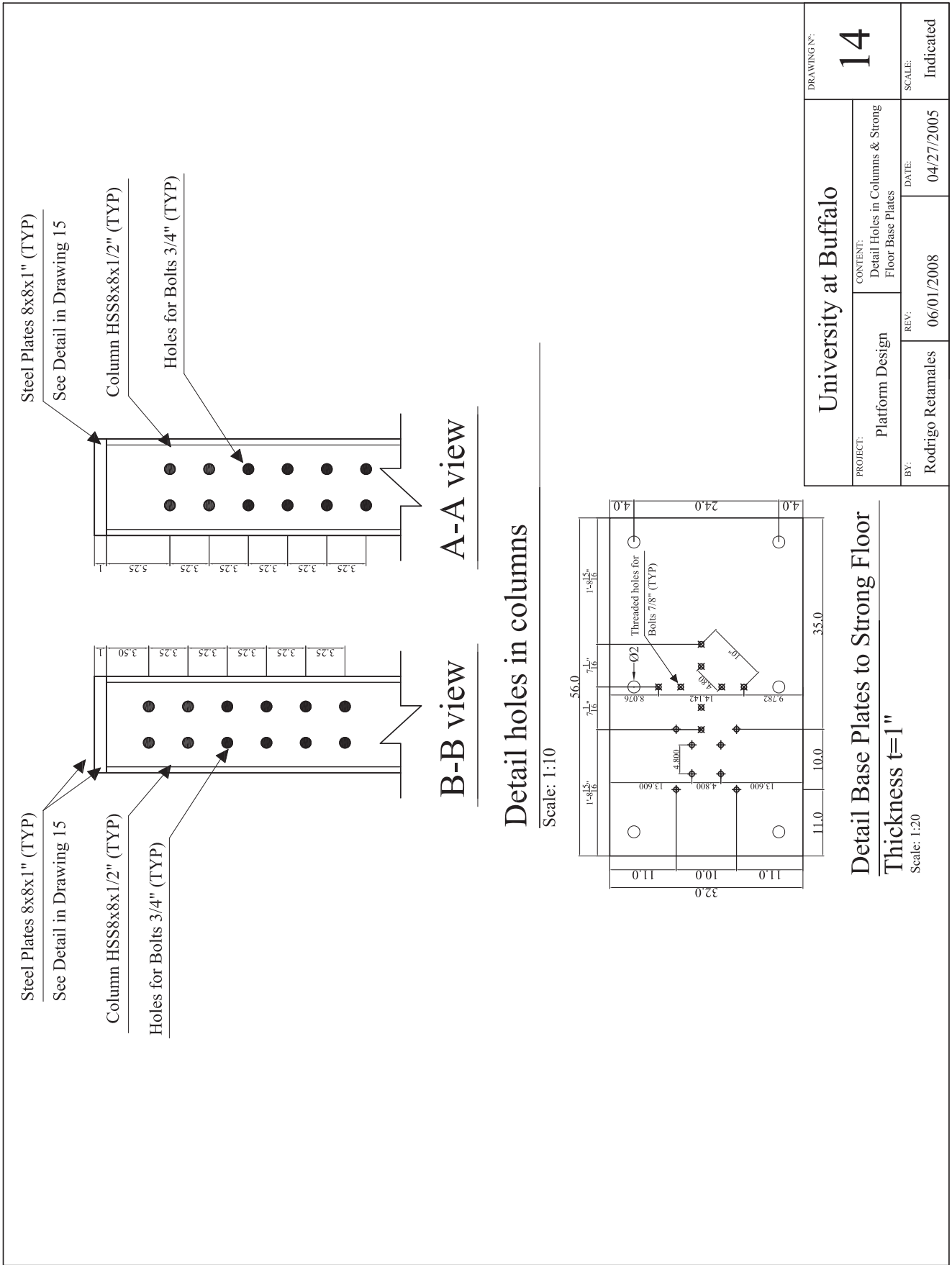
Figure A.14. Detail holes in columns & strong floor base plates
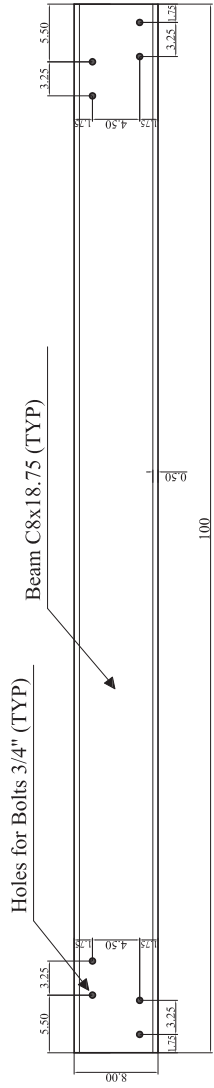
Detail Transverse Beam (4 Units)
Scale: 1:16
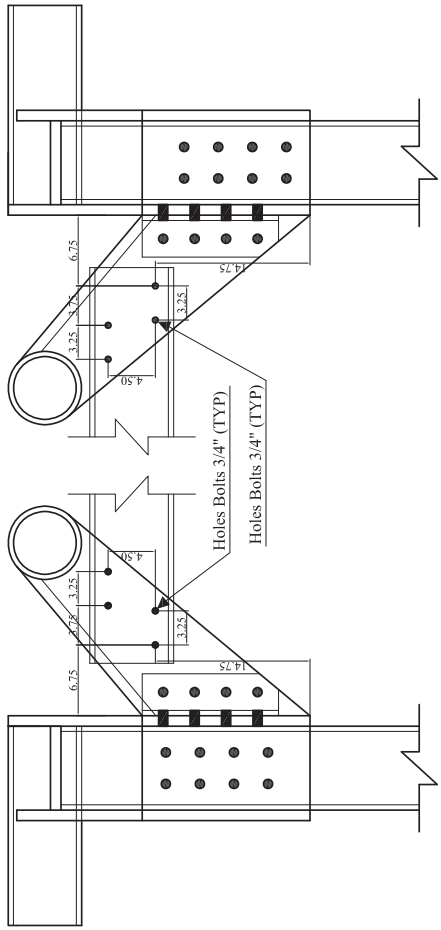
View A-A (TYP)
Scale: 1:16

View B-B (TYP)
Scale: 1:16

Detail Additional Holes for Transverse Beam Connection
Scale: 1:16

Holes for Bolts 3/4" (TYP)

Beam C8x18.75 (TYP)

Holes Bolts 3/4" (TYP)

Holes Bolts 3/4" (TYP)

University at Buffalo

PROJECT:	CONTENT:		DRAWING Nº:
Platform Design	Detail Transverse Beams		15
BY:	REV:	DATE:	SCALE:
Rodrigo Retamales	06/01/2008	05/23/2005	Indicated

Figure A.15. Detail transverse beams

290

Figure A.16. Diagonal braces

The drawing sheet contains the following text:

Steel plate t=3/8" Top

L2.5x2.5x1/4" Top

2 Holes for Bolts 3/4"

Steel plate t=3/8" Bottom

L2.5x2.5x1/4" Bottom

1 Hole for Bolt 3/4"

2 Holes for Bolts 3/4"
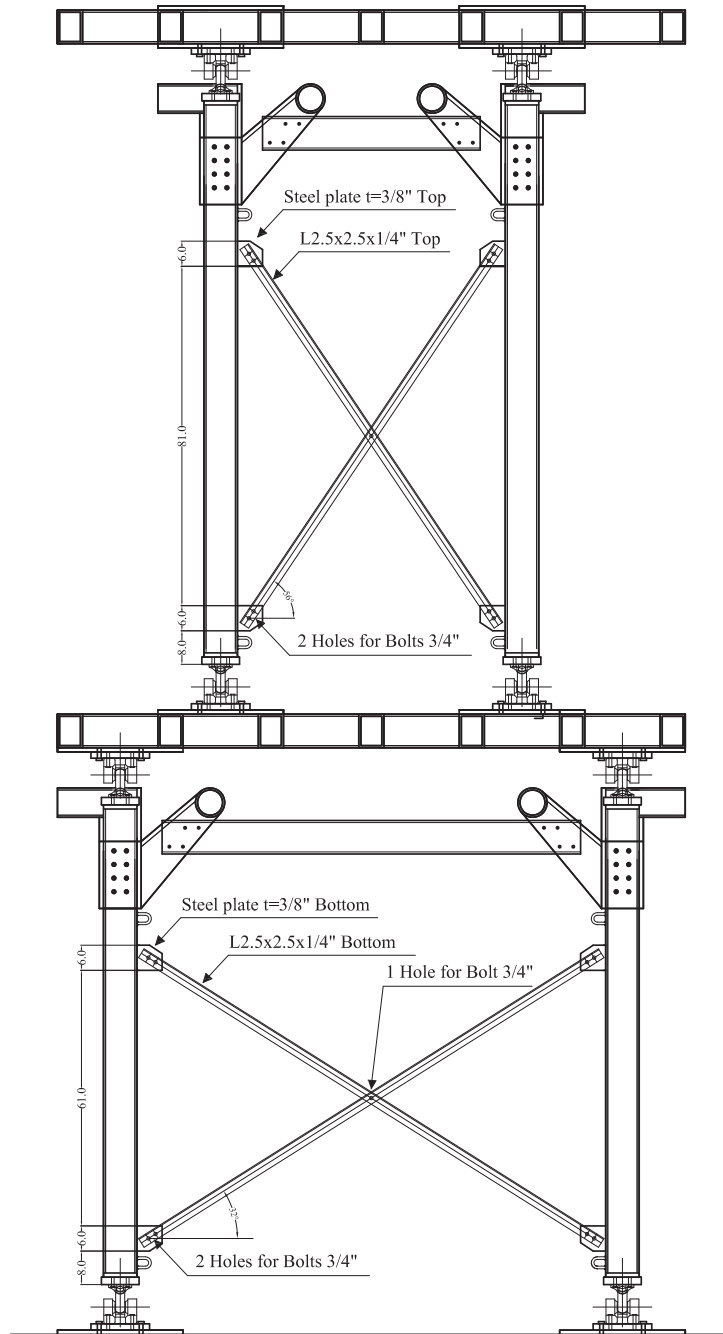
UB-NCS Rigid Braces System
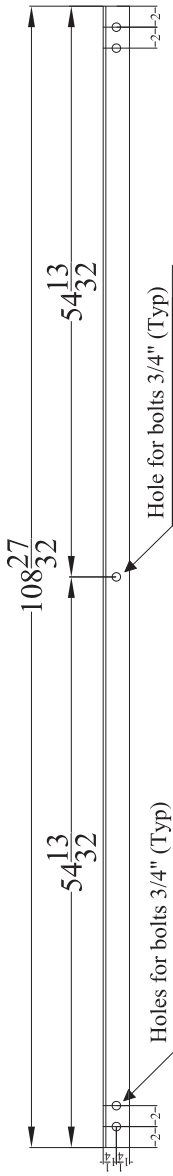
Scale: 1:40

Detail Braces L2.5x2.5x1/4" top level (4 units)
Scale: 1:16

Holes for bolts 3/4" (Typ)

Hole for bolts 3/4" (Typ)

$108\frac{27}{32}$

$54\frac{13}{32}$

$54\frac{13}{32}$

L-2-2
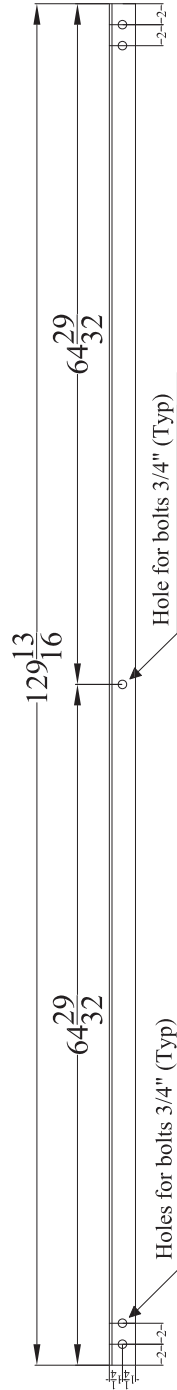
Detail Braces L2.5x2.5x1/4" bottom level (4 units)
Scale: 1:16

Holes for bolts 3/4" (Typ)

Hole for bolts 3/4" (Typ)

$129\frac{13}{16}$

$64\frac{29}{32}$

$64\frac{29}{32}$

L-2-2

Detail Connection to Column
Scale: 1:10

Column HSS8x8x1/2"

L2.5x2.5x1/4" (Typ)

Steel plate t=3/8" (Typ)

1/4 (TYP)
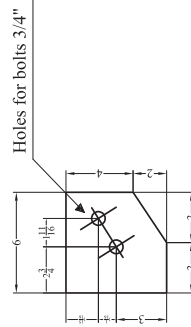
Detail Gousset Steel plate t=3/8" Bottom level (8 units)
Scale: 1:10

Holes for bolts 3/4"
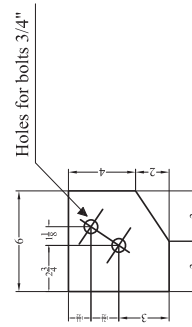
Detail Gousset Steel plate t=3/8" Top level (8 units)
Scale: 1:10

Holes for bolts 3/4"

University at Buffalo

DRAWING Nº: 17
SCALE: Indicated
CONTENT: Detail Diagonal Braces
DATE: 04/27/2005
PROJECT: Platform Design
REV: 06/01/2008
BY: Rodrigo Retamales

Figure A.17. Detail diagonal braces

292

DRAWING N°: 18

SCALE: Indicated

University at Buffalo

CONTENT: Front View Gate System

DATE: 05/23/2005

PROJECT: Platform Design

REV: 06/01/2008

BY: Rodrigo Retamales

EL 360.00

Transverse Beam

Clevis to Frame
See Detail 2

15.0

30.0

14

13

Plate to Reaction Wall
See Detail 3

12

11

168.0

Steel Section
HSS4x4x3/16" (TYP)

10

9

8

Plate to Reaction Wall
See Detail 3

Clevis to Frame
See Detail 2

7

6

Plate to Reaction Wall
See Detail 3

5

144.0

4

3

2

Plate to Strong Floor
See Detail 4

1

EL 000.00

192.0

Front View Gate System

Scale: 1:40

Figure A.18. Front view gate system
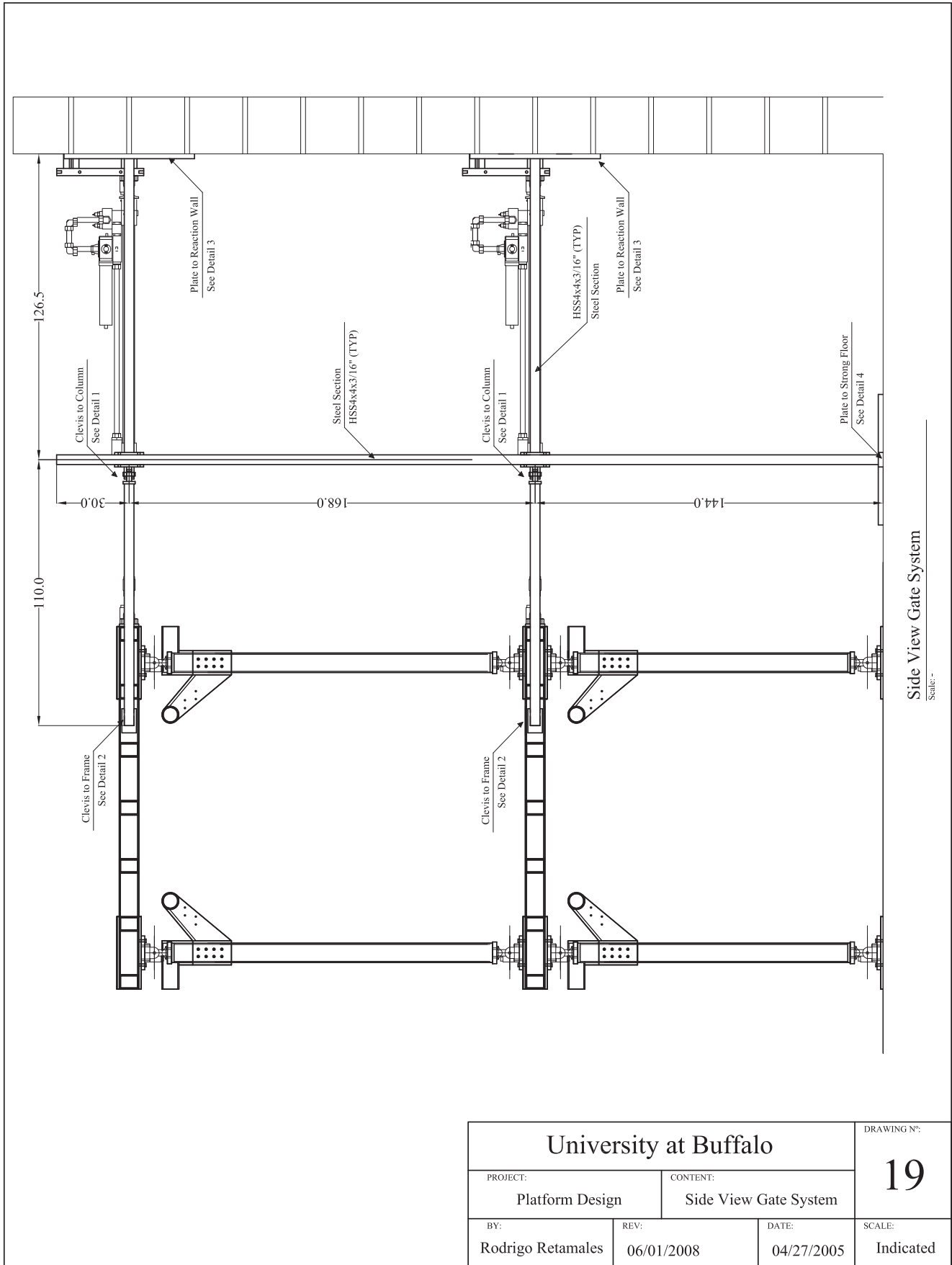
Figure A.19. Side view gate system
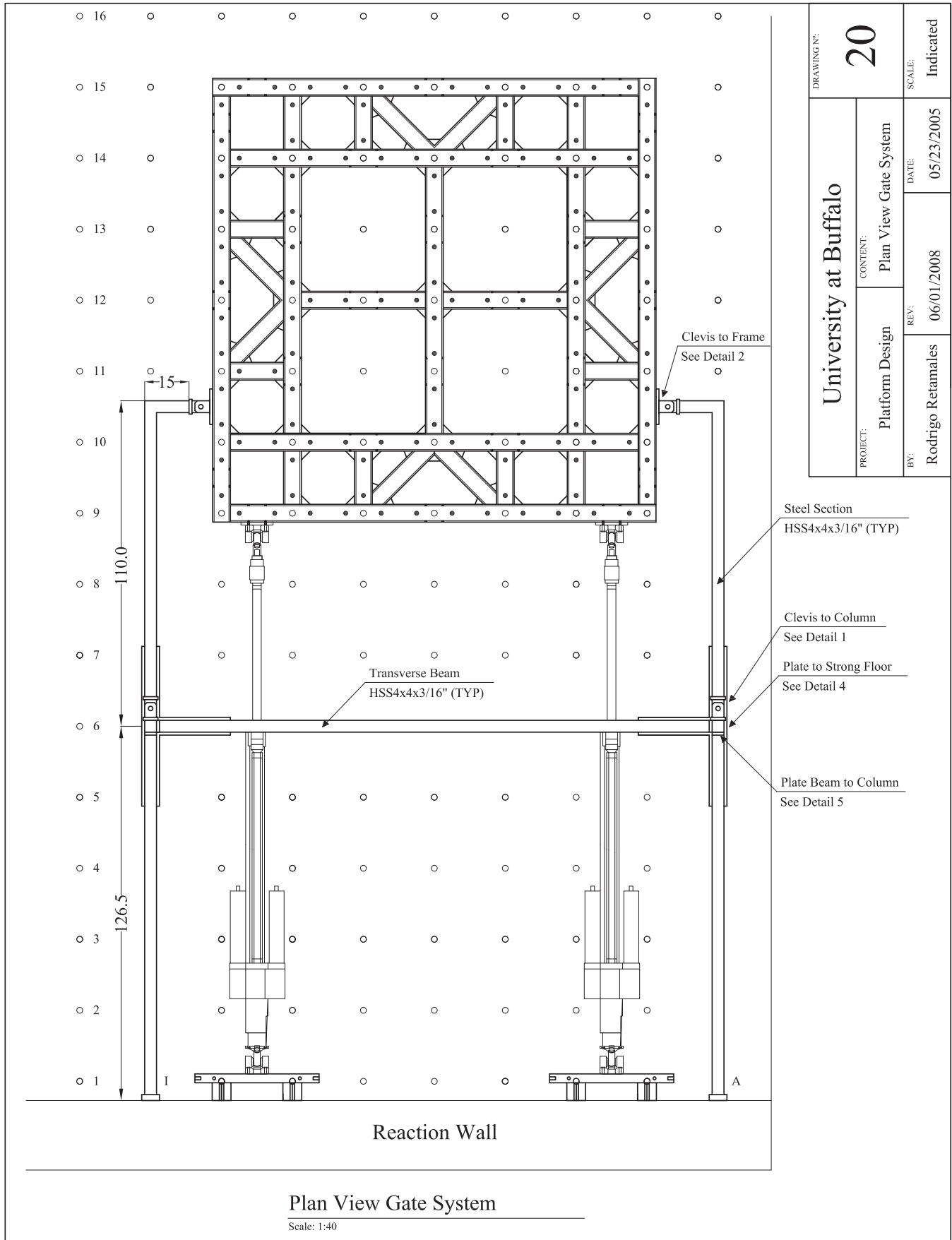
Within the drawing:

- 126.5
- Plate to Reaction Wall See Detail 3
- Clevis to Column See Detail 1
- Steel Section HSS4x4x3/16" (TYP)
- HSS4x4x3/16" (TYP) Steel Section
- Plate to Reaction Wall See Detail 3
- Clevis to Column See Detail 1
- Plate to Strong Floor See Detail 4
- 30.0
- 168.0
- 144.0
- 110.0
- Clevis to Frame See Detail 2
- Clevis to Frame See Detail 2
- Side View Gate System
- Scale: -

Title block:

University at Buffalo		DRAWING Nº: 19
PROJECT: Platform Design	CONTENT: Side View Gate System	
BY: Rodrigo Retamales	REV: 06/01/2008	DATE: 04/27/2005	SCALE: Indicated

294

Figure A.20. Plan view gate system

University at Buffalo

CONTENT: Details Gate System

DATE: 04/27/2005

PROJECT: Platform Design

REV: 06/01/2008

BY: Rodrigo Retamales

Detail 1. Clevis to Column (4 Units)
Scale: 1:10

Detail 2. Clevis to Frame (4 Units)
Scale: 1:10

Detail Steel Alloy Pin (8 Units)
Scale: 1:10

Detail Plate 10x6x1" (4 Units)
Scale: 1:10

Detail Plate 12x5x1" (4 Units)
Scale: 1:10

Detail 3. Plate to Reaction Wall (4 Units)
Scale: 1:16

Detail 5. Connection Beam to Column (6 Units)
Scale: 1:10

Detail 4. Plate to Strong Floor (2 Units)
Scale: 1:16

Detail Plate 12x4x1" Connection Beam to Column (6 Units)
Scale: 1:10

Figure A.21. Details gate system
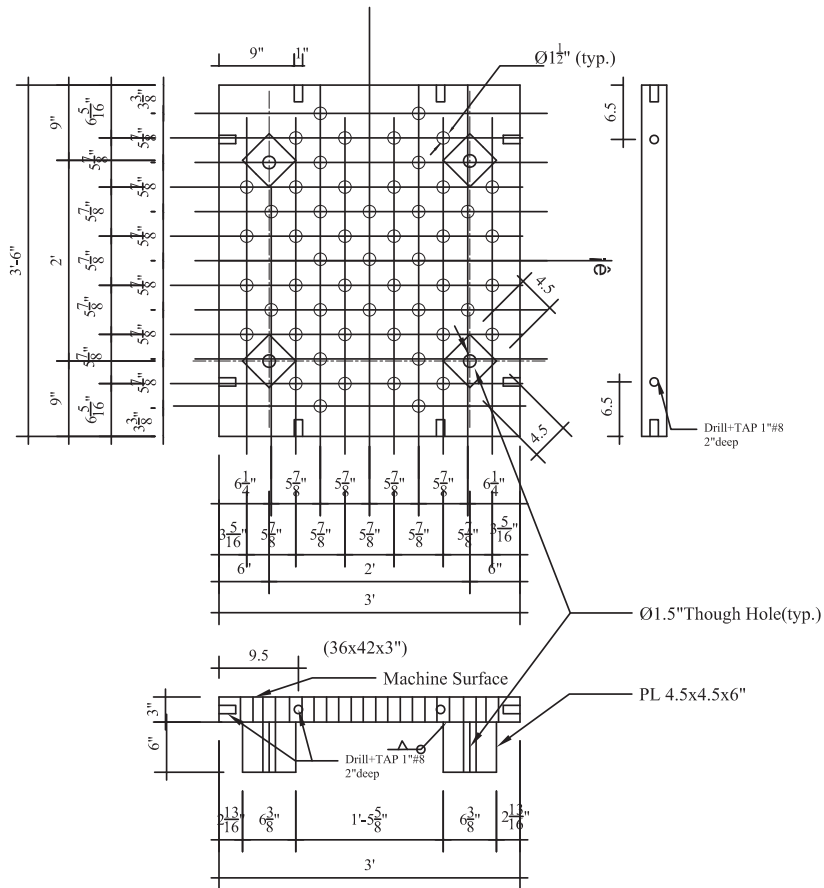
Actuators Connection Plate (100 Tons)

Scale: 1:20

	DRAWING N°:
University at Buffalo	**22**

PROJECT:	CONTENT:
Platform Design	Plate to Reaction Wall

BY:	REV:	DATE:	SCALE:
Rodrigo Retamales	06/01/2008	04/27/2005	Indicated

Figure A.22. Plate to reaction wall

MCEER Technical Reports

MCEER publishes technical reports on a variety of subjects written by authors funded through MCEER. These reports are available from both MCEER Publications and the National Technical Information Service (NTIS). Requests for reports should be directed to MCEER Publications, MCEER, University at Buffalo, State University of New York, Red Jacket Quadrangle, Buffalo, New York 14261. Reports can also be requested through NTIS, 5285 Port Royal Road, Springfield, Virginia 22161. NTIS accession numbers are shown in parenthesis, if available.

NCEER-87-0001   "First-Year Program in Research, Education and Technology Transfer," 3/5/87, (PB88-134275, A04, MF-A01).

NCEER-87-0002   "Experimental Evaluation of Instantaneous Optimal Algorithms for Structural Control," by R.C. Lin, T.T. Soong and A.M. Reinhorn, 4/20/87, (PB88-134341, A04, MF-A01).

NCEER-87-0003   "Experimentation Using the Earthquake Simulation Facilities at University at Buffalo," by A.M. Reinhorn and R.L. Ketter, to be published.

NCEER-87-0004   "The System Characteristics and Performance of a Shaking Table," by J.S. Hwang, K.C. Chang and G.C. Lee, 6/1/87, (PB88-134259, A03, MF-A01). This report is available only through NTIS (see address given above).

NCEER-87-0005   "A Finite Element Formulation for Nonlinear Viscoplastic Material Using a Q Model," by O. Gyebi and G. Dasgupta, 11/2/87, (PB88-213764, A08, MF-A01).

NCEER-87-0006   "Symbolic Manipulation Program (SMP) - Algebraic Codes for Two and Three Dimensional Finite Element Formulations," by X. Lee and G. Dasgupta, 11/9/87, (PB88-218522, A05, MF-A01).

NCEER-87-0007   "Instantaneous Optimal Control Laws for Tall Buildings Under Seismic Excitations," by J.N. Yang, A. Akbarpour and P. Ghaemmaghami, 6/10/87, (PB88-134333, A06, MF-A01). This report is only available through NTIS (see address given above).

NCEER-87-0008   "IDARC: Inelastic Damage Analysis of Reinforced Concrete Frame - Shear-Wall Structures," by Y.J. Park, A.M. Reinhorn and S.K. Kunnath, 7/20/87, (PB88-134325, A09, MF-A01). This report is only available through NTIS (see address given above).

NCEER-87-0009   "Liquefaction Potential for New York State: A Preliminary Report on Sites in Manhattan and Buffalo," by M. Budhu, V. Vijayakumar, R.F. Giese and L. Baumgras, 8/31/87, (PB88-163704, A03, MF-A01). This report is available only through NTIS (see address given above).

NCEER-87-0010   "Vertical and Torsional Vibration of Foundations in Inhomogeneous Media," by A.S. Veletsos and K.W. Dotson, 6/1/87, (PB88-134291, A03, MF-A01). This report is only available through NTIS (see address given above).

NCEER-87-0011   "Seismic Probabilistic Risk Assessment and Seismic Margins Studies for Nuclear Power Plants," by Howard H.M. Hwang, 6/15/87, (PB88-134267, A03, MF-A01). This report is only available through NTIS (see address given above).

NCEER-87-0012   "Parametric Studies of Frequency Response of Secondary Systems Under Ground-Acceleration Excitations," by Y. Yong and Y.K. Lin, 6/10/87, (PB88-134309, A03, MF-A01). This report is only available through NTIS (see address given above).

NCEER-87-0013   "Frequency Response of Secondary Systems Under Seismic Excitation," by J.A. HoLung, J. Cai and Y.K. Lin, 7/31/87, (PB88-134317, A05, MF-A01). This report is only available through NTIS (see address given above).

NCEER-87-0014   "Modelling Earthquake Ground Motions in Seismically Active Regions Using Parametric Time Series Methods," by G.W. Ellis and A.S. Cakmak, 8/25/87, (PB88-134283, A08, MF-A01). This report is only available through NTIS (see address given above).

NCEER-87-0015   "Detection and Assessment of Seismic Structural Damage," by E. DiPasquale and A.S. Cakmak, 8/25/87, (PB88-163712, A05, MF-A01). This report is only available through NTIS (see address given above).

NCEER-87-0016   "Pipeline Experiment at Parkfield, California," by J. Isenberg and E. Richardson, 9/15/87, (PB88-163720, A03, MF-A01). This report is available only through NTIS (see address given above).

NCEER-87-0017   "Digital Simulation of Seismic Ground Motion," by M. Shinozuka, G. Deodatis and T. Harada, 8/31/87, (PB88-155197, A04, MF-A01). This report is available only through NTIS (see address given above).

NCEER-87-0018   "Practical Considerations for Structural Control: System Uncertainty, System Time Delay and Truncation of Small Control Forces," J.N. Yang and A. Akbarpour, 8/10/87, (PB88-163738, A08, MF-A01). This report is only available through NTIS (see address given above).

NCEER-87-0019   "Modal Analysis of Nonclassically Damped Structural Systems Using Canonical Transformation," by J.N. Yang, S. Sarkani and F.X. Long, 9/27/87, (PB88-187851, A04, MF-A01).

NCEER-87-0020   "A Nonstationary Solution in Random Vibration Theory," by J.R. Red-Horse and P.D. Spanos, 11/3/87, (PB88-163746, A03, MF-A01).

NCEER-87-0021   "Horizontal Impedances for Radially Inhomogeneous Viscoelastic Soil Layers," by A.S. Veletsos and K.W. Dotson, 10/15/87, (PB88-150859, A04, MF-A01).

NCEER-87-0022   "Seismic Damage Assessment of Reinforced Concrete Members," by Y.S. Chung, C. Meyer and M. Shinozuka, 10/9/87, (PB88-150867, A05, MF-A01). This report is available only through NTIS (see address given above).

NCEER-87-0023   "Active Structural Control in Civil Engineering," by T.T. Soong, 11/11/87, (PB88-187778, A03, MF-A01).

NCEER-87-0024   "Vertical and Torsional Impedances for Radially Inhomogeneous Viscoelastic Soil Layers," by K.W. Dotson and A.S. Veletsos, 12/87, (PB88-187786, A03, MF-A01).

NCEER-87-0025   "Proceedings from the Symposium on Seismic Hazards, Ground Motions, Soil-Liquefaction and Engineering Practice in Eastern North America," October 20-22, 1987, edited by K.H. Jacob, 12/87, (PB88-188115, A23, MF-A01). This report is available only through NTIS (see address given above).

NCEER-87-0026   "Report on the Whittier-Narrows, California, Earthquake of October 1, 1987," by J. Pantelic and A. Reinhorn, 11/87, (PB88-187752, A03, MF-A01). This report is available only through NTIS (see address given above).

NCEER-87-0027   "Design of a Modular Program for Transient Nonlinear Analysis of Large 3-D Building Structures," by S. Srivastav and J.F. Abel, 12/30/87, (PB88-187950, A05, MF-A01). This report is only available through NTIS (see address given above).

NCEER-87-0028   "Second-Year Program in Research, Education and Technology Transfer," 3/8/88, (PB88-219480, A04, MF-A01).

NCEER-88-0001   "Workshop on Seismic Computer Analysis and Design of Buildings With Interactive Graphics," by W. McGuire, J.F. Abel and C.H. Conley, 1/18/88, (PB88-187760, A03, MF-A01). This report is only available through NTIS (see address given above).

NCEER-88-0002   "Optimal Control of Nonlinear Flexible Structures," by J.N. Yang, F.X. Long and D. Wong, 1/22/88, (PB88-213772, A06, MF-A01).

NCEER-88-0003   "Substructuring Techniques in the Time Domain for Primary-Secondary Structural Systems," by G.D. Manolis and G. Juhn, 2/10/88, (PB88-213780, A04, MF-A01).

NCEER-88-0004   "Iterative Seismic Analysis of Primary-Secondary Systems," by A. Singhal, L.D. Lutes and P.D. Spanos, 2/23/88, (PB88-213798, A04, MF-A01).

NCEER-88-0005   "Stochastic Finite Element Expansion for Random Media," by P.D. Spanos and R. Ghanem, 3/14/88, (PB88-213806, A03, MF-A01).

NCEER-88-0006   "Combining Structural Optimization and Structural Control," by F.Y. Cheng and C.P. Pantelides, 1/10/88, (PB88-213814, A05, MF-A01).

NCEER-88-0007   "Seismic Performance Assessment of Code-Designed Structures," by H.H-M. Hwang, J-W. Jaw and H-J. Shau, 3/20/88, (PB88-219423, A04, MF-A01). This report is only available through NTIS (see address given above).

NCEER-88-0008   "Reliability Analysis of Code-Designed Structures Under Natural Hazards," by H.H-M. Hwang, H. Ushiba and M. Shinozuka, 2/29/88, (PB88-229471, A07, MF-A01). This report is only available through NTIS (see address given above).

NCEER-88-0009   "Seismic Fragility Analysis of Shear Wall Structures," by J-W Jaw and H.H-M. Hwang, 4/30/88, (PB89-102867, A04, MF-A01).

NCEER-88-0010   "Base Isolation of a Multi-Story Building Under a Harmonic Ground Motion - A Comparison of Performances of Various Systems," by F-G Fan, G. Ahmadi and I.G. Tadjbakhsh, 5/18/88, (PB89-122238, A06, MF-A01). This report is only available through NTIS (see address given above).

NCEER-88-0011   "Seismic Floor Response Spectra for a Combined System by Green's Functions," by F.M. Lavelle, L.A. Bergman and P.D. Spanos, 5/1/88, (PB89-102875, A03, MF-A01).

NCEER-88-0012   "A New Solution Technique for Randomly Excited Hysteretic Structures," by G.Q. Cai and Y.K. Lin, 5/16/88, (PB89-102883, A03, MF-A01).

NCEER-88-0013   "A Study of Radiation Damping and Soil-Structure Interaction Effects in the Centrifuge," by K. Weissman, supervised by J.H. Prevost, 5/24/88, (PB89-144703, A06, MF-A01).

NCEER-88-0014   "Parameter Identification and Implementation of a Kinematic Plasticity Model for Frictional Soils," by J.H. Prevost and D.V. Griffiths, to be published.

NCEER-88-0015   "Two- and Three- Dimensional Dynamic Finite Element Analyses of the Long Valley Dam," by D.V. Griffiths and J.H. Prevost, 6/17/88, (PB89-144711, A04, MF-A01).

NCEER-88-0016   "Damage Assessment of Reinforced Concrete Structures in Eastern United States," by A.M. Reinhorn, M.J. Seidel, S.K. Kunnath and Y.J. Park, 6/15/88, (PB89-122220, A04, MF-A01). This report is only available through NTIS (see address given above).

NCEER-88-0017   "Dynamic Compliance of Vertically Loaded Strip Foundations in Multilayered Viscoelastic Soils," by S. Ahmad and A.S.M. Israil, 6/17/88, (PB89-102891, A04, MF-A01).

NCEER-88-0018   "An Experimental Study of Seismic Structural Response With Added Viscoelastic Dampers," by R.C. Lin, Z. Liang, T.T. Soong and R.H. Zhang, 6/30/88, (PB89-122212, A05, MF-A01). This report is available only through NTIS (see address given above).

NCEER-88-0019   "Experimental Investigation of Primary - Secondary System Interaction," by G.D. Manolis, G. Juhn and A.M. Reinhorn, 5/27/88, (PB89-122204, A04, MF-A01).

NCEER-88-0020   "A Response Spectrum Approach For Analysis of Nonclassically Damped Structures," by J.N. Yang, S. Sarkani and F.X. Long, 4/22/88, (PB89-102909, A04, MF-A01).

NCEER-88-0021   "Seismic Interaction of Structures and Soils: Stochastic Approach," by A.S. Veletsos and A.M. Prasad, 7/21/88, (PB89-122196, A04, MF-A01). This report is only available through NTIS (see address given above).

NCEER-88-0022   "Identification of the Serviceability Limit State and Detection of Seismic Structural Damage," by E. DiPasquale and A.S. Cakmak, 6/15/88, (PB89-122188, A05, MF-A01). This report is available only through NTIS (see address given above).

NCEER-88-0023   "Multi-Hazard Risk Analysis: Case of a Simple Offshore Structure," by B.K. Bhartia and E.H. Vanmarcke, 7/21/88, (PB89-145213, A05, MF-A01).

NCEER-88-0024   "Automated Seismic Design of Reinforced Concrete Buildings," by Y.S. Chung, C. Meyer and M. Shinozuka, 7/5/88, (PB89-122170, A06, MF-A01). This report is available only through NTIS (see address given above).

NCEER-88-0025   "Experimental Study of Active Control of MDOF Structures Under Seismic Excitations," by L.L. Chung, R.C. Lin, T.T. Soong and A.M. Reinhorn, 7/10/88, (PB89-122600, A04, MF-A01).

NCEER-88-0026   "Earthquake Simulation Tests of a Low-Rise Metal Structure," by J.S. Hwang, K.C. Chang, G.C. Lee and R.L. Ketter, 8/1/88, (PB89-102917, A04, MF-A01).

NCEER-88-0027   "Systems Study of Urban Response and Reconstruction Due to Catastrophic Earthquakes," by F. Kozin and H.K. Zhou, 9/22/88, (PB90-162348, A04, MF-A01).

NCEER-88-0028   "Seismic Fragility Analysis of Plane Frame Structures," by H.H-M. Hwang and Y.K. Low, 7/31/88, (PB89-131445, A06, MF-A01).

NCEER-88-0029   "Response Analysis of Stochastic Structures," by A. Kardara, C. Bucher and M. Shinozuka, 9/22/88, (PB89-174429, A04, MF-A01).

NCEER-88-0030   "Nonnormal Accelerations Due to Yielding in a Primary Structure," by D.C.K. Chen and L.D. Lutes, 9/19/88, (PB89-131437, A04, MF-A01).

NCEER-88-0031   "Design Approaches for Soil-Structure Interaction," by A.S. Veletsos, A.M. Prasad and Y. Tang, 12/30/88, (PB89-174437, A03, MF-A01). This report is available only through NTIS (see address given above).

NCEER-88-0032   "A Re-evaluation of Design Spectra for Seismic Damage Control," by C.J. Turkstra and A.G. Tallin, 11/7/88, (PB89-145221, A05, MF-A01).

NCEER-88-0033   "The Behavior and Design of Noncontact Lap Splices Subjected to Repeated Inelastic Tensile Loading," by V.E. Sagan, P. Gergely and R.N. White, 12/8/88, (PB89-163737, A08, MF-A01).

NCEER-88-0034   "Seismic Response of Pile Foundations," by S.M. Mamoon, P.K. Banerjee and S. Ahmad, 11/1/88, (PB89-145239, A04, MF-A01).

NCEER-88-0035   "Modeling of R/C Building Structures With Flexible Floor Diaphragms (IDARC2)," by A.M. Reinhorn, S.K. Kunnath and N. Panahshahi, 9/7/88, (PB89-207153, A07, MF-A01).

NCEER-88-0036   "Solution of the Dam-Reservoir Interaction Problem Using a Combination of FEM, BEM with Particular Integrals, Modal Analysis, and Substructuring," by C-S. Tsai, G.C. Lee and R.L. Ketter, 12/31/88, (PB89-207146, A04, MF-A01).

NCEER-88-0037   "Optimal Placement of Actuators for Structural Control," by F.Y. Cheng and C.P. Pantelides, 8/15/88, (PB89-162846, A05, MF-A01).

NCEER-88-0038   "Teflon Bearings in Aseismic Base Isolation: Experimental Studies and Mathematical Modeling," by A. Mokha, M.C. Constantinou and A.M. Reinhorn, 12/5/88, (PB89-218457, A10, MF-A01). This report is available only through NTIS (see address given above).

NCEER-88-0039   "Seismic Behavior of Flat Slab High-Rise Buildings in the New York City Area," by P. Weidlinger and M. Ettouney, 10/15/88, (PB90-145681, A04, MF-A01).

NCEER-88-0040   "Evaluation of the Earthquake Resistance of Existing Buildings in New York City," by P. Weidlinger and M. Ettouney, 10/15/88, to be published.

NCEER-88-0041   "Small-Scale Modeling Techniques for Reinforced Concrete Structures Subjected to Seismic Loads," by W. Kim, A. El-Attar and R.N. White, 11/22/88, (PB89-189625, A05, MF-A01).

NCEER-88-0042   "Modeling Strong Ground Motion from Multiple Event Earthquakes," by G.W. Ellis and A.S. Cakmak, 10/15/88, (PB89-174445, A03, MF-A01).

NCEER-88-0043   "Nonstationary Models of Seismic Ground Acceleration," by M. Grigoriu, S.E. Ruiz and E. Rosenblueth, 7/15/88, (PB89-189617, A04, MF-A01).

NCEER-88-0044   "SARCF User's Guide: Seismic Analysis of Reinforced Concrete Frames," by Y.S. Chung, C. Meyer and M. Shinozuka, 11/9/88, (PB89-174452, A08, MF-A01).

NCEER-88-0045   "First Expert Panel Meeting on Disaster Research and Planning," edited by J. Pantelic and J. Stoyle, 9/15/88, (PB89-174460, A05, MF-A01).

NCEER-88-0046   "Preliminary Studies of the Effect of Degrading Infill Walls on the Nonlinear Seismic Response of Steel Frames," by C.Z. Chrysostomou, P. Gergely and J.F. Abel, 12/19/88, (PB89-208383, A05, MF-A01).

NCEER-88-0047   "Reinforced Concrete Frame Component Testing Facility - Design, Construction, Instrumentation and Operation," by S.P. Pessiki, C. Conley, T. Bond, P. Gergely and R.N. White, 12/16/88, (PB89-174478, A04, MF-A01).

NCEER-89-0001   "Effects of Protective Cushion and Soil Compliancy on the Response of Equipment Within a Seismically Excited Building," by J.A. HoLung, 2/16/89, (PB89-207179, A04, MF-A01).

NCEER-89-0002   "Statistical Evaluation of Response Modification Factors for Reinforced Concrete Structures," by H.H-M. Hwang and J-W. Jaw, 2/17/89, (PB89-207187, A05, MF-A01).

NCEER-89-0003   "Hysteretic Columns Under Random Excitation," by G-Q. Cai and Y.K. Lin, 1/9/89, (PB89-196513, A03, MF-A01).

NCEER-89-0004   "Experimental Study of `Elephant Foot Bulge' Instability of Thin-Walled Metal Tanks," by Z-H. Jia and R.L. Ketter, 2/22/89, (PB89-207195, A03, MF-A01).

NCEER-89-0005   "Experiment on Performance of Buried Pipelines Across San Andreas Fault," by J. Isenberg, E. Richardson and T.D. O'Rourke, 3/10/89, (PB89-218440, A04, MF-A01). This report is available only through NTIS (see address given above).

NCEER-89-0006   "A Knowledge-Based Approach to Structural Design of Earthquake-Resistant Buildings," by M. Subramani, P. Gergely, C.H. Conley, J.F. Abel and A.H. Zaghw, 1/15/89, (PB89-218465, A06, MF-A01).

NCEER-89-0007   "Liquefaction Hazards and Their Effects on Buried Pipelines," by T.D. O'Rourke and P.A. Lane, 2/1/89, (PB89-218481, A09, MF-A01).

NCEER-89-0008   "Fundamentals of System Identification in Structural Dynamics," by H. Imai, C-B. Yun, O. Maruyama and M. Shinozuka, 1/26/89, (PB89-207211, A04, MF-A01).

NCEER-89-0009   "Effects of the 1985 Michoacan Earthquake on Water Systems and Other Buried Lifelines in Mexico," by A.G. Ayala and M.J. O'Rourke, 3/8/89, (PB89-207229, A06, MF-A01).

NCEER-89-R010   "NCEER Bibliography of Earthquake Education Materials," by K.E.K. Ross, Second Revision, 9/1/89, (PB90-125352, A05, MF-A01). This report is replaced by NCEER-92-0018.

NCEER-89-0011   "Inelastic Three-Dimensional Response Analysis of Reinforced Concrete Building Structures (IDARC-3D), Part I - Modeling," by S.K. Kunnath and A.M. Reinhorn, 4/17/89, (PB90-114612, A07, MF-A01). This report is available only through NTIS (see address given above).

NCEER-89-0012   "Recommended Modifications to ATC-14," by C.D. Poland and J.O. Malley, 4/12/89, (PB90-108648, A15, MF-A01).

NCEER-89-0013   "Repair and Strengthening of Beam-to-Column Connections Subjected to Earthquake Loading," by M. Corazao and A.J. Durrani, 2/28/89, (PB90-109885, A06, MF-A01).

NCEER-89-0014   "Program EXKAL2 for Identification of Structural Dynamic Systems," by O. Maruyama, C-B. Yun, M. Hoshiya and M. Shinozuka, 5/19/89, (PB90-109877, A09, MF-A01).

NCEER-89-0015   "Response of Frames With Bolted Semi-Rigid Connections, Part I - Experimental Study and Analytical Predictions," by P.J. DiCorso, A.M. Reinhorn, J.R. Dickerson, J.B. Radziminski and W.L. Harper, 6/1/89, to be published.

NCEER-89-0016   "ARMA Monte Carlo Simulation in Probabilistic Structural Analysis," by P.D. Spanos and M.P. Mignolet, 7/10/89, (PB90-109893, A03, MF-A01).

NCEER-89-P017   "Preliminary Proceedings from the Conference on Disaster Preparedness - The Place of Earthquake Education in Our Schools," Edited by K.E.K. Ross, 6/23/89, (PB90-108606, A03, MF-A01).

NCEER-89-0017   "Proceedings from the Conference on Disaster Preparedness - The Place of Earthquake Education in Our Schools," Edited by K.E.K. Ross, 12/31/89, (PB90-207895, A012, MF-A02). This report is available only through NTIS (see address given above).

NCEER-89-0018   "Multidimensional Models of Hysteretic Material Behavior for Vibration Analysis of Shape Memory Energy Absorbing Devices, by E.J. Graesser and F.A. Cozzarelli, 6/7/89, (PB90-164146, A04, MF-A01).

NCEER-89-0019   "Nonlinear Dynamic Analysis of Three-Dimensional Base Isolated Structures (3D-BASIS)," by S. Nagarajaiah, A.M. Reinhorn and M.C. Constantinou, 8/3/89, (PB90-161936, A06, MF-A01). This report has been replaced by NCEER-93-0011.

NCEER-89-0020   "Structural Control Considering Time-Rate of Control Forces and Control Rate Constraints," by F.Y. Cheng and C.P. Pantelides, 8/3/89, (PB90-120445, A04, MF-A01).

NCEER-89-0021   "Subsurface Conditions of Memphis and Shelby County," by K.W. Ng, T-S. Chang and H-H.M. Hwang, 7/26/89, (PB90-120437, A03, MF-A01).

NCEER-89-0022   "Seismic Wave Propagation Effects on Straight Jointed Buried Pipelines," by K. Elhmadi and M.J. O'Rourke, 8/24/89, (PB90-162322, A10, MF-A02).

NCEER-89-0023   "Workshop on Serviceability Analysis of Water Delivery Systems," edited by M. Grigoriu, 3/6/89, (PB90-127424, A03, MF-A01).

NCEER-89-0024   "Shaking Table Study of a 1/5 Scale Steel Frame Composed of Tapered Members," by K.C. Chang, J.S. Hwang and G.C. Lee, 9/18/89, (PB90-160169, A04, MF-A01).

NCEER-89-0025   "DYNA1D: A Computer Program for Nonlinear Seismic Site Response Analysis - Technical Documentation," by Jean H. Prevost, 9/14/89, (PB90-161944, A07, MF-A01). This report is available only through NTIS (see address given above).

NCEER-89-0026   "1:4 Scale Model Studies of Active Tendon Systems and Active Mass Dampers for Aseismic Protection," by A.M. Reinhorn, T.T. Soong, R.C. Lin, Y.P. Yang, Y. Fukao, H. Abe and M. Nakai, 9/15/89, (PB90-173246, A10, MF-A02). This report is available only through NTIS (see address given above).

NCEER-89-0027   "Scattering of Waves by Inclusions in a Nonhomogeneous Elastic Half Space Solved by Boundary Element Methods," by P.K. Hadley, A. Askar and A.S. Cakmak, 6/15/89, (PB90-145699, A07, MF-A01).

NCEER-89-0028   "Statistical Evaluation of Deflection Amplification Factors for Reinforced Concrete Structures," by H.H.M. Hwang, J-W. Jaw and A.L. Ch'ng, 8/31/89, (PB90-164633, A05, MF-A01).

NCEER-89-0029   "Bedrock Accelerations in Memphis Area Due to Large New Madrid Earthquakes," by H.H.M. Hwang, C.H.S. Chen and G. Yu, 11/7/89, (PB90-162330, A04, MF-A01).

NCEER-89-0030   "Seismic Behavior and Response Sensitivity of Secondary Structural Systems," by Y.Q. Chen and T.T. Soong, 10/23/89, (PB90-164658, A08, MF-A01).

NCEER-89-0031   "Random Vibration and Reliability Analysis of Primary-Secondary Structural Systems," by Y. Ibrahim, M. Grigoriu and T.T. Soong, 11/10/89, (PB90-161951, A04, MF-A01).

NCEER-89-0032   "Proceedings from the Second U.S. - Japan Workshop on Liquefaction, Large Ground Deformation and Their Effects on Lifelines, September 26-29, 1989," Edited by T.D. O'Rourke and M. Hamada, 12/1/89, (PB90-209388, A22, MF-A03).

NCEER-89-0033   "Deterministic Model for Seismic Damage Evaluation of Reinforced Concrete Structures," by J.M. Bracci, A.M. Reinhorn, J.B. Mander and S.K. Kunnath, 9/27/89, (PB91-108803, A06, MF-A01).

NCEER-89-0034   "On the Relation Between Local and Global Damage Indices," by E. DiPasquale and A.S. Cakmak, 8/15/89, (PB90-173865, A05, MF-A01).

NCEER-89-0035   "Cyclic Undrained Behavior of Nonplastic and Low Plasticity Silts," by A.J. Walker and H.E. Stewart, 7/26/89, (PB90-183518, A10, MF-A01).

NCEER-89-0036   "Liquefaction Potential of Surficial Deposits in the City of Buffalo, New York," by M. Budhu, R. Giese and L. Baumgrass, 1/17/89, (PB90-208455, A04, MF-A01).

NCEER-89-0037   "A Deterministic Assessment of Effects of Ground Motion Incoherence," by A.S. Veletsos and Y. Tang, 7/15/89, (PB90-164294, A03, MF-A01).

NCEER-89-0038   "Workshop on Ground Motion Parameters for Seismic Hazard Mapping," July 17-18, 1989, edited by R.V. Whitman, 12/1/89, (PB90-173923, A04, MF-A01).

NCEER-89-0039   "Seismic Effects on Elevated Transit Lines of the New York City Transit Authority," by C.J. Costantino, C.A. Miller and E. Heymsfield, 12/26/89, (PB90-207887, A06, MF-A01).

NCEER-89-0040   "Centrifugal Modeling of Dynamic Soil-Structure Interaction," by K. Weissman, Supervised by J.H. Prevost, 5/10/89, (PB90-207879, A07, MF-A01).

NCEER-89-0041   "Linearized Identification of Buildings With Cores for Seismic Vulnerability Assessment," by I-K. Ho and A.E. Aktan, 11/1/89, (PB90-251943, A07, MF-A01).

NCEER-90-0001   "Geotechnical and Lifeline Aspects of the October 17, 1989 Loma Prieta Earthquake in San Francisco," by T.D. O'Rourke, H.E. Stewart, F.T. Blackburn and T.S. Dickerman, 1/90, (PB90-208596, A05, MF-A01).

NCEER-90-0002   "Nonnormal Secondary Response Due to Yielding in a Primary Structure," by D.C.K. Chen and L.D. Lutes, 2/28/90, (PB90-251976, A07, MF-A01).

NCEER-90-0003   "Earthquake Education Materials for Grades K-12," by K.E.K. Ross, 4/16/90, (PB91-251984, A05, MF-A05). This report has been replaced by NCEER-92-0018.

NCEER-90-0004   "Catalog of Strong Motion Stations in Eastern North America," by R.W. Busby, 4/3/90, (PB90-251984, A05, MF-A01).

NCEER-90-0005   "NCEER Strong-Motion Data Base: A User Manual for the GeoBase Release (Version 1.0 for the Sun3)," by P. Friberg and K. Jacob, 3/31/90 (PB90-258062, A04, MF-A01).

NCEER-90-0006   "Seismic Hazard Along a Crude Oil Pipeline in the Event of an 1811-1812 Type New Madrid Earthquake," by H.H.M. Hwang and C-H.S. Chen, 4/16/90, (PB90-258054, A04, MF-A01).

NCEER-90-0007   "Site-Specific Response Spectra for Memphis Sheahan Pumping Station," by H.H.M. Hwang and C.S. Lee, 5/15/90, (PB91-108811, A05, MF-A01).

NCEER-90-0008   "Pilot Study on Seismic Vulnerability of Crude Oil Transmission Systems," by T. Ariman, R. Dobry, M. Grigoriu, F. Kozin, M. O'Rourke, T. O'Rourke and M. Shinozuka, 5/25/90, (PB91-108837, A06, MF-A01).

NCEER-90-0009   "A Program to Generate Site Dependent Time Histories: EQGEN," by G.W. Ellis, M. Srinivasan and A.S. Cakmak, 1/30/90, (PB91-108829, A04, MF-A01).

NCEER-90-0010   "Active Isolation for Seismic Protection of Operating Rooms," by M.E. Talbott, Supervised by M. Shinozuka, 6/8/9, (PB91-110205, A05, MF-A01).

NCEER-90-0011   "Program LINEARID for Identification of Linear Structural Dynamic Systems," by C-B. Yun and M. Shinozuka, 6/25/90, (PB91-110312, A08, MF-A01).

NCEER-90-0012   "Two-Dimensional Two-Phase Elasto-Plastic Seismic Response of Earth Dams," by A.N. Yiagos, Supervised by J.H. Prevost, 6/20/90, (PB91-110197, A13, MF-A02).

NCEER-90-0013   "Secondary Systems in Base-Isolated Structures: Experimental Investigation, Stochastic Response and Stochastic Sensitivity," by G.D. Manolis, G. Juhn, M.C. Constantinou and A.M. Reinhorn, 7/1/90, (PB91-110320, A08, MF-A01).

NCEER-90-0014   "Seismic Behavior of Lightly-Reinforced Concrete Column and Beam-Column Joint Details," by S.P. Pessiki, C.H. Conley, P. Gergely and R.N. White, 8/22/90, (PB91-108795, A11, MF-A02).

NCEER-90-0015   "Two Hybrid Control Systems for Building Structures Under Strong Earthquakes," by J.N. Yang and A. Danielians, 6/29/90, (PB91-125393, A04, MF-A01).

NCEER-90-0016   "Instantaneous Optimal Control with Acceleration and Velocity Feedback," by J.N. Yang and Z. Li, 6/29/90, (PB91-125401, A03, MF-A01).

NCEER-90-0017   "Reconnaissance Report on the Northern Iran Earthquake of June 21, 1990," by M. Mehrain, 10/4/90, (PB91-125377, A03, MF-A01).

NCEER-90-0018   "Evaluation of Liquefaction Potential in Memphis and Shelby County," by T.S. Chang, P.S. Tang, C.S. Lee and H. Hwang, 8/10/90, (PB91-125427, A09, MF-A01).

NCEER-90-0019   "Experimental and Analytical Study of a Combined Sliding Disc Bearing and Helical Steel Spring Isolation System," by M.C. Constantinou, A.S. Mokha and A.M. Reinhorn, 10/4/90, (PB91-125385, A06, MF-A01). This report is available only through NTIS (see address given above).

NCEER-90-0020   "Experimental Study and Analytical Prediction of Earthquake Response of a Sliding Isolation System with a Spherical Surface," by A.S. Mokha, M.C. Constantinou and A.M. Reinhorn, 10/11/90, (PB91-125419, A05, MF-A01).

NCEER-90-0021   "Dynamic Interaction Factors for Floating Pile Groups," by G. Gazetas, K. Fan, A. Kaynia and E. Kausel, 9/10/90, (PB91-170381, A05, MF-A01).

NCEER-90-0022   "Evaluation of Seismic Damage Indices for Reinforced Concrete Structures," by S. Rodriguez-Gomez and A.S. Cakmak, 9/30/90, PB91-171322, A06, MF-A01).

NCEER-90-0023   "Study of Site Response at a Selected Memphis Site," by H. Desai, S. Ahmad, E.S. Gazetas and M.R. Oh, 10/11/90, (PB91-196857, A03, MF-A01).

NCEER-90-0024   "A User's Guide to Strongmo: Version 1.0 of NCEER's Strong-Motion Data Access Tool for PCs and Terminals," by P.A. Friberg and C.A.T. Susch, 11/15/90, (PB91-171272, A03, MF-A01).

NCEER-90-0025   "A Three-Dimensional Analytical Study of Spatial Variability of Seismic Ground Motions," by L-L. Hong and A.H.-S. Ang, 10/30/90, (PB91-170399, A09, MF-A01).

NCEER-90-0026   "MUMOID User's Guide - A Program for the Identification of Modal Parameters," by S. Rodriguez-Gomez and E. DiPasquale, 9/30/90, (PB91-171298, A04, MF-A01).

NCEER-90-0027   "SARCF-II User's Guide - Seismic Analysis of Reinforced Concrete Frames," by S. Rodriguez-Gomez, Y.S. Chung and C. Meyer, 9/30/90, (PB91-171280, A05, MF-A01).

NCEER-90-0028   "Viscous Dampers: Testing, Modeling and Application in Vibration and Seismic Isolation," by N. Makris and M.C. Constantinou, 12/20/90 (PB91-190561, A06, MF-A01).

NCEER-90-0029   "Soil Effects on Earthquake Ground Motions in the Memphis Area," by H. Hwang, C.S. Lee, K.W. Ng and T.S. Chang, 8/2/90, (PB91-190751, A05, MF-A01).

NCEER-91-0001   "Proceedings from the Third Japan-U.S. Workshop on Earthquake Resistant Design of Lifeline Facilities and Countermeasures for Soil Liquefaction, December 17-19, 1990," edited by T.D. O'Rourke and M. Hamada, 2/1/91, (PB91-179259, A99, MF-A04).

NCEER-91-0002   "Physical Space Solutions of Non-Proportionally Damped Systems," by M. Tong, Z. Liang and G.C. Lee, 1/15/91, (PB91-179242, A04, MF-A01).

NCEER-91-0003   "Seismic Response of Single Piles and Pile Groups," by K. Fan and G. Gazetas, 1/10/91, (PB92-174994, A04, MF-A01).

NCEER-91-0004   "Damping of Structures: Part 1 - Theory of Complex Damping," by Z. Liang and G. Lee, 10/10/91, (PB92-197235, A12, MF-A03).

NCEER-91-0005   "3D-BASIS - Nonlinear Dynamic Analysis of Three Dimensional Base Isolated Structures: Part II," by S. Nagarajaiah, A.M. Reinhorn and M.C. Constantinou, 2/28/91, (PB91-190553, A07, MF-A01). This report has been replaced by NCEER-93-0011.

NCEER-91-0006   "A Multidimensional Hysteretic Model for Plasticity Deforming Metals in Energy Absorbing Devices," by E.J. Graesser and F.A. Cozzarelli, 4/9/91, (PB92-108364, A04, MF-A01).

NCEER-91-0007   "A Framework for Customizable Knowledge-Based Expert Systems with an Application to a KBES for Evaluating the Seismic Resistance of Existing Buildings," by E.G. Ibarra-Anaya and S.J. Fenves, 4/9/91, (PB91-210930, A08, MF-A01).

NCEER-91-0008   "Nonlinear Analysis of Steel Frames with Semi-Rigid Connections Using the Capacity Spectrum Method," by G.G. Deierlein, S-H. Hsieh, Y-J. Shen and J.F. Abel, 7/2/91, (PB92-113828, A05, MF-A01).

NCEER-91-0009   "Earthquake Education Materials for Grades K-12," by K.E.K. Ross, 4/30/91, (PB91-212142, A06, MF-A01). This report has been replaced by NCEER-92-0018.

NCEER-91-0010   "Phase Wave Velocities and Displacement Phase Differences in a Harmonically Oscillating Pile," by N. Makris and G. Gazetas, 7/8/91, (PB92-108356, A04, MF-A01).

NCEER-91-0011   "Dynamic Characteristics of a Full-Size Five-Story Steel Structure and a 2/5 Scale Model," by K.C. Chang, G.C. Yao, G.C. Lee, D.S. Hao and Y.C. Yeh," 7/2/91, (PB93-116648, A06, MF-A02).

NCEER-91-0012   "Seismic Response of a 2/5 Scale Steel Structure with Added Viscoelastic Dampers," by K.C. Chang, T.T. Soong, S-T. Oh and M.L. Lai, 5/17/91, (PB92-110816, A05, MF-A01).

NCEER-91-0013   "Earthquake Response of Retaining Walls; Full-Scale Testing and Computational Modeling," by S. Alampalli and A-W.M. Elgamal, 6/20/91, to be published.

NCEER-91-0014   "3D-BASIS-M: Nonlinear Dynamic Analysis of Multiple Building Base Isolated Structures," by P.C. Tsopelas, S. Nagarajaiah, M.C. Constantinou and A.M. Reinhorn, 5/28/91, (PB92-113885, A09, MF-A02).

NCEER-91-0015   "Evaluation of SEAOC Design Requirements for Sliding Isolated Structures," by D. Theodossiou and M.C. Constantinou, 6/10/91, (PB92-114602, A11, MF-A03).

NCEER-91-0016   "Closed-Loop Modal Testing of a 27-Story Reinforced Concrete Flat Plate-Core Building," by H.R. Somaprasad, T. Toksoy, H. Yoshiyuki and A.E. Aktan, 7/15/91, (PB92-129980, A07, MF-A02).

NCEER-91-0017   "Shake Table Test of a 1/6 Scale Two-Story Lightly Reinforced Concrete Building," by A.G. El-Attar, R.N. White and P. Gergely, 2/28/91, (PB92-222447, A06, MF-A02).

NCEER-91-0018   "Shake Table Test of a 1/8 Scale Three-Story Lightly Reinforced Concrete Building," by A.G. El-Attar, R.N. White and P. Gergely, 2/28/91, (PB93-116630, A08, MF-A02).

NCEER-91-0019   "Transfer Functions for Rigid Rectangular Foundations," by A.S. Veletsos, A.M. Prasad and W.H. Wu, 7/31/91, to be published.

NCEER-91-0020   "Hybrid Control of Seismic-Excited Nonlinear and Inelastic Structural Systems," by J.N. Yang, Z. Li and A. Danielians, 8/1/91, (PB92-143171, A06, MF-A02).

NCEER-91-0021   "The NCEER-91 Earthquake Catalog: Improved Intensity-Based Magnitudes and Recurrence Relations for U.S. Earthquakes East of New Madrid," by L. Seeber and J.G. Armbruster, 8/28/91, (PB92-176742, A06, MF-A02).

NCEER-91-0022   "Proceedings from the Implementation of Earthquake Planning and Education in Schools: The Need for Change - The Roles of the Changemakers," by K.E.K. Ross and F. Winslow, 7/23/91, (PB92-129998, A12, MF-A03).

NCEER-91-0023   "A Study of Reliability-Based Criteria for Seismic Design of Reinforced Concrete Frame Buildings," by H.H.M. Hwang and H-M. Hsu, 8/10/91, (PB92-140235, A09, MF-A02).

NCEER-91-0024   "Experimental Verification of a Number of Structural System Identification Algorithms," by R.G. Ghanem, H. Gavin and M. Shinozuka, 9/18/91, (PB92-176577, A18, MF-A04).

NCEER-91-0025   "Probabilistic Evaluation of Liquefaction Potential," by H.H.M. Hwang and C.S. Lee," 11/25/91, (PB92-143429, A05, MF-A01).

NCEER-91-0026   "Instantaneous Optimal Control for Linear, Nonlinear and Hysteretic Structures - Stable Controllers," by J.N. Yang and Z. Li, 11/15/91, (PB92-163807, A04, MF-A01).

NCEER-91-0027   "Experimental and Theoretical Study of a Sliding Isolation System for Bridges," by M.C. Constantinou, A. Kartoum, A.M. Reinhorn and P. Bradford, 11/15/91, (PB92-176973, A10, MF-A03).

NCEER-92-0001   "Case Studies of Liquefaction and Lifeline Performance During Past Earthquakes, Volume 1: Japanese Case Studies," Edited by M. Hamada and T. O'Rourke, 2/17/92, (PB92-197243, A18, MF-A04).

NCEER-92-0002   "Case Studies of Liquefaction and Lifeline Performance During Past Earthquakes, Volume 2: United States Case Studies," Edited by T. O'Rourke and M. Hamada, 2/17/92, (PB92-197250, A20, MF-A04).

NCEER-92-0003   "Issues in Earthquake Education," Edited by K. Ross, 2/3/92, (PB92-222389, A07, MF-A02).

NCEER-92-0004   "Proceedings from the First U.S. - Japan Workshop on Earthquake Protective Systems for Bridges," Edited by I.G. Buckle, 2/4/92, (PB94-142239, A99, MF-A06).

NCEER-92-0005   "Seismic Ground Motion from a Haskell-Type Source in a Multiple-Layered Half-Space," A.P. Theoharis, G. Deodatis and M. Shinozuka, 1/2/92, to be published.

NCEER-92-0006   "Proceedings from the Site Effects Workshop," Edited by R. Whitman, 2/29/92, (PB92-197201, A04, MF-A01).

NCEER-92-0007   "Engineering Evaluation of Permanent Ground Deformations Due to Seismically-Induced Liquefaction," by M.H. Baziar, R. Dobry and A-W.M. Elgamal, 3/24/92, (PB92-222421, A13, MF-A03).

NCEER-92-0008   "A Procedure for the Seismic Evaluation of Buildings in the Central and Eastern United States," by C.D. Poland and J.O. Malley, 4/2/92, (PB92-222439, A20, MF-A04).

NCEER-92-0009   "Experimental and Analytical Study of a Hybrid Isolation System Using Friction Controllable Sliding Bearings," by M.Q. Feng, S. Fujii and M. Shinozuka, 5/15/92, (PB93-150282, A06, MF-A02).

NCEER-92-0010   "Seismic Resistance of Slab-Column Connections in Existing Non-Ductile Flat-Plate Buildings," by A.J. Durrani and Y. Du, 5/18/92, (PB93-116812, A06, MF-A02).

NCEER-92-0011   "The Hysteretic and Dynamic Behavior of Brick Masonry Walls Upgraded by Ferrocement Coatings Under Cyclic Loading and Strong Simulated Ground Motion," by H. Lee and S.P. Prawel, 5/11/92, to be published.

NCEER-92-0012   "Study of Wire Rope Systems for Seismic Protection of Equipment in Buildings," by G.F. Demetriades, M.C. Constantinou and A.M. Reinhorn, 5/20/92, (PB93-116655, A08, MF-A02).

NCEER-92-0013   "Shape Memory Structural Dampers: Material Properties, Design and Seismic Testing," by P.R. Witting and F.A. Cozzarelli, 5/26/92, (PB93-116663, A05, MF-A01).

NCEER-92-0014   "Longitudinal Permanent Ground Deformation Effects on Buried Continuous Pipelines," by M.J. O'Rourke, and C. Nordberg, 6/15/92, (PB93-116671, A08, MF-A02).

NCEER-92-0015   "A Simulation Method for Stationary Gaussian Random Functions Based on the Sampling Theorem," by M. Grigoriu and S. Balopoulou, 6/11/92, (PB93-127496, A05, MF-A01).

NCEER-92-0016   "Gravity-Load-Designed Reinforced Concrete Buildings: Seismic Evaluation of Existing Construction and Detailing Strategies for Improved Seismic Resistance," by G.W. Hoffmann, S.K. Kunnath, A.M. Reinhorn and J.B. Mander, 7/15/92, (PB94-142007, A08, MF-A02).

NCEER-92-0017   "Observations on Water System and Pipeline Performance in the Limón Area of Costa Rica Due to the April 22, 1991 Earthquake," by M. O'Rourke and D. Ballantyne, 6/30/92, (PB93-126811, A06, MF-A02).

NCEER-92-0018   "Fourth Edition of Earthquake Education Materials for Grades K-12," Edited by K.E.K. Ross, 8/10/92, (PB93-114023, A07, MF-A02).

NCEER-92-0019   "Proceedings from the Fourth Japan-U.S. Workshop on Earthquake Resistant Design of Lifeline Facilities and Countermeasures for Soil Liquefaction," Edited by M. Hamada and T.D. O'Rourke, 8/12/92, (PB93-163939, A99, MF-E11).

NCEER-92-0020   "Active Bracing System: A Full Scale Implementation of Active Control," by A.M. Reinhorn, T.T. Soong, R.C. Lin, M.A. Riley, Y.P. Wang, S. Aizawa and M. Higashino, 8/14/92, (PB93-127512, A06, MF-A02).

NCEER-92-0021   "Empirical Analysis of Horizontal Ground Displacement Generated by Liquefaction-Induced Lateral Spreads," by S.F. Bartlett and T.L. Youd, 8/17/92, (PB93-188241, A06, MF-A02).

NCEER-92-0022   "IDARC Version 3.0: Inelastic Damage Analysis of Reinforced Concrete Structures," by S.K. Kunnath, A.M. Reinhorn and R.F. Lobo, 8/31/92, (PB93-227502, A07, MF-A02).

NCEER-92-0023   "A Semi-Empirical Analysis of Strong-Motion Peaks in Terms of Seismic Source, Propagation Path and Local Site Conditions, by M. Kamiyama, M.J. O'Rourke and R. Flores-Berrones, 9/9/92, (PB93-150266, A08, MF-A02).

NCEER-92-0024   "Seismic Behavior of Reinforced Concrete Frame Structures with Nonductile Details, Part I: Summary of Experimental Findings of Full Scale Beam-Column Joint Tests," by A. Beres, R.N. White and P. Gergely, 9/30/92, (PB93-227783, A05, MF-A01).

NCEER-92-0025   "Experimental Results of Repaired and Retrofitted Beam-Column Joint Tests in Lightly Reinforced Concrete Frame Buildings," by A. Beres, S. El-Borgi, R.N. White and P. Gergely, 10/29/92, (PB93-227791, A05, MF-A01).

NCEER-92-0026   "A Generalization of Optimal Control Theory: Linear and Nonlinear Structures," by J.N. Yang, Z. Li and S. Vongchavalitkul, 11/2/92, (PB93-188621, A05, MF-A01).

NCEER-92-0027   "Seismic Resistance of Reinforced Concrete Frame Structures Designed Only for Gravity Loads: Part I - Design and Properties of a One-Third Scale Model Structure," by J.M. Bracci, A.M. Reinhorn and J.B. Mander, 12/1/92, (PB94-104502, A08, MF-A02).

NCEER-92-0028   "Seismic Resistance of Reinforced Concrete Frame Structures Designed Only for Gravity Loads: Part II - Experimental Performance of Subassemblages," by L.E. Aycardi, J.B. Mander and A.M. Reinhorn, 12/1/92, (PB94-104510, A08, MF-A02).

NCEER-92-0029   "Seismic Resistance of Reinforced Concrete Frame Structures Designed Only for Gravity Loads: Part III - Experimental Performance and Analytical Study of a Structural Model," by J.M. Bracci, A.M. Reinhorn and J.B. Mander, 12/1/92, (PB93-227528, A09, MF-A01).

NCEER-92-0030   "Evaluation of Seismic Retrofit of Reinforced Concrete Frame Structures: Part I - Experimental Performance of Retrofitted Subassemblages," by D. Choudhuri, J.B. Mander and A.M. Reinhorn, 12/8/92, (PB93-198307, A07, MF-A02).

NCEER-92-0031   "Evaluation of Seismic Retrofit of Reinforced Concrete Frame Structures: Part II - Experimental Performance and Analytical Study of a Retrofitted Structural Model," by J.M. Bracci, A.M. Reinhorn and J.B. Mander, 12/8/92, (PB93-198315, A09, MF-A03).

NCEER-92-0032   "Experimental and Analytical Investigation of Seismic Response of Structures with Supplemental Fluid Viscous Dampers," by M.C. Constantinou and M.D. Symans, 12/21/92, (PB93-191435, A10, MF-A03). This report is available only through NTIS (see address given above).

NCEER-92-0033   "Reconnaissance Report on the Cairo, Egypt Earthquake of October 12, 1992," by M. Khater, 12/23/92, (PB93-188621, A03, MF-A01).

NCEER-92-0034   "Low-Level Dynamic Characteristics of Four Tall Flat-Plate Buildings in New York City," by H. Gavin, S. Yuan, J. Grossman, E. Pekelis and K. Jacob, 12/28/92, (PB93-188217, A07, MF-A02).

NCEER-93-0001   "An Experimental Study on the Seismic Performance of Brick-Infilled Steel Frames With and Without Retrofit," by J.B. Mander, B. Nair, K. Wojtkowski and J. Ma, 1/29/93, (PB93-227510, A07, MF-A02).

NCEER-93-0002   "Social Accounting for Disaster Preparedness and Recovery Planning," by S. Cole, E. Pantoja and V. Razak, 2/22/93, (PB94-142114, A12, MF-A03).

NCEER-93-0003   "Assessment of 1991 NEHRP Provisions for Nonstructural Components and Recommended Revisions," by T.T. Soong, G. Chen, Z. Wu, R-H. Zhang and M. Grigoriu, 3/1/93, (PB93-188639, A06, MF-A02).

NCEER-93-0004   "Evaluation of Static and Response Spectrum Analysis Procedures of SEAOC/UBC for Seismic Isolated Structures," by C.W. Winters and M.C. Constantinou, 3/23/93, (PB93-198299, A10, MF-A03).

NCEER-93-0005   "Earthquakes in the Northeast - Are We Ignoring the Hazard? A Workshop on Earthquake Science and Safety for Educators," edited by K.E.K. Ross, 4/2/93, (PB94-103066, A09, MF-A02).

NCEER-93-0006   "Inelastic Response of Reinforced Concrete Structures with Viscoelastic Braces," by R.F. Lobo, J.M. Bracci, K.L. Shen, A.M. Reinhorn and T.T. Soong, 4/5/93, (PB93-227486, A05, MF-A02).

NCEER-93-0007   "Seismic Testing of Installation Methods for Computers and Data Processing Equipment," by K. Kosar, T.T. Soong, K.L. Shen, J.A. HoLung and Y.K. Lin, 4/12/93, (PB93-198299, A07, MF-A02).

NCEER-93-0008   "Retrofit of Reinforced Concrete Frames Using Added Dampers," by A. Reinhorn, M. Constantinou and C. Li, to be published.

NCEER-93-0009   "Seismic Behavior and Design Guidelines for Steel Frame Structures with Added Viscoelastic Dampers," by K.C. Chang, M.L. Lai, T.T. Soong, D.S. Hao and Y.C. Yeh, 5/1/93, (PB94-141959, A07, MF-A02).

NCEER-93-0010   "Seismic Performance of Shear-Critical Reinforced Concrete Bridge Piers," by J.B. Mander, S.M. Waheed, M.T.A. Chaudhary and S.S. Chen, 5/12/93, (PB93-227494, A08, MF-A02).

NCEER-93-0011   "3D-BASIS-TABS: Computer Program for Nonlinear Dynamic Analysis of Three Dimensional Base Isolated Structures," by S. Nagarajaiah, C. Li, A.M. Reinhorn and M.C. Constantinou, 8/2/93, (PB94-141819, A09, MF-A02).

NCEER-93-0012   "Effects of Hydrocarbon Spills from an Oil Pipeline Break on Ground Water," by O.J. Helweg and H.H.M. Hwang, 8/3/93, (PB94-141942, A06, MF-A02).

NCEER-93-0013   "Simplified Procedures for Seismic Design of Nonstructural Components and Assessment of Current Code Provisions," by M.P. Singh, L.E. Suarez, E.E. Matheu and G.O. Maldonado, 8/4/93, (PB94-141827, A09, MF-A02).

NCEER-93-0014   "An Energy Approach to Seismic Analysis and Design of Secondary Systems," by G. Chen and T.T. Soong, 8/6/93, (PB94-142767, A11, MF-A03).

NCEER-93-0015   "Proceedings from School Sites: Becoming Prepared for Earthquakes - Commemorating the Third Anniversary of the Loma Prieta Earthquake," Edited by F.E. Winslow and K.E.K. Ross, 8/16/93, (PB94-154275, A16, MF-A02).

NCEER-93-0016   "Reconnaissance Report of Damage to Historic Monuments in Cairo, Egypt Following the October 12, 1992 Dahshur Earthquake," by D. Sykora, D. Look, G. Croci, E. Karaesmen and E. Karaesmen, 8/19/93, (PB94-142221, A08, MF-A02).

NCEER-93-0017   "The Island of Guam Earthquake of August 8, 1993," by S.W. Swan and S.K. Harris, 9/30/93, (PB94-141843, A04, MF-A01).

NCEER-93-0018   "Engineering Aspects of the October 12, 1992 Egyptian Earthquake," by A.W. Elgamal, M. Amer, K. Adalier and A. Abul-Fadl, 10/7/93, (PB94-141983, A05, MF-A01).

NCEER-93-0019   "Development of an Earthquake Motion Simulator and its Application in Dynamic Centrifuge Testing," by I. Krstelj, Supervised by J.H. Prevost, 10/23/93, (PB94-181773, A-10, MF-A03).

NCEER-93-0020   "NCEER-Taisei Corporation Research Program on Sliding Seismic Isolation Systems for Bridges: Experimental and Analytical Study of a Friction Pendulum System (FPS)," by M.C. Constantinou, P. Tsopelas, Y-S. Kim and S. Okamoto, 11/1/93, (PB94-142775, A08, MF-A02).

NCEER-93-0021   "Finite Element Modeling of Elastomeric Seismic Isolation Bearings," by L.J. Billings, Supervised by R. Shepherd, 11/8/93, to be published.

NCEER-93-0022   "Seismic Vulnerability of Equipment in Critical Facilities: Life-Safety and Operational Consequences," by K. Porter, G.S. Johnson, M.M. Zadeh, C. Scawthorn and S. Eder, 11/24/93, (PB94-181765, A16, MF-A03).

NCEER-93-0023   "Hokkaido Nansei-oki, Japan Earthquake of July 12, 1993, by P.I. Yanev and C.R. Scawthorn, 12/23/93, (PB94-181500, A07, MF-A01).

NCEER-94-0001   "An Evaluation of Seismic Serviceability of Water Supply Networks with Application to the San Francisco Auxiliary Water Supply System," by I. Markov, Supervised by M. Grigoriu and T. O'Rourke, 1/21/94, (PB94-204013, A07, MF-A02).

NCEER-94-0002   "NCEER-Taisei Corporation Research Program on Sliding Seismic Isolation Systems for Bridges: Experimental and Analytical Study of Systems Consisting of Sliding Bearings, Rubber Restoring Force Devices and Fluid Dampers," Volumes I and II, by P. Tsopelas, S. Okamoto, M.C. Constantinou, D. Ozaki and S. Fujii, 2/4/94, (PB94-181740, A09, MF-A02 and PB94-181757, A12, MF-A03).

NCEER-94-0003   "A Markov Model for Local and Global Damage Indices in Seismic Analysis," by S. Rahman and M. Grigoriu, 2/18/94, (PB94-206000, A12, MF-A03).

NCEER-94-0004   "Proceedings from the NCEER Workshop on Seismic Response of Masonry Infills," edited by D.P. Abrams, 3/1/94, (PB94-180783, A07, MF-A02).

NCEER-94-0005   "The Northridge, California Earthquake of January 17, 1994: General Reconnaissance Report," edited by J.D. Goltz, 3/11/94, (PB94-193943, A10, MF-A03).

NCEER-94-0006   "Seismic Energy Based Fatigue Damage Analysis of Bridge Columns: Part I - Evaluation of Seismic Capacity," by G.A. Chang and J.B. Mander, 3/14/94, (PB94-219185, A11, MF-A03).

NCEER-94-0007   "Seismic Isolation of Multi-Story Frame Structures Using Spherical Sliding Isolation Systems," by T.M. Al-Hussaini, V.A. Zayas and M.C. Constantinou, 3/17/94, (PB94-193745, A09, MF-A02).

NCEER-94-0008   "The Northridge, California Earthquake of January 17, 1994: Performance of Highway Bridges," edited by I.G. Buckle, 3/24/94, (PB94-193851, A06, MF-A02).

NCEER-94-0009   "Proceedings of the Third U.S.-Japan Workshop on Earthquake Protective Systems for Bridges," edited by I.G. Buckle and I. Friedland, 3/31/94, (PB94-195815, A99, MF-A06).

NCEER-94-0010   "3D-BASIS-ME: Computer Program for Nonlinear Dynamic Analysis of Seismically Isolated Single and Multiple Structures and Liquid Storage Tanks," by P.C. Tsopelas, M.C. Constantinou and A.M. Reinhorn, 4/12/94, (PB94-204922, A09, MF-A02).

NCEER-94-0011   "The Northridge, California Earthquake of January 17, 1994: Performance of Gas Transmission Pipelines," by T.D. O'Rourke and M.C. Palmer, 5/16/94, (PB94-204989, A05, MF-A01).

NCEER-94-0012   "Feasibility Study of Replacement Procedures and Earthquake Performance Related to Gas Transmission Pipelines," by T.D. O'Rourke and M.C. Palmer, 5/25/94, (PB94-206638, A09, MF-A02).

NCEER-94-0013   "Seismic Energy Based Fatigue Damage Analysis of Bridge Columns: Part II - Evaluation of Seismic Demand," by G.A. Chang and J.B. Mander, 6/1/94, (PB95-18106, A08, MF-A02).

NCEER-94-0014   "NCEER-Taisei Corporation Research Program on Sliding Seismic Isolation Systems for Bridges: Experimental and Analytical Study of a System Consisting of Sliding Bearings and Fluid Restoring Force/Damping Devices," by P. Tsopelas and M.C. Constantinou, 6/13/94, (PB94-219144, A10, MF-A03).

NCEER-94-0015   "Generation of Hazard-Consistent Fragility Curves for Seismic Loss Estimation Studies," by H. Hwang and J-R. Huo, 6/14/94, (PB95-181996, A09, MF-A02).

NCEER-94-0016   "Seismic Study of Building Frames with Added Energy-Absorbing Devices," by W.S. Pong, C.S. Tsai and G.C. Lee, 6/20/94, (PB94-219136, A10, A03).

NCEER-94-0017   "Sliding Mode Control for Seismic-Excited Linear and Nonlinear Civil Engineering Structures," by J. Yang, J. Wu, A. Agrawal and Z. Li, 6/21/94, (PB95-138483, A06, MF-A02).

NCEER-94-0018   "3D-BASIS-TABS Version 2.0: Computer Program for Nonlinear Dynamic Analysis of Three Dimensional Base Isolated Structures," by A.M. Reinhorn, S. Nagarajaiah, M.C. Constantinou, P. Tsopelas and R. Li, 6/22/94, (PB95-182176, A08, MF-A02).

NCEER-94-0019   "Proceedings of the International Workshop on Civil Infrastructure Systems: Application of Intelligent Systems and Advanced Materials on Bridge Systems," Edited by G.C. Lee and K.C. Chang, 7/18/94, (PB95-252474, A20, MF-A04).

NCEER-94-0020   "Study of Seismic Isolation Systems for Computer Floors," by V. Lambrou and M.C. Constantinou, 7/19/94, (PB95-138533, A10, MF-A03).

NCEER-94-0021   "Proceedings of the U.S.-Italian Workshop on Guidelines for Seismic Evaluation and Rehabilitation of Unreinforced Masonry Buildings," Edited by D.P. Abrams and G.M. Calvi, 7/20/94, (PB95-138749, A13, MF-A03).

NCEER-94-0022   "NCEER-Taisei Corporation Research Program on Sliding Seismic Isolation Systems for Bridges: Experimental and Analytical Study of a System Consisting of Lubricated PTFE Sliding Bearings and Mild Steel Dampers," by P. Tsopelas and M.C. Constantinou, 7/22/94, (PB95-182184, A08, MF-A02).

NCEER-94-0023   "Development of Reliability-Based Design Criteria for Buildings Under Seismic Load," by Y.K. Wen, H. Hwang and M. Shinozuka, 8/1/94, (PB95-211934, A08, MF-A02).

NCEER-94-0024   "Experimental Verification of Acceleration Feedback Control Strategies for an Active Tendon System," by S.J. Dyke, B.F. Spencer, Jr., P. Quast, M.K. Sain, D.C. Kaspari, Jr. and T.T. Soong, 8/29/94, (PB95-212320, A05, MF-A01).

NCEER-94-0025   "Seismic Retrofitting Manual for Highway Bridges," Edited by I.G. Buckle and I.F. Friedland, published by the Federal Highway Administration (PB95-212676, A15, MF-A03).

NCEER-94-0026   "Proceedings from the Fifth U.S.-Japan Workshop on Earthquake Resistant Design of Lifeline Facilities and Countermeasures Against Soil Liquefaction," Edited by T.D. O'Rourke and M. Hamada, 11/7/94, (PB95-220802, A99, MF-E08).

NCEER-95-0001 "Experimental and Analytical Investigation of Seismic Retrofit of Structures with Supplemental Damping: Part 1 - Fluid Viscous Damping Devices," by A.M. Reinhorn, C. Li and M.C. Constantinou, 1/3/95, (PB95-266599, A09, MF-A02).

NCEER-95-0002 "Experimental and Analytical Study of Low-Cycle Fatigue Behavior of Semi-Rigid Top-And-Seat Angle Connections," by G. Pekcan, J.B. Mander and S.S. Chen, 1/5/95, (PB95-220042, A07, MF-A02).

NCEER-95-0003 "NCEER-ATC Joint Study on Fragility of Buildings," by T. Anagnos, C. Rojahn and A.S. Kiremidjian, 1/20/95, (PB95-220026, A06, MF-A02).

NCEER-95-0004 "Nonlinear Control Algorithms for Peak Response Reduction," by Z. Wu, T.T. Soong, V. Gattulli and R.C. Lin, 2/16/95, (PB95-220349, A05, MF-A01).

NCEER-95-0005 "Pipeline Replacement Feasibility Study: A Methodology for Minimizing Seismic and Corrosion Risks to Underground Natural Gas Pipelines," by R.T. Eguchi, H.A. Seligson and D.G. Honegger, 3/2/95, (PB95-252326, A06, MF-A02).

NCEER-95-0006 "Evaluation of Seismic Performance of an 11-Story Frame Building During the 1994 Northridge Earthquake," by F. Naeim, R. DiSulio, K. Benuska, A. Reinhorn and C. Li, to be published.

NCEER-95-0007 "Prioritization of Bridges for Seismic Retrofitting," by N. Basöz and A.S. Kiremidjian, 4/24/95, (PB95-252300, A08, MF-A02).

NCEER-95-0008 "Method for Developing Motion Damage Relationships for Reinforced Concrete Frames," by A. Singhal and A.S. Kiremidjian, 5/11/95, (PB95-266607, A06, MF-A02).

NCEER-95-0009 "Experimental and Analytical Investigation of Seismic Retrofit of Structures with Supplemental Damping: Part II - Friction Devices," by C. Li and A.M. Reinhorn, 7/6/95, (PB96-128087, A11, MF-A03).

NCEER-95-0010 "Experimental Performance and Analytical Study of a Non-Ductile Reinforced Concrete Frame Structure Retrofitted with Elastomeric Spring Dampers," by G. Pekcan, J.B. Mander and S.S. Chen, 7/14/95, (PB96-137161, A08, MF-A02).

NCEER-95-0011 "Development and Experimental Study of Semi-Active Fluid Damping Devices for Seismic Protection of Structures," by M.D. Symans and M.C. Constantinou, 8/3/95, (PB96-136940, A23, MF-A04).

NCEER-95-0012 "Real-Time Structural Parameter Modification (RSPM): Development of Innervated Structures," by Z. Liang, M. Tong and G.C. Lee, 4/11/95, (PB96-137153, A06, MF-A01).

NCEER-95-0013 "Experimental and Analytical Investigation of Seismic Retrofit of Structures with Supplemental Damping: Part III - Viscous Damping Walls," by A.M. Reinhorn and C. Li, 10/1/95, (PB96-176409, A11, MF-A03).

NCEER-95-0014 "Seismic Fragility Analysis of Equipment and Structures in a Memphis Electric Substation," by J-R. Huo and H.H.M. Hwang, 8/10/95, (PB96-128087, A09, MF-A02).

NCEER-95-0015 "The Hanshin-Awaji Earthquake of January 17, 1995: Performance of Lifelines," Edited by M. Shinozuka, 11/3/95, (PB96-176383, A15, MF-A03).

NCEER-95-0016 "Highway Culvert Performance During Earthquakes," by T.L. Youd and C.J. Beckman, available as NCEER-96-0015.

NCEER-95-0017 "The Hanshin-Awaji Earthquake of January 17, 1995: Performance of Highway Bridges," Edited by I.G. Buckle, 12/1/95, to be published.

NCEER-95-0018 "Modeling of Masonry Infill Panels for Structural Analysis," by A.M. Reinhorn, A. Madan, R.E. Valles, Y. Reichmann and J.B. Mander, 12/8/95, (PB97-110886, MF-A01, A06).

NCEER-95-0019 "Optimal Polynomial Control for Linear and Nonlinear Structures," by A.K. Agrawal and J.N. Yang, 12/11/95, (PB96-168737, A07, MF-A02).

NCEER-95-0020 "Retrofit of Non-Ductile Reinforced Concrete Frames Using Friction Dampers," by R.S. Rao, P. Gergely and R.N. White, 12/22/95, (PB97-133508, A10, MF-A02).

NCEER-95-0021 "Parametric Results for Seismic Response of Pile-Supported Bridge Bents," by G. Mylonakis, A. Nikolaou and G. Gazetas, 12/22/95, (PB97-100242, A12, MF-A03).

NCEER-95-0022 "Kinematic Bending Moments in Seismically Stressed Piles," by A. Nikolaou, G. Mylonakis and G. Gazetas, 12/23/95, (PB97-113914, MF-A03, A13).

NCEER-96-0001 "Dynamic Response of Unreinforced Masonry Buildings with Flexible Diaphragms," by A.C. Costley and D.P. Abrams," 10/10/96, (PB97-133573, MF-A03, A15).

NCEER-96-0002 "State of the Art Review: Foundations and Retaining Structures," by I. Po Lam, to be published.

NCEER-96-0003 "Ductility of Rectangular Reinforced Concrete Bridge Columns with Moderate Confinement," by N. Wehbe, M. Saiidi, D. Sanders and B. Douglas, 11/7/96, (PB97-133557, A06, MF-A02).

NCEER-96-0004 "Proceedings of the Long-Span Bridge Seismic Research Workshop," edited by I.G. Buckle and I.M. Friedland, to be published.

NCEER-96-0005 "Establish Representative Pier Types for Comprehensive Study: Eastern United States," by J. Kulicki and Z. Prucz, 5/28/96, (PB98-119217, A07, MF-A02).

NCEER-96-0006 "Establish Representative Pier Types for Comprehensive Study: Western United States," by R. Imbsen, R.A. Schamber and T.A. Osterkamp, 5/28/96, (PB98-118607, A07, MF-A02).

NCEER-96-0007 "Nonlinear Control Techniques for Dynamical Systems with Uncertain Parameters," by R.G. Ghanem and M.I. Bujakov, 5/27/96, (PB97-100259, A17, MF-A03).

NCEER-96-0008 "Seismic Evaluation of a 30-Year Old Non-Ductile Highway Bridge Pier and Its Retrofit," by J.B. Mander, B. Mahmoodzadegan, S. Bhadra and S.S. Chen, 5/31/96, (PB97-110902, MF-A03, A10).

NCEER-96-0009 "Seismic Performance of a Model Reinforced Concrete Bridge Pier Before and After Retrofit," by J.B. Mander, J.H. Kim and C.A. Ligozio, 5/31/96, (PB97-110910, MF-A02, A10).

NCEER-96-0010 "IDARC2D Version 4.0: A Computer Program for the Inelastic Damage Analysis of Buildings," by R.E. Valles, A.M. Reinhorn, S.K. Kunnath, C. Li and A. Madan, 6/3/96, (PB97-100234, A17, MF-A03).

NCEER-96-0011 "Estimation of the Economic Impact of Multiple Lifeline Disruption: Memphis Light, Gas and Water Division Case Study," by S.E. Chang, H.A. Seligson and R.T. Eguchi, 8/16/96, (PB97-133490, A11, MF-A03).

NCEER-96-0012 "Proceedings from the Sixth Japan-U.S. Workshop on Earthquake Resistant Design of Lifeline Facilities and Countermeasures Against Soil Liquefaction, Edited by M. Hamada and T. O'Rourke, 9/11/96, (PB97-133581, A99, MF-A06).

NCEER-96-0013 "Chemical Hazards, Mitigation and Preparedness in Areas of High Seismic Risk: A Methodology for Estimating the Risk of Post-Earthquake Hazardous Materials Release," by H.A. Seligson, R.T. Eguchi, K.J. Tierney and K. Richmond, 11/7/96, (PB97-133565, MF-A02, A08).

NCEER-96-0014 "Response of Steel Bridge Bearings to Reversed Cyclic Loading," by J.B. Mander, D-K. Kim, S.S. Chen and G.J. Premus, 11/13/96, (PB97-140735, A12, MF-A03).

NCEER-96-0015 "Highway Culvert Performance During Past Earthquakes," by T.L. Youd and C.J. Beckman, 11/25/96, (PB97-133532, A06, MF-A01).

NCEER-97-0001 "Evaluation, Prevention and Mitigation of Pounding Effects in Building Structures," by R.E. Valles and A.M. Reinhorn, 2/20/97, (PB97-159552, A14, MF-A03).

NCEER-97-0002 "Seismic Design Criteria for Bridges and Other Highway Structures," by C. Rojahn, R. Mayes, D.G. Anderson, J. Clark, J.H. Hom, R.V. Nutt and M.J. O'Rourke, 4/30/97, (PB97-194658, A06, MF-A03).

NCEER-97-0003   "Proceedings of the U.S.-Italian Workshop on Seismic Evaluation and Retrofit," Edited by D.P. Abrams and G.M. Calvi, 3/19/97, (PB97-194666, A13, MF-A03).

NCEER-97-0004   "Investigation of Seismic Response of Buildings with Linear and Nonlinear Fluid Viscous Dampers," by A.A. Seleemah and M.C. Constantinou, 5/21/97, (PB98-109002, A15, MF-A03).

NCEER-97-0005   "Proceedings of the Workshop on Earthquake Engineering Frontiers in Transportation Facilities," edited by G.C. Lee and I.M. Friedland, 8/29/97, (PB98-128911, A25, MR-A04).

NCEER-97-0006   "Cumulative Seismic Damage of Reinforced Concrete Bridge Piers," by S.K. Kunnath, A. El-Bahy, A. Taylor and W. Stone, 9/2/97, (PB98-108814, A11, MF-A03).

NCEER-97-0007   "Structural Details to Accommodate Seismic Movements of Highway Bridges and Retaining Walls," by R.A. Imbsen, R.A. Schamber, E. Thorkildsen, A. Kartoum, B.T. Martin, T.N. Rosser and J.M. Kulicki, 9/3/97, (PB98-108996, A09, MF-A02).

NCEER-97-0008   "A Method for Earthquake Motion-Damage Relationships with Application to Reinforced Concrete Frames," by A. Singhal and A.S. Kiremidjian, 9/10/97, (PB98-108988, A13, MF-A03).

NCEER-97-0009   "Seismic Analysis and Design of Bridge Abutments Considering Sliding and Rotation," by K. Fishman and R. Richards, Jr., 9/15/97, (PB98-108897, A06, MF-A02).

NCEER-97-0010   "Proceedings of the FHWA/NCEER Workshop on the National Representation of Seismic Ground Motion for New and Existing Highway Facilities," edited by I.M. Friedland, M.S. Power and R.L. Mayes, 9/22/97, (PB98-128903, A21, MF-A04).

NCEER-97-0011   "Seismic Analysis for Design or Retrofit of Gravity Bridge Abutments," by K.L. Fishman, R. Richards, Jr. and R.C. Divito, 10/2/97, (PB98-128937, A08, MF-A02).

NCEER-97-0012   "Evaluation of Simplified Methods of Analysis for Yielding Structures," by P. Tsopelas, M.C. Constantinou, C.A. Kircher and A.S. Whittaker, 10/31/97, (PB98-128929, A10, MF-A03).

NCEER-97-0013   "Seismic Design of Bridge Columns Based on Control and Repairability of Damage," by C-T. Cheng and J.B. Mander, 12/8/97, (PB98-144249, A11, MF-A03).

NCEER-97-0014   "Seismic Resistance of Bridge Piers Based on Damage Avoidance Design," by J.B. Mander and C-T. Cheng, 12/10/97, (PB98-144223, A09, MF-A02).

NCEER-97-0015   "Seismic Response of Nominally Symmetric Systems with Strength Uncertainty," by S. Balopoulou and M. Grigoriu, 12/23/97, (PB98-153422, A11, MF-A03).

NCEER-97-0016   "Evaluation of Seismic Retrofit Methods for Reinforced Concrete Bridge Columns," by T.J. Wipf, F.W. Klaiber and F.M. Russo, 12/28/97, (PB98-144215, A12, MF-A03).

NCEER-97-0017   "Seismic Fragility of Existing Conventional Reinforced Concrete Highway Bridges," by C.L. Mullen and A.S. Cakmak, 12/30/97, (PB98-153406, A08, MF-A02).

NCEER-97-0018   "Loss Asssessment of Memphis Buildings," edited by D.P. Abrams and M. Shinozuka, 12/31/97, (PB98-144231, A13, MF-A03).

NCEER-97-0019   "Seismic Evaluation of Frames with Infill Walls Using Quasi-static Experiments," by K.M. Mosalam, R.N. White and P. Gergely, 12/31/97, (PB98-153455, A07, MF-A02).

NCEER-97-0020   "Seismic Evaluation of Frames with Infill Walls Using Pseudo-dynamic Experiments," by K.M. Mosalam, R.N. White and P. Gergely, 12/31/97, (PB98-153430, A07, MF-A02).

NCEER-97-0021   "Computational Strategies for Frames with Infill Walls: Discrete and Smeared Crack Analyses and Seismic Fragility," by K.M. Mosalam, R.N. White and P. Gergely, 12/31/97, (PB98-153414, A10, MF-A02).

NCEER-97-0022   "Proceedings of the NCEER Workshop on Evaluation of Liquefaction Resistance of Soils," edited by T.L. Youd and I.M. Idriss, 12/31/97, (PB98-155617, A15, MF-A03).

MCEER-98-0001   "Extraction of Nonlinear Hysteretic Properties of Seismically Isolated Bridges from Quick-Release Field Tests," by Q. Chen, B.M. Douglas, E.M. Maragakis and I.G. Buckle, 5/26/98, (PB99-118838, A06, MF-A01).

MCEER-98-0002   "Methodologies for Evaluating the Importance of Highway Bridges," by A. Thomas, S. Eshenaur and J. Kulicki, 5/29/98, (PB99-118846, A10, MF-A02).

MCEER-98-0003   "Capacity Design of Bridge Piers and the Analysis of Overstrength," by J.B. Mander, A. Dutta and P. Goel, 6/1/98, (PB99-118853, A09, MF-A02).

MCEER-98-0004   "Evaluation of Bridge Damage Data from the Loma Prieta and Northridge, California Earthquakes," by N. Basoz and A. Kiremidjian, 6/2/98, (PB99-118861, A15, MF-A03).

MCEER-98-0005   "Screening Guide for Rapid Assessment of Liquefaction Hazard at Highway Bridge Sites," by T. L. Youd, 6/16/98, (PB99-118879, A06, not available on microfiche).

MCEER-98-0006   "Structural Steel and Steel/Concrete Interface Details for Bridges," by P. Ritchie, N. Kauhl and J. Kulicki, 7/13/98, (PB99-118945, A06, MF-A01).

MCEER-98-0007   "Capacity Design and Fatigue Analysis of Confined Concrete Columns," by A. Dutta and J.B. Mander, 7/14/98, (PB99-118960, A14, MF-A03).

MCEER-98-0008   "Proceedings of the Workshop on Performance Criteria for Telecommunication Services Under Earthquake Conditions," edited by A.J. Schiff, 7/15/98, (PB99-118952, A08, MF-A02).

MCEER-98-0009   "Fatigue Analysis of Unconfined Concrete Columns," by J.B. Mander, A. Dutta and J.H. Kim, 9/12/98, (PB99-123655, A10, MF-A02).

MCEER-98-0010   "Centrifuge Modeling of Cyclic Lateral Response of Pile-Cap Systems and Seat-Type Abutments in Dry Sands," by A.D. Gadre and R. Dobry, 10/2/98, (PB99-123606, A13, MF-A03).

MCEER-98-0011   "IDARC-BRIDGE: A Computational Platform for Seismic Damage Assessment of Bridge Structures," by A.M. Reinhorn, V. Simeonov, G. Mylonakis and Y. Reichman, 10/2/98, (PB99-162919, A15, MF-A03).

MCEER-98-0012   "Experimental Investigation of the Dynamic Response of Two Bridges Before and After Retrofitting with Elastomeric Bearings," by D.A. Wendichansky, S.S. Chen and J.B. Mander, 10/2/98, (PB99-162927, A15, MF-A03).

MCEER-98-0013   "Design Procedures for Hinge Restrainers and Hinge Sear Width for Multiple-Frame Bridges," by R. Des Roches and G.L. Fenves, 11/3/98, (PB99-140477, A13, MF-A03).

MCEER-98-0014   "Response Modification Factors for Seismically Isolated Bridges," by M.C. Constantinou and J.K. Quarshie, 11/3/98, (PB99-140485, A14, MF-A03).

MCEER-98-0015   "Proceedings of the U.S.-Italy Workshop on Seismic Protective Systems for Bridges," edited by I.M. Friedland and M.C. Constantinou, 11/3/98, (PB2000-101711, A22, MF-A04).

MCEER-98-0016   "Appropriate Seismic Reliability for Critical Equipment Systems: Recommendations Based on Regional Analysis of Financial and Life Loss," by K. Porter, C. Scawthorn, C. Taylor and N. Blais, 11/10/98, (PB99-157265, A08, MF-A02).

MCEER-98-0017   "Proceedings of the U.S. Japan Joint Seminar on Civil Infrastructure Systems Research," edited by M. Shinozuka and A. Rose, 11/12/98, (PB99-156713, A16, MF-A03).

MCEER-98-0018   "Modeling of Pile Footings and Drilled Shafts for Seismic Design," by I. PoLam, M. Kapuskar and D. Chaudhuri, 12/21/98, (PB99-157257, A09, MF-A02).

MCEER-99-0001 "Seismic Evaluation of a Masonry Infilled Reinforced Concrete Frame by Pseudodynamic Testing," by S.G. Buonopane and R.N. White, 2/16/99, (PB99-162851, A09, MF-A02).

MCEER-99-0002 "Response History Analysis of Structures with Seismic Isolation and Energy Dissipation Systems: Verification Examples for Program SAP2000," by J. Scheller and M.C. Constantinou, 2/22/99, (PB99-162869, A08, MF-A02).

MCEER-99-0003 "Experimental Study on the Seismic Design and Retrofit of Bridge Columns Including Axial Load Effects," by A. Dutta, T. Kokorina and J.B. Mander, 2/22/99, (PB99-162877, A09, MF-A02).

MCEER-99-0004 "Experimental Study of Bridge Elastomeric and Other Isolation and Energy Dissipation Systems with Emphasis on Uplift Prevention and High Velocity Near-source Seismic Excitation," by A. Kasalanati and M. C. Constantinou, 2/26/99, (PB99-162885, A12, MF-A03).

MCEER-99-0005 "Truss Modeling of Reinforced Concrete Shear-flexure Behavior," by J.H. Kim and J.B. Mander, 3/8/99, (PB99-163693, A12, MF-A03).

MCEER-99-0006 "Experimental Investigation and Computational Modeling of Seismic Response of a 1:4 Scale Model Steel Structure with a Load Balancing Supplemental Damping System," by G. Pekcan, J.B. Mander and S.S. Chen, 4/2/99, (PB99-162893, A11, MF-A03).

MCEER-99-0007 "Effect of Vertical Ground Motions on the Structural Response of Highway Bridges," by M.R. Button, C.J. Cronin and R.L. Mayes, 4/10/99, (PB2000-101411, A10, MF-A03).

MCEER-99-0008 "Seismic Reliability Assessment of Critical Facilities: A Handbook, Supporting Documentation, and Model Code Provisions," by G.S. Johnson, R.E. Sheppard, M.D. Quilici, S.J. Eder and C.R. Scawthorn, 4/12/99, (PB2000-101701, A18, MF-A04).

MCEER-99-0009 "Impact Assessment of Selected MCEER Highway Project Research on the Seismic Design of Highway Structures," by C. Rojahn, R. Mayes, D.G. Anderson, J.H. Clark, D'Appolonia Engineering, S. Gloyd and R.V. Nutt, 4/14/99, (PB99-162901, A10, MF-A02).

MCEER-99-0010 "Site Factors and Site Categories in Seismic Codes," by R. Dobry, R. Ramos and M.S. Power, 7/19/99, (PB2000-101705, A08, MF-A02).

MCEER-99-0011 "Restrainer Design Procedures for Multi-Span Simply-Supported Bridges," by M.J. Randall, M. Saiidi, E. Maragakis and T. Isakovic, 7/20/99, (PB2000-101702, A10, MF-A02).

MCEER-99-0012 "Property Modification Factors for Seismic Isolation Bearings," by M.C. Constantinou, P. Tsopelas, A. Kasalanati and E. Wolff, 7/20/99, (PB2000-103387, A11, MF-A03).

MCEER-99-0013 "Critical Seismic Issues for Existing Steel Bridges," by P. Ritchie, N. Kauhl and J. Kulicki, 7/20/99, (PB2000-101697, A09, MF-A02).

MCEER-99-0014 "Nonstructural Damage Database," by A. Kao, T.T. Soong and A. Vender, 7/24/99, (PB2000-101407, A06, MF-A01).

MCEER-99-0015 "Guide to Remedial Measures for Liquefaction Mitigation at Existing Highway Bridge Sites," by H.G. Cooke and J. K. Mitchell, 7/26/99, (PB2000-101703, A11, MF-A03).

MCEER-99-0016 "Proceedings of the MCEER Workshop on Ground Motion Methodologies for the Eastern United States," edited by N. Abrahamson and A. Becker, 8/11/99, (PB2000-103385, A07, MF-A02).

MCEER-99-0017 "Quindío, Colombia Earthquake of January 25, 1999: Reconnaissance Report," by A.P. Asfura and P.J. Flores, 10/4/99, (PB2000-106893, A06, MF-A01).

MCEER-99-0018 "Hysteretic Models for Cyclic Behavior of Deteriorating Inelastic Structures," by M.V. Sivaselvan and A.M. Reinhorn, 11/5/99, (PB2000-103386, A08, MF-A02).

MCEER-99-0019   "Proceedings of the 7th U.S.- Japan Workshop on Earthquake Resistant Design of Lifeline Facilities and Countermeasures Against Soil Liquefaction," edited by T.D. O'Rourke, J.P. Bardet and M. Hamada, 11/19/99, (PB2000-103354, A99, MF-A06).

MCEER-99-0020   "Development of Measurement Capability for Micro-Vibration Evaluations with Application to Chip Fabrication Facilities," by G.C. Lee, Z. Liang, J.W. Song, J.D. Shen and W.C. Liu, 12/1/99, (PB2000-105993, A08, MF-A02).

MCEER-99-0021   "Design and Retrofit Methodology for Building Structures with Supplemental Energy Dissipating Systems," by G. Pekcan, J.B. Mander and S.S. Chen, 12/31/99, (PB2000-105994, A11, MF-A03).

MCEER-00-0001   "The Marmara, Turkey Earthquake of August 17, 1999: Reconnaissance Report," edited by C. Scawthorn; with major contributions by M. Bruneau, R. Eguchi, T. Holzer, G. Johnson, J. Mander, J. Mitchell, W. Mitchell, A. Papageorgiou, C. Scaethorn, and G. Webb, 3/23/00, (PB2000-106200, A11, MF-A03).

MCEER-00-0002   "Proceedings of the MCEER Workshop for Seismic Hazard Mitigation of Health Care Facilities," edited by G.C. Lee, M. Ettouney, M. Grigoriu, J. Hauer and J. Nigg, 3/29/00, (PB2000-106892, A08, MF-A02).

MCEER-00-0003   "The Chi-Chi, Taiwan Earthquake of September 21, 1999: Reconnaissance Report," edited by G.C. Lee and C.H. Loh, with major contributions by G.C. Lee, M. Bruneau, I.G. Buckle, S.E. Chang, P.J. Flores, T.D. O'Rourke, M. Shinozuka, T.T. Soong, C-H. Loh, K-C. Chang, Z-J. Chen, J-S. Hwang, M-L. Lin, G-Y. Liu, K-C. Tsai, G.C. Yao and C-L. Yen, 4/30/00, (PB2001-100980, A10, MF-A02).

MCEER-00-0004   "Seismic Retrofit of End-Sway Frames of Steel Deck-Truss Bridges with a Supplemental Tendon System: Experimental and Analytical Investigation," by G. Pekcan, J.B. Mander and S.S. Chen, 7/1/00, (PB2001-100982, A10, MF-A02).

MCEER-00-0005   "Sliding Fragility of Unrestrained Equipment in Critical Facilities," by W.H. Chong and T.T. Soong, 7/5/00, (PB2001-100983, A08, MF-A02).

MCEER-00-0006   "Seismic Response of Reinforced Concrete Bridge Pier Walls in the Weak Direction," by N. Abo-Shadi, M. Saiidi and D. Sanders, 7/17/00, (PB2001-100981, A17, MF-A03).

MCEER-00-0007   "Low-Cycle Fatigue Behavior of Longitudinal Reinforcement in Reinforced Concrete Bridge Columns," by J. Brown and S.K. Kunnath, 7/23/00, (PB2001-104392, A08, MF-A02).

MCEER-00-0008   "Soil Structure Interaction of Bridges for Seismic Analysis," I. PoLam and H. Law, 9/25/00, (PB2001-105397, A08, MF-A02).

MCEER-00-0009   "Proceedings of the First MCEER Workshop on Mitigation of Earthquake Disaster by Advanced Technologies (MEDAT-1), edited by M. Shinozuka, D.J. Inman and T.D. O'Rourke, 11/10/00, (PB2001-105399, A14, MF-A03).

MCEER-00-0010   "Development and Evaluation of Simplified Procedures for Analysis and Design of Buildings with Passive Energy Dissipation Systems, Revision 01," by O.M. Ramirez, M.C. Constantinou, C.A. Kircher, A.S. Whittaker, M.W. Johnson, J.D. Gomez and C. Chrysostomou, 11/16/01, (PB2001-105523, A23, MF-A04).

MCEER-00-0011   "Dynamic Soil-Foundation-Structure Interaction Analyses of Large Caissons," by C-Y. Chang, C-M. Mok, Z-L. Wang, R. Settgast, F. Waggoner, M.A. Ketchum, H.M. Gonnermann and C-C. Chin, 12/30/00, (PB2001-104373, A07, MF-A02).

MCEER-00-0012   "Experimental Evaluation of Seismic Performance of Bridge Restrainers," by A.G. Vlassis, E.M. Maragakis and M. Saiid Saiidi, 12/30/00, (PB2001-104354, A09, MF-A02).

MCEER-00-0013   "Effect of Spatial Variation of Ground Motion on Highway Structures," by M. Shinozuka, V. Saxena and G. Deodatis, 12/31/00, (PB2001-108755, A13, MF-A03).

MCEER-00-0014   "A Risk-Based Methodology for Assessing the Seismic Performance of Highway Systems," by S.D. Werner, C.E. Taylor, J.E. Moore, II, J.S. Walton and S. Cho, 12/31/00, (PB2001-108756, A14, MF-A03).

MCEER-01-0001 "Experimental Investigation of P-Delta Effects to Collapse During Earthquakes," by D. Vian and M. Bruneau, 6/25/01, (PB2002-100534, A17, MF-A03).

MCEER-01-0002 "Proceedings of the Second MCEER Workshop on Mitigation of Earthquake Disaster by Advanced Technologies (MEDAT-2)," edited by M. Bruneau and D.J. Inman, 7/23/01, (PB2002-100434, A16, MF-A03).

MCEER-01-0003 "Sensitivity Analysis of Dynamic Systems Subjected to Seismic Loads," by C. Roth and M. Grigoriu, 9/18/01, (PB2003-100884, A12, MF-A03).

MCEER-01-0004 "Overcoming Obstacles to Implementing Earthquake Hazard Mitigation Policies: Stage 1 Report," by D.J. Alesch and W.J. Petak, 12/17/01, (PB2002-107949, A07, MF-A02).

MCEER-01-0005 "Updating Real-Time Earthquake Loss Estimates: Methods, Problems and Insights," by C.E. Taylor, S.E. Chang and R.T. Eguchi, 12/17/01, (PB2002-107948, A05, MF-A01).

MCEER-01-0006 "Experimental Investigation and Retrofit of Steel Pile Foundations and Pile Bents Under Cyclic Lateral Loadings," by A. Shama, J. Mander, B. Blabac and S. Chen, 12/31/01, (PB2002-107950, A13, MF-A03).

MCEER-02-0001 "Assessment of Performance of Bolu Viaduct in the 1999 Duzce Earthquake in Turkey" by P.C. Roussis, M.C. Constantinou, M. Erdik, E. Durukal and M. Dicleli, 5/8/02, (PB2003-100883, A08, MF-A02).

MCEER-02-0002 "Seismic Behavior of Rail Counterweight Systems of Elevators in Buildings," by M.P. Singh, Rildova and L.E. Suarez, 5/27/02. (PB2003-100882, A11, MF-A03).

MCEER-02-0003 "Development of Analysis and Design Procedures for Spread Footings," by G. Mylonakis, G. Gazetas, S. Nikolaou and A. Chauncey, 10/02/02, (PB2004-101636, A13, MF-A03, CD-A13).

MCEER-02-0004 "Bare-Earth Algorithms for Use with SAR and LIDAR Digital Elevation Models," by C.K. Huyck, R.T. Eguchi and B. Houshmand, 10/16/02, (PB2004-101637, A07, CD-A07).

MCEER-02-0005 "Review of Energy Dissipation of Compression Members in Concentrically Braced Frames," by K.Lee and M. Bruneau, 10/18/02, (PB2004-101638, A10, CD-A10).

MCEER-03-0001 "Experimental Investigation of Light-Gauge Steel Plate Shear Walls for the Seismic Retrofit of Buildings" by J. Berman and M. Bruneau, 5/2/03, (PB2004-101622, A10, MF-A03, CD-A10).

MCEER-03-0002 "Statistical Analysis of Fragility Curves," by M. Shinozuka, M.Q. Feng, H. Kim, T. Uzawa and T. Ueda, 6/16/03, (PB2004-101849, A09, CD-A09).

MCEER-03-0003 "Proceedings of the Eighth U.S.-Japan Workshop on Earthquake Resistant Design f Lifeline Facilities and Countermeasures Against Liquefaction," edited by M. Hamada, J.P. Bardet and T.D. O'Rourke, 6/30/03, (PB2004-104386, A99, CD-A99).

MCEER-03-0004 "Proceedings of the PRC-US Workshop on Seismic Analysis and Design of Special Bridges," edited by L.C. Fan and G.C. Lee, 7/15/03, (PB2004-104387, A14, CD-A14).

MCEER-03-0005 "Urban Disaster Recovery: A Framework and Simulation Model," by S.B. Miles and S.E. Chang, 7/25/03, (PB2004-104388, A07, CD-A07).

MCEER-03-0006 "Behavior of Underground Piping Joints Due to Static and Dynamic Loading," by R.D. Meis, M. Maragakis and R. Siddharthan, 11/17/03, (PB2005-102194, A13, MF-A03, CD-A00).

MCEER-04-0001 "Experimental Study of Seismic Isolation Systems with Emphasis on Secondary System Response and Verification of Accuracy of Dynamic Response History Analysis Methods," by E. Wolff and M. Constantinou, 1/16/04 (PB2005-102195, A99, MF-E08, CD-A00).

MCEER-04-0002 "Tension, Compression and Cyclic Testing of Engineered Cementitious Composite Materials," by K. Kesner and S.L. Billington, 3/1/04, (PB2005-102196, A08, CD-A08).

MCEER-04-0003   "Cyclic Testing of Braces Laterally Restrained by Steel Studs to Enhance Performance During Earthquakes," by O.C. Celik, J.W. Berman and M. Bruneau, 3/16/04, (PB2005-102197, A13, MF-A03, CD-A00).

MCEER-04-0004   "Methodologies for Post Earthquake Building Damage Detection Using SAR and Optical Remote Sensing: Application to the August 17, 1999 Marmara, Turkey Earthquake," by C.K. Huyck, B.J. Adams, S. Cho, R.T. Eguchi, B. Mansouri and B. Houshmand, 6/15/04, (PB2005-104888, A10, CD-A00).

MCEER-04-0005   "Nonlinear Structural Analysis Towards Collapse Simulation: A Dynamical Systems Approach," by M.V. Sivaselvan and A.M. Reinhorn, 6/16/04, (PB2005-104889, A11, MF-A03, CD-A00).

MCEER-04-0006   "Proceedings of the Second PRC-US Workshop on Seismic Analysis and Design of Special Bridges," edited by G.C. Lee and L.C. Fan, 6/25/04, (PB2005-104890, A16, CD-A00).

MCEER-04-0007   "Seismic Vulnerability Evaluation of Axially Loaded Steel Built-up Laced Members," by K. Lee and M. Bruneau, 6/30/04, (PB2005-104891, A16, CD-A00).

MCEER-04-0008   "Evaluation of Accuracy of Simplified Methods of Analysis and Design of Buildings with Damping Systems for Near-Fault and for Soft-Soil Seismic Motions," by E.A. Pavlou and M.C. Constantinou, 8/16/04, (PB2005-104892, A08, MF-A02, CD-A00).

MCEER-04-0009   "Assessment of Geotechnical Issues in Acute Care Facilities in California," by M. Lew, T.D. O'Rourke, R. Dobry and M. Koch, 9/15/04, (PB2005-104893, A08, CD-A00).

MCEER-04-0010   "Scissor-Jack-Damper Energy Dissipation System," by A.N. Sigaher-Boyle and M.C. Constantinou, 12/1/04 (PB2005-108221).

MCEER-04-0011   "Seismic Retrofit of Bridge Steel Truss Piers Using a Controlled Rocking Approach," by M. Pollino and M. Bruneau, 12/20/04 (PB2006-105795).

MCEER-05-0001   "Experimental and Analytical Studies of Structures Seismically Isolated with an Uplift-Restraint Isolation System," by P.C. Roussis and M.C. Constantinou, 1/10/05 (PB2005-108222).

MCEER-05-0002   "A Versatile Experimentation Model for Study of Structures Near Collapse Applied to Seismic Evaluation of Irregular Structures," by D. Kusumastuti, A.M. Reinhorn and A. Rutenberg, 3/31/05 (PB2006-101523).

MCEER-05-0003   "Proceedings of the Third PRC-US Workshop on Seismic Analysis and Design of Special Bridges," edited by L.C. Fan and G.C. Lee, 4/20/05, (PB2006-105796).

MCEER-05-0004   "Approaches for the Seismic Retrofit of Braced Steel Bridge Piers and Proof-of-Concept Testing of an Eccentrically Braced Frame with Tubular Link," by J.W. Berman and M. Bruneau, 4/21/05 (PB2006-101524).

MCEER-05-0005   "Simulation of Strong Ground Motions for Seismic Fragility Evaluation of Nonstructural Components in Hospitals," by A. Wanitkorkul and A. Filiatrault, 5/26/05 (PB2006-500027).

MCEER-05-0006   "Seismic Safety in California Hospitals: Assessing an Attempt to Accelerate the Replacement or Seismic Retrofit of Older Hospital Facilities," by D.J. Alesch, L.A. Arendt and W.J. Petak, 6/6/05 (PB2006-105794).

MCEER-05-0007   "Development of Seismic Strengthening and Retrofit Strategies for Critical Facilities Using Engineered Cementitious Composite Materials," by K. Kesner and S.L. Billington, 8/29/05 (PB2006-111701).

MCEER-05-0008   "Experimental and Analytical Studies of Base Isolation Systems for Seismic Protection of Power Transformers," by N. Murota, M.Q. Feng and G-Y. Liu, 9/30/05 (PB2006-111702).

MCEER-05-0009   "3D-BASIS-ME-MB: Computer Program for Nonlinear Dynamic Analysis of Seismically Isolated Structures," by P.C. Tsopelas, P.C. Roussis, M.C. Constantinou, R. Buchanan and A.M. Reinhorn, 10/3/05 (PB2006-111703).

MCEER-05-0010   "Steel Plate Shear Walls for Seismic Design and Retrofit of Building Structures," by D. Vian and M. Bruneau, 12/15/05 (PB2006-111704).

MCEER-05-0011 "The Performance-Based Design Paradigm," by M.J. Astrella and A. Whittaker, 12/15/05 (PB2006-111705).

MCEER-06-0001 "Seismic Fragility of Suspended Ceiling Systems," H. Badillo-Almaraz, A.S. Whittaker, A.M. Reinhorn and G.P. Cimellaro, 2/4/06 (PB2006-111706).

MCEER-06-0002 "Multi-Dimensional Fragility of Structures," by G.P. Cimellaro, A.M. Reinhorn and M. Bruneau, 3/1/06 (PB2007-106974, A09, MF-A02, CD A00).

MCEER-06-0003 "Built-Up Shear Links as Energy Dissipators for Seismic Protection of Bridges," by P. Dusicka, A.M. Itani and I.G. Buckle, 3/15/06 (PB2006-111708).

MCEER-06-0004 "Analytical Investigation of the Structural Fuse Concept," by R.E. Vargas and M. Bruneau, 3/16/06 (PB2006-111709).

MCEER-06-0005 "Experimental Investigation of the Structural Fuse Concept," by R.E. Vargas and M. Bruneau, 3/17/06 (PB2006-111710).

MCEER-06-0006 "Further Development of Tubular Eccentrically Braced Frame Links for the Seismic Retrofit of Braced Steel Truss Bridge Piers," by J.W. Berman and M. Bruneau, 3/27/06 (PB2007-105147).

MCEER-06-0007 "REDARS Validation Report," by S. Cho, C.K. Huyck, S. Ghosh and R.T. Eguchi, 8/8/06 (PB2007-106983).

MCEER-06-0008 "Review of Current NDE Technologies for Post-Earthquake Assessment of Retrofitted Bridge Columns," by J.W. Song, Z. Liang and G.C. Lee, 8/21/06 (PB2007-106984).

MCEER-06-0009 "Liquefaction Remediation in Silty Soils Using Dynamic Compaction and Stone Columns," by S. Thevanayagam, G.R. Martin, R. Nashed, T. Shenthan, T. Kanagalingam and N. Ecemis, 8/28/06 (PB2007-106985).

MCEER-06-0010 "Conceptual Design and Experimental Investigation of Polymer Matrix Composite Infill Panels for Seismic Retrofitting," by W. Jung, M. Chiewanichakorn and A.J. Aref, 9/21/06 (PB2007-106986).

MCEER-06-0011 "A Study of the Coupled Horizontal-Vertical Behavior of Elastomeric and Lead-Rubber Seismic Isolation Bearings," by G.P. Warn and A.S. Whittaker, 9/22/06 (PB2007-108679).

MCEER-06-0012 "Proceedings of the Fourth PRC-US Workshop on Seismic Analysis and Design of Special Bridges: Advancing Bridge Technologies in Research, Design, Construction and Preservation," Edited by L.C. Fan, G.C. Lee and L. Ziang, 10/12/06 (PB2007-109042).

MCEER-06-0013 "Cyclic Response and Low Cycle Fatigue Characteristics of Plate Steels," by P. Dusicka, A.M. Itani and I.G. Buckle, 11/1/06 06 (PB2007-106987).

MCEER-06-0014 "Proceedings of the Second US-Taiwan Bridge Engineering Workshop," edited by W.P. Yen, J. Shen, J-Y. Chen and M. Wang, 11/15/06 (PB2008-500041).

MCEER-06-0015 "User Manual and Technical Documentation for the REDARS™ Import Wizard," by S. Cho, S. Ghosh, C.K. Huyck and S.D. Werner, 11/30/06 (PB2007-114766).

MCEER-06-0016 "Hazard Mitigation Strategy and Monitoring Technologies for Urban and Infrastructure Public Buildings: Proceedings of the China-US Workshops," edited by X.Y. Zhou, A.L. Zhang, G.C. Lee and M. Tong, 12/12/06 (PB2008-500018).

MCEER-07-0001 "Static and Kinetic Coefficients of Friction for Rigid Blocks," by C. Kafali, S. Fathali, M. Grigoriu and A.S. Whittaker, 3/20/07 (PB2007-114767).

MCEER-07-0002 "Hazard Mitigation Investment Decision Making: Organizational Response to Legislative Mandate," by L.A. Arendt, D.J. Alesch and W.J. Petak, 4/9/07 (PB2007-114768).

MCEER-07-0003 "Seismic Behavior of Bidirectional-Resistant Ductile End Diaphragms with Unbonded Braces in Straight or Skewed Steel Bridges," by O. Celik and M. Bruneau, 4/11/07 (PB2008-105141).

MCEER-07-0004   "Modeling Pile Behavior in Large Pile Groups Under Lateral Loading," by A.M. Dodds and G.R. Martin, 4/16/07(PB2008-105142).

MCEER-07-0005   "Experimental Investigation of Blast Performance of Seismically Resistant Concrete-Filled Steel Tube Bridge Piers," by S. Fujikura, M. Bruneau and D. Lopez-Garcia, 4/20/07 (PB2008-105143).

MCEER-07-0006   "Seismic Analysis of Conventional and Isolated Liquefied Natural Gas Tanks Using Mechanical Analogs," by I.P. Christovasilis and A.S. Whittaker, 5/1/07.

MCEER-07-0007   "Experimental Seismic Performance Evaluation of Isolation/Restraint Systems for Mechanical Equipment – Part 1: Heavy Equipment Study," by S. Fathali and A. Filiatrault, 6/6/07 (PB2008-105144).

MCEER-07-0008   "Seismic Vulnerability of Timber Bridges and Timber Substructures," by A.A. Sharma, J.B. Mander, I.M. Friedland and D.R. Allicock, 6/7/07 (PB2008-105145).

MCEER-07-0009   "Experimental and Analytical Study of the XY-Friction Pendulum (XY-FP) Bearing for Bridge Applications," by C.C. Marin-Artieda, A.S. Whittaker and M.C. Constantinou, 6/7/07 (PB2008-105191).

MCEER-07-0010   "Proceedings of the PRC-US Earthquake Engineering Forum for Young Researchers," Edited by G.C. Lee and X.Z. Qi, 6/8/07.

MCEER-07-0011   "Design Recommendations for Perforated Steel Plate Shear Walls," by R. Purba and M. Bruneau, 6/18/07, (PB2008-105192).

MCEER-07-0012   "Performance of Seismic Isolation Hardware Under Service and Seismic Loading," by M.C. Constantinou, A.S. Whittaker, Y. Kalpakidis, D.M. Fenz and G.P. Warn, 8/27/07, (PB2008-105193).

MCEER-07-0013   "Experimental Evaluation of the Seismic Performance of Hospital Piping Subassemblies," by E.R. Goodwin, E. Maragakis and A.M. Itani, 9/4/07, (PB2008-105194).

MCEER-07-0014   "A Simulation Model of Urban Disaster Recovery and Resilience: Implementation for the 1994 Northridge Earthquake," by S. Miles and S.E. Chang, 9/7/07, (PB2008-106426).

MCEER-07-0015   "Statistical and Mechanistic Fragility Analysis of Concrete Bridges," by M. Shinozuka, S. Banerjee and S-H. Kim, 9/10/07, (PB2008-106427).

MCEER-07-0016   "Three-Dimensional Modeling of Inelastic Buckling in Frame Structures," by M. Schachter and AM. Reinhorn, 9/13/07, (PB2008-108125).

MCEER-07-0017   "Modeling of Seismic Wave Scattering on Pile Groups and Caissons," by I. Po Lam, H. Law and C.T. Yang, 9/17/07 (PB2008-108150).

MCEER-07-0018   "Bridge Foundations: Modeling Large Pile Groups and Caissons for Seismic Design," by I. Po Lam, H. Law and G.R. Martin (Coordinating Author), 12/1/07 (PB2008-111190).

MCEER-07-0019   "Principles and Performance of Roller Seismic Isolation Bearings for Highway Bridges," by G.C. Lee, Y.C. Ou, Z. Liang, T.C. Niu and J. Song, 12/10/07.

MCEER-07-0020   "Centrifuge Modeling of Permeability and Pinning Reinforcement Effects on Pile Response to Lateral Spreading," by L.L Gonzalez-Lagos, T. Abdoun and R. Dobry, 12/10/07 (PB2008-111191).

MCEER-07-0021   "Damage to the Highway System from the Pisco, Perú Earthquake of August 15, 2007," by J.S. O'Connor, L. Mesa and M. Nykamp, 12/10/07, (PB2008-108126).

MCEER-07-0022   "Experimental Seismic Performance Evaluation of Isolation/Restraint Systems for Mechanical Equipment – Part 2: Light Equipment Study," by S. Fathali and A. Filiatrault, 12/13/07 (PB2008-111192).

MCEER-07-0023   "Fragility Considerations in Highway Bridge Design," by M. Shinozuka, S. Banerjee and S.H. Kim, 12/14/07 (PB2008-111193).

MCEER-07-0024   "Performance Estimates for Seismically Isolated Bridges," by G.P. Warn and A.S. Whittaker, 12/30/07 (PB2008-112230).

MCEER-08-0001   "Seismic Performance of Steel Girder Bridge Superstructures with Conventional Cross Frames," by L.P. Carden, A.M. Itani and I.G. Buckle, 1/7/08, (PB2008-112231).

MCEER-08-0002   "Seismic Performance of Steel Girder Bridge Superstructures with Ductile End Cross Frames with Seismic Isolators," by L.P. Carden, A.M. Itani and I.G. Buckle, 1/7/08 (PB2008-112232).

MCEER-08-0003   "Analytical and Experimental Investigation of a Controlled Rocking Approach for Seismic Protection of Bridge Steel Truss Piers," by M. Pollino and M. Bruneau, 1/21/08 (PB2008-112233).

MCEER-08-0004   "Linking Lifeline Infrastructure Performance and Community Disaster Resilience: Models and Multi-Stakeholder Processes," by S.E. Chang, C. Pasion, K. Tatebe and R. Ahmad, 3/3/08 (PB2008-112234).

MCEER-08-0005   "Modal Analysis of Generally Damped Linear Structures Subjected to Seismic Excitations," by J. Song, Y-L. Chu, Z. Liang and G.C. Lee, 3/4/08 (PB2009-102311).

MCEER-08-0006   "System Performance Under Multi-Hazard Environments," by C. Kafali and M. Grigoriu, 3/4/08 (PB2008-112235).

MCEER-08-0007   "Mechanical Behavior of Multi-Spherical Sliding Bearings," by D.M. Fenz and M.C. Constantinou, 3/6/08 (PB2008-112236).

MCEER-08-0008   "Post-Earthquake Restoration of the Los Angeles Water Supply System," by T.H.P. Tabucchi and R.A. Davidson, 3/7/08 (PB2008-112237).

MCEER-08-0009   "Fragility Analysis of Water Supply Systems," by A. Jacobson and M. Grigoriu, 3/10/08 (PB2009-105545).

MCEER-08-0010   "Experimental Investigation of Full-Scale Two-Story Steel Plate Shear Walls with Reduced Beam Section Connections," by B. Qu, M. Bruneau, C-H. Lin and K-C. Tsai, 3/17/08.

MCEER-08-0011   "Seismic Evaluation and Rehabilitation of Critical Components of Electrical Power Systems," S. Ersoy, B. Feizi, A. Ashrafi and M. Ala Saadeghvaziri, 3/17/08 (PB2009-105546).

MCEER-08-0012   "Seismic Behavior and Design of Boundary Frame Members of Steel Plate Shear Walls," by B. Qu and M. Bruneau, 4/26/08.

MCEER-08-0013   "Development and Appraisal of a Numerical Cyclic Loading Protocol for Quantifying Building System Performance," by A. Filiatrault, A. Wanitkorkul and M. Constantinou, 4/27/08.

MCEER-08-0014   "Structural and Nonstructural Earthquake Design: The Challenge of Integrating Specialty Areas in Designing Complex, Critical Facilities," by W.J. Petak and D.J. Alesch, 4/30/08.

MCEER-08-0015   "Seismic Performance Evaluation of Water Systems," by Y. Wang and T.D. O'Rourke, 5/5/08.

MCEER-08-0016   "Seismic Response Modeling of Water Supply Systems," by P. Shi and T.D. O'Rourke, 5/5/08.

MCEER-08-0017   "Numerical and Experimental Studies of Self-Centering Post-Tensioned Steel Frames," by D. Wang and A. Filiatrault, 5/12/08.

MCEER-08-0018   "Development, Implementation and Verification of Dynamic Analysis Models for Multi-Spherical Sliding Bearings," by D.M. Fenz and M.C. Constantinou, 8/15/08.

MCEER-08-0019   "Performance Assessment of Conventional and Base Isolated Nuclear Power Plants for Earthquake Blast Loadings," by Y.N. Huang, A.S. Whittaker and N. Luco, 10/28/08.

MCEER-08-0020   "Remote Sensing for Resilient Multi-Hazard Disaster Response – Volume I: Introduction to Damage Assessment Methodologies," by B.J. Adams and R.T. Eguchi, 11/17/08.

MCEER-08-0021 "Remote Sensing for Resilient Multi-Hazard Disaster Response – Volume II: Counting the Number of Collapsed Buildings Using an Object-Oriented Analysis: Case Study of the 2003 Bam Earthquake," by L. Gusella, C.K. Huyck and B.J. Adams, 11/17/08.

MCEER-08-0022 "Remote Sensing for Resilient Multi-Hazard Disaster Response – Volume III: Multi-Sensor Image Fusion Techniques for Robust Neighborhood-Scale Urban Damage Assessment," by B.J. Adams and A. McMillan, 11/17/08.

MCEER-08-0023 "Remote Sensing for Resilient Multi-Hazard Disaster Response – Volume IV: A Study of Multi-Temporal and Multi-Resolution SAR Imagery for Post-Katrina Flood Monitoring in New Orleans," by A. McMillan, J.G. Morley, B.J. Adams and S. Chesworth, 11/17/08.

MCEER-08-0024 "Remote Sensing for Resilient Multi-Hazard Disaster Response – Volume V: Integration of Remote Sensing Imagery and VIEWS[TM] Field Data for Post-Hurricane Charley Building Damage Assessment," by J.A. Womble, K. Mehta and B.J. Adams, 11/17/08.

MCEER-08-0025 "Building Inventory Compilation for Disaster Management: Application of Remote Sensing and Statistical Modeling," by P. Sarabandi, A.S. Kiremidjian, R.T. Eguchi and B. J. Adams, 11/20/08.

MCEER-08-0026 "New Experimental Capabilities and Loading Protocols for Seismic Qualification and Fragility Assessment of Nonstructural Systems," by R. Retamales, G. Mosqueda, A. Filiatrault and A. Reinhorn, 11/24/08.